Advances in Experimental Medicine and Biology 860

Chris Peers
Prem Kumar
Christopher N. Wyatt
Estelle Gauda
Colin A. Nurse
Nanduri Prabhakar *Editors*

# Arterial Chemoreceptors in Physiology and Pathophysiology

Springer

# Advances in Experimental Medicine and Biology

## Volume 860

More information about this series at http://www.springer.com/series/5584

Chris Peers • Prem Kumar
Christopher N. Wyatt • Estelle Gauda
Colin A. Nurse • Nanduri Prabhakar
Editors

# Arterial Chemoreceptors in Physiology and Pathophysiology

Springer

*Editors*
Chris Peers
Leeds Institute of Cardiovascular and Metabolic Medicine
Faculty of Medicine and Health
University of Leeds
Leeds, UK

Christopher N. Wyatt
Department of Neuroscience
Cell Biology and Physiology
Wright State University
Dayton, OH, USA

Colin A. Nurse
Department of Biology
McMaster University
Hamilton, ON, Canada

Prem Kumar
College of Medical and Dental Sciences
University of Birmingham
Birmingham, UK

Estelle Gauda
Department of Pediatrics
Johns Hopkins Medical Institutions
Baltimore, MD, USA

Nanduri Prabhakar
Institute for Integrative Physiology and Center for Systems Biology of O(2) Sensing
Biological Sciences Division
University of Chicago
Chicago, IL, USA

ISSN 0065-2598 ISSN 2214-8019 (electronic)
Advances in Experimental Medicine and Biology
ISBN 978-3-319-18439-5 ISBN 978-3-319-18440-1 (eBook)
DOI 10.1007/978-3-319-18440-1

Library of Congress Control Number: 2015947563

Springer Cham Heidelberg New York Dordrecht London


Printed on acid-free paper

Springer International Publishing AG Switzerland is part of Springer Science+Business Media (www.springer.com)

# Preface

This volume of *Advances in Experimental Medicine and Biology* holds the proceedings of the XVIIIth meeting of the International Society for Arterial Chemoreception, which was held in Leeds, UK, from June 30 to July 3, 2014. The collection of chapters represents the contributions – either as oral presentations or posters – of almost all of the attendees at the meeting. The meeting was made possible by the generous support of the University of Leeds (particularly the Faculty of Medicine and Health), the Company of Biologists, and Galleon Pharmaceuticals, and we are most grateful for their support.

In her concluding remarks at the end of this volume, Professor Estelle Gauda gives a comprehensive and engrossing account of the scientific content of the meeting, along with the social aspects which always make ISAC meetings so unique and enjoyable, so there is no need to repeat any such information here. However, we must thank each and every contributor without whom the meeting would not have been such a success. In particular, we are grateful to the plenary speakers: Mike Spyer, Nanduri Prabhakar, Keith Buckler, Bob Fitzgerald, Jose Lopez-Barneo, Harold Schultz, and Julian Paton, each of whom made an important impact at the start of each scientific session. Most of these are presented in this volume, and collectively, they present a concise and readable account of the present state of chemoreceptor research, ranging from cellular and molecular aspects through to clinical intervention.

The meeting as a whole ran very smoothly, thanks to the efforts of some dedicated individuals. Sue Tattersall from Meet in Leeds was the main organizer and go-to person for any problems, but help was at hand from local scientists; Dr Moza Al-Owais, Dr Jacob Elies, and Emily Johnson from Chris Peers' group were always around to provide local knowledge and support. Also working tirelessly throughout the meeting (as well as before and since!) was Prem Kumar, the co-organizer and perfect host, whose efforts were made twice as challenging due to Chris Peers' untimely absence through illness. It was apparent from the feeling at the meeting and subsequent correspondence that he ensured everyone had a memorable and worthwhile time.

The Heymans-De Castro-Neil Prize for early career scientists was selected by a broad-ranging panel of symposiasts. There were many excellent contributions to select from, and after careful deliberation, it was awarded to Maria Joao Ribeiro with Mª Carmen Fernandez-Aguera Rodriguez and Jessica Kohlin gaining runner-up awards. Their contributions are within this volume and we wish them all success with their future careers.

At the ISAC Business Meeting, the decision was confirmed that the next (XIXth) meeting of the society would be held in Baltimore, USA, in 2017, with Professor Estelle Gauda installed as ISAC and Meeting President.

| | |
|---|---|
| Leeds, UK | Chris Peers |
| Birmingham, UK | Prem Kumar |
| Dayton, OH, USA | Chris Wyatt |
| Baltimore, MD, USA | Estelle Gauda |
| Hamilton, ON, Canada | Colin Nurse |
| Chicago, IL, USA | Nanduri Prabhakar |

# Contents

# Epigenetic Regulation of Carotid Body Oxygen Sensing: Clinical Implications

1

Jayasri Nanduri and Nanduri R. Prabhakar

**Abstract**

Recurrent apnea with intermittent hypoxia (IH) is a major clinical problem in infants born preterm. Recent epidemiological studies showed that adults who were born preterm exhibit increased incidence of sleep-disordered breathing and hypertension. Thus, apnea of prematurity predisposes individuals to autonomic dysfunction in adulthood. Experimental studies showed that adult rats exposed to IH as neonates exhibit augmented carotid body and adrenal chromaffin cells (AMC) response to hypoxia and irregular breathing with apneas and hypertension. The enhanced hypoxic sensitivity of the carotid body and AMC in adult rats exposed to neonatal IH was associated with increased oxidative stress, decreased expression of genes encoding anti-oxidant enzymes, and increased expression of pro-oxidant enzymes. Epigenetic mechanisms including DNA methylation leads to long-term changes in gene expression. The decreased expression of the *Sod2* gene, which encodes the anti-oxidant enzyme, superoxide dismutase 2, was associated with DNA hypermethylation of a single CpG dinucleotide close to the transcription start site. Treating neonatal rats with decitabine, an inhibitor of DNA methylation, during IH exposure prevented the oxidative stress, enhanced hypoxic sensitivity, and autonomic dysfunction in adult rats. These findings suggest that epigenetic mechanisms, especially DNA methylation contributes to neonatal programming of hypoxic sensitivity and the ensuing autonomic dysfunction in adulthood.

J. Nanduri
Biological Science Division, Institute for Integrative Physiology, 5841 S. Maryland Avenue, MC 5068, Room N-711, University of Chicago, Chicago, IL 60637, USA
e-mail: jnanduri@uchicago.edu

N.R. Prabhakar (✉)
Biological Science Division, Institute for Integrative Physiology and Center for Systems Biology of O(2) Sensing, University of Chicago, Chicago, IL USA
e-mail: nanduri@uchicago.edu



C. Peers et al. (eds.), *Arterial Chemoreceptors in Physiology and Pathophysiology*, Advances in Experimental Medicine and Biology 860, DOI 10.1007/978-3-319-18440-1_1

**Keywords**
$O_2$ sensing • Apnea • Epigenetic mechanisms • DNA hypermethylation • Exocytosis • Oxidative stress

## 1.1 Introduction

Recurrent apnea (i.e., brief cessation of breathing) with intermittent hypoxia (IH) is a major clinical problem affecting a substantial population of infants born preterm (Nock et al. 2004; Poets et al. 1994). Infants with apnea of prematurity exhibit autonomic dysfunction manifested by clinical signs of increased sympathetic nerve activity (Lagercrantz et al. 1990), defective sympatho-adrenal function (Lagercrantz and Sjöquist 1980) and augmented ventilatory response to hypoxia (Nock et al. 2004). These comorbidities are attributed to augmented chemosensory reflex arising from the carotid body, the principal sensory organ for monitoring arterial blood $O_2$ levels (Kumar and Prabhakar 2012). Recent studies reported augmented hypoxic sensory response of the carotid body in neonatal rats exposed to IH (Pawar et al. 2008). Increased catecholamine (CA) secretion from adrenal medullary chromaffin cells (AMC) is another important homeostatic mechanism for preserving cardiovascular function in neonates under hypoxia (Lagercrantz and Bistoletti 1977; Seidler and Slotkin 1985). IH also enhances hypoxia-evoked CA secretion from AMC in neonatal rats (Souvannakitti et al. 2009a). Remarkably, the effects of neonatal IH on the carotid body and AMC persist into adult life (Pawar et al. 2008; Souvannakitti et al. 2009b). While these findings demonstrate that neonatal IH leads to long-lasting changes in $O_2$ sensing by the carotid body and AMC, little is known about the underlying molecular mechanisms.

It is being increasingly appreciated that epigenetic mechanisms, especially during development, lead to long-term changes in gene expression, which have been implicated in adult diseases resulting from perturbations in fetal/neonatal period (Feinberg 2007). Classic examples include association of low birth weight to risk for developing adult onset of cardiovascular disease (Barker et al. 1993) and type 2 diabetes (Ravelli et al. 1998). Epigenetic changes are heritable modifications of DNA that do not involve changes in DNA primary sequence. Three mechanisms contribute to epigenetic modifications: (a) silencing RNAs, (b) DNA methylation and (c) histone modifications (Feinberg 2007), which either singularly or conjointly determine whether a gene is activated or silenced. Of the three mechanisms, DNA methylation is a key mechanism mediating fetal/neonatal-based adult disease (Niculescu et al. 2005; Waterland and Jirtle 2003). This article describes recent studies showing the involvement of epigenetic mechanisms, especially DNA methylation, in the neonatal programing of $O_2$ sensing by the carotid body and AMC and its impact on cardiorespiratory homeostasis.

## 1.2 Neonatal IH Augments Carotid Body and AMC Responses to Hypoxia

Neonatal rat pups are neurologically immature and resemble prematurely born human infants. The effects of IH on the carotid body responses to hypoxia were examined in neonatal rats. Rat pups with the dams were exposed to IH (15 s of hypoxia followed by 5 min of normoxia, 9 episodes/h, 8 h/day) from ages P0-P10 (Pawar et al. 2009). During each episode of IH, blood $O_2$ saturation decreased from 98 to 82 % (Nanduri et al. 2012). Carotid bodies from control pups reared under normoxia responded poorly to hypoxia, and the response was relatively slow in onset. In striking contrast, carotid bodies from IH exposed pups exhibited robust sensory response to hypoxia, much similar to the adult carotid bodies, and the response was fast occurred within few seconds after the onset of hypoxia (Peng et al. 2004; Pawar et al. 2008; Fig. 1.1).

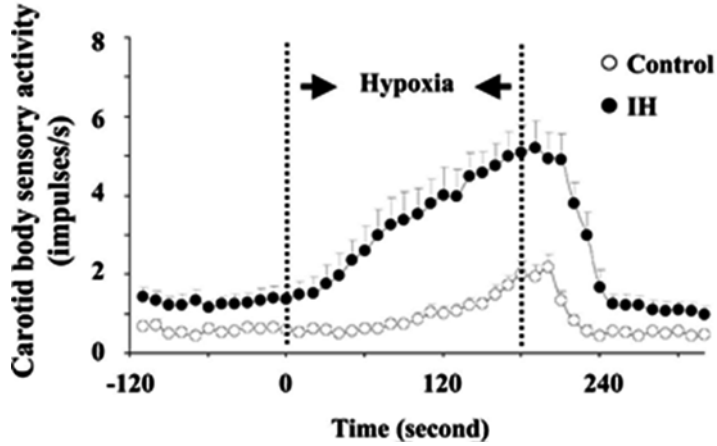


**Fig. 1.1** Time course of the hypoxic sensory response of carotid bodies *ex vivo* from intermittent hypoxia (IH)-exposed and control rat pups reared under normoxia (n = 6 pups in each group; age P5; medium $PO_2 = 32–34 \pm 2$ Torr). Area between *dashed lines* indicates duration of hypoxic challenges (Modified from Peng et al. 2004)

A number of studies reported that hypoxia by directly acting on AMC evokes CA secretion in neonatal rats (Lagercrantz and Bistoletti 1977; Seidler and Slotkin 1985; Takeuchi et al. 2001; Thompson et al. 1997). In IH exposed neonatal rats, the number of AMC responding to hypoxia and the magnitude of CA secretion for a given level of hypoxia were greater than control rat pups (Souvannakitti et al. 2009b). Further analysis showed that the increased CA secretion by hypoxia was due to more number of secretory events as well as the amount of CA released per secretory event. In addition, IH also increased both norepinephrine and epinephrine contents in neonatal adrenal medullae. In striking contrast, hypoxia-evoked CA secretion was reduced in rat pups exposed to continuous hypobaric hypoxia (0.4 ATM), suggesting that the augmented secretory response of AMC is unique to IH (Souvannakitti et al. 2009a and b; Fig. 1.2). These findings demonstrate that exposing neonatal rats to IH, simulating the blood $O_2$ saturation profiles occurring in recurrent apnea augments the hypoxic sensing by the carotid body and AMC.

### 1.2.1 The Effects of Neonatal IH on the Carotid Body and AMC Persist into Adult Life and Their Consequences on Cardio-Respiratory Functions

IH exposed rat pups showed augmented hypoxic ventilatory response (Peng et al. 2004), a hallmark of carotid body chemosensory reflex, which is similar to the heightened HVR seen in preterm infants (Nock et al. 2004). The heightened HVR was associated with higher incidence of apneas in neonatal rat pups (Julien et al. 2008). Remarkably, adult rats treated with neonatal IH exhibited: (a) augmented carotid body response and CA secretion to hypoxia, (b) elevated plasma CA levels, (c) high incidence of apneas, and (d) hypertension as compared to control rats reared under room air (Nanduri et al. 2012). These observations suggest that neonatal IH leads to long-lasting increase in hypoxic sensitivity of the carotid body and AMC and results in serious abnormalities in cardio-respiratory function.

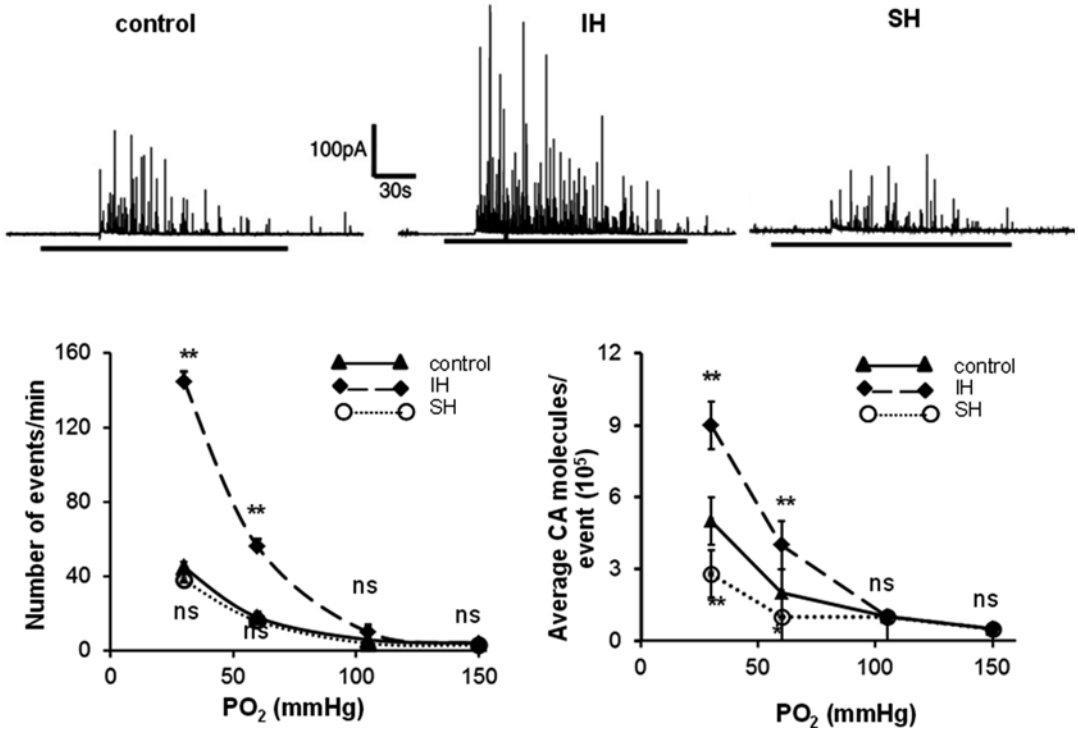


**Fig. 1.2** Effects of intermittent (IH) and sustained hypoxia (SH) on hypoxia–evoked catecholamine (CA) secretion from neonatal adrenal medullary chromaffin cells (AMC). *Top panels*: examples of hypoxia-evoked CA secretion from AMC derived from postnatal day 5 (P5) rats reared under normoxia (control) or IH or SH. *Horizontal black bar* represents the duration of the hypoxia ($PO_2 \simeq 30$ mmHg). *Bottom panels*: average data on the effects of graded hypoxia on the number of secretory events/min (*left*) and the average CA molecules released/event (*right*). $PO_2$, partial pressure of oxygen (mmHg) in the superfusing medium. Data shown are means ± SE. Control = 17 cells, IH = 20 cells and SH = 18 cells (SH) obtained from three different litters in each group. *P < 0.01; **P < 0.001; n.s., not significant (P > 0.05) (Modified from Souvannakitti et al. 2009b)

The above findings from neonatal IH rats are reminiscent of recent clinical studies in human subjects. Adults born with apnea of prematurity exhibit higher incidence of sleep-disordered breathing with several co-morbidities including systemic hypertension and metabolic syndrome (Rosen et al. 2003; Paavonen et al. 2007; Dalziel et al. 2007).

## 1.3 Reactive Oxygen Species (ROS) – A Major Cellular Mechanism Mediating the Effects of Neonatal IH

Adverse physiological consequences of neonatal IH prompted the examination of the underlying mechanisms. Increased reactive oxygen species (ROS) and the ensuing oxidative stress is an important cellular mechanism mediating cardiorespiratory changes caused by IH in experimental models and in patients with recurrent apneas (Christou et al. 2003; Grebe et al. 2006; Prabhakar 2011; Suzuki et al. 2006). Previous studies have shown that ROS mediate cellular responses to IH (Prabhakar et al. 2007). The following observations demonstrate that ROS mediate the neonatal IH-induced augmented hypoxic sensing in the carotid body and AMC: (1) IH increased ROS levels in neonatal carotid bodies and adrenal medullae as evidenced by elevated malondialdehyde (MDA) levels (Pawar et al. 2009; Souvannakitti et al. 2010), which represent oxidized lipids and proteins (Hiroshi et al. 1979; Peng et al. 2003). (2) Rats treated with a stable

superoxide dismutase mimetic (MnTMPyP), a potent scavenger of ROS blocked IH-evoked increases in ROS in the carotid body and abolished sensitization of the hypoxic response (Pawar et al. 2009); and (3) Anti-oxidants prevented the effects of IH on hypoxia-evoked CA secretion and exaggerated $[Ca^{2+}]_i$ responses in neonatal AMC (Souvannakitti et al. 2010).

The elevated ROS levels by IH could be due to either increased generation by pro-oxidant enzymes and/or decreased degradation by anti-oxidant enzymes. The family of NADPH oxidases (NOX) constitutes one of the major sources of ROS generation in mammalian cells (Bedard and Krause 2007). NADPH oxidase 2 and 4 (Nox2 and 4) mRNAs as well as the enzyme activities were up regulated in neonatal adrenal medulla. Similar up regulation of Nox2 and 4 was also seen in IH exposed carotid bodies (Peng et al. 2009). Anti-oxidant enzymes including the manganese superoxide dismutase or SOD-2, catalase (*CAS1*), and glutathione peroxidase 1 (*GPX2*) are down regulated in carotid bodies and adrenal medullae in adult rats exposed to neonatal IH (Nanduri et al. 2012). These observations suggest that both decreased degradation by anti-oxidant enzymes and increased generation by NADPH oxidases contribute to elevated ROS levels by neonatal IH, facilitating the hypoxic sensing by the carotid body and the AMC. These findings further demonstrate that neonatal IH leads to long-lasting changes in genes encoding pro-, and anti-oxidant enzyme leading to persistent oxidative stress in the carotid bodies and adrenal medullae in adult rats.

## 1.4 Neonatal IH Initiates Epigenetic Programming of Redox State by DNA Methylation

DNA methylation is a key mechanism mediating the long-term regulation of gene expression (Niculescu et al. 2005; Waterland and Jirtle 2003). DNA methylation involves covalent addition of a methyl group to the fifth carbon of the cytosine to form 5-methyl cytosine (5meC). Methylation occurs predominantly in cytosine located at 5′ of guanine, known as CpG dinucleotides (CpG), which occur in clusters in the promoter region of genes often referred as "CpG islands". In general, an inverse relationship exists between the extent of methylation of regulatory CpG island(s) and gene transcription (Gardiner-Garden and Frommer 1987; Illingworth and Bird 2009). Thus, DNA hypermethylation leads to repression of gene transcription and hypomethylation causes transcriptional activation.

A recent study by Nanduri et al. (2012) reported that the persistent oxidative stress in adult rats exposed to neonatal IH is in part due to long-lasting down regulation of genes encoding anti-oxidant enzymes in both the carotid body and adrenal medullae involving DNA hypermethylation. Neonatal IH increases DNA hypermethylation of a single CpG dinucleotide within the *Sod2* gene close to the transcription initiation site and was associated with reduced *Sod2* mRNA, protein and enzyme activity.

### 1.4.1 Role of DNA Methyl Transferases in Regulating Anti-oxidant Gene Methylation

DNA methylation is catalyzed by the DNA methyltransferases Dnmt1, Dnmt3a, and Dnmt3b. Whereas Dnmt1 is responsible for the maintenance of methylation, Dnmt3a and Dnmt3b are *de novo* methylases (Miranda and Jones 2007). The expression of Dnmts were analyzed in carotid bodies and adrenal medullae in adult rats exposed to IH during neonatal period (Nanduri et al. 2012). The levels of Dnmt1 and Dnmt3b mRNA and protein were elevated in adult rats exposed to neonatal IH, whereas, Dnmt3a mRNA expression was unchanged.

### 1.4.2 DNA Methyl Transferase Inhibitors Prevent the Long-Lasting Effects of Neonatal IH

Recent studies revealed direct interactions of Dnmt3a and Dnmt3b with specific transcription

factors as an important mechanism for gene regulation by DNA methylation (Hervouet et al. 2009). Dnmts can be inhibited pharmacologically by the nucleoside analog 5-aza-2′-deoxycytidine (decitabine), which irreversibly binds to the Dnmts once incorporated into DNA, resulting in global demethylation after several cell divisions (Bird and Wolffe 1999).

Treating neonatal rats with decitabine, during IH exposure, prevented hypermethylation of the *Sod2 DNA,* oxidative stress, the enhanced hypoxic sensitivity of the carotid body and AMC, and the cardio-respiratory abnormalities in adult rats. The effects of decitabine are unlikely to be due to non-selective actions because: (a) basal hypoxic responses of the carotid body and adrenal medulla were unaffected in decitabine treated rats; (b) decitabine had no effect on responses of the carotid body and adrenal medulla to stimuli other than hypoxia; and (c) in control rats, decitabine had no effect on breathing, and blood pressure, redox status and pro-, and anti-oxidant enzyme expressions.

## 1.5 Summary and Perspective

The findings described above demonstrate a hitherto uncharacterized role for epigenetic modulation of $O_2$ sensing via DNA hypermethylation in neonates, pre-disposing them to disrupted cardio-respiratory homeostasis in adulthood. Genes encoding anti-oxidant enzymes other than *Sod2* were also down regulated in rats treated with neonatal IH (Nanduri et al. 2012); whether DNA methylation contributes to these changes remains to be investigated.

In addition to DNA methylation, post-translational modifications of histones (methylation, acetylation, phosphorylation, and ubiquination) can change chromatin structure, altering the access of RNA polymerase and transcription factors to the DNA and thereby modulating gene expression (Chi et al. 2010). In particular, the relative activities of histone methyltransferases and histone demethylases (JHDMs) provide a dynamic mechanism of transcriptional regulation (Siddiqi et al. 2010). HIF-1 activates the transcription of several *JHDM* genes including *JMJD1A (KDM3A), JMJD2B (KDM4B), and JMJD2C (KDM4C)* (Pollard et al. 2008) and recent studies suggest that JHDMs are important for increasing or maintaining the expression of specific genes that are known to be up-regulated by HIF-1 (Krieg et al. 2010; Xia et al. 2009). Whether HIF-1 activated JHDMs contribute to persistent changes in pro-oxidant gene expression like NADPH oxidase in response to neonatal IH requires further investigation.

Clinical studies also show that epigenetic modifications may constitute an important determinant of inflammatory phenotype in OSA. The levels of DNA methylation of 24 inflammatory related genes were studied in children with OSA with and without high levels of C-reactive protein and it was concluded that FOXP3 DNA methylation levels may provide a potential biomarker for end-organ vulnerability (Kim et al. 2012). In addition, abnormal eNOS-dependent vascular responses in children with OSA was also reported and this phenotype was associated with epigenetic modifications in the eNOS gene (Kheirandish-Gozal et al. 2013).

The current findings of epigenetic modulation of hypoxic sensing may also be of considerable relevance for understanding the impact of long-term IH on autonomic function in adult life. Clinically, this is of great importance because a subset of obstructive sleep apnea (OSA) patients are resistant to continuous positive airway pressure (CPAP) treatment. It is likely that reprogramming by epigenetic mechanisms render these OSA patients resistant to CPAP therapy. Assessing this possibility might lead to the use of DNA hypomethylating drugs as a novel therapeutic intervention to prevent the CPAP resistant co-morbidities in OSA patients.

**Acknowledgement** This research was supported by grants from National Institutes of Health, Heart, Lung and Blood Institute PO1-HL-90554 and UH2- HL-123610.

## References

Barker DJ, Osmond C, Simmonds SJ, Wield GA (1993) The relation of small head circumference and thinness at birth to death from cardiovascular disease in adult life. BMJ 306(6875):422–426

Bedard K, Krause KH (2007) The NOX family of ROS-generating NADPH oxidases: physiology and pathophysiology. Physiol Rev 87(1):245–313

Bird AP, Wolffe AP (1999) Methylation-induced repression–belts, braces, and chromatin. Cell 99(5):451–454

Chi P, Allis CD, Wang GG (2010) Covalent histone modifications–miswritten, misinterpreted and mis-erased in human cancers. Nat Rev Cancer 10(7):457–469

Christou K, Moulas AN, Pastaka C, Gourgoulianis KI (2003) Antioxidant capacity in obstructive sleep apnea patients. Sleep Med 4(3):225–228

Dalziel SR, Parag V, Rodgers A, Harding JE (2007) Cardiovascular risk factors at age 30 following preterm birth. Int J Epidemiol 36(4):907–915

Feinberg AP (2007) Phenotypic plasticity and the epigenetics of human disease. Nature 447(7143):433–440

Gardiner-Garden M, Frommer M (1987) CpG islands in vertebrate genomes. J Mol Biol 196(2):261–282

Grebe M, Eisele HJ, Weissmann N, Schaefer C, Tillmanns H, Seeger W, Schulz R (2006) Antioxidant vitamin C improves endothelial function in obstructive sleep apnea. Am J Respir Crit Care Med 173(8):897–901

Hervouet E, Vallette FM, Cartron PF (2009) Dnmt3/transcription factor interactions as crucial players in targeted DNA methylation. Epigenetics 4(7):487–499

Hiroshi O, Nobuko O, Kunio Y (1979) Assay for lipid peroxidases in animal tissues by thiobarbituric acid reaction. Anal Biochem 95:351–358

Illingworth RS, Bird AP (2009) CpG islands–'a rough guide'. FEBS Lett 583(11):1713–1720

Julien C, Bairam A, Joseph V (2008) Chronic intermittent hypoxia reduces ventilatory long-term facilitation and enhances apnea frequency in newborn rats. Am J Physiol Regul Integr Comp Physiol 294(4):R1356–R1366

Kheirandish-Gozal L, Khalyfa A, Gozal D, Bhattacharjee R, Wang Y (2013) Endothelial dysfunction in children with obstructive sleep apnea is associated with epigenetic changes in the eNOS gene. Chest 143(4):971–977

Kim J, Bhattacharjee R, Khalyfa A, Kheirandish-Gozal L, Capdevila OS, Wang Y, Gozal D (2012) DNA methylation in inflammatory genes among children with obstructive sleep apnea. Am J Respir Crit Care Med 185(3):330–338

Krieg AJ, Rankin EB, Chan D, Razorenova O, Fernandez S, Giaccia AJ (2010) Regulation of the histone demethylase JMJD1A by hypoxia-inducible factor 1 alpha enhances hypoxic gene expression and tumor growth. Mol Cell Biol 30(1):344–353

Kumar P, Prabhakar NR (2012) Peripheral chemoreceptors: function and plasticity of the carotid body. Compr Physiol 2:141–219

Lagercrantz H, Bistoletti P (1977) Catecholamine release in the newborn infant at birth. Pediatr Res 11(8):889–893

Lagercrantz H, Sjöquist B (1980) Deficient sympathoadrenal activity-a cause of apnoea? Urinary excretion of catecholamines and their metabolites in preterm infants. Early Hum Dev 4(4):405–409

Lagercrantz H, Edwards D, Henderson-Smart D, Hertzberg T, Jeffery H (1990) Autonomic reflexes in preterm infants. Acta Paediatr Scand 79(8–9):721–728

Miranda TB, Jones PA (2007) DNA methylation: the nuts and bolts of repression. J Cell Physiol 213(2):384–390

Nanduri J, Makarenko V, Reddy VD, Yuan G, Pawar A, Wang N, Khan SA, Zhang X, Kinsman B, Peng YJ, Kumar GK, Fox AP, Godley LA, Semenza GL, Prabhakar NR (2012) Epigenetic regulation of hypoxic sensing disrupts cardiorespiratory homeostasis. Proc Natl Acad Sci U S A 109(7):2515–2520

Niculescu MD, Craciunescu CN, Zeisel SH (2005) Gene expression profiling of choline-deprived neural precursor cells isolated from mouse brain. Brain Res Mol Brain Res 134(2):309–322

Nock ML, Difiore JM, Arko MK, Martin RJ (2004) Relationship of the ventilatory response to hypoxia with neonatal apnea in preterm infants. J Pediatr 144(3):291–295

Paavonen EJ, Strang-Karlsson S, Räikkönen K, Heinonen K, Pesonen AK, Hovi P, Andersson S, Järvenpää AL, Eriksson JG, Kajantie E (2007) Very low birth weight increases risk for sleep-disordered breathing in young adulthood: the Helsinki Study of Very Low Birth Weight Adults. Pediatrics 120(4):778–784

Pawar A, Peng YJ, Jacono FJ, Prabhakar NR (2008) Comparative analysis of neonatal and adult rat carotid body responses to chronic intermittent hypoxia. J Appl Physiol 104(5):1287–1294

Pawar A, Nanduri J, Yuan G, Khan SA, Wang N, Kumar GK, Prabhakar NR (2009) Reactive oxygen species-dependent endothelin signaling is required for augmented hypoxic sensory response of the neonatal carotid body by intermittent hypoxia. Am J Physiol Regul Integr Comp Physiol 296(3):R735–R742

Peng YJ, Overholt JL, Kline D, Kumar GK, Prabhakar NR (2003) Induction of sensory long-term facilitation in the carotid body by intermittent hypoxia: implications for recurrent apneas. Proc Natl Acad Sci U S A 100(17):10073–10078

Peng YJ, Rennison J, Prabhakar NR (2004) Intermittent hypoxia augments carotid body and ventilatory response to hypoxia in neonatal rat pups. J Appl Physiol 97(5):2020–2025

Peng YJ, Nanduri J, Yuan G, Wang N, Deneris E, Pendyala S, Natarajan V, Kumar GK, Prabhakar NR (2009) NADPH oxidase is required for the sensory plasticity of the carotid body by chronic intermittent hypoxia. J Neurosci 29(15):4903–4910

Poets CF, Samuels MP, Southall DP (1994) Epidemiology and pathophysiology of apnoea of prematurity. Biol Neonate 65(3–4):211–219

Pollard PJ, Loenarz C, Mole DR, McDonough MA, Gleadle JM, Schofield CJ, Ratcliffe PJ (2008) Regulation of Jumonji-domain-containing histone demethylases by hypoxia-inducible factor (HIF)-1alpha. Biochem J 416(3):387–394

Prabhakar NR (2011) Sensory plasticity of the carotid body: role of reactive oxygen species and physio-

logical significance. Respir Physiol Neurobiol 178(3):375–380

Prabhakar NR, Kumar GK, Nanduri J, Semenza GL (2007) ROS signaling in systemic and cellular responses to chronic intermittent hypoxia. Antioxid Redox Signal 9(9):1397–1403

Ravelli AC, van der Meulen JH, Michels RP, Osmond C, Barker DJ, Hales CN, Bleker OP (1998) Glucose tolerance in adults after prenatal exposure to famine. Lancet 351(9097):173–177

Rosen CL, Larkin EK, Kirchner HL, Emancipator JL, Bivins SF, Surovec SA, Martin RJ, Redline S (2003) Prevalence and risk factors for sleep-disordered breathing in 8- to 11-year-old children: association with race and prematurity. J Pediatr 142(4):383–389

Seidler FJ, Slotkin TA (1985) Adrenomedullary function in the neonatal rat: responses to acute hypoxia. J Physiol 358:1–16

Siddiqi S, Mills J, Matushansky I (2010) Epigenetic remodeling of chromatin architecture: exploring tumor differentiation therapies in mesenchymal stem cells and sarcomas. Curr Stem Cell Res Ther 5(1):63–73

Souvannakitti D, Kumar GK, Fox A, Prabhakar NR (2009a) Contrasting effects of intermittent and continuous hypoxia on low O(2) evoked catecholamine secretion from neonatal rat chromaffin cells. Adv Exp Med Biol 648:345–349

Souvannakitti D, Kumar GK, Fox A, Prabhakar NR (2009b) Neonatal intermittent hypoxia leads to long-lasting facilitation of acute hypoxia-evoked catecholamine secretion from rat chromaffin cells. J Neurophysiol 101(6):2837–2846

Souvannakitti D, Nanduri J, Yuan G, Kumar GK, Fox AP, Prabhakar NR (2010) NADPH oxidase-dependent regulation of T-type $Ca^{2+}$ channels and ryanodine receptors mediate the augmented exocytosis of catecholamines from intermittent hypoxia-treated neonatal rat chromaffin cells. J Neurosci 30(32):10763–10772

Suzuki YJ, Jain V, Park AM, Day RM (2006) Oxidative stress and oxidant signaling in obstructive sleep apnea and associated cardiovascular diseases. Free Radic Biol Med 40(10):1683–1692

Takeuchi Y, Mochizuki-Oda N, Yamada H, Kurokawa K, Watanabe Y (2001) Nonneurogenic hypoxia sensitivity in rat adrenal slices. Biochem Biophys Res Commun 289(1):51–56

Thompson RJ, Jackson A, Nurse CA (1997) Developmental loss of hypoxic chemosensitivity in rat adrenomedullary chromaffin cells. J Physiol 498(Pt 2):503–510

Waterland RA, Jirtle RL (2003) Transposable elements: targets for early nutritional effects on epigenetic gene regulation. Mol Cell Biol 23(15):5293–5300

Xia X, Lemieux ME, Li W, Carroll JS, Brown M, Liu XS, Kung AL (2009) Integrative analysis of HIF binding and transactivation reveals its role in maintaining histone methylation homeostasis. Proc Natl Acad Sci U S A 106(11):4260–4265

# 2 Experimental Observations on the Biological Significance of Hydrogen Sulfide in Carotid Body Chemoreception

T. Gallego-Martin, T. Agapito, M. Ramirez, E. Olea, S. Yubero, A. Rocher, A. Gomez-Niño, A. Obeso, and C. Gonzalez

**Abstract**

The cascade of transduction of hypoxia and hypercapnia, the natural stimuli to chemoreceptor cells, is incompletely understood. A particular gap in that knowledge is the role played by second messengers, or in a most ample term, of modulators. A recently described modulator of chemoreceptor cell responses is the gaseous transmitter hydrogen sulfide, which has been proposed as a specific activator of the hypoxic responses in the carotid body, both at the level of the chemoreceptor cell response or at the level of the global output of the organ. Since sulfide behaves in this regard as cAMP, we explored the possibility that sulfide effects were mediated by the more classical messenger. Data indicate that exogenous and endogenous sulfide inhibits adenyl cyclase finding additionally that inhibition of adenylyl cyclase does not modify chemoreceptor cell responses elicited by sulfide. We have also observed that transient receptor potential cation channels A1 (TRPA1) are not regulated by sulfide in chemoreceptor cells.

**Keywords**

Carotid body • Sulfide • Catecholamine • cAMP • TRPA1

## 2.1 Introduction

Normal functioning of the CB consists of the detection of arterial blood gases levels by chemoreceptor cells, the transduction into a neurosecretory response and synaptic transmission to the CSN endings which generate action potentials that reach the nucleus of the tractus solitarius. This medullar nucleus is the first relay of the chemosensory activity and, from there on, information is channelled to different brain stem nuclei to

T. Gallego-Martin (✉) • T. Agapito • M. Ramirez
E. Olea • S. Yubero • A. Rocher • A. Gomez-Niño
A. Obeso • C. Gonzalez
Department of Biochemistry, Molecular Biology and Physiology, Medicine School, University of Valladolid and IBGM/CSIC, Valladolid, Spain

CIBERES. Instituto de Salud Carlos III, Madrid, Spain
e-mail: tgallego@ibgm.uva.es



C. Peers et al. (eds.), *Arterial Chemoreceptors in Physiology and Pathophysiology*,
Advances in Experimental Medicine and Biology 860, DOI 10.1007/978-3-319-18440-1_2

generate integrated respiratory, cardiovascular and hormonal responses. If the central integration and mechanisms of reflex genesis of systemic responses are not well known, the initial steps of the whole chemoreceptor reflex, i.e., the detection-transduction of blood gases levels in chemoreceptor cells and synaptic transmission to CSN nerve endings is comparably poorly understood.

The transduction machinery is complex, and probably dual, that is, there is a machinery to detect arterial blood oxygen levels leading to chemoreceptor cell activation in hypoxic hypoxia and probably another to detect arterial hypercapnia and/or acidosis (Gonzalez et al. 1992, 2010). Likely, hypoxia and hypercapnia share some steps in the chain of events leading to cell activation (Buckler et al. 2000). Many primary molecular entities have been proposed as the primary $O_2$-sensor including a non-identified hemoprotein (Lopez-Lopez and Gonzalez 1992; Riesco-Fagundo et al. 2001; Park et al. 2009), mitochondrial cytochrome oxidase (Biscoe and Duchen 1990; Buckler and Turner 2013) NADPH-oxidase (Cross et al. 1990), hemoxoygenase-1 (Williams et al. 2004) adenosine-monophosphate activated protein kinase (Evans et al. 2005; Evans 2006), and potassium channels (McCartney et al. 2005). When $PO_2$ diminishes in the internal milieu bathing chemoreceptor cells, the molecular putative $O_2$-sensor(s), through ill-defined coupling mechanisms, diminish the opening probability of diverse $O_2$-sensitive $K^+$ channels leading to cell depolarization, activation of voltage operated $Ca^{2+}$ channels, entry of $Ca^{2+}$ and triggering of the release of several neurotransmitters which, in addition to activating the sensory nerve endings of the CSN, feedback control chemoreceptor cell activity via autoreceptors (Gonzalez et al. 1994; Conde et al. 2009; Nurse 2010). At every step from $O_2$-sensing to the release of neurotransmitters, there are second messengers which fine shape the exocytosis and other neurotransmitter releasing mechanisms, and therefore the level of activity generated in the CSN (e.g., Pérez-García et al. 1990, 1991; Gómez-Niño et al. 1994a, b; Rocher et al. 2009; He et al. 2007; Nunes et al. 2010; Kemp and Telezhkin 2014).

Among these second messengers there is one, namely hydrogen sulfide, whose potential capacity to modulate chemoreceptor activity, mechanisms of action, and physiological significance are not well defined (Anichkov and Belen'kii 1963; Telezhkin et al. 2009; Li et al. 2010; Peng et al. 2010; Fitzgerald et al. 2011; Olson 2011; Haouzi et al. 2011; Buckler 2012; Makarenko et al. 2012; Kemp and Telezhkin 2014). Main observations include that sulfide, applied in the form of NaSH, inhibits $K^+$ channels (Telezhkin et al. 2009; Buckler 2012), increases intracellular $Ca^{2+}$ in a voltage dependent and dihydropyridine sensitive $Ca^{2+}$-dependent manner (Buckler 2012; Makarenko et al. 2012) and augments CSN activity and ventilation (Peng et al. 2010; Anichkov and Belen'kii 1963; Van de Louw and Haouzi 2012). Additional observations include that cystathionine-γ-lyase (CSE; one of the enzymes involved in sulfide synthesis) knockout mice exhibit a greatly diminished hypoxic ventilatory response, without alteration of the response to hypercapnia, and a diminished chemoreceptor cells $Ca^{2+}$ response without alteration of the response to high extracellular $K^+$ (Peng et al. 2010; Makarenko et al. 2012). These data would indicate that in mouse the main sulfide synthesizing enzyme in the CB seems to be CSE. In rat, the enzyme responsible for sulfide generation in the CB seems to be cystathionine β-synthase (CBS) as its inhibition reproduces in their major the effects of CSE knockouts mice (Li et al. 2010).

In the present study we have explored the possible contribution of cAMP in sulfide signalling because, cAMP as sulfide production increases during hypoxia, and both messengers positively modulate the responses to hypoxia without affecting those elicited by high $K^+$ (Pérez-García et al. 1990, 1991); also, sulfide dose-dependently increases cAMP levels in rat retinal pigment epithelial cells (Njie-Mbye et al. 2012). In addition, the recent description that sulfide inhibits L-type voltage dependent $Ca^{2+}$ channels in several tissues (Zhang et al. 2012; Streeter et al. 2012; Tang et al. 2013; Avanzato et al. 2014) does not support the notion that the positive modulation of the hypoxic response is linked to $Ca^{2+}$ entry via L-type $Ca^{2+}$ channels. Therefore we have

explored the possibility that sulfide activates alternative pathways for $Ca^{2+}$ entry into chemoreceptor cells, namely transient receptor potential cation channel A1 (TRPA 1), a cationic channel with high $Ca^{2+}$ permeability (Guimaraes and Jordt 2007) activated by many stimuli included sulfide and their derived polysulphates (see Kimura 2014). Additionally, TRPA1 can also be activated by hypoxia (Takahashi et al. 2012).

## 2.2 Material and Methods

### 2.2.1 Animals and Anaesthesia. Surgical Procedures

Experiments were performed with tissues obtained from male adult Wistar rats (280–350 g body weight). Animals were anaesthetized with sodium pentobarbital (60 mg/kg, i.p.) and euthanized by an intracardiac overdose of sodium-pentobarbital. We have followed the European Community Council directive of 24 November 1986 (86/609/EEC) for the Care and Use of Laboratory Animals with protocols for the experiments being approved by the Institutional Committee of the University of Valladolid for Animal Care and Use.

Anaesthetized animals were tracheotomised and bilateral blocks of tissue containing the carotid bifurcations were removed and placed in a dissecting chamber filled with ice-cold $O_2$-saturated Tyrode solution (in mM: NaCl, 140; KCl, 5; $CaCl_2$, 2; $MgCl_2$, 1.1; HEPES, 10; glucose, 5; pH 7.40). The CBs were cleaned of surrounding tissues with the aid of a dissecting microscope. Cleaned CB, were collected and saved in glass vials containing $O_2$-saturated ice-cold Tyrode until use.

### 2.2.2 $^3$H-Catecholamine ($^3$H-CA) Release Experiments Using Intact CBs

General procedures used to label chemoreceptor cells CA deposits and to later study their release have been described in previous publications (Vicario et al. 2000) and analytical methods have been described in detail in Conde et al. (2006). In brief, the CBs were incubated (2 h; 37 °C) in Tyrode solution containing $^3$H-tyrosine (40–50 Ci/mmol; Perkin-Elmer España), 6-methyl-tetrahydropterine (100 μM) and ascorbic acid (1 mM). Following $^3$H-CA labelling incubation, individual CBs were transferred to glass vials containing 2 ml of precursor-free Tyrode bicarbonate solution. Initial incubation in precursor-free normoxic (20 % $O_2$, 5 % $CO_2$, balance $N_2$) solution lasted 1 h, with solutions renewed every 20 min and discarded. Thereafter, incubating solutions were renewed every 10 min and collected for the analysis in their $^3$H-CA content. Specific protocols for drug application are given in the Results sections. Drug solutions were freshly prepared as stock solutions and maintained at 0–4 °C in capped vials.

### 2.2.3 cAMP Measurement

Individual CBs were incubated (30 min) in Tyrode bicarbonate equilibrated with 95 % $O_2$/5 % $CO_2$. Thereafter the incubating solutions were renewed with an identical solution (control) or with test solutions as specified in the Results section; in every instance this second incubation lasted 20 min and contained IBMX 0.5 mM. At the end of the incubation, the organs were placed in homogenizers (0 °C) containing 150 μl of 6 % TCA and after 30 min were homogenized and centrifuged (2,000 × g; 15 min; 4 °C). The supernatant was extracted four times with 500 μl of diethyl ether saturated water. The upper diethyl ether layer from each extraction was discarded and the aqueous layer combined and lyophilized. Samples were stored at −80 °C until assay. Samples were reconstituted in a sodium acetate buffer (0.05 M; pH 5.8) containing BSA at 0.01 %. cAMP was measured using 96 wells commercial kit Healthcare Biosciences (EIA, RPN 2255, GE Healthcare Biosciences) following the instructions of the supplier. The standard curve (12.5–3,200 fmole), tissue extracts and blanks were assayed in duplicated. Tissue contents of cAMP, calculated by interpolation, are expressed as pmole/mg tissue.

#### 2.2.4 Statistics

All data are expressed as the mean ± S.E.M. Statistical analysis were performed by two tails student t-test for unpaired data to compare two groups. Values of $p < 0.05$ indicate statistical significance.

## 2.3 Results

### 2.3.1 Sulfide and cAMP

Hydroxocobalamin is a vitamin B12 analogue that reacts with sulfide according to the reaction: $HS^- + H^+ + HO\text{-}Co\text{-}R \rightarrow HS\text{-}Co\text{-}R + H_2O$. As a result, it has been demonstrated both in vivo and in vitro models that hydroxocobalamin prevents the toxic effects of sulfide (Truong et al. 2007) and in our in vitro CB preparation fully prevents the release of CA elicited by NaSH. Hydroxocobalamin, at the concentration of 300 μM, augmented basal normoxic cAMP from 14.4 ± 1.8 (n = 10) to 27.0 ± 5.2 (n = 6) ($p < 0.01$) pmole/mg tissue and hypoxic cAMP from 47.4 ± 4.9 (n = 5) to 64.4 ± 5.2 (n = 5) ($p < 0.05$). These findings would imply that endogenous sulfide moderately inhibits adenylyl cyclase(s) (Fig. 2.1a). Consistent with these findings we also observed that NaSH (200 μM), diminished normoxic cAMP levels to 8.5 ± 0.8 pmole/mg tissue (n = 5; $p < 0.05$), with hydroxocobalamin fully reversing the effects of the sulfide donor, rising cAMP to 21.9 ± 2.8 pmole/mg tissue.

Figure 2.2 shows the effects of SQ22536, an inhibitor of adenylyl cyclase, on the release of $^3$H-CA elicited by NaSH (200 μM). In panel A it can be seen that the inhibitor (80 μM) did not alter the time course of the NaSH elicited release response. Figure 2.2 panel B shows that the $^{3H\text{-}CA}$ evoked release, equivalent to the area under the curve in panel A, was nearly identical in CBs treated with NaSH and NaSH + SQ22536 and amounted to 8.0 ± 2.7 and 8.1 ± 2.7 (n = 6) percent of the total tissue $^3$H-CA content.

### 2.3.2 Effects of TRPA1 Channel Inhibition of NaSH Elicited $^3$H-CA Release

Using a slightly different protocol we tested the effect of the selective inhibitor of TRPA1 channel HC030031 at a concentration of 60 μM. Control CBs were stimulated twice with 200 μM NaSH and experimental CBs were similarly stimulated, but prior to and during the second stimulus the TRPA1 inhibitor was also present. Figure 2.3a shows the time course of the release of both control and experimental organs showing the apparent absence of effects of the inhibitor. Figure 2.3b shows the ratios of the evoked release in the second to the first stimulus (S2/S1) of both control and experimental CBs. The ratios were, respectively, 0.9 ± 0.1 (n = 4) and 1.1 ± 0.2 (n = 4) in control and HC030031 treated organs, confirming that TRPA1 does not participate in the NaSH response.

## 2.4 Discussion

Present experiments show that, contrary to the hypoxic natural stimulus, NaSH, the most commonly used sulfide donor, decreases the rate of cAMP accumulation in CBs incubated in the presence of the phosphodiesterase inhibitor IBMX. Therefore, our data indicate that sulfide inhibits adenylyl cyclase, the cAMP synthesizing enzyme (Pérez-García et al. 1990). Consistent with this effect of exogenous sulfide the hydroxyl form of vitamin B12 or hyroxocobalamin, which reacts with sulfide (Truong et al. 2007; as well as it reacts with HCN; Borron et al. 2007) reverses the effect produced by exogenous sulfide. Further, hydroxocobalamin which enters inside cells and mitochondria (Begley et al. 1993; Buccellato et al. 2004; see Depeint et al. 2006) and would purportedly react with endogenously generated sulfide, increases basal and hypoxic-stimulated accumulation of cAMP, implying that endogenous sulfide physiologically inhibits cAMP. It should be emphasized, however, that the inhibition

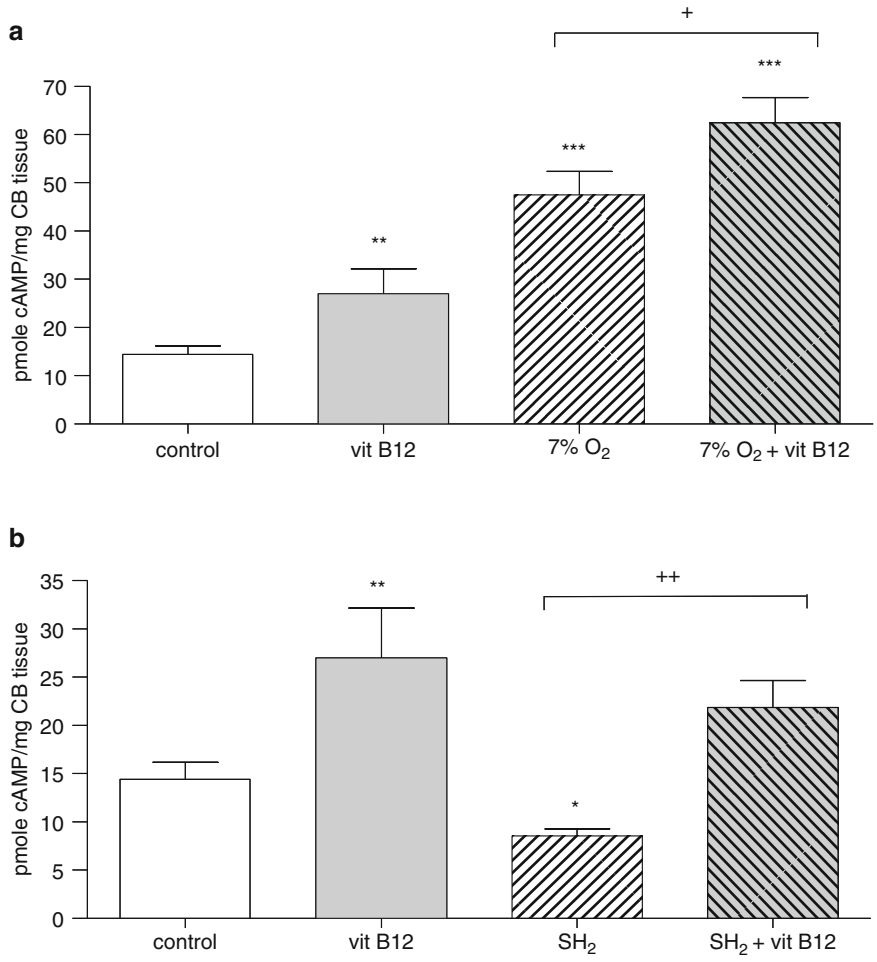


**Fig. 2.1** Effects of different experimental manoeuvres on the rate of cAMP accumulation in the CB (See text for details)

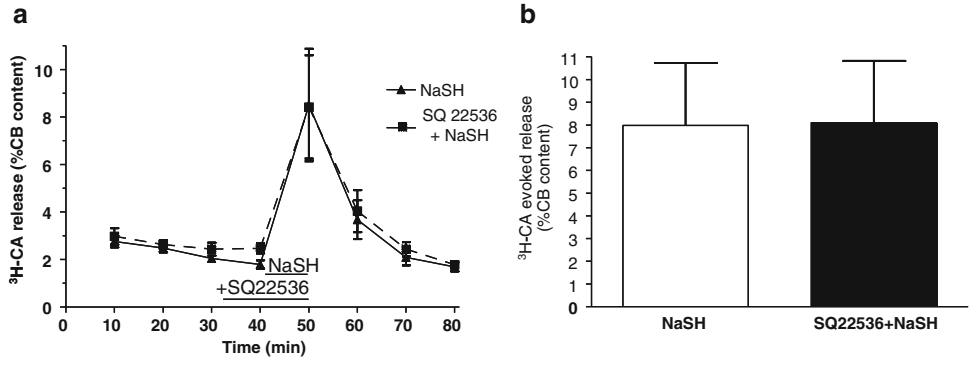


**Fig. 2.2** Effects of the adenylyl cyclase inhibitor SQ22538 on the $^{3}$H-CA release induced by sulphide

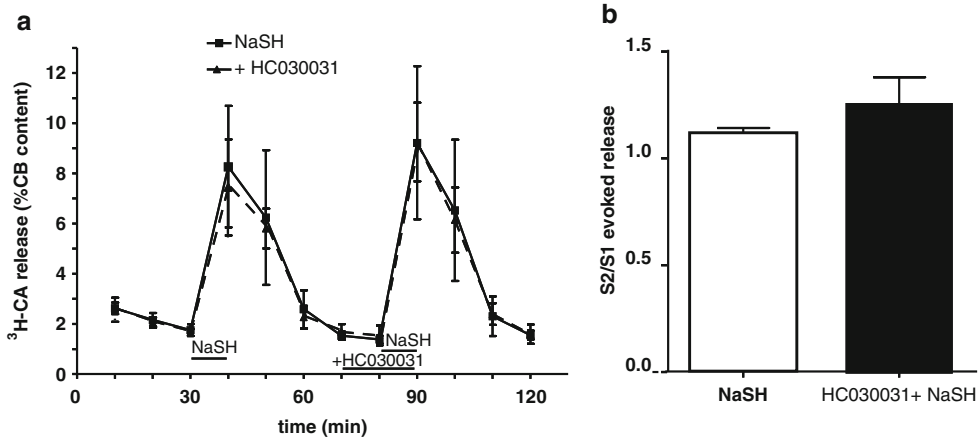


**Fig. 2.3** Effects of the TRPA1 channel inhibitor HC030031 (See text)

exerted by endogenous sulfide, is quantitatively comparable in normoxia and hypoxia, implying that it does not interfere with the intimate mechanism used by hypoxia to activate the cycling enzyme.

The adenylyl cyclase inhibitor, SQ22536, which inhibits the release of $^3$H-CA elicited by hypoxia by around 50 % (Rocher et al. 2009) does not alter the release response elicited by exogenous sulfide, behaving in this regard like the release response elicited by high external $K^+$ which is not affected by cAMP (Pérez-García et al. 1991). Thus, although hypoxia and high external $K^+$ share many steps in the cascade leading to activation of exocytosis (Gonzalez et al. 1994) they are fundamentally different stimulus. Similarly, sulfide and cyanide produce chemoreceptor cell depolarization, promote voltage dependent $Ca^{2+}$ entry to chemoreceptor cells (Buckler 2012) and have a comparable $IC_{50}$ for cytochrome oxidase (Wallace and Starkov 2000; Cooper and Brown 2008), yet cyanide-induced release response is modulated by cAMP while sulfide response is not. These considerations lead us to conclude that even if chemoreceptor cell depolarization and triggering of voltage dependent $Ca^{2+}$ entry shared by many stimuli, each one seems to activate a specific second messenger system, shaping specificity to the responses (Pérez-García et al. 1991; Gómez-Niño et al. 1994a, b).

We also have explored the possibility that TRPA1 represented an alternative or additional pathway to voltage dependent L-type $Ca^{2+}$ channel (Buckler 2012; Makarenko et al. 2012) for $Ca^{2+}$ entry in chemoreceptor cells. The rationale for this search rests on two different observations: one, sulfide activates TRPA1, a $Ca^{2+}$ selective cationic channel, in many structures (Guimaraes and Jordt 2007; Kimura 2014); and, two, sulfide inhibits L-type channels in many preparations (Zhang et al. 2012; Streeter et al. 2012; Tang et al. 2013; Avanzato et al. 2014) making possible that sulphide activates chemoreceptor cells by pathways alternative to L-type channels. Our findings did not support our working hypothesis: either chemoreceptor cells do not express TRPA1 or it is not amenable to sulfide regulation.

In conclusion, exogenous and endogenously produced sulfide inhibits adenylyl cyclase in the carotid body, behaving in this regard in an opposite manner to hypoxia. Similarly, inhibition of adenylyl cyclase does not affect the release response elicited by exogenous sulfide, while that elicited by hypoxia is greatly diminished.

**Acknowledgements** This work was supported by Grants BFU2012-37459 from the Ministry of Economy and Competitiveness (Spain) of and Grant CIBER CB06/06/0050 from the Institute of Health Carlos III (Spain) to C. G.

## References


Anichkov SV, Belen'kii ML (1963) Pharmacology of the carotid body chemoreceptors. Macmillan, New York

Avanzato D, Merlino A, Porrera S, Wang R, Munaron L, Mancardi D (2014) Role of calcium channels in the protective effect of hydrogen sulfide in rat cardiomyoblasts. Cell Physiol Biochem 33(4):1205–1214

Begley JA, Colligan PD, Chu RC, Hall CA (1993) Cobalamin metabolism in cultured human chorionic villus cells. J Cell Physiol 156(1):43–47

Biscoe TJ, Duchen MR (1990) Responses of type I cells dissociated from the rabbit carotid body to hypoxia. J Physiol Lond 428:39–59

Borron SW, Baud FJ, Mégarbane B, Bismuth C (2007) OH-Cbl for severe acute cyanide poisoning by ingestion or inhalation. Am J Emerg Med 25(5):551–558

Buccellato FR, Foi L, Veber D, Pravettoni G, Scalabrino G (2004) Different uptake of cobalamin (vitamin B12) by astrocytes and oligodendrocytes isolated from rat spinal cord. Glia 45(4):406–411

Buckler KJ (2012) Effects of exogenous hydrogen sulfide on calcium signalling, background (TASK) K channel activity and mitochondrial function in chemoreceptor cells. Pflugers Arch 463(5):743–754

Buckler KJ, Turner PJ (2013) Oxygen sensitivity of mitochondrial function in rat arterial chemoreceptor cells. J Physiol 591:3549–3563

Buckler KJ, Williams BA, Honore E (2000) An oxygen-, acid- and anaesthetic-sensitive TASK-like background potassium channel in rat arterial chemoreceptor cells. J Physiol 525:135–142

Conde SV, Obeso A, Vicario I, Rigual R, Rocher A, Gonzalez C (2006) Caffeine inhibition of rat carotid body chemoreceptors is mediated by A2A and A2B adenosine receptors. J Neurochem 98(2):616–628

Conde SV, Monteiro EC, Obeso A, Gonzalez C (2009) Adenosine in peripheral chemoreception: new insights into a historically overlooked molecule. Adv Exp Med Biol 648:145–159

Cooper CE, Brown GC (2008) The inhibition of mitochondrial cytochrome oxidase by the gases carbon monoxide, nitric oxide, hydrogen cyanide and hydrogen sulfide: chemical mechanism and physiological significance. J Bioenerg Biomembr 40(5):533–539

Cross AR, Henderson L, Jones OT, Delpiano MA, Hentschel J, Acker H (1990) Involvement of an NAD(P)H oxidase as a $Po_2$ sensor protein in the rat carotid body. Biochem J 272(3):743–747

Depeint F, Bruce WR, Shangari N, Mehta R, O'Brien PJ (2006) Mitochondrial function and toxicity: role of B vitamins on the one-carbon transfer pathways. Chem Biol Interact 163(1-2):113–132

Evans AM (2006) AMP-activated protein kinase and the regulation of $Ca^{2+}$ signalling in $O_2$-sensing cells. J Physiol 574:113–123

Evans AM, Mustard KJ, Wyatt CN, Peers C, Dipp M, Kumar P, Kinnear NP, Hardie DG (2005) Does AMP-activated protein kinase couple inhibition of mitochondrial oxidative phosphorylation by hypoxia to calcium signaling in $O_2$-sensing cells? J Biol Chem 280(50):41504–41511

Fitzgerald RS, Shirahata M, Chang I, Kostuk E, Kiihl S (2011) The impact of hydrogen sulfide ($H_2S$) on neurotransmitter release from the cat carotid body. Respir Physiol Neurobiol 176(3):80–89

Gómez-Niño A, Almaraz L, González C (1994a) In vitro activation of cyclo-oxygenase in the rabbit carotid body: effect of its blockade on [$^3$H]catecholamine release. J Physiol 476(2):257–267

Gómez-Niño A, López-López JR, Almaraz L, González C (1994b) Inhibition of [$^3$H]catecholamine release and $Ca^{2+}$ currents by prostaglandin E2 in rabbit carotid body chemoreceptor cells. J Physiol 476(2):269–277

Gonzalez C, Almaraz L, Obeso A, Rigual R (1992) Oxygen and acid chemoreception in the carotid body chemoreceptors. Trends Neurosci 15(4):146–153

Gonzalez C, Almaraz L, Obeso A, Rigual R (1994) Carotid body chemoreceptors: from natural stimuli to sensory discharges. Physiol Rev 74(4):829–898

Gonzalez C, Agapito MT, Rocher A, Gomez-Niño A, Rigual R, Castañeda J, Conde SV, Obeso A (2010) A revisit to $O_2$ sensing and transduction in the carotid body chemoreceptors in the context of reactive oxygen species biology. Respir Physiol Neurobiol 174(3):317–330

Guimaraes MZP, Jordt S-E (2007) TRPA1: a sensory channel of many talents (chapter 11). In: Liedtke WB, Heller S (eds) TRP ion channel function in sensory transduction and cellular signaling cascades. Frontiers in neuroscience. CRC Press, Boca Raton

Haouzi P, Bell H, Philmon M (2011) Hydrogen sulfide oxidation and the arterial chemoreflex: effect of methemoglobin. Respir Physiol Neurobiol 177(3):273–283

He L, Chen J, Liu X, Dinger B, Fidone S (2007) Enhanced nitric oxide-mediated chemoreceptor inhibition and altered cyclic GMP signaling in rat carotid body following chronic hypoxia. Am J Physiol Lung Cell Mol Physiol 293(6):L1463–L1468

Kemp PJ, Telezhkin V (2014) Oxygen sensing by the carotid body: is it all just rotten eggs? Antioxid Redox Signal 20(5):794–804

Kimura H (2014) The physiological role of hydrogen sulfide and beyond. Nitric Oxide 41:4–10

Li Q, Sun B, Wang X, Jin Z, Zhou Y, Dong L, Jiang LH, Rong W (2010) A crucial role for hydrogen sulfide in oxygen sensing via modulating large conductance calcium-activated potassium channels. Antioxid Redox Signal 12(10):1179–1189

Lopez-Lopez JR, Gonzalez C (1992) Tissue course of $K^+$ current inhibition by low oxygen in chemoreceptors cells of adult rabbit carotid body. Effects of carbon monoxide. FEBS Lett 299(3):251–254

Makarenko VV, Nanduri J, Raghuraman G, Fox AP, Gadalla MM, Kumar GK, Snyder SH, Prabhakar NR (2012) Endogenous $H_2S$ is required for hypoxic sensing by carotid body glomus cells. Am J Physiol Cell Physiol 303(9):C916–C923

McCartney CE, McClafferty H, Huibant JM, Rowan EG, Shipston MJ, Rowe IC (2005) A cysteine-rich motif confers hypoxia sensitivity to mammalian large conductance voltage- and Ca-activated K (BK) channel alpha-subunits. Proc Natl Acad Sci U S A 102(49):17870–17876

Njie-Mbye YF, Kulkarni M, Opere CA, Ohia SE (2012) Mechanism of action of hydrogen sulfide on cyclic AMP formation in rat retinal pigment epithelial cells. Exp Eye Res 98:16–22

Nunes AR, Batuca JR, Monteiro EC (2010) Acute hypoxia modifies cAMP levels induced by inhibitors of phosphodiesterase-4 in rat carotid bodies, carotid arteries and superior cervical ganglia. Br J Pharmacol 159(2):353–361

Nurse CA (2010) Neurotransmitter and neuromodulatory mechanisms at peripheral arterial chemoreceptors. Exp Physiol 95(6):657–667

Olson KR (2011) Hydrogen sulfide is an oxygen sensor in the carotid body. Respir Physiol Neurobiol 179:103–110

Park SJ, Chun YS, Park KS, Kim SJ, Choi SO, Kim HL, Park JW (2009) Identification of subdomains in NADPH oxidase-4 critical for the oxygen-dependent regulation of TASK-1 K+ channels. Am J Physiol Cell Physiol 297(4):C855–C864

Peng YJ, Nanduri J, Raghuraman G, Souvannakitti D, Gadalla MM, Kumar GK, Snyder SH, Prabhakar NR (2010) $H_2S$ mediates $O_2$ sensing in the carotid body. Proc Natl Acad Sci U S A 107(23):10719–10724

Pérez-García MT, Almaraz L, Gonzalez C (1990) Effects of different types of stimulation on cyclic AMP content in the rabbit carotid body: functional significance. J Neurochem 55(4):1287–1293

Pérez-García MT, Almaraz L, Gonzalez C (1991) Cyclic AMP modulates differentially the release of dopamine induced by hypoxia and other stimuli and increases dopamine synthesis in the rabbit carotid body. J Neurochem 57(6):1992–2000

Riesco-Fagundo A, Pérez-García MT, Gonzalez C, López-López JR (2001) $O_2$ modulates large-conductance $Ca^{2+}$-dependent $K^+$ channels of rat chemoreceptor cells by a membrane-restricted and CO-sensitive mechanism. Circ Res 89(5):430–436

Rocher A, Caceres AI, Almaraz L, Gonzalez C (2009) EPAC signalling pathways are involved in low $PO_2$ chemoreception in carotid body chemoreceptor cells. J Physiol 587:4015–4027

Streeter E, Hart J, Badoer E (2012) An investigation of the mechanisms of hydrogen sulfide-induced vasorelaxation in rat middle cerebral arteries. Naunyn Schmiedebergs Arch Pharmacol 385(10):991–1002

Takahashi N, Kozai D, Mori Y (2012) TRP channels: sensors and transducers of gasotransmitter signals. Front Physiol 3:324

Tang G, Zhang L, Yang G, Wu L, Wang R (2013) Hydrogen sulfide-induced inhibition of L-type $Ca^{2+}$ channels and insulin secretion in mouse pancreatic beta cells. Diabetologia 56(3):533–541

Telezhkin V, Brazier SP, Cayzac S, Müller CT, Riccardi D, Kemp PJ (2009) Hydrogen sulfide inhibits human BK(Ca) channels. Adv Exp Med Biol 648:65–72

Truong DH, Mihajlovic A, Gunness P, Hindmarsh W, O'Brien PJ (2007) Prevention of hydrogen sulfide ($H_2S$)-induced mouse lethality and cytotoxicity by OH-Cbl (vitamin B12a). Toxicology 242(1-3):16–22

Van de Louw A, Haouzi P (2012) Inhibitory effects of hyperoxia and methemoglobinemia on H(2)S induced ventilatory stimulation in the rat. Respir Physiol Neurobiol 181(3):326–334

Vicario I, Rigual R, Obeso A, Gonzalez C (2000) Characterization of the synthesis and release of catecholamine in the rat carotid body in vitro. Am J Physiol Cell Physiol 278(3):C490–C499

Wallace KB, Starkov AA (2000) Mitochondrial targets of drug toxicity. Annu Rev Pharmacol Toxicol 40:353–388

Williams SE, Wootton P, Mason HS, Bould J, Iles DE, Riccardi D, Peers C, Kemp PJ (2004) Hemoxygenase-2 is an oxygen sensor for a calcium-sensitive potassium channel. Science 306(5704):2093–2097

Zhang R, Sun Y, Tsai H, Tang C, Jin H, Du J (2012) Hydrogen sulfide inhibits L-type calcium currents depending upon the protein sulfhydryl state in rat cardiomyocytes. PLoS One 7(5), e37073

# 3 The CamKKβ Inhibitor STO609 Causes Artefacts in Calcium Imaging and Selectively Inhibits $BK_{Ca}$ in Mouse Carotid Body Type I Cells

Jennifer G. Jurcsisn, Richard L. Pye, Jon Ali, Barbara L. Barr, and Christopher N. Wyatt

**Abstract**

It has previously been reported that AMP-activated protein kinase (AMPK) may be critical for hypoxic chemotransduction in carotid body type I cells. This study sought to determine the importance of the regulatory upstream kinase of AMPK, CamKKβ, in the acute response to hypoxia in isolated mouse type I cells.

Initial data indicated several previously unreported artefacts associated with using the CamKKβ inhibitor STO609 and $Ca^{2+}$ imaging techniques. Most importantly Fura-2 and X-Rhod1 imaging revealed that STO609 quenched emission fluorescence even in the absence of intracellular $Ca^{2+}$ ($[Ca^{2+}]_i$). Furthermore, STO609 (100 μM) rapidly inhibited outward macroscopic currents and this inhibition was abolished in the presence of the selective $BK_{Ca}$ inhibitor paxilline.

Taken together these data suggest that ST0609 should be used with caution during $Ca^{2+}$ imaging studies as it can directly interact with $Ca^{2+}$ binding dyes. The rapid inhibitory effect of STO609 on $BK_{Ca}$ was unexpected as the majority of studies using this compound required an incubation of approximately 10 min to inhibit the kinase. Furthermore, as AMPK activation inhibits $BK_{Ca,}$ inhibiting AMPK's upstream kinases would, if anything, be predicted to have the opposite effect on $BK_{Ca}$. Future work will determine if the inhibition of $BK_{Ca}$ is via CamKKβ or via an off target action of STO609 on the channel itself.

J.G. Jurcsisn • R.L. Pye • J. Ali • B.L. Barr
C.N. Wyatt (✉)
Department of Neuroscience, Cell Biology and Physiology, Wright State University,
3640 Colonel Glenn Hwy, Dayton, OH 45435, USA
e-mail: christopher.wyatt@wright.edu



C. Peers et al. (eds.), *Arterial Chemoreceptors in Physiology and Pathophysiology*,
Advances in Experimental Medicine and Biology 860, DOI 10.1007/978-3-319-18440-1_3

**Keywords**
Carotid body • Type I cells • CamKKβ • STO609

## 3.1 Introduction

Adenosine monophosphate-activated protein kinase (AMPK) has been identified as a master regulator of energy balance throughout the body (Hardie 2008). Recent evidence suggests that AMPK can also influence neuronal excitability by regulating ion channels (Ross et al. 2011). Moreover, there is increasing evidence that AMPK is critical in the transduction cascade whereby hypoxic inhibition of $K^+$ channels causes depolarization and subsequent neurotransmitter release from carotid body (CB) Type I cells (Wyatt and Evans 2007). Activation of AMPK is dependent on one of its three known upstream kinases: LKB1 (Hawley et al. 2003; Woods et al. 2003), CamKKβ (Hawley et al. 2005; Woods et al. 2005), and TAK1 (Momcilovic et al. 2006). These upstream kinases phosphorylate AMPK at the threonine-172 (Thr-172) location on the catalytic alpha subunit (Carling et al. 2008; Fogarty et al. 2010). Once activated, AMPK phosphorylates multiple different targets, including ion channels. Therefore it is conceivable that inhibition of the upstream kinases of AMPK may attenuate the hypoxic response in CB Type I cells.

The compound STO-609 has been widely used as a selective pharmacological inhibitor of CamKKβ in a variety of preparations (Hawley et al. 2005; Tamás et al. 2006; Tokumitsu et al. 2002). The crystallized structure of the STO-609-CamKKβ complex shows that STO-609 binds near the ATP-binding site of the kinase, inducing structural changes that result in a closed conformation state (Kukimoto-Niino et al. 2011). This specific inhibitor has been used in conjunction with $Ca^{2+}$ imaging experiments (Monteiro et al. 2008; Wayman et al. 2004) as well as electrophysiological recordings (Tamás et al. 2006; Schmitt et al. 2005). Therefore, STO-609 seemed suitable for examining the potential role of CamKKβ as a regulator of hypoxic chemotransduction in carotid body type I cells. If CamKKβ was inhibited by STO-609, the AMPK activation cascade would be disrupted, allowing the chemosensitive $K^+$ channels that would normally close under hypoxic circumstances to stay open, inhibiting depolarization of the cell membrane and subsequent influx of $Ca^{2+}$. The hypoxic response would then ultimately be attenuated.

## 3.2 Methods

All studies were performed in accordance with protocols approved by the Wright State University Institutional Laboratory Animal Care and Use Committee (IACUC). These protocols are in accordance with the National Institute of Health guide for the care and use of laboratory animals (NIH publications No. 80-23) revised 1996.

### 3.2.1 Type I Cell Isolation

On the day of experimentation two to five adult mice (25–35 g) were euthanized with a rising concentration of $CO_2$. Carotid artery bifurcations were removed and the carotid bodies excised. Carotid bodies were then dissociated and type I cells isolated as has previously been described for neonatal rat type I cells (Burlon et al. 2009). Isolated type I cells were maintained in tissue culture for up to 8 h.

### 3.2.2 N2A Cell Culture

Mouse neuroblastoma cells (N2A) lines were maintained, split (1:20 ratio), and grown the week prior to usage. On the day of experimentation, the 75 $mm^2$ Tissue Culture flask (Corning) containing the cells was removed from the 37 °C, humidified, 5 % $CO_2$/air incubator. The remaining growth media in the flask taken from a stock

comprised of 250 ml DMEM with high glucose (Gibco Life Technologies), 250 ml Opti-MEM + GlutaMAX (Gibco Life Technologies), 25 ml 5 % Fetal Bovine Serum (BioWest) and 5 ml penicillin/streptomycin solution (10,000 units/ml penicillin 10,000 µg/ml streptomycin) (Gibco Life Technologies) was removed and the cells were rinsed with 5 ml Phosphate Buffered Saline (Gibco Life Technologies). 2 ml of 0.25 % Trypsin-EDTA (Gibco Life Technologies) was added and allowed to incubate at 37 °C for 2 min to loosen the cells from the flask. 5 ml of the growth media was added to stop digestion and the cells were drawn up and placed in a 50 ml tube. The cells were centrifuged at 750 rpm for 5 min. After removing the supernatant, the pellet was resuspended in 10 ml of the growth media and plated in 50 µl increments onto glass coverslips coated with poly-d-lysine (0.01 % w/v).

### 3.2.3 $Ca^{2+}$ Imaging

For experiments recording intracellular calcium ($[Ca^{2+}]_i$) type I cells were loaded with 5 µM FURA-2 AM (Invitrogen) for 30 min at room temperature. The dye was excited with 340/380 nm light and emitted light was recorded at 510 nm using a Coolsnap HQ2 CCD camera (Photometrics). Image acquisition was controlled by Metafluor software (Molecular Devices) and cells were visualized using a Nikon TE2000-U microscope with a X40 objective. Extracellular solution was HEPES buffered salt solution (in mM): 140 NaCl, 4.5 KCl, 2.5 $CaCl_2$, 1, $MgCl_2$, 11 glucose, 10 HEPES, adjusted to pH 7.4 with NaOH at 37 °C. The high potassium stimulus was (in mM): 64.5 NaCl, 80 KCl, 2.5 $CaCl_2$, 1, $MgCl_2$, 11 glucose, 10 HEPES adjusted to pH 7.4 with KOH at 37 °C.

Isolated type I cells were loaded with the $Ca^{2+}$-sensitive fluorescent dye X-Rhod-1-AM (5 µM, Invitrogen) using the same procedure as Fura-2. The X-Rhod-1 loaded cells were excited with 50 msec exposures to 580 nm light at 0.2 Hz reflected up to the cells by way of a Texas Red dichroic mirror (Chroma). The emitted fluorescence measured at 602 nm was then allowed to pass through the dichroic mirror and be captured using a CoolSNAP HQ2 CCD camera. Fluorescence emission was measured before, during, and after perfusing STO-609 (100 µM, Tocris) over the cells for approximately 10 min. In some of these experiments, type I cells were excited by a high $K^+$ extracellular solution of composition (in mM): NaCl, 64; KCl, 80; $CaCl_2$, 2.5; $MgCl_2$, 1; glucose, 11; HEPES, 11; pH 7.4 at 37 °C with KOH were used. All other imaging and recording parameters were identical to those used for the Fura-2 experiments.

Experiments were also conducted both in N2A cells loaded with Fura-2 and X-Rhod-1 at zero $[Ca^{2+}]_i$ by perfusing cells with the extracellular solution described previously, but with $Ca^{2+}$ removed and 10 mM EGTA and 2 µM of the calcium ionophore ionomycin added. After applying the solution containing ionomycin, $Ca^{2+}$ levels were allowed to reach a zero baseline before applying STO-609 (100 µM, Tocris, Fig. 3.3).

### 3.2.4 Electrophysiology

Isolated type I cells were mounted in a chamber (0.4 ml, RC-25F, Warner Instruments) and perfused at 8 ml/min with extracellular solution of composition (in mM): NaCl, 117; KCl, 4.6; $CaCl_2$, 2.5; $MgCl_2$, 1; glucose, 11; $NaHCO_3$, 23; pH 7.4 via bubbling with 5 % $CO_2$/95 % air. Cells were visualized with a Nikon TE 2000U inverted microscope. The traditional whole-cell configuration of the patch clamp technique was used. Data were acquired using an Axopatch 200B amplifier (Molecular Devices). Currents were digitized at 5 kHz and filtered at 1 kHz. Experiments were performed at 35–37 °C. Results were not leak subtracted, seal resistance was typically >5 GΩ, access resistance was typically 20–30 MΩ and was not compensated, and holding currents were typically less than 20 pA throughout the recordings. All data were recorded using Clampex v10.0 software and analyzed using Clampfit v10.0 software (Molecular Devices). All experiments were carried out on an anti-vibration microscopy table (TMC).

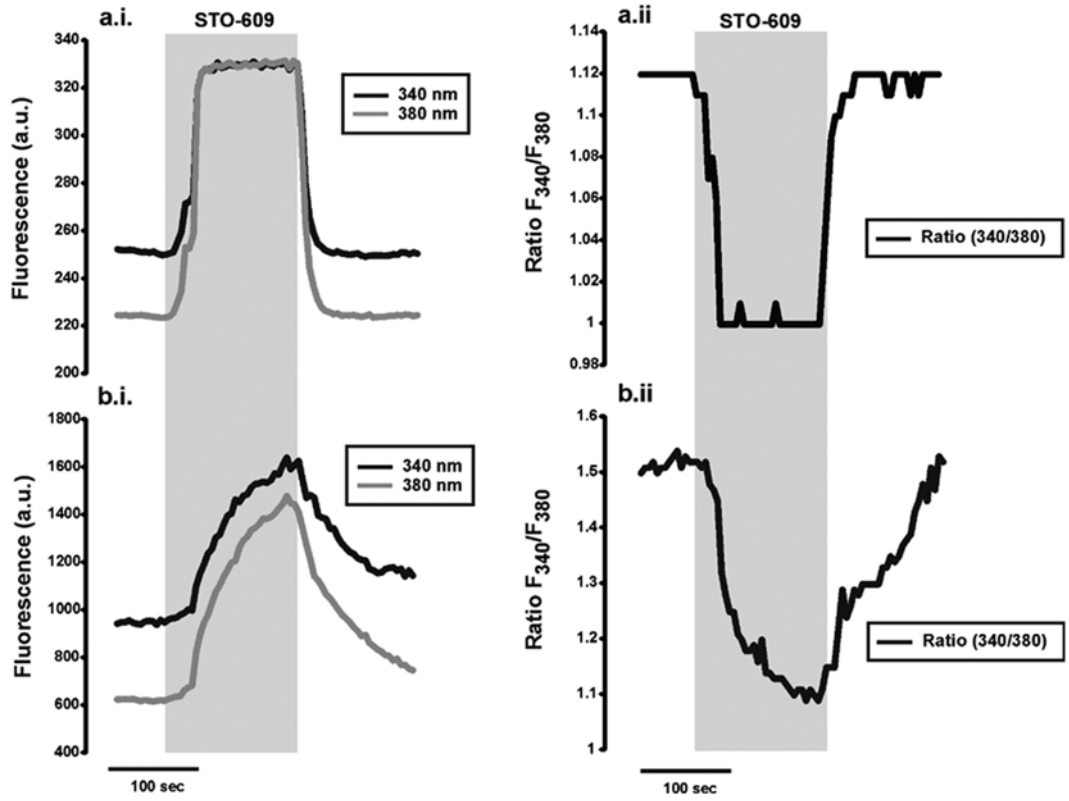


**Fig. 3.1** Autofluorescence of STO609 and its effect on Fura-2 emission intensity. (**a.i**) No cell, raw trace. Autofluorescence at 510 nm increases with application of STO-609 and decreases upon removal. (**a.ii**) No cell, ratio 340/380. The ratio of the raw traces decreases with drug application and increases upon removal. (**b.i**) Type I Cell, raw trace. Emission fluorescence at 510 nm increases with application of STO-609 and decreases upon removal. (**b.ii**) Type I Cell, ratio 340/380. The ratio of the raw traces decreases with drug application and increases upon removal

Microelectrodes were made from 1.5 mm O.D. × 0.86 mm I.D. borosilicate glass capillaries (Harvard Apparatus) inserted into a Narishige PC-10 Puller. The tips were polished using a Narishige MF-900 Microforge. Only microelectrodes with tip resistances between 5 and 12 MΩ were used. After carefully dipping the tips in an intracellular solution of composition (in MM): NaCl, 10; KCl, 130; $CaCl_2$, 1; $MgSO_4$, 2; EGTA, 11; HEPES, 11; ATP, 2; pH 7.2 with KOH, micropipettes were back-filled with the same solution.

Once a stable whole-cell configuration was achieved, recordings were taken every minute. STO-609 (100 μM, Tocris) was applied after achieving several stable baseline recordings. In later experiments, the $BK_{Ca}$ channel blocker paxilline (1 μM, Sigma) was applied prior to, and in conjunction with STO-609.

## 3.3 Results

### 3.3.1 $Ca^{2+}$ Imaging

Isolated type I cells loaded with Fura-2 (5 μM) were perfused with normoxic solution. Application of STO-609 (100 μM) caused an increase in fluorescence at 510 nm when excited with 340 and 380 nm light in both the presence and absence (blank area of coverslip) of cells and decreased upon drug removal (see Fig. 3.1a.i, b.i). Bizarrely both the 340 and 380 nm signals increased upon drug application instead of opposing one another as is typical. The 380 nm fluorescence increased faster and more robustly than 340 nm fluorescence in both instances, resulting in an overall decrease in signal ratio (Fig. 3.1a.ii, b.ii). The changes in fluorescence

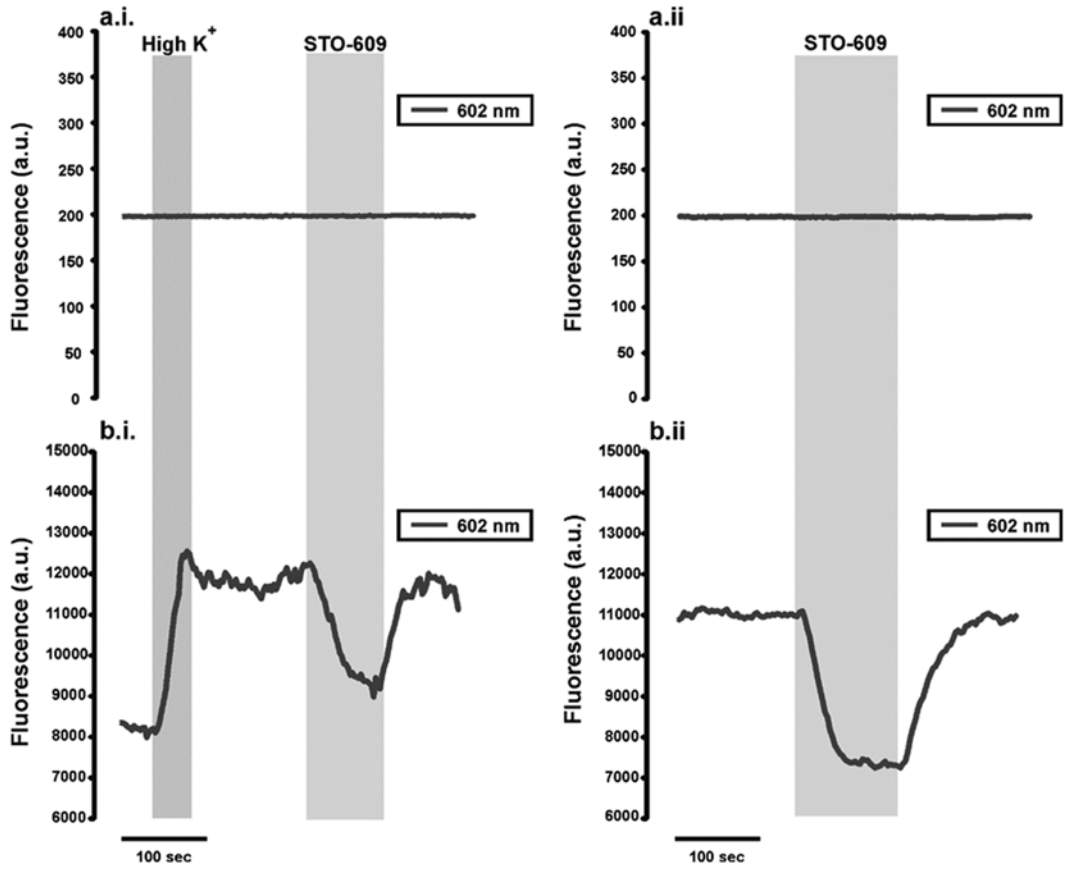


**Fig. 3.2** Autofluorescence of STO609 and its effect on X-Rhod-1 emission intensity (**a.i**) and (**a.ii**) No Cell. High $K^+$ perfusion or application of STO609 resulted in no fluorescence change at 602 nm. (**b.i**) Type I cell. The cell is depolarized with a high $K^+$ perfusion, but fails to recover. Application of STO-609 caused a reversible decrease in X-Rhod-1 fluorescence. (**b.ii**) N2A Cell. X-Rhod-1 fluorescence decreased reversibly with STO-609 application

were observed within seconds of STO-609 application, which is uncharacteristically rapid (Hawley et al. 2003).

Isolated Type I cells loaded with the red calcium-fluorescent dye X-Rhod-1(5 μM) were perfused. The autofluorescence of STO609 seen in Fig. 3.1a.i was not observed when it was exposed to 580 nm light and emission at 602 nm recorded (Fig. 3.2a.i, a.ii). A high $K^+$ challenge was used to depolarize the type I cell. Though in the example shown (Fig. 3.2b.i) the rise in emission signal did not recover, STO-609 (100 μM) was applied. The drug caused a rapid decrease in X-Rhod-1 emission fluorescence and reversed upon removal. Because the rise in signal caused by a high $K^+$ depolarization should not operate via the CamKKβ pathway, it was not expected that STO-609 would have caused a decrease in fluorescence signal.

At this point, it became clear that the apparent decrease in emission signals (emission ratio for Fura-2) may be due, at least in part, to interactions between STO-609 and the dyes *independent* of the cell. Since hypoxic depolarization is not required to examine this effect, the remaining calcium imaging experiments were carried out in mouse neuroblastoma cells (N2A), which are easy to divide and culture, instead of mouse type I cells which are fragile and have upsettingly low yields. Application of STO-609 (100 μM) caused a rapid decrease in emission fluorescence and reversal upon drug removal (Fig. 3.2b.ii). Resting

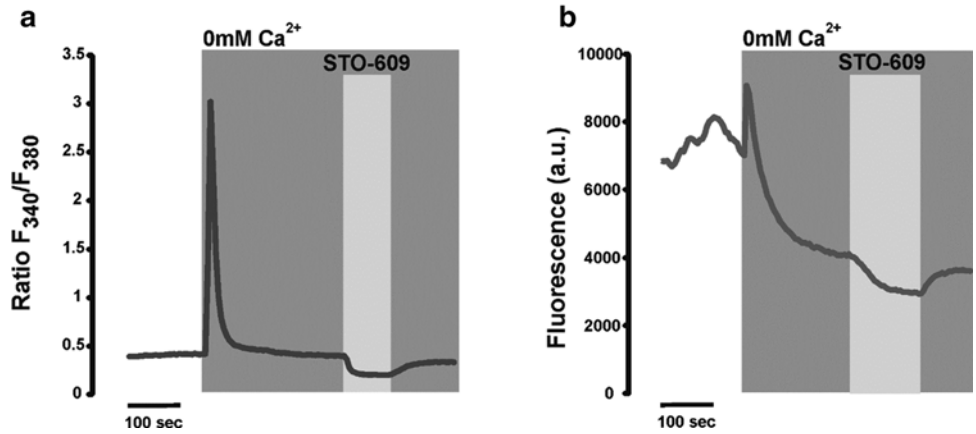


**Fig. 3.3** Effect of STO609 on the Fura-2 ratio signal and X-Rhod-1 emission signal in the absence of intracellular calcium in N2A cells (**a**) Background subtracted data of N2A cells loaded with Fura-2. Application of STO-609 decreased emission signal in the presence of 0 mM $Ca^{2+}$. (**b**) Background subtracted data of N2A cells loaded with X-Rhod-1. Application of STO-609 decreased emission signal in the presence of 0 mM $Ca^{2+}$

cells characteristically have low intracellular $Ca^{2+}$ levels, thus again such a dramatic decrease in fluorescence seen here was not expected.

Changes in calcium-fluorescent dye emissions correlate directly with changes in intracellular [$Ca^{2+}$]. If $Ca^{2+}$ is eliminated as an experimental variable, then any fluorescence changes seen after application of STO-609 must be artefactual – possibly due to direct drug-dye interaction. To investigate this, a $Ca^{2+}$ ionophore Ionomycin (2 μM) was used to perforate the cell membrane, allowing free passage of $Ca^{2+}$. This, in conjunction with a 0 mM $Ca^{2+}$ solution, was perfused over N2A cells loaded with Fura-2 and repeated in N2A cells loaded with X-Rhod-1. After a 0 $Ca^{2+}$ baseline was reached, STO-609 (100 μM) was applied. Fluorescence emission signals immediately decreased upon drug application and subsequently recovered upon drug removal for both experiments (see Fig. 3.3). The Fura-2 data were background subtracted to account for the STO-609 autofluorescence in the 510 nm range.

### 3.3.2 Electrophysiology

A programmed voltage step protocol from −80 mV to +60 mV in 10 mV steps with 200 ms duration per step was used. Protocols were executed at 1 min intervals. Once a gigaseal patch was achieved and several stable baseline recordings made, STO-609 was applied to the cells for several minutes.

Application of STO-609 (100 μM) caused a decrease in evoked outward current (see Fig. 3.4a). Measured at +10 mV, currents were reduced by an average of 38.0 ± 7.4 % (n = 5, P < 0.03, mean ± SEM). The recordings did not last long enough to observe any effects of drug removal. Notably, the raw traces observed after STO-609 application appeared smoother. This could indicate that STO-609 may be inhibiting large-conductance $Ca^{2+}$-activated potassium channels ($BK_{Ca}$), the opening and closing of which is visible on raw traces, making them appear noisy. If STO-609 is selectively inhibiting these channels, then applying a $BK_{Ca}$ blocker prior to and in conjunction with STO-609 should prevent any further channel inhibition and current reduction by the drug.

Paxilline is blocker of large-conductance calcium-activated potassium channels ($BK_{Ca}$). Application of this inhibitor will reduce outward currents by blocking these channels. If STO-609 is responsible for any inhibition of $BK_{Ca}$ channels, then application of it after and in conjunction with paxilline should result in no further reduction in current. Application of paxilline (1 μM) caused a decrease in outward current (see Fig. 3.4b). Measured at +20 mV, currents were

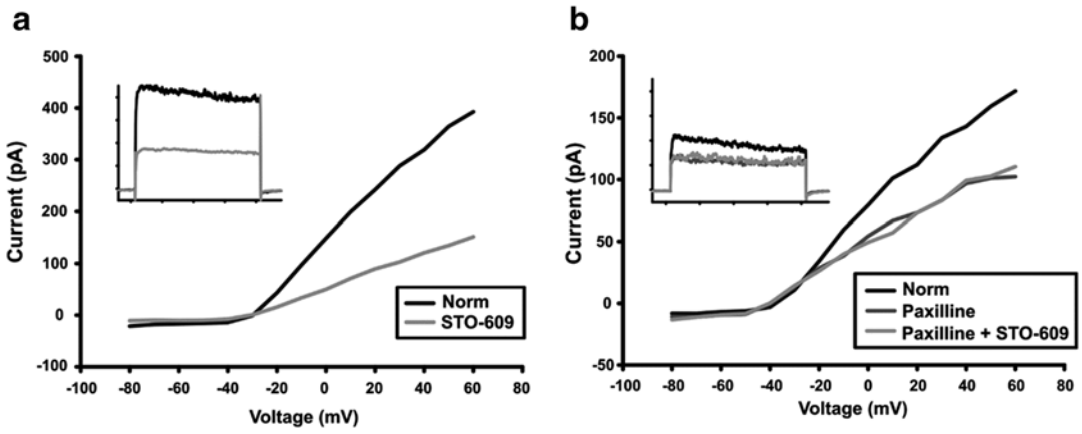


**Fig. 3.4** (**a**) Example I-V plot from an isolated type I cell. Application of STO-609 caused a decrease in outward current. Corresponding raw current traces at +20 mV shown inset. (**b**) Example I-V plot from an isolated type I cell. Application of the $BK_{Ca}$ channel inhibitor Paxilline caused a decrease in current. Application of Paxilline and STO-609 caused no further decrease in current. Corresponding raw traces at +20 mV shown inset

reduced by an average of 25.4 ± 4.3 % (n = 3) and this decrease was statistically significant ($P < 0.03$). Once no further reduction was observed, STO-609 (100 μM) was applied in conjunction with the paxilline (1 μM). In the presence of paxilline STO609 did not significantly decrease the remaining currents.

## 3.4 Discussion

These results illustrate two major findings: STO-609 directly interacts with and alters the fluorescent properties of the $Ca^{2+}$-fluorescent dyes Fura-2 and X-Rhod-1, and that STO-609 selectively inhibits $BK_{Ca}$ channels. For these reasons we were unable to use STO609 to assess the contribution of CamKKβ to the acute hypoxic response of isolated mouse type I cells.

The calcium imaging data show that the application of STO-609 caused artefactual changes in the fluorescent emissions of both Fura-2 and X-Rhod-1. The ionomycin experiments, which eliminated $Ca^{2+}$ as a variable, confirmed that the drug may be directly interacting with the dyes and quenching fluorescence rather than actually reducing intracellular $Ca^{2+}$. Interestingly, the electrophysiology data showed that STO-609 selectively interacts with and inhibits $BK_{Ca}$ channels. This was surprising as it was predicted that STO-609 would have the opposite effect on $K^+$ currents when applied during normoxic conditions, possibly via relief of any tonic regulation of $BK_{Ca}$ by AMPK.

This pattern of direct interaction and inhibition with calcium sensitive dyes and channels raises the possibility that STO-609 could potentially be acting via the $Ca^{2+}$-binding domains on these kinases, dyes, and channels. The drug may be binding competitively at the active sites for $Ca^{2+}$ interaction or binding near the active site and altering the shape and functionality of the dyes and channels, as it does with CamKKβ (Kukimoto-Niino et al. 2011). It is therefore recommended that STO-609 not be used in conjunction with calcium imaging techniques, and caution should be taken when using STO-609 in the presence of other molecules that bind $Ca^{2+}$, as it may interfere with their function, although this remains to be exhaustively tested.

Future experiments will seek to determine if the novel effect of STO609 on $BK_{Ca}$ is by a direct action on the channel or is in fact via its inhibitory actions on CamKKβ.

**Acknowledgements** This work was supported by NIH-1RO1HL091836

## References


Burlon DC, Jordan HL, Wyatt CN (2009) Presynaptic regulation of isolated neonatal rat carotid body type I cells by histamine. Respir Physiol Neurobiol 168(3):218–223

Carling D, Sanders MJ, Woods A (2008) The regulation of AMP-activated protein kinase by upstream kinases. Int J Obes (Lond) 32(4):55–59

Fogarty S, Hawley SA, Green KA, Saner N, Mustard KJ, Hardie DG (2010) Calmodulin-dependent protein kinase kinase-beta activates AMPK without forming a stable complex: synergistic effects of $Ca^{2+}$ and AMP. Biochem J 426(1):109–118

Hardie DG (2008) AMPK: a key regulator of energy balance in the single cell and the whole organism. Int J Obes (Lond) 32:S7–S12

Hawley SA, Boudeau J, Reid JL, Mustard KJ, Udd L, Ma¨kela¨ TP et al (2003) Complexes between the LKB1 tumor suppressor, STRAD alpha/beta and MO25 alpha/beta are upstream kinases in the AMP-activated protein kinase cascade. J Biol 2:28

Hawley SA, Pan DA, Mustard KJ, Ross L, Bain J, Edelman AM et al (2005) Calmodulin-dependent protein kinase kinase-beta is an alternative upstream kinase for AMP-activated protein kinase. Cell Metab 2:9–19

Kukimoto-Niino M et al (2011) Crystal structure of the $Ca^{2+}$/calmodulin-dependent protein kinase kinase in complex with the inhibitor STO-609. J Biol Chem 286:22570–22579

Momcilovic M, Hong SP, Carlson M (2006) Mammalian TAK1 activates Snf1 protein kinase in yeast and phosphorylates AMP-activated protein kinase in vitro. J Biol Chem 281(35):25336–25343

Monteiro P, Gilot D, Langouet S, Fardel O (2008) Activation of the aryl hydrocarbon receptor by the calcium/calmodulin-dependent protein kinase kinase inhibitor 7-Oxo-7H-benzimidazo[2,1-a]benz[de]isoquinoline-3-carboxylic acid (STO-609). Drug Metab Dispos 36(12):2556–2563

Ross FA, Rafferty JN, Dallas ML, Ogunbayo O, Ikematsu N, McClafferty H, Tian L, Widmer H, Rowe ICM, Wyatt CN, Shipston MJ, Peers C, Hardie DG, Evans AM (2011) Selective expression in carotid body type I cells of a single splice variant of the large conductance calcium- and voltage-activated potassium channel confers regulation by AMP-activated protein kinase. J Biol Chem 286(14):11929–11936

Schmitt JM, Guire ES, Saneyoshi T, Soderling TR (2005) Calmodulin-dependent kinase kinase/calmodulin kinase I activity gates extracellular-regulated kinase-dependent long-term potentiation. J Neurosci 25(5):1281–1290

Tamás P, Hawley SA, Clarke RG, Mustard KJ, Green K, Hardie DG, Cantrell DA (2006) Regulation of the energy sensor AMP-activated protein kinase by antigen receptor and $Ca^{2+}$ in T lymphocytes. J Exp Med 203(7):1665–1670

Tokumitsu H, Inuzuka H, Ishikawa Y, Ikeda M, Saji I, Kobayashi R (2002) STO-609, a specific inhibitor of the $Ca^{(2+)}$/calmodulin-dependent protein kinase kinase. J Biol Chem 277:15813–15818

Wayman GA, Kaech S, Grant WF, Davare M, Impey S, Tokumitsu H, Nozaki N, Banker G, Soderling TR (2004) Regulation of axonal extension and growth cone motility by calmodulin-dependent protein kinase I. J Neurosci 24(15):3786–3794

Woods A, Johnstone SR, Dickerson K, Leiper FC, Fryer LG, Neumann D et al (2003) LKB1 is the upstream kinase in the AMP-activated protein kinase cascade. Curr Biol 13:2004–2008

Woods A, Dickerson K, Heath R, Hong SP, Momcilovic M, Johnstone SR et al (2005) $Ca^{2+}$/calmodulin-dependent protein kinase kinase-beta acts upstream of AMP-activated protein kinase in mammalian cells. Cell Metab 2:21–33

Wyatt CN, Evans AM (2007) AMP-activated protein kinase and chemotransduction in the carotid body. Respir Physiol Neurobiol 157:22–29

# Tissue Dynamics of the Carotid Body Under Chronic Hypoxia: A Computational Study

4

Andrea Porzionato, Diego Guidolin, Veronica Macchi, Gloria Sarasin, Andrea Mazzatenta, Camillo Di Giulio, José López-Barneo, and Raffaele De Caro

**Abstract**

The carotid body (CB) increases in volume in response to chronic continuous hypoxia and the mechanisms underlying this adaptive response are not fully elucidated. It has been proposed that chronic hypoxia could lead to the generation of a sub-population of type II cells representing precursors, which, in turn, can give rise to mature type I cells. To test whether this process could explain not only the observed changes in cell number, but also the micro-anatomical pattern of tissue rearrangement, a mathematical modeling approach was devised to simulate the hypothetical sequence of cellular events occurring within the CB during chronic hypoxia. The modeling strategy involved two steps. In a first step a "population level" modeling approach was followed, in order to estimate, by comparing the model results with the available experimental data, "macroscopic" features of the cell system, such as cell population expansion rates and differentiation rates. In the second step, these results represented key parameters to build a "cell-centered" model simulating the self-organization of a system of CB cells under a chronic hypoxic stimulus and including cell adhesion, cytoskeletal rearrangement, cell proliferation, differentiation, and apoptosis. The cell patterns generated by the model showed consistency (from both a qualitative and quantitative point of view) with the observations performed on real tissue samples obtained from rats exposed to 16 days hypoxia,

Andrea Porzionato and Diego Guidolin contributed equally to this work

A. Porzionato (✉) • D. Guidolin • V. Macchi
G. Sarasin • R. De Caro
Section of Human Anatomy, Department of Molecular Medicine, University of Padova, Via A. Gabelli 65, 35121 Padova, Italy
e-mail: andrea.porzionato@unipd.it

A. Mazzatenta • C. Di Giulio
Department of Neurosciences, Imaging and Clinical Science, University 'G. d'Annunzio' of Chieti–Pescara, Via dei Vestini 31, 66100 Chieti, Italy
e-mail: amazzatenta@yahoo.com

J. López-Barneo
Instituto de Biomedicina de Sevilla (IBiS), Hospital Universitario Virgen del Rocío/CSIC/Universidad de Sevilla, Avenida Manuel Siurot s/n, 41013 Seville, Spain



C. Peers et al. (eds.), *Arterial Chemoreceptors in Physiology and Pathophysiology*, Advances in Experimental Medicine and Biology 860, DOI 10.1007/978-3-319-18440-1_4

indicating that the hypothesized sequence of cellular events was adequate to explain not only changes in cell number, but also the tissue architecture acquired by CB following a chronic hypoxic stimulus.

**Keywords**
Carotid body • Hypoxia • Morphogenesis • Mathematical modeling • Stem cells • Peripheral neurogenesis

## 4.1 Introduction

Carotid body (CB) is a neural crest-derived paired organ located in the carotid bifurcation (Jiang et al. 2000), where it represents a principal component of the homeostatic $O_2$ sensing system, required to activate the brainstem respiratory center to produce hyperventilation during hypoxemia (López-Barneo et al. 1988). The CB parenchyma appears organized in clusters of type I cells (chief-cells) that are the primary $O_2$-sensing elements in the CB. They are electrically excitable and depolarize in response to hypoxia, releasing vesicles with neurotransmitters that activate sensory nerve fibers projecting to the solitary tract nucleus. The type I cell clusters are enveloped by type II (sustentacular) cells, which are classically believed to have only a structural role, although they probably also co-ordinate chemosensory transduction through interactions with the other cells of the CB (Tse et al. 2012). The CB also shows a complex microvascularization and local changes in blood flow have been considered to be involved in CB chemoreceptor discharge (Joels and Neil 1963; Kirby and McQueen 1984; Porzionato et al. 2006, 2011).

Unlike most neural organs, CB exhibits a quite remarkable level of structural plasticity. It undergoes structural and functional changes during perinatal development (e.g., Porzionato et al. 2008a, b; De Caro et al. 2013), ageing (e.g., Di Giulio et al. 2012; Zara et al. 2013) and in response to a variety of environmental stimuli. In particular, upon exposure to chronic continuous hypoxia, as it occurs during acclimation to high altitude (Wang and Bisgard 2002) or in patients with cardiopulmonary diseases involving hypoxemia (Heat et al. 1982), the CB may undergo a large increase in volume. The mechanisms underlying this adaptive morphogenetic response are not fully elucidated. Recently, however, it has been proposed (Pardal et al. 2007; Platero-Luengo et al. 2014) that, as a consequence of a chronic hypoxic stimulus, type II cells, selectively expressing glial markers (such as glial fibrillary acidic protein and S100), could differentiate into precursor neural cells (also expressing nestin) that give rise to mature glomus cells. Cell fate experiments *in vitro* and *in vivo* (see Pardal et al. 2007) have confirmed that this process can significantly contribute to the generation of new glomus cells in animals exposed to sustained hypoxia. On return to normoxia, proliferation and differentiation of the intermediate progenitors ceased, and most of them acquired the usual sustentacular cell phenotype.

To test whether this process could explain not only the observed changes in cell number, but also the micro anatomical pattern of tissue rearrangement, in the present study a mathematical modeling approach was followed. It was based on the abovementioned findings, and aimed at simulating the hypothetical sequence of cellular events occurring within the CB during chronic hypoxia. The modeling strategy involved two steps. In a first step a "population level" modeling approach was followed, in which the time change of the cell number was simulated using partial differential equations. By comparing the model results with the real experimental data provided by Pardal et al. (2007), "macroscopic" features of the cell system, such as cell population expansion rates and differentiation rates, were estimated. This approach is unable to provide detailed information at a "microscale" concerning the actual structure and morphology of the CB tissue. The results obtained, however, provided key parameters to build a "cell-centered"

model (Merks and Glazier 2005; Guidolin et al. 2011) simulating the self-organization of a system of CB cells under a chronic hypoxic stimulus lasting 16 days. This second step of the modeling process was based on a simulation technique known as "Cellular Potts Model" (Glazier and Graner 1993; Merks and Glazier 2005), in which cell adhesion, cytoskeletal rearrangement, cell proliferation, differentiation, and apoptosis were considered. The tissue patterns obtained with such a simulation procedure were finally compared with those observed on real tissue sections to assess whether the hypothesized sequence of cellular events was adequate to explain the tissue architecture acquired by CB following a chronic hypoxic stimulus.

## 4.2 Materials and Methods

### 4.2.1 Animals and Experimental Procedure of Hypoxia Exposure

Wistar rats were housed and treated according to the animal care guidelines of the European Community Council (86/609/ECC), and all the procedures were approved by the local Ethical Committee. Animals were chronically exposed to 10 % $O_2$ (hypoxic group) or 21 % $O_2$ (normoxic group) for 16 days using a hermetic isobaric chamber with $O_2$ and $CO_2$ controls and temperature and humidity monitoring.

### 4.2.2 Tissue Samples and Immunohistochemistry

At the end of the treatment three animals per group were sacrificed by intraperitoneal injection of sodium pentobarbital (65 mg/Kg), and specimens were taken of the carotid bifurcations. All procedures for animal handling and tissue dissection were carried out according to the ECC and the local Ethical Committee guidelines. Tissues were fixed in 10 % phosphate-buffered formalin for 72 h, dehydrated through ascending alcohols and xylene, and paraffin embedded. Sections, 5 μm thick, were then obtained, de-waxed (xylene and alcohol progressively at lower concentrations), and processed for immunohistochemical analysis. To detect the cell pool formed by type II and precursor cells, slides were incubated in the presence of polyclonal rabbit anti-S100 (primary antibody dilution 1:7,000) (DakoCytomation, Glostrup, Denmark; Z 0311), and then in the presence of specific HRP-conjugated secondary antibodies. Peroxidase was developed using diaminobenzidin chromogen (DAB) and nuclei were hematoxylin counterstained. Negative controls were performed by omitting the primary antibody.

### 4.2.3 Morphometry

Bright-field images of the immunohistochemical preparations were acquired by using a Leica DMR microscope (Leica Microsystems, Wetzlar, Germany) and a high resolution digital camera (DC 200, Leica Microsystems, Wetzlar, Germany). At a primary magnification of ×20 one field per section (covering 0.0231 $mm^2$) randomly chosen within the CB tissue was selected and its image acquired in full colors (RGB, 24-bit), processed to correct shading, then filed TIFF.

Since it showed the best contrast between immune-positive cells and the other, counterstained, tissue components, the blue component of each acquired RGB image was selected for the analysis. The main steps of the computer-assisted image analysis procedure are illustrated in Fig. 4.1. It was performed by using the ImageJ software (Schneider et al. 2012), powered by macro routines specifically developed by the authors. For the identification of the S100-positive cells a top-hat transform (Jenné et al. 2007) was first applied. This transform is performed by subtracting from the original grey-scale image the result of a grey-scale closing. After a rescaling of the brightness values (see Fig. 4.1b), S100-positive cells can be easily segmented with conventional thresholding methods (Fig. 4.1c) and the percent area they occupy calculated. This dimensional parameter, however, cannot fully characterize the architecture of the pattern of type II cells, since patterns very similar in size can correspond to very different spatial

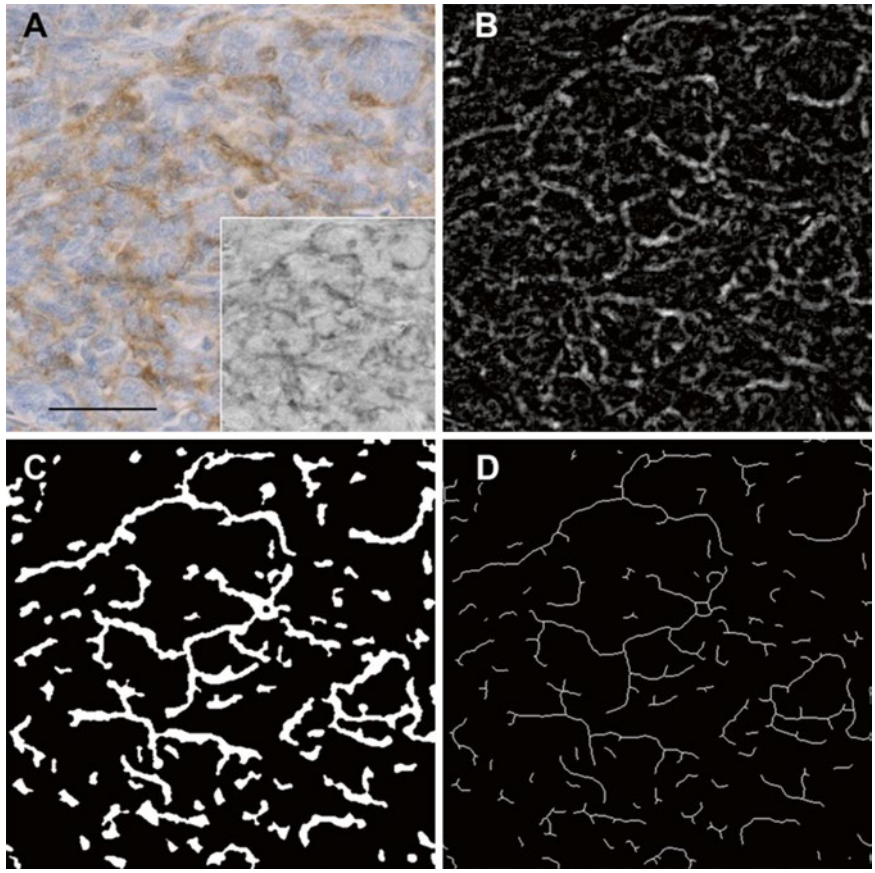


**Fig. 4.1** Main steps of the image analysis procedure. (**a**) Full color (RGB, 24-bit) digital image of a microscope field stained for S100 and counterstained with hematoxylin (primary magnification × 20). In the inset the *blue* component is shown. After the application of a top-hat filter and a rescaling of the brightness values (**b**), the image was thresholded, to identify the S100-positive structures (**c**) and measure the percent area they occupied. The binary skeleton was then calculated (**d**) and its fractal dimension estimated. Scale bar: 40 μm

textures (Guidolin et al. 2004). For this reason, the binary skeleton of the S100-positive cells was derived (Fig. 4.1d) and its fractal dimension was evaluated by using the 'box counting' method at multiple origins (Smith et al. 1996). This parameter, in fact, was previously shown to efficiently describe the changes in spatial complexity of a binary pattern (Guidolin et al. 2004) and, in particular, of the connective tissue component of the CB (Guidolin et al. 2014).

The same image analysis procedure was also applied to the simulated patterns (see Sect. 2.2.5) and the obtained results compared with those observed in the real tissue samples in order to assess the accuracy of the simulations.

### 4.2.4 "Population Level" Modeling of the Carotid Body Changes Under Hypoxia

To describe the CB growth and the changes its cell composition undergoes under chronic hypoxic conditions, a "population level" modeling approach (Bassingthwaighte 2000) was first followed, in which only cell numbers are considered and their changes in time estimated using partial differential equations. Continuum models of this type average out the behavior of the individual elements and are capable of efficiently capturing features of the cell system at a

"macroscale" (such as cell population expansion rate, differentiation rates etc.).

According to Pardal et al. (2007) the modeled system involved the following set of cell populations:

$$\mathrm{CB} = \{\mathrm{T1}, \mathrm{T2}, \mathrm{Pc}\}$$

where:

- T1 represents the glomus type I or chief cells.
- T2 represents the type II or sustentacular cells of the CB.
- Pc indicates a population of precursor cells expressing glial markers, but able to differentiate to both chief and sustentacular cells (Pardal et al. 2007).

CB stem and precursor cells may also generate smooth muscle actin-positive myofibroblasts and endothelial cells, playing a potential role in angiogenesis and connective tissue changes in response to chronic hypoxia. At the moment, however, these cell types and these possible differentiations were not taken into account.

The proposed general dynamics involving the abovementioned cell populations is schematically shown in Fig. 4.2a, and corresponds to the following set of partial differential equations:

$$\frac{\partial N_1}{\partial t} = \left(k_{11} - k_1 - k_{1p}\right) N_1 + k_{p1} N_p = \left(\delta_1 - k_{1p}\right) N_1 + k_{p1} N_p$$
$$\frac{\partial N_2}{\partial t} = \left(k_{22} - k_2 - k_{2p}\right) N_2 + k_{p2} N_p = \left(\delta_2 - k_{2p}\right) N_2 + k_{p2} N_p$$
$$\frac{\partial N_p}{\partial t} = \left(k_{pp} - k_p - k_{p2}\right) N_p + k_{1p} N_1 + k_{2p} N_2 = \left(\delta_p - k_{p2}\right) N_p + k_{1p} N_1 + k_{2p} N_2$$

where $N_1$, $N_2$, and $N_p$ are the number of type I, type II and precursor cells respectively. The parameters $k_{ii}$ and $k_i$ represent the mitosis and apoptosis rate of population i respectively, and $k_{ij}$ is the rate at which cell type i differentiates to type j.

For what the parameters of the model are concerned, all the values were taken from literature as far as possible. Both $k_{11}$ and $k_{1p}$ were set to 0, since neither significant type I cells mitosis nor back differentiation of type I to precursor cells were observed under hypoxic conditions (Pardal et al. 2007). Some BrdU+/TH+ cells appear after exposure to hypoxia but these cells may be considered immature type I cells which are activated by hypoxia to complete their differentiation. The net population expansion rates of T1 ($\delta_1 = k_{11} - k_1$), T2 ($\delta_2 = k_{22} - k_2$), Pc ($\delta_p = k_{pp} - k_p$), and the differentiation rates ($k_{2p}$, $k_{p2}$, $k_{p1}$) were estimated by a sensitivity analysis (Merks et al. 2006). According to this procedure the parameter space is systematically scanned to find a set of values leading to a simulated time course representing a good fit of the experimental trend reported by Pardal et al. (2007), and involving a first period (5/6 days), in which mainly type II cell number increase was observed, followed by a second phase (~15 days) in which the complete pattern of cell behaviors develops. Simulations were then performed according to this scheme. The open source software platform for numerical computation SCILAB 5.2.0 (The SCILAB Consortium, France, www.scilab.org) was used to solve numerically the equation system according to a finite-difference procedure (LeVeque 2007), in which each time step corresponded to 1 h of real time.

### 4.2.5 "Cell-Centered" Model of Carotid Body Changes Under Hypoxia

The just described modeling strategy, however, is unable to provide detailed information at a "microscale" concerning the actual structure and

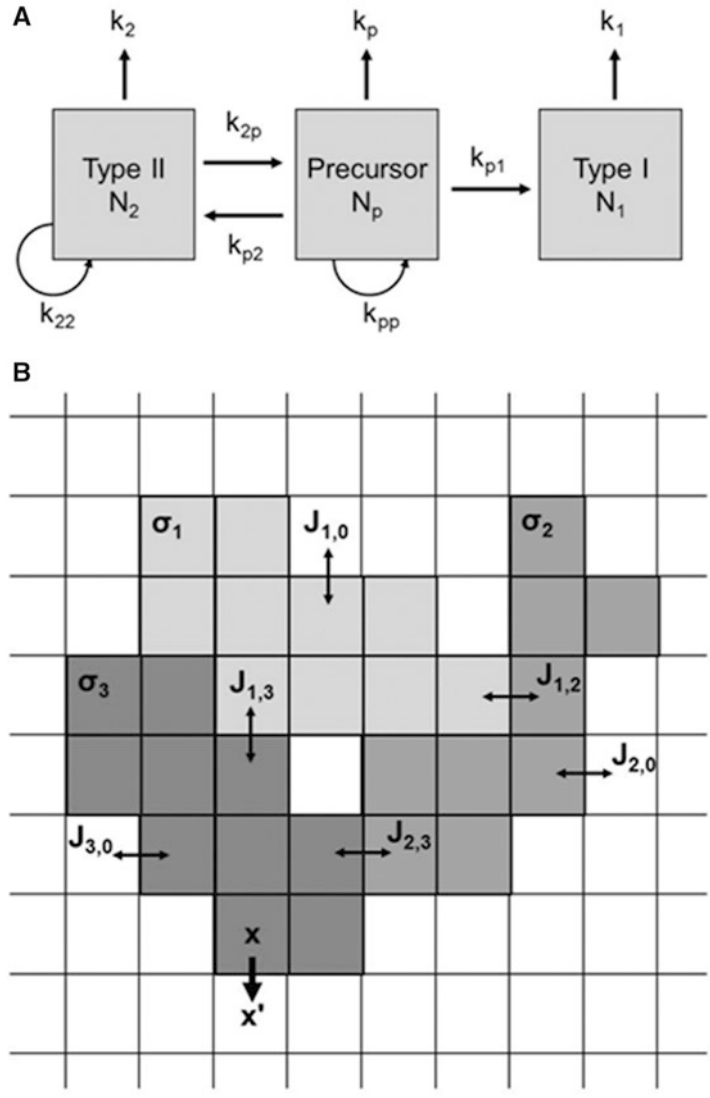


**Fig. 4.2** Schematic representation of the modeling strategies applied. (**a**) Sequence of cellular events implemented in the "population level" model used to describe the changes in cell composition of the CB under chronic hypoxic conditions (see text). $N_1$, $N_2$, and $N_p$ are the number of type I, type II and precursor cells respectively. The parameters $k_{ii}$ and $k_i$ represent the mitosis and apoptosis rate of the population i respectively, and $k_{ij}$ is the rate at which cell type i differentiates to type j. (**b**) In the "Cellular Potts Model" (see text) cells are represented on a numerical grid as domains of pixels with identical index (shown as a specific shade of *gray*), while the extracellular matrix is the set of the remaining pixels (*white* pixels). Connections between neighboring lattice sites of unlike index (some of them are indicated with *double-headed arrows*) represent membrane bonds, with a characteristic bond energy *J*, which depends on the pair of objects in contact and determine the strength of their adhesion. Furthermore, because biological cells generally have a fixed range of sizes and shapes, additional elastic energy terms are considered whenever deviations from a target volume or elongation occur. All these contributions lead to Eq. (4.1), representing the "energy" of the system at each time instant. Cytoskeletally driven membrane fluctuations can be mimicked by randomly choosing a lattice site $x$ and copying its index into a randomly chosen neighboring lattice site $x'$ (*single-head arrow*)

morphology of the CB tissue. In fact, the self-organization of the cells leading to the microscopic appearance of the tissue is mainly the result of several intimately linked single-cell behaviors. In this respect, "cell-centered" approaches (Merks and Glazier 2005), working at a "mesoscopic scale" and treating the cell as the fundamental module, can be particularly useful to simulate the rearrangement of the glomic tissue under a chronic hypoxic stimulus.

Thus, a modeling approach based on the well-known Cellular Potts Model (CPM) (Merks and Glazier 2005; Guidolin and Albertin 2012) was devised.

Briefly, CPM is a simulation technique (see Fig. 4.2b) representing cells as domains of lattice sites, x, with identical non-zero indices ($\sigma_x$), while the index value 0 identifies the extracellular matrix (ECM). Thus, cell volume and shape can be described. A further basic characteristic of the CPM is to represent the cell behaviors of interest in the form of terms within a generalized energy function which also includes the interactions with the ECM and parameters constraining individual cell behaviour. With reference to Fig. 4.2b, for instance, grid points at patch interfaces represent cell surfaces, and the interaction between cell surfaces is modeled by defining coupling constants $J\sigma_x,\sigma_x'$ representing the adhesion energy involved in the specified interaction. Each cell also has a set of attributes, including a "target" area and elongation, which poses some constraint on the possible cell shape changes. Thus, the following "energy function" can be defined for this system:

$$H = \sum_{x,x'} J_{\sigma_x,\sigma_{x'}} \left(1-\delta_{\sigma_x,\sigma_{x'}}\right) + \lambda_A \sum_{\sigma} \left(a_\sigma - A_\sigma\right)^2 + \lambda_L \sum_{\sigma} \left(l_\sigma - L_\sigma\right)^2 \qquad (4.1)$$

where **x** represents the eight neighbors of x′, $\lambda_A$ and $\lambda_L$ represent resistances to changes in size and elongation respectively, Aσ and Lσ are the "target" values for cell area and length, aσ and lσ are the actual cell area and length values, and the Kronecker delta is $\delta_{x,y}$ = (1 if x = y; 0 if x ≠ y).

By repeatedly replacing a value at a cell interface by a neighboring grid point's value (see Fig. 4.2b), it is possible to mimic active, random extensions and retractions of filopodia and lamellipodia. If the resulting variation in effective energy (ΔH) is negative, then the cell change will be accepted; conversely, if ΔH is positive, then the cell change will be accepted with Boltzmann-weighted probability.

CPM was originally developed by Glazier and Graner (1993) to simulate the cell rearrangement resulting from cell adhesion, in order to quantitatively simulate cell-sorting experiments. However, a number of cell behaviors can be quite easily implemented in this computational framework, and improvements to the CPM included the possibility to model cell growth, cell division, apoptosis and cell differentiation (Merks and Glazier 2005).

In particular, the preferential extension of filopodia in the direction of chemo attractant gradients can be implemented by including in (4.1) an extra reduction of energy whenever the cell protrudes into an area with a higher concentration of chemo attractant:

$$\Delta H_{\text{chemotaxis}} = \chi\left(c(x) - c(x')\right) \qquad (4.2)$$

where x′ is the neighbor into which site x moves (i.e., copies its value), χ is the strength of the chemo tactic response, and c(x) is the local concentration of the chemo attractant. At each time step it is possible to estimate the concentrations c(x) from the following diffusion equation:

$$\frac{\partial c}{\partial t} = \alpha\left(1-\delta_{\sigma_x,0}\right) - \delta_{\sigma_x,0} \cdot \varepsilon \cdot c + D\nabla^2 c \qquad (4.3)$$

where α is the rate at which the cells release chemo attractant, ε is the clearance rate of the chemo attractant, and D its diffusion coefficient. The Kronecker delta simply indicates that the release occurs at the cell locations, while the factor is cleared in the extracellular space.

The framework *CompuCell3D* (Cickovski et al. 2007) (www.compucell3d.org), providing the basic engine and user interface to run this type of approach to modeling, and Python scripts specifically developed by the authors to customize the models were used for the simulation of CB tissue dynamics. A 100×100 CPM lattice, where each lattice site represents an area of 2.25 μm$^2$, was always used. Thus, it corresponded to a simulated field area of 0.0225 mm$^2$, comparable to the area of the images from real samples (see Sect. 4.2.3). The simulations evolved through discrete time steps (Monte-Carlo steps, mcs) each corresponding to 5 min of real time.

#### 4.2.5.1 Simulation of the Initial (Normoxic) Pattern

The cell composition of the normal CB parenchyma involves ~75 % of type I cells, organized in clusters enveloped by processes of sustentacular type II cells (see Fig. 4.1a), representing the remaining ~25 % of the total cell number. As suggested by Pardal et al. (2007), however, ~20 % of the glia-like sustentacular cells (i.e. ~5 % of the total) can be considered multipotent precursor cells, able to differentiate to mature type I cells when needed. In particular, they would represent a key population in the course of tissue remodeling under chronic hypoxia.

To obtain simulated tissue patterns qualitatively similar to those observed in real normoxic CB samples, the CPM lattice was randomly filled with virtual cells of the three types in an amount fulfilling the abovementioned proportions. Cell attributes, such as target size and elongation, were defined based on measurements performed on real tissue samples, and cell resistances ($\lambda_A$ and $\lambda_L$ in Eq. (4.1)) were chosen large enough to maintain the size and elongation close to the observed values. As far as intercellular adhesion was concerned, the *surface tensions* ($\gamma_{T1,T2} = J_{T1,T2} - (J_{T1,T1} + J_{T2,T2})/2$) (Merks and Glazier 2005) were set to favor heterotypic bonds ($\gamma_{T1,T2} < 0$). Furthermore, a preferential movement of T1 cells towards T2 and Pc cells along a chemotactic gradient was hypothesized. The diffusion characteristics of the hypothetic chemotactic factor secreted by T2 (and Pc) cells and recognized by T1 cells were assumed to be consistent with those reported (see Duchesne et al. 2012) for a typical growth factor (such as FGF-2). As illustrated in Fig. 4.3, these conditions can allow the generation of cell patterns qualitatively and quantitatively very similar to those observed in real normoxic samples. The number of mcs to apply to achieve such a result was established by a parameter study, in which a range of values for the total number of mcs was tested to find the one leading to the best simulation of the experimental cell arrangement.

A detailed view of the parameters used for the simulation is reported in Table 4.1, including references. Ten simulations were performed, and the resulting patterns recorded. They were then used as initial conditions for the simulation of the cell rearrangement under chronic hypoxia.

#### 4.2.5.2 Simulation of the Tissue Remodeling Under Hypoxic Conditions

The cell features used to simulate the tissue changes due to hypoxic conditions are detailed in Table 4.1, and the simulation was set to cover 4,600 mcs, corresponding to 16 days of real time. Chemotaxis was strongly reduced, but processes of mitosis, differentiation and apoptosis were included in the simulation. The amount and frequency of these events were based on the rate constants obtained from the "population level" model (see Sect. 4.2.4). Since that model was evolving by time steps of 1 h, in the "cell-centered" simulation the update of the cell populations was performed with this frequency, corresponding to 12 mcs. Thus, every 12 mcs the cell populations were updated as follows:

- From each cell population $\delta_i N_i$ cells were random selected, where $\delta_i$ is the net expansion rate of the population i. They were assigned to mitosis if $\delta_i > 0$, or to apoptosis if $\delta_i < 0$. Furthermore, from each population $k_{ij} N_i$ cells (where $k_{ij}$ is the differentiation rate from cell type i to type j) were random selected for differentiation.
- Each cell selected for mitosis was divided in two child cells through its center of mass along the axis of minimum length (Mombach and Glazier 1996). The two child cells (of approximately the same size) inherited the characteristics

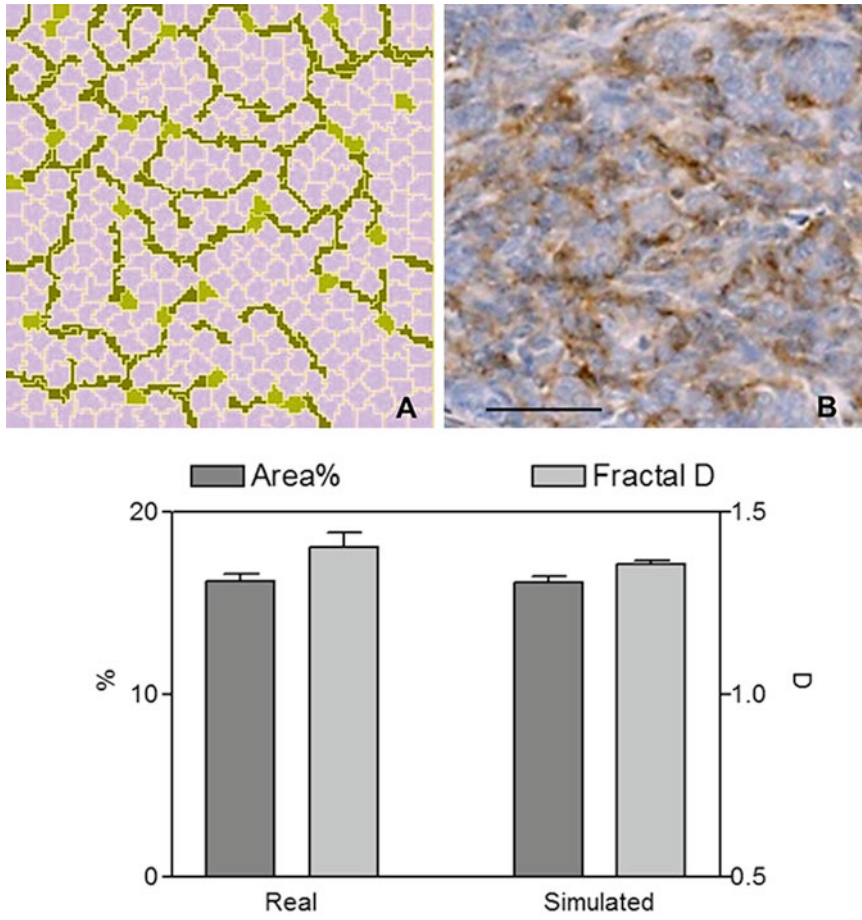


**Fig. 4.3** *Upper panels*. Typical pattern generated by the cell-centered model tuned to simulate the CB tissue organization in normoxic conditions (**a**). Type I, type II and precursor cells appear in *violet*, *brown* and *green* respectively. A real tissue pattern is shown in (**b**). Scale bar: 40 μm. *Lower panel*. Simulated patterns (n=6) underwent the same morphometric analysis performed on real samples (n=6). As shown, no significant differences were detected both in terms of percent area covered by S100-positive cells and in the fractal dimension of their spatial arrangement

of adhesion, target size, and elongation of the parent cell and evolved accordingly.

- To the cells selected for apoptosis a target volume of 0 was assigned (leading to a progressive shrinkage of the cell), and they were removed from the global cell list.
- A different cell type was assigned to differentiating cells, that inherited all the characteristics of the new type and started evolving accordingly.

Each simulation run started from a normoxic-like pattern obtained as detailed before, and the final cell arrangement was recorded to be morphometrically analyzed and compared with images from real samples of CB exposed to a 16 days hypoxic stimulus.

## 4.3 Results

### 4.3.1 "Population Level" Model and Changes in Cell Composition

As shown in Fig. 4.4, with the proper choice of the parameters the time course of cell changes predicted by the continuum model fitted quite

**Table 4.1** Cell-centered model parameters

| Parameter | Symbol | Model value | References |
|---|---|---|---|
| *Type I cell features:* | | | |
| Initial number | $N_1$ | 300 | Pardal et al. (2007) |
| Number change rates | $\delta_1$, $k_{1j}$ | | |
| Normoxia | | 0 | |
| Hypoxia | | see Table 4.2 | *From continuum model* |
| Target area | $A_1$ | 60 μm$^2$ | *Measurement on tissue sections* |
| Target elongation | $L_1$ | 10 μm | |
| Resistance to changes in size | $\lambda_{A1}$ | 25 | |
| Resistance to changes in elongation | $\lambda_{L1}$ | 20 | |
| *Type II cell features:* | | | |
| Initial number | $N_2$ | 80 | Pardal et al. (2007) |
| Number change rates | $\delta_2$, $k_{2j}$ | | |
| Normoxia | | 0 | |
| Hypoxia | | see Table 4.2 | *From continuum model* |
| Target area | $A_2$ | 36 μm$^2$ | *Measurement on tissue sections* |
| Target elongation | $L_2$ | 20 μm | |
| Resistance to changes in size | $\lambda_{A2}$ | 25 | |
| Resistance to changes in elongation | $\lambda_{L2}$ | 20 | |
| *Precursor cell features:* | | | |
| Initial number | $N_p$ | 20 | Pardal et al. (2007) |
| Number change rates | $\Delta_p$, $k_{pj}$ | | |
| Normoxia | | 0 | |
| Hypoxia | | see Table 4.2 | *From continuum model* |
| Target area | $A_p$ | 36 μm$^2$ | *Measurement on tissue sections* |
| Target elongation | $L_p$ | 8 μm | |
| Resistance to changes in size | $\lambda_{Ap}$ | 25 | |
| Resistance to changes in elongation | $\lambda_{Lp}$ | 20 | |
| *Adhesion:* | | | |
| Type I-Type I | $J_{11}$ | 10 | Merks and Glazier (2005) |
| Type II-TypeII, Type II-PC, PC-PC | $J_{22}$, $J_{2p}$, $J_{pp}$ | 16 | |
| Type I-Type II, Type I-PC | $J_{12}$, $J_{1p}$ | 11 | |
| Cell-Matrix | $J_{10}$, $J_{20}$, $J_{30}$ | 20 | |
| *Chemotaxis:* | | | |
| Diffusion | D | 0.01 μ$^2$s$^{-1}$ | Duchesne et al. (2012) |
| Source | α | $10^{-4}$ s$^{-1}$ | |
| Clearance | ε | $10^{-4}$ s$^{-1}$ | |
| Strength of chemotactic response | χ | | |
| Normoxia | | 1,000 | |
| Hypoxia | | 100 | |

well the experimental data provided by Pardal et al. (2007). The estimated population expansion rates and differentiation rates leading to the best fit are reported in Table 4.2. As expected, precursor cells were predicted to exhibit the most dynamic behavior, in which about 2.5 % cells per hour undergo mitosis and an additional 2.5 % differentiate to a type I phenotype. On such a differentiation process is mainly based the increase in number of the type I cells population, since these cells do not proliferate, and a small rate of cell removal

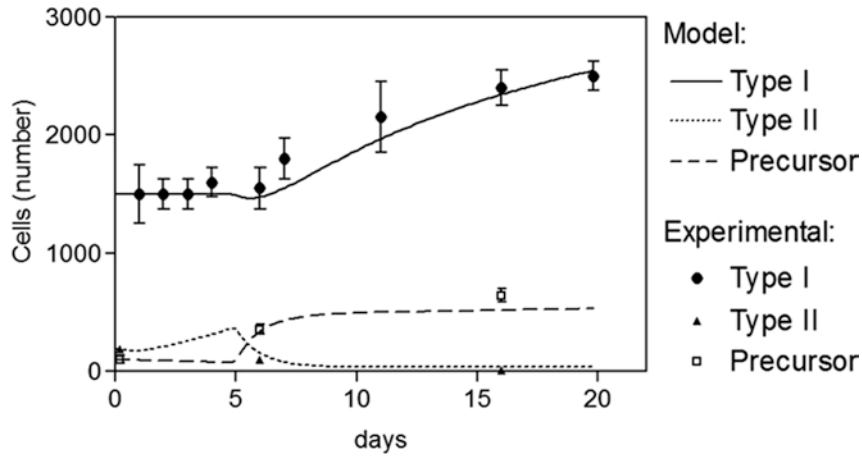


**Fig. 4.4** Time course of cell changes predicted by the continuum model customized with the parameters reported in Table 4.2 (*lines*), together with the experimental data (*dots*) provided by Pardal et al. (2007)

**Table 4.2** Population expansion rates and differentiation rates

| Cell type | Expansion rate (δ) | Differentiation rates ($k_{ij}$) |
|---|---|---|
| Type I | –0.0045 | $k_{1p}=0.0000$ |
| Type II | 0.0070 | $k_{2p}=0.0430$ |
| Precursors | 0.0248 | $k_{p1}=0.0250$ |
| | | $k_{p2}=0.0025$ |

Values represent the ratio of cells undergoing mitosis ($\delta>0$) or apoptosis ($\delta<0$), and differentiation ($k_{ij}$) at each time step (1 h)

(~0.4 % cells/h) seems to be needed to fit the experimental data.

### 4.3.2 "Cell-Centered" Model and Changes in Tissue Architecture

CB coming from rats exposed to 16 days chronic hypoxia appeared of increased size when compared to samples obtained from control animals (see Fig. 4.5). The tissue architecture was characterized by an increased relative amount of type I cells, and a reduced relative presence of S100-positive structures that often do not completely envelop the type I cell clusters. As illustrated in Fig. 4.6 the cell-centered model customized to simulate the hypoxia-induced morphogenetic process generated cell patterns qualitatively very similar to those observed in the immunohistochemical preparations.

The morphometric analysis confirmed these findings. When compared with normoxic samples, chronic hypoxia induced a decrease of both the S100-positive volume fraction ($\Delta\% \cong -25$ %, $p=0.0038$) and the fractal dimension of the S100-positive pattern ($\Delta\% \cong -10$ %, $p=0.0116$). A comparison between experimental and simulated tissue architectures is illustrated in Fig. 4.7a. As shown, no significant differences can be observed in terms of both volume fraction occupied by S100-positive structures and overall complexity of their spatial arrangement.

As expected, in terms of cell numbers (Fig. 4.7b) the prediction of the cell-centered model was consistent with the one of the "population level" model, with type I cells exhibiting a ~70 % increase, and type II a ~80 % decrease in number, a result fitting (see Fig. 4.4) the experimental data by Pardal et al. (2007).

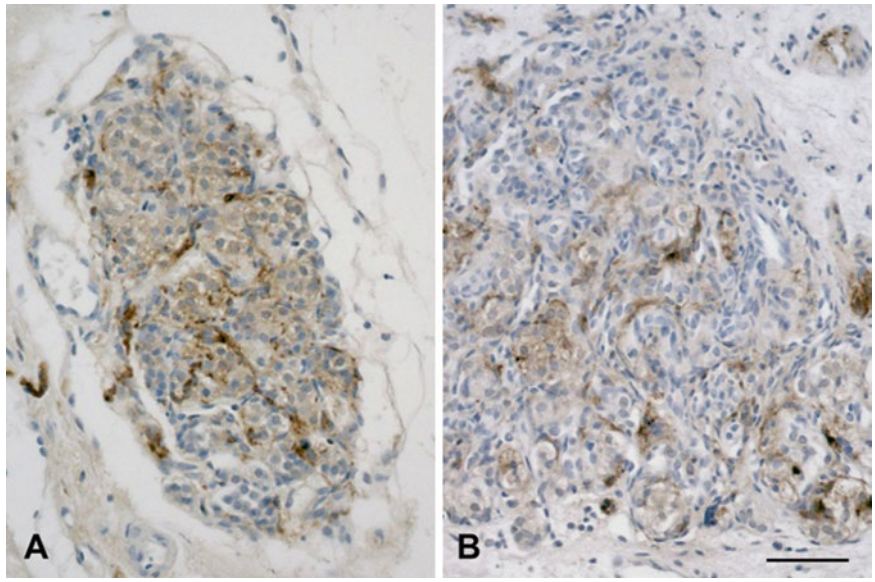


**Fig. 4.5** Immunohistochemical visualization of S100-positive structures in control rat CB (**a**) and in CB from an animal exposed to 16 days chronic hypoxia (**b**). Scale bar: 50 μm

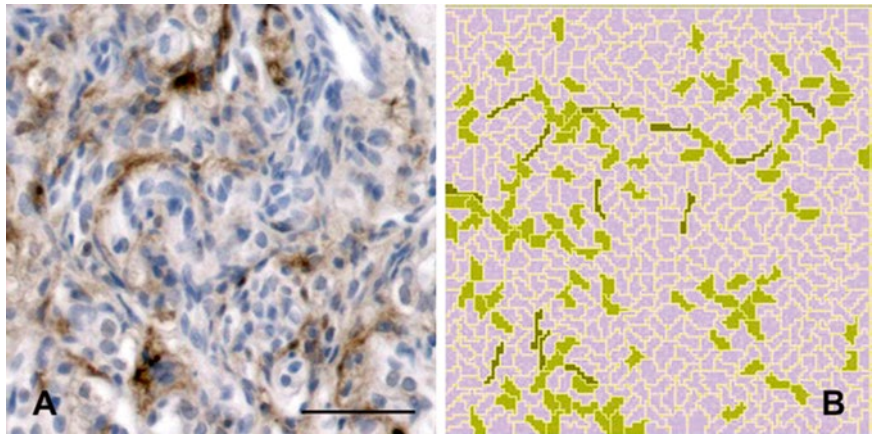


**Fig. 4.6** Typical cell pattern experimentally observed in CB following 16 days chronic hypoxia (**a**), and pattern generated by the cell-centered model tuned to simulate the CB tissue organization under hypoxic conditions (**b**). Type I, type II and precursor cells appear in *violet*, *brown* and *green* respectively. Scale bar: 40 μm

## 4.4 Discussion

As observed in several human and animal studies (see Lahiri 2000; Wang and Bisgard 2002), chronic hypoxia causes enlargement of the CB. A detailed experimental analysis of the tissue components involved in such a morphogenetic process was recently reported (Pardal et al. 2007; Ortega-Sáenz et al. 2013; Platero-Luengo et al. 2014). In these studies the chronic hypoxia-induced CB hypertrophy was paralleled by a significant increase in type I cells, whose number resulted ~1.7-fold the number of chief cells characterizing the normoxic condition. Interestingly, the increase of type I cells was not simply due to type I cell proliferation (as indicated by BrdU incorporation experiments), suggesting the existence in the CB of precursor cells,

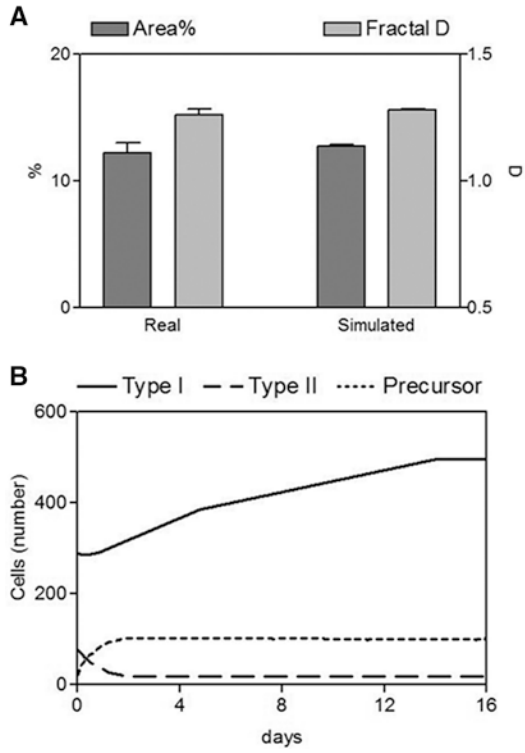


**Fig. 4.7** (**a**) Morphometric analysis comparing experimental cell arrangements (N = 6) observed under chronic hypoxia and patterns generated by the cell-centered model (N = 10). As shown, no significant differences were detected both in terms of percent area covered by S100-positive cells and in the fractal dimension of their spatial arrangement. (**b**) Time course of the cell numbers predicted by the cell-centered model

whose proliferation in hypoxia preceded their differentiation to type I cells. In this respect, cell fate experiments indicated that, upon exposure to hypoxia, intermediate progenitors were derived from glia-like (GFAP+/nestin-) type II cells, whose number progressively vanished as the number of GFAP+/nestin + cells increased to generate new chief cells. In the present study, a "population level" mathematical model (see Merks and Glazier 2005; Guidolin et al. 2011) was devised to simulate the observed changes in cell number. It was tuned to fit the experimental data by Pardal et al. (2007) and allowed the estimate of the rate constants of the involved cellular events (mitosis, differentiation and cell death). Interestingly, the model suggested that some, quite limited, process of type I cells removal (~0.4 % cells/h) would be needed to better fit the available experimental results. In this respect, almost no experimental studies investigated apoptosis or cell death caused by chronic hypoxia in the CB. Unpublished data on the possible presence of DNA fragmentation (as indicated by the TUNEL assay) were mentioned by Wang and Bisgard (2002), and this approach did not seem to provide evidence of cell death within the CB. Such a preliminary analysis, however, was limited to 1 week of continuous hypoxia. Thus, the model prediction concerning cell death would deserve further and more deep investigation in future experimental work.

A modeling approach of the abovementioned type, however, although able to capture the behavior of the system at a "macroscale", cannot provide detailed information at the "microscale" (Merks and Glazier 2005; Guidolin et al. 2011) concerning the architecture and the morphology assumed by the CB tissue. In fact, the pattern of morphogenetic changes a tissue undergoes is always the result of several intimately linked single-cell behaviors (Donovan et al. 2001). Thus, to accurately simulate processes of tissue rearrangement a cell-centered approach to modeling (Merks and Glazier 2005; Guidolin et al. 2011) is likely more appropriate, since it often reproduces experimental observations missing from "population level" models. Cell-centered models were successfully used to investigate *in vitro* (Merks et al. 2006; Guidolin et al. 2007, 2009) and tumor-induced (Bauer et al. 2007; Mahoney et al. 2008) angiogenesis, lumen formation (Boas and Merks 2014), cardiac valve morphogenesis (Lagendijk et al. 2013), and skeletogenesis of the vertebrate limb (Chaturvedi et al. 2004). In the present study an approach of this type was used to verify whether the proposed sequence of cell events triggered by chronic hypoxia in the CB could not only explain the changes in cell number, but also the microanatomical pattern exhibited by the tissue. This specific point, indeed, was never addressed in previous studies. The devised cell-centered model included three cell populations (type I, type II and precursor cells) undergoing differential processes of mitosis, differentiation and death, whose kinetics was regulated by the rate constants derived from the "population level" model

and fitting the experimental results by Pardal et al. (2007). Furthermore, single cell features, such as cell adhesion and cytoskeletal rearrangement, were considered. The obtained results indicated that this set of cell behaviors sufficed to quantitatively reproduce the hypoxia-induced changes of the CB tissue morphology. It is worth noting that the inclusion in the model of some degree of hypertrophy for type I cells was not needed to obtain such an agreement between simulated patterns and real samples. Hypertrophy of type I cells was reported in some of the earlier studies on CB tissue rearrangement following chronic hypoxia (Pequignot et al. 1984; Mills and Nurse 1993). More recent studies (Clarke et al. 2000), however, did not confirm this observation, showing that in rats exposed to 31 days hypoxia the size of the type I cells fell in the normal range.

In conclusion, the results of the present study further support cell-centered modeling as a particularly well suited quantitative framework to generate and test hypotheses in developmental biology, helping to understand which cell behaviors are essential to structure tissues. In particular, such a research effort may represent an important target for future work aimed at exploring the plastic responses of CB to stimuli other than chronic sustained hypoxia, as, for instance, chronic intermittent hypoxia and hyperoxia, in a suitable combination of experiment and computation acting in concert. Moreover, further structural components of the CB, such as microvascularization and angiogenetic responses, could be add in the future to the present mathematical model, together with further implementations concerning the generation of smooth muscle and endothelial cells from CB stem and precursor cells.

## References


Bassingthwaighte JB (2000) Strategies for the physiome project. Ann Biomed Eng 28:1043–1058

Bauer AL, Jackson TL, Jiang Y (2007) A cell-based model exhibiting branching and anastomosis during tumor-induced angiogenesis. Biophys J 92:3105–3121

Boas SEM, Merks RMH (2014) Synergy of cell-cell repulsion and vacuolation in a computational model of lumen formation. J R Soc Interface 11:20131049

Chaturvedi R, Huang C, Izaguirre JA, Newman SA, Glazier JA (2004) A hybrid discrete-continuum model for 3D skeletogenesis of the vertebrate limb. LNCS 3305:543–552

Clarke JA, Daly MB, Marshall JM, Ead HW, Hennessy EM (2000) Quantitative studies of the vasculature of the carotid body in the chronically hypoxic rat. Braz J Med Biol Res 33:331–340

Cickovski T, Aras K, Alber MS, Izaguirre JA, Swat M, Glazier JA, Merks RM, Glimm T, Hentschel HG, Newman SA (2007) From genes to organisms via the cell: a problem-solving environment for multicellular development. Comput Sci Eng 9:50–60

De Caro R, Macchi V, Sfriso MM, Porzionato A (2013) Structural and neurochemical changes in the maturation of the carotid body. Respir Physiol Neurobiol 185:9–19

Di Giulio C, Zara S, Cataldi A, Porzionato A, Pokorski M, De Caro R (2012) Human carotid body HIF and NGB expression during human development and aging. Adv Exp Med Biol 758:265–271

Donovan D, Brown NJ, Bishop ET, Lewis CE (2001) Comparison of three in vitro human 'angiogenesis' assays with capillaries formed in vivo. Angiogenesis 4:113–121

Duchesne L, Octeau V, Bearon RN, Beckett A, Prior IA, Lounis B, Fernig DG (2012) Transport of fibroblast growth factor 2 in the pericellular matrix is controlled by the spatial distribution of its binding sites in heparin sulfate. PLoS Biol 10:e1001361

Glazier JA, Graner F (1993) Simulation of the differential adhesion driven rearrangement of biological cells. Phys Rev E 47:2128–2154

Guidolin D, Albertin A (2012) Tube formation in vitro angiogenesis assay. Methods Cell Biol 112:281–293

Guidolin D, Vacca A, Nussdorfer GG, Ribatti D (2004) A new image analysis method based on topological and fractal parameters to evaluate the angiostatic activity of docetaxel by using the Matrigel assay in vitro. Microvasc Res 67:117–124

Guidolin D, Nico B, Belloni AS, Nussdorfer GG, Vacca A, Ribatti D (2007) Morphometry and mathematical modeling of the capillary-like patterns formed in vitro by bone marrow macrophages of patients with multiple myeloma. Leukemia 21:2201–2203

Guidolin D, Albertin G, Sorato E, Oselladore B, Mascarin A, Ribatti D (2009) Mathematical modeling of capillary-like pattern generated by adrenomedullin-treated human vascular endothelial cells in vitro. Dev Dyn 238:1951–1963

Guidolin D, Rebuffat P, Albertin G (2011) Cell-oriented modeling of angiogenesis. Sci World J 11:1735–1748

Guidolin D, Porzionato A, Tortorella C, Macchi V, De Caro R (2014) Fractal analysis of the structural complexity of the connective tissue in human carotid bodies. Front Physiol 5:432

Heat D, Smith P, Jago R (1982) Hyperplasia of the carotid body. J Pathol 138:115–127

Jenné R, Banadda EN, Smets I, Deurinck J, Van Impe J (2007) Detection of filamentous bulking problems:

developing an image analysis system for sludge composition monitoring. Microsc Microanal 13:36–41
Jiang X, Rowitch DH, Soriano P, McMahon AP, Sucov HM (2000) Fate of the mammalian cardiac neural crest. Development 127:1606–1616
Joels N, Neil E (1963) The excitation mechanisms of the carotid body. Br Med Bull 19:21–24
Kirby GC, McQueen DS (1984) Effects of the antagonists MDL 7222 and ketanserin on responses of cat carotid body chemoreceptors to 5-hydroxytryptamine. Br J Pharmacol 83:259–269
Lagendijk AK, Szabo A, Merks RHM, Bakkers J (2013) Hyaluronan: a critical regulator of endothelial-to-mesenchimal transition during cardiac valve formation. Trends Cardiovasc Med 23:135–142
Lahiri S (2000) Plasticity and multiplicity in the mechanisms of oxygen sensing. Adv Exp Med Biol 475:13–23
LeVeque RJ (2007) Finite difference methods for ordinary and partial differential equations: steady state and time-dependent problems. SIAM, Philadelphia
López-Barneo J, Lopez-Lopez JR, Urena J, Gonzales C (1988) Chemotransduction in the carotid body: $K^+$ current modulated by $PO_2$ in type I chemoreceptor cells. Science 241:580–582
Mahoney AW, Smith BG, Flann NS, Podgorski GJ (2008) Discovering novel cancer therapies: a computational modeling and search approach. In: Proceedings of the IEEE symposium on computational intelligence in bioinformatics and computational biology, (CIBCB'08), pp 233–240
Merks RMH, Glazier JA (2005) A cell-centered approach to developmental biology. Phys A 352(1):113–130
Merks RM, Brodsky SV, Goligorksy MS, Newman SA, Glazier JA (2006) Cell elongation is key to in silico replication of in vitro vasculogenesis and subsequent remodeling. Dev Biol 289:44–54
Mills L, Nurse C (1993) Chronic hypoxia in vitro increases volume of dissociated carotid body chemoreceptors. NeuroReport 4:619–622
Mombach JCM, Glazier JA (1996) Single cell motion in aggregates of embryonic cells. Phys Rev Lett 76:3032–3035
Ortega-Sáenz P, Pardal R, Levitsky K, Villadiego J, Muñoz-Manchado AB, Durán R, Bonilla-Henao V, Arias-Mayenco I, Sobrino V, Ordóñez A, Oliver M, Toledo-Aral JJ, López-Barneo J (2013) Cellular properties and chemosensory responses of the human carotid body. J Physiol 591:6157–6173
Pardal R, Ortega-Sàenz P, Duràn R, Lòpez-Barneo J (2007) Glia-like stem cells sustain physiologic neurogenesis in the adult mammalian carotid body. Cell 131:364–377
Pequignot JM, Hellstrom S, Johansson C (1984) Intact and sympathectomized carotid bodies of long-term hypoxic rats: a morphometric ultrastructural study. J Neurocytol 13:481–493
Platero-Luengo A, Gonzàlez-Granero S, Duràn R, Dìaz-Castro B, Piruat JI, Garcìa-Verdugo JM, Pardal R, Lòpez-Barneo J (2014) An $O_2$-sensitive glomus cell-stem cell synapse induces carotid body growth in chronic hypoxia. Cell 156:291–303
Porzionato A, Macchi V, Belloni AS, Parenti A, De Caro R (2006) Adrenomedullin immunoreactivity in the human carotid body. Peptides 27:69–73
Porzionato A, Macchi V, Parenti A, Matturri L, De Caro R (2008a) Peripheral chemoreceptors: postnatal development and cytochemical findings in Sudden Infant Death Syndrome. Histol Histopathol 23:351–365
Porzionato A, Macchi V, Parenti A, De Caro R (2008b) Trophic factors in the carotid body. Int Rev Cell Mol Biol 269:1–58
Porzionato A, Rucinski M, Macchi V, Stecco C, Castagliuolo I, Malendowicz LK, De Caro R (2011) Expression of leptin and leptin receptor isoforms in the rat and human carotid body. Brain Res 1385:56–67
Schneider CA, Rasband WS, Eliceiri KW (2012) NIH Image to ImageJ: 25 years of image analysis. Nat Methods 9:671–675
Smith TG, Lange GD, Marks WB (1996) Fractal methods and results in cellular morphology – dimensions, lacunarity and multifractals. J Neurosci Methods 69:123–136
Tse A, Yan L, Lee AK, Tse FW (2012) Autocrine and paracrine actions of ATP in rat carotid body. Can J Physiol Pharmacol 90:705–711
Wang ZY, Bisgard GE (2002) Chronic hypoxia-induced morphological and neurochemical changes in the carotid body. Microsc Res Tech 59:168–177
Zara S, Pokorski M, Cataldi A, Porzionato A, De Caro R, Antosiewicz J, Di Giulio C (2013) Development and aging are oxygen-dependent and correlate with VEGF and NOS along life span. Adv Exp Med Biol 756:223–228

# Paracrine Signaling in Glial-Like Type II Cells of the Rat Carotid Body

5

Sindhubarathi Murali, Min Zhang, and Colin A. Nurse

**Abstract**

The carotid body (CB) chemosensory complex uses ATP as a key excitatory neurotransmitter that is the main contributor to the sensory discharge during acute hypoxia. The complex includes receptor type I cells, which depolarize and release various neurochemicals including ATP during hypoxia, and contiguous glial-like type II cells which express purinergic P2Y2 receptors (P2Y2R). We previously showed that activation of P2Y2R on rat type II cells led to the opening of pannexin-1 (Panx-1) channels, which acted as conduits for the further release of ATP. More recently, we considered the possibility that other CB neuromodulators may have a similar paracrine role, leading to the activation of type II cells. Here, we examine the evidence that angiotensin II (ANG II), endothelin- (ET-1), and muscarinic agonists (e.g. acetylcholine, ACh) may activate intracellular $Ca^{2+}$ signals in type II cells and, in the case of ANG II and ACh, Panx-1 currents as well. Using ratiometric $Ca^{2+}$ imaging, we found that a substantial population of type II cells responded to 100 nM ANG II with a robust rise in intracellular $Ca^{2+}$ and activation of Panx-1 current. Both effects of ANG II were mediated via $AT_1$ receptors ($AT_1$Rs) and current activation could be inhibited by the Panx-1 channel blocker, carbenoxolone (CBX; 5 μM). Additionally, low concentrations of ET-1 (1 nM) evoked robust intracellular $Ca^{2+}$ responses in subpopulations of type II cells. The mAChR agonist muscarine (10 μM) also induced a rise in intracellular $Ca^{2+}$ in some type II cells, and preliminary perforated-patch, whole-cell recordings revealed that ACh (10 μM) may activate Panx-1-like currents. These data suggest that paracrine activation of type II cells by endogenous neuromodulators may be a common feature of signal processing in the rat CB.

S. Murali • M. Zhang • C.A. Nurse (✉)
Department of Biology, McMaster University,
Hamilton, ON L8S 4K1, Canada
e-mail: nursec@mcmaster.ca



C. Peers et al. (eds.), *Arterial Chemoreceptors in Physiology and Pathophysiology*,
Advances in Experimental Medicine and Biology 860, DOI 10.1007/978-3-319-18440-1_5

**Keywords**

ATP • Gliotransmission • Angiotensin II • Endothelin-1 • Acetylcholine • Pannexin-1 channels

## 5.1 Introduction

In the carotid body (CB), **g**lial **f**ibrillary **a**cidic **p**rotein (GFAP)-positive glial-like type II cells occur in intimate association with chemoreceptor (type I) cells in the ratio of approximately 1:4 (McDonald 1981). The elongated cell bodies of type II cells extend cytoplasmic processes that ensheath type I clusters, suggesting paracrine interactions may occur between these two cell types (Tse et al. 2012; Nurse and Piskuric 2013). So far, most of the paracrine mechanisms investigated in the CB have targeted the chemoreceptor type I cells, which express a variety of G-protein coupled receptors for endogenous neuromodulators (Kumar and Prabhakar 2012; Nurse 2010; Nurse and Piskuric 2013). By comparison, the potential role of paracrine signaling via glial-like type II cells has been less well studied (Tse et al. 2012). Glial cells in the central nervous system may monitor, respond to, and participate in synaptic activity by releasing neuroactive substances in a process known as 'gliotransmission' (Eroglu and Barres 2010; Parpura et al. 2012). Zhang et al. (2012) proposed that within the rat CB, type I cells, sensory nerve endings, and glial-like type II cells may communicate within a tripartite synaptic complex, where sensory transmission is modulated, in part by purinergic mechanisms. In support of this schema, activation of purinergic P2Y2 receptors on type II cells led to the opening of gap-junction-like, pannexin 1 (Panx-1) channels and release of ATP (Zhang et al. 2012). Given the central role of ATP as a key excitatory neurotransmitter released from type I cells during chemoexcitation (Zhang et al. 2000; Nurse 2010; Nurse and Piskuric 2013), the study of Zhang et al. (2012) suggested a novel pathway whereby paracrine stimulation of type II cells during chemoexcitation might help boost the excitatory signal, ATP.

In a more recent search for other CB neurochemicals that might be capable of similarly stimulating type II cells, we tested the effects of the vasoactive neuropeptides, angiotensin II (ANG II) and endothelin-1 (ET-1), as well as the putative CB neurotransmitter, acetylcholine (ACh). In agreement with an earlier preliminary report (Tse et al. 2012), we found that type II cells of the rat CB can respond to both ANG II (Murali et al. 2014) and muscarinic agonists, leading to a rise in intracellular $Ca^{2+}$ concentration. A novel finding was that low, nanomolar concentrations of ET-1 can also elicit robust intracellular $Ca^{2+}$ responses in a subpopulation of type II cells and that, similar to ATP and ANG II (Murali et al. 2014), the effects of ACh may lead to the activation of Panx-1 channels.

## 5.2 Materials and Methods

### 5.2.1 Cell Culture

Dissociated rat CBs were cultured as previously described (Zhang et al. 2000, 2012). Briefly, CBs were removed from juvenile (P9-14) rats and placed in ice-cold L15 medium. All procedures for animal handling were carried out according to the guidelines of the Canadian Council on Animal Care (CCAC) and institutional guidelines. The excised CBs were enzymatically dissociated for 1 h, then mechanically dissociated with forceps. The cells were then triturated and plated on culture dishes with modified F-12 medium.

### 5.2.2 Fura-2 Ratiometric $Ca^{2+}$ Imaging

Intracellular $Ca^{2+}$ measurements were performed as previously described (Piskuric and Nurse 2012; Murali et al. 2014). Briefly, CBs were loaded with 2.5 μM fura-2 diluted in standard bicarbonate-buffered solution (BBS) for 20 min at 37 °C, and subsequently washed for ~15 min to remove free dye. The dish was placed on the stage of an inverted microscope and perfused with BBS buffered with 95 % air/5 % $CO_2$ at 37 °C.

### 5.2.3 Electrophysiology

Nystatin perforated-patch, whole cell-recording was used to monitor ionic currents in type II cells as previously described (Zhang et al. 2012). All recordings were carried out at ~35 °C and the cells were perfused with standard BBS. Agonists (ANG II, ET-1, ACh) were applied by a 'fast perfusion' system utilizing a double-barreled pipette assembly as previous described (Zhang et al. 2012).

### 5.2.4 Solutions and Drugs

For calcium imaging, the BBS contained (in mM): $NaHCO_3$, 24; NaCl, 115; glucose, 5; KCl, 5; $CaCl_2$, 2 and $MgCl_2$, 1, at 37 °C and the pH was kept at 7.4 by bubbling the solution with a 95 % air/5 % $CO_2$ gas mixture. For electrophysiology, the BBS contained (in mM): $NaHCO_3$, 24; NaCl, 115; glucose, 10; KCl, 5; $CaCl_2$, 2; $MgCl_2$, 1, and sucrose, 12. The pipette solution contained (mM): potassium gluconate, 115; KCl, 25; NaCl, 5; $CaCl_2$, 1; Hepes, 10, and nystatin 200 $\mu g.ml^{-1}$; at pH 7.2.

## 5.3 Results

Experiments were carried out on isolated 'solitary' type II cells to minimize cross-talk arising from neurosecretion by neighbouring type I cells. In $Ca^{2+}$ imaging experiments, type II cells were identified by the presence of an increase in intracellular $Ca^{2+}$ ($\Delta[Ca^{2+}]_i$) during stimulation with UTP, a selective P2Y2 receptor agonist (Xu et al. 2003; Piskuric and Nurse 2012; Tse et al. 2012; Zhang et al. 2012). In these experiments, the absence of cross-talk was indicated when type II cells failed to elicit a $\Delta[Ca^{2+}]_i$ response during perfusion with the depolarizing stimulus high $K^+$, which stimulates neurosecretion from type I cells (Buttigieg and Nurse 2004; Livermore and Nurse 2013). In voltage clamp experiments, solitary type II cells were identified by their elongated morphology and electrophysiological profile (Duchen et al. 1988; Zhang et al. 2012; Murali et al. 2014).

### 5.3.1 Angiotensin II (ANG II) Stimulates a Rise in $[Ca^{2+}]_i$ and Activates Panx-1 Currents in Type II Cells via $AT_1$ Receptors

It is well established that ANG II elicits a rise in intracellular $Ca^{2+}$ ($[Ca^{2+}]_i$) in at least a subpopulation of rat type I cells (Fung et al. 2001). In a recent study (Murali et al. 2014), we confirmed this finding and further showed that type II cells also respond to ANG II (see also, Tse et al. 2012), and with an even larger increase in $[Ca^{2+}]_i$. Figure 5.1a illustrates an example where ANG II (100 nM) elicited a $Ca^{2+}$ response in both a type I and type II cell in the same culture. Interestingly, in the presence of suramin (100 μM) which should block any cross-talk from type I to type II cells mediated via P2Y2R stimulation, the $\Delta[Ca^{2+}]_i$ response to ANG II was unaffected as exemplified in Fig. 5.1a; summary data from one experimental series supporting this point are shown in Fig. 5.1b (n = 3 dishes; 30–100 cells sampled per dish). These data support a direct interaction between ANG II and AT receptors on type II cells, without type I cell involvement. Results from a recent study of >500 UTP-sensitive type II cells revealed that ~75 % of them were also sensitive to ANG II (Murali et al. 2014). The intracellular $Ca^{2+}$ signal elicited by

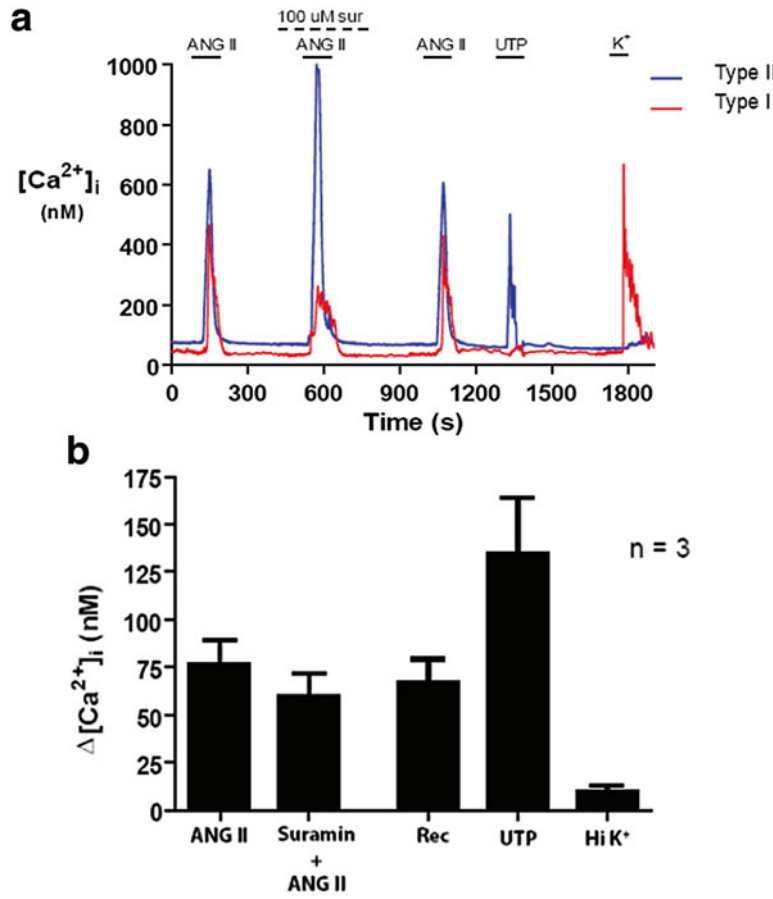


**Fig. 5.1 Angiotensin II (ANG II) elicits intracellular $Ca^{2+}$ responses in both type I and type II cells**. In (**a**) ANG II-induced $Ca^{2+}$ responses occur with similar latencies in type I and type II cells. Suramin (100 μM) failed to block ANG II-evoked $Ca^{2+}$ responses in type II cells (**a**, **b**), suggesting these responses were not secondary to release of ATP from type I cells (n = 3 dishes; 30–100 cells sample per dish). Note UTP and high $K^+$ (30 mM) selectively elicit $Ca^{2+}$ responses in type II and type I cells respectively

ANG II in type II cells arose from intracellular stores, and was mediated via $AT_1$ receptors ($AT_1R$) because it could be reversibly abolished by the specific $AT_1R$ blocker, 1 μM losartan (Murali et al. 2014).

To determine whether stimulation of $AT_1R$ by ANG II also led to the activation of Panx-1 currents in type II cells, similar to P2Y2R activation by ATP or UTP (Zhang et al. 2012), we used voltage clamp. Indeed, at a holding potential of −60 mV, ANG II (100 μM) induced an inward current in type II cells that was reversibly abolished by 5 μM carbenoxolone (CBX), a selective Panx-1 channel blocker (Ma et al. 2009; Murali et al. 2014). This inward current was also reversibly abolished by losartan (1 μM), confirming that both the rise in $[Ca^{2+}]_i$ and activation of Panx-1 current were mediated via $AT_1R$ in type II cells (Murali et al. 2014).

### 5.3.2 Endothelin 1 (ET-1) Stimulates a Rise in $[Ca^{2+}]_i$ in Type II Cells

In addition to ANG II, endothelin 1 (ET-1) is another vasoactive neuropeptide expressed in rat CB type I cells, and its expression is upregulated during whole animal exposure to chronic hypoxia

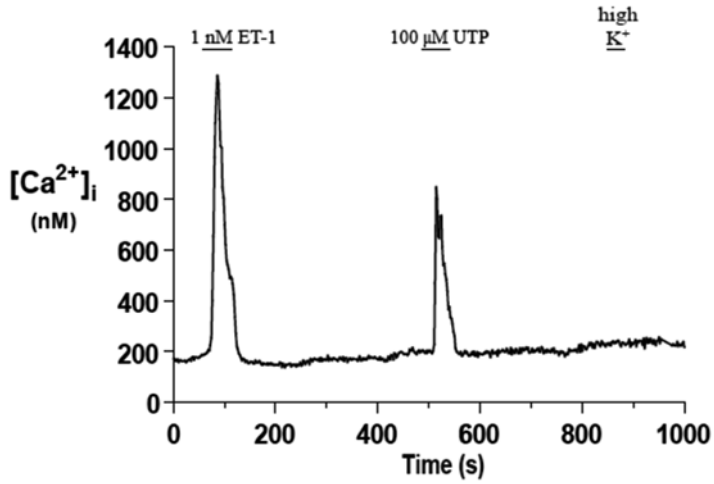


**Fig. 5.2 Effects of endothelin-1 (ET-1) on intracellular $Ca^{2+}$ in carotid body type II cells**. The sample trace shows a rise in $[Ca^{2+}]_i$ in response to 1 nM ET-1 and 100 μM UTP in a type II cell. The ET-1 response was typical of 60/100 cells that were sensitive to UTP

(Chen et al. 2002a, b). Moreover, there is recent evidence that release of ET-1 from type I cells can stimulate proliferation of CB cells by acting mainly at ET(B) receptors on $GFAP^+$, glial-like progenitors (Platero-Luengo et al. 2014). Though in the latter study, weak expression of ET(A) receptors was also found on a subpopulation of $GFAP^+$ cells, the possibility is raised that CB type II cells may express ET(A) and/or ET(B) receptors. Indeed, as exemplified in Fig. 5.2, exposure of type II cells to a relatively low dose of ET-1 (1 nM) caused a robust rise in $[Ca^{2+}]_i$, comparable to that seen with much higher concentrations of ANG II (100 nM) and UTP (100 μM). The mean $\Delta[Ca^{2+}]_i$ response induced by 1 nM ET-1 in solitary type II cells was 96.7 ± 9.8 nM (n = 60 cells). Future experiments will determine which subtype(s) of ET-receptors mediate(s) these $\Delta[Ca^{2+}]_i$ responses, as well as the intracellular signaling pathway involved.

### 5.3.3 ACh Mobilizes $Ca^{2+}$ and Activates Panx-1-Like Currents in Type II Cells

In a preliminary study, stimulation of muscarinic ACh receptors (mAChRs) on rat type II cells led a rise in intracellular $Ca^{2+}$ (Tse et al. 2012). Figure 5.3a confirms that stimulation of mAChR with 10 μM muscarine caused a rise in $[Ca^{2+}]_i$ in the same type II cell that was responsive to 100 μM UTP. We found that ~53 % (149/280 cells) of UTP-sensitive type II cells were also sensitive to 10 μM muscarine; the mean $\Delta[Ca^{2+}]_i$ response induced by muscarine was ~36 nM in type II cells. This $Ca^{2+}$ response to mAChR stimulation appeared much smaller in comparison with responses to ATP/UTP (Zhang et al. 2012) and ANG II (see above). To determine whether mAChR stimulation can lead to Panx-1 channel opening we used voltage clamp. In preliminary studies, rapid perfusion of 10 μM ACh resulted in the activation of Panx-1-like currents in a subpopulation of type II cells. An example is shown in Fig. 5.3b, where both ATP (Fig. 5.3b1) and ACh (Fig. 5.3b2) activated Panx-1-like currents in the *same* type II cell; recordings are typical of n = 5 cells.

## 5.4 Discussion

In this study we consider the evidence for paracrine signaling in the rat carotid body involving the action of neurochemicals at glial-like type II cells. Previous studies demonstrated that type II cells express P2Y2 receptors (P2Y2R) which,

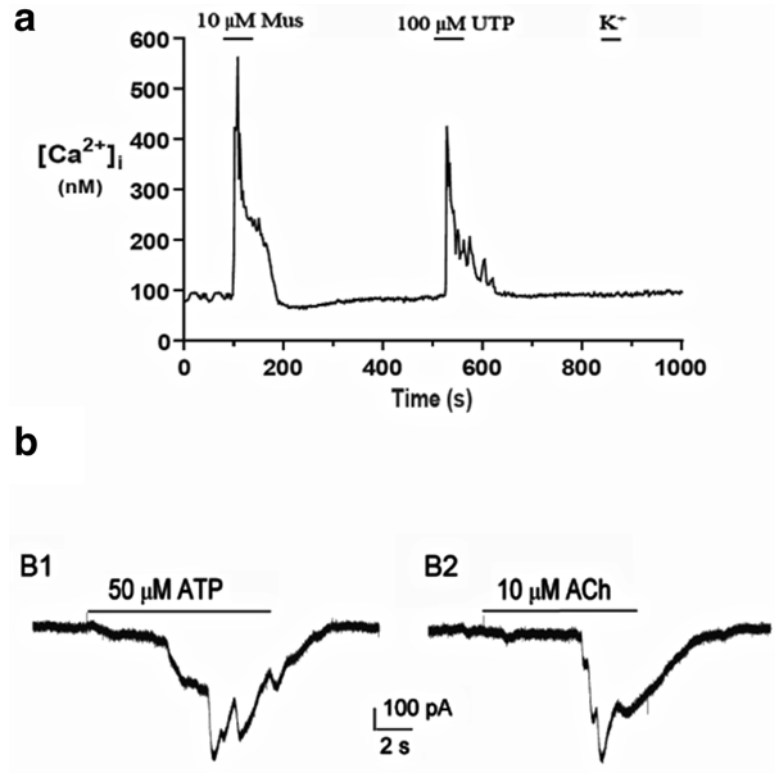


**Fig. 5.3 Muscarine (Mus) elicits $Ca^{2+}$ responses and acetylcholine (ACh) activates pannexin-1 (Panx-1) currents in rat carotid body type II cells**. Sample trace shows a rise in $Ca^{2+}$ evoked by 10 µM Mus and 100 µM UTP in a type II cell (**a**). The response to Mus was present in 53 % (150/280) of UTP-sensitive type II cells. Both ATP (**b1**) and ACh (**b2**) activated Panx-1-like currents in the same cell (n = 5)

when stimulated by agonists such as ATP and UTP, elicited a rise in intracellular $Ca^{2+}$ (Xu et al. 2003; Tse et al. 2012; Zhang et al. 2012). Moreover, activation of this signaling pathway led to a $Ca^{2+}$-dependent opening of Panx-1 channels that allowed further release of ATP (Zhang et al. 2012; Murali et al. 2014). In the study by Zhang et al. (2012), stimulation of type II cells alone with UTP could trigger release of ATP that was sufficient to excite afferent petrosal neurons in co-culture. Together, these studies suggest that purinergic signaling pathways in type II cells may contribute to sensory processing in the carotid body.

Recent evidence, including preliminary data described in the present study, point to the type II cell as a likely target for other neurochemicals released by type I cells during chemotransduction. For example, the vasoactive neuropeptides angiotensin II (ANG II) (Tse et al. 2012; Murali et al. 2014) and endothelin-1 (ET-1) (this study), which are known to be expressed in chemoreceptor type I cells, evoke a robust rise in intracellular $Ca^{2+}$ in type II cells. Similar to ATP acting via P2Y2R, the signaling pathway activated by ANG II led to a $Ca^{2+}$-dependent opening of Panx-1 channels (Murali et al. 2014). Further studies are required to determine whether ET-1 can act similarly. Nevertheless, our preliminary data suggest that another neurochemical ACh, whose cellular localization and role in CB physiology remains controversial (Nurse 2010; Nurse and Piskuric 2013), is capable of eliciting a rise in intracellular $Ca^{2+}$ and Panx-1 channel opening in at least a subpopulation of type II cells. This pathway involves activation of G-protein coupled mAChR

receptors (Tse et al. 2012; this study). Taken together, these studies demonstrate that several CB neurochemicals synthesized in type I cells may trigger intracellular $Ca^{2+}$ responses in type II cells. These paracrine pathways may also lead to the opening of Panx-1 channels and release of ATP, a 'gliotransmitter' capable of exciting afferent petrosal neurons (Zhang et al. 2012). However, it still remains to be formally demonstrated that these proposed signaling pathways do in fact play a significant role in synapse integration in the CB during chemotransduction.

**Acknowledgements** This work was supported by an operating grant from the Canadian Institutes of Health Research (CIHR) and a Discovery grant from the Natural Sciences and Engineering Research Council of Canada (NSERC) to C.A.N. S.M. was supported in part by a CIHR/NSERC CGS-M graduate scholarship award.

## References

Buttigieg J, Nurse CA (2004) Detection of hypoxia-evoked ATP release from chemoreceptor cells of the rat carotid body. Biochem Biophys Res Commun 322(1):82–87

Chen J, He L, Dinger B, Stensaas L, Fidone S (2002a) Role of endothelin and endothelin A-type receptor in adaptation of the carotid body to chronic hypoxia. Am J Physiol Lung Cell Mol Physiol 282(6):L1314–L1323

Chen Y, Tipoe GL, Liong E, Leung P, Lam S-Y, Iwase R, Tjong Y-W, Fung M-L (2002b) Chronic hypoxia enhances endothelin-1-induced intracellular calcium elevation in rat carotid body chemoreceptors and up-regulates ETA receptor expression. Pflugers Arch 443(4):565–573

Duchen M, Caddy K, Kirby G, Patterson D, Ponte J, Biscoe T (1988) Biophysical studies of the cellular elements of the rabbit carotid body. Neuroscience 26(1):291–311

Eroglu C, Barres BA (2010) Regulation of synaptic connectivity by glia. Nature 468(7321):223–231

Fung M-L, Lam S-Y, Chen Y, Dong X, Leung PS (2001) Functional expression of angiotensin II receptors in type-I cells of the rat carotid body. Pflugers Arch 441(4):474–480

Kumar P, Prabhakar NR (2012) Peripheral chemoreceptors: function and plasticity of the carotid body. Compr Physiol 2(1):141–219

Livermore S, Nurse CA (2013) Enhanced adenosine A2b receptor signaling facilitates stimulus-induced catecholamine secretion in chronically hypoxic carotid body type I cells. Am J Physiol Cell Physiol 305(7):C739–C750

Ma W, Hui H, Pelegrin P, Surprenant A (2009) Pharmacological characterization of pannexin-1 currents expressed in mammalian cells. J Pharmacol Exp Ther 328(2):409–418

McDonald DM (1981) Peripheral chemoreceptors: structure-function relationships of the carotid body. In: Horbein TF (ed) Regulation of breathing, part 1. Marcel Dekker Inc., New York, pp 105–319

Murali S, Zhang M, Nurse CA (2014) Angiotensin II mobilizes intracellular calcium and activates pannexin-1 channels in rat carotid body type II cells via AT1 receptors. J Physiol 592(21):4747–4762

Nurse CA (2010) Neurotransmitter and neuromodulatory mechanisms at peripheral arterial chemoreceptors. Exp Physiol 95(6):657–667

Nurse CA, Piskuric NA (2013) Signal processing at mammalian carotid body chemoreceptors. Semin Cell Dev Biol 24(1):22–30

Parpura V, Heneka MT, Montana V, Oliet SH, Schousboe A, Haydon PG, Stout RF, Spray DC, Reichenbach A, Pannicke T (2012) Glial cells in (patho) physiology. J Neurochem 121(1):4–27

Platero-Luengo A, González-Granero S, Durán R, Díaz-Castro B, Piruat JI, García-Verdugo JM, Pardal R, López-Barneo J (2014) An $O_2$-sensitive glomus cell-stem cell synapse induces carotid body growth in chronic hypoxia. Cell 156(1–2):291–303

Piskuric NA, Nurse CA (2012) Effects of chemostimuli on [Ca2+]i responses of rat aortic body type I cells and endogenous local neurons: comparison with carotid body cells. J Physiol 590(9):2121–2135

Tse A, Yan L, Lee AK, Tse FW (2012) Autocrine and paracrine actions of ATP in rat carotid body. Can J Physiol Pharmacol 90(6):705–711

Xu J, Frederick WT, Tse A (2003) ATP triggers intracellular $Ca^{2+}$ release in type II cells of the rat carotid body. J Physiol 549(3):739–747

Zhang M, Zhong H, Vollmer C, Nurse CA (2000) Co-release of ATP and ACh mediates hypoxic signalling at rat carotid body chemoreceptors. J Physiol 525(1):143–158

Zhang M, Piskuric NA, Vollmer C, Nurse CA (2012) P2Y2 receptor activation opens pannexin-1 channels in rat carotid body type II cells: potential role in amplifying the neurotransmitter ATP. J Physiol 590(17):4335–4350

# 6 Selective mu and kappa Opioid Agonists Inhibit Voltage-Gated $Ca^{2+}$ Entry in Isolated Neonatal Rat Carotid Body Type I Cells

Ellen M. Ricker, Richard L. Pye, Barbara L. Barr, and Christopher N. Wyatt

**Abstract**

It is known that opioids inhibit the hypoxic ventilatory response in part via an action at the carotid body, but little is known about the cellular mechanisms that underpin this. This study's objectives were to examine which opioid receptors are located on the oxygen-sensing carotid body type I cells from the rat and determine the mechanism by which opioids might inhibit cellular excitability.

Immunocytochemistry revealed the presence of μ and κ opioid receptors on type I cells. The μ-selective agonist DAMGO (10 μM) and the κ-selective agonist U50-488 (10 μM) inhibited high $K^+$ induced rises in intracellular $Ca^{2+}$ compared with controls. After 3 h incubation (37 °C) with pertussis toxin (150 ng $ml^{-1}$), DAMGO (10 μM) and U50-488 (10 μM) had no significant effect on the $Ca^{2+}$ response to high $K^+$.

These results indicate that opioids acting at μ and κ receptors inhibit voltage-gated $Ca^{2+}$ influx in rat carotid body type I cells via $G_i$-coupled mechanisms. This mechanism may contribute to opioid's inhibitory actions in the carotid body.

**Keywords**

Carotid body • Type I cells • Opioid receptors • $Ca^{2+}$ imaging

## 6.1 Introduction

The drive to breathe is generated in the brainstem and is modulated by inputs from the cortex, central chemoreceptors located in the brainstem, and peripheral chemoreceptors, such as the carotid body (CB) and the aortic bodies. It has been

E.M. Ricker • R.L. Pye • B.L. Barr • C.N. Wyatt (✉)
Department of Neuroscience, Cell Biology and Physiology, Wright State University,
3640 Colonel Glenn Hwy, Dayton, OH 45435, USA
e-mail: christopher.wyatt@wright.edu



C. Peers et al. (eds.), *Arterial Chemoreceptors in Physiology and Pathophysiology*,
Advances in Experimental Medicine and Biology 860, DOI 10.1007/978-3-319-18440-1_6

shown that there is a high concentration of opioid receptors in areas of the brain related to respiration (Mutolo et al. 2007; Mansour and Watson 1993). Activation of opioid receptors in these respiratory centers of the brain and brainstem affects ion channels through $G_i$ proteins, which can alter the excitability of neurons and ultimately affect respiration patterns. Interestingly at low doses, opioids change the respiratory patterns whereas at high doses, they reduce tidal volume (Lalley 2003).

Critically, μ opioid receptor activation decreases respiratory rate and can lead to complete apnea upon overdose (Feng et al. 2012). The μ opioid receptor agonist, DAMGO caused a naloxone-reversible dose-dependent decrease in the frequency of respiratory rhythmic discharge when applied to the bathing solutions of the neonatal rat brainstem (Greer et al. 1995). Furthermore, the activation of μ opioid receptors in the NTS eliminated the hypoxic ventilatory response in rats (Zhang et al. 2011). Overall, these studies show that opioids can affect the acute hypoxic response and ultimately the respiration patterns in rodents via the central nervous system.

However, in the peripheral nervous system, little opioid signaling research has been done on isolated chemosensitive carotid body (CB) type I cells; only whole CBs have been examined in detail. The common opioid fentanyl decreased the canine carotid chemoreceptor reflex (Mayer et al. 1989) and it was also shown that activation of opioid receptors in the peripheral nervous system inhibited the acute hypoxic chemoreceptor response in the cat, although cellular mechanisms underpinning this effect were not explored (Kirby and McQueen 1986).

This study tested the hypothesis that activation of opioid receptors on the type I cells of the rat CB may inhibit the influx of $Ca^{2+}$ via $G_i$-protein coupled receptors potentially reducing neurotransmitter release, decreasing the firing rate of the CSN and ultimately inhibiting the acute hypoxic response.

## 6.2 Methods

### 6.2.1 Type I Cell Isolation

Neonatal Sprague-Dawley rats (12–19 days old) were deeply anesthetized with isoflurane (4.5 % in oxygen) and their carotid bodies removed. Type I cells were isolated as previously described (Burlon et al. 2009).

### 6.2.2 Immunocytochemistry

Coverslips with adhered type I cells were fixed by immersion in methanol at −20 °C for 15 min. Cells were then washed 3 × 5 min with a permeabilization and blocking solution (0.3 % triton X-100 and 1 % bovine serum albumin in phosphate buffered saline (PBS)). Specific primary antibodies were used to identify the different three opioid receptors while an anti-TH antibody identified the cells as type I cells.

The anti-δ opioid and the anti-μ opioid receptor 1° antibodies (Santa Cruz Biotechnology: sc-9111, sc-15310) were rabbit polyclonal antibodies diluted to 1:200 with the blocking solution, whereas the anti-κ opioid receptor 1° antibody (USBiological, O7030-31A) was a rabbit polyclonal antibody diluted to 1:1000 with the blocking solution. All primary antibodies were added to the appropriate coverslips with the anti-TH 1° antibody (Sigma, 1:1000 dilution) and incubated at 4 °C for 16 h.

Following the incubation with the 1° antibodies, coverslips were washed 2 × 10 min with the blocking solution and then incubated for 2 h in the dark at room temperature with the 2° antibodies diluted to 1:200 with the blocking solution. Rhodamine Red-X-conjugated AffiniPure donkey anti-rabbit IgG 2° antibody marked the opioid receptor antibodies and a Fluorescein (FITC)-conjugated donkey anti-mouse IgG 2° antibody allowed identification of TH. All 2° antibodies were supplied by Jackson Immunoresearch.

### 6.2.3 $Ca^{2+}$ Imaging

For experiments recording intracellular calcium type I cells were loaded with 5 μM FURA-2 AM (Invitrogen) for 30 min at room temperature. The dye was excited with 340/380 nm light and emitted light was recorded at 510 nm using a Coolsnap HQ2 CCD camera (Photometrics). Image acquisition was controlled by Metafluor software (Molecular Devices) and cells were visualized using a Nikon TE2000-U microscope with a X40 objective. Extracellular solution was HEPES buffered salt solution (in mM): 140 NaCl, 4.5 KCl, 2.5 $CaCl_2$, 1, $MgCl_2$, 11 glucose, 10 HEPES, adjusted to pH 7.4 with NaOH at 37 °C. The high potassium stimulus was (in mM): 64.5 NaCl, 80 KCl, 2.5 $CaCl_2$, 1, $MgCl_2$, 11 glucose, 10 HEPES adjusted to pH 7.4 with KOH at 37 °C. To examine the importance of opioid-activated $G_i$-mediated inhibition of $Ca^{2+}$ influx CB cells were incubated for 3 h in the presence of 150 ng/ml of pertussis toxin (PTX, 37 °C, in culture medium) and $Ca^{2+}$ imaging examined the effects on voltage-gated $Ca^{2+}$ influx.

## 6.3 Results

### 6.3.1 Immunocytochemistry

Immunofluorescence was used to identify which of the opioid receptors (μ, κ, or δ) were present on the membranes of rat CB cells type I cells. TH identified the cells as type I cells while DAPI identified the nucleus. Control experiments were only treated with the 2° antibodies. Images were acquired using a DeltaVision microscope and each image represents an example z-section through the cell. Staining was observed for both the μ and the κ opioid receptors, but only very faint staining was seen for the δ opioid receptors (Fig. 6.1). The brightest staining for the μ and κ opioid receptors was in the cytoplasm and on the cell membrane. The control images were clear of any nonselective 2° antibody staining. The absence of δ receptor staining could have been due to a poor quality antibody. However, under the same conditions the δ antibody stained δ receptors in rat dorsal root ganglion cells indicating that this was unlikely (data not shown). These images confirmed that μ and κ receptors are present in rat type I cells whereas δ receptors are not.

### 6.3.2 $Ca^{2+}$ Imaging

Cells were depolarized with 80 mM $K^+$ to ensure that they were viable. Only cells that responded to the stimulus with a rapid and reversible rise in $[Ca^{2+}]_i$ were chosen. Cells were then exposed to the agonist (DAMGO for the μ opioid receptor; U50-488 for the κ opioid receptor) for 4 min before a second 80 mM $K^+$ stimulus was applied in the presence of the agonist. Finally, a third 80 mM $K^+$ stimulus was applied to the cell to ensure that the cell was still viable. The control cells did not have an opioid agonist applied.

Isolated rat CB type I cells experienced a reduction in voltage-gated $Ca^{2+}$ influx upon repetitive stimulation by the 80 mM $K^+$ stimulus. Among 12 cells, there was an average reduction of 12.99 ± 1.46 % between the first and second $K^+$ responses (Fig. 6.2a, d). Therefore, to analyze the effect of an agonist, the percent reduction in the controls was compared to the percent inhibition in the presence of the agonist, using an unpaired student's t-test. At a concentration of 10 μM, the μ selective agonist DAMGO significantly inhibited voltage-gated $Ca^{2+}$ influx by 26.23 ± 2.92 % ($N = 11$, $p < 0.0004$, Fig. 6.2b, d) compared with controls. Similarly, at a concentration of 10 μM, the selective κ receptor agonist U50-488 elicited a significant inhibition of voltage-gated $Ca^{2+}$ influx of 22.22 ± 2.47 % ($N = 11$, $p < 0.003$, Fig. 6.2c, d) compared to controls.

Finally, incubation with PTX did not alter control responses to high potassium (Fig. 6.3a, d) but the inhibition of $Ca^{2+}$ entry in the presence of both opioid agonists was abolished (Fig. 6.3b–d).

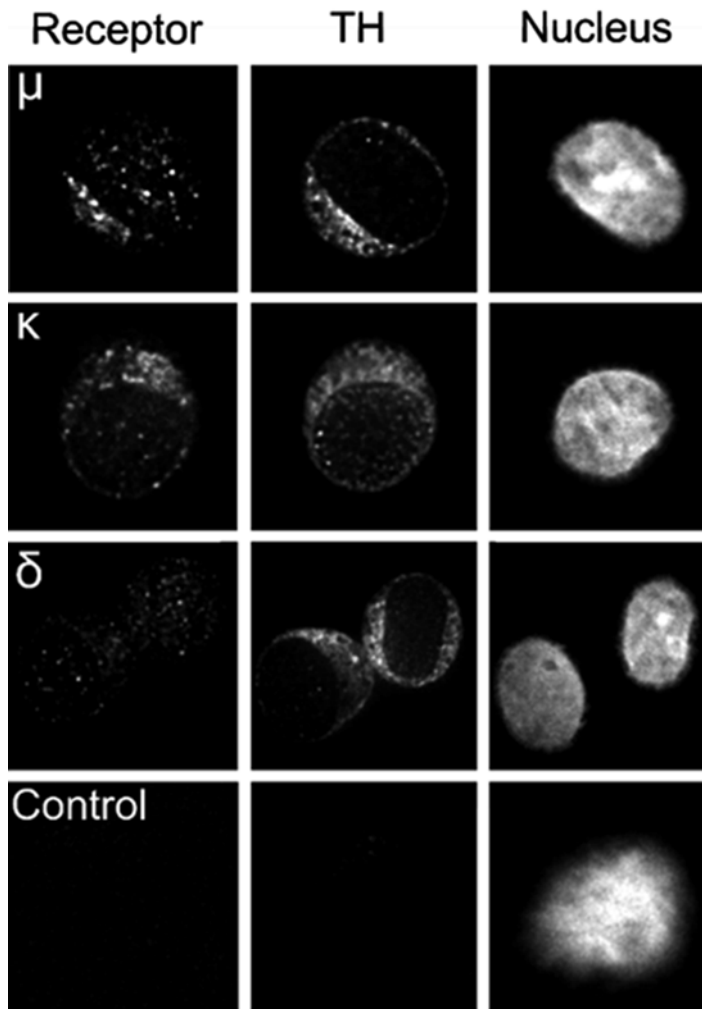


**Fig. 6.1** Opioid receptor staining in isolated rat CB type I cells using double immunofluorescence. The receptors, tyrosine hydroxylase (TH), and the nucleus are all shown in 16-bit *greyscale*. Staining is present for μ and κ opioid receptors and is not present for δ opioid receptors. TH is seen throughout the cytoplasm of μ, κ, and δ stained cells. Control images show absence of 2° antibody staining when 1° antibodies were absent. Images for the controls, μ, and κ are scaled to 15 μm width. Images for δ staining are scaled to 20 μm width

## 6.4 Discussion

It was discovered that μ and κ opioid receptors were present on the rat type I CB cells, whereas δ opioid receptors were not present. The μ agonist DAMGO and the κ agonist U50-488 both significantly inhibited voltage-gated $Ca^{2+}$ entry into type I cells. Following a 3 h incubation with PTX, a $G_i$ protein inhibitor, neither DAMGO nor U50-488 inhibited voltage-gated $Ca^{2+}$ entry into the cells. Therefore, it can be concluded that the opioid receptor-mediated inhibition of voltage-gated $Ca^{2+}$ influx occurs via PTX-sensitive $G_i$ proteins. Interestingly, a previous study by eSilva and Lewis (1995) suggested that activation of opioid receptors on CB type I cells (n = 3, data not shown) did not inhibit voltage-gated $Ca^{2+}$ influx. Importantly, those experiments were conducted in adult rats and no immunocytochemistry was performed. Thus it is possible that a

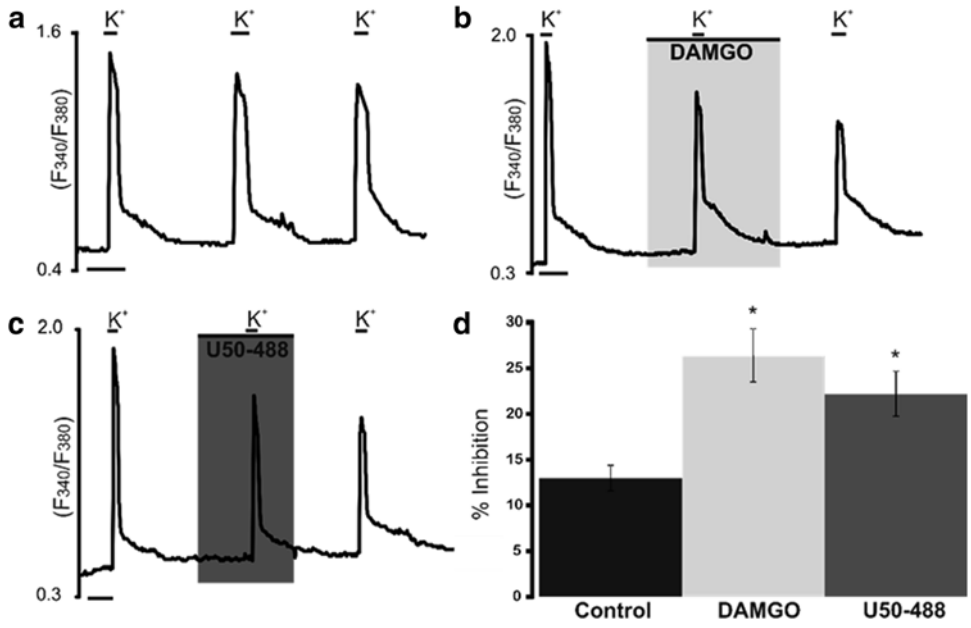


**Fig. 6.2** Effects of 10 μM DAMGO and 10 μM U50-488 on type I CB cell Fura-2 Fluorescence ratios. (**a**) Control responses to 80 mM $K^+$ in an example cell. (**b**) Responses to 80 mM $K^+$ in an example cell exposed to 10 μM DAMGO. (**c**) Responses to 80 mM $K^+$ in an example cell exposed to 10 μM U50-488. (**d**) The *bar chart* shows the average percent inhibitions for the second $K^+$ response compared to the first. Controls (12.99 ± 1.34 %), in the presence of 10 μM DAMGO (26.43 ± 2.92 %) and in the presence of 10 μM U50-488 (22.22 ± 2.47 %). *Scale bars* indicate 2 min

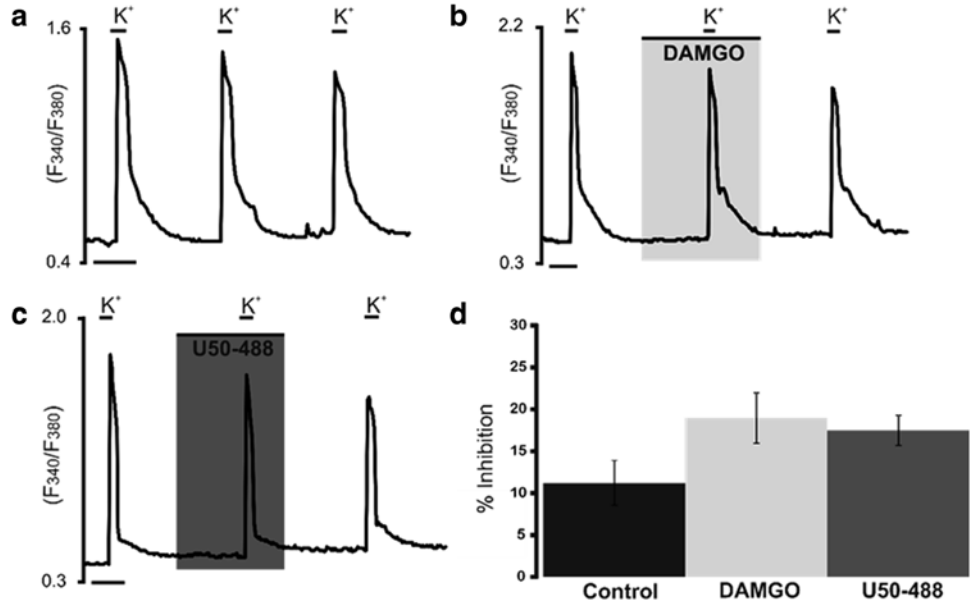


**Fig. 6.3** Effects of 10 μM DAMGO and 10 μM U50-488 on type I CB cell Fura-2 Fluorescence ratios after incubation with PTX. (**a**) Control responses to 80 mM $K^+$ in an example cell. (**b**) Responses to 80 mM $K^+$ in an example cell exposed to 10 μM DAMGO. (**c**) Responses to 80 mM $K^+$ in an example cell exposed to 10 μM U50-488. (**d**) The *bar chart* shows the average percent inhibitions for the second $K^+$ response compared to the first. Controls (11.21 ± 2.66 %) 10 μM DAMGO (18.95 ± 3.02 %) and 10 μM U50-488 (17.47 ± 1.81 %). *Scale bars* indicate 2 min

developmental change may occur in rat CB whereby younger animals are more sensitive to the effects of opioids but this sensitivity decreases with age. The possible mechanisms for this developmental change are not known at this time.

## References

Burlon DC, Jordan HL, Wyatt CN (2009) Presynaptic regulation of isolated neonatal rat carotid body type I cells by histamine. Respir Physiol Neurobiol 168(3):218–223

eSilva MJM, Lewis DL (1995) L- and N-type $Ca^{2+}$ channels in adult carotid body chemoreceptor type I cells. J Physiol 489(3):689–699

Feng Y, He X, Yang Y, Chao D, Lazarus L, Xia Y (2012) Current research on opioid receptor function. Curr Drug Targets 13(2):230–246

Greer JJ, Carter JE, Al-Zubaidy Z (1995) Opioid depression of respiration in neonatal rats. J Physiol 485(3):845–855

Kirby GC, McQueen DS (1986) Characterization of opioid receptors in the cat carotid body involved in chemosensory depression in vivo. Br J Pharmacol 88:889–898

Lalley PM (2003) Mu-opioid receptor agonist effects on medullary respiratory neurons in the cat: evidence for involvement in certain types of ventilatory disturbances. Am J Physiol Regul Integr Comp Physiol 285:1287–1304

Mansour A, Watson SJ (1993) Anatomical distribution of opioid receptors in mammalians: an overview. Handb Exp Pharmacol 104:79–105

Mayer N, Zimpfer M, Raberger G, Beck A (1989) Fentanyl inhibits canine carotid chemoreceptor reflex. Anesth Analg 69:756–762

Mutolo D, Bongianni F, Einum J, Dubuc R, Pantaleo T (2007) Opioid-induced depression in the lamprey respiratory network. Neuroscience 150:720–729

Zhang Z, Zhuang J, Zhang C, Xu F (2011) Activation of opioid μ-receptors in the commissural subdivision of the nucleus tractus solitarius abolishes the ventilatory response to hypoxia in anesthetized rats. Anesthesiology 115(2):353–363

# 7 Measurement of ROS Levels and Membrane Potential Dynamics in the Intact Carotid Body Ex Vivo

Andre Bernardini, Ulf Brockmeier, Eric Metzen, Utta Berchner-Pfannschmidt, Eva Harde, Amparo Acker-Palmer, Dmitri Papkovsky, Helmut Acker, and Joachim Fandrey

**Abstract**

Reactive oxygen species (ROS) generated by the NADPH oxidase have been proposed to play an important role in the carotid body (CB) oxygen sensing process (Cross et al. 1990). Up to now it remains unclear whether hypoxia causes an increase or decrease of CB ROS levels. We transfected CBs with the ROS sensitive HSP-FRET construct and subsequently measured the intracellular redox state by means of Förster resonance energy transfer (FRET) microscopy. In a previous study we found both increasing and decreasing ROS levels under hypoxic conditions. The transition from decreasing to increasing ROS levels coincided with the change of the caging system from ambient environment caging (AEC) to individually ventilated caging (IVC) (Bernardini A, Brockmeier U, Metzen E, Berchner-Pfannschmidt U, Harde E, Acker-Palmer A, Papkovsky D, Acker H, Fandrey J, Type I cell ROS kinetics under hypoxia in the intact mouse carotid body ex vivo: a FRET based study. Am J Physiol Cell Physiol. doi:10.1152/ajpcell.00370.2013, 2014). In this work we analyze hypoxia induced ROS reaction of animals from an IVC system that had been exposed to AEC conditions for 5 days. The results further support the hypothesis of an important impact of the caging system on CB ROS reaction.

A. Bernardini (✉) • U. Brockmeier • E. Metzen • H. Acker • J. Fandrey
Institute of Physiology, University of Duisburg-Essen, Hufelandstr. 55, 45122 Essen, Germany
e-mail: andre.bernardini@uni-due.de

U. Berchner-Pfannschmidt
Department of Opthalmology, University of Duisburg-Essen, Hufelandstr. 55, 45122 Essen, Germany

E. Harde • A. Acker-Palmer
Institute for Cell Biology and Neuroscience and Buchmann Institute for Molecular Life Sciences, Goethe University Frankfurt, Max-von-Laue-Str. 15, 60438 Frankfurt am Main, Germany

D. Papkovsky
Biochemistry Department, University College Cork, College Road, Cork, Ireland



C. Peers et al. (eds.), *Arterial Chemoreceptors in Physiology and Pathophysiology*, Advances in Experimental Medicine and Biology 860, DOI 10.1007/978-3-319-18440-1_7

**Keywords**

Carotid body • ROS • Tissue-oxygen • Membrane potential • FRET microscopy • NADPH oxidase

## 7.1 Introduction

ROS originating from the NADPH oxidase (NOX) have been shown to play a central role in transforming changes in partial oxygen pressure ($pO_2$) to nervous activity in type I CB cells (Acker 2005). The question whether the cellular ROS level increases or decreases during hypoxia in type I CB cells is, however, still controversially discussed. Mouse studies demonstrated CB hypersensitivity when $p47_{phox}$ an essential regulatory subunit of NOX was genetically deleted (Sanders et al. 2002) or pharmacologically inhibited (Dinger et al. 2007). This is in line with the hypothesis that low ROS levels favor increased CB activity. Conflicting with these findings there are publications that found increasing ROS levels under hypoxic conditions using synthetic ROS indicators like dihydroethidium (DHE) (He et al. 2005).

The subject of ROS measurements itself is controversially discussed. The problem with the widely used synthetic probes like DHE and dichlorofluorescein (DCF) is that they are irreversibly oxidized by ROS and hence unsuitable for kinetic measurements. Moreover, there are some examples throughout the literature, where a reversal of the signal is shown (He et al. 2005). Since the oxidation of the dye is not reversible, it seems obvious that there must be a ROS independent mechanism (e.g. a transport mechanism) contributing to the course of the signal. All together this shows how problematic the usage of synthetic dyes in ROS imaging is. Our aim was therefore to establish a methodology that can be used to reliably assess intracellular ROS kinetics of type I CB cells in their native environment (i.e. in the intact CB) and help to elucidate the question whether ROS levels increase or decrease during hypoxia.

Using the genetically encoded, ROS sensitive HSP-FRET biosensor we successfully followed intracellular ROS kinetics in type I cells of mouse CB. Recent work from our group (Bernardini et al. 2014) showed that both ROS results (increase and decrease) can be observed in mouse CB preparations. We suspected differences in the used caging systems to be the cause for the observed heterogeneity. Indeed, a recent publication reveals that mice from individually ventilated cages (IVC) suffer from chronic low grade hypoxia as compared to ambient environment caging (AEC) (York et al. 2012). In this work we show data, suggesting the used caging system as an important contributing factor to the observed ROS results.

## 7.2 Methods

### 7.2.1 CB Preparation

Preparations of CBs were made as previously described (Bernardini et al. 2014). Briefly, animals were euthanized by isoflurane inhalation and the bifurcation of the common carotid artery dissected immediately thereafter and kept in icecold phosphate buffered saline until fine preparation was done, where connective and fat tissues were removed. Transfection with the HSP-FRET construct was achieved using a Gene Pulser II (Bio-Rad, Germany) with settings 200 Ω, 25 µF, 200 V. The preparation was then put in DMEM supplemented with 10 % FBS, 4.5 g glucose, 4 mM l-glutamine 100 U/ml penicillin and 100 µg/ml streptomycin and stored for 48 h in a humidified 5 % $CO_2$ in air atmosphere at 37 °C.

### 7.2.2 Microscopy

Förster resonance energy transfer (FRET) microscopy was carried out using a custom-built system. Two diode-pumped solid state lasers (Crystalaser, USA) of wavelengths 440 and 532 nm were coupled to a QLC100 spinning disc (Visitech Int. Ltd, UK) mounted to the side-port of a Nikon Ti-E inverted microscope. Excitation light is guided through the pinholes of the spinning disc and focused by a 20×/0.75NA or a 40×/1.3NA objective on the specimen that resides inside a temperature controlled chamber (Luigs&Neumann GmbH, Germany) on the microscope stage. Attached to the chamber is a gas mixing device enabling the controlled application of different gas mixtures to the specimen. Emission light is then collected by the objective, guided through the Nipkow disc and a DualView beamsplitter (Optical Insights, USA). Finally emission light is registered by an Orca ER-G (Hamamatsu Photonics Deutschland GmbH, Germany) 12 bit CCD camera. Sensitized emission image processing and evaluation is done using a custom made software described in detail elsewhere (Bernardini et al. 2010).

### 7.2.3 ROS Sensitive HSP-FRET Construct

The HSP-FRET construct encodes for a protein where enhanced cyan and yellow fluorescent protein (ECFP and EYFP) are linked by the redox-sensitive domain of heatshock protein 33 from Escherichia coli (Waypa et al. 2006). The resulting protein exhibits a fairly high FRET signal as long as it is not oxidized. When oxidized, the conformation of HSP-FRET changes, resulting in a larger distance between both fluorophores and consequently a decrease of the FRET signal. As this conformational change is reversible, the HSP-FRET construct facilitates real time monitoring of intracellular ROS levels inside living cells. The HSP-FRET construct was kindly provided by Paul Schumacker (Chicago).

## 7.3 Results and Discussion

As recently shown by our group through FRET measurements using the HSP-FRET construct CB type I cells can show both an increase and a decrease as response to hypoxic challenges (Bernardini et al. 2014). Figure 7.1 shows an example of a successful transfection of HSP-FRET into CB type I cells (Fig. 7.1a–c) as well as CB cells stained for membrane potential measurements with the voltage sensitive dye di-4-ANEPPDHQ (Fig. 7.1d).

The heterogeneity in the hypoxia induced ROS response seems to be influenced by the type of the used caging system for breeding the mice. Throughout this study 2 different caging systems have been in use: Use of ambient environment caging (AEC) coincided with hypoxia inducible ROS decrease while animals from individually ventilated caging (IVC) systems were much more likely to show a hypoxia induced ROS increase. As recently shown, mice from AEC conditions have normoxic blood parameters whereas animals from IVC systems suffer from chronic low grade hypoxia evidenced by corresponding blood parameters such as increased hematocrit, red blood cell count etc. (York et al. 2012).

In accordance with our findings, pulmonary smooth muscle cells exhibit a ROS decrease under acute hypoxia while responding with a ROS increase to chronic hypoxia (Wu et al. 2007). It has been shown by York and colleagues that 2 days of AEC conditions is sufficient to recover the blood parameters of animals from IVC systems back to normoxic values (York et al. 2012).

We therefore continued with our CB measurements to elucidate whether the ROS response of animals from IVC systems can also be reversed to the acute hypoxic ROS decrease as seen under AEC conditions. We therefore exposed three mice that were bred in an IVC system to AEC conditions for 5 days. As a result of these procedure, Fig. 7.2a shows a remarkable heterogeneity in the hypoxic ROS response of type I cells. 3 CBs responded with an increase in ROS levels as recently shown for animals from IVC systems (Bernardini et al. 2014). 1 CB did not show any notable change in ROS levels and 2 CBs

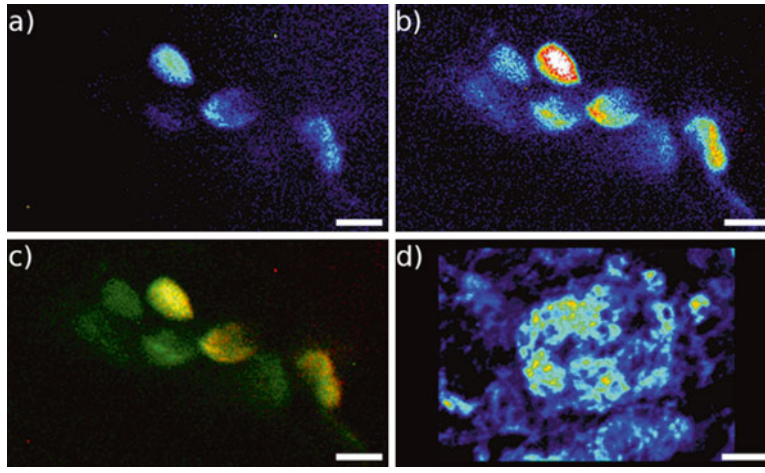


**Fig. 7.1** Example of HSP-FRET transfected CB type I cells. (**a**) HSP-FRET transfected cells as identified by staining with anti-GFP antibody, (**b**) CB type I cells as identified by anti-tyrosinhydroxilase staining, (**c**) *red-green* overlay of **a** and **b** identifying HSP-FRET expressing type I cells, (**d**) di-4-ANEPPDHQ stained carotid body cells for membrane potential measurement. *White bar* indicates 10 μm (**a**–**c**) or 50 μm (**d**)

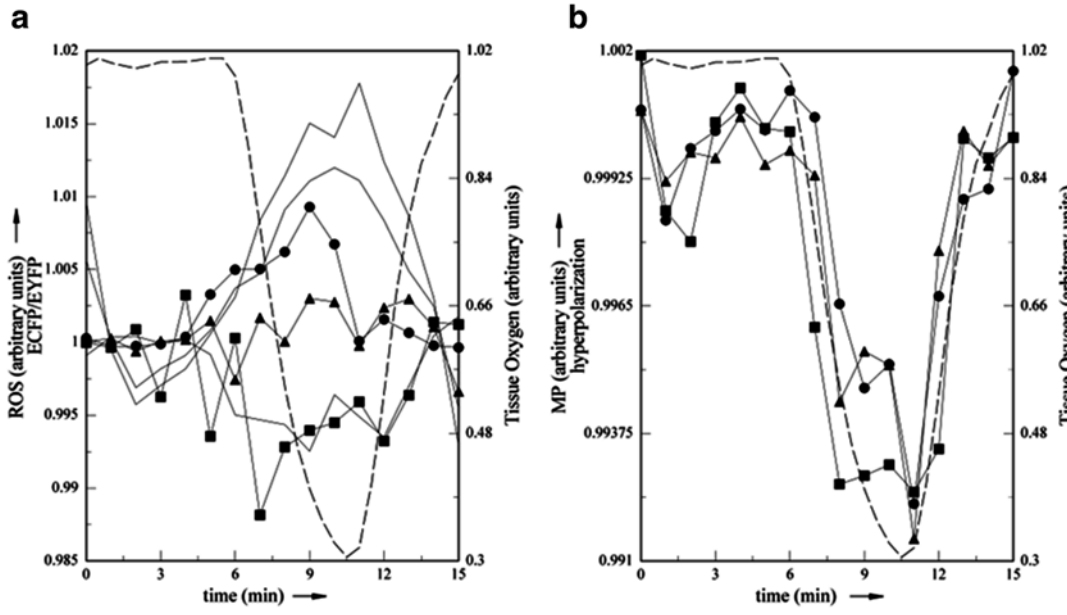


**Fig. 7.2** Measurement of ROS and membrane potential in CB type I cells from IVC animals exposed to AEC conditions for 5 days. (**a**) hypoxic ROS response of 6 CBs. 3 CBs responded with an increase of intracellular ROS levels, 1 CB with no reaction and 2 with a decrease of ROS. (**b**) membrane potential measurement from 3 CBs from **a**. Equal symbols correspond to equal CBs

responded with a decrease of intracellular ROS as already seen in other AEC animals.

The reversal of chronic hypoxic into normoxic animals (as far as the CB ROS response is concerned) seems to have been partially successful and might require therefore more adaptation time for a full transition. One CB for each type of ROS response (increase, decrease and no reaction) was subjected to membrane potential measurement. Equal CBs can be identified by equal symbols. In no case did we see a difference in the hypoxic membrane potential response. All analyzed CBs show the expected membrane potential depolarization under hypoxia as described (Bernardini et al. 2014).

Our study underlines the complexity of ROS interaction with targets like ion channels. It has been shown that NOX and potassium channels are closely co-localized (Buttigieg et al. 2012). Therefore it has to be discussed whether ROS or one of the subunits of NOX interact with the ion channels. 4-(2-Aminoethyl)benzensulfonylfluorid (AEBSF), a specific inhibitor of the $p47_{phox}$ subunit leads to an inhibition of the hypoxia induced ROS decrease but has no influence on a hypoxia induced ROS increase. Furthermore AEBSF inhibits the hypoxia induced membrane potential depolarization independently of the observed ROS kinetics (Bernardini et al. 2014). From these data we conclude that ion channels can be regulated by localized action of NOX that is independent of the overall cellular ROS level. We have to investigate in further studies the supposed localized interaction of ROS or $p47_{phox}$ with potassium channels in order to establish a model for transferring redox sensitivity (and ultimately oxygen sensitivity) to ion channels of type I cells.

## References

Acker H (2005) The oxygen sensing signal cascade under the influence of reactive oxygen species. Philos Trans R Soc Lond Ser B Biol Sci 360(1464):2201–2210. doi:10.1098/rstb.2005.1760

Bernardini A, Wotzlaw C, Lipinski H-G, Fandrey J (2010) An automated real-time microscopy system for analysis of fluorescence resonance energy transfer. In: Schelkens P, Ebrahimi T, Cristóbal G, Truchetet F, Saarikko P (eds) Proc SPIE 7723, 772311. doi:10.1117/12.854027

Bernardini A, Brockmeier U, Metzen E, Berchner-Pfannschmidt U, Harde E, Acker-Palmer A, Papkovsky D, Acker H. Fandrey J (2014) Type I cell ROS kinetics under hypoxia in the intact mouse carotid body ex vivo: a FRET based study. Am J Physiol Cell Physiol. doi:10.1152/ajpcell.00370.2013

Buttigieg J, Pan J, Yeger H, Cutz E (2012) NOX2 (gp91phox) is a predominant $O_2$ sensor in a human airway chemoreceptor cell line: biochemical, molecular, and electrophysiological evidence. Am J Physiol Lung Cell Mol Physiol 303(7):L598–L607. doi:10.1152/ajplung.00170.2012

Cross A, Henderson L, Jones OTG, Delpiano MA, Hentschel J, Acker H (1990) Involvement of an NAD(P)H oxidase as a pO2 sensor protein in the rat carotid body. Biochem J 272(3):743–747

Dinger B, He L, Chen J, Liu X, Gonzalez C, Obeso A, Sanders K, Hoidal J, Stensaas L, Fidone S (2007) The role of NADPH oxidase in carotid body arterial chemoreceptors. Respir Physiol Neurobiol 157(1):45–54. doi:10.1016/j.resp.2006.12.003

He L, Dinger B, Sanders K, Hoidal J, Obeso A, Stensaas L, Fidone S, Gonzalez C (2005) Effect of p47phox gene deletion on ROS production and oxygen sensing in mouse carotid body chemoreceptor cells. Am J Physiol Lung Cell Mol Physiol 289(6):L916–L924. doi:10.1152/ajplung.00015.2005

Sanders KA, Sundar KM, He L, Dinger B, Fidone S, Hoidal JR (2002) Role of components of the phagocytic NADPH oxidase in oxygen sensing. J Appl Physiol (Bethesda, Md. : 1985) 93(4):1357–1364. doi:10.1152/japplphysiol.00564.2001

Waypa GB, Guzy R, Mungai PT, Mack MM, Marks JD, Roe MW, Schumacker PT (2006) Increases in mitochondrial reactive oxygen species trigger hypoxia-induced calcium responses in pulmonary artery smooth muscle cells. Circ Res 99(9):970–978. doi:10.1161/01.RES.0000247068.75808.3f

Wu W, Platoshyn O, Firth AL, Yuan JX-J (2007) Hypoxia divergently regulates production of reactive oxygen species in human pulmonary and coronary artery smooth muscle cells. Am J Physiol Lung Cell Mol Physiol 293(4):L952–L959. doi:10.1152/ajplung.00203.2007

York JM, McDaniel AW, Blevins NA, Guillet RR, Allison SO, Cengel KA, Freund GG (2012) Individually ventilated cages cause chronic low-grade hypoxia impacting mice hematologically and behaviorally. Brain Behav Immun 26(6):951–958. doi:10.1016/j.bbi.2012.04.008

# 8 Acutely Administered Leptin Increases $[Ca^{2+}]_i$ and $BK_{Ca}$ Currents But Does Not Alter Chemosensory Behavior in Rat Carotid Body Type I Cells

Richard L. Pye, Eric J. Dunn, Ellen M. Ricker, Jennifer G. Jurcsisn, Barbara L. Barr, and Christopher N. Wyatt

**Abstract**

Obesity related pathologies are the health care crisis of our generation. The fat cell derived adipokine leptin has been shown to be a central stimulant of respiration. Very high levels of leptin, however, are associated with the depressed ventilatory phenotype observed in obesity hypoventilation syndrome. Leptin receptors have been identified on carotid body type I cells but how their activation might influence the physiology of these cells is not known.

The acute application of leptin evoked calcium signaling responses in isolated type I cells. Cells increased their Fura 2 ratio by $0.074 \pm 0.010$ ratio units ($n = 39$, $P < 0.001$). Leptin also increased the peak membrane currents in 6 of 9 cells increasing the peak macroscopic currents at +10 mV by $61 \pm 14$ % ($p < 0.02$). Leptin administered in the presence of the selective $BK_{Ca}$ channel inhibitor Paxilline (0.5 μM) failed to increase membrane currents ($n = 5$). Interestingly, leptin did not significantly alter the resting membrane potential of isolated type I cells ($n = 9$) and anoxic/acidic depolarizations were unaffected by leptin ($n = 7$, $n = 6$).

These data suggest that leptin receptors are functional in type I cells but that their acute activation does not alter chemosensory properties. Future studies will use chronic models of leptin dysregulation.

R.L. Pye • E.J. Dunn • E.M. Ricker
J.G. Jurcsisn • B.L. Barr • C.N. Wyatt (✉)
Department of Neuroscience, Cell Biology and Physiology, Wright State University,
3640 Colonel Glenn Hwy, Dayton, OH 45435, USA
e-mail: christopher.wyatt@wright.edu



C. Peers et al. (eds.), *Arterial Chemoreceptors in Physiology and Pathophysiology*,
Advances in Experimental Medicine and Biology 860, DOI 10.1007/978-3-319-18440-1_8

**Keywords**

Carotid body • Type I cells • Leptin • $Ca^{2+}$ imaging • Voltage-clamp • Current-clamp

## 8.1 Introduction

Pathologies associated with obesity are wide ranging and present huge challenges to healthcare. The adipokine leptin is considered to be a central stimulant of respiration as focal central, as well as systemic, administration of leptin stimulate ventilation (Inyushkin et al. 2009; Chang et al. 2013). Leptin may therefore have an adaptive compensatory role in responding to altered respiratory requirements associated with weight gain. Very high levels of leptin, paradoxically, are associated with the depressed ventilatory phenotype observed in obesity hypoventilation syndrome (Piper 2011) potentially due to compromised central leptin access (Burguera et al. 2000). Recently leptin and leptin receptors have been identified on type I cells (Porzionato et al. 2011) and have been shown to be functional (Messenger et al. 2012). Carotid body exposure to systemic leptin is not constrained by the blood brain barrier and paracrine release of leptin could also contribute to high local concentrations of leptin in the CB, however the physiological significance of leptin signaling in the CB is not known. This study sought to determine the acute effects of obese levels of leptin (200 $ng.mL^{-1}$) on isolated carotid body type I cells from neonatal rats (12–19 days old) using calcium imaging and electrophysiological techniques.

## 8.2 Methods

### 8.2.1 Type I Cell Isolation

Neonatal Sprague-Dawley rats (12–19 days old) were deeply anesthetized with isoflurane (4.5 % in oxygen) and their carotid bodies removed. Type I cells were isolated as previously described (Burlon et al. 2009).

### 8.2.2 $Ca^{2+}$ Imaging

For experiments recording intracellular calcium type I cells were loaded with 5 μM FURA-2 AM (Invitrogen) for 30 min at room temperature. The dye was excited with 340/380 nm light and emitted light was recorded at 510 nm using a Coolsnap HQ2 CCD camera (Photometrics). Image acquisition was controlled by Metafluor software (Molecular Devices) and cells were visualized using a Nikon TE2000-U microscope with a X40 objective.

### 8.2.3 Electrophysiology

The amphotericin perforated patch configuration of the whole-cell patch clamp technique was used using pipettes with a resistance of 6.5–9.5 MΩ. Data were acquired using an axopatch 200B amplifier (Molecular Devices) controlled by Clampex 10 (Molecular Devices). Currents were digitized at 5 kHz and filtered at 1 kHz. Results were not leak-subtracted, seal resistance was >2 GΩ, access resistance was typically 20–50 MΩ and was not compensated, holding currents were less than 25 pA. All data were analysed using Clampfit 10 (Molecular Devices).

### 8.2.4 Solutions

Extracellular solution was HEPES buffered salt solution (in mM): 140 NaCl, 4.5 KCl, 2.5 $CaCl_2$, 1, $MgCl_2$, 11 glucose, 10 HEPES, adjusted to pH 7.4 with NaOH at 37 °C. The low extracellular calcium solution was identical except $CaCl_2$ was lowered from 2.5 mM to 0.5 μM. The high potassium stimulus was (in mM): 64.5 NaCl, 80 KCl, 2.5 $CaCl_2$, 1, $MgCl_2$, 11 glucose,

10 HEPES adjusted to pH 7.4 with KOH at 37 °C. The pipette solution was (in mM): 130 KCl; 5 $MgCl_2$; 1 EGTA; 0 glucose; 10 HEPES, adjusted to pH 7.2 with KOH. Pipette solution contained amphotericin B (250 μg $ml^{-1}$, Sigma). Anoxic stimulus was made by bubbling HEPES buffered salt solution with 100 % $N_2$, adding sodium dithionate to scavenge $O_2$ (final concentration 1 mM) before readjusting pH to match control solution. All experiments were performed at 35–37 °C.

Recombinant rat leptin (R&D systems) and Paxilline (0.5 μM – Sigma) solutions were made up in HEPES buffered salt solutions described above.

### 8.2.5 Statistics

Two tailed Student's paired t-tests were used to analyze data with significance set at $p<0.05$. Data are presented as means ± standard error of the mean.

## 8.3 Results

### 8.3.1 $Ca^{2+}$ Imaging Experiments

The acute (6–10 min) application of leptin (200 ng.$ml^{-1}$) evoked calcium signaling responses in isolated type I cells (Fig. 8.1a). Cells increased

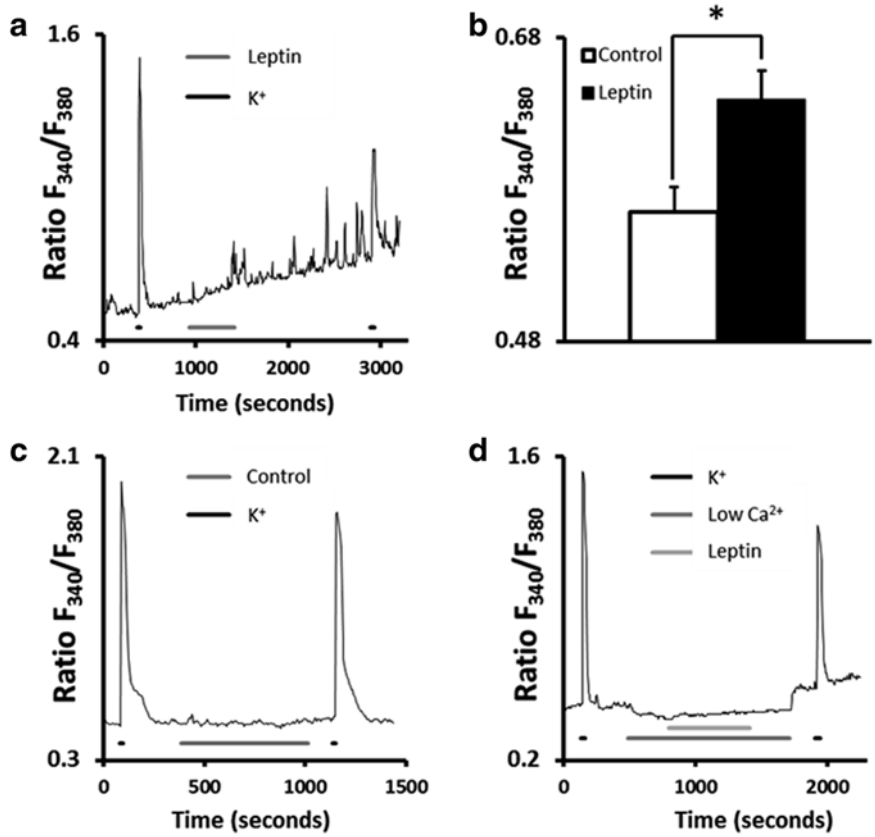


**Fig. 8.1** Leptin causes an increase in $[Ca^{2+}]_i$ in isolated neonatal rat carotid body type I cells. (**a**) An example recording from an isolated rat type I cell loaded with FURA-2. Leptin (200 ng.$mL^{-1}$) causes a persistent increase in $[Ca^{2+}]_i$. (**b**) Summary of $Ca^{2+}$ imaging data. Acute (8–10 min) application of leptin (200 ng.$ml^{-1}$) evoked calcium signaling responses in isolated type I cells. (**c**) An example control recording showing no increase in $Ca^{2+}$ signal during 10 min switch to control solution. (**d**) An example recording showing absence of spiking activity when leptin administered in presence of low (0.5 μM) extracellular $Ca^{2+}$ HEPES solution

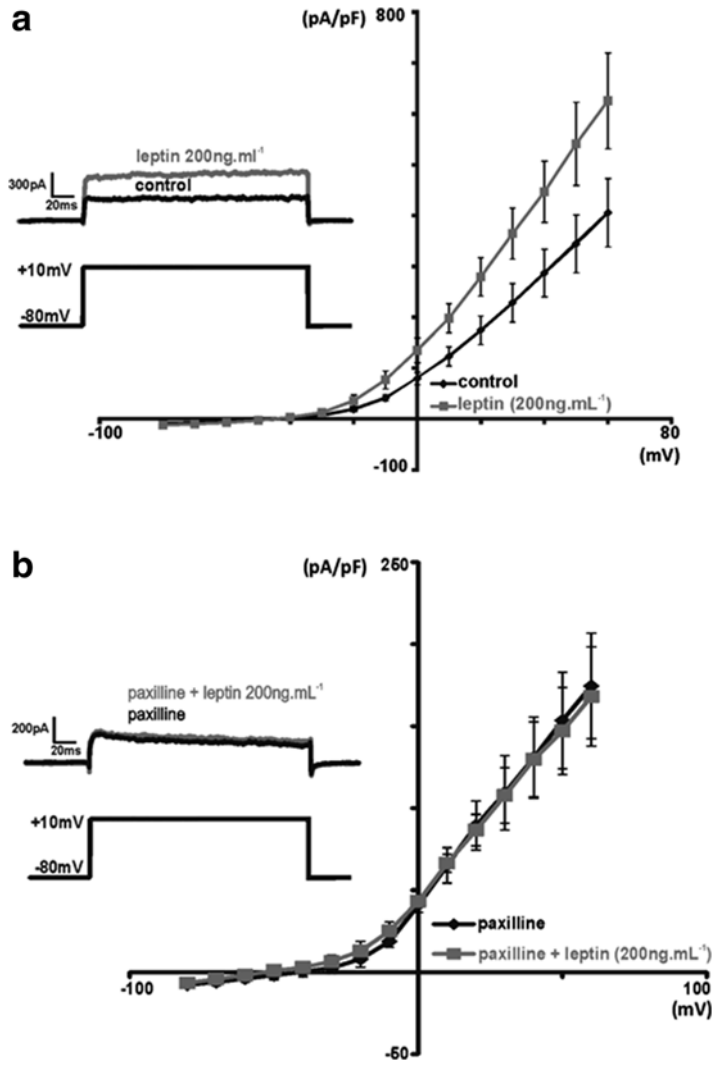


**Fig. 8.2** Leptin increases membrane conductance in rat CB type I cells but not in the presence of paxilline, a $BK_{Ca}$ specific channel blocker. (**a**) Graph of membrane potential vs. current density acquired using whole-cell perforated patch. (**b**) Leptin (200 ng.mL$^{-1}$) does not increase the membrane conductance of type I cells in the presence of paxilline (0.5 μM), a selective $BK_{Ca}$ channel inhibitor (n = 5)

their Fura 2 $F_{340}/F_{380}$ ratio by 0.074 ± 0.010 ratio units (n = 39, P < 0.001, Fig. 8.1b) and the increase in $Ca^{2+}$ signal was not reversible within 30 min. Control cells did not spontaneously demonstrate rises in the Fura 2 ratio (Fig. 8.1c) and spiking activity was abolished in the presence of low extracellular $Ca^{2+}$ (Fig. 8.1d).

### 8.3.2 Voltage Clamp Experiments

Acute application of leptin (200 ng.mL$^{-1}$) significantly increased the membrane conductance in a subset (6 out of 9) of isolated type I cells between −10 mV and +60 mV (n = 6, p < 0.02, Fig. 8.2a). The peak macroscopic

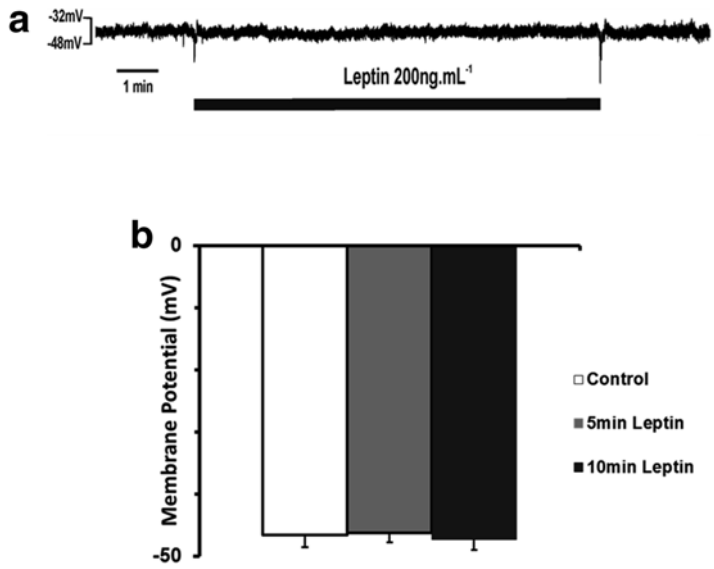


**Fig. 8.3** Leptin does not alter the resting membrane potential of type I cells. (**a**) Sample current clamp recording showing 10 min Leptin (200 ng.mL$^{-1}$) exposure. (**b**) Leptin did not significantly alter the resting membrane potential of isolated type I cells after 5 and 10 min exposure when compared to baseline (n = 9)

currents at +10 mV increased by 61 ± 14 % ($p < 0.02$). When leptin was administered in the presence of the selective $BK_{Ca}$ channel inhibitor Paxilline (0.5 μM) increases in membrane conductance were abolished (n = 5, Fig. 8.2b).

### 8.3.3 Current Clamp Experiments

Leptin did not significantly alter the resting membrane potential of isolated type I cells after 5 and 10 min when compared to baseline (n = 9 $p = 0.66$ & $p = 0.42$ respectively, Fig. 8.3a, b). Acidic challenges (pH 6.9) evoked depolarizations of 8.3 ± 1.1 mV and in the presence of acute leptin these depolarizations were not statistically altered (n = 6, $p = 0.4$, Fig. 8.4a, b). Similarly, anoxic depolarizations of 7.6 ± 0.9 mV were unaffected by acute administration of leptin (n = 7, $p = 0.51$, Fig. 8.4a, b).

## 8.4 Discussion

The adipokine leptin has an established role in energy regulation and in recent years has also been shown to modulate respiratory behavior (Malli et al. 2010). However, its potential role in regulating the peripheral chemoreceptors and therefore ventilatory responses has not been studied. The data presented here focused on the acute application of obese levels of leptin to isolated type I cells. It was discovered that leptin induced a significant rise in intracellular $Ca^{2+}$ and additionally significantly increased $BK_{Ca}$ currents. However, these leptin induced changes in cellular physiology were without effect on the resting membrane potential or the ability of type I cells to respond to acidic or anoxic chemostimuli.

The ability of leptin to modulate $[Ca^{2+}]_i$ and also $BK_{Ca}$ has been demonstrated in numerous tissues including hippocampal and cortical neurons (Shanley et al. 2002; Mancini et al. 2014). In carotid body type I cells leptin caused a slow increase in $[Ca^{2+}]_i$ with occasional spiking behavior observed, this rise in $[Ca^{2+}]_i$ was not reversible. The signaling mechanisms that underpinned the rise in $Ca^{2+}$ were not examined in detail but experiments using low extracellular $Ca^{2+}$ solutions induced a small reduction in baseline $[Ca^{2+}]_i$ and abolished the $Ca^{2+}$ spiking behavior. Thus acute leptin must be causing $Ca^{2+}$ influx. At pres-

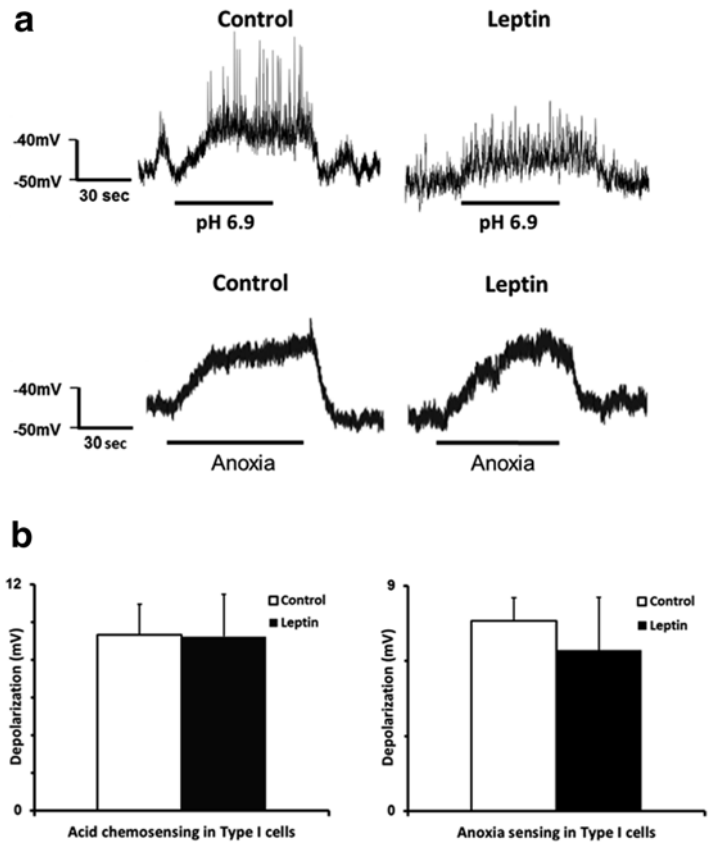


**Fig. 8.4** Leptin does not alter chemosensory depolarization of isolated rat CB type I cells. (**a**) Sample traces of depolarizations induced by acid (pH = 6.9) and anoxic challenges before and after 8–10 min of leptin (200 ng.mL$^{-1}$) exposure. (**b**) Averaged depolarizations before and after leptin (200 ng.mL$^{-1}$) exposure in response to pH = 6.9 and anoxic depolarizations

ent it is not known if the leptin induced $Ca^{2+}$ influx is sufficient to cause the enhanced $BK_{Ca}$ currents or if leptin may be acting via phosphatidylinositol-3-kinase to promote channel expression at the membrane, as has been observed in other neuronal preparations (O'Malley et al. 2005). Although the latter is unlikely given the acute time course of the type I cell experiments.

Current-clamp recordings revealed that despite its effect on $BK_{Ca}$ currents leptin was without effect on resting membrane potential (RMP). This result indicated that $BK_{Ca}$ is not contributing to the RMP of these type I cells, a finding that is in contrast to earlier work that demonstrated $BK_{Ca}$ does contribute to type I cell RMP (Wyatt and Peers 1995) but is in agreement with the work from Keith Buckler's laboratory which showed that leak $K^+$ channels, not $BK_{Ca}$ channels, were responsible for setting RMP in type I cells (Buckler 1997). Furthermore, the lack of effect on RMP suggested that leptin can only modulate open $BK_{Ca}$ channels and is incapable of opening a closed channel.

Given the critical role of the carotid bodies in chemoreception and the control of breathing, the effect of acute leptin on acid and anoxic responses of the type I cells was tested. Leptin was found to be without any significant effect on depolarization induced by acid or anoxia. Augmented responses to hypoxia were, however, recently reported in *in vitro* mouse carotid sinus nerve preparations following acute leptin exposure (Shirahata et al. 2014). Leptin receptors have

been reported in petrosal ganglion neurons (Messenger et al. 2012) and it is conceivable that these neurons, which convey sensory responses away from the carotid body, may mediate observed changes in whole CB recordings. Future experiments will therefore investigate the acute effects of leptin on whole nerve recordings from *in vitro* rat whole CB/CSN preparations. If positive responses to leptin are found in rats at the level of the whole carotid body then the effect of leptin on petrosal ganglion neurons should be evaluated.

In conclusion, whilst acute leptin does cause physiological changes in isolated type I cells it does not alter the way these cells respond to chemostimuli. Future work will focus on chronic models of leptin dysregulation to determine if leptin might be acting via the carotid body to contribute to the ventilatory problems observed in these obese models (O'Donnell et al. 1999; Lee et al. 2005).

**Acknowledgements** This work was supported by NIH-1RO1HL091836

## References

Buckler KJ (1997) A novel oxygen-sensitive potassium current in rat carotid body type I cells. J Physiol 498(Pt 3):649–662

Burguera B, Couce ME, Curran GL, Jensen MD, Lloyd RV, Cleary MP, Poduslo JF (2000) Obesity is associated with a decreased leptin transport across the blood–brain barrier in rats. Diabetes 49(7):1219–1223

Burlon DC, Jordan HL, Wyatt CN (2009) Presynaptic regulation of isolated neonatal rat carotid body type I cells by histamine. Respir Physiol Neurobiol 168(3):218–223

Chang Z, Ballou E, Jiao W, McKenna KE, Morrison SF, McCrimmon DR (2013) Systemic leptin produces a long-lasting increase in respiratory motor output in rats. Front Physiol 4:16

Inyushkin AN, Inyushkina EM, Merkulova NA (2009) Respiratory responses to microinjections of leptin into the solitary tract nucleus. Neurosci Behav Physiol 39(3):231–240

Lee SD, Nakano H, Farkas GA (2005) Adenosinergic modulation of ventilation in obese zucker rats. Obes Res 13(3):545–555

Malli F, Papaioannou AI, Gourgoulianis KI, Daniil Z (2010) The role of leptin in the respiratory system: an overview. Respir Res 11:152

Mancini M, Soldovieri MV, Gessner G, Wissuwa B, Barrese V, Boscia F, Secondo A, Miceli F, Franco C, Ambrosino P, Canzoniero LM, Bauer M, Hoshi T, Heinemann SH, Taglialatela M (2014) Critical role of large-conductance calcium- and voltage-activated potassium channels in leptin-induced neuroprotection of N-methyl-d-aspartate-exposed cortical neurons. Pharmacol Res 87C:80–86

Messenger SA, Moreau JM, Ciriello J (2012) Intermittent hypoxia and systemic leptin administration induces pSTAT3 and Fos/Fra-1 in the carotid body. Brain Res 1446:56–70

O'Donnell CP, Schaub CD, Haines AS, Berkowitz DE, Tankersley CG, Schwartz AR, Smith PL (1999) Leptin prevents respiratory depression in obesity. Am J Respir Crit Care Med 159(5 Pt 1):1477–1484

O'Malley D, Irving AJ, Harvey J (2005) Leptin-induced dynamic alterations in the actin cytoskeleton mediate the activation and synaptic clustering of BK channels. FASEB J 19(13):1917–1919

Piper AJ (2011) Obesity hypoventilation syndrome – the big and the breathless. Sleep Med Rev 15(2):79–89

Porzionato A, Rucinski M, Macchi V, Stecco C, Castagliuolo I, Malendowicz LK, De Caro R (2011) Expression of leptin and leptin receptor isoforms in the rat and human carotid body. Brain Res 1385:56–67

Shanley LJ, Irving AJ, Rae MG, Ashford ML, Harvey J (2002) Leptin inhibits rat hippocampal neurons via activation of large conductance calcium-activated K+ channels. Nat Neurosci 5(4):299–300

Shirahata M, Shin M, Polotsky V (2014) Metabolic monitoring by the carotid body (873.8). FASEB J 28(1 Supplement)

Wyatt CN, Peers C (1995) $Ca^{2+}$-activated $K^+$ channels in isolated type I cells of the neonatal rat carotid body. J Physiol 483(Pt 3):559–565

# Functional Properties of Mitochondria in the Type-1 Cell and Their Role in Oxygen Sensing

9

Keith J. Buckler and Philip J. Turner

**Abstract**

The identity of the oxygen sensor in arterial chemoreceptors has been the subject of much speculation. One of the oldest hypotheses is that oxygen is sensed through oxidative phosphorylation. There is a wealth of data demonstrating that arterial chemoreceptors are excited by inhibitors of oxidative phosphorylation. These compounds mimic the effects of hypoxia inhibiting TASK1/3 potassium channels causing membrane depolarisation calcium influx and neurosecretion. The TASK channels of Type-I cells are also sensitive to cytosolic MgATP. The existence of a metabolic signalling pathway in Type-1 cells is thus established; the contentious issue is whether this pathway is also used for acute oxygen sensing. The main criticism is that because cytochrome oxidase has a high affinity for oxygen ($P_{50} \approx 0.2$ mmHg) mitochondrial metabolism should be insensitive to physiological hypoxia. This argument is however predicated on the assumption that chemoreceptor mitochondria are analogous to those of other tissues. We have however obtained new evidence to support the hypothesis that type-1 cell mitochondria are not like those of other cells in that they have an unusually low affinity for oxygen (Mills E, Jobsis FF, J Neurophysiol 35(4):405–428, 1972; Duchen MR, Biscoe TJ, J Physiol 450:13–31, 1992a). Our data confirm that mitochondrial membrane potential, NADH, electron transport and cytochrome oxidase activity in the Type-1 cell are all highly sensitive to hypoxia. These observations not only provide exceptionally strong support for the metabolic hypothesis but also reveal an unknown side of mitochondrial behaviour.

**Keywords**

Oxygen sensing • Hypoxia • Mitochondria • NADH • Mitochondrial potential • ATP • Potassium channel • TASK channel • Carotid body

K.J. Buckler (✉) • P.J. Turner
Department of Physiology Anatomy and Genetics,
University of Oxford, Oxford OX1 3PT, UK
e-mail: keith.buckler@dpag.ox.ac.uk



C. Peers et al. (eds.), *Arterial Chemoreceptors in Physiology and Pathophysiology*,
Advances in Experimental Medicine and Biology 860, DOI 10.1007/978-3-319-18440-1_9

## 9.1 Introduction: Acute Oxygen Sensing

Acute oxygen sensing is only recognised in a limited number of tissues including blood vessels (e.g. pulmonary, placental, systemic & ductus arteriosus) neonatal chromaffin cells, neuroepithelial bodies in the lung and the peripheral chemoreceptors (Weir et al. 2005). It is characterised by a rapid (i.e. within seconds to minutes) response to relatively modest hypoxia which, in most cases, has a well-defined homeostatic role in defending against hypoxemia. It is however possible that acute oxygen sensitivity may be a more widespread phenomenon that has not been recognised in other tissues either because it is only evident at much lower oxygen levels and/or because its effects are easily overlooked. At present however acute oxygen sensing is only clearly demonstrable in the above tissues and it is only through their study that our understanding of this process has made much advance. Of these tissues the carotid body is perhaps the archetypal acute oxygen sensor.

The mechanisms by which the carotid body senses oxygen are only partially understood. Ion channels play a central role in the stimulus secretion coupling pathway but the nature of the primary oxygen sensor itself is unresolved. There have been many hypotheses as to the identity of this sensor, this chapter however deals directly with only one, the oldest and most enduring of all the "metabolic hypothesis".

## 9.2 Stimulus Secretion Coupling in the Type-1 Cell

Much of what is known about the stimulus secretion coupling pathway for hypoxia has come from *in vitro* experiments using acutely isolated type-1 cells, cultured type-1 cells and carotid body slices. The consensus model tells a familiar story common to many receptors. The stimulus, in this case hypoxia, modulates specific ion channels in the cell to elicit a depolarising receptor potential which can then trigger spontaneous action potentials. These electrical events incorporate the activation of voltage-gated calcium channels which mediate a large influx of calcium ions resulting in a substantive elevation of the intracellular calcium ion concentration (Buckler and Vaughan Jones 1994b; Buckler 1997). Hypoxia also causes a marked increase in the release/exocytosis of neurotransmitters (Fidone et al. 1982) (Perez Garcia et al. 1991, 1992; Pardal et al. 2000). Since both the elevation of intracellular calcium and the exocytosis of neurotransmitters are dependent upon extracellular calcium and inhibited by calcium channel antagonists (Perez Garcia et al. 1991, 1992; Buckler and Vaughan Jones 1994a; Buckler 1997; Pardal et al. 2000) it is taken as axiomatic that the rise of calcium drives the exocytosis. The main transmitter responsible for exciting sensory nerve endings appears to be ATP which acts through postsynaptic P2X2/P2X3 receptors (Zhang et al. 2000; Prasad et al. 2001; Rong et al. 2003). Other transmitters that may also play a role in exciting afferent nerves include acetylcholine and 5HT (Nurse 2014; Zhang et al. 2000).

## 9.3 Role of Ion Channels

Ion channels play a central role in the transduction process and, in the case of those ion channels modulated by hypoxia, currently represent the events most proximal to the oxygen sensor of which we can be reasonably certain. Type 1 cells express a number of different types of ion channel including TASK channels, an uncharacterised background Na conductance, Cl channels, a calcium activated cation channel, L & N type voltage gated calcium channels, voltage-gated Na-channels (in some species), voltage-gated (delayed rectifier) K channels and large conductance calcium activated $K^+$ channels (maxi K channels, $BK_{Ca}$) (Duchen et al. 1988; Stea and Nurse 1989, 1991; Urena et al. 1989; Peers 1990a; Peers and O'Donnell 1990; Lopez Lopez et al. 1993, 1997; e Silva and Lewis 1995; Carpenter et al. 1996; Buckler 1997; Carpenter and Peers 1997, 2001; Buckler et al. 2000; Rocher et al. 2005; Kang et al. 2014).

The resting membrane potential of type-1 cells *in vitro* is approximately −50 to −60 mV (Buckler and Vaughan Jones 1994a, b; Wyatt and Buckler 2003; Rocher et al. 2005; Buckler 2012) and is maintained by a balance between inward currents, carried by $Na^+$ ions, and outward currents carried by $K^+$ ions and the Na/K ATPase. $K^+$ ion efflux/outward potassium current at the resting membrane potential is mediated predominantly by TASK channels of which most are TASK1:TASK3 heterodimers (Kim et al. 2009; Turner and Buckler 2013). In response to hypoxia this resting background $K^+$ conductance is inhibited by up to 50–80 % (Buckler 1997) (Buckler et al. 2000; Kim et al. 2009) with a $P_{50}$ ($K_{1/2}$) for $O_2$ of around 12 mmHg. The inhibition of background K-channels by hypoxia creates an imbalance between resting Na, K and Na/K ATPase currents resulting in a net inward current. The resultant membrane depolarisation is thus primarily a consequence of background (TASK) $K^+$-channel inhibition but is probably driven by $Na^+$-ion influx.

Recent studies using TASK-1/TASK-3 double knockout animals suggest that there may yet be other pathways capable of initiating depolarisation in type-1 cells since the deletion of these two genes led to a complete loss of TASK channels yet some cells retained the ability to respond to hypoxia (Turner and Buckler 2013). Given the high input impendence of type-1 cells from such animals however (Ortega-Saenz et al. 2010) it is possible that such additional $O_2$-sensitive currents could be very small.

Whilst the cause of the onset of membrane depolarisation in response to hypoxia has been defined, the determinants of the magnitude of the receptor potential and any resultant electrical activity are unknown since there have been no direct electrophysiological studies of this state. One may however surmise the following sequence of events. As the cell begins to depolarise beyond −50 mV high threshold voltage-gated $Ca^{2+}$ channels will activate adding significant inward current and elevating intracellular [$Ca^{2+}$] (Urena et al. 1989; Buckler and Vaughan Jones 1994a, b; e Silva and Lewis 1995). This would add a further drive to depolarisation with positive feedback between depolarisation and $Ca^{2+}$ channel activation possibly resulting in an action potential (in some species a similar process involving voltage gated Na-channels may also occur). The rise in $[Ca^{2+}]_i$ will activate a non-selective cation channel adding further inward current (Kang et al. 2014). Note that the combination of a voltage activated Ca channel and a calcium activated cation channel constitute another form of positive feedback generating depolarisation and $[Ca^{2+}]_i$ elevation. Countering these depolarising influences the activation of delayed rectifier K channels and large conductance calcium activated $K^+$ channels ($BK_{Ca}$) are likely to participate in action potential repolarisation and oppose sustained depolarisation and elevation of $[Ca^{2+}]_i$. It is notable however that $BK_{Ca}$ channels are also inhibited by hypoxia (Peers 1990b) which may play a permissive role in allowing sustained depolarisation and elevation of intracellular calcium. Thus a state of perpetual depolarisation, electrical activity and voltage-gated $Ca^{2+}$ influx may be maintained until the stimulus is removed and the oxygen sensitive potassium channels repolarise the cell. This is however to a large extent speculative. Electrical signalling in type-1 cells is an area that deserves much further investigation since these events will effectively define the neurosecretory response and thus the output from the carotid body in response to any given stimulus. This makes ion channels prime targets for mediating chemoreceptor plasticity.

## 9.4 Role of Mitochondria in Oxygen Sensing

It has been known for over a century that both cyanide and sulphide, two inhibitors of cytochrome oxidase, are potent stimulants of breathing. The site of action of these poisons was traced to the carotid body by Heymans et al. (1931). This was followed by the discovery that mitochondrial uncouplers were also potent stimulants (Shen and Hauss 1939). Anichkov and Belen'kii reported similar observations and proposed a linkage between cellular ATP levels and

chemoreceptor excitation i.e. the metabolic hypothesis (Anichkov and Belen'kii 1963). Subsequent studies extended the number and type of inhibitors of oxidative phosphorylation which produce chemoreceptor excitation to include high levels of carbon monoxide (a photo labile inhibitor of cytochrome oxidase) (Wilson et al. 1994) inhibitors of complex III (e.g. antimycin) and inhibitors of the ATP synthase (oligomycin) (Mulligan et al. 1981; Mulligan and Lahiri 1982).

More recently we and others have investigated the mechanisms by which these agents mediate the excitation of type-1 cells. The main steps involved are identical to those of hypoxia beginning with the inhibition of potassium channels, principally TASK channels, followed by membrane depolarisation, voltage gated calcium entry and neurosecretion (Buckler and Vaughan-Jones 1998; Ortega Saenz et al. 2003; Wyatt and Buckler 2004). The observation that such a wide range of agents with disparate modes of action all excite the type-1 cells immediately suggests a role for ATP production in the signalling process as it is the only obvious common factor.

There is therefore robust evidence for a metabolic sensing pathway in the carotid body/type-1 cell that leads to excitation. An important question is whether this pathway is the means by which the cell also senses hypoxia. In isolated type-1 cells it can be demonstrated that the modulation of background K-currents by hypoxia can be occluded by the presence of high levels of rotenone or cyanide or FCCP (Wyatt and Buckler 2004). This mutual exclusivity suggests that both metabolic and oxygen sensing pathways at least converge on a common, saturable, pathway.

## 9.5 Mitochondrial Oxygen Sensitivity

The main conceptual problem with the metabolic hypothesis has always been the argument that cytochrome oxidase lacks the sensitivity to oxygen that would be required for it to act as an oxygen sensor in the context of the carotid body (Coxon 1966). For example the partial pressure at which oxygen consumption is reduced by 50 % ($P_{50}$) in muscle & liver mitochondria is typically 0.1–0.3 mmHg (Gnaiger 2001). In comparison (a) chemoreceptor activity *in vivo* increases markedly as arterial $PO_2$ falls below about 70 mmHg (Fidone and Gonzalez 1986) although there is no absolute threshold (Biscoe et al. 1970): (b) measurements of microvascular $PO_2$ indicate that chemoreceptor output increases at $PO_2 < 40$–30 mmHg (Lahiri et al. 1993): and (c) type-1 cells *in vitro* are excited at $PO_2 \leq 40$ mmHg (Biscoe and Duchen 1990; Perez Garcia et al. 1992; Buckler and Vaughan Jones 1994a, b; Montoro et al. 1996; Dasso et al. 1997; Buckler and Turner 2013). Thus although oxygen sensitivity at the cellular level is not as great as that seen in the whole organ (from the perspective of arterial $PO_2$) there is still a substantive difference between the oxygen sensing capacity of the type-1 cell and the oxygen requirements of mitochondrial respiration in any other known tissue.

One possible solution to this problem was presented in the 1960s by Mills & Jobsis. Using absorption spectroscopy to monitor the oxidation state of cytochrome a3 in cat carotid body they observed that about 50 % of cytochrome a3 became reduced at high perfusate $PO_2$ ($P_{50} = 90$ mmHg). They also observed that changes in the oxidation state of some of the cytochrome a3 within the carotid body was concurrent with chemoreceptor activation. These observations supported the metabolic hypothesis. By way of explanation they proposed that the carotid body contains two forms of cytochrome $a_3$ a normal high affinity form and a low affinity form (Mills and Jobsis 1970, 1972). Since tissue $P_{O2}$ was unknown however this data cannot unequivocally be interpreted as evidence for a low affinity form of cytochrome a3, similar observations could result from regions of low $PO_2$ due to poor perfusion and/or high oxygen consumption.

In the 1990s Duchen & Biscoe investigated mitochondrial function in isolated type-1 cells and reported that mitochondrial membrane potential ($\psi_m$) depolarised and NADH levels increased when $PO_2$ was reduced below about 20 mmHg (Duchen and Biscoe 1992a, b). These

studies supported the view that mitochondrial respiration in type-1 cells is de facto unusually oxygen sensitive. Questions were however raised around issues of cause and effect (Gonzalez et al. 1994) i.e. were the changes observed caused by a low affinity form of cytochrome oxidase and therefore a manifestation of primary oxygen sensing or were they a result of hypoxic excitation of the cell. For example since hypoxia excites type-1 cells this could increase demand for ATP synthesis leading to increased proton influx through complex V thus depolarising $\psi_m$. In addition hypoxia evoked elevation of cytosolic $[Ca^{2+}]_I$ (Buckler and Vaughan Jones 1994a, b) could promote mitochondrial $Ca^{2+}$ uptake (Werth and Thayer 1994; Park et al. 1996) further depolarising $\psi_m$ and activating mitochondrial dehydrogenases thus increasing NADH (McCormack and Denton 1989; Hajnoczky et al. 1995).

## 9.6 New Evidence for High Oxygen Sensitivity in Type-1 Cell Mitochondria

We have recently re-investigated the oxygen dependence of mitochondrial respiration in isolated type-1 cells (Buckler and Turner 2013). Our data confirm that both $\psi_m$ and NADH are sensitive to hypoxia over a very wide range of $PO_2$ (from 80 mmHg and below) (see Fig. 9.1). These effects are independent of change in cytosolic calcium i.e. similar results are obtained in calcium free medium and in the presence of a calcium channel blocker (2 mM $Ni^{2+}$). Mitochondrial depolarisation and increase in NADH levels are therefore unlikely to be secondary to mitochondrial $Ca^{2+}$ uptake.

We further examined the effects of oxygen on electron transport in the presence of oligomycin and 75 nM FCCP (an uncoupler). In this experiment oligomycin inhibits ATP synthase such that ATP demand no longer influences mitochondrial proton influx. Instead the low level of FCCP induces a non-specific proton leak which will be roughly proportional to $\psi_m$. Under these conditions proton translocation by complexes I, III & IV works against this passive proton leak to establish a steady state $\psi_m$ the value of which reflects the rate of electron transport. As can be seen in Fig. 9.2 $\psi_m$ is highly sensitive to changes in oxygen level under these conditions demonstrating that hypoxia can inhibit electron transport even at quite high $PO_2$.

We have also investigated the oxygen sensitivity of cytochrome oxidase. In this experiment (Fig. 9.3) complexes I and III are blocked using rotenone, myxothiazol and antimycin A (as is ATP synthase using oligomycin). This stops all electron transport coupled proton translocation, since complex IV activity is dependent upon reduction of cytochrome C by complex III, and results in full mitochondrial depolarisation. At this point the introduction of tetramethyl-p-phenylenediamine (TMPD) facilitates mitochondrial repolarisation by donating electrons directly to cytochrome C which is then oxidised by cytochrome oxidase with electron transfer to oxygen and the translocation of protons out of the mitochondrion. Under these conditions mitochondrial potential is supported entirely by the activity of cytochrome oxidase i.e. this is now a direct assay of cytochrome oxidase activity alone. The subsequent application of hypoxic solutions clearly show that $\psi_m$ is again highly sensitive to changes in oxygen levels thus confirming the low apparent affinity of cytochrome oxidase for oxygen in the type-1 cell.

In this series of experiments we obtained $P_{50}$ values for the effects of oxygen on NADH, electron transport and cytochrome oxidase activity of 40, 5.4 and 2.6 mmHg in the rat type-1 cell (Buckler and Turner 2013). We have recently confirmed the high oxygen sensitivity of NADH levels in the mouse type-1 cell which has a $P_{50}$ of about 10 mmHg. These values are at least an order of magnitude greater than those reported in other tissues and are compatible with a role for mitochondrial metabolism in oxygen sensing. Consequently our studies not only provide exceptionally strong support for the metabolic hypothesis but also reveal a hitherto unknown side of mitochondrial behaviour.

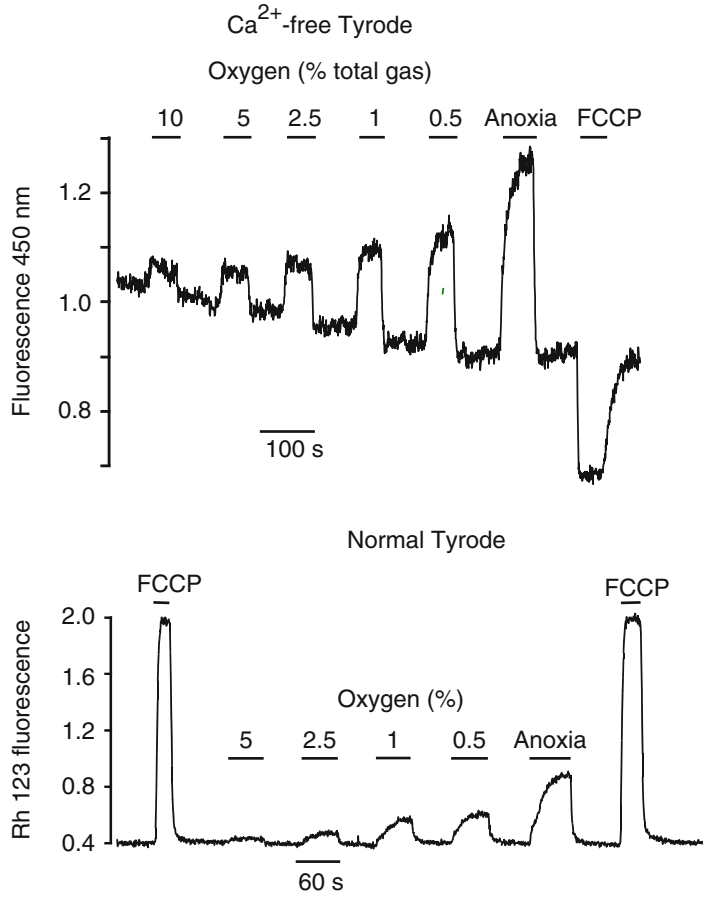


**Fig. 9.1** *Upper panel*, recording of NADH autofluorescence in a small cluster of type-1 cells in a calcium free bicarbonate buffered Tyrode at 37 °C. NADH fluorescence was excited at 340 nm and recorded at 450 nm. *Lower panel*, recording of mitochondrial membrane potential using rhodamine 123 in the de-quench mode. Note that under these conditions an increase in Rh 123 fluorescence represents mitochondrial depolarisation. Maximal depolarisation is shown in response to 1 μM FCCP. Tyrodes are equilibrated with a gas mix containing either 5 % $CO_2$/95 % air (control approx. 20 % oxygen) or 5 % $CO_2$ and the indicated level of oxygen shown in the figure (balance of gas is nitrogen). Bath $PO_2$ levels for solutions equilibrated with 5, 2.5, 1 & 0.5 % $O_2$ were approximately 38, 19, 8 & 4 mmHg respectively (Figure redrawn from Buckler and Turner 2013)

## 9.7 Potential Mechanisms for Enhanced Mitochondrial Oxygen Sensitivity

As far as we are aware the extreme oxygen sensitivity of mitochondrial function and cytochrome oxidase activity in the type-1 cell is without precedent. There are, therefore, no established mechanisms to account for it. Consequently we can only offer hypothetical explanations.

### 9.7.1 Competitive Inhibitors: Nitric Oxide and Carbon Monoxide

NO is a well-known competitive inhibitor of cytochrome oxidase (Mason et al. 2006; Cooper and Giulivi 2007). Theoretically it has the capacity to increase the apparent Km for oxygen utilisation significantly even at low levels e.g. given values for the equilibrium constants $K_{O2} = 0.21$ μM and $K_{NO} = 0.225$ nM (Mason et al. 2006; Hall and Garthwaite 2009) as little as 2 nM NO could

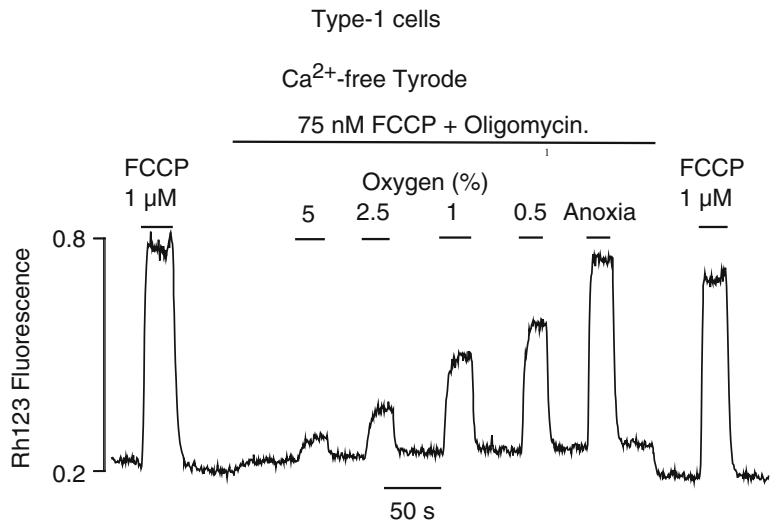


**Fig. 9.2** Recording of mitochondrial membrane potential ($\psi_m$) using rhodamine 123 in the de-quench mode. Experiment is conducted in a Ca-free media in the presence of oligomycin and a low level of FCCP. Under these conditions $\psi_m$ is uncoupled from ATP synthesis and cytosolic calcium signalling such that electron transport is just working against an enhanced proton leak to maintain $\psi_m$ (Figure redrawn from Buckler and Turner 2013)

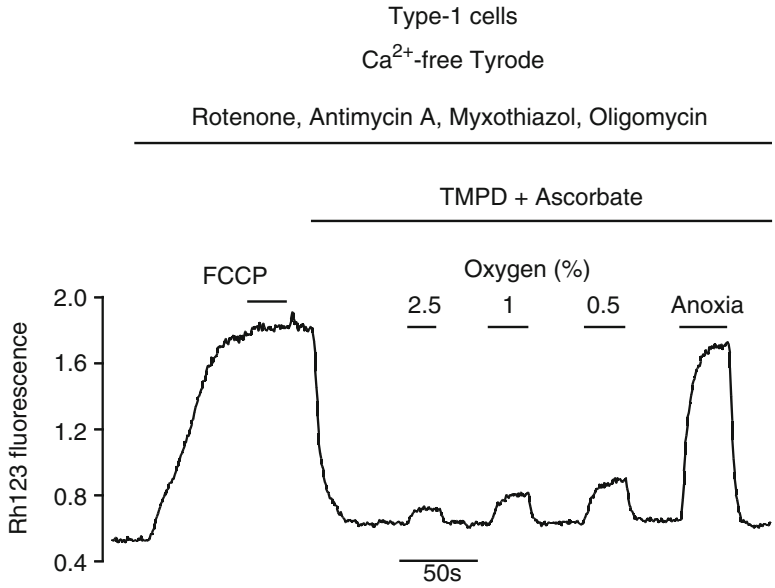


**Fig. 9.3** Recording of cytochrome oxidase through changes in mitochondrial potential. Block of complex I, III and V (ATP synthase) is achieved with the combination of drugs illustrated in the figure. Indirect block of complex IV (cytochrome oxidase) also occurs by preventing reduction of cytochrome c by complex III. The resulting total block of active proton translocation across the inner mitochondrial membrane fully depolarises the mitochondria (this is confirmed by the lack of any additional effect of 1 μM FCCP). The application of the artificial electron donors TMPD and ascorbate then directly reduces cytochrome C allowing reactivation of complex IV and repolarisation of mitochondrial membrane potential. Subsequent effects of hypoxia on $\psi_m$ therefore reflect the inhibition of cytochrome oxidase activity in isolation (Figure redrawn from Buckler and Turner 2013)

increase the apparent Km for oxygen tenfold. Constitutive NO production could therefore easily re-set the oxygen sensitivity of mitochondrial function. Whether this is indeed the case in the type-1 cell remains to be tested. Carbon monoxide is another competitive inhibitor of cytochrome oxidase which is produced endogenously by heme-oxygenases (Cooper and Brown 2008). CO is however about 1,000-fold less potent than NO as an inhibitor of cytochrome oxidase (the $K_i$ for CO is approximately 0.3 μM (Cooper and Brown 2008)). Again CO production would not need to be regulated by oxygen to enhance the oxygen sensitivity of mitochondrial function but an implausibly high level of constitutive production would likely be necessary to maintain micro molar levels within the cell.

### 9.7.2 Another "Master" Oxygen Sensing Pathway: Hydrogen Sulphide

It has recently been hypothesised that endogenous $H_2S$ accumulation mediates oxygen sensing in the carotid body and other tissues (Olson 2011; Olson and Whitfield 2010; Olson et al. 2008; Peng et al. 2010). Given that sulfide is an inhibitor of cytochrome oxidase it is pertinent to consider whether mitochondrial inhibition could be secondary to a sulfide based oxygen sensor/signalling system.

We have recently demonstrated that the concentration dependence of $H_2S$ mediated excitation of type-1 cells is directly comparable with that of $H_2S$ mediated inhibition of mitochondrial function and ATP depletion in type-1 cells. The effects of micro molar levels of sulphide are therefore likely to be mediated by the metabolic signalling pathway, indeed it is hard to see how this could be avoided (note excitation of type-1 cells by sulphide follows the same pathway as described for other mitochondrial inhibitors). Whether endogenous sulfide plays a role in oxygen sensing and mitochondrial function in type-1 cells is however open to debate. A number of different scenarios for sulphide signalling in hypoxia have been proposed. It is of interest to consider how they might fit in with our observations of mitochondrial function.

In the hypothesis originally put forward for vascular oxygen sensing and trout gill chemoreceptors (Olson et al. 2006, 2008) it is proposed that $H_2S$ is constitutively produced by the metabolism of the sulphur containing amino acids cysteine and homocysteine by the enzymes cystathionine β-synthase (CBS) and cystathionine γ-lyase (CSE) but its breakdown by sulfide quinone oxidoreductase (SQR) and sulphur dioxygenase is oxygen dependent such that $H_2S$ levels rise in hypoxia. This process of $H_2S$ oxidation is dependent upon mitochondrial electron transport to re oxidise the ubiquinone. Oxygen sensing in this model is therefore mediated by cytochrome oxidase with $H_2S$ functioning as a signalling molecule. So this does not offer an explanation of mitochondrial oxygen sensitivity.

In the model of Peng et al. (2010) heme-oxygenase II is hypothesised to play the role of oxygen sensor generating carbon monoxide which then activates CSE thus increasing $H_2S$. In this model mitochondrial/metabolic signalling could be seen as a downstream consequence of $H_2S$ signalling. It is however notable that genomic deletion of heme-oxygenase II does not alter oxygen sensing in the mouse (Ortega-Saenz et al. 2006). Moreover the levels of sulfide required to inhibit mitochondrial function and excite chemoreceptors to a level comparable to that induced by hypoxia appear to be in the 10's of micro molar. It is difficult to see how an isolated type-1 cell in vitro could sustain such levels without some form of barrier to free $H_2S$ diffusion (Buckler 2012).

### 9.7.3 An Alternative Cytochrome Oxidase

Finally it is possible that the type-1 cell expresses a different, possibly unique, form of cytochrome oxidase that has an intrinsically diminished oxygen sensitivity compared to that of other cells (as originally postulated by Mills & Jobsis). The Km for oxygen utilisation by cytochrome oxidase is determined in part through kinetic trapping.

Oxygen binding to the Heme-a3-Cu-B binuclear centre in subunit I is actually quite weak but the subsequent intramolecular electron transfer from haem-a to the binuclear centre results in rapid partial reduction of oxygen and a low apparent Km (Verkhovsky et al. 1996). Whilst the core subunits of cytochrome oxidase (I, II & III) are encoded by mitochondrial genes there are also many accessory subunits encoded by nuclear genes. Studies in yeast have shown that different isoforms of subunit 5 (Va & Vb, equivalent to Cox4-1 & Cox4-2 in Mammalia) can alter rates of intramolecular electron transfer (Waterland et al. 1991; Allen et al. 1995). Thus accessory subunits encoded by nuclear genes could, in principle, alter the Km for oxygen.

## 9.8 Signalling Between Mitochondria and Ion Channels

Two mechanisms have been proposed whereby metabolism might regulate TASK channel activity in the type-1 cell; one proposes that channel activity is regulated via an AMP dependent protein kinase (AMPK) and the other that channel activity is regulated by cytosolic ATP. AMPK is a metabolic sensor involved in the regulation of metabolism. It is activated by a rise in AMP which occurs whenever ATP breakdown exceeds ATP re-synthesis (see (Hardie 2011)). It is however unclear whether AMPK is responsible for modulating TASK channels in the context of hypoxia. Dallas et al. have reported that TASK 3 alone can be regulated by AMPK (Dallas et al. 2009) whereas Kréneisz et al. reported that the AMPK activator AICAR had no effect upon TASK1, TASK3 or the TASK1/3 concatamer (Kreneisz et al. 2009). It should be noted that all 3 forms of TASK channel (TASK-1, TASK-3 and TASK1/3 heterodimers) are regulated by hypoxia in the type-1 cell (Turner and Buckler 2013). Furthermore original reports that AICAR stimulates the carotid body/type-1 cell; and that compound C (and AMPK inhibitor) attenuates responses to both AICAR and hypoxia (Evans et al. 2005; Wyatt et al. 2007) appear to be contradicted by a more recent study which found no effect of AMPK activators (AICAR and A769662) on TASK channel activity or $Ca^{2+}$ signalling in type-1 cells nor any effect of compound C upon TASK channel inhibition by hypoxia (Kim et al. 2014). The importance of AMPK in regulating type-1 cell TASK channels is therefore currently uncertain.

The other hypothesis is that TASK1/3 channel activity might be regulated by cytosolic ATP levels directly. This is based on the observation that type-1 cell TASK channels rundown rapidly upon patch excision but can be partially reactivated by applying MgATP to the inside of the patch. The Km for MgATP activation of TASK channel activity in the type-1 cell is approximately 2.3 mM, well within the physiological range. Cytosolic MgATP levels could therefore directly regulate channel activity. Indirect measurements of changes in MgATP, using $Mg^{2+}$-sensitive dyes to detect the release of $Mg^{2+}$ as Mg. ATP is broken down first to ADP and then AMP, suggest a relatively rapid fall in $[MgATP]_i$ upon metabolic inhibition or exposure to hypoxia. Thus signalling by MgATP would seem feasible. What is currently unknown is how MgATP activates these channels, there are no known/reported ATP binding domains present in either TASK-1 or TASK-3. Moreover it is possible that other, unknown, cytosolic signalling factors may also be involved since MgATP alone cannot fully restore the loss in channel activity caused by patch excision.

## 9.9 Conclusions

Whilst there is very strong evidence for a metabolic signalling pathway in type-1 cells that is highly oxygen sensitive there are still a great many unanswered questions. How is the highly unusual oxygen sensitivity of type-1 cell cytochrome oxidase brought about? Can it be reversed or prevented, and, if so, will this result in the loss of downstream responses to hypoxia? Is the link between mitochondrial function and TASK channel activity entirely mediated by MgATP or are other factors also involved? At present there is no sign of any recognisable MgATP binding domain

in either TASK-1 or TASK-3. Finding answers to these questions is vital if we are to confirm, or reject, the metabolic hypothesis as the primary means of acute oxygen sensing in type-1 cells.

## References


Allen LA, Zhao XJ, Caughey W, Poyton RO (1995) Isoforms of yeast cytochrome c oxidase subunit V affect the binuclear reaction center and alter the kinetics of interaction with the isoforms of yeast cytochrome c. J Biol Chem 270(1):110–118

Anichkov S, Belen'kii M (1963) Pharmacology of the carotid body chemoreceptors. Pergamon Press, Oxford

Biscoe TJ, Duchen MR (1990) Responses of type I cells dissociated from the rabbit carotid body to hypoxia. J Physiol 428:39–59

Biscoe TJ, Purves MJ, Sampson SR (1970) The frequency of nerve impulses in single carotid body chemoreceptor afferent fibres recorded in vivo with intact circulation. J Physiol 208(1):121–131

Buckler KJ (1997) A novel oxygen-sensitive potassium current in rat carotid body type I cells. J Physiol 498(Pt 3):649–662

Buckler KJ (2012) Effects of exogenous hydrogen sulphide on calcium signalling, background (TASK) K channel activity and mitochondrial function in chemoreceptor cells. Pflugers Arch 463(5):743–754

Buckler KJ, Turner PJ (2013) Oxygen sensitivity of mitochondrial function in rat arterial chemoreceptor cells. J Physiol 591(Pt 14):3549–3563

Buckler KJ, Vaughan Jones RD (1994a) Effects of hypercapnia on membrane potential and intracellular calcium in rat carotid body type I cells. J Physiol 478(Pt 1):157–171

Buckler KJ, Vaughan Jones RD (1994b) Effects of hypoxia on membrane potential and intracellular calcium in rat neonatal carotid body type I cells. J Physiol 476(3):423–428

Buckler KJ, Vaughan-Jones RD (1998) Effects of mitochondrial uncouplers on intracellular calcium, pH and membrane potential in rat carotid body type I cells. J Physiol 513(Pt 3):819–833

Buckler KJ, Williams BA, Honore E (2000) An oxygen-, acid- and anaesthetic-sensitive TASK-like background potassium channel in rat arterial chemoreceptor cells. J Physiol 525(Pt 1):135–142

Carpenter E, Peers C (1997) Swelling- and cAMP-activated Cl- currents in isolated rat carotid body type I cells. J Physiol 503(Pt 3):497–511

Carpenter E, Peers C (2001) A standing $Na^+$ conductance in rat carotid body type I cells. Neuroreport 12(7):1421–1425

Carpenter E, Wyatt CN, Hatton CJ, Bee D, Peers C (1996) $Ca^{2+}$ channel currents in type I carotid body cells from normoxic and chronically hypoxic rats. Adv Exp Med Biol 410:105–108

Cooper CE, Brown GC (2008) The inhibition of mitochondrial cytochrome oxidase by the gases carbon monoxide, nitric oxide, hydrogen cyanide and hydrogen sulfide: chemical mechanism and physiological significance. J Bioenerg Biomembr 40(5):533–539

Cooper CE, Giulivi C (2007) Nitric oxide regulation of mitochondrial oxygen consumption II: molecular mechanism and tissue physiology. Am J Physiol Cell Physiol 292(6):C1993–C2003

Coxon RV (1966) Regulation of biochemical reactions by oxygen and carbon dioxide. Blackwell, Oxford

Dallas ML, Scragg JL, Wyatt CN, Ross F, Hardie DG, Evans AM, Peers C (2009) Modulation of O(2) sensitive K(+) channels by AMP-activated protein kinase. Adv Exp Med Biol 648:57–63

Dasso LL, Buckler KJ, Vaughan Jones RD (1997) Muscarinic and nicotinic receptors raise intracellular $Ca^{2+}$ levels in rat carotid body type I cells. J Physiol 498(Pt 2):327–338

Duchen MR, Biscoe TJ (1992a) Mitochondrial function in type I cells isolated from rabbit arterial chemoreceptors. J Physiol 450:13–31

Duchen MR, Biscoe TJ (1992b) Relative mitochondrial membrane potential and $[Ca^{2+}]i$ in type I cells isolated from the rabbit carotid body. J Physiol 450:33–61

Duchen MR, Caddy KW, Kirby GC, Patterson DL, Ponte J, Biscoe TJ (1988) Biophysical studies of the cellular elements of the rabbit carotid body. Neuroscience 26(1):291–311

e Silva MJ, Lewis DL (1995) L- and N-type $Ca^{2+}$ channels in adult rat carotid body chemoreceptor type I cells. J Physiol 489(Pt 3):689–699

Evans AM, Mustard KJ, Wyatt CN, Peers C, Dipp M, Kumar P, Kinnear NP, Hardie DG (2005) Does AMP-activated protein kinase couple inhibition of mitochondrial oxidative phosphorylation by hypoxia to calcium signaling in $O_2$-sensing cells? J Biol Chem 280(50):41504–41511

Fidone SJ, Gonzalez C (1986) Initiation and control of chemoreceptor activity in the carotid body. American Physiological Society, Bethesda

Fidone S, Gonzalez C, Yoshizaki K (1982) Effects of low oxygen on the release of dopamine from the rabbit carotid body in vitro. J Physiol 333:93–110

Gnaiger E (2001) Bioenergetics at low oxygen: dependence of respiration and phosphorylation on oxygen and adenosine diphosphate supply. Respir Physiol 128(3):277–297

Gonzalez C, Almaraz L, Obeso A, Rigual R (1994) Carotid body chemoreceptors: from natural stimuli to sensory discharges. Physiol Rev 74(4):829–898

Hajnoczky G, Robb-Gaspers LD, Seitz MB, Thomas AP (1995) Decoding of cytosolic calcium oscillations in the mitochondria. Cell 82(3):415–424

Hall CN, Garthwaite J (2009) What is the real physiological NO concentration in vivo? Nitric Oxide 21(2):92–103

Hardie DG (2011) AMP-activated protein kinase: an energy sensor that regulates all aspects of cell function. Genes Dev 25(18):1895–1908

Heymans C, Bouckaert JJ, Dautrebande L (1931) Sinus carotidien et reflexes respiratoires: sensibilite des sinus carotidiens aux substances chimiques. Action stimulante respiratoire reflexe du sulfure de sodium, du cyanure de potassium, de la nicotine et de la lobeline. Arch Int Pharmacodyn Ther 40:54–91

Kang D, Wang J, Hogan JO, Vennekens R, Freichel M, White C, Kim D (2014) Increase in cytosolic $Ca^{2+}$ produced by hypoxia and other depolarizing stimuli activates a non-selective cation channel in chemoreceptor cells of rat carotid body. J Physiol 592(Pt 9):1975–1992

Kim D, Cavanaugh EJ, Kim I, Carroll JL (2009) Heteromeric TASK-1/TASK-3 is the major oxygen-sensitive background $K^+$ channel in rat carotid body glomus cells. J Physiol 587(Pt 12):2963–2975

Kim D, Kang D, Martin EA, Kim I, Carroll JL (2014) Effects of modulators of AMP-activated protein kinase on TASK-1/3 and intracellular Ca(2+) concentration in rat carotid body glomus cells. Respir Physiol Neurobiol 195:19–26

Kreneisz O, Benoit JP, Bayliss DA, Mulkey DK (2009) AMP-activated protein kinase inhibits TREK channels. J Physiol 587(Pt 24):5819–5830

Lahiri S, Rumsey WL, Wilson DF, Iturriaga R (1993) Contribution of in vivo microvascular $PO_2$ in the cat carotid body chemotransduction. J Appl Physiol 75(3):1035–1043

Lopez Lopez JR, De Luis DA, Gonzalez C (1993) Properties of a transient $K^+$ current in chemoreceptor cells of rabbit carotid body. J Physiol 460:15–32

Lopez Lopez JR, Gonzalez C, Perez Garcia MT (1997) Properties of ionic currents from isolated adult rat carotid body chemoreceptor cells: effect of hypoxia. J Physiol 499(Pt 2):429–441

Mason MG, Nicholls P, Wilson MT, Cooper CE (2006) Nitric oxide inhibition of respiration involves both competitive (heme) and noncompetitive (copper) binding to cytochrome c oxidase. Proc Natl Acad Sci U S A 103(3):708–713

McCormack JG, Denton RM (1989) The role of $Ca^{2+}$ ions in the regulation of intramitochondrial metabolism and energy production in rat heart. Mol Cell Biochem 89(2):121–125

Mills E, Jobsis FF (1970) Simultaneous measurement of cytochrome a3 reduction and chemoreceptor afferent activity in the carotid body. Nature 225(238):1147–1149

Mills E, Jobsis FF (1972) Mitochondrial respiratory chain of carotid body and chemoreceptor response to changes in oxygen tension. J Neurophysiol 35(4):405–428

Montoro RJ, Urena J, Fernandez Chacon R, Alvarez de Toledo G, Lopez Barneo J (1996) Oxygen sensing by ion channels and chemotransduction in single glomus cells. J Gen Physiol 107(1):133–143

Mulligan E, Lahiri S (1982) Separation of carotid body chemoreceptor responses to $O_2$ and $CO_2$ by oligomycin and by antimycin A. Am J Physiol 242(3):C200–C206

Mulligan E, Lahiri S, Storey BT (1981) Carotid body $O_2$ chemoreception and mitochondrial oxidative phosphorylation. J Appl Physiol 51(2):438–446

Nurse CA (2014) Synaptic and paracrine mechanisms at carotid body arterial chemoreceptors. J Physiol 592(16):3419–3426

Olson KR (2011) Hydrogen sulfide is an oxygen sensor in the carotid body. Respir Physiol Neurobiol 179(2–3):103–110

Olson KR, Whitfield NL (2010) Hydrogen sulfide and oxygen sensing in the cardiovascular system. Antioxid Redox Signal 12(10):1219–1234

Olson KR, Dombkowski RA, Russell MJ, Doellman MM, Head SK, Whitfield NL, Madden JA (2006) Hydrogen sulfide as an oxygen sensor/transducer in vertebrate hypoxic vasoconstriction and hypoxic vasodilation. J Exp Biol 209(Pt 20):4011–4023

Olson KR, Healy MJ, Qin Z, Skovgaard N, Vulesevic B, Duff DW, Whitfield NL, Yang G, Wang R, Perry SF (2008) Hydrogen sulfide as an oxygen sensor in trout gill chemoreceptors. Am J Physiol Regul Integr Comp Physiol 295(2):R669–R680

Ortega Saenz P, Pardal R, Garcia Fernandez M, Lopez Barneo J (2003) Rotenone selectively occludes sensitivity to hypoxia in rat carotid body glomus cells. J Physiol 548(Pt 3):789–800

Ortega-Saenz P, Pascual A, Gomez-Diaz R, Lopez-Barneo J (2006) Acute oxygen sensing in heme oxygenase-2 null mice. J Gen Physiol 128(4):405–411

Ortega-Saenz P, Levitsky KL, Marcos-Almaraz MT, Bonilla-Henao V, Pascual A, Lopez-Barneo J (2010) Carotid body chemosensory responses in mice deficient of TASK channels. J Gen Physiol 135(4):379–392

Pardal R, Ludewig U, Garcia Hirschfeld J, Lopez Barneo J (2000) Secretory responses of intact glomus cells in thin slices of rat carotid body to hypoxia and tetraethylammonium. Proc Natl Acad Sci U S A 97(5):2361–2366

Park YB, Herrington J, Babcock DF, Hille B (1996) $Ca^{2+}$ clearance mechanisms in isolated rat adrenal chromaffin cells. J Physiol 492(Pt 2):329–346

Peers C (1990a) Effect of lowered extracellular pH on Ca2(+)-dependent $K^+$ currents in type I cells from the neonatal rat carotid body. J Physiol 422:381–395

Peers C (1990b) Hypoxic suppression of $K^+$ currents in type I carotid body cells: selective effect on the Ca2(+)-activated $K^+$ current. Neurosci Lett 119(2):253–256

Peers C, O'Donnell J (1990) Potassium currents recorded in type I carotid body cells from the neonatal rat and their modulation by chemoexcitatory agents. Brain Res 522(2):259–266

Peng YJ, Nanduri J, Raghuraman G, Souvannakitti D, Gadalla MM, Kumar GK, Snyder SH, Prabhakar NR (2010) H2S mediates $O_2$ sensing in the carotid body. Proc Natl Acad Sci U S A 107(23):10719–10724

Perez Garcia MT, Almaraz L, Gonzalez C (1991) Cyclic AMP modulates differentially the release of dopamine induced by hypoxia and other stimuli and increases dopamine synthesis in the rabbit carotid body. J Neurochem 57(6):1992–2000

Perez Garcia MT, Obeso A, Lopez Lopez JR, Herreros B, Gonzalez C (1992) Characterization of cultured chemoreceptor cells dissociated from adult rabbit carotid body. Am J Physiol 263(6 Pt 1):C1152–C1159

Prasad M, Fearon IM, Zhang M, Laing M, Vollmer C, Nurse CA (2001) Expression of P2X2 and P2X3 receptor subunits in rat carotid body afferent neurones: role in chemosensory signalling. J Physiol 537(Pt 3):667–677

Rocher A, Geijo Barrientos E, Caceres AI, Rigual R, Gonzalez C, Almaraz L (2005) Role of voltage-dependent calcium channels in stimulus-secretion coupling in rabbit carotid body chemoreceptor cells. J Physiol 562(Pt 2):407–420

Rong W, Gourine AV, Cockayne DA, Xiang Z, Ford AP, Spyer KM, Burnstock G (2003) Pivotal role of nucleotide P2X2 receptor subunit of the ATP-gated ion channel mediating ventilatory responses to hypoxia. J Neurosci 23(36):11315–11321

Shen TCR, Hauss WH (1939) Influence of dinitrophenol, dinitroortocresol and paranitrophenol upon the carotid sinus chemoreceptors of the dog. Arch Int Pharmacodyn Ther 63:251–258

Stea A, Nurse CA (1989) Chloride channels in cultured glomus cells of the rat carotid body. Am J Physiol 257(2 Pt 1):C174–C181

Stea A, Nurse CA (1991) Whole-cell and perforated-patch recordings from $O_2$-sensitive rat carotid body cells grown in short- and long-term culture. Pflugers Arch 418(1–2):93–101

Turner PJ, Buckler KJ (2013) Oxygen and mitochondrial inhibitors modulate both monomeric and heteromeric TASK-1 and TASK-3 channels in mouse carotid body type-1 cells. J Physiol 591(Pt 23):5977–5998

Urena J, Lopez Lopez J, Gonzalez C, Lopez Barneo J (1989) Ionic currents in dispersed chemoreceptor cells of the mammalian carotid body. J Gen Physiol 93(5):979–999

Verkhovsky MI, Morgan JE, Puustein A, Wikstrom M (1996) Kinetic trapping of oxygen in cell respiration. Nature 380(6571):268–270

Waterland RA, Basu A, Chance B, Poyton RO (1991) The isoforms of yeast cytochrome c oxidase subunit V alter the in vivo kinetic properties of the holoenzyme. J Biol Chem 266(7):4180–4186

Weir EK, Lopez-Barneo J, Buckler KJ, Archer SL (2005) Acute oxygen-sensing mechanisms. N Engl J Med 353(19):2042–2055

Werth JL, Thayer SA (1994) Mitochondria buffer physiological calcium loads in cultured rat dorsal root ganglion neurons. J Neurosci 14(1):348–356

Wilson DF, Mokashi A, Chugh D, Vinogradov S, Osanai S, Lahiri S (1994) The primary oxygen sensor of the cat carotid body is cytochrome a3 of the mitochondrial respiratory chain. FEBS Lett 351(3):370–374

Wyatt CN, Buckler KJ (2003) Effect of mitochondrial inhibitors on type I cells. Adv Exp Med Biol 536:55–58

Wyatt CN, Buckler KJ (2004) The effect of mitochondrial inhibitors on membrane currents in isolated neonatal rat carotid body type I cells. J Physiol 556(Pt 1):175–191

Wyatt CN, Mustard KJ, Pearson SA, Dallas ML, Atkinson L, Kumar P, Peers C, Hardie DG, Evans AM (2007) AMP-activated protein kinase mediates carotid body excitation by hypoxia. J Biol Chem 282(11):8092–8098

Zhang M, Zhong H, Vollmer C, Nurse CA (2000) Co-release of ATP and ACh mediates hypoxic signalling at rat carotid body chemoreceptors. J Physiol 525(Pt 1):143–158

# 10

# Potentiation of Hypoxic Pulmonary Vasoconstriction by Hydrogen Sulfide Precursors 3-Mercaptopyruvate and D-Cysteine Is Blocked by the Cystathionine γ Lyase Inhibitor Propargylglycine

Jesus Prieto-Lloret and Philip I. Aaronson

**Abstract**

Although the gasotransmitter hydrogen sulfide ($H_2S$) generally dilates systemic arteries in mammals, it causes constriction of pulmonary arteries. In isolated rat pulmonary arteries, we have shown that the $H_2S$ precursor cysteine enhances both hypoxic pulmonary vasoconstriction and tension development caused by the agonist prostaglandin $F_{2\alpha}$ under normoxic conditions. These effects were blocked by propargylglycine (PAG), a blocker of the enzyme cystathionine γ lyase which metabolises cysteine to sulfide. In the present study, we evaluated whether 3-mercaptopyruvate (3-MP), a sulfide precursor which is thought to give rise to sulfide when it is metabolised by the enzyme mercaptopyruvate sulfurtransferase, also enhanced contraction. Application of 3-MP prior to hypoxic challenge caused a marked enhancement of HPV which was completely blocked by both L- and D,L-PAG (both 1 mM). Cumulative application of 3–1,000 μM 3-MP during an ongoing contraction to $PGF_{2\alpha}$ under normoxic conditions also caused a marked increase in tension. Application of D-cysteine (1 mM) also enhanced HPV, and this effect was prevented by both the D-amino acid oxidase inhibitor sodium benzoate (500 μM) and 1 mM L-PAG.

**Keywords**

Hypoxic pulmonary vasoconstriction • 3-mercaptopyruvate • D-cysteine

J. Prieto-Lloret • P.I. Aaronson (✉)
Division of Asthma, Allergy & Lung Biology, Faculty of Life Sciences and Medicine, King's College London, London WC2R 2LS, UK
e-mail: philip.aaronson@kcl.ac.uk



C. Peers et al. (eds.), *Arterial Chemoreceptors in Physiology and Pathophysiology*, Advances in Experimental Medicine and Biology 860, DOI 10.1007/978-3-319-18440-1_10

## 10.1 Introduction

The gasotransmitter $H_2S$ (hereafter 'sulfide') is produced in cells *via* both enzymatic and non-enzymatic pathways (*e.g.* mobilization by reductants of sulfane sulphur bound to proteins). Three enzymes, cystathionine γ lyase (CSE), cystathionine β synthase (CBS), and mercaptopyruvate sulfurtransferase (MST), which acts in concert with cysteine aminotransferase(CAT), produce sulfide from cysteine. Of these, CSE is thought to be the most important enzymatic source of sulfide in the cardiovascular system (Wang 2012).

We reported that application of cysteine to rat pulmonary arteries (PA) causes further tension development during an ongoing vasoconstriction to the agonist $PGF_{2\alpha}$, and also potentiates hypoxic pulmonary vasoconstriction (HPV), the unique response of pulmonary arteries which functions to match pulmonary perfusion to ventilation during hypoxia (Prieto-Lloret et al. 2014). Both effects were blocked by the CSE antagonist PAG, implying that cysteine induced potentiation of contraction was due to the production of sulfide, which causes contraction in these arteries (Olson et al. 2006).

We have recently observed that these effects of L-cysteine are mimicked by exogenously applied 3-mercaptopyruvate (3-MP), a substance which is produced when cysteine is metabolised by CAT, and which can then be further processed by MST to form sulfide. However, 3-MP binds to MST with a rather low affinity (Km = ~1.5 mM), whereas we find that application of as little 10 μM exogenous 3-MP causes tension development.

However, CAT is a reversible enzyme (Singh and Banerjee 2011), and the possibility therefore exists that it can use 3-MP to generate L-cysteine which is then metabolised to sulfide by CSE. In the current study we explored this possibility by examining the effect of 3-MP on HPV in the presence and absence of PAG. Similar experiments were carried using D-cysteine, which can be metabolised to 3-MP via the enzyme D-amino acid oxidase (DAO).

## 10.2 Methods

### 10.2.1 Ethical Approval and Myography

This study conforms with the *Guide for the Care and Use of Laboratory Animals* published by the US National Institutes of Health (NIH Publication No. 85–23, revised 1996) and is in accordance with UK Home Office regulations (Animals (Scientific Procedures) Act, 1986). Male Wistar rats (200–300 g) were killed by lethal injection (*i.p.*) of sodium thiopental. The heart and lungs were excised and placed in cold physiological salt solution (PSS) containing (in mmol/L): 118 NaCl, 24 $NaHCO_3$, 1 $MgSO_4$, 0.435 $NaH_2PO_4$, 5.56 glucose, 1.8 $CaCl_2$, and 4 KCl. Rings of small PA (inner diameter 0.5–1.0 mm) were cleaned of adventitia and parenchyma under a dissection microscope, mounted on an isometric small vessel wire myograph, and stretched to a basal tension of 5–6 mN (equivalent to an internal pressure of ~15 mmHg). They were then equilibrated with three brief exposures to PSS containing 80 mmol/L KCl (80KPSS; isotonic replacement of NaCl by KCl). The pH of the solution was maintained at 7.4 by gassing with 20 %$O_2$, 5 %$CO_2$, balance $N_2$.

### 10.2.2 HPV Experimental Protocol, Data Representation and Statistical Analysis

PA were challenged with hypoxia to evoke HPV three times, with each 45 min hypoxic episode being separated from the others by ≥35 min. Hypoxia was applied by gassing the myograph solution with 0 % $O_2$, which caused a rapid fall in $pO_2$ in the solution to a stable level of 6–9 mmHg. Tension was measured just before hypoxia was imposed, every 5 min during the hypoxic periods, and then 5 min after re-oxygenation when HPV had almost completely subsided.

As described in Connolly et al. (2013) we used the 2nd HPV as the control response and experimental interventions (*e.g.* applying 3-MP)

were made 30 min prior to the 3rd challenge with hypoxia. When we examined the effect on HPV of a combination of two agents (e.g. PAG and 3-MP), the first was applied 30 min before the 2nd hypoxic challenge and remained present during the 3rd hypoxic challenge and the second was then applied after the 2nd HPV, 30 min prior to the 3rd hypoxic challenge. For calculating effects of drugs on HPV, increases in tension above baseline throughout the 2nd and 3rd hypoxic challenges were expressed as a percentage of the increase in force above baseline recorded at 45 min of hypoxia during the 2nd (control) response The amplitudes of the control and intervention HPVs were compared every 5 min using repeated measures ANOVA followed by a Bonferroni posthoc test in order to determine whether the intervention had significantly changed the response.

In other experiments, 3-MP or D-cysteine were applied cumulatively in ascending concentrations during an ongoing stable contraction to 5 μM $PGF_{2\alpha}$. The resulting increase in force was expressed as a percent of the maximal (80KPSS) contraction in that artery. When used to study this response, inhibitors were applied 30 min before $PGF_{2\alpha}$; their effects were assessed using Student's unpaired t-test. The threshold for statistical significance for all comparisons was set at $P<0.05$.

## 10.3 Results

As shown in Fig. 10.1a, a low concentration of 3-MP (30 μM) markedly enhanced HPV. This response was abolished by the CSE blocker PAG (1 mM) in both its L and racemic forms (Fig. 10.1b, c).

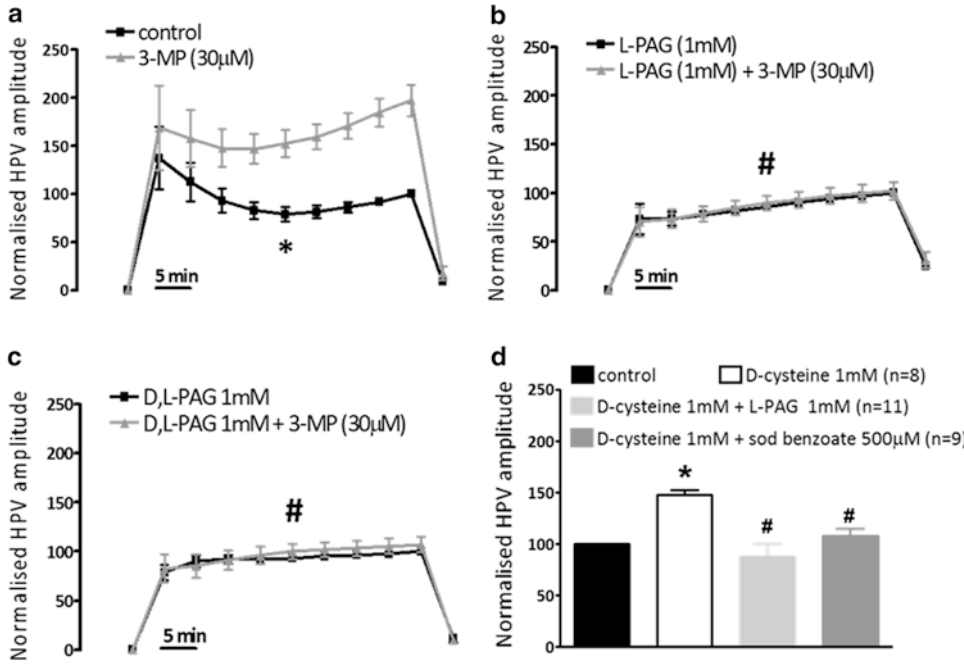


**Fig. 10.1** 3-MP – induced enhancement of HPV is blocked by PAG. HPV to 6–9 mmHg $O_2$ before (*black squares*) and after (*grey triangles*) incubation of PAs with 30 μM 3-MP (**a**, n = 11), 30 μM 3-MP in the additional presence of 1 mM L-PAG (**b**, n = 8) and 30 μM 3-MP in the additional presence of D,L-PAG (**c**, n = 9). Results are shown as mean ± SEM; * indicates a significant ($p<0.05$) effect of 3-MP on HPV, # indicates a significant block of the effect of 3-MP by PAG. (**d**) Effect of 1 mM D-cysteine on HPV, measured after 45 min of hypoxia, under control conditions and in the presence of 1 mM PAG or 500 μM sodium benzoate. D-cysteine significantly ($p<0.05$) increased HPV amplitude (*), and this effect was significantly suppressed by PAG and sodium benzoate (#)

Similarly, D-cysteine (1 mM) caused a significant increase in the amplitude of HPV (Fig. 10.1d; the amplitude of HPV measured after 45 of hypoxia is shown). This effect of D-cysteine was abolished by L-PAG, and also by the DAO inhibitor sodium benzoate (500 μM). Neither of these blockers had any effect on HPV in the absence of D-cysteine (not shown).

Under normoxic conditions, 3-MP (3–1,000 μM) caused a concentration-dependent increase in tension when applied during a stable ongoing contraction to 5 μM $PGF_{2\alpha}$ (Fig. 10.2a, b). 1 mM 3-MP applied on its own also caused a contraction, and this was reversed by the reducing agent dithiothreitol (DTT, 1 mM) (Fig. 10.2c). Like 3-MP, D-cysteine also caused an increase in tension when applied during a contraction to 5 μM $PGF_{2\alpha}$, although this was smaller than that induced by 3-MP (Fig. 10.2d) and reached a maximum level before appearing to fall at higher concentrations. Like its effect on HPV, the increase in the $PGF_{2\alpha}$ contraction caused by D-cysteine was significantly attenuated by sodium benzoate (Fig. 10.2d).

## 10.4 Discussion

The key novel finding of these experiments is that the putative sulfide precursor 3-MP enhances both HPV and the contraction to $PGF_{2\alpha}$ under normoxic conditions. D-cysteine, which can be converted to 3-MP by D-amino acid oxidase, also caused a PAG-sensitive enhancement of HPV.

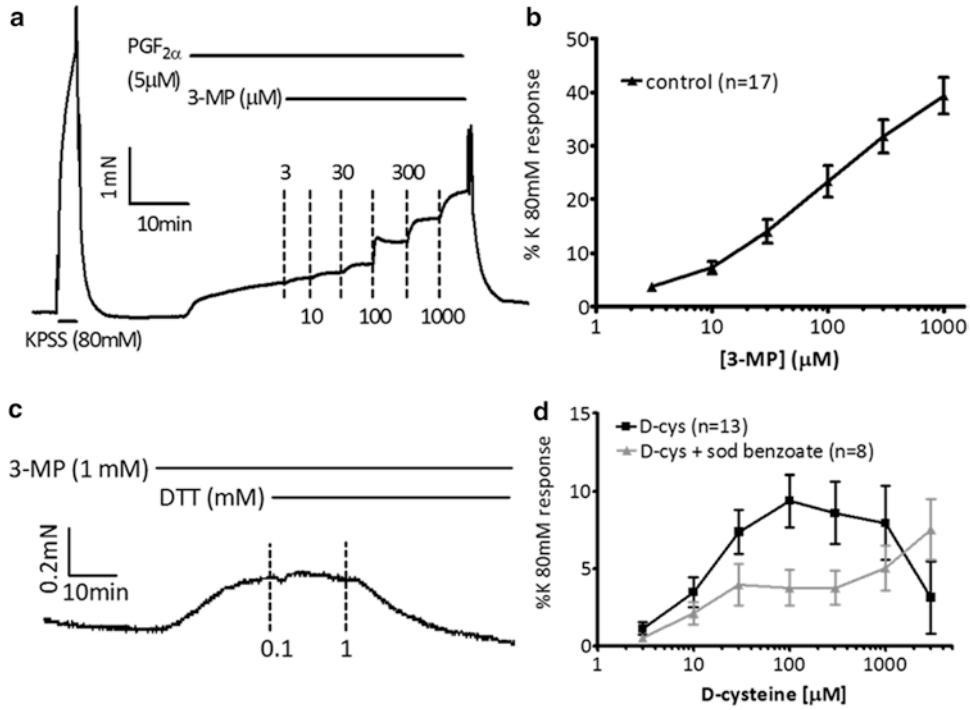


**Fig. 10.2** 3-MP and D-cysteine enhance, and DTT inhibits, the contraction induced by 5 μM $PGF_{2\alpha}$ under normoxic conditions. (**a**) Typical experiment showing that cumulative application of 3-MP (3–1,000 μM) during an ongoing contraction to 5 μM $PGF_{2\alpha}$ caused a progressive further increase in tension. (**b**) Mean ± SEM increase in tension caused by 3-MP in 17 experiments using the protocol described for panel A (*solid triangles*). Tension is expressed as a percent of that evoked by 80KPSS in that artery, which represents the maximal contraction. (**c**) Effect of 0.1 and 1 mM DTT on the contraction evoked by 1 mM 3-MP. Trace shown is representative of 5 similar experiments. (**d**) Effect of on tension cumulative application of D-cysteine (3–3,000 μM) during an ongoing contraction to 5 μM $PGF_{2\alpha}$ in the absence (*black squares*) and presence (*grey triangles*) of 500 μM sodium benzoate

Sulfide can be synthesised from L-cysteine by enzymatic pathways involving CBS, CSE, and CAT/MST. CSE, which is strongly expressed in rat PA (Prieto-Lloret et al. 2014), is generally thought of as being the important sulfide-synthesising pathway in the vasculature (Liu et al. 2012). MST is also expressed in rat pulmonary arteries (Olson et al. 2010; Prieto-Lloret et al. 2014), whereas CBS is not (Prieto-Lloret et al. 2014).

Although it is unclear whether D-cysteine is produced in the body, a significant proportion of L-cysteine is converted to the D form during food processing and can enter the body that way (Shibuya et al. 2013). D-cysteine can then be converted to 3-MP by D-amino acid oxidase, which is strongly expressed in the kidney and parts of the brain (Kimura 2014).

PA are unusual in that they are constricted by sulfide, which generally dilates systemic arteries (Olson and Whitfield 2010). We have reported that pre-incubation of isolated rat pulmonary artery segments in 1 mM L-cysteine increased the magnitude of both HPV and the contraction to $PGF_{2a}$ under normoxic conditions. These effects were reversed by blocking CSE with PAG but not by the CAT blocker aspartate, implying that they were most likely due to an increased production of sulfide via CSE (Prieto-Lloret et al. 2014).

On the other hand, application of 1 mM α-ketoglutarate together with 1 mM cysteine also caused an enhancement of HPV which was markedly attenuated by aspartate as well as PAG, leading us to speculate that in the presence of exogenous α-ketoglutarate, which is required for the metabolism of cysteine by CAT, cysteine might also yield sulfide via the CAT/MST (Prieto-Lloret et al. 2014).

CAT, which is found both in the mitochondria and the cytoplasm, is also referred to as aspartate aminotransferase (AAT). It catalyses the following reversible reactions,

$$\text{L cysteine} + \text{PLP-CAT} \leftrightarrow \text{3-MP} + \text{PMP-CAT} \tag{10.1}$$

$$\text{aspartate} + \text{PLP-CAT} \leftrightarrow \text{oxaloacetate} + \text{PMP-CAT} \tag{10.2}$$

$$\alpha\text{-ketoglutarate} + \text{PMP-CAT} \leftrightarrow \text{glutamate} + \text{PLP-CAT} \tag{10.3}$$

in which pyridoxal-5′-phosphate (PLP) acts as a co-factor which accepts an amino acid from cysteine or aspartate, becoming pyridoxamine-5′-phosphate (PMP), and then donates it to α-ketoglutarate to form glutamate (Singh and Banerjee 2011).

MST then metabolises 3-MP, resulting in the transfer of sulfane sulphur to form MST-SSH. This then gives rise to sulfide owing to the action of reductants such as dihydrolipoic acid (Olson et al. 2013).

Notably, however, the $K_m$ for the metabolism of 3-MP by MST is high (>1 mM) even under the highly alkaline conditions which favour this reaction (Singh and Banerjee 2011). The extent to which the CAT/MST pathway synthesises sulfide in cells of the vasculature at normal intracellular concentrations of cysteine is therefore questionable (Kimura 2014).

To further explore whether the CAT/MST pathway plays any role in promoting contraction in pulmonary arteries, we examined whether 3-MP was able to mimic L-cysteine in enhancing both HPV and the contraction to $PGF_{2\alpha}$ evoked under normoxic conditions, and found that 30 μM 3-MP had an effect similar to, and indeed somewhat larger than, L-cysteine (see Prieto-Lloret et al. 2014 for the effect of cysteine).

There are currently no well-characterised pharmacological antagonists of MST with which to assess the effects on cells of its metabolism of 3-MP. However, given that the production of sulfide by the CAT/MST pathway is facilitated by

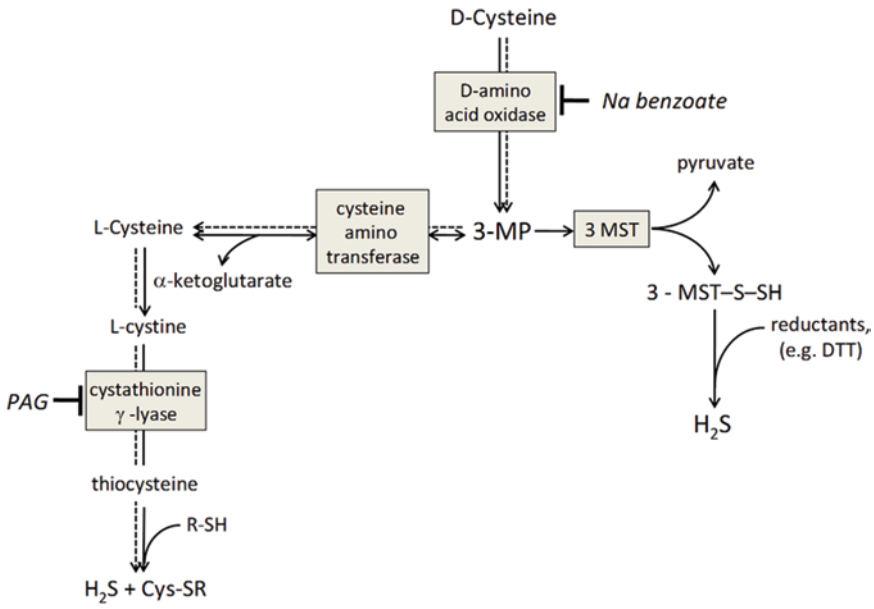


**Fig. 10.3** Enzymatic pathways by which sulfide may be synthesized from 3-MP and D-cysteine. The scheme illustrated is based on information presented in Wang (2012), Olson et al. (2013) and Kimura (2014). The *dashed line* shows the proposed pathway by which sulfide may be synthesized from D-cysteine and 3-MP under hypoxic conditions

reductants (Olson et al. 2013), it might be predicted that the reductant dithiothreitol (DTT) would increase the contractile effect of 3-MP. However, as shown in Fig. 10.2c, 1 mM DTT inhibited rather than increased the contraction caused 1 mM 3-MP. Although this was not a conclusive experiment, as DTT might cause relaxation through effects independent of sulfide, it suggested that 3-MP might give rise to sulfide via another pathway, i.e. the production of L-cysteine by the reversal of CAT and its subsequent metabolism by CSE to sulfide.

In this case, it would be predicted that PAG should block the enhancement of HPV and of the $PGF_{2\alpha}$ – induced contraction by 3-MP. The results shown in Fig. 10.1 are in accord with this prediction, since 1 mM PAG, which would not be expected to block MST, abolished the potentiating effect of 30 μM 3-MP on HPV.

Since 3-MP can also be produced in cells through the metabolism of D-cysteine by DAO, it would be expected that D-cysteine should mimic the effects of 3-MP, and that these effects should be inhibited by blocking DAO or PAG. As shown in Fig. 10.1d, both PAG and the DAO blocker sodium benzoate prevented the enhancement of HPV induced by 1 mM D-cysteine. D-cysteine also increased tension in the presence of $PGF_{2\alpha}$ and this was attenuated by sodium benzoate (Fig. 10.2d).

In summary, both 3-MP and D-cysteine promote HPV in rat PA, and this effect is blocked by PAG. Since both can give rise to L-cysteine, which also enhances HPV in a PAG-sensitive manner, we speculate that under hypoxic conditions sulfide can be produced by the reversal of CAT and the pathway illustrated by the dashed line in Fig. 10.3, at least when cells are supplied with sufficient D-cysteine or 3-MP. However, the extent to which this pathway is operative in these arteries under physiological conditions remains to be determined.

**Acknowledgements** This study was supported by a Wellcome Trust Programme grant (087776) to PIA and Jeremy Ward.

## References

Connolly MJ, Prieto-Lloret J, Becker S, Ward JP, Aaronson PI (2013) Hypoxic pulmonary vasoconstriction in the absence of pretone: essential role for intracellular $Ca^{2+}$ release. J Physiol 591:4473–4498

Kimura H (2014) The physiological role of hydrogen sulfide and beyond. Nitric Oxide 41C:4–10

Liu YH, Lu M, Hu LF, Wong PT, Webb GD, Bian JS (2012) Hydrogen sulfide in the mammalian cardiovascular system. Antioxid Redox Signal 17:141–185

Olson KR, Whitfield NL (2010) Hydrogen sulfide and oxygen sensing in the cardiovascular system. Antioxid Redox Signal 12:1219–1234

Olson KR, Dombkowski RA, Russell MJ, Doellman MM, Head SK, Whitfield NL et al (2006) Hydrogen sulfide as an oxygen sensor/transducer in vertebrate hypoxic vasoconstriction and hypoxic vasodilation. J Exp Biol 209:4011–4023

Olson KR, Whitfield NL, Bearden SE, St Leger LJ, Nilson E, Gao Y, Madden JA (2010) Hypoxic pulmonary vasodilation: a paradigm shift with a hydrogen sulfide mechanism. Am J Physiol Regul Integr Comp Physiol 298:R51–R60

Olson KR, Deleon ER, Gao Y, Hurley K, Sadauskas V, Batz C et al (2013) Thiosulfate: a readily accessible source of hydrogen sulfide in oxygen sensing. Am J Physiol egul Integr Comp Physiol 305:R592–R603

Prieto-Lloret J, Shaifta Y, Ward JPT, Aaronson PI (2014) Hypoxic pulmonary vasoconstriction in isolated rat pulmonary arteries is not inhibited by antagonists of $H_2S$-synthesizing pathways. J Physiol 593:385–401

Shibuya N, Kioke S, Tanaka M, Ishigami-Yuasa M, Kimura Y, Ogasawara K et al (2013) A novel pathway for the production of hydrogen sulfide from D-cysteine in mammalian cells. Nat Commun 4:1366–1372

Singh S, Banerjee R (2011) PLP-dependent H(2)S biogenesis. Biochim Biophys Acta 1814:1518–1527

Wang R (2012) Physiological implications of hydrogen sulfide: a whiff exploration that blossomed. Physiol Rev 92:791–896

# 11 Modulation of the LKB1-AMPK Signalling Pathway Underpins Hypoxic Pulmonary Vasoconstriction and Pulmonary Hypertension

A. Mark Evans, Sophronia A. Lewis, Oluseye A. Ogunbayo, and Javier Moral-Sanz

**Abstract**

Perhaps the defining characteristic of pulmonary arteries is the process of hypoxic pulmonary vasoconstriction (HPV) which, under physiological conditions, supports ventilation-perfusion matching in the lung by diverting blood flow away from oxygen deprived areas of the lung to oxygen rich regions. However, when alveolar hypoxia is more widespread, either at altitude or with disease (e.g., cystic fibrosis), HPV may lead to hypoxic pulmonary hypertension. HPV is driven by the intrinsic response to hypoxia of pulmonary arterial smooth muscle and endothelial cells, which are acutely sensitive to relatively small changes in $pO_2$ and have evolved to monitor oxygen supply and thus address ventilation-perfusion mismatch. There is now a consensus that the inhibition by hypoxia of mitochondrial oxidative phosphorylation represents a key step towards the induction of HPV, but the precise nature of the signalling pathway(s) engaged thereafter remains open to debate. We will consider the role of the AMP-activated protein kinase (AMPK) and liver kinase B1 (LKB1), an upstream kinase through which AMPK is intimately coupled to changes in oxygen supply via mitochondrial metabolism. A growing body of evidence, from our laboratory and others, suggests that modulation of the LKB1-AMPK signalling pathway underpins both hypoxic pulmonary vasoconstriction and the development of pulmonary hypertension.

A.M. Evans (✉) • S.A. Lewis • O.A. Ogunbayo
J. Moral-Sanz
Centre for Integrative Physiology, College of Medicine and Veterinary Medicine, Hugh Robson Building, University of Edinburgh, Edinburgh EH8 9XD, UK
e-mail: mark.evans@ed.ac.uk



C. Peers et al. (eds.), *Arterial Chemoreceptors in Physiology and Pathophysiology*, Advances in Experimental Medicine and Biology 860, DOI 10.1007/978-3-319-18440-1_11

**Keywords**

LKB1 • AMPK • Hypoxia • Pulmonary artery • Vasoconstriction • Kv1.5

## 11.1 Introduction

Although there had been some prior comment, the first definitive description of hypoxic pulmonary vasoconstriction (HPV) was provided by Bradford and Dean in 1894 (Bradford and Dean 1894). They described not only a rise in pulmonary vascular pressure upon asphyxia, but concluded that this was driven by the reaction to asphyxia of the blood vessels themselves, because the measured increase in pressure upon asphyxia persisted after transection of the spinal cord. Fifty years later, von Euler and Liljestrand showed that hypoxia without hypercapnia induced pulmonary vasoconstriction, and hypothesised that HPV may assist ventilation-perfusion matching in the lung (von Euler and Liljestrand 1946); by contrast, systemic arteries dilate in response to tissue hypoxemia, in order to match local perfusion to local metabolism (Roy and Sherrington 1890).

That HPV was largely, or entirely independent of the autonomic nervous system (Nisell 1951) was evident after chemical sympathectomy (using 6-hydroxy-dopamine), surgical denervation of the carotid and aortic chemoreceptors or after bilateral cervical vagotomy (Lejeune et al. 1989; Naeije et al. 1989). Most significantly, bilateral lung transplants established that HPV remains unaffected following denervation in man (Robin et al. 1987). Therefore, neither central nor local regulation of the autonomic nervous system plays a role in mediating HPV.

In 1951 it was demonstrated that HPV was not induced when the lung was perfused with hypoxic blood at a constant, normoxic alveolar oxygen tension (Duke and Killick 1952), and later work confirmed that a fall in airway/alveolar $pO_2$ triggered a pronounced increase in pulmonary vascular perfusion pressure (Bergofsky et al. 1968). Consistent with this, Kato and Staub demonstrated, using unilobar hypoxia, that the small precapillary resistance arteries contributed most to the increase in pulmonary vascular perfusion pressure during alveolar hypoxia, and that the magnitude of HPV was inversely related to pulmonary artery diameter (Kato and Staub 1966). In isolated arteries HPV is biphasic (see Fig. 11.2a) with a threshold for initiation of ~60 mmHg (Dipp and Evans 2001). Thereafter the magnitude of constriction increases in a manner proportional to the degree of hypoxia, until it fails under near anoxic conditions (Dipp et al. 2003). The two phases of HPV observed in isolated arteries are discrete, comprising a transient constriction (Phase 1; 5–10 min) followed by a slow tonic constriction (Phase 2; peak after 30–40 min), both of which are initiated immediately upon exposure to hypoxia (Dipp et al. 2001; Leach et al. 1994).

It is generally accepted that hypoxia triggers pulmonary artery constriction via signalling pathways intrinsic to the smooth muscle and endothelial cells. Initially, HPV is driven by calcium release from the smooth muscle sarcoplasmic reticulum via ryanodine receptors and in a manner that does not require calcium influx (Dipp et al. 2001), although it is clear that subsequent activation of the store-refilling current aids the maintenance of constriction (Evans et al. 2005; Lu et al. 2008; Wang et al. 2004; Wilson et al. 2002). Thereafter, constriction is augmented via myofilament calcium sensitisation, which is initiated in response to the release of a vasoconstrictor from the endothelium (Evans and Dipp 2002; Robertson et al. 2000, 2001). At the molecular level, there is also clear evidence that hypoxia modulates the activity of voltage-gated potassium channels ($K_V$) in the plasma membrane of the smooth muscle cells, although the functional consequence of potassium channel regulation remains unclear (Archer et al. 1993; Dipp et al. 2001; Post et al. 1992; Remillard et al. 2007). That aside, the nature of the principle signalling

pathway(s) involved remains open to debate (Evans et al. 2011), but clearly relies on the modulation by hypoxia of mitochondrial metabolism (see for example Sommer et al. 2010).

## 11.2 Mitochondria and Oxygen Sensing

A requirement for functional mitochondria in the process of oxygen-sensing was first identified by investigations into the function of the carotid bodies, which noted that cyanide (Cooper and Brown 2008) mimicked and occluded activation by hypoxia of the carotid body (Heymans et al. 1930). The first direct evidence of this fact was provided by spectrophotometric analysis of the respiratory chain redox status and fluorometric measurement of the NAD(P)H/NAD(P)$^+$ ratio (Mills and Jobsis 1972). By relating outcomes to afferent sinus nerve discharge during hypoxia it was shown that an increase in the NAD(P)H/NAD(P)$^+$ ratio correlated with afferent fibre discharge frequency over what is considered to be the physiological range of arterial $pO_2$. It was therefore proposed that mitochondria of most cells may utilise a high affinity (i.e. normal) cytochrome $a_3$, while the cytochrome $a_3$ incorporated in mitochondria of oxygen-sensing cells may have a low affinity for oxygen. This proposal gained support from the work of Duchen and Biscoe (1992a, b) and has gathered further momentum of late, not least due to the detailed investigations of Buckler and co-workers (Turner and Buckler 2013; Wyatt and Buckler 2004). However, the strongest evidence in favour of an absolute requirement for functional mitochondria in oxygen-sensing comes from studies on immortalised neonatal adrenomedullary chromaffin cells that incorporate or lack functional mitochondria (Buttigieg et al. 2006; Thompson et al. 1997, 2007). Those with functional mitochondria were found to respond to hypoxia and to inhibitors of mitochondrial oxidative phosphorylation. By contrast, those cells lacking functional mitochondria failed to respond to either stimulus. Allied to these findings, it has been shown that pulmonary arterial smooth muscle cells depleted, by ethidium bromide, of mitochondrial DNA and thus a functional mitochondrial electron transport chain, do not respond to hypoxia (Waypa et al. 2001). Moreover, comprehensive data indicate that inhibitors of mitochondria (either uncouplers or blockers of specific respiratory chain complexes) mimic hypoxia in their ability to regulate ion channel function in a variety of oxygen-sensing cells, including pulmonary arterial smooth muscle cells (Leach et al. 2001; Weissmann et al. 2003). It should be noted, however, that we have yet to determine effectively the extent to which mitochondria of oxygen-sensing cells are uniquely sensitive to a fall in oxygen supply, or subject to the modulation of their activities, either directly or indirectly, by "local" metabolic intermediates (e.g. $O_2$ gradients, ATP, ADP; Brown 1992; Gnaiger et al. 1998; Jones 1986) and/or the signalling systems that they may modulate mitochondrial function. Nevertheless the weight of evidence suggests that the inhibition of mitochondrial oxidative phosphorylation is a key step towards the initiation of HPV.

## 11.3 The AMP-Activated Protein Kinase Mediates Hypoxic Pulmonary Vasoconstriction

Ten years ago the LKB1-AMPK signalling pathway was proposed to couple inhibition by hypoxia of mitochondrial metabolism to HPV (Evans 2006; Evans et al. 2005, 2006). This seemed logical not least because AMPK activity is intimately coupled to mitochondrial oxidative phosphorylation through the action of LKB1, the principle upstream kinase contributing to the activation of AMPK in response to metabolic stress (Hardie 2007; Oakhill et al. 2011). Moreover, AMPK is ubiquitously expressed and comprises catalytic α and regulatory β and γ subunits, of which there are multiple isoforms (Hardie 2007) (Fig. 11.1), that may confer at least 12 different subunit combinations and thus the capacity for the modulation of both substrate- and cell-specific functions (Steinberg and Kemp 2009). In response to metabolic stresses, such as the inhibition of mitochondrial oxidative

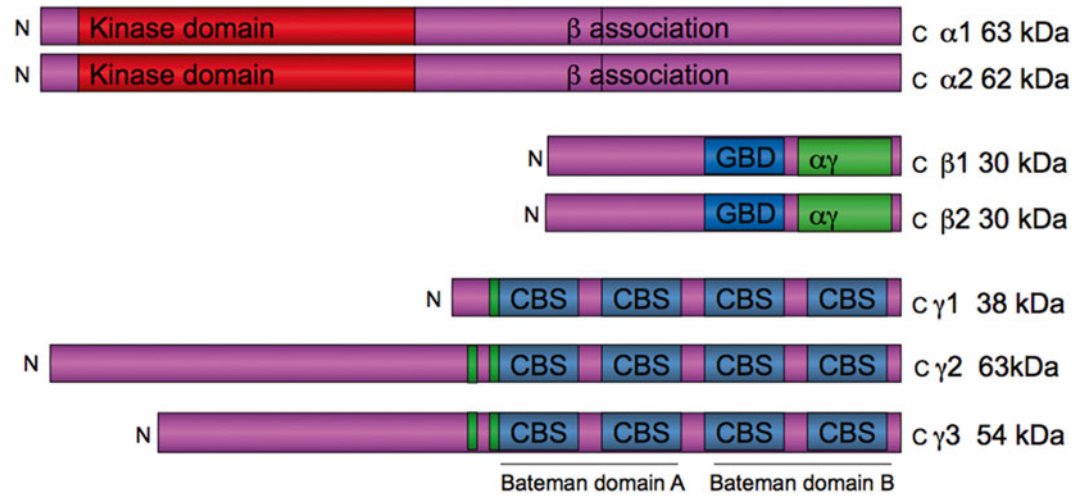


**Fig. 11.1** The AMPK alpha, beta and gamma subunit isoforms GBD, Glycogen binding domain

phosphorylation, AMPK is activated by an increase in the ADP/ATP ratio, which is amplified by adenylate kinase into a much larger increase in the AMP/ATP ratio (Gowans et al. 2013; Hawley et al. 1995). Allosteric activation of AMPK by AMP binding to the γ subunit may confer a 10-fold increase in activity (Gowans et al. 2013). That aside, activation of AMPK by more than 100-fold is conferred by phosphorylation at Thr-172 within the α subunit by upstream kinases, of which the most important is the tumor suppressor, LKB1 (Hawley et al. 2003). LKB1 appears to phosphorylate Thr-172 constitutively, but in manner facilitated by binding of AMP to the γ subunit (Gowans et al. 2013). Moreover, binding of AMP or ADP to exchangeable sites (Oakhill et al. 2011; Xiao et al. 2011) on the γ subunit of AMPK inhibits dephosphorylation of Thr-172, thus augmenting the switch to the active, phosphorylated form. This multiplexing mechanism of AMPK activation ensures great sensitivity, with the combinatorial effects delivering graded activation up to 1,000-fold from very low activities observed in unstressed cells when ATP is bound to the γ subunit sites. Alternatively, AMPK may be activated by increases in intracellular calcium via CaMKK-β, which also phosphorylates Thr-172 and likely acts to increase energy supply, for example, during periods of high cellular activity (Woods et al. 2005). By these mechanisms AMPK can be activated within seconds (Tamas et al. 2006) in order to up-regulate catabolic processes and suppress non-essential ATP-consuming reactions in order to maintain ATP supply; even without any measurable fall in cellular ATP. AMPK is therefore rightly considered to act as a 'guardian' or 'fuel gauge' of cellular metabolism (Hardie 2007). Pertinent to this Chapter, however, is the concept that AMPK may contribute to the regulation of oxygen and thereby energy (ATP) supply at the whole-body level and in doing so may contribute to hypoxia-response coupling by regulating cell and system physiology (Evans 2006). That AMPK may regulate aspects of cell function other than metabolism in all cell types brings us back to the mitochondrial/metabolic hypothesis for oxygen sensing.

As mentioned above, all mitochondrial inhibitors tested thus far mimic the effects of hypoxia on pulmonary arterial smooth muscle cells at the level of the oxygen-sensitive delayed rectifier potassium ($K_V$) current (Firth et al. 2008). However only some mitochondrial inhibitors have been shown to mimic and occlude HPV in the perfused lung, while others have been shown to block but not mimic HPV in the perfused lung and isolated pulmonary arteries

(Leach et al. 2001; Weissmann et al. 2003). This has been a bone of contention in the field and has been cast as being inconsistent with the view that HPV may be triggered by inhibition of mitochondrial oxidative phosphorylation. In this respect it is important to note that HPV fails under near anoxic conditions (<1 % oxygen), i.e., there is a $pO_2$ window within which pulmonary artery constriction may be initiated by hypoxia. It is therefore notable, for example, that the NAD(P)H/NAD(P)$^+$ ratio in dorsal root ganglion neurones, which do not serve to monitor oxygen supply, exhibits no shift until the $pO_2$ falls to near anoxic levels (~5 mm Hg); i.e., the $pO_2$ at which HPV begins to fail (Dipp et al. 2003). Why might this be significant? Strictly speaking, it is the "anoxic" and not the "hypoxic" condition that mitochondrial inhibitors would mimic at concentrations that ablate oxidative phosphorylation. Therefore, an explanation for the inconsistency of outcome with respect to the effects of mitochondrial inhibitors on HPV, and the $pO_2$ window within which HPV is triggered, may ultimately be provided by a greater understanding of the impact on pulmonary vascular function of degrees of metabolic stress. After all, dilating pulmonary arteries in response to anoxia might be the "last gasp" for optimal gaseous exchange within the lungs and thereby oxygen supply to the body. These considerations bring us back nicely to AMPK, which is activated by all mitochondrial inhibitors in a manner dependent of the degree of inhibition of mitochondrial oxidative phosphorylation (Hawley et al. 2010).

Consider the possibility that physiological levels of hypoxia may activate AMPK and thereby precipitate, for example, HPV (Evans et al. 2005). It is quite possible that during more extreme metabolic stress, such as anoxia, AMPK may play its now classical role and "switch off" non-essential ATP-consuming processes in order to ensure cell survival, and may not under these conditions function itself to drive constriction. A case in point with respect to mitochondrial inhibitors may be that one such agent, metformin, provides for effective therapy of type II diabetes via AMPK activation, whereas a closely related and more potent inhibitor of mitochondrial respiration, phenformin, is no longer prescribed because of related contra-indications.

What of the evidence supporting a role for AMPK in HPV? Our initial studies (Evans et al. 2005) showed that exposure of pulmonary arterial smooth muscle to hypoxia (15–20 mm Hg) precipitates an increase in the AMP/ATP ratio (Fig. 11.2), concomitant activation of AMPK and phosphorylation of acetyl-CoA carboxylase (ACC; an established marker for AMPK action), despite the fact that cellular ATP levels remain remarkably stable in the presence of hypoxia (Fig. 11.3a). Moreover, inhibition of mitochondrial oxidative phosphorylation by phenformin (Owen et al. 2000), evoked increases in NAD(P)H autofluorescence (Fig. 11.3b), AMPK activation and ACC phosphorylation (Fig. 11.3a) in pulmonary arterial smooth muscle cells. AMPK activation and ACC phosphorylation were also induced by AICAR (Fig. 11.3c), which activates AMPK not by inhibiting the mitochondrial electron transport chain (Fig. 11.3b) but by uptake into cells and subsequent metabolism to the AMP mimetic, ZMP (AICAR monophosphate; Corton et al. 1995). Regardless of their respective mechanism of action, each agent induced an increase in the intracellular calcium concentration in acutely isolated pulmonary arterial smooth muscle cells and did so by mobilising sarcoplasmic reticulum stores via ryanodine receptors as does hypoxia (Fig. 11.4). Most significantly, AMPK activation by AICAR evoked a slow, sustained and reversible constriction of pulmonary artery rings (Fig. 11.5a, b); an action not mimicked by phenformin due to confounding effects on smooth muscle function (Evans, unpublished observation). Moreover the sustained phase of HPV and pulmonary artery constriction in response to AICAR exhibited strikingly similar characteristics, namely a requirement for smooth muscle SR calcium release via ryanodine receptors, and calcium influx into and vasoconstrictor release from the endothelium (Fig. 11.5c). Consistent with these findings HPV was blocked by the non-selective AMPK antagonist, compound C (Robertson et al. 2008).

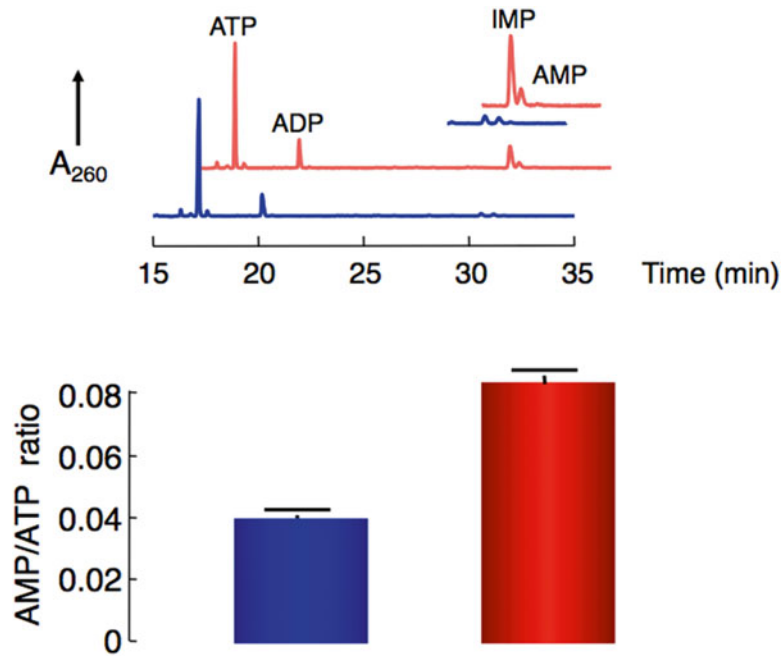


**Fig. 11.2** Hypoxia increases the AMP/ATP ratio in pulmonary arterial smooth muscle. *Upper panel* shows an idealised representation of the assessment of relative nucleotide levels by capillary electrophoresis. *Lower panel* show the AMP/ATP ratio of pulmonary arterial smooth muscle during normoxia (*blue*) and hypoxia (*red*)

Most recently we have gathered further significant support for our original proposals by use of pharmacological activators of AMPK (e.g., A769662) and recombinant, thiophosphorylated and thus active, human α2β2γ1 heterotrimers. Intracellular dialysis of the activated human AMPK or extracellular application of A769662 resulted in the inhibition of recombinant currents carried by $K_V1.5$ channels (not shown) and, like hypoxia, inhibited $K_V$ currents in acutely isolated pulmonary arterial smooth muscle cells (Fig. 11.6). Therefore, AMPK activation mimics the effects of hypoxia on pulmonary arterial smooth muscle cells, at the molecular, cellular and system level. This leaves us with perhaps the most important question – is the LKB1-AMPK signalling cascade necessary for HPV?

## 11.4 The Lkb1-AMPK Signalling Cascade and HPV

We have recently studied mice in which the genes for either LKB1, CaMKK-β or AMPK have been deleted in smooth muscles. Experimental outcomes from a range of studies on these mice are entirely consistent with the view that the LKB1-AMPK signalling pathway is required for HPV, including the response to hypoxia of the pulmonary vasculature and acutely isolated smooth muscle cells. By contrast, we find no evidence to suggest that CaMKK-β contributes to HPV. Nor have we found any evidence for the direct regulation of AMPK by hydrogen peroxide (Emerling et al. 2009), which appears to activate AMPK through inhibition of mitochondrial oxidative phosphorylation (Hawley et al. 2010).

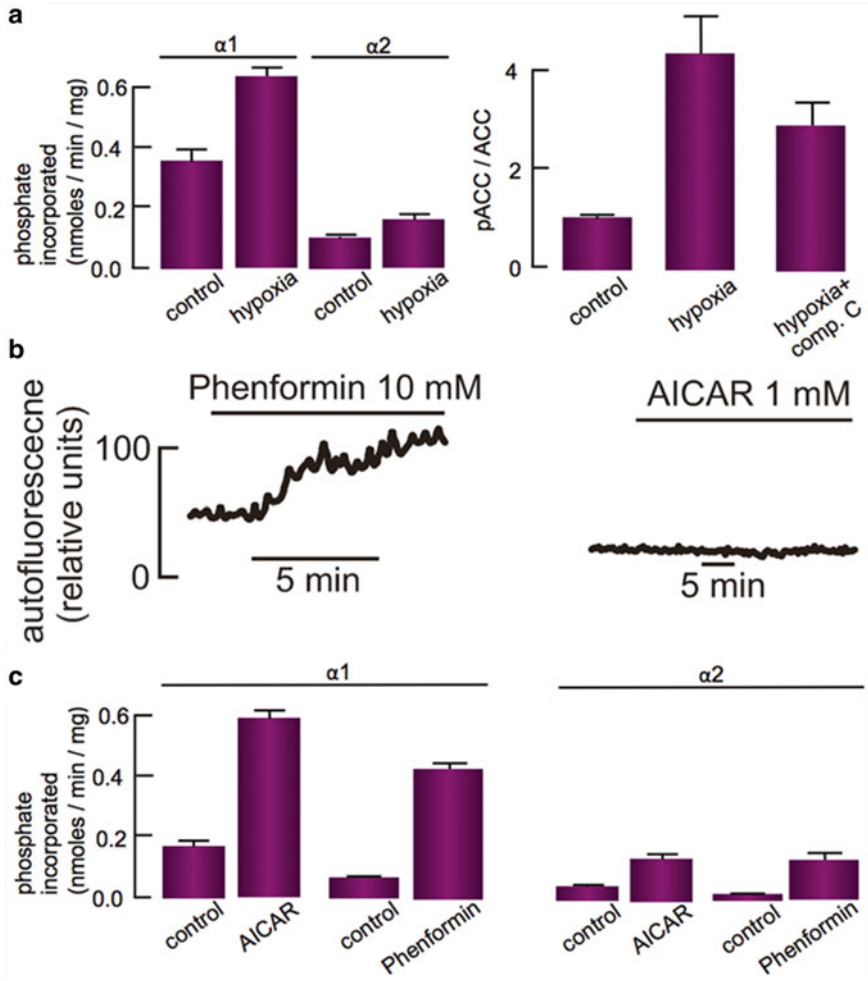


**Fig. 11.3** AMPK activation and acetyl CoA carboxylase phosphorylation in response to hypoxia, mitochondrial inhibition and direct pharmacological activation. (**a**) *Left panel* shows the increases in activity of AMPK-α1 and AMPK-α2 containing heterotrimers during hypoxia, as determined by immunoprecipitate kinase assay. *Right panel* shows the increased phosphorylation of acetyl CoA carboxylase during hypoxia in the presence and absence of compound C, the non-selective AMPK antagonist. (**b**) NAD(P)H autofluorescence of pulmonary arterial smooth muscle cells is increased by phenformin but not AICAR. (**c**) Effect of AICAR and phenformin on the activity of AMPK-α1 (*left panel*) and AMPK-α2 (*right panel*) containing heterotrimers, as determined by immunoprecipitate kinase assay

## 11.5 The Lkb1-AMPK Signalling Cascade and the Development of Hypoxic Pulmonary Hypertension

Consistent with our findings, Zhou and co-workers have demonstrated that acute hypoxia-induced pulmonary hypertension may be prevented and partially reversed by the non-selective AMPK antagonist compound C (Ibe et al. 2013). Moreover they suggest that AMPK activation promotes pulmonary arterial smooth muscle survival and thus proliferation during hypoxia by a dual mechanism. Briefly, it was suggested that activation of autophagy by AMPK-α1 reduced cell death and that reduced apoptosis resulted from AMPK-α2 activation. Contrary to this latter proposal, however, upregulation of mTORC2 signalling has been proposed to underpin smooth muscle proliferation and the

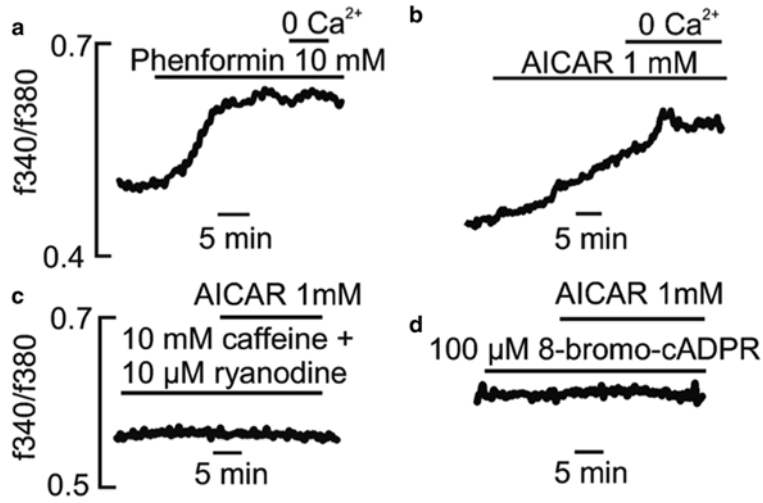


**Fig. 11.4** AMPK activation initiates cADPR-dependent calcium release from the sarcoplasmic reticulum via ryanodine receptors. Activation of AMPK by either phenformin (**a**) or AICAR (**b**) increases the FURA-2 fluorescence ratio in acutely isolated pulmonary arterial smooth muscle cells, in a manner that is abolished by prior block of ryanodine receptors (**c**) or cADPR (**d**)

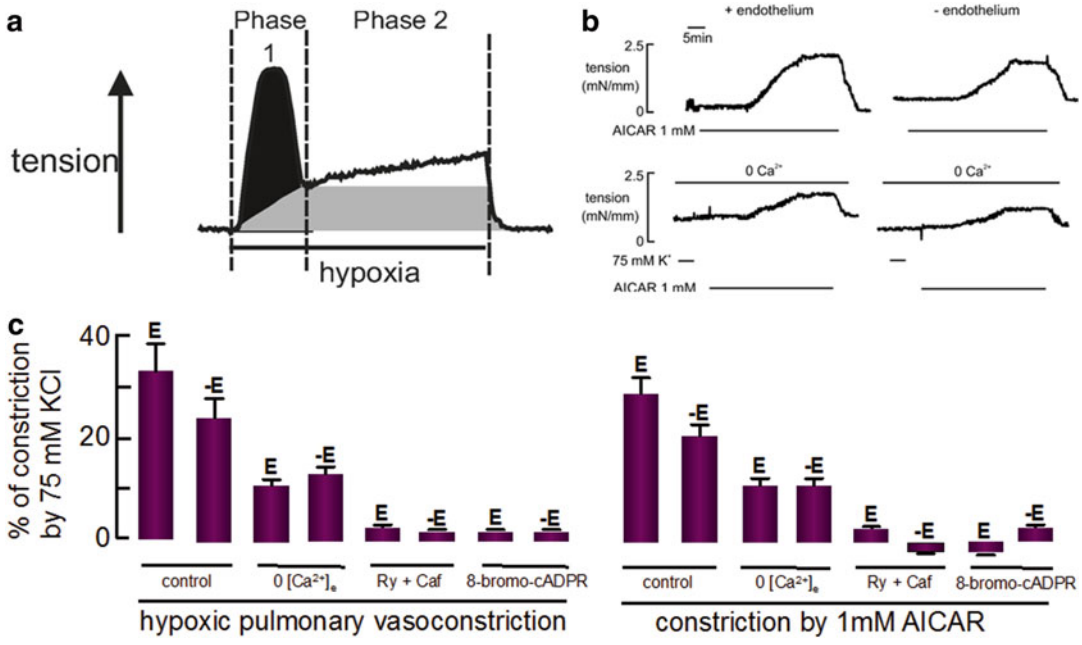


**Fig. 11.5** Hypoxia and AMPK activation induce pulmonary artery constriction by similar mechanisms. (**a**) Record of Phase 1 and Phase 2 of hypoxia-induced constriction of a rat pulmonary artery ring, indicating the contribution to constriction of two components of calcium release from the smooth muscle sarcoplasmic reticulum (*black and grey*) and 3rd component driven by the release of a vasoconstrictor from the pulmonary artery endothelium (*white*). (**b**) Constriction of a pulmonary artery ring by AMPK activation with AICAR, in the presence and absence of the endothelium, with and without extracellular calcium. (**c**) Comparison of hypoxic pulmonary vasoconstriction and constriction by AICAR following the indicated experimental interventions: removal of the endothelium (-E); removal of extracellular calcium (0[$Ca^{2+}$]$_e$); block of ryanodine receptors with caffeine and ryanodine; block of cADPR with 8-bromo-cADPR

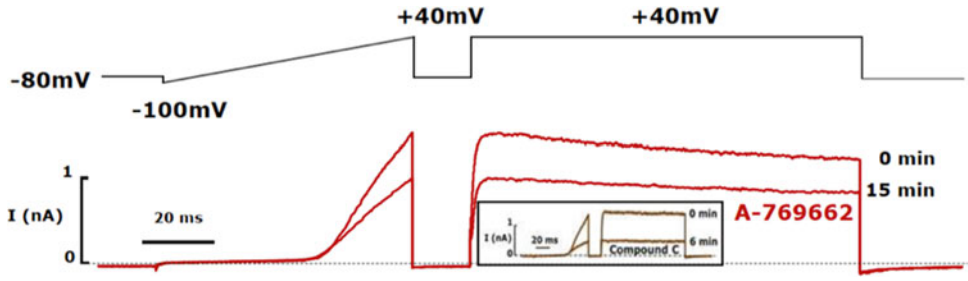


**Fig. 11.6** AMPK activation by A769662 inhibits Kv current in pulmonary arterial smooth muscle cells. The effect of AMPK activation by A769662 on $K_V$ currents recorded in acutely isolated pulmonary arterial smooth muscle cells. *Left*, current voltage relationship obtained by use of a ramp protocol between −100 mV and +40 mV, from a holding potential of −80 mV. *Right*, current activated by a voltage step to +40 mV from −80 mV. Insert shows confounding inhibition of Kv current by the AMPK antagonist compound C

progression of both idiopathic and hypoxic pulmonary arterial hypertension (Goncharov et al. 2014), by promoting smooth muscle cell survival in a manner, at least in part, dependent on down-regulation of AMPK and consequent activation of mTORC1. One possible explanation for these contrary findings could be that AMPK activation may be context-dependent and/or that the progression of pulmonary hypertension at different stages is governed by temporal fluctuations in AMPK activity.

## 11.6 Summary

We conclude that the inhibition of mitochondrial oxidative phosphorylation by acute hypoxia is coupled to pulmonary vasoconstriction through the LKB1-AMPK signalling pathway, which drives HPV by initiating and maintaining intracellular calcium release from the smooth muscle sarcoplasmic reticulum, promoting concomitant inhibition of the smooth muscle $K_V$ current and by initiating vasoconstrictor release from the pulmonary artery endothelium. Thereafter modulation of the LKB1-AMPK signalling pathway may determine the progression of pulmonary hypertension. Further detailed characterisation of the regulation and role of AMPK signalling in the pulmonary vasculature is therefore vital to our understanding of the progression HPV and pulmonary hypertension, and may provide greater insight into those tissue-specific responses that are key to oxygen homeostasis.

**Acknowledgements** The work described was supported by Programme Grants from the Wellcome Trust (81195), and the British Heart Foundation (29885).

## References

Archer SL, Huang J, Henry T, Peterson D, Weir EK (1993) A redox-based $O_2$ sensor in rat pulmonary vasculature. Circ Res 73:1100–1112

Bergofsky EH, Haas F, Porcelli R (1968) Determination of the sensitive vascular sites from which hypoxia and hypercapnia elicit rises in pulmonary arterial pressure. Fed Proc 27:1420–1425

Bradford JR, Dean HP (1894) The pulmonary circulation. J Physiol 16:34–158 25

Brown GC (1992) Control of respiration and ATP synthesis in mammalian mitochondria and cells. Biochem J 284:1–13

Buttigieg J, Zhang M, Thompson R, Nurse C (2006) Potential role of mitochondria in hypoxia sensing by adrenomedullary chromaffin cells. Adv Exp Med Biol 580:79–85, discussion 351–9

Cooper CE, Brown GC (2008) The inhibition of mitochondrial cytochrome oxidase by the gases carbon monoxide, nitric oxide, hydrogen cyanide and hydrogen sulfide: chemical mechanism and physiological significance. J Bioenerg Biomembr 40:533–539

Corton JM, Gillespie JG, Hawley SA, Hardie DG (1995) 5-aminoimidazole-4-carboxamide ribonucleoside. A specific method for activating AMP-activated protein kinase in intact cells? Eur J Biochem/FEBS 229:558–565

Dipp M, Evans AM (2001) Cyclic ADP-ribose is the primary trigger for hypoxic pulmonary vasoconstriction in the rat lung in situ. Circ Res 89:77–83

Dipp M, Nye PC, Evans AM (2001) Hypoxic release of calcium from the sarcoplasmic reticulum of pulmonary artery smooth muscle. Am J Physiol Lung Cell Mol Physiol 281:L318–L325

Dipp M, Thomas JM, Galione A, Evans AM (2003) A PO2 window for smooth muscle cADPR accumulation and constriction by hypoxia in rabbit pulmonary artery smooth muscle. Proc Physiol Soc 547P:C72

Duchen MR, Biscoe TJ (1992a) Mitochondrial function in type I cells isolated from rabbit arterial chemoreceptors. J Physiol 450:13–31

Duchen MR, Biscoe TJ (1992b) Relative mitochondrial membrane potential and $[Ca^{2+}]i$ in type I cells isolated from the rabbit carotid body. J Physiol 450:33–61

Duke HN, Killick EM (1952) Pulmonary vasomotor responses of isolated perfused cat lungs to anoxia. J Physiol 117:303–316

Emerling BM, Weinberg F, Snyder C, Burgess Z, Mutlu GM, Viollet B et al (2009) Hypoxic activation of AMPK is dependent on mitochondrial ROS but independent of an increase in AMP/ATP ratio. Free Radic Biol Med 46:1386–1391

Evans AM (2006) AMP-activated protein kinase and the regulation of $Ca^{2+}$ signalling in $O_2$-sensing cells. J Physiol 574:113–123

Evans AM, Dipp M (2002) Hypoxic pulmonary vasoconstriction: cyclic adenosine diphosphate-ribose, smooth muscle Ca(2+) stores and the endothelium. Respir Physiol Neurobiol 132:3–15

Evans AM, Mustard KJ, Wyatt CN, Peers C, Dipp M, Kumar P et al (2005) Does AMP-activated protein kinase couple inhibition of mitochondrial oxidative phosphorylation by hypoxia to calcium signaling in $O_2$-sensing cells? J Biol Chem 280:41504–41511

Evans AM, Hardie DG, Galione A, Peers C, Kumar P, Wyatt CN (2006) AMP-activated protein kinase couples mitochondrial inhibition by hypoxia to cell-specific $Ca^{2+}$ signalling mechanisms in oxygen-sensing cells. Novartis Found Symp 272:234–252, discussion 52–8, 74–9

Evans AM, Hardie DG, Peers C, Mahmoud A (2011) Hypoxic pulmonary vasoconstriction: mechanisms of oxygen-sensing. Curr Opin Anaesthesiol 24:13–20

Firth AL, Yuill KH, Smirnov SV (2008) Mitochondria-dependent regulation of Kv currents in rat pulmonary artery smooth muscle cells. Am J Physiol Lung Cell Mol Physiol 295:L61–L70

Gnaiger E, Lassnig B, Kuznetsov A, Rieger G, Margreiter R (1998) Mitochondrial oxygen affinity, respiratory flux control and excess capacity of cytochrome c oxidase. J Exp Biol 201:1129–1139

Goncharov DA, Kudryashova TV, Ziai H, Ihida-Stansbury K, DeLisser H, Krymskaya VP et al (2014) Mammalian target of rapamycin complex 2 (mTORC2) coordinates pulmonary artery smooth muscle cell metabolism, proliferation, and survival in pulmonary arterial hypertension. Circulation 129:864–874

Gowans GJ, Hawley SA, Ross FA, Hardie DG (2013) AMP is a true physiological regulator of AMP-activated protein kinase by both allosteric activation and enhancing net phosphorylation. Cell Metab 18:556–566

Hardie DG (2007) AMP-activated/SNF1 protein kinases: conserved guardians of cellular energy. Nat Rev Mol Cell Biol 8:774–785

Hawley SA, Selbert MA, Goldstein EG, Edelman AM, Carling D, Hardie DG (1995) 5′-AMP activates the AMP-activated protein kinase cascade, and $Ca^{2+}$/calmodulin activates the calmodulin-dependent protein kinase I cascade, via three independent mechanisms. J Biol Chem 270:27186–27191

Hawley SA, Boudeau J, Reid JL, Mustard KJ, Udd L, Makela TP et al (2003) Complexes between the LKB1 tumor suppressor, STRAD alpha/beta and MO25 alpha/beta are upstream kinases in the AMP-activated protein kinase cascade. J Biol 2:28

Hawley SA, Ross FA, Chevtzoff C, Green KA, Evans A, Fogarty S et al (2010) Use of cells expressing gamma subunit variants to identify diverse mechanisms of AMPK activation. Cell Metab 11:554–565

Heymans C, Bouckaert JJ, Dautrebande L (1930) Sinus carotidien et refléxes respiratoires. II. Influences respiratoires réflexes de l'acidose, de l'alcalose, de l'anhydride carbonique, de l'ion hydrogéne et de l'anoxémie: sinus carotidiens et échanges respiratoires dans les poumons et au dela poumons. Arch Int Pharmacodyn Ther 39:400–408

Ibe JC, Zhou Q, Chen T, Tang H, Yuan JX, Raj JU et al (2013) Adenosine monophosphate-activated protein kinase is required for pulmonary artery smooth muscle cell survival and the development of hypoxic pulmonary hypertension. Am J Respir Cell Mol Biol 49:609–618

Jones DP (1986) Intracellular diffusion gradients of $O_2$ and ATP. Am J Physiol 250:C663–C675

Kato M, Staub NC (1966) Response of small pulmonary arteries to unilobar hypoxia and hypercapnia. Circ Res 19:426–440

Leach RM, Robertson TP, Twort CH, Ward JP (1994) Hypoxic vasoconstriction in rat pulmonary and mesenteric arteries. Am J Physiol 266:L223–L231

Leach RM, Hill HM, Snetkov VA, Robertson TP, Ward JP (2001) Divergent roles of glycolysis and the mitochondrial electron transport chain in hypoxic pulmonary vasoconstriction of the rat: identity of the hypoxic sensor. J Physiol 536:211–224

Lejeune P, Vachiery JL, Leeman M, Brimioulle S, Hallemans R, Melot C et al (1989) Absence of parasympathetic control of pulmonary vascular pressure-flow plots in hyperoxic and hypoxic dogs. Respir Physiol 78:123–133

Lu W, Wang J, Shimoda LA, Sylvester JT (2008) Differences in STIM1 and TRPC expression in proximal and distal pulmonary arterial smooth muscle are associated with differences in $Ca^{2+}$ responses to

hypoxia. Am J Physiol Lung Cell Mol Physiol 295:L104–L113
Mills E, Jobsis FF (1972) Mitochondrial respiratory chain of carotid body and chemoreceptor response to changes in oxygen tension. J Neurophysiol 35:405–428
Naeije R, Lejeune P, Leeman M, Melot C, Closset J (1989) Pulmonary vascular responses to surgical chemodenervation and chemical sympathectomy in dogs. J Appl Physiol 66:42–50
Nisell O (1951) The influence of blood gases on the pulmonary vessels of the cat. Acta Physiol Scand 23:85–90
Oakhill JS, Steel R, Chen ZP, Scott JW, Ling N, Tam S et al (2011) AMPK is a direct adenylate charge-regulated protein kinase. Science 332:1433–1435
Owen MR, Doran E, Halestrap AP (2000) Evidence that metformin exerts its anti-diabetic effects through inhibition of complex 1 of the mitochondrial respiratory chain. Biochem J 348:607–614
Post JM, Hume JR, Archer SL, Weir EK (1992) Direct role for potassium channel inhibition in hypoxic pulmonary vasoconstriction. Am J Physiol 262:C882–C890
Remillard CV, Tigno DD, Platoshyn O, Burg ED, Brevnova EE, Conger D et al (2007) Function of Kv1.5 channels and genetic variations of KCNA5 in patients with idiopathic pulmonary arterial hypertension. Am J Physiol Cell Physiol 292:C1837–C1853
Robertson TP, Dipp M, Ward JP, Aaronson PI, Evans AM (2000) Inhibition of sustained hypoxic vasoconstriction by Y-27632 in isolated intrapulmonary arteries and perfused lung of the rat. Br J Pharmacol 131:5–9
Robertson TP, Ward JP, Aaronson PI (2001) Hypoxia induces the release of a pulmonary-selective, Ca(2+)-sensitising, vasoconstrictor from the perfused rat lung. Cardiovasc Res 50:145–150
Robertson TP, Mustard KJ, Lewis TH, Clark JH, Wyatt CN, Blanco EA et al (2008) AMP-activated protein kinase and hypoxic pulmonary vasoconstriction. Eur J Pharmacol 595:39–43
Robin ED, Theodore J, Burke CM, Oesterle SN, Fowler MB, Jamieson SW et al (1987) Hypoxic pulmonary vasoconstriction persists in the human transplanted lung. Clin Sci 72:283–287
Roy CS, Sherrington CS (1890) On the regulation of the blood-supply of the brain. J Physiol 11(85–158):17
Sommer N, Pak O, Schorner S, Derfuss T, Krug A, Gnaiger E et al (2010) Mitochondrial cytochrome redox states and respiration in acute pulmonary oxygen sensing. Eur Respir J 36:1056–1066
Steinberg GR, Kemp BE (2009) AMPK in health and disease. Physiol Rev 89:1025–1078
Tamas P, Hawley SA, Clarke RG, Mustard KJ, Green K, Hardie DG et al (2006) Regulation of the energy sensor AMP-activated protein kinase by antigen receptor and $Ca^{2+}$ in T lymphocytes. J Exp Med 203:1665–1670
Thompson RJ, Jackson A, Nurse CA (1997) Developmental loss of hypoxic chemosensitivity in rat adrenomedullary chromaffin cells. J Physiol 498:503–510
Thompson RJ, Buttigieg J, Zhang M, Nurse CA (2007) A rotenone-sensitive site and $H_2O_2$ are key components of hypoxia-sensing in neonatal rat adrenomedullary chromaffin cells. Neuroscience 145:130–141
Turner PJ, Buckler KJ (2013) Oxygen and mitochondrial inhibitors modulate both monomeric and heteromeric TASK-1 and TASK-3 channels in mouse carotid body type-1 cells. J Physiol 591:5977–5998
von Euler US, Liljestrand G (1946) Observations on the pulmonary arterial blood pressure in the cat. Acta Physiol Scand 12:301–320
Wang J, Shimoda LA, Sylvester JT (2004) Capacitative calcium entry and TRPC channel proteins are expressed in rat distal pulmonary arterial smooth muscle. Am J Physiol Lung Cell Mol Physiol 286:L848–L858
Waypa GB, Chandel NS, Schumacker PT (2001) Model for hypoxic pulmonary vasoconstriction involving mitochondrial oxygen sensing. Circ Res 88:1259–1266
Weissmann N, Ebert N, Ahrens M, Ghofrani HA, Schermuly RT, Hanze J et al (2003) Effects of mitochondrial inhibitors and uncouplers on hypoxic vasoconstriction in rabbit lungs. Am J Respir Cell Mol Biol 29:721–732
Wilson SM, Mason HS, Smith GD, Nicholson N, Johnston L, Janiak R et al (2002) Comparative capacitative calcium entry mechanisms in canine pulmonary and renal arterial smooth muscle cells. J Physiol 543:917–931
Woods A, Dickerson K, Heath R, Hong SP, Momcilovic M, Johnstone SR et al (2005) $Ca^{2+}$/calmodulin-dependent protein kinase kinase-beta acts upstream of AMP-activated protein kinase in mammalian cells. Cell Metab 2:21–33
Wyatt CN, Buckler KJ (2004) The effect of mitochondrial inhibitors on membrane currents in isolated neonatal rat carotid body type I cells. J Physiol 556:175–191
Xiao B, Sanders MJ, Underwood E, Heath R, Mayer FV, Carmena D et al (2011) Structure of mammalian AMPK and its regulation by ADP. Nature 472:230–233

# Organismal Responses to Hypoxemic Challenges

12

Robert S. Fitzgerald, Gholam A. Dehghani, and Samara Kiihl

**Abstract**

As a counterpoint to the volumes of beautiful work exploring how the carotid bodies (CBs) sense and transduce stimuli into neural traffic, this study explored one organismal reflex response to such stimulation. We challenged the anesthetized, paralyzed, artificially ventilated cat with two forms of acute hypoxemia: 10 % $O_2$/balance $N_2$ (hypoxic hypoxia [HH] and carbon monoxide hypoxia [COH]). HH stimulates both CBs and aortic bodies (ABs), whereas COH stimulates only the ABs. Our design was to stimulate both with HH (HHint), then to stimulate only the ABs with COH (COHint); then, after aortic depressor nerve transaction, only the CBs with HH (HHabr), and finally neither with COH (COHabr). We recorded whole animal responses from Group 1 cats (e.g., cardiac output, arterial blood pressure, pulmonary arterial pressure/and vascular resistance) before and after sectioning the aortic depressor nerves. From Group 2 cats (intact) and Group 3 cats (aortic body resected) we recorded the vascular resistance in several organs (e.g., brain, heart, spleen, stomach, pancreas, adrenal glands, eyes). The HHint challenge was the most effective at keeping perfusion pressures adequate to maintain homeostasis in the face of a systemic wide hypoxemia with locally mediated vasodilation. The spleen and pancreas, however, showed a vasoconstrictive response.

R.S. Fitzgerald (✉)
Departments of Environmental Health Sciences, The Johns Hopkins University Medical Institutions, Baltimore, MD 21205, USA

Departments of Physiology, The Johns Hopkins University Medical Institutions, Baltimore, MD 21205, USA

Departments of Medicine, The Johns Hopkins University Medical Institutions, Baltimore, MD 21205, USA
e-mail: rfitzger@jhsph.edu

G.A. Dehghani
Departments of Environmental Health Sciences, The Johns Hopkins University Medical Institutions, Baltimore, MD 21205, USA

S. Kiihl
Departments of Biostatistics, The Johns Hopkins University Medical Institutions, Baltimore, MD 21205, USA


C. Peers et al. (eds.), *Arterial Chemoreceptors in Physiology and Pathophysiology*, Advances in Experimental Medicine and Biology 860, DOI 10.1007/978-3-319-18440-1_12

The adrenals and eyes showed a CB-mediated vasodilation. The ABs appeared to have a significant impact on the pulmonary vasculature as well as the stomach. Chemoreceptors via the sympathetic nervous system play the major role in this organism's response to hypoxemia.

**Keywords**
Hypoxemia • Chemoreceptors • Organ vascular resistances

## 12.1 Introduction

Volumes of beautiful work have been done over the last 20–25 years exploring how the CBs and ABs work … cellular, subcellular, genetic mechanisms. We wondered if it might not be instructive and entertaining to reverse out of the reductionist mode to look at what stimulation of the carotid/aortic bodies do at the organ/systems level of the organism. We chose the feline model because its genome is reported to approximate the human genome more closely than any other mammal except for primates. For example, with respect to the α3 and α4 neuronal ACh receptor subunits, the cDNA sequences reveal 91 % and 93 % identities with the human respectively. And the deduced amino acid sequences show 96 % identities to the human for both subunits. For the β2 subunit the identity to human cDNA is 93 %, and amino acid sequence is 98 % identical.

A major stimulus to both the carotid and aortic bodies is, of course, hypoxia. A major challenge to the organism is to confront its cardiopulmonary system with a decrease in oxygen, the very molecule this system, provided by evolutionary progress, must capture from the environment and deliver to the mitochondria.

Many consider the CB the most important interoreceptor in the organism, and understandably so. For stimulation of the CB generates reflex responses in the respiratory, cardiovascular, endocrine, and renal systems. For example, increases in respiratory tidal volume and airway secretions, increases in cardiac output and systemic vasoconstriction, increases in plasma renin and ADH, and increases in fractional urinary and sodium excretion are just a few such responses.

The goal of our study was to determine the response to a hypoxemic challenge when both CBs and ABs were simultaneously sending increased neural activity to the nucleus tractus solitarii (NTS), when only the CBs were sending increased neural activity to NTS, when only the ABs were sending increased neural activity to NTS, and when neither chemoreceptor was sending increased neural activity to NTS.

To do so we used two forms of hypoxemia: (1) Hypoxic hypoxia (HH; ventilated on 10 % $O_2$, lowering $S_aO_2$ to ~45–47 %); (2) Carbon monoxide hypoxia (COH; ventilated on a mixture of CO and air mildly enriched with $O_2$ reducing $S_aO_2$ to ~45–47 %). We did this in three groups of cats.

Group 1 cats (n = 15) were initially intact; we tested cardiovascular systemic responses. Challenges were HHint and COHint. After transecting the aortic depressor nerves (aortic bodies resected) we repeated the protocol (HHabr and COHabr).

Group 2 cats (n = 5) were tested for the vascular resistances in several organs. They were completely intact. Challenges: HHint and COHint.

Group 3 cats (n = 5) had their bilateral aortic depressor nerves sectioned, eliminating the apparently major increase in neural activity to the NTS from the ABs; so challenges were HHabr and COHabr. Organ vascular resistances were again determined.

## 12.2 Materials and Methods for Group 1 Cats

1. Preparation: Anesthetized, paralyzed, artificially ventilated cat with tracheal cannula, catheters in both femoral arteries, right/left atria, pulmonary artery, left ventricle, flow probe around ascending aorta.
2. Agents: room air (r.a.), enriched with 30 % $O_2$; CO (initially 2 %, then 0.1 % in r.a.),
3. Assumptions: (1) Because CO stimulates only the ABs and not CBs had been demonstrated in previous studies (Fitzgerald and Traystman 1980; Lahiri et al. 1981), we assumed the same phenomenon in this study as well. (2) The major, if not exclusive, connection between the ABs and the NTS is via the aortic depressor nerves traveling juxtaposed to the vagus in the cat. This rests on observations from a previous study suggesting that during the COHabr challenge virtually all cardiovascular responses to CO had no detectable input from chemoreceptor action on the autonomic nervous system.
4. The schema below presents the experimental design based on characteristics of the CBs and ABs and showing chemoreceptor involvement

| Intact | | Aortic body denervated | |
|---|---|---|---|
| HH | COH | HH | COH |
| AB + CB | AB only | CB only | none |

5. Protocol: for Intact cat: (1) control (ctl for 5 min); (2) HHint for 15 min; (3) recovery/rest for 60 min; (4) ctl for 5 min; (5) COHint for 15 min. Hyperventilation on $O_2$ with $CO_2$ while transecting aortic depressor nerves.

   For Aortic Body Denervated cat (bilateral aortic depressor nerves had been transected) followed exactly the same chronology of events as for the intact cats.
6. Statistical Analysis: Within groups Repeated Measures ANOVA with an All Pairwise Multiple Comparison Procedure (Tukey Test) was used for both primary data and for normalized data. Between groups comparison analysis was made with Student's t Test…testing for significance between samples.

## 12.3 Materials and Methods for Groups 2, 3 Cats

1. Preparation: Anesthetized, paralyzed, artificially ventilated cats; five intact (int) and five with aortic depressor nerves sectioned (abr). Surgery and catheter placement was the same as in the Group 1 cats except for a catheter in the right femoral artery. This was advanced into the thoracic aorta for collecting a reference sample for microsphere measurements. Handling of the animals was the same as with the Group 1 animals except for the injection of the radiolabeled microspheres.
2. Agents: room air (r.a.), enriched with 30 % $O_2$; CO (initially 2 % then 0.1 % in r.a.); carbonized microspheres (diameter: 15 ± 3 μm labeled with scandium-46, strontium-85, tin-113, or cerium-141.
3. Assumptions: These were the same as with the Group 1 animals regarding what receptors are stimulated by CO, and the route of traffic from the aortic bodies to NTS.
4. Protocol: For both intact and aortic bodies denervated cats: (1) control (ctl) for 5 min; (2) HH for 15 min; (3) recovery/rest for 60 min; (4) ctl for 5 min; (5) COH for 15 min; (6) End of experiment. During the last minute of the control period and the last minute of the 15 min exposure period 3 mL of saline containing 0.2 mL of the sphere-containing solutions (~800,000 spheres) were injected into the left atrial appendage over a 20 s interval. Reference blood sample was taken with a constant flow Harvard pump for at least 90 s after injection.

   Blood Flow Equation: $Flow_T = (A_T/A_r) \times (Flow_r/wt) \times 100$, where FlowT is tissue blood

flow (mL/min per 100 g tissue), Flowr is withdrawal rate of reference sample (mL/min), AT and Ar are total tissue counts and total reference counts respectively, and Wt is weight of the organ of interest in grams. Further details of this methodology have been published (Fitzgerald et al. 2013a, b).

5. Statistical Analysis: The same methods were used with the data from these animals as were used with the Group 1 animals; mostly Repeated Measures ANOVA.

## 12.4 Results for Group 1 Cats (Before and After Aortic Nerve Cutting)

1. Stimulus: As mentioned above, one stimulus for the arterial chemoreceptors is hypoxemia. Hypoxic hypoxia (10 % $O_2$/balance $N_2$) provokes an increase in ventilation, whereas carbon monoxide does not…at least at the levels we used. With the use of this stimulus many factors can influence/modulate the effect *per se* of hypoxia on the cardiovascular system (Marshall 1994): e.g., lung volume, lung stretch receptor activity, status of the organism (sleep, anesthesia), $pH_a$ $P_aCO_2$. In this study the table below shows that we have had some success in eliminating at least some of these factors: our $pH_a$ $P_aCO_2$ after 15 min of hypoxia remain relatively unchanged from the control condition, and rather constant between challenges in both the intact and aortic body resected conditions. And since the animals were paralyzed and on a ventilator, the impact on the pulmonary stretch receptors was constant (Table 12.1)
2. Responses:
   (a) Figure 12.1a. Cardiac Output (C.O.). Here presented as % of its own control is the 15 min value to one of four hypoxemic challenges. Control values in mL/min for HHint (CB + AB, solid blocks) was 272; for HHabr (CB only, solid upright triangles) was 270; for COHint (AB only, solid downward triangles) was 280; for COHabr (none, solid diamonds) was 290. The C.O. in response to HHint (CB + AB) is significantly greater than the response to all other challenges; maximum is reached at 5 min (429 mL/min). And the C.O. in response to the HHabr (CBs only), with a maximum in the 5–7 min period of 381 mL/min, is significantly greater than during the COHint challenge from 3 to 10 min (ABs only); maximum of 390 mL/min at 15 min. The COHabr challenge did not significantly increase C.O. from the control value of 290 mL/min. The four traces differ significantly from each other from about 2–3 min to 10 min when HHabr and COHint become indistin-

**Table 12.1** Blood gas values for group 1 cats

| n = 15 | Intact | | | | |
|---|---|---|---|---|---|
| Condition | $pH_a$ | $P_aCO_2$ (mmHg) | $P_aO_2$ (mmHg) | $S_aO_2$ (%) | Hb (gm%) |
| Control | 7.44 ± 0.02 | 33.8 ± 1.2 | 170.1 ± 4.0 | 99.0 ± 0.4 | 8.4 ± 0.5 |
| HH (15 min) | 7.36 ± 0.02 | 36.5 ± 1.1 | 28.1 ± 2.0* | 43.7 ± 3.9* | 9.7 ± 0.6 |
| Control | 7.42 ± 0.01 | 35.8 ± 1.0 | 121.0 ± 5.1 | 100.0 ± 0.0 | 8.5 ± 0.5 |
| COH (15 min) | 7.41 ± 0.02 | 34.3 ± 1.1 | 130.0 ± 5.1 | 44.8 ± 2.5* | 9.0 ± 0.5 |
| | Aortic bodies resected | | | | |
| Control | 7.49 ± 0.01 | 33.1 ± 0.9 | 124.1 ± 4.0 | 99.3 ± 0.3 | 7.6 ± 0.5 |
| HH (15 min) | 7.38 ± 0.02 | 34.3 ± 1.1 | 33.0 ± 3.1* | 47.4 ± 4.0* | 8.3 ± 0.6 |
| Control | 7.43 ± 0.02 | 35.1 ± 0.8 | 128.0 ± 5.1 | 99.1 ± 0.4 | 7.0 ± 0.5 |
| COH (15 min) | 7.39 ± 0.02 | 32.4 ± 1.7 | 125.0 ± 4.1 | 40.2 ± 3.7* | 7.4 ± 0.5 |

*: $P \leq 0.05$

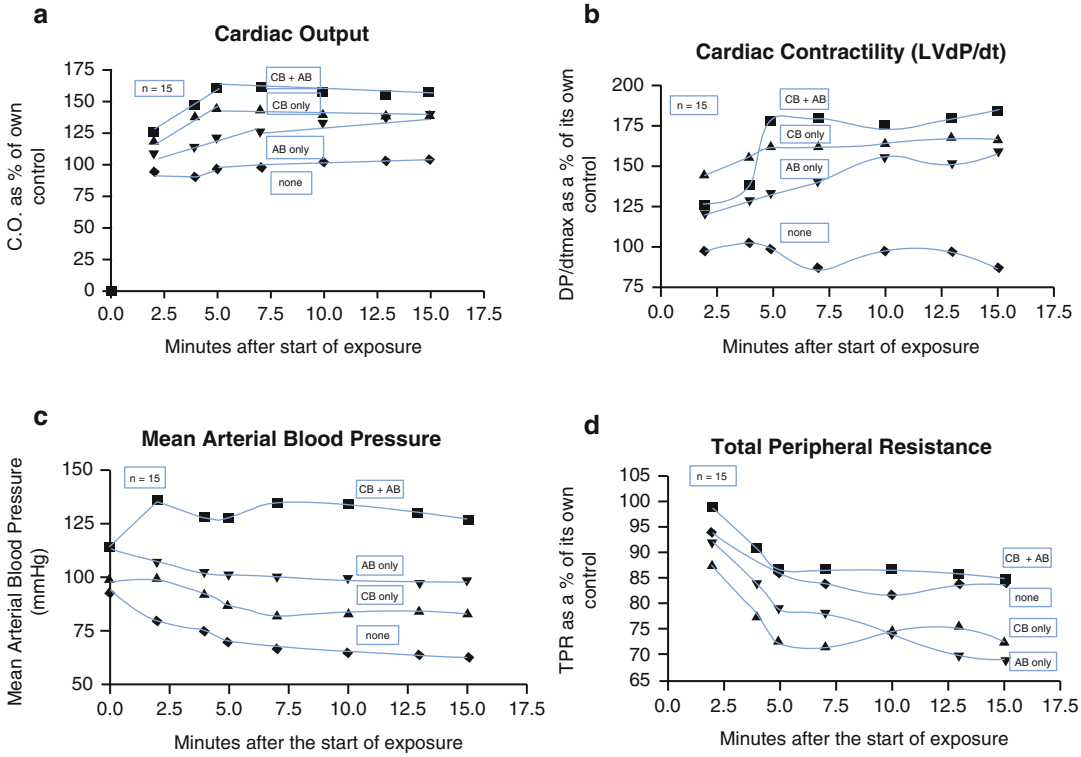


**Fig. 12.1** (**a**) Cardiac output (C.O.). (**b**) Left ventricular contractility (LVdP/dt). (**c**) Mean arterial pressure (MAP). (**d**) Total peripheral resistance (TPR)

guishable, but remain less than HHint. All three top traces are significantly greater than COHabr.

(b) Figure 12.1b. Left Ventricular Contractility (LVdP/dt). Again significant variability recommended that the values be normalized, each 15′ value of the challenge to its own control. The HHint challenges did not differ significantly (P = 0.055) from the HHabr challenge. Both differed significantly (P = 0.024) from the COHint challenge. Clearly these three challenges differed significantly from the COHabr challenge.

(c) Figure 12.1c. Mean Arterial Pressure (MAP). The responses to HHint (CB + AB) differs significantly from all others. The responses to HHabr (CB only) and to COHint (AB only) are statistically indistinguishable; but both decrease from their respective control values, and are significantly greater than the response to COHabr (none).

(d) Figure 12.1d. Total Peripheral Resistance (TPR). This variable decreased in response to all four hypoxemic challenges. The outcome is the result of several factors from the organismal-wide vasodilation in response to the systemic hypoxemia, to sympathetic nervous system output due to both chemo- and baroreceptor stimulation. Mean TPR over the seven time points (mmHg/mL/min) was calculated to be for the HHint challenge 0.385 resistance units (mmHg/mL/min), 0.325 units for COHint, 0.296 units for HHabr, and 0.270 units for COHabr. A Repeated Measures

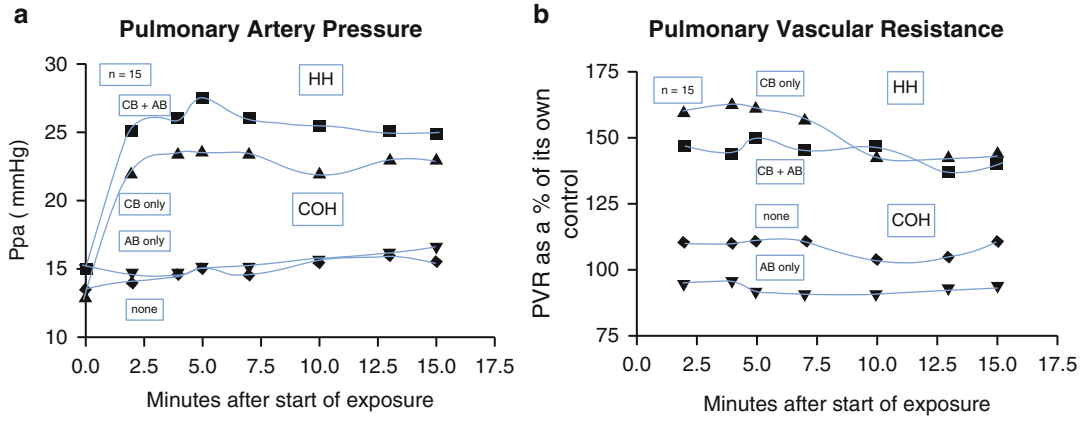


**Fig. 12.2** (**a**) Pulmonary artery pressure ($P_{pa}$). (**b**) Pulmonary vascular resistance (PVR)

**Table 12.2** Blood gas values for groups 2, 3 Cats

| n = 5 | Intact (int; Group 2) | | | | |
|---|---|---|---|---|---|
| Condition | $pH_a$ | $P_aCO_2$ (mmHg) | $P_aO_2$ (mmHg) | $S_aO_2$ (%) | Hb (gm%) |
| Control | 7.43 ± 0.02 | 32.5 ± 1.7 | 129.1 ± 13 | 100 | 10.2 ± 0.9 |
| HH(15 min) | 7.35 ± 0.04 | 34.0 ± 1.7 | 24.1 ± 2.0* | 36.2 ± 1.6* | 12.6 ± 0.7 |
| Control | 7.40 ± 0.09 | 34.0 ± 0.7 | 133.0 ± 12 | 100 | 11.6 ± 0.6 |
| COH(15 min) | 7.40 ± 0.03 | 34.2 ± 1.9 | 147.0 ± 13 | 39.7 ± 2.6* | 11.7 ± 0.6 |
| n = 5 | Aortic bodies resected (abr; Group 3) | | | | |
| Control | 7.42 ± 0.01 | 33.7 ± 0.7 | 136.1 ± 6 | 99.8 ± 0.2 | 10.6 ± 0.9 |
| HH(15 min) | 7.37 ± 0.03 | 32.8 ± 1.7 | 19.0 ± 1.0* | 32.3 ± 3.4* | 12.0 ± 0.6 |
| Control | 7.39 ± 0.02 | 32.9 ± 2.2 | 142.0 ± 6.1 | 100 | 10.8 ± 0.7 |
| COH(15 min) | 7.39 ± 0.01 | 31.9 ± 1.8 | 141.0 ± 10 | 35.8 ± 1.4* | 11.3 ± 0.5 |

*: $P \leq 0.05$

ANOVA on Ranks revealed the four values differed from each other ($P < 0.001$).

(e) Figure 12.2a. Pulmonary Artery Pressure ($P_{pa}$). The well known hypoxic pulmonary vasoconstrictor response in the face of alveolar hypoxia is clearly evident. But during COH exposure no significant change is present.

(f) Figure 12.2b. Pulmonary Vascular Resistance (PVR). PVR in response to HHint (CB + AB) which produced a greater Ppa showed a lower PVR, at least initially, than HHabr (CB only). During COHint (AB only) PVR was significantly lower than during COHabr (none).

## 12.5 Results for Group 2 (Intact), 3 (Aortic Nerves Transected) Cats

1. Stimulus: Again with .Groups 2 and 3 cats the table below shows that we have had some success in eliminating at least some of the modulating factors: our pHa, $P_aCO_2$ after 15 min of hypoxia remain relatively unchanged from the control condition, and rather constant between challenges in both the intact and aortic body resected animals. And since the animals were paralyzed and on a ventilator, the impact on the pulmonary stretch receptors was constant (Table 12.2).

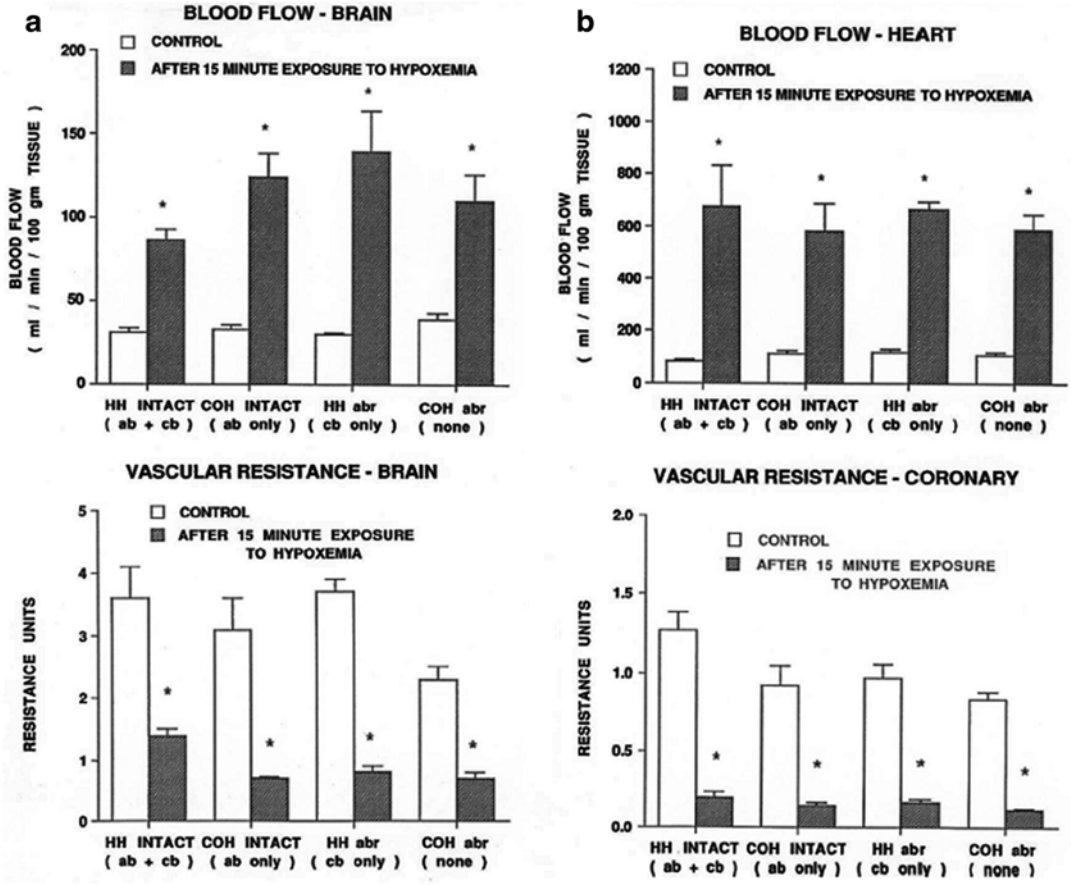


**Fig. 12.3** (**a**) Brain blood flow/vascular resistance. (**b**) Coronary blood flow/vascular resistance

2. Responses:
   (a) Figure 12.3a. Brain Blood Flow/Vascular Resistance. In Group 2 the Figure shows, during the HHint challenge flow increased about threefold; during COHint, roughly fourfold. In the Group 3 cats HHabr increased the flow more than fourfold, and in the COHabr condition, just less than threefold. RMANOVA analysis of vascular resistance values for the Group 2 cats showed that the two control values did not differ, nor did the 15 min exposure values. In the Group 3 cats the control values were different ($P<0.001$), while the 15 min exposure values did not differ. When the 15 min values for HH and for COH were normalized each to its own control, HHint was significantly higher than COHint (data not shown).
   (b) Figure 12.3b. Coronary Blood Flow/Vascular Resistance. Significant increases in Flow and with decreases in Resistance are easily seen. No significant differences among the changes could be found either in the initial or normalized data.
   (c) Figure 12.4a. Splenic Blood Flow/Vascular Resistance. The figure shows significant decreases in splenic Blood Flow for both Groups of cats as well as significant increases in vascular resistance for both Groups. Normalized value (data not shown) for the HHint challenge is significantly greater than that for the COHint challenge. But with the CB and

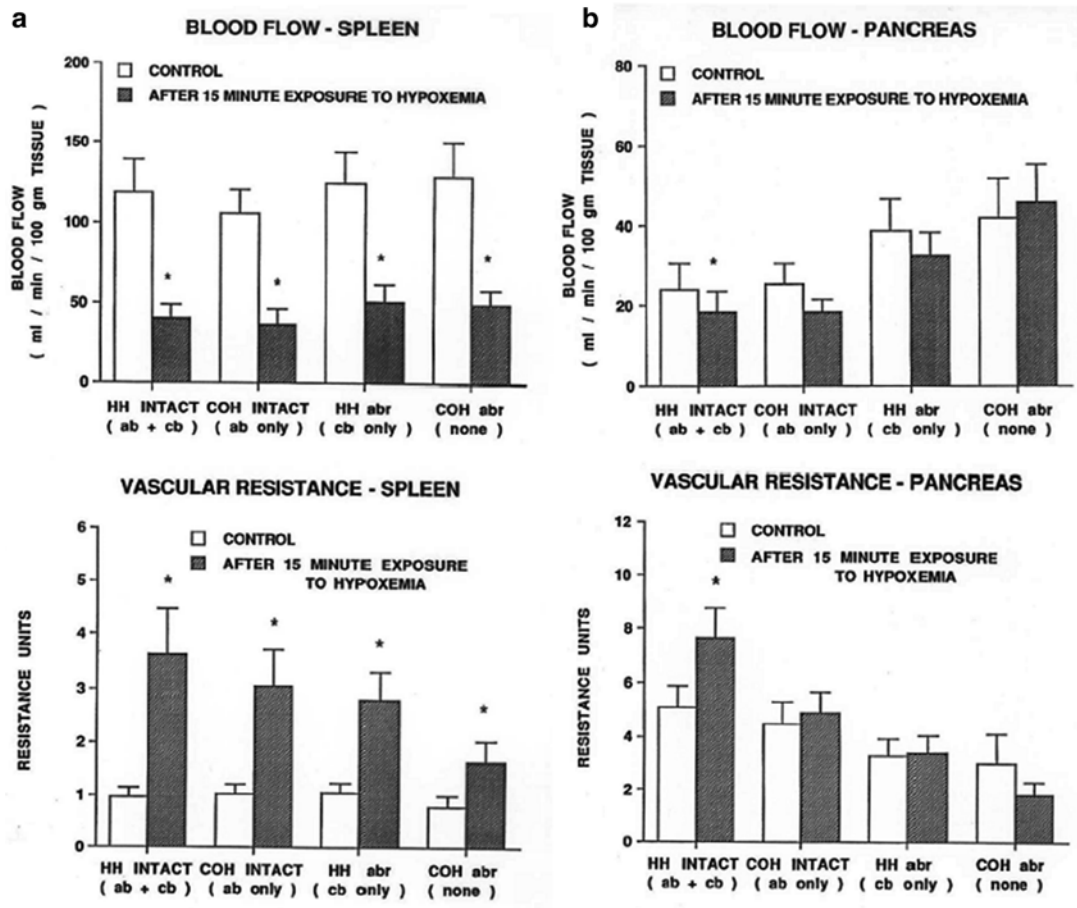


**Fig. 12.4** (**a**) Splenic blood flow/vascular resistance. (**b**) Pancreatic blood flow/vascular resistance

AB acting singly the increases in resistances do not differ.

(d) Figure 12.4b. Pancreatic Blood Flow/Vascular Resistance. The figure shows another instance of a vasoconstricting bed in the face of systemic hypoxemia. Blood flow decreased significantly in the Group 2 cats. Vascular resistance increased when both chemoreceptors were stimulated. And each acting alone offsets the vasodilation when compared to the result during the COHabr challenge (Group 3).

(e) Figure 12.5a. Stomach Blood Flow/Vascular Resistance. Blood flow increased significantly in three of the four conditions by 66 %, 58 %, and 90 % of their respective controls. The 36 % increase with only the ABs acting was not significant. The decrease in resistance during the HHint challenge was not significant whereas during the other challenges the decreases were significant.

(f) Figure 12.5b. Small Intestine Blood Flow/Vascular Resistance. The figure shows a significant 74 % increase in flow during the HHint challenge as well as a significant 36 % increase during the COHabr challenge. This is somewhat puzzling in terms of trying to identify chemoreceptor involvement. Resistance drops significantly when the CB alone was acting or when none was acting.

(g) Figure 12.6a. Adrenals Blood Flow/Vascular Resistance. Apparently unique

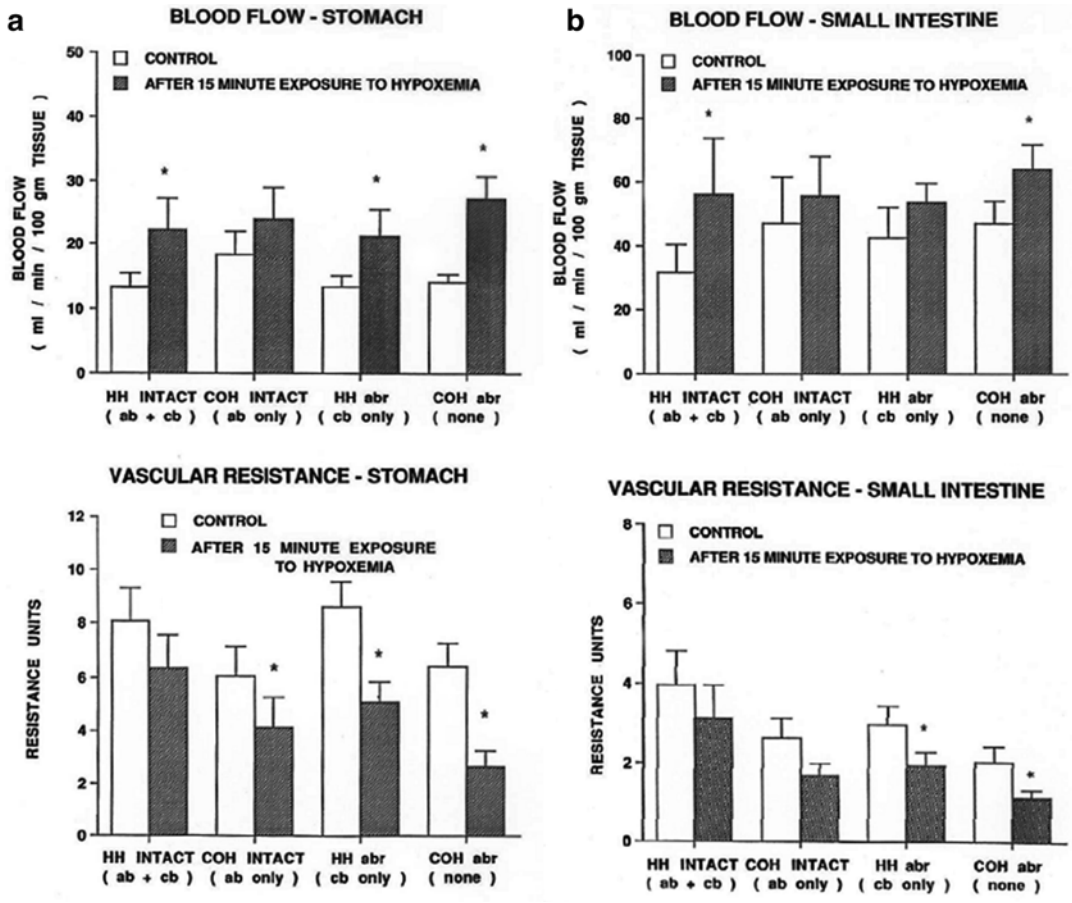


**Fig. 12.5** (**a**) Stomach blood flow/vascular resistance. (**b**) Small intestine blood flow/vascular resistance

to CB activity is both flow and resistance since the only significant changes occur when the CB is active, though the AB is also active during HHint. However, AB acting alone does not have any significant effect. This appears to be a unique effect of CB input; AB input seems negligible

(h) Figure 12.6b. Eyes Blood Flow/Vascular Resistance. The pattern for this vascular bed repeats what was seen above in the adrenals. CB influence is again unique to the response

Neither the kidney nor the liver showed a significant change in flow or resistance in the two Groups of cats. There was, of course, an increase in flow with a decrease in resistance; but they were inconsistent and not significant.

Diaphragmatic blood flow increased significantly in all four challenges: 979, 576, 570, and 350 %. Vascular resistance also decreased significantly in this non-working muscle. There were no significant differences within or among the four normalized 15 min values.

## 12.6 Discussion

Figure 12.1a. CARDIAC OUTPUT. The data suggest that C.O.'s increases depend on the arterial chemoreceptors, probably acting principally through the sympathetic nervous system (SNS).

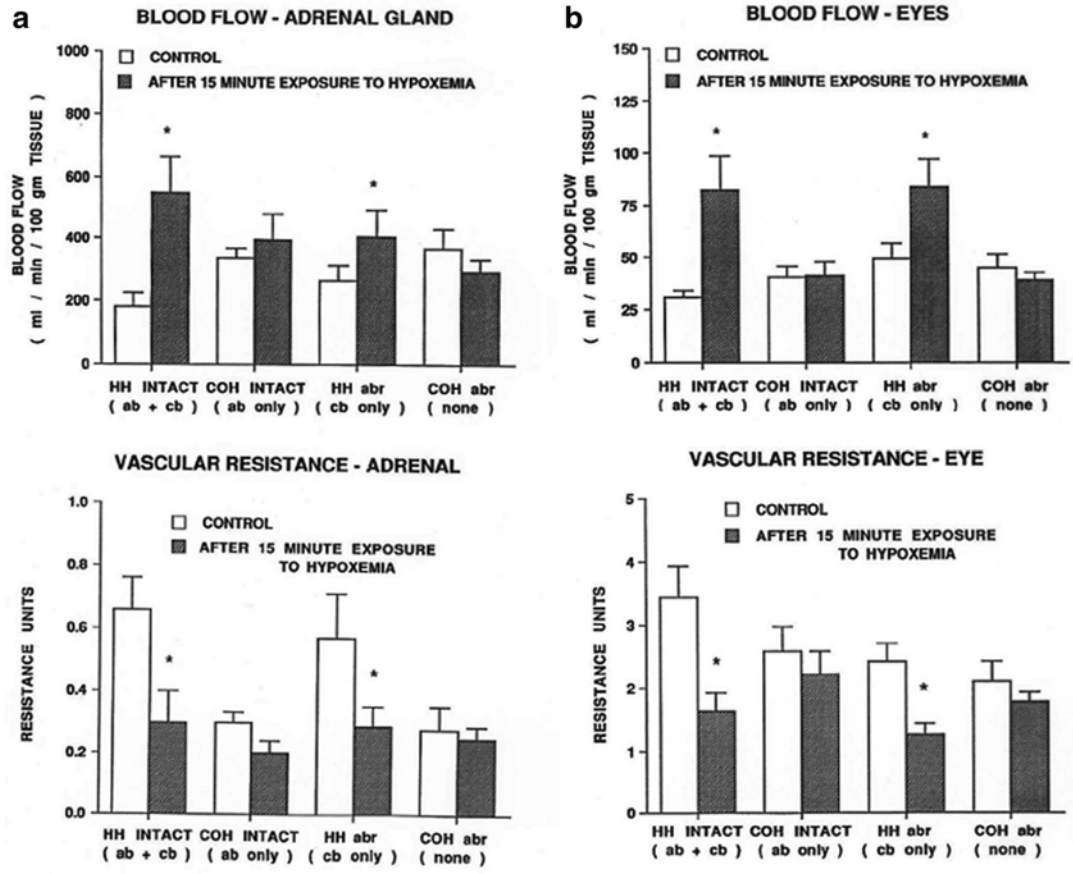


**Fig. 12.6** (**a**) Adrenals blood flow/vascular resistance. (**b**) Eyes blood flow/vascular resistance

However, the significant increase in arterial pressure would have increased the afterload on the left ventricle, stretching its fibers. This would increase stroke volume according to the Frank-Starling law of the heart.

Figure 12.1b. CARDIAC CONTRACTILITY. Results of left ventricular contractility (LVdP/dt) seem to confirm the results above, even though the variability was somewhat larger than expected. The four median values for the LVdP/dt responses were as follows: CB + AB, 137 % of control; CB only, 134 % of control; AB only, 125 % of control. The first two values were just short of significantly different ($P = 0.055$), whereas they both differed from the third ($P = 0.024$). Clearly, all three values differed significantly from COHabr (none) where no significant change occurred until the significant decrease at the end. Cardiac frequency is also a factor in C.O. But the mean frequency across the 15 min of exposure did not vary (RMANOVA); nor did this variable differ significantly among the four challenges, in beats/min: CB + AB showed 175; CB only showed 183; AB only showed 180; none showed 188. This last could have been higher due to input from the carotid sinus baroreceptors inhibition of the SNS being attenuated/removed by the lower blood pressure.

Figure 12.1c. MEAN ARTERIAL PRESSURE. The data suggest that both chemoreceptors are needed to elevate perfusion pressures to offset the system-wide vasodilation. Indeed the response to HHint (CB + AB) differs significantly from the other three. But the responses to COHint and HHabr are statistically indistinguishable, suggesting that each chemoreceptor's recruitment of

the SNS is about the same. Each, however, does differ from the COHabr challenge. And the fact that pressure in the intact preparations (HHint and COHint) is higher than in the abr preparations (HHabr and COHabr) suggests that aortic mechanisms have a role in maintaining normal blood pressures.

Figure 12.1d. TOTAL PERIPHERAL RESISTANCE. Data suggests input from both chemoreceptors to vasoconstrict systemically overrides the attenuating input from both baroreceptors. COHint generated 0.325 units, suggesting the action of the aortic mechanisms with the carotid sinus baroreceptors provided a more powerful vasoconstrictor action than during the HHabr challenge which generated 0.296 units, where the CBs and carotid baroreceptors, but no aortic mechanisms were inputting to the sympathetic neural output. The COHabr challenge generated 0.270 units. Here only the carotid baroreceptors were freeing up the SNS to increase output.

Figure 12.2a. PULMONARY ARTERIAL PRESSURE. Clearly alveolar hypoxia (HH) provokes the well-known hypoxic vasoconstrictor response (HPVR), elevating the perfusion pressure (Ppa). Other studies have shown that a stimulated carotid body tends to vasodilate the pulmonary bed. And Fig. 12.2b clearly shows that aortic body stimulation vasodilates the pulmonary bed. The higher increase in Ppa during HHint is probably due to the larger increase in C.O. than during the HHabr challenge. The HPVR would be the same in both challenges. With COH there is no HPVR. The slow, small, but significant rise (10–15 min) during the COHint challenge is presently unexplained.

Figure 12.2b. PULMONARY VASCULAR RESISTANCE. AB stimulation during both HH and COH challenges seems to influence pulmonary vascular resistance. With the HH challenges PVR with CB + AB is lower than with CB only. And with the COH challenges the PVR during COHint (AB only) is lower than during COHabr (none). A test (RMANOVAR) of the several time points shows that CB + AB is significantly less than CB only ($P = 0.003$). And AB only is less than none ($P = 0.001$). Arterial chemoreceptor input into pulmonary vascular control has been reported previously (deB Daly and deB Daly 1957; Fitzgerald et al. 1992; Levitzky 1979; Levitzky et al. 1977; Wilson and Levitzky 1989).

Figure 12.3a. BRAIN. Blood flow/vascular resistance exhibit significant increases in the flow and decreases in the resistance. Whether chemoreceptors influence this vascular bed or not remains controversial. Normalizing each response to its respective control value shows that HH response (~42 % of control) in the Group 2 cats was significantly larger than was the response (~23 % of control) to the COH challenge. This could result from some CB-generated sympathetic nervous system (SNS)-mediated vasoconstriction. But C.O. was larger during HHint than during COHint; arterial pressure was also higher. Autoregulation of the bed could be a possibility. Normalizing the 15 min values to their controls (data not shown) suggests that the operation of the CB and AB is more effective in overcoming the organism-wide vasodilation than the operation of CB and AB singly; these two normalized values do not differ.

Figure 12.3b. HEART. Data suggest the chemoreceptors have little to no significant impact on this organ's vasculature during the hypoxemic challenges. This is consistent with the findings of Marshall and Metcalfe (1990). The increased afterload due to increased arterial pressure during HHint could increase oxygen demand and account for the increased flow with decreased resistance.

Figure 12.4a. SPLEEN. Data suggests a very strong influence of the chemoreceptors on the SNS control of the spleen's vascular bed. The most significant reduction in blood flow occurs during the HH challenge in the Group 2 cats. The increased resistance is significantly greater than during the COHint challenge. This latter response does not differ significantly from the HH challenge in the Group 3 cats. But this latter response is significantly greater than that to the COHabr challenge.

Figure 12.4b. PANCREAS. The only significant changes in flow and resistance occurred during the HHint challenge with both AB and CB acting in concert. Yet this effect on the SNS had to have been attenuated by the baroreceptor input,

increased because of the elevated arterial blood pressure. Each set of chemoreceptors acting singly was able to offset the systemic vasodilation.

Figure 12.5a. STOMACH. The response to HHint suggests that CB and AB acting in concert can offset the systemic wide hypoxemic induced vasodilation, whereas each acting on its own cannot. Normalized response to HHint (~77 % of control) does not differ from the normalized response to COHint (~64 % of control), but is significantly greater than the normalized response to HHabr (~54 % of control). This suggests that possibly the ABs act more powerfully in this bed than do the CBs.

Figure 12.5b. SMALL INTESTINE. The small intestine undergoes a significant increase in blood flow (~76 % above control) during the HHint challenge. But vascular resistance is maintained in both the HHint and COHint challenges, but not during the HHabr challenge. This suggests that the CB + AB stimulation and the AB stimulation of the SNS can offset the systemic vasodilation in this bed. However, baroreceptor activity reduction during COHint might have helped produce the effect. Weissman et al. (1976) produce similar data from the cat; i.e., no change. And again our data are consistent with Marshall and Metcalfe (1990) in the rat. Stimulating the CBs of the normoxic cat also increased resistance (Little and Oberg 1975).

Figure 12.6a. ADRENALS. The significant reduction in resistance is also found in the normalized values (data not shown). During the HHint challenge the decrease in resistance might have been facilitated by the increased baroreceptor output attenuating SNS output. Results are again consistent with the data of Marshall and Metcalfe (1990).

Figure 12.6b. EYES. Pattern in this bed reproduces that of the adrenal bed, CB producing a vasodilation. Both beds' response seems counterintuitive in that stimulation of the CB produces an increase in SNS output, a vasoconstrictive result is the usual outcome. But the pulmonary vasculature is another instance of a CB-mediated vasodilatation (cf. Levitzky et al. 1977; Levitzky 1979; Wilson and Levitzky 1989; Fitzgerald et al. 1992, Fitzgerald et al. 2013a, b).

DIAPHRAGM: Local tissue hypoxia was the controlling factor. These data correspond to flow and conductance data in rats (Marshall and Metcalfe 1990).

Marshall and Metcalfe (1989) reported a significant drop in renal conductance and blood flow in their cats. Weissman et al. (1976), however, did report a small but significant increase in renal resistance in their hypoxia-challenged cats. The liver response was somewhat surprising since Alvarez and de Alvarez (1988) reported CB stimulation provoked a sharp release of liver glucose elevating both hepatic venous and arterial concentrations

## 12.7 Summary and Conclusions

This preparation, when confronted with the hypoxemic challenge, seemed to generate responses critically dependent on the two arterial chemoreceptors, CBs and ABs, stimulating the SNS via the NTS. Cardiac output was much greater when both were involved (HHint) than when either one, the other, or neither was stimulated. But baroreceptor influence cannot be disregarded. The response of cardiac output, for example, would probably have been greater if arterial pressure would have been held constant. But the increase in pressure acted to attenuate the SNS output via the baroreceptors. Additionally one cannot forget that the SNS would also act to promote the release of catecholamines from the adrenals which would help offset the system-wide hypoxemia-induced vasodilation.

1. The data seem to point out the heterogeneous nature of the CB-generated SNS output to the various organs and their behavior in the presence of systemic hypoxemia.
2. Changes in pressures, flows, vascular resistances are larger when both CBs and ABs are working in concert.
3. There also seem to be in this preparation several roles played by the ABs…dilating pulmonary vasculature, more dominant in controlling stomach and small intestine vasculature.

**Acknowledgement** The authors gratefully acknowledge the support of the National Institutes of Health (NHLBI; HL 0-50712-13) for this study.

## References

Alvarez R, de Alvarez E (1988) Carotid sinus receptors participate in glucose homeostasis. Respir Physiol 72:347–360

deB Daly IB, deB Daly MB (1957) The effects of stimulation of the carotid body chemoreceptors on pulmonary vascular resistance in the dog. J Physiol Lond 137:436–446

Fitzgerald RS, Traystman RJ (1980) Peripheral chemoreceptors and the cerebral vascular response to hypoxemia. Fed Proc 39:2674–2676

Fitzgerald RS, Dehghani GA, Sham JSK, Shirahata M, Mitzner WA (1992) Peripheral chemoreceptor modulation of the pulmonary vasculature in the cat. J Appl Physiol 73:20–29

Fitzgerald RS, Dehghani GA, Kiihl S (2013a) Autonomic control of the cardiovascular system in the cat during hypoxemia. Auton Neurosci Basic Clin 174:21–30

Fitzgerald RS, Dehghani GA, Kiihl S (2013b) Autonomic regulation of organ vascular resistances during hypoxemia. Auton Neurosci Basic Clin 177:181–193

Lahiri S, Mulligan E, Nishino T, Mokashi A, Davies RO (1981) Relative responses of aortic body and carotid body chemoreceptors to carboxyhemoglobinemia. J Appl Physiol 50:580–586

Levitzky MG (1979) Chemoreceptor stimulation and hypoxic pulmonary vasoconstriction in conscious dogs. Respir Physiol 37:151–160

Levitzky MG, Newell JC, Krasney JA, Dutton RE (1977) Chemoreceptor influence on pulmonary blood flow during unilateral hypoxia in dogs. Respir Physiol 31:345–356

Little R, Oberg B (1975) Circulatory responses to stimulation of the carotid body chemoreceptors in the cat. Acta Physiol Scand 93:34–51

Marshall JM (1994) Peripheral chemoreceptors and cardiovascular regulation. Physiol Rev 74:543–594

Marshall JM, Metcalfe JD (1989) Analysis of factors that contribute to cardiovascular changes induced in the cat by graded levels of systemic hypoxia. J Physiol 412:429–448

Marshall JM, Metcalfe JD (1990) Effects of systemic hypoxia on the distribution of cardiac output in the rat. J Physiol 426:335–353

Weissman ML, Rubinstein EH, Sonnenschein RR (1976) Vascular responses to short-term systemic hypoxia, hypercapnia, and asphyxia in the cat. Am J Physiol 230:595–601

Wilson LB, Levitzky MG (1989) Chemoreflex blunting of hypoxic pulmonary vasoconstriction is vagally mediated. J Appl Physiol 66:782–791

# 13 Effect of Lipopolysaccharide Exposure on Structure and Function of the Carotid Body in Newborn Rats

Z.R. Master, K. Kesavan, A. Mason, M. Shirahata, and Estelle B. Gauda

**Abstract**

Premature infants are vulnerable to infections and have unstable breathing (Di Fiore JM, Martin RJ, Gauda EB, Respir Physiol Neurobiol 189:213–222, 2013). Inflammation adversely modifies carotid body (CB) structure and chemosensitivity in adult animals. We determined the effect of inflammation on CB structure and function in newborn rat pups. Pups were given LPS (0.1 mg/kg; IP) or saline at postnatal day 2 (P2). At P9-10 (1 week after exposure) various studies were done including ventilation, carotid sinus nerve (CSN) activity and histology. Using whole body plethysmography, we found that LPS exposure attenuates the change in interbreath (IBI) interval in response to changes in oxygen tension 1 week after LPS exposure. The response of the CSN to hypoxia was attenuated and delayed in onset in LPS-treated animals as compared to controls. Histological sections of the CB were examined for inflammatory cells at P4 (n = 7) and P9-12 (n = 6). After LPS exposure, only mast cells were seen, often encircling the CB, and clustered within the CSN as it entered the CB. Mast cells per section (mean ± SEM) were higher at P9-12 in LPS (7.4 ± 1.5) vs saline (5.4 ± 1.4) exposed animals (p = 0.04). Surprisingly, more mast cells were seen at 7–10 days vs 48 h after LPS exposure. In a newborn model of inflammation, breathing is altered which is associated with changes in structure and function of the carotid body.

Z.R. Master • K. Kesavan
A. Mason • E.B. Gauda (✉)
Department of Pediatrics, Johns Hopkins University School of Medicine, Baltimore, MD 21205, USA
e-mail: egauda@jhmi.edu

M. Shirahata
Department of Environmental Health Sciences, Johns Hopkins University, Baltimore, MD, USA



C. Peers et al. (eds.), *Arterial Chemoreceptors in Physiology and Pathophysiology*, Advances in Experimental Medicine and Biology 860, DOI 10.1007/978-3-319-18440-1_13

**Keywords**

Carotid body (CB) • Lipopolysaccharide (LPS) • Mast cells • Premature infants

## 13.1 Introduction

The CB is a multimodal sensor which is excited by decreases in oxygen tension, pH, and glucose and increases in carbon dioxide and temperature in the arterial blood. Excitation of the CB increases neural activity of the CSN and the information is integrated in the nucleus tractus solitarii in the brainstem leading to increases in respiration, heart rate, blood pressure and sympathetic tone. Since the input from the CB rapidly modifies ventilation in response to changes in oxygen and carbon dioxide tension, hypersensitivity or hyposensitivity of the CB to changes in arterial gases destabilizes breathing (reviewed in Gauda et al. 2004, 2007). The CB continues to develop structurally and functionally during the first several weeks after birth. Hyperoxic exposure during development causes CB hypoplasia, CSN axon degeneration, and diminished glomus cells oxygen sensitivity, all contributing to impaired hypoxic ventilatory response (reviewed in Bavis et al. 2013). LPS exposure (intravenously or topically) increases expression of pro-inflammatory cytokines, causes infiltration of immature cells associated with disruption of glomic lobules and increased intralobular connective tissue in the adult cat CB 5 h after exposure (Fernandez et al. 2008). Thus, we hypothesize that early ex utero exposures such as inflammation could modify the development of the CB leading to sustained alterations in structure and function contributing to unstable breathing.

## 13.2 Methods

Sprague-Dawley newborn rat pups exposed to LPS were used as a translational model for apnea of prematurity in the setting of early postnatal inflammation (previously described in Gauda et al. 2013). Experiments were approved by the Animal Care and Use Committee at the Johns Hopkins University and were performed in accordance with the NIH 'Guide for the care and use of laboratory animals' of the U.S. Department of Health and Human Services 85-23, 2011. Newborn rat pups were intraperitoneally (IP) injected with LPS (0.1 mg/kg, IP; E. Coli 0111:B4; Millipore) or saline on P2. At P9-12, a separate group of animals were used to assess (1) the ventilatory responses at different levels of oxygen tension, (2) the hypoxic sensitivity of the CB by recording from the CSN (in vitro) using a superfused preparation, and (3) the histological changes within the CB.

### 13.2.1 Ventilation

Newborn rat pups (n = 12 for each saline and LPS group) were given LPS (0.1 mg/kg; IP) or saline at P2. At P9-10 days of age, 1 week after LPS exposure ventilation was measured using a whole body plethysmography in freely moving, unsedated animals. Chamber temperature was monitored and maintained within 30–32 °C. Breathing frequency was measured for 2 min during normoxia (21% $O_2$/Bal $N_2$) and hypoxia (15 % $O_2$/Bal $N_2$) and for 90 s during hyperoxia (100 % $O_2$). Data were analyzed for Interbreath interval (IBI) measured in seconds using Acqknowledge Data Requisition and Analysis Software.

### 13.2.2 Carotid Sinus Nerve Activity

Preparation of the CSN recording was done as previously described (Igarashi et al. 2002). At P9-10 days of age, 1 week after LPS (n = 8) or saline (n = 9) exposure, rat pups were anesthetized

with urethane (1.25 mg/kg, IP), the carotid bifurcation was quickly removed, and with the aid of a dissecting microscope, the CB with the CSN was cleaned and exposed while being continuously superfused with Krebs (in mM: 120 NaCl, 4.7 KCl, 1.2, $CaCl_2$ 1.8 mM, Mg $SO_4 \cdot 7H_2O$, 1.2, $Na_2HPO_4$, 22 $NaHCO_3$, and 11.1 Glucose) solution equilibrated with 95 % $O_2$/5 % $CO_2$. Afterwards the CSN was placed in the suction pipette, and the recording chamber was bubbled with 95 % $O_2$/5 % $CO_2$ enclosed by a plastic chamber maintained at 35–36 °C. During the hypoxic challenge, Krebs was switched to the solution equilibrated with 95 % $N_2$/5 % $CO_2$, and the gas to the recording chamber was changed to 95 % $N_2$/5 % $CO_2$. Data were initially expressed as impulse per second, and normalized between groups by expressing the percent change in activity from baseline which was obtained during hyperoxia. Data were analyzed using single-factor ANOVA; $p<0.05$ was considered statistically significant.

### 13.2.3 Histology

At P9-10 days of age, 1 week after LPS or saline exposure, animals were anesthetized with isoflurane and then intracardially infused with phosphate buffered saline (pH 7.4; 11.9 mM phosphates, 137 mM sodium chloride and 2.7 mM potassium chloride) to flush the blood, followed by fixation with 4 % paraformaldehyde. The bifurcation of the carotid artery, CB, superior cervical ganglion, nodose, petrosal and jugular ganglia were removed *en bloc*, post-fixed in 4 % paraformaldehyde for 2 h and cryoprotected in 30 % sucrose in PBS overnight. Tissue was embedded in Tissue-Tek OCT media and stored at −80 °C until further processing. Some carotid bodies were embedded in plastic (*JB*-4 embedding kit; Polysciences) and cut on a microtome to obtain 4 μm sections for better identification of cellular morphology. Ten μm frozen sections were cut on a cryostat (Leica cryostat CM 3050S), and sections were stained with toluidine blue to identify mast cells. Additional tissue sections were stained with cresyl violet to identify other immune cells. The number of mast cells was counted per section, and 3–5 sections were analyzed per animal. Low and high power images were captured using Olympus BX51TF microscope with DP70 software and number of mast cells was counted by a person who was unaware of the treatment groups. The mean number of mast cells/section was determined for each animal. Differences between the number of mast cells for the LPS and saline exposed animals at 48 h and 7–10 days after the exposure was determined using Students unpaired t-test.

## 13.3 Results

### 13.3.1 Ventilation

During exposure to normoxia (21 % $O_2$) and hyperoxia (100 %) the mean IBI for the group was different between the two treatments. While the IBI during hypoxia (15 % $O_2$) did not differ between the groups, LPS animals had a small but consistently longer IBI during normoxia but a shorter IBI during hyperoxia compared to saline treated controls (Table 13.1). In LPS treated animals, IBI did not change until the lowest level of oxygen exposure (hyperoxia: 0.41 ± 0.06, normoxia: 0.40 ± 0.05, and hypoxia: 0.33 ± 0.03; LPS/hyperoxia vs. LPS/hypoxia $p<0.001$). However, saline treated animals had a graded reduction in IBI when transitioning from hyperoxia (0.47 ± 0.56) to normoxia (0.41 ± 0.05) to hypoxia (0.33 ± 0.03); $p<0.001$ for saline/hyperoxia vs saline/hypoxia and $p<0.01$ for saline/hyperoxia vs saline/normoxia.

**Table 13.1** Ventilatory changes expressed as IBI during normoxia, hyperoxia and hypoxia

| Treatment group | Normoxia | Hyperoxia | Hypoxia |
|---|---|---|---|
| Saline-exposed | 0.40 ± 0.17 | 0.46 ± 0.26* | 0.33 ± 0.08 |
| LPS-exposed | 0.40 ± 0.16 | 0.42 ± 0.17 | 0.33 ± 0.09 |

n = 12, LPS and saline treated animals; Data (sec) presented as Mean ± SE, *p-value < 0.05, Saline vs LPS

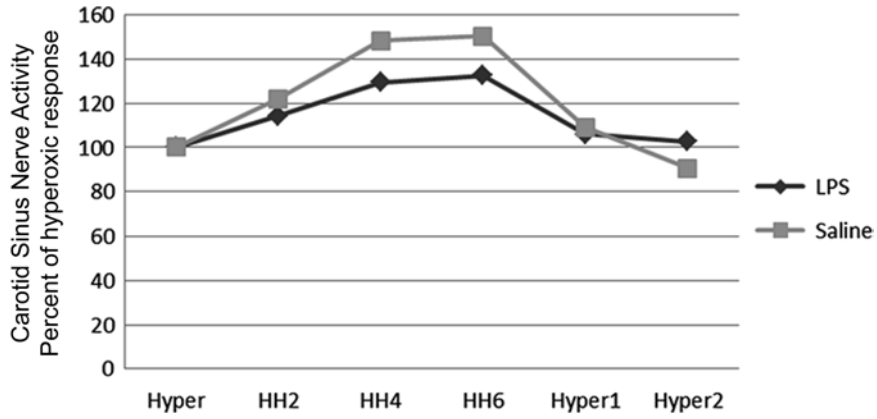


**Fig. 13.1** Graph representing CSN activity for LPS and saline animals expressed as the % of Hyperoxia. Legends: *Hyper* initial hyperoxia, *HH2* 2 min of hypoxia, *HH4* 4 min of hypoxia, *HH6* 6 min of hypoxia, *Hyper1* 1 min of hyperoxia, *Hyper2* 2 min of hyperoxia

### 13.3.2 Carotid Sinus Nerve Activity

As shown in Fig. 13.1, the response of the CSN to hypoxia was attenuated and delayed in onset in LPS-treated animals as compared to saline treated animals.

On-response: Transitioning the superfusate from hyperoxia to hypoxia, in preparations from saline treated animals, CSN activity increased by 50 %, ($p<0.05$; ANOVA) while in preparations from LPS exposed animals, CSN activity did not change ($p=0.8$; ANOVA).

Off-response: Transitioning the superfusate from hypoxia to hyperoxia, in preparations from saline treated animals, CSN activity had returned to control levels by 2 min of hyperoxia. Thus, CSN activity, in preparations from saline treated animals, decreased from a maximum of 150 % of control (HH6) by 2 mins after returning to hyperoxia whereas CSN activity did not change in response to hyperoxia in preparations from LPS treated animals.

### 13.3.3 Histology

LPS exposure at P2 disrupts CB architecture at P9 as shown in Fig. 13.2 using frozen and plastic sections stained with toluidine blue. The CB in LPS exposed animals appeared to have less cellular density as compared to tissues sections of the CB from saline treated littermates.

In order to study the immune cells, frozen sections were stained with toluidine blue and cresyl violet. As shown in Fig. 13.3, only mast cells were found in the vicinity of the CB and no additional immune cells were identified on sections stained with cresyl violet. At P9-12, mast cells per section ($M \pm SEM$) was greater in sections from animals exposed to LPS ($7.4 \pm 1.5$) vs those exposed to saline ($5.4 \pm 1.4$; $p=0.04$). More mast cells were seen at 7–10 days vs 48 h after LPS exposure.

## 13.4 Discussion

Premature birth is associated with immaturity and instability of the respiratory network and intrauterine inflammation/infection is a major inciting event that precipitates premature delivery. A subset of premature infants will have persistent breathing instability that is greater than what would be predicted based on the infants' postconceptional age. While we know that *acute* inflammation/infection is associated with increase in the number and severity of apneic episodes in premature infants, the long term consequences of previous infection on respiratory

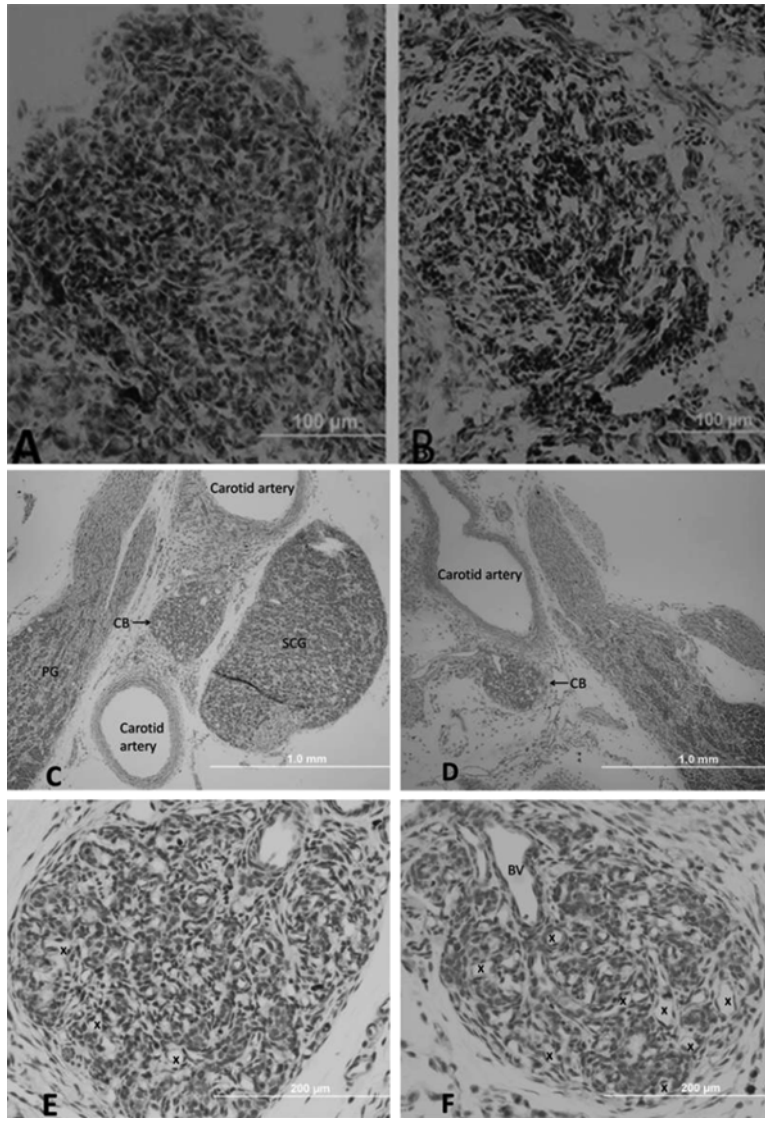


**Fig. 13.2** LPS treatment at P2 disrupts histology of the carotid CB at P9. Thick (10 micron) frozen sections from saline (**A**) and LPS (**B**) treated animals. Sections from LPS treated animals is less dense appearing with more clear spaces (x) than that from Saline treated animals. Low power images of the tissue block of thin (4 microns) plastic sections of the CB from LPS (**C**) and Saline (**D**) exposed animals. High power image of thin sections stained with toluidine blue (**E**, **F**) gives the appearance of less cellular density in tissue sections from LPS (**E**) vs Saline exposed animals (**F**). *SCG* is superior cervical ganglion, *PG* is petrosal ganglion, *BV* is blood vessel

control has not been explored. Our preliminary data show that 1 week after LPS exposure at P2, newborn rats at P9 have (1) blunted breathing and CSN nerve responses to graded changes in oxygen tension, (2) disrupted histological architecture of the carotid body, and (3) increase in mast cell infiltration within the CB.

In adult animals, LPS and inflammatory cytokines acutely influences the CB function (Fernandez et al. 2008). Little is known about the effects of LPS exposure during the neonatal period during which CB is still undergoing maturation. In our experiments, we measured CB function using CSN activity, and in saline treated

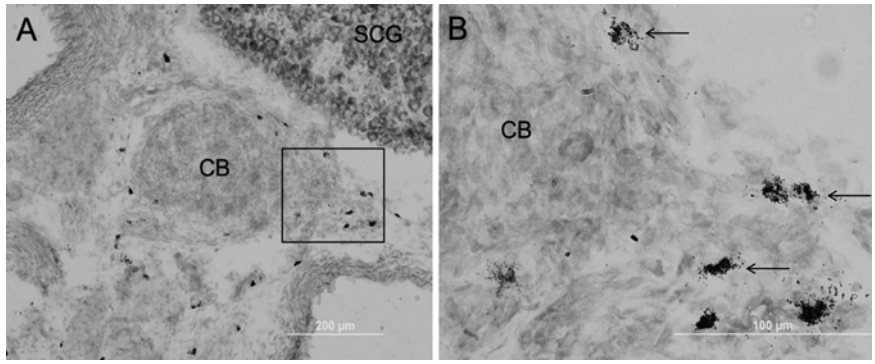


**Fig. 13.3** Photomicrographs of frozen *CB* sections stained with toluidine blue. Mast cells (*Black arrows*) are often seen encircling the *CB* (**A**) and associated with the CSN as it enters the *CB* (**B** magnified area in the *inset*)

animals, the CSN activity increases promptly with hypoxic and decreases with hyperoxic exposure. In contrast, in LPS treated animals, the response of CSN to hypoxia was delayed and attenuated. In rat models of Parkinson disease, in whom LPS is given systemically or intranigrally, the development of dopaminergic (DA) neurons in substantia nigra and serotonergic (5-HT) neurons in the dorsal raphe is inhibited (Wang et al. 2009). In adult animals, intranigral injection of LPS causes selective degeneration of DA neurons (Herrera et al. 2005). While chemoafferents contain DA, type I cells in the CB contain DA and 5-HT, theoretically making them more vulnerable to cellular toxicity induced by LPS, preliminary data (not presented) suggest that type 1 cells are not significantly reduced in our model. Thus, the altered responses of CSN activity that we observed is not likely related to a reduction in type 1 cells.

Nevertheless, we observed that LPS disrupts the histology of the CB. Increased infiltration of polymorphonuclear cells in the vascular bed and tissue parenchyma of adult rat CB was seen after the LPS exposure (Fernandez et al. 2008). In our newborn rat model, LPS induced-inflammation produces only mast cell infiltration in the CB without evidence of macrophage or neutrophil infiltration. It is well known that mast cells release pro and anti-inflammatory cytokines, growth factors, tryptase, histamine and other neuromodulators which modify the microenvironment and sensitivity of sensory neurons. Blair et al. 1997 using cell culture techniques showed that tryptase from mast cells has angiogenic properties and leads to augmentation of capillary growth and proliferation of human dermal microvascular endothelial cell tube formation. In thin plastic sections from LPS exposed animals, we observed more blood vessels as compared to saline-exposed animals (preliminary data not shown). Histamine is present in abundance in the Type I cells of rat CB and its release is enhanced during hypoxia (Koerner et al. 2004). Mast cells are multifunctional cells of the immune lineage. Since mast cells are present in the CB and the number increases with LPS exposure, mast cells may be contributing to tissue injury, repair and/or neuromodulation of hypoxic chemosensitivity of the CSN. Further studies are needed to characterize role of mast cells on CB chemosensitivity. One speculation is that mast cells may be modifying the sensitivity of the CSN to hypoxia, similar to their role in other sensory systems such as pain (Diest et al. 2012).

While we have described the effects of inflammation on CSN activity, we understand that breathing instability observed in the rat pups is not solely due to altered CB function. Other important contributors include, the central circuits affected by systemic inflammation and LPS induced lung inflammation leading to alteration in lung capacity and lung mechanics (Hakansson et al. 2012). Inflammation is likely contributing

to metaplasticity of multiple organs that control breathing. Our data suggest that early postnatal exposure to inflammation may adversely alter CB structure and function, contributing to breathing instability. We speculate that a subset of premature infants with persistent and protracted apnea presenting as intermittent hypoxia (Martin et al. 2011) may be secondary to changes in hypoxic chemosensitivity of the CB induced by previous inflammatory episode.

## References


Bavis RW, Fallon SC, Dmitrieff EF (2013) Chronic hyperoxia and the development of the carotid body. Respir Physiol Neurobiol 185:94–104

Blair RJ, Meng H, Marchese MJ, Ren S, Schwartz LB, Tonnesen MG (1997) Human mast cells stimulate vascular tube formation. J Clin Invest 99–11:2691–2700

Di Fiore JM, Martin RJ, Gauda EB (2013) Apnea of prematurity – perfect storm. Respir Physiol Neurobiol 189:213–222

Diest SA, Stanisor OI, Boeckxstaens GE, Jonge WJ, Wijngaard RM (2012) Relevance of mast cell-nerve interactions in intestinal nociception. Mol Basis Dis 1822(1):74–81

Fernandez R, Gonzalez S, Rey S, Cortes PP, Maisey KR, Reyes EP, Larrain C, Zapata P (2008) Lipopolysaccharide-induced carotid body inflammation in cats: functional manifestations, histopathology and involvement of tumor necrosis factor-alpha. Exp Physiol 93(7):892–907

Gauda EB, McLemore GL, Tolosa J, Marston-Nelson J, Kwak D (2004) Maturation of peripheral arterial chemoreceptors in relation to neonatal apnoea. Semin Neonatol 9:181–194

Gauda EB, Cristofalo E, Nunez J (2007) Peripheral arterial chemoreceptors and sudden infant death syndrome. Respir Physiol Neurobiol 157:162–170

Gauda EB, Shirahata M, Mason A, Pichard LE, Kostuk EW, Chavez-Valdez R (2013) Inflammation in the carotid body during development and its contribution to apnea of prematurity. Respir Physiol Neurobiol 185:120–131

Hakansson HF, Smailagic A, Brunmark C, Miller-Larsson A, Lal H (2012) Altered lung function relates to inflammation in an acute LPS mouse model. Pulm Pharmacol Ther 25:399–406

Herrera AJ, Tomas-Camardiel M, Venero JL, Cano J, Machado A (2005) Inflammatory process as a determinant factor for the degeneration of substantia nigra dopaminergic neurons. J Neural Transm 112:111–119

Igarashi A, Amagasa S, Horikawa H, Shirahata M (2002) Vecuronium directly inhibits hypoxia neurotransmission of the rat carotid body. Anesth Analg 94:117–122

Koerner P, Hesslinger C, Schaefermeyer A, Printz C, Gratzi M (2004) Evidence for histamine as a transmitter in rat carotid body sensor cells. J Neurochem 91:493–500

Martin RJ, Wang K, Koroglu O, Di Fiore J, Prabha KC (2011) Intermittent hypoxic episodes in preterm infant: do they matter? Neonatology 100(3):303–310

Wang S, Yan JY, Lo YK, Carvey PM, Ling Z (2009) Dopaminergic and serotoninergic deficiencies in young adult rats prenatally exposed to the bacterial lipopolysaccharide. Brain Res 1265:196–204

# Hypoxic Ventilatory Reactivity in Experimental Diabetes

14

M. Pokorski, M. Pozdzik, J. Antosiewicz, A. Dymecka, A. Mazzatenta, and C. Di Giulio

**Abstract**

Diabetes, apart from generalized neuropathy and microangiopathy, involves tissue hypoxia, which may drive chronic proinflammatory state. However, studies on the ventilatory control in diabetes are sparse and conflicting. In this study we examined the function and morphology of diabetic carotid bodies (CBs). Diabetes was evoked in Wistar rats with streptozotocin (70 mg/kg, i.p.). The acute hypoxic ventilatory responses (HVR) to 12 and 8 % $O_2$ were investigated in conscious untreated rats after 2 and 4 weeks in a plethysmographic chamber. CBs were dissected and subjected to morphologic investigations: (1) electron transmission microscopy for ultrastructure and (2) laser scanning confocal microscopy to visualize the microvascular bed in sections labeled with the lectin Griffonia simplicifolia-I (GSI), an endothelial cell marker, and fluorescein isothiocyanate (FITC). All findings were referenced to the normal healthy rats. We found that diabetes distinctly dampened the HVR. At the ultrastructural level, the diabetic CB displayed proliferation of connective tissue and neovascularization deranging the interglomal structure, and lengthening the $O_2$ diffusion path from capillaries to chemoreceptor cells. The chemoreceptor cells remained largely unchanged. The endothelial cell labeling

M. Pokorski (✉)
Laboratory of Electrophysiology, Clinical Research Center, Murayama Medical Center, 2-37-1 Gakuen, MusashiMurayama City, Tokyo 208-0011 Japan

Public Higher Medical Professional School, 68 Katowicka St., 45-060 Opole, Poland

Institute of Psychology, Opole University, Opole, Poland
e-mail: m_pokorski@hotmail.com

M. Pozdzik • J. Antosiewicz • A. Dymecka
Medical Research Center, Polish Academy of Sciences, Warsaw, Poland

A. Mazzatenta • C. Di Giulio
Department of Neurosciences, Imaging and Clinical Science, University 'G. d'Annunzio' of Chieti–Pescara, Via dei Vestini 31, 66100 Chieti, Italy
e-mail: amazzatenta@yahoo.com



C. Peers et al. (eds.), *Arterial Chemoreceptors in Physiology and Pathophysiology*, Advances in Experimental Medicine and Biology 860, DOI 10.1007/978-3-319-18440-1_14

confirmed the intensive angiopathy and the induction of microvessel growth. We conclude that diabetes hampers the chemical regulation of ventilation due to remodeling of CB parenchyma, which may facilitate chronic hypoxia and inflammation in the organ.

**Keywords**
Angiopathy • Carotid body • Chemoreceptor cells • Diabetes • Endothelial cells • Hypoxic ventilatory response • Microvasculature • Neovascularization

## 14.1 Introduction

Diabetes entails the long-term complications related to generalized neuropathy (Ellenberg 1958), or occasionally isolated such as phrenic neuropathy (White et al. 1992), and microangiopathy (Devaraj et al. 2007). The disease also is underlain by enhanced oxidative stress, due mostly to hyperglycemia-driven increase in free radicals (Sano et al. 1998) and enhanced circulating levels of proinflammatory cytokines and acute phase proteins, exemplified by interleukins 1β and IL-6, and by C-reactive protein (Donath and Shoelson 2011). There are reasons to presume that the stimulating ventilatory responses could be blunted in diabetes due to metabolic and physical strain they are involved with. In addition, the ventilatory responses might be affected by dysfunction of the carotid body, a paired sensory organ of neuronal crest origin which generates such responses. The chemosensing ability of the carotid body has undoubtedly to do with its being highly vascularized and having an extremely high blood flow (Clarke et al. 1993). However, function of the hypoxic chemoreflex in diabetes is a contentious issue; the reports vary from respiratory arrest due to carotid body denervation-like state (Kageyama et al. 1985) through blunting (Weisbrod et al. 2005; Yamazaki et al. 2002), or having the responses unaffected (Saiki et al. 2005). The functional and morphological status of the diabetic carotid body remains by far conjectural. The issue is further confounded by the glomus cells being considered a combined sensor of hypoxia and hypoglycemia, sharing the same mechanism of excitation, consisting of $Ca^{2+}$ influx, $K^+$ channel inhibition, and plasma membrane depolarization (López-Barneo 2003). The hyperventilatory response that follows carotid chemoreceptor excitation may be considered a mitigator of the potential hypoxic neuronal damage, as hyperventilation increases delivery of oxygen with breathing.

To clarify the diabetes-associated changes in the chemical regulation of ventilation, acute ventilatory responses to hypoxia were compared between streptozotocin-induced diabetic and normal conscious rats. To get insight into the plausible parenchymal changes in the carotid body caused by diabetes, the organs were dissected and subjected to a two-pronged morphological examination aimed at the ultrastructure and microvasculature.

## 14.2 Methods

The study conforms to the good publishing practice in physiology (Persson and Henriksson 2011) and the protocol was accepted by the 4th Local Ethics Committee on Animal Experiments in Warsaw, Poland (Permit 24/2012). The study consisted of two separate parts: functional and morphological; with a total of 15 adult, male, Wistar rats used, weighing 294.1 ± 2.2(SE) g. All animals were kept on a 12/12 h light/dark cycle, were fed with a standard animal chow, and had water *ad libitum*. There were 12 rats; each subjected to sequential ventilatory studies in three experimental conditions: control, 2 weeks' diabetes, and 4 weeks' untreated

diabetes. The last condition included only six animals, since the other six were used for another study ramification dealing with diabetic pharmacotherapy, herein unreported. Ventilation ($V_E$, l/min, BTPS) and its responses to acute 3-min hypoxic poikilocapnic tests were measured breath-by-breath in conscious rats in a plethysmographic chamber (PLY3223; Buxco Electronix Inc., Wilmington, NC). The method was based on the pressure difference between the experimental and reference chamber measured with a differential pressure transducer. A bias flow at a rate of 2.5 l/min was employed between the tests to remove the $CO_2$ build-up from the chamber.

### 14.2.1 Protocol of Functional Studies

The animals were allowed to acclimatize to the chamber condition for 20–30 min. Then, the gas in the chamber was switched randomly to 8 % $O_2$ or 12 % $O_2$ in $N_2$. The chamber gas equilibrium was achieved in 40 s and the test started, with 15–20 min intervals in ambient air between tests. After the control hypoxic tests, each animal was injected with streptozotocin (70 mg/kg, i.p.) to induce diabetes. Diabetes was left untreated and the hypoxic tests were repeated after 2 and 4 weeks. The dose of streptozotocin above outlined was chosen as being placed in-between of the range usually used to induce experimental diabetes in rodents, ranging from 50 to 75 mg/kg (Eleayu et al. 2013; Saiki et al. 2005) for the intraperitoneal administration in the rat. The streptozotocin mode mimics neuropathic and angiopathic complications of human diabetes, with hyperglycemia similar to either type 1 or type II diabetes (Eleayu et al. 2013). Streptozotocin-induced diabetes also is associated with enhanced oxidative stress, due mostly to hyperglycemia-driven increase in free radicals (Sano et al. 1998).

Data were processed off-line and are shown at 30 s time marks of the hypoxic ventilatory course; each point being an average of a 10 s bin preceding the time mark. The analysis focused on three time marks of greatest interest along the ventilatory response profile: baseline (0 s), peak response (30 s), and end-test fall-off (180 s).

Three diabetic rats, after the completion of functional studies, and three additional healthy rats were anesthetized with α-chloralose and urethane (35 and 800 mg/kg, i.p., respectively), tracheostomized, and the carotid bodies were surgically exposed in the neck and prepared for a two-pronged morphological study.

### 14.2.2 Transmission Electron Microscopy

A fixative mixture consisting of 2 % paraformaldehyde and 2.5 % glutaraldehyde in 0.1 M cacodylate buffer, pH 7.4 was perfused through the left ventricle of the heart to euthanize the animals. Carotid bodies were dissected and post-fixed in the same fixative for 24 h at 4 °C. In some instances carotid bodies were rapidly dissected *in vivo* and immediately immersed in the fixative. The animal was then euthanized by an overdose of the anesthetics. The tissue was incubated in 2 % $OsO_4$ and after graded dehydration in ethyl alcohol and propylene oxide, it was embedded in Spurr resin. Ultrathin serial sections of 50 nm were cut, mounted on copper grids, and examined randomly under with a JEM 1200Ex transmission electron microscope (Jeol, Tokyo, Japan).

### 14.2.3 Laser Scanning Confocal Microscopy

Carotid bodies were dissected from healthy and diabetic rats. Specimens were routinely processed into paraffin. Paraffin sections (30 μ thick) were stained with hematoxylin-eosin and labeled with Griffonia simplicifolia I (GSI) lectin, a tracer that selectively binds to the endothelial cells in microcirculatory vessels, conjugated with fluorescein isothiocyanate (FITC) (Sigma-Aldrich, St. Louis, MO). Slides were examined under a laser scanning confocal microscope, with a 40× or 63× objective, coupled with Laser Pix 2000 software (BioRad, Hemel Hempstead, Hertfordshire, UK).

On average, 10–15 fields per carotid body were randomly sampled. A spatial reconstruction of the carotid body capillary bed was made. Specimens were examined layer-by-layer every 0.5 μ downward in a given area of intact volume of thick tissue sections, yielding a stack of 20–50 digital images of successive optical sections. Green fluorescence was excited with argon (488 nm) laser to visualize the capillary configuration. The parameter describing the capillary frequency was number of capillaries per unit section (averaged from 5 square areas of 275×275 μ). Capillary luminal diameter was measured morphometrically. In addition, capillary geometry, tortuosity, and formation of new microvessels were assessed by observation.

Functional ventilatory and morphological ordinal data (number of capillaries and their lumen's diameter) were compared statistically between diabetic and healthy carotid bodies with the Wilcoxon signed-rank test; significant changes were defined as $p<0.05$. Morphological cardinal data in photomicrographs presenting the ultrastructure and the capillary profile in carotid body parenchyma, related to diabetic changes, were determined by visual inspection by at least two independent observers to determine reproducibility and intraobserver variability.

## 14.3 Results and Discussion

The rats showed clear diabetic symptoms from about 10 days on after streptozotocin injection (blood glucose levels were tested every 5 days), with polyuria and polydipsia, apathy, decreased locomotion, and skin and hair coat consisting of increased grayness and easily epilated hair. The baseline data 4 weeks into the untreated diabetes are summarized in Table 14.1. Severe hyperglycemia was accompanied by hypoxia and a drop in resting ventilation.

The hypoxic ventilatory response was classically biphasic, stimulatory/inhibitory, in both healthy and diabetic conditions (Fig. 14.1a, b). The peak ventilatory stimulation occurred 30 s from the hypoxic test onset, with a gradual ventilatory fall-off thereafter. The response to hypoxia was distinctly dampened in diabetes already after 2 weeks, the dampening tended to deepen after another 2 weeks. The magnitude of peak hyperventilation in response to 12 % hypoxia, on average, amounted to about 80 % of that present in the healthy condition. Hypoxic hyperventilation was expectedly accentuated in response to the stronger 8 % hypoxic stimulus. The magnitude of the inhibitory effect on the hypoxic responses of diabetes was here similar to that observed in 12 % hypoxia (Table 14.1).

The functional findings of the present study were that untreated diabetes appreciably impaired the hypoxic ventilatory responses. The impairment is in agreement with other studies in both animals (Rasche et al. 2010; Hein et al. 1994) and humans (Weisbrod et al. 2005; Nishimura et al. 1989), although there also are sporadic reports showing no effects of diabetes on hypoxic ventilation (Saiki et al. 2005). The underlying mechanisms of the impairment are unclear. Generalized diabetic neuropathy, causing dysfunction of the respiratory muscle pump, may factor in the ventilatory impairment. There are reports showing that the hypoxic ventilatory increase is dampened in diabetic patients even without autonomic neuropathy, although the dampening is enhanced in the setting of the accompanying neuropathy (Montserrat et al. 1985).

The role of deficient respiratory muscle system in the diabetic-related impairment of ventilatory responses may be, to an extent, supported by a decrease in resting ventilation in diabetes observed in the present study, but it is at variance with a well maintained (Hein et al. 1994) or even enhanced (Nishimura et al. 1989) hyperventilatory response to severe hypercapnia, which we also confirmed in the present study (data not shown). The hypoxic ventilatory drive also seems well preserved in diabetic autonomic neuropathy (Calverley et al. 1982). Therefore, the respiratory system seems able to meet the strenuous mechanistic ventilatory challenge. The resolution of the issue of the role of deficient respiratory muscle pump, as opposed to defunct hypoxic drive emanating from the carotid body chemoreceptors, in hypoventilatory responses requires alternative study designs in which respiration would be

**Table 14.1** Baseline data 4 weeks after induction of diabetes compared with the healthy condition

| | | | 12 % Hypoxia – $V_E$ (L/min/kg) | | | 8 % Hypoxia – $V_E$ (L/min/kg) | | |
|---|---|---|---|---|---|---|---|---|
| | Glycemia (mg/dL) | $PaO_2$ (mmHg) | Resting | Peak | Fall-off | Resting | Peak | Fall-off |
| Diabetes | 506.7 ± 18.1* | 77.7 ± 1.7* | 0.59 ± 0.05* | 1.01 ± 0.06* | 1.01 ± 0.07* | 0.66 ± 0.04* | 1.35 ± 0.10* | 0.95 ± 0.29* |
| Healthy | 117.0 ± 7.5 | 95.9 ± 2.0 | 0.95 ± 0.05 | 1.43 ± 0.05 | 1.28 ± 0.06 | 0.86 ± 0.04 | 1.92 ± 0.07 | 1.87 ± 0.10 |

Data are means ± SE. Diabetic data refer to 4 weeks' untreated diabetes (n = 6), healthy (n = 12). $V_E$ – minute ventilation, *p < 0.05 between the two conditions

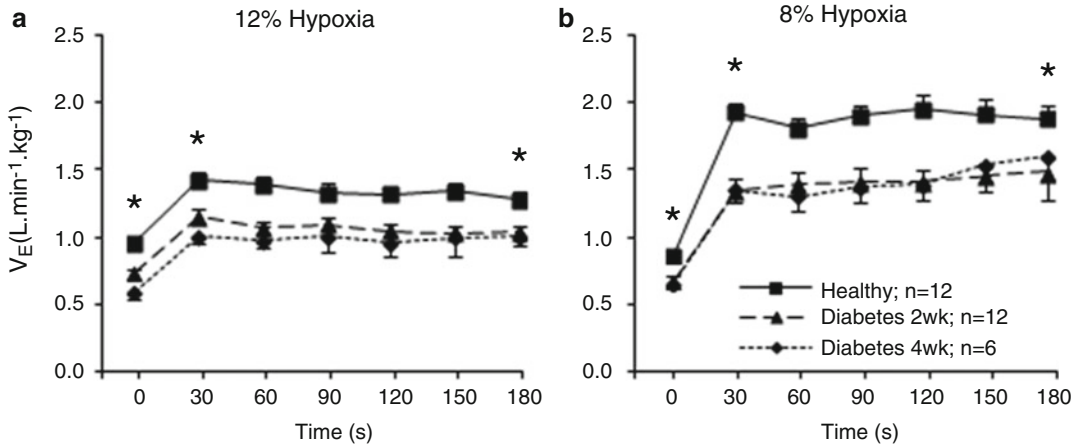


**Fig. 14.1** Ventilatory responses to acute 12 % hypoxia (Panel **a**) and 8 % hypoxia (Panel **b**) in the healthy condition and after 2 and 4 weeks of untreated diabetes in the same rats. Diabetes decreased both resting and hypoxic ventilation. *p < 0.05 for the difference between the healthy and either hypoxic ventilatory level at the marked time points (*vertical*)

recorded from the phrenic nerve activity, along with chemoreceptor cell discharge, in paralyzed ventilated animals.

In the present study, to get insight into chemoreceptor function, we examined diabetes-induced morphological changes in carotid body parenchyma, which has not yet been reported in the literature. At the ultrastructural level, carotid bodies from healthy rats show clusters of chemoreceptor cells with characteristic dense-cored secretory vesicles. Figure 14.2 demonstrates cross-sections of several chemoreceptor cells from a healthy carotid body. Since the cells are cut through at different levels, the nuclei are of different size or are not visible in some of them. The cells contain numerous mitochondria and Golgi apparatuses. Nerve fibers are placed between the cells. A capillary seen in the upper right corner presents a layer of normal endothelial cells. Diabetes caused little ultrastructural changes in chemoreceptor cells, consisting of occasional vacuolization and thinning of the inner mitochondrial cristae (Fig. 14.3a). However, the Golgi apparatus was distinctly hyperactive showing distended cisternae of its reticular structure and enlarged stacks of vesicles in their proximity (Fig. 14.3b), which points to enhanced processing and packaging of molecules for secretion from the cell. The most notable change in the diabetic carotid body was proliferation of connective tissue pushing aside the chemoreceptor cells and disorganizing otherwise regular arrangement of the cell cluster (Fig. 14.4). The diffusion pathway for oxygen from capillaries to chemoreceptor cells became clearly elongated in diabetes. The capillaries themselves were patho-

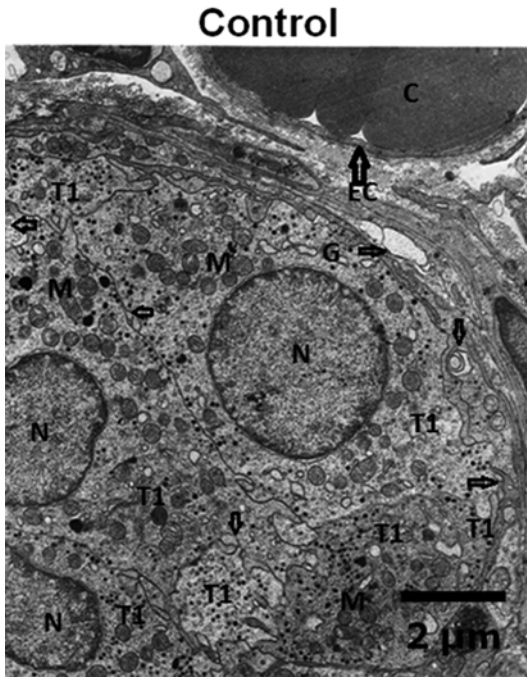


**Fig. 14.2** Photomicrograph of a healthy rat carotid body. Cross-section of a cluster of chemoreceptor cells (T1 – type 1 cells) is shown. There are nuclei in three of the cells, not visible in other cells due to the cutting the cells through at different levels. The cells contain a typical pattern of dense-cored secretory vesicles (appear as *black dots* inside the chemoreceptor cells), mitochondria (*M*), and Golgi cisternae (*G*). A capillary (*C*) filled with erythrocytes is seen in the *upper right* corner, with a layer of normal endothelial cells (EC with a *thick arrow*). Occasional nerve fibers (NF) squeezed between type 1 cells or in the cluster periphery are seen (*short arrows*)

logically changed. The endothelial cells were swollen, showed enhanced pinocytosis, rarefied mitochondrial content (Fig. 14.4a), and breaks in the endothelial layer (Fig. 14.4b). There were signs of neovascularization in carotid body parenchyma. Figure 14.5 demonstrates the ongoing splitting of a capillary into a two-channel microvessel. The microvessel, however, before being fully formed, seems dysfunctional having a highly pathological appearance, with degenerated endothelial cells. There is an apoptotic nucleus in the endothelial cell visible in the central part of the image; the cell is shared by both vessel channels.

Angiopathy was a dominant feature in diabetic carotid bodies. Therefore, we set out to perform a spatial reconstruction of the capillary bed in the carotid body using laser scanning confocal microscopy. To this end, we used GSI lectin conjugated with a fluorophore, which selective binds to the endothelial cells and thus is a tracer of microcirculatory vessels in both perfused and non-perfused capillaries (Greene et al. 1990). The green fluorescent GSI staining distinctly visualized capillaries surrounding the clusters of chemoreceptor cells (black islets of cells) and cutting in through normal carotid body parenchyma (Figs. 14.6a, 14.7a). The number of microvessels was significantly greater in the diabetic than that in the healthy carotid body; $43.0 \pm 5.4$ *vs.* $32.0 \pm 2.4$, respectively ($P < 0.05$). The microvessels' diameter remained unchanged; diabetic – $6.08 \pm 0.37$ µm ($n = 36$) *vs*. healthy – $6.35 \pm 0.28$ µm ($n = 104$). In the diabetic carotid body, microvessels were visibly elongated, of greater tortuosity, entwined together, and occasionally forming braids (Fig. 14.6b). There were signs of neovascularization consisting of splitting of microvessels into 2- or 3-channel vessels, and the connective tissue stroma was clearly outgrown pushing the chemoreceptor cells into the cluster's periphery (Fig. 14.7b).

## 14.4 Summary and Conclusions

In view of the paucity of studies on, and controversies surrounding the issue of, the ventilatory control in diabetes mellitus, in the present study we attempted to clarify the influence of diabetes on the carotid body generated hypoxic chemoreflex. We further proceeded to examine morphologically the diabetic carotid body in search for the plausible mechanisms underlying changes in the ventilatory control. We addressed these issues in a model of streptozotocin-induced diabetes in the rat; the model which closely imitates human diabetes in terms of increased oxidative stress, chronic inflammation, neuropathy, and angiogenic changes (Eleayu et al. 2013; Sano et al. 1998). The major finding was that the hypoxic ventilatory responses were progressively diminished in diabetes. Furthermore, diabetic carotid bodies displayed profound

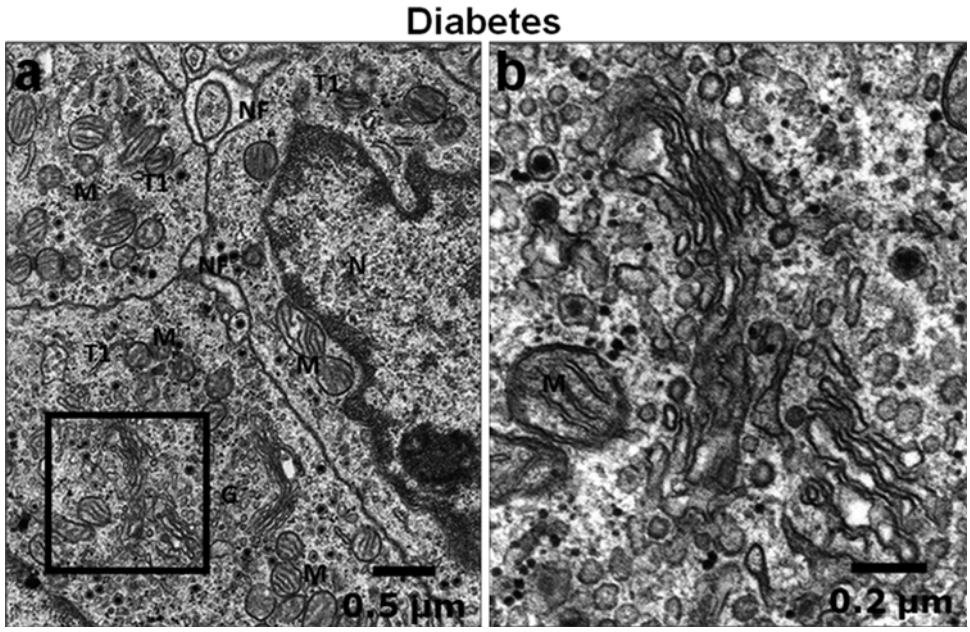


**Fig. 14.3** Photomicrograph showing three chemoreceptor cells (T1 – type 1 cells) in a diabetic rat carotid body (*left panel*). The cells seem functionally intact, with subtle changes in the organelles (*M* mitochondria, *N* nucleus of type 1 cell). Nerve fibers (NF) are visible between the cells. The area of the *black square* contains a hyperactive Golgi area. This area is blown up in the *right panel* (see text for details)

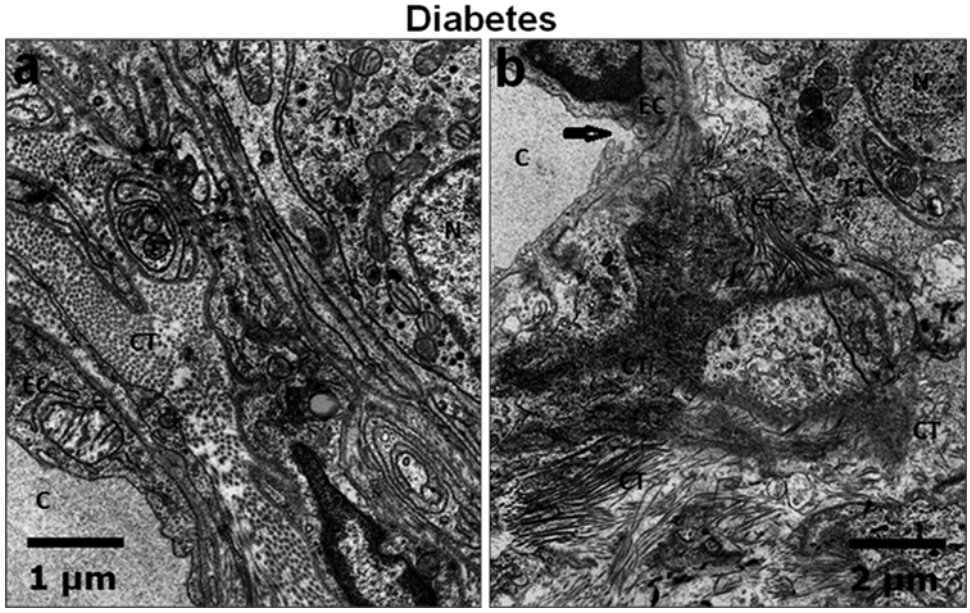


**Fig. 14.4** Heavy proliferation of connective tissue (CT) in diabetic carotid body parenchyma seen in both photomicrographs. Chemoreceptor cells are pushed away toward the cluster periphery. Swollen endothelial cells (EC) in the capillaries (*C – lower left* in the *left panel* and *upper left* in the *right panel*) and a break in the endothelial layer continuity in the capillary of the *right panel* pointed to by the *arrow*

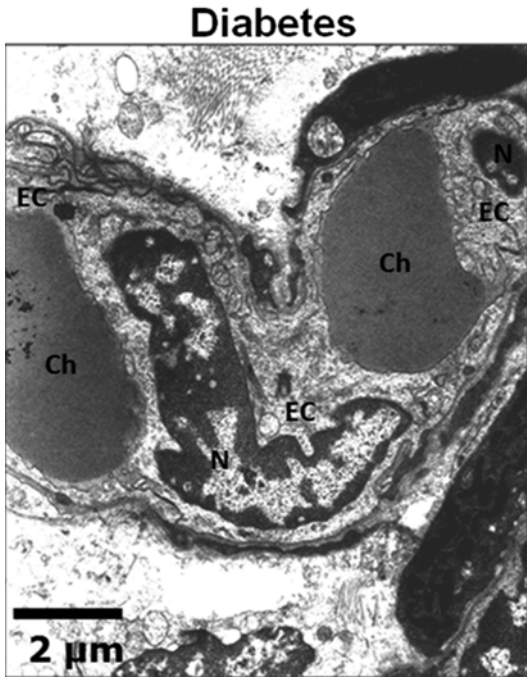


**Fig. 14.5** Photomicrograph showing the splitting of a microvessel in diabetic carotid body parenchyma into a two-channel pathologically changed vessel; *EC* endothelial cells, *N* nucleus of endothelial cell, *Ch* channels of the splitting blood capillary (see text for details)

morphological restructuring, most notably consisting of proliferation of interglomal connective tissue and the induction of blood-microvessel growth. We show evidence of angiopathic changes in the carotid body microvasculature which also included newly formed vessels. The morphological alterations outlined above clearly derange the otherwise regular glomal structure and raise the possibility of the development of chronic hypoxia in the organ. Studies show that sustained hypoxia is associated with upregulation of proinflammatory cytokines and their receptors in the carotid body (Liu et al. 2009; Lam et al. 2008). Diabetes may thus lead to chronic inflammation of the carotid body; a trait that may have underpinned both morphological and functional alterations of the organ.

The ultrastructural examination of the present study supplies evidence that the chemoreceptor cells were grossly unchanged in diabetes. Although ultrastructurally intact, the chemoreceptor cells' function may have been impaired by the parenchymal impediment, in terms of the ability to respond, in size and extent, to the hypoxic stimulus. Our study lends support to

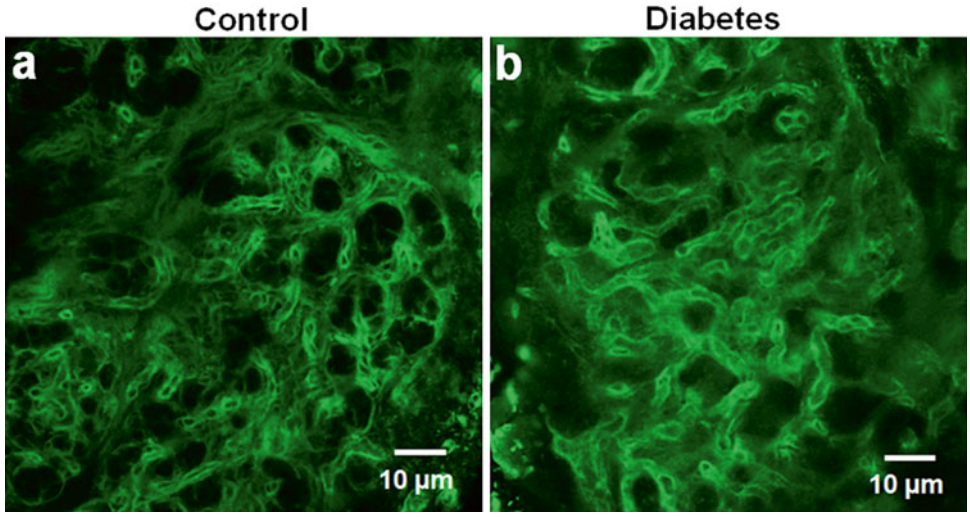


**Fig. 14.6** Laser scanning confocal microscopy showing reconstruction of the microvascular bed in healthy (Panel **a**) and diabetic (Panel **b**) carotid bodies. Green fluorescence depicts the endothelial layers that encircle the lumen of capillaries. Capillaries surround islets of chemoreceptor cells (*black cell* groupings). In diabetes, microvessels are elongated, tortuous, and entwined

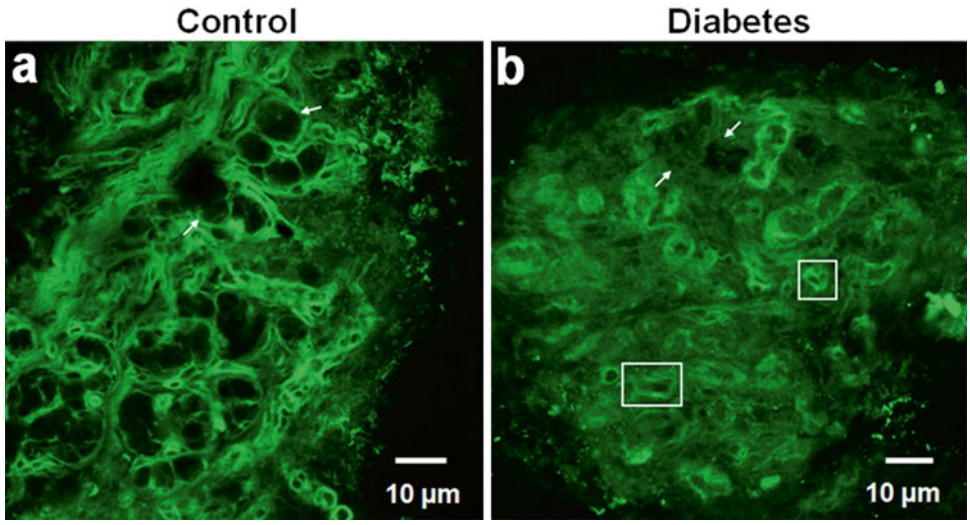


**Fig. 14.7** Laser scanning confocal microscopy presenting another example of the microvascular bed in healthy (Panel **a**) and diabetic (Panel **b**) carotid bodies. *White arrows* in both panels exemplify the black islets of chemoreceptor cells surrounded by greenly fluorescent endothelial layers of capillaries. *White rectangles* in Panel **b** exemplify neovascularization consisting of splitting of microvessels into two-channel vessels in diabetic carotid body. Note, disordered structure of diabetic carotid body parenchyma congruous with connective tissue proliferation observed in transmission electron microscopy (Fig. 14.4)

those previous reports which show deficient ventilatory responses to hypoxia in diabetes. The deficient ventilatory control of diabetes is indubitably multifactorial. Although we observed unfavorable effects of hyperglycemia on carotid body parenchymal organization, which makes it difficult for the chemoreceptor cells to guide the hypoxic ventilatory response, we believe the deficient responses cannot be solely explained by the disturbed peripheral chemoreceptor function. The central component of respiratory regulation and that related to the neuropathic restrain of motor pathways running to the respiratory muscle pump should be taken into consideration. Finally, the role of chronic diabetic inflammation of the carotid body remains to be clarified.

**Conflicts of Interest** The authors declare no conflicts of interest in relation to this article.

## References

Calverley PM, Ewing AJ, Campbell IW, Wraith PK, Brash HM, Clarke BF, Flenley DC (1982) Preservation of the hypoxic drive to breathing in diabetic autonomic neuropathy. Clin Sci (Lond) 63(1):17–22

Clarke JA, de Burgh Daly M, Ead HW, Kreclović G (1993) A morphological study of the size of the vascular compartment of the carotid body in a non-human primate (*Cercopithecus ethiopus*), and a comparison with the cat and rat. Acta Anat (Basel) 147(4):240–247

Devaraj S, Cheung AT, Jialal I, Griffen SC, Nguyen D, Glaser N, Aoki T (2007) Evidence of increased inflammation and microcirculatory abnormalities in patients with type 1 diabetes and their role in microvascular complications. Diabetes 56(11):2790–2796

Donath MY, Shoelson SE (2011) Type 2 diabetes as an inflammatory disease. Nat Rev Immunol 11(2):98–107

Eleayu CO, Eleayu KC, Chukwuma S, Essien E (2013) Review of the mechanism of cell death resulting from streptozotocin challenge in experimental animals, its practical use and potential risk to humans. J Diabetes Metab Disord 12:60. doi:10.1186/2251-6581-12-60

Ellenberg M (1958) Diabetic neuropathy presenting as the initial clinical manifestation of diabetes. Ann Intern Med 49(3):620–631

Greene AS, Lombard JH, Cowley AW Jr, Hansen-Smith FM (1990) Microvessel changes in hypertension measured by Griffonia simplicifolial lectin. Hypertension 15(6 Pt 2):779–783

Hein MS, Schlenker EH, Patel KP (1994) Altered control of ventilation in streptozotocin-induced diabetic rats. Proc Soc Exp Biol Med 207(2):213–219

Kageyama S, Sasoh F, Taniguchi I, Homma I, Saito H, Isogai Y (1985) Cardiorespiratory arrest in a patient with advanced diabetic autonomic neuropathy. Diabetes Res Clin Pract 1(4):243–246

Lam SY, Tipoe GL, Liong EC, Fung ML (2008) Chronic hypoxia upregulates the expression and function of

proinflammatory cytokines in the rat carotid body. Histochem Cell Biol 130(3):549–559

Liu X, He L, Stensaas L, Dinger B, Fidone S (2009) Adaptation to chronic hypoxia involves immune cell invasion and increased expression of inflammatory cytokines in rat carotid body. Am J Physiol Lung Cell Mol Physiol 296(2):158–166

López-Barneo J (2003) Oxygen and glucose sensing by carotid body glomus cells. Curr Opin Neurobiol 13(4):493–499

Montserrat JM, Cochrane GM, Wolf C, Picado C, Roca J, Augusti Vidal A (1985) Ventilatory control in diabetes mellitus. Eur J Respir Dis 67(2):112–117

Nishimura M, Miyamoto K, Suzuki A, Yamamoto H, Tsuji M, Kishi F, Kawakami Y (1989) Ventilatory and heart rate responses to hypoxia and hypercapnia in patients with diabetes mellitus. Thorax 44(4):251–257

Persson PB, Henriksson J (2011) Good publication practise in physiology. Acta Physiol 203(4):403–407

Rasche K, Kelner T, Tautz B, Hader C, Hergenc G, Antosiewicz J, Di Giulio C, Pokorski M (2010) Obstructive sleep apnea and type 2 diabetes. Eur J Med Res 15(Suppl 2):152–156

Saiki C, Seki N, Furuya H, Matsumoto S (2005) The acute effects of insulin on the cardiorespiratory responses to hypoxia in streptozotocin-induced diabetic rats. Acta Physiol Scand 183(1):107–115

Sano T, Umeda F, Hashimoto T, Nawata H, Utsumi H (1998) Oxidative stress measurement by *in vivo* electron spin resonance spectroscopy in rats with streptozotocin-induced diabetes. Diabetologia 41(11):1355–1360

Weisbrod CJ, Eastwood PR, O'Driscoll G, Green DJ (2005) Abnormal ventilatory responses to hypoxia in type 2 diabetes. Diabet Med 22(5):563–568

White JE, Bullock RE, Hudgson P, Home PD, Gibson GJ (1992) Phrenic neuropathy in association with diabetes. Diabet Med 9(10):954–956

Yamazaki H, Okazaki M, Takeda R, Haji A (2002) Hypercapnic and hypoxic ventilatory responses in long-term streptozotocin-diabetic rats during conscious and pentobarbital-induced anesthetic states. Life Sci 72(1):79–89

# 15 Adenosine Receptor Blockade by Caffeine Inhibits Carotid Sinus Nerve Chemosensory Activity in Chronic Intermittent Hypoxic Animals

J.F. Sacramento, C. Gonzalez, M.C. Gonzalez-Martin, and S.V. Conde

**Abstract**

Adenosine is a key excitatory neurotransmitter at the synapse between $O_2$-sensing chemoreceptor cells-carotid sinus nerve (CSN) endings in the carotid body (CB). Herein, we have investigated the significance of adenosine, through the blockade of its receptors with caffeine, on the CB hypoxic sensitization induced by chronic intermittent hypoxia (CIH) in the rat. CIH animals were obtained by submitting rats during 15 days from 8:00 to 16:00 to 10 %$O_2$ for 40 s and 20 % $O_2$ for 80 s (i.e., 30 episodes/h). Caffeine (1 mM) was tested in spontaneous and 5 %$O_2$ evoked-CSN chemosensory activity in normoxic and CIH animals. CIH decreased basal spontaneous activity but increased significantly CSN activity evoked by acute hypoxia. Caffeine did not modify basal spontaneous activity in normoxic rats, but decreased significantly by 47.83 % basal activity in CIH animals. In addition, acute application of caffeine decreased 49.31 % and 56.01 % the acute hypoxic response in normoxic and CIH animals, respectively. We demonstrate that adenosine contributes to fix CSN basal activity during CIH, being also involved in hypoxic CB chemotransduction. It is concluded that adenosine participates in CB sensitization during CIH.

**Keywords**

Chronic intermittent hypoxia • Hypoxic sensitization • Adenosine • Carotid sinus nerve activity • Caffeine

J.F. Sacramento • S.V. Conde (✉)
CEDOC, Centro de Estudos Doenças Crónicas, Nova Medical School, Faculdade de Ciências Médicas, Universidade Nova de Lisboa,
Campo Mártires da Pátria, 130, 1169-056 Lisbon, Portugal
e-mail: silvia.conde@fcm.unl.pt

C. Gonzalez • M.C. Gonzalez-Martin
Departamento de Bioquímica y Biología Molecular y Fisiología, Universidad de Valladolid, Facultad de Medicina, Instituto de Biología y Genética Molecular, CSIC. Ciber de Enfermedades Respiratorias, CIBERES, Instituto de Salud Carlos III,
47005 Valladolid, Spain



C. Peers et al. (eds.), *Arterial Chemoreceptors in Physiology and Pathophysiology*,
Advances in Experimental Medicine and Biology 860, DOI 10.1007/978-3-319-18440-1_15

## 15.1 Introduction

Chronic intermittent hypoxia (CIH) is a characteristic feature of obstructive sleep apnea (OSA). Nowadays, it is consensual that OSA, increase carotid body (CB) peripheral drive being this reflected by enhanced ventilatory and cardiovascular reflex responses to acute hypoxia and by an enhanced sympathetic tone (Somers et al. 1995; Narkiewicz et al. 1999). In fact, in the last decade several studies in animal models of CIH have strengthened the idea that CIH leads to an overactivation of the CB, which is manifested by its increased sensitivity to hypoxia (Rey et al. 2004; Prabhakar et al. 2007). In fact, the recording of carotid sinus nerve (CSN) discharge *in vitro* and *in situ* showed that exposure of animals to CIH increased CSN basal discharge and enhanced the chemosensory response evoked by acute hypoxia (Peng et al. 2003; Rey et al. 2004; Gonzalez-Martín et al. 2011). Nevertheless, the mechanisms underlying the CB hypoxic sensitization induced by CIH are not well understood. Herein, we have investigated the role of adenosine, a key excitatory neurotransmitter at the synapse between $O_2$-sensing chemoreceptor cells- CSN endings in the carotid body (Conde et al. 2009, 2012a) on CB hypoxic sensitization during CIH. The role of adenosine was studied by testing acutely caffeine, which is a non-selective adenosine receptor antagonist, that blocks $A_{2A}$ and $A_{2B}$ receptors at the CB (Conde et al. 2006, 2012b) on CSN chemosensory activity in basal conditions and in response to hypoxia in normoxic and CIH animals. We have found that, in contrast with what happens in normoxic animals, adenosine contributes to fix CSN basal activity during CIH. Also, we showed that adenosine, as it has been described in normoxic animals, is a key player involved in hypoxic CB chemotransduction.

## 15.2 Methods

Experiments were performed in Wistar adult rats (300–380 g) obtained from *vivarium* of the Faculty of Medicine of the University of Valladolid. The Institutional Committee of the University of Valladolid for Animal Care and Use approved the protocols. Control animals were maintained in room air atmosphere and CIH animals were submitted during 15 days from 8:00 to 16:00 to the following IH pattern: 10 %$O_2$ for 40 s and 20 % $O_2$ for 80 s (i.e., 30 episodes/h) as previously described by Gonzalez-Martín et al. (2011). The experiments were performed approximately 16 h after the completion of their last IH episode.

Rats were anaesthetized with sodium pentobarbital (Sigma, Madrid, Spain) (60 mg/kg i.p.), tracheostomized and the carotid arteries were dissected past the carotid bifurcation. The preparation CB-CSN was identified and processed for CSN recordings as previously described by Rigual et al. (2002) and Conde et al. (2012a, b). In all instances animals were killed by intracardiac overdoses of sodium pentobarbital until the beating of their hearts ceased.

Recordings of either a single or a few fibers of CSN were made using a suction electrode. The pipette potential was amplified (NeuroLog; Digimiter, Hertfordshire, England), filtered (1 kHz), digitized at 6 kHz (Axonscope; Axon Instruments, Molecular Devices, Wokingham, UK) and stored on a computer. Chemoreceptor activity was identified (as the spontaneous generation of action potentials at irregular intervals) and confirmed by its increase in response to hypoxia (normoxia: 20 % $O_2$ + 5 % $O_2$ + 75 % $N_2$; hypoxia: 5 %$O_2$ + 5 %$CO_2$ + balanced $N_2$). CSN unit activity was converted to logic pulses, which were summed every second and converted in a voltage proportional to the sum. The effect of caffeine (1 mM) on the CSN activity was studied while perfusing the preparations with normoxic (20 % $O_2$-equilibrated) and hypoxic (5 % $O_2$-equilibrated) solutions.

Data was evaluated using Graph Pad Prism Software, version 5 and was presented as mean ± SEM. The significance of the differences between the means was calculated by One and Two-Way Analysis of Variance (ANOVA) with Dunnett's and Bonferroni multiple comparison tests, respectively. *P* values of 0.05 or less were considered to represent significant differences.

## 15.3 Results

Figure 15.1 illustrates the effect of caffeine (1 mM), a non-selective adenosine receptor antagonist, on spontaneous and hypoxic-evoked CSN chemosensory activity in control rats and in rats submitted to CIH. Although it is not evident from Fig. 15.1a, mean basal CSN chemosensory activity decreased by 58.11 % with CIH (Fig. 15.1d). Blockade of adenosine receptors by caffeine did not modify the basal CSN chemosensory activity in normoxic animals (Fig. 15.1b, d), but decreased by 47.33 % in CIH rats (Fig. 15.1c, d; $p<0.01$). Mean basal activity for each paradigm was: control – 4.51 ± 0.62 impulses/s; control + acute caffeine – 4.46 ± 0.48 impulses/s; CIH rats – 1.89 ± 0.20 impulses/s; CIH rats + acute caffeine – 0.99 ± 0.23 impulses/s.

In order to correct the activity of CSN in response to any given stimulus, the activity was expressed as times over basal. As it can be seen in Fig. 15.1a, e, exposure to CIH induced a significantly increase by 277.66 % in CSN activity in response to moderate hypoxia, 5 % $O_2$ (CSN activity in normoxic animals = 7.72 ± 1.03 times over basal; CSN activity in CIH animals = 28.99 ± 2.42 times over basal). Blockade of adenosine receptors decreased by 49.31 % CSN activity evoked by 5 %$O_2$ in normoxic animals (Fig. 15.1b, e) and by 56.04 % in CIH animals (Fig. 15.1c, e). For each given stimulus we also measured the latency of the response and the time to peak response. Acute caffeine application did not delay the onset of the response (latency time) either in normoxic or in CIH animals (normoxic animals = 22.72 ± 5.58 s; normoxic + caffeine = 32.46 ± 2.93 s; CIH animals = 26.07 ± 6.98 s; CIH + caffeine = 29.61 ± 4.02 s, data not shown). The times to reach the maximal activity (time to peak) are depicted in Fig. 15.1f. CIH exposure increased significantly time to peak to 121.20 ± 17.5 s from a control value of 47.13 ± 4.59 s (normoxic animals). Acute caffeine application in normoxic animals increased significantly time to peak 75.22 ± 7.05 s, although no significant statistical differences were observed for acute caffeine application in CIH animals (time to peak = 11.58 ± 16.37 s).

## 15.4 Discussion

The present study demonstrates, for the first time, that adenosine is involved in CB sensitization during CIH. We have showed that acute caffeine administration, blocking adenosine receptors, decreased spontaneous CSN chemosensory activity in CIH animals, meaning that adenosine contributes to fix basal CSN activity during CIH. In addition, caffeine also reduced CSN chemosensory activity evoked by acute hypoxia, demonstrating that adenosine is a key player in hypoxic chemotransduction during CIH.

The concentration of caffeine tested in the present work was compatible with the antagonism of adenosine receptors and with the inhibition of phosphodiesterases (Fredholm et al. 1999), although we have attributed all the effects to the antagonism of adenosine receptors as we previously described that caffeine action on CSN activity is due to a mixed $A_{2A}$ and $A_{2B}$ receptor-mediated effect (Conde et al. 2006).

In accordance with other groups and with our previous findings we have observed that CIH induced an increase in CB sensitization that is manifested by its increased sensitivity to hypoxia (Rey et al. 2004; Prabhakar et al. 2007; Gonzalez-Martín et al. 2011). In addition, we have shown that adenosine receptors blockade by caffeine decreased basal CSN activity, as well as the CSN activity evoked by acute hypoxia in CIH animals, indicating that apart from mediating acute hypoxic signalling in CIH, adenosine also contributes to fix CSN basal activity in CIH. The effect of caffeine on CSN basal activity contrasts with what happens in normoxic animals where caffeine did not modify basal CSN activity (Fig. 15.1; Conde et al. 2006) and with the absence of effect of chronic caffeine administration in chronic sustained hypoxia in basal CSN action potential frequency (Conde et al. 2012b). Nevertheless, caffeine action on CSN activity evoked by acute hypoxia during CIH was consistent with previous findings that show that adenosine have excitatory effects on the CB, being a key neurotransmitter involved in hypoxic CB chemotransduction both in normoxic animals as in chronic sustained hypoxia (Conde et al. 2009,

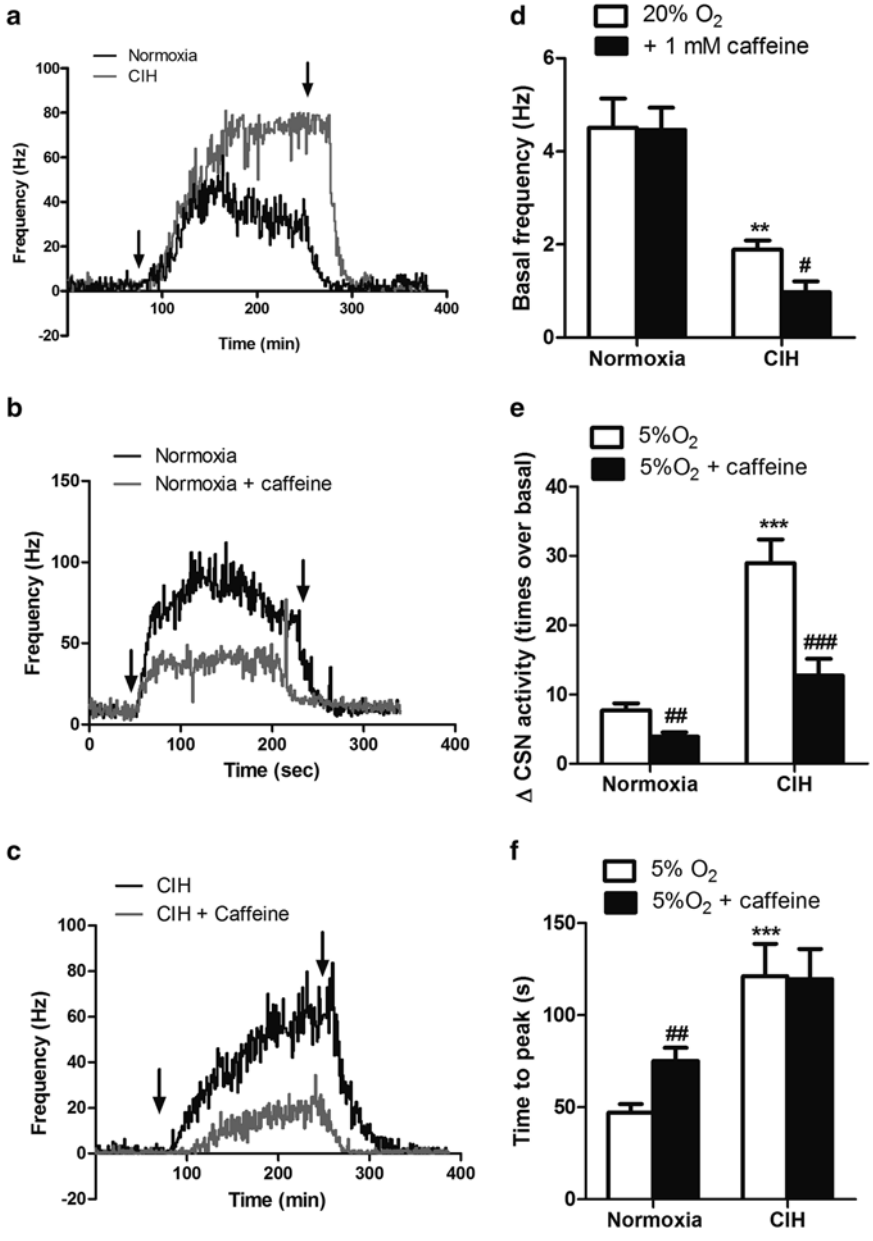


**Fig. 15.1** Effect of caffeine (1 mM) in basal and hypoxia evoked-carotid sinus nerve (CSN) chemosensory activity in normoxic and chronically intermittent hypoxic (CIH) animals. (**a**) Typical recording of the frequency of action potentials of CSN in response to hypoxia (5 % $O_2$) in normoxic and CIH rats. (**b**) Typical recording for the effect of acute caffeine application on the frequency of actions potentials of CSN in basal and in response to 5 %$O_2$ in normoxic rats. (**c**) Typical recording for the effect of acute caffeine application on the frequency of actions potentials of CSN in basal and in response to 5 %$O_2$ in CIH rats. *Arrows* indicate the period of application of acute hypoxic stimulus (5 %$O_2$). Animals were submitted to 15 days of chronic intermittent hypoxia (10 %$O_2$ for 40 s and 20 % $O_2$ for 80 s (i.e., 30 episodes/h)). Panels **d** and **e** represent, respectively, the effect of caffeine on means of basal CSN activity and on means of increases in peak frequencies, in normoxic rats and in rats exposed to CIH. Panel **f** represent the time required to reach maximal activity during stimulation (time to peak). Data represent means ± SEM of n individual values given in the drawing. *P < 0.05, **P < 0.01, ***P < 0.001 vs. control values, #P < 0.05, ##P < 0.01 vs. CIH values

2012a, b). It is well known that hypoxia induces the release of adenosine from the CB in normoxic animals (Conde and Monteiro 2004), therefore it is expected that the contribution of adenosine to CB sensitization during CIH and thereby to the CSN activity in basal conditions and in response to acute hypoxia be correlated with alterations in adenosine release. In fact, it has been described that plasma adenosine levels are increased in OSA patients (Lavie 2003) suggesting that alterations in adenosine release and adenosine dynamics are involved in the mechanisms underlying the pathophysiological alterations observed in OSA and with the increased CB sensitization. Additionally, changes in the density and/or affinity of their receptors in the sensory nerve endings should also be considered.

**Acknowledgements** The work was supported by FCT Grant (Ref: EXPL/NEU-SCC/2183/2013) from Portugal and by the Spanish Grants BFU2012-37459 and CIBERES to C.G.

## References

Conde SV, Monteiro EC (2004) Hypoxia induces adenosine release from the rat carotid body. J Neurochem 89:1148–1156

Conde SV, Obeso A, Vicario I, Rigual R, Rocher A, Gonzalez C (2006) Caffeine inhibition of rat carotid body chemoreceptors is mediated by A2A and A2B adenosine receptors. J Neurochem 98:616–628

Conde SV, Monteiro EC, Obeso A, Gonzalez C (2009) Adenosine in peripheral chemoreception: new insights into a historically overlooked molecule. Adv Exp Med Biol 648:159–174

Conde SV, Monteiro EC, Rigual R, Obeso A, Gonzalez C (2012a) Hypoxic intensity: a determinant for the contribution of ATP and adenosine to the genesis of carotid body chemosensory activity. J Appl Physiol 112:2002–2010

Conde SV, Ribeiro MJ, Obeso A, Rigual R, Monteiro EC, Gonzalez C (2012b) Chronic caffeine intake in adult rat inhibits carotid body sensitization produced by chronic sustained hypoxia but maintains intact chemoreflex output. Mol Pharmacol 82:1056–1065

Fredholm BB, Battig K, Holemn J, Nehlig A, Zvartau EE (1999) Actions of caffeine in the brain with special reference to factors that contribute to its widespread use. Pharmacol Rev 51:83–133

Gonzalez-Martín MC, Vega-Agapito MV, Conde SV, Castañeda J, Bustamante R, Olea E, Perez-Vizcaino F, Gonzalez C, Obeso A (2011) Carotid body function and ventilatory responses in intermittent hypoxia. Evidence for anomalous brainstem integration of arterial chemoreceptor input. J Cell Physiol 226:1961–1969

Lavie L (2003) Obstructive sleep apnoea syndrome – an oxidative stress disorder. Sleep Med Rev 7:35–51

Narkiewicz K, van de Borne PJ, Pesek CA, Dyken ME, Montano N, Somers VK (1999) Selective potentiation of peripheral chemoreflex sensitivity in obstructive sleep apnea. Circulation 99:1183–1189

Peng YJ, Overholt JL, Kline D, Kumar GK, Prabhakar NR (2003) Induction of sensory longterm facilitation in the carotid body by intermittent hypoxia: implications for recurrent apneas. Proc Natl Acad Sci U S A 100:10073–10078

Prabhakar NR, Dick TE, Nanduri J, Kumar GK (2007) Systemic, cellular and molecular analysis of chemoreflex-mediated sympathoexcitation by chronic intermittent hypoxia. Exp Physiol 92:39–44

Rey S, Del Rio R, Alcayaga J, Iturriaga R (2004) Chronic intermittent hypoxia enhances cat chemosensory and ventilatory responses to hypoxia. J Physiol 560:577–586

Rigual R, Rico AJ, Prieto-Lloret J, de Felipe C, Gonzalez C, Donnelly DF (2002) Chemoreceptor activity is normal in mice lacking the NK1 receptor. Eur J Neurosci 16:2078–2084

Somers VK, Dyken ME, Clary MP, Abboud FM (1995) Sympathetic neural mechanisms in obstructive sleep apnea. J Clin Invest 96:1897–1904

# 16 Neurotrophic Properties, Chemosensory Responses and Neurogenic Niche of the Human Carotid Body

Patricia Ortega-Sáenz, Javier Villadiego, Ricardo Pardal, Juan José Toledo-Aral, and José López-Barneo

**Abstract**

The carotid body (CB) is a polymodal chemoreceptor that triggers the hyperventilatory response to hypoxia necessary for the maintenance of $O_2$ homeostasis essential for the survival of organs such as the brain or heart. Glomus cells, the sensory elements in the CB, are also sensitive to hypercapnia, acidosis and, although less generally accepted, hypoglycemia. Current knowledge on CB function is mainly based on studies performed on lower mammals, but the information on the human CB is scant. Here we describe the structure, neurotrophic properties, and cellular responses to hypoxia and hypoglycemia of CBs dissected from human cadavers. The adult CB parenchyma contains clusters of chemosensitive glomus (type I) and sustentacular (type II) cells as well as nestin-positive progenitor cells. This organ also expresses high levels of the dopaminotrophic glial cell line-derived neurotrophic factor (GDNF). GDNF production and the number of progenitor and glomus cells were preserved in the CBs of human subjects of advanced age. As reported for other mammalian species, glomus cells responded to hypoxia by external $Ca^{2+}$-dependent increase of cytosolic [$Ca^{2+}$] and quantal catecholamine release. Human glomus cells are also responsive to hypoglycemia and together the two stimuli, hypoxia

P. Ortega-Sáenz • J. Villadiego • R. Pardal
J.J. Toledo-Aral • J. López-Barneo (✉)
Instituto de Biomedicina de Sevilla (IBiS), Hospital Universitario Virgen del Rocío/CSIC/Universidad de Sevilla, Avenida Manuel Siurot s/n,
41013 Seville, Spain

Departamento de Fisiología Médica y Biofísica, Facultad de Medicina, Universidad de Sevilla, Sevilla, Spain

Centro de Investigación Biomédica en Red sobre Enfermedades Neurodegenerativas (CIBERNED), Madrid, Spain
e-mail: lbarneo@us.es



C. Peers et al. (eds.), *Arterial Chemoreceptors in Physiology and Pathophysiology*,
Advances in Experimental Medicine and Biology 860, DOI 10.1007/978-3-319-18440-1_16

and hypoglycemia, can potentiate each other's effects. The chemo-sensory responses of glomus cells are also preserved at an advanced age. Interestingly, a neurogenic niche similar to that recently described in rodents is also preserved in the adult human CB. These new data on the cellular and molecular physiology of the CB pave the way for future pathophysiological studies involving this organ in humans.

**Keywords**

Human carotid body • Chemosensory response • Hypoxia • Hypoglycemia • Glomus cells • Neurotrophic factors • GDNF • Cell therapy • Neuroprotection • Peripheral neurogenic niche • Neural crest-derived stem cells

## Abbreviations

| | |
|---|---|
| CB | carotid body |
| GDNF | glial cell line-derived neurotrophic factor |
| TH | tyrosine hydroxylase |
| GFAP | glial fibrillary acidic protein |
| DDC | dopa-decarboxylase |
| DAPI | 4′,6-diamidino-2-phenylindole |
| BDNF | brain derived neurotrophic factor |
| IGF-1 | insulin-like growth factor-1 |
| HVA | Hypoxic ventilatory acclimatization |

## 16.1 Introduction

The carotid body (CB) is a main arterial chemoreceptor responsible for activation of the brainstem respiratory center to produce hyperventilation and sympathetic activation during hypoxemia. Together with other organs, the CB constitutes a homeostatic acute $O_2$-sensing system, which is required for adaptation to acute hypoxia (Lopez-Barneo et al. 2008; Teppema and Dahan 2010; Weir et al. 2005). Although low $O_2$ tension ($PO_2$) is the main stimulus for CB activation, it functions as a polymodal peripheral chemoreceptor that is also sensitive to increased $CO_2$, low pH, and low glucose as well as other less studied stimuli (Kumar and Prabhakar 2012; Lopez-Barneo 2003). The CB parenchyma is organized in clusters of cells (glomeruli) in close contact with a profuse network of capillaries. The most abundant cells within the CB glomeruli are the neuron-like, type I or glomus cells, which are the $O_2$-sensitive neurosecretory elements of the organ. Glomus cells are electrically excitable and release neurotransmitters upon exposure to environmental low $PO_2$. Type I cells have numerous secretory vesicles containing dopamine and other neurotransmitters (particularly acetylcholine and ATP) as well as several peptides. These cells are enveloped by the processes of glia-like, sustentacular or type II cells, which were classically considered to belong to the peripheral glia and to play a supportive role. Recent data have suggested that type II cells may behave as stem cells that contribute to CB growth in response to chronic hypoxia (Pardal et al. 2007; Platero-Luengo et al. 2014) (see below). Alterations of CB development or function have been implicated in several respiratory diseases, particularly in the newborn (reviewed by (Lopez-Barneo et al. 2008)). On the other hand, CB over-activation appears to contribute to the autonomic imbalance characteristic of several highly prevalent disorders, such as obesity, hypertension, obstructive sleep apnea, metabolic syndrome, cardiac failure, and diabetes (Cramer et al. 2014; Iturriaga 2013; Nair et al. 2013; Narkiewicz et al. 1998; Prabhakar and Semenza

2012; Ribeiro et al. 2013; Schultz et al. 2013). Recently, ablation of this organ has been proposed for the treatment of neurogenic hypertension (Paton et al. 2013).

Although the understanding of the physiological function of the CB at the molecular and cellular levels has increased considerably during the last 25 years due to studies performed on lower mammals (mainly rodents), the information about the human CB is scant (Conde and Peers 2013). The anatomy and ultrastructure of the human CB in normal subjects, as well as in high altitude dwellers and patients with chronic lung or cardiac diseases has been reported (Arias-Stella and Valcarcel 1976; Heath et al. 1970). Several papers have also described the systemic cardio-respiratory alterations caused by bilateral CB resection (Timmers et al. 2003) or ageing (Di Giulio et al. 2012; Pokorski et al. 2004) in humans. However, with the exception of two recent publications on the gene expression profile of the human CB (Fagerlund et al. 2010; Mkrtchian et al. 2012), its functional characteristics have remained practically unknown. Herein we summarize and discuss the data recently obtained by our group regarding the basic anatomical, neurochemical and physiological properties of CBs dissected from human cadavers, of different age and gender, registered with the Organ Donation Program at our institution (Ortega-Saenz et al. 2013).

## 16.2 Structure and GDNF Content of the Human CB

The human CB is located at the carotid bifurcation in close contact with the arterial adventitia and normally surrounded by abundant fat and connective tissue, which must be carefully removed before a clean CB can be dissected out (Fig. 16.1a). The estimated volume of the adult human CB in our cohort is $20.7 \pm 3.8$ mm$^3$ (n = 16 carotid bodies; 11 donors), a value within the range reported by other studies (Heath et al. 1970; Shamblin et al. 1971; Arias-Stella and Valcarcel 1976). However, large differences in sizes are observed among the different individuals or even between the right and left CBs of the same subject (Ortega-Saenz et al. 2013). Although there is a trend for CBs from males to be larger than those of females, no statistically significant differences was found associated to sex (Fig. 16.1b). In addition, the average CB volume is similar in young (<50 years) and older (>50 years) donors (Fig. 16.1c). We have performed detailed immunohistochemical analyses to study the presence of the main cell types existing in the CB: type I or glomus cells, which are highly dopaminergic and express specific markers as tyrosine hydroxylase (TH) or dopa-decarboxylase (DDC), and type II or sustentacular cells that can be identified by the expression of glial markers such as the glial fibrillary acidic protein (GFAP) (Lopez-Barneo et al. 2009). We have found the typical clusters of TH+ cells in the human CB (Fig. 16.1d), although as previously reported (Lazarov et al. 2009), the number of these cells was surprisingly low (~1–2 % of the cell population) in comparison with values (>20 %) described in rodent CBs (Ortega-Saenz et al. 2006; Pardal et al. 2007). However, the actual number of human glomus cells is clearly higher (>10 %) than that revealed by TH immunofluorescence, as demonstrated by the staining of sections with antibodies against DDC, which also shows the typical appearance of clusters of glomus cells (Fig. 16.1e). The fact that TH is a highly regulated enzyme whose expression depends on numerous factors (Kroll and Czyzyk-Krzeska 1998) could be the explanation for the different percentage of glomus cells obtained by these dopaminergic markers, TH and DDC, in our cohort of subjects. Notably, the levels of TH or DDC expression appeared similar among individuals of different ages or gender (Fig. 16.1g, h, j, k). GFAP immunoreactivity was found on the soma of type II cells as well as in their long processes covering extensive areas of the organ. However, the estimated number of GFAP+ cells (in comparison with the total number of DAPI+ nuclei) is only ~1 % and no significant differences have been observed associated to age or gender (Fig. 16.1i, l).

A special neurochemical feature of the CB is the high levels of neurotrophic factors contained

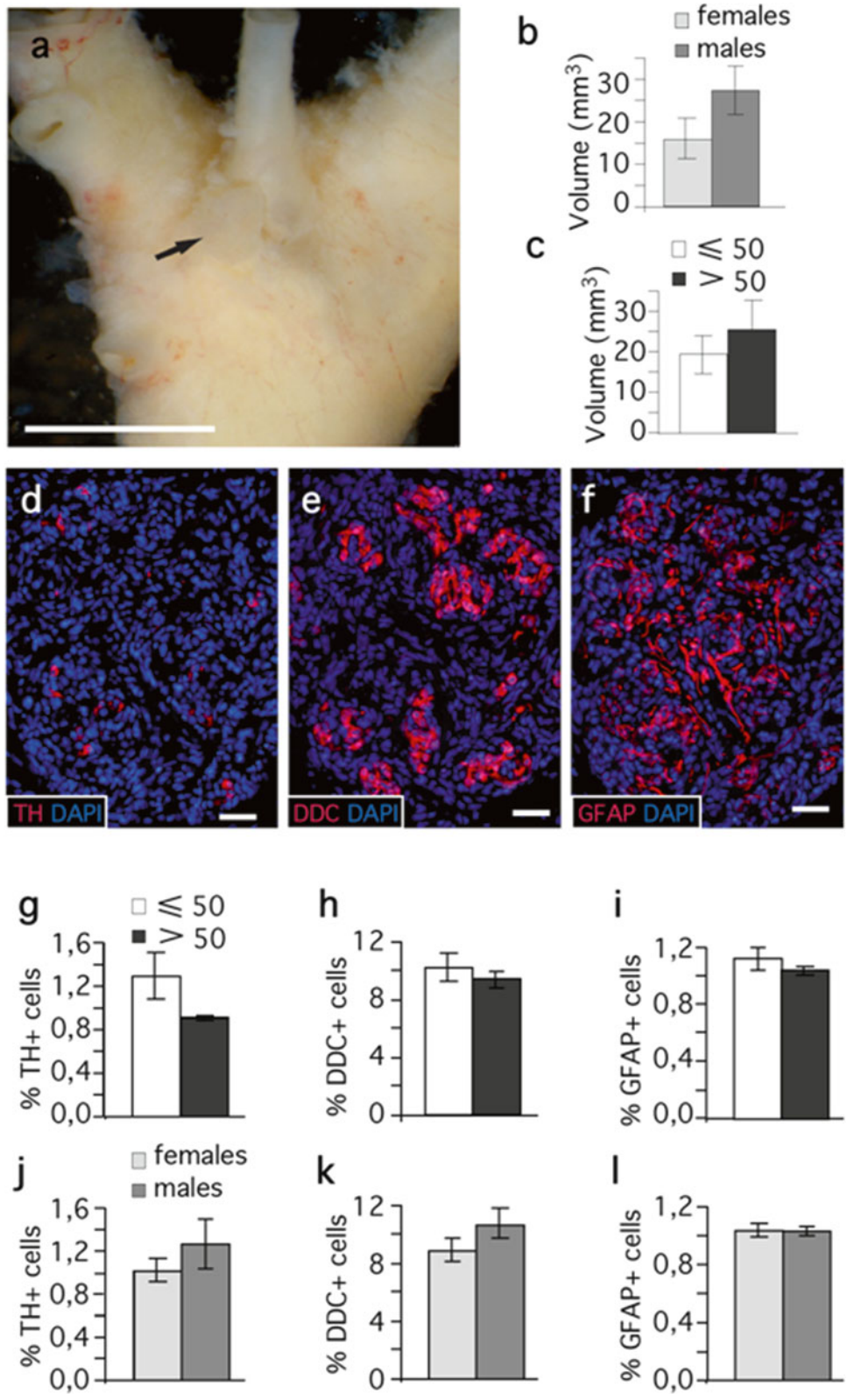


**Fig. 16.1** Morphology of the human carotid body. (**a**) Photograph of the human carotid artery bifurcation. Connective and adipose tissues have been removed to reveal the carotid body (*black arrow*). Scale bar: 1 cm. (**b** and **c**)

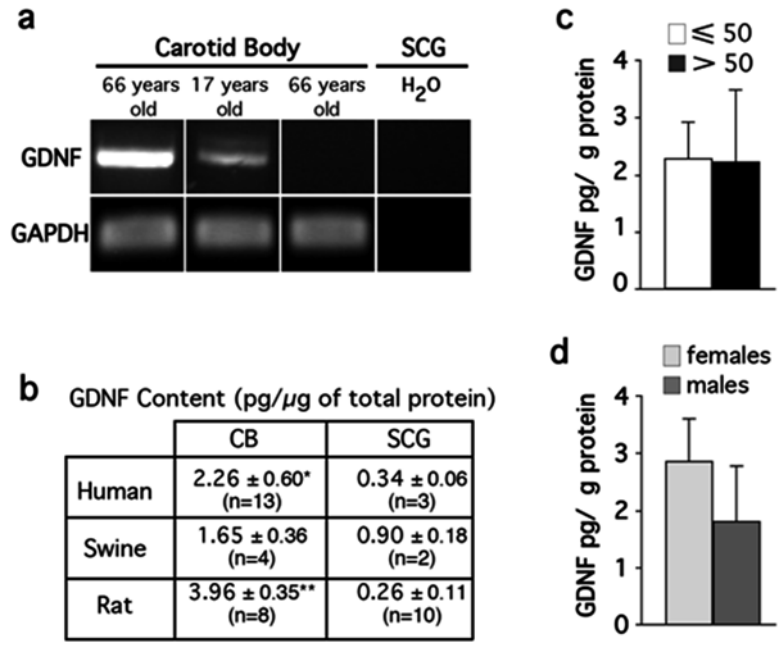


| | CB | SCG |
|---|---|---|
| Human | 2.26 ± 0.60* (n=13) | 0.34 ± 0.06 (n=3) |
| Swine | 1.65 ± 0.36 (n=4) | 0.90 ± 0.18 (n=2) |
| Rat | 3.96 ± 0.35** (n=8) | 0.26 ± 0.11 (n=10) |

**Fig. 16.2** GDNF expression in human carotid body cells. (**a**) GDNF mRNA expression in human CB samples from 66- and 17-year-old subjects. Note the lack of expression of GDNF in the SCG tissue (66-year-old subject). Glyceraldehyde 3-phosphate dehydrogenase (*GAPDH*) was used as housekeeping gene to normalise mRNA. (**b**) GDNF content (in picograms per microgram of total protein) measured by ELISA in human, swine and rat CB and SCG. (**c** and **d**) GDNF protein levels in CBs from subjects below (n = 8) and above (n = 5) 50 years of age (**c**) and females (n = 6) and males (n = 7) (**d**). * $p < 0.05$ and ** $p < 0.01$ (Mann-Whitney U test) (Modified from Ortega-Saenz et al. 2013)

by the adult organ. Among the various trophic factors identified in rodent CBs are brain derived neurotrophic factor (BDNF), glial cell line neurotrophic factor (GDNF), insulin growth factor-1 (IGF-1) and artemin (Erickson et al. 2001; Izal-Azcarate et al. 2008; Leitner et al. 2005; Porzionato et al. 2008; Villadiego et al. 2005). Interestingly, the CB is among the tissues with the highest level of GDNF in the adult rodent nervous system (Villadiego et al. 2005). The main sources of GDNF are the dopaminergic neuron-like glomus cells (Villadiego et al. 2005) and a similar distribution (preferential location in neurons) is also found in the central nervous system (Hidalgo-Figueroa et al. 2012). In humans, selective GDNF mRNA expression is also observed by PCR in CBs of young and aged adult individuals (Fig. 16.2a). In contrast, no GDNF mRNA signal was seen in the human superior cervical ganglion (SCG). The amount of GDNF protein, estimated by ELISA, was significantly higher (~10-fold) in the human CB than in the SCG. The levels of GDNF encountered in the human CB and SCG are in the range of those found in equivalent rat or swine tissues processed in parallel using the same experimental protocol (Fig. 16.2b). Surprisingly, no quantitative difference has been observed between

**Fig. 16.1** (continued) Volumes of human carotid bodies grouped by gender (**b**) and donor age (≤50 years, >50 years) (**c**). (**d, e** and **f**) Fluorescence immunohistochemistry with antibodies against the glomus cell markers TH (**d**) and DDC (**e**), and the type II cell marker GFAP (**f**), in thin sections of a human carotid body. Scale bars: 50 μm. (**g, h, I, j, k** and **l**) Quantification of immunopositive cells versus total number of cells estimated in human carotid body sections. Tissues have been grouped by donor age (≤50 years, >50 years) (**d, e** and **f**) and gender (**j, k** and **l**). No significant changes with age or sex were detected for any of the cell types quantified (Modified from Ortega-Saenz et al. 2013)

GDNF protein content in CBs from young and aged individuals (Fig. 16.2c) or linked to the sex of the donors (Fig. 16.2d).

The role that GDNF plays in CB homeostasis is poorly known. A plausible hypothesis is that the trophic factor exerts an autocrine/paracrine protective effect on glomus cells, which have a particularly high $O_2$ consumption and therefore are exposed to oxidative stress. It is well established that GDNF can increase the activity of detoxifying enzymes as superoxide dismutase, catalase or glutathione peroxidase and therefore protects cells from oxidative damage (Chao and Lee 1999; Cheng et al. 2004; Saavedra et al. 2008; Smith and Cass 2007). In accord with this concept, conditional deletion of GDNF in adult mice results in a marked cell death in the CB (Pascual et al. 2008). Together, these observations strongly support a paracrine protective role of GDNF. Maintenance of high GDNF production in the adult human CB may explain the preservation of CB structure in aged subjects. The high level of GDNF encountered on the CB tissue could be also responsible for the neuroprotective effect of intrastriatal CB transplants on substantia nigra neurons in animals models of Parkinson's disease (Espejo et al. 1998; Luquin et al. 1999; Munoz-Manchado et al. 2013; Toledo-Aral et al. 2003). Glomus cells are envisaged and biological pumps appropriate for synergistic delivery of dopamine and GDNF of potential applicability in antiparkinsonian cell therapy. Indeed, two pilot phase I/II open clinical trials have shown that CB autotransplantation is a safe and feasible procedure with some clinical benefit on PD patients (Arjona et al. 2003; Minguez-Castellanos et al. 2007). However, transplantation of a single CB does not seem to provide enough tissue for a robust and sustainable neuroprotective effect in humans. Expansion of the CB tissue *in vitro*, before transplantation, could probably increase the likelihood that these techniques are effectively translated to the clinical setting.

## 16.3 Cellular Responses to Hypoxia

Chemotransduction in $O_2$-sensitive glomus cells depend on the expression of $O_2$-regulated voltage-gated and background $K^+$ channels whose activity is inhibited in hypoxia (reviewed by (Lopez-Barneo et al. 2001)). This leads to cell depolarization, $Ca^{2+}$ influx and transmitter release (Buckler and Honore 2004; Urena et al. 1994). Although this model of sensory transduction has been demonstrated in several animal models, it has not been studied in human tissues. We have prepared slices of human CB, to measure the secretory responses to hypoxia by amperometry, as well as dispersed CB cells to monitor the changes of cytosolic [$Ca^{2+}$] by microfluorimetry (Garcia-Fernandez et al. 2007; Ortega-Saenz et al. 2010; Pardal et al. 2000; Urena et al. 1994). Representative recordings of catecholamine release from individual glomus cells subjected to low $O_2$ tension ($PO_2$, ≈15 mmHg) and high (40 mM) potassium are illustrated in Fig. 16.3a (upper panel). The cumulative secretion signal obtained by the sum of the time integral of successive amperometric events is represented in Fig. 16.3a (lower panel). About 85 % of the cells recorded (n = 15) presented a potent secretory response to both hypoxia and high $K^+$. To estimate the magnitude of the cell secretory responses to hypoxia and other stimuli, we calculated the secretion rate (in picocoulombs/min) as the amount of charge transferred to the recording electrode during the 60 s after the solutions were equilibrated in the recording chamber. Quantitative estimates of the secretion rate induced by hypoxia (~2,000 pC/min) or high $K^+$ (~7,000 pC/min) yielded results (Fig. 16.3b, c) that are within the range of those calculated for similar responses in rats or mice with the same methodology (Ortega-Saenz et al. 2003; Piruat et al. 2004). Besides catecholamines, recent experiments have also shown the release of ATP

**Fig. 16.3** (continued) 40 mM KCl: 6,821 ± 2,290 fC/min; Hypoxia: 1,910 ± 521 fC/min; $n = 13$ recordings, 8 donors, aged from 27 to 62 years). Secretion rate is expressed in pC/min (mean ± S.E.M.). (**d**) Representative recordings of the increase in cytosolic [$Ca^{2+}$] elicited by hypoxia and high $K^+$ in dispersed glomus cells loaded with Fura-2 (67-year-old donor). Note in (**d**) that the hypoxia-induced increase of cytosolic $Ca^{2+}$ was reversibly abolished by the application of extracellular $Cd^{2+}$ (0.5 mM) (Modified from Ortega-Saenz et al. 2013)

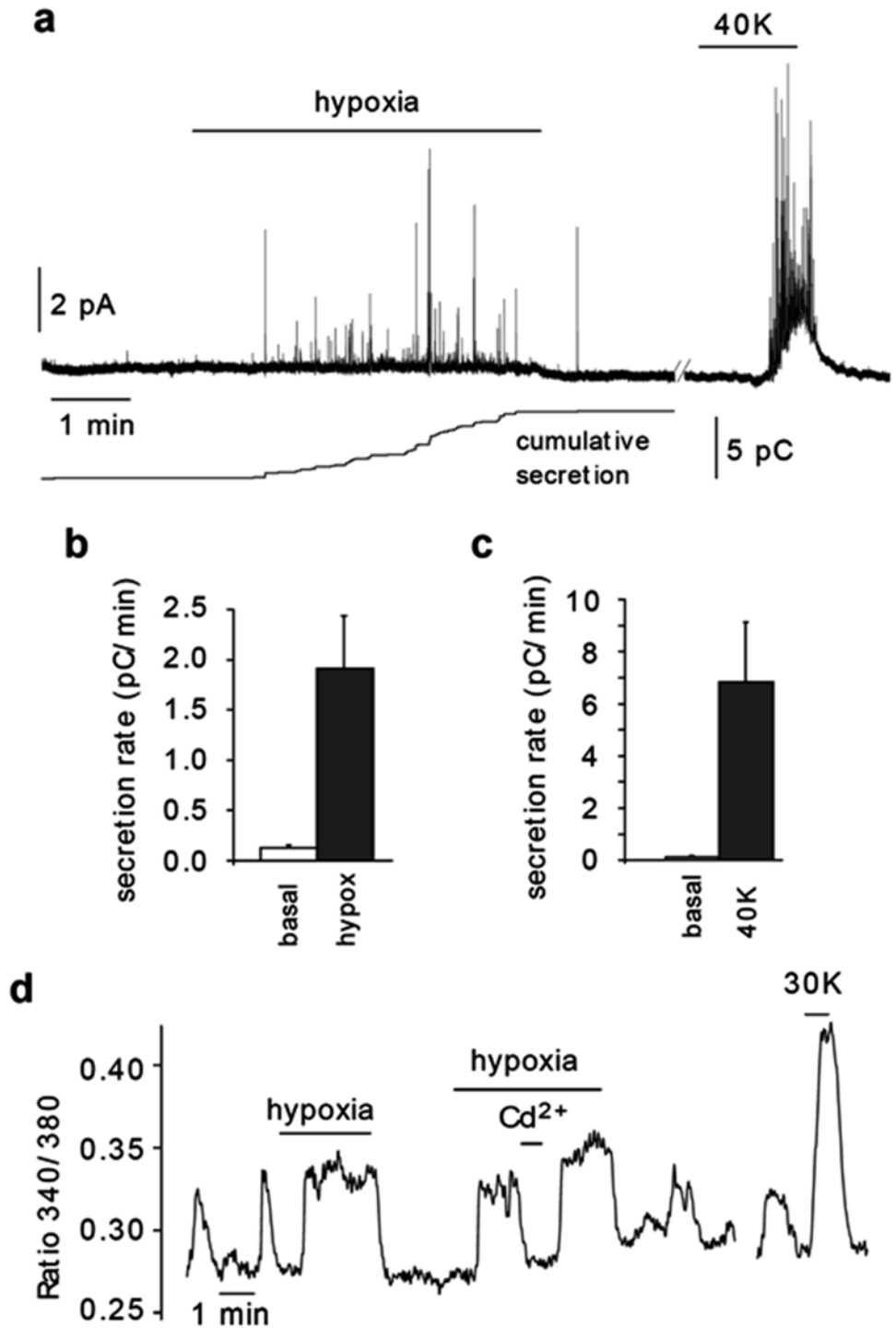


**Fig. 16.3** Secretory response of glomus cells to hypoxia in human carotid body slices. (**a**) *Top* Amperometric signal showing catecholamine release from a glomus cell in a human carotid body slice (27-year-old subject) exposed to low $PO_2$ (≈10 mmHg) and 40 mM $K^+$. Each spike represents a single exocytotic event. *Bottom* cumulative secretion signal (in picocoulombs, pC), resulting from the time integral of the amperometric recording. (**b** and **c**) Average secretion rate measured under basal conditions and in response to high $K^+$ and hypoxia. (Basal: 120±36 fC/min;

and acetylcholine form human glomus cells (Kahlin et al. 2014), which, as in lower mammalian species (Zhang et al. 2000), could be the mediators of the glomus cell-afferent fiber synapse. Although the protocol designed to obtain dispersed cells from human CB is still susceptible to improvement, we were able to get some cultures of healthy isolated human glomus cells in which hypoxia-evoked a robust increase in cytosolic [$Ca^{2+}$]. Nonetheless, the time courses of the $Ca^{2+}$ signals greatly varied from cell to cell (Ortega-Saenz et al. 2013). In cells with spontaneous $Ca^{2+}$ oscillations, hypoxia normally elicited a sustained elevation of [$Ca^{2+}$] that was reversibly abolished by 0.5 mM extracellular $Cd^{2+}$ (Fig. 16.3d). About 70 % of the human glomus cells that exhibited a clear increase in cytosolic $Ca^{2+}$ concentration in response to 30 mM $K^+$ (n = 17), also responded to hypoxia with a peak $Ca^{2+}$ signal amplitude that was 14.4 ± 4 % of that observed during exposure to high $K^+$.

## 16.4 Cellular Responses to Hypoglycemia

Participation of CB cells in glucose homeostasis has been suggested by previous work in non-primate mammals (Alvarez-Buylla and de Alvarez-Buylla 1988; Koyama et al. 2000; Koyama et al. 2001). We have shown that glomus cells are glucose sensitive and that low glucose induces depolarization, increase of cytosolic [$Ca^{2+}$] and secretion of transmitters from these cells. Glomus cell sensitivity to hypoglycemia seems to be mainly due to activation of an inward cationic current (Garcia-Fernandez et al. 2007; Pardal and Lopez-Barneo 2002). The responsiveness of mammalian CB cells to hypoglycemia has been confirmed in the *in vitro* CB–petrosal ganglion preparation (Zhang et al. 2007) and in dispersed cat glomus cells (Fitzgerald et al. 2009). Nonetheless, other authors have failed to find any responsiveness of explanted whole CB preparations to low glucose (Bin-Jaliah et al. 2004; Conde et al. 2007) or any significant changes in cytosolic [$Ca^{2+}$] in dispersed glomus cells in response to rapid glucose removal (Gallego-Martin et al. 2012). In contrast to these last observations, we have found that, as in the rat (Garcia-Fernandez et al. 2007), human glomus cells can also depolarize and release transmitters in response to a decrease in the extracellular glucose concentration (Ortega-Saenz et al. 2013). Under normoxic conditions ($PO_2$ ~ 150 mmHg), removal of extracellular glucose produced membrane depolarization, an increase in cytosolic [$Ca^{2+}$] and a secretory response in human glomus cells similar to that obtained in rodent cells subjected to the same experimental protocol (Fig. 16.4a–d) (Garcia-Fernandez et al. 2007; Zhang et al. 2007). The average membrane potential recorded in dialysed human glomus cells (whole cell patch clamp recording) was −44 ± 3 mV ($n$ = 10). In 75 % of the cells tested, removal of the glucose from the bathing medium elicited a reversible depolarization averaging 4.2 ± 0.4 mV ($n$ = 5 exposures in three cells; Fig. 16.4a). In 67 % of the human glomus cells tested glucose removal induced a rise of cytosolic $Ca^{2+}$ with a peak signal amplitude that was 15.2 ± 3 % of that observed for the exposure to 30 mM $K^+$ (Fig. 16.4b). In parallel experiments performed on rat cells, the peak $Ca^{2+}$ signal in response to hypoglycemia was 34.5 ± 6 % of that seen with 30 mM $K^+$ ($n$ = 13). The secretory response induced by hypoglycaemia in human CB slices is illustrated in Fig. 16.4c, d. Stimulation of CB glomus cells by low glucose is markedly potentiated in hypoxia, and both stimuli (glucose deficiency and hypoxia) act additively to induce transmitter release (Fig. 16.4e) or rises of intracellular [$Ca^{2+}$] (Fig. 16.4f).

**Fig. 16.4** (continued) (44-year-old subject). Bottom cumulative secretion signal (in picocoulombs, pC) resulting from the time integral of the amperometric recording. (d) Quantification of the increase in secretion rate induced by hypoglycemia (n = 2 recordings; 2 donors of 27 and 44 years of age). (e) Top Potentiation of the secretory response to low glucose induced by mild hypoxia (6 % $O_2$). Bottom Cumulative secretion signal (in picocoulombs, pC) resulting from the time integral of the amperometric recording. (f) Representative recording of the reversible increase of cytosolic [$Ca^{2+}$] in a Fura-2-loaded glomus cell in response to hypoxia and hypoglycaemia. Note the potentiation by hypoxia of the response to low glucose (67-year-old subject) (Modified from Ortega-Saenz et al. 2013)

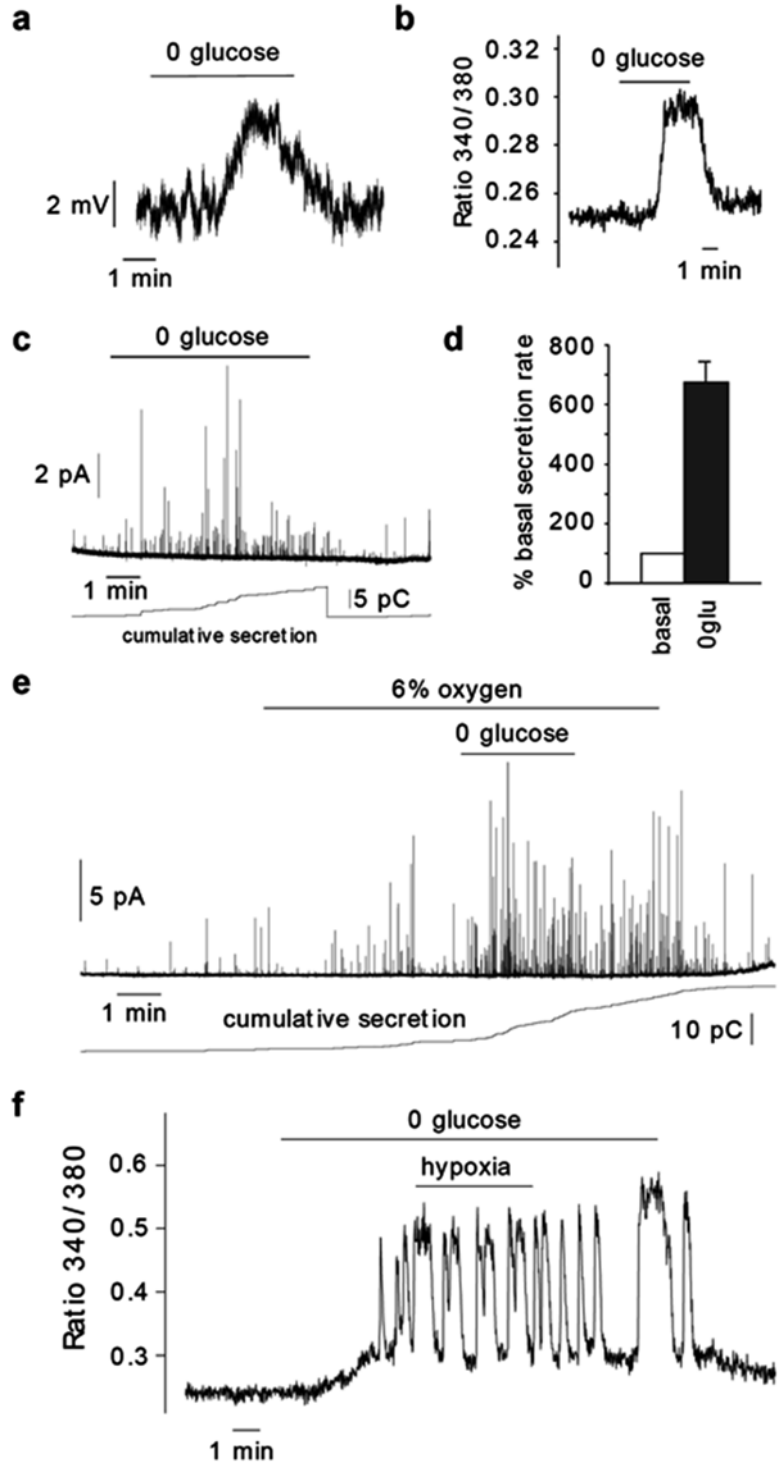


**Fig. 16.4** Responses of human glomus cells to low glucose and hypoxia. (**a**) Depolarising receptor potential recorded in a current-clamped human glomus cell in response to glucopenia (72-year-old subject). (**b**) Reversible increase of cytosolic [$Ca^{2+}$] in a Fura-2-loaded glomus cell exposed to low glucose (76-year-old subject). (**c**) *Top* Secretory response to low glucose of a glomus cell in a CB slice recorded by amperometry

## 16.5 Neurogenic Niche in the Human Carotid Body

Hypoxic ventilatory acclimatization (HVA) to long-term hypoxia is an adaptive hyperventilatory response that facilitates survival of sojourners at high altitude or patients with cardio-respiratory diseases with reduced gas exchange in the lungs (Arias-Stella and Valcarcel 1976; Heath et al. 1970). It has been suggested that HVA acclimatization is due, at least in part, to the enhancement of glomus cell excitability (Chen et al. 2002; Stea et al. 1995) and the increase of CB size induced by chronic hypoxia (Arias-Stella and Valcarcel 1976; McGregor et al. 1984). The ability of the CB to grow in response to sustained hypoxia is an intriguing property that makes it unique among other organs of the adult peripheral nervous system. Although a population of glomus cells can undergo mitosis (Chen et al. 2007; Pardal et al. 2007; Wang et al. 2008), it has been reported that the CB shares properties with neurogenic centers in the adult brain and that the glia-like type II cells, or a subpopulation of them, are indeed stem cells which contribute to the growth of the CB in response to chronic hypoxia (Kokovay and Temple 2007; Pardal et al. 2007). CB stem cells are quiescent in normoxia but upon exposure to hypoxia they evolve into nestin-positive intermediate progenitor cells, which in turn proliferate and, eventually, differentiate into new glomus cells and other cell types (Pardal et al. 2007). Moreover, we have recently shown that hypoxia does not directly activates stem cells to proliferate but this depends on synaptic-like contacts between glomus cells and stem cells ("chemoproliferative synapse") in which transmitters released from glomus cells during hypoxia (particularly endothelin 1) activate the stem cells (Platero-Luengo et al. 2014). Our histological analyses in the human CB (Ortega-Saenz et al. 2013) indicated that the neurogenic niche is present even at advance age. Both GFAP+ (~1 %) and nestin+ (~7 %) cells lie next to TH+/DDC+ neuronal cells (Fig. 16.5a–c), suggesting that a chemo-proliferative synapse structure, similar to the one described in rodents (Platero-Luengo et al. 2014), may exist within the human CB parenchyma. These human neural progenitors are able to grow in culture forming clonal and spherical colonies called neurospheres (Fig. 16.5d), similar to those described in the rat CB (Pardal et al. 2007). Human CB neurospheres have a core enriched in nestin+ progenitor cells and these progenitors are able to differentiate into TH+ neuronal cells forming blebs at the edge of the neurosphere (Fig. 16.5e). As reported previously for the rat (Pardal et al. 2007), human neurospheres are also obtained in cultures in which a single cell per well is plated, thus confirming the single stem cell (clonal) origin of these neurosphere colonies.

## 16.6 Conclusions

We have shown that human CB glomus cells have functional properties that are similar to their lower mammals counterparts (Kahlin et al. 2014; Ortega-Saenz et al. 2013). Although the relative size of the human CB parenchyma seems to be smaller than that of other non-primate mammalian species, CB progenitor cells and chemosensitive glomus cells appear to be preserved in human subjects of advanced age (Ortega-Saenz et al. 2013). Our research demonstrates that functional studies at the cellular and molecular levels are feasible in CBs removed from human donors, meaning that the association between CB function and human pathology can be now systematically investigated. These findings are particularly relevant since in recent times the CB is attracting renewed medical interest. Systemic studies in man have yielded results compatible with CB involvement in the counter-regulatory response to hypoglycemia, a process that could be altered in diabetic patients (Wehrwein et al. 2010). In addition, cumulative evidence indicates that abnormal CB over-activation may contribute to autonomic imbalance underlying several human diseases, such as sleep apnea, hypertension, heart failure or diabetes (Iturriaga 2013; Narkiewicz et al. 1998; Paton et al. 2013; Prabhakar and Semenza 2012; Ribeiro et al. 2013; Schultz et al. 2013). Indeed, modulation of CB function is

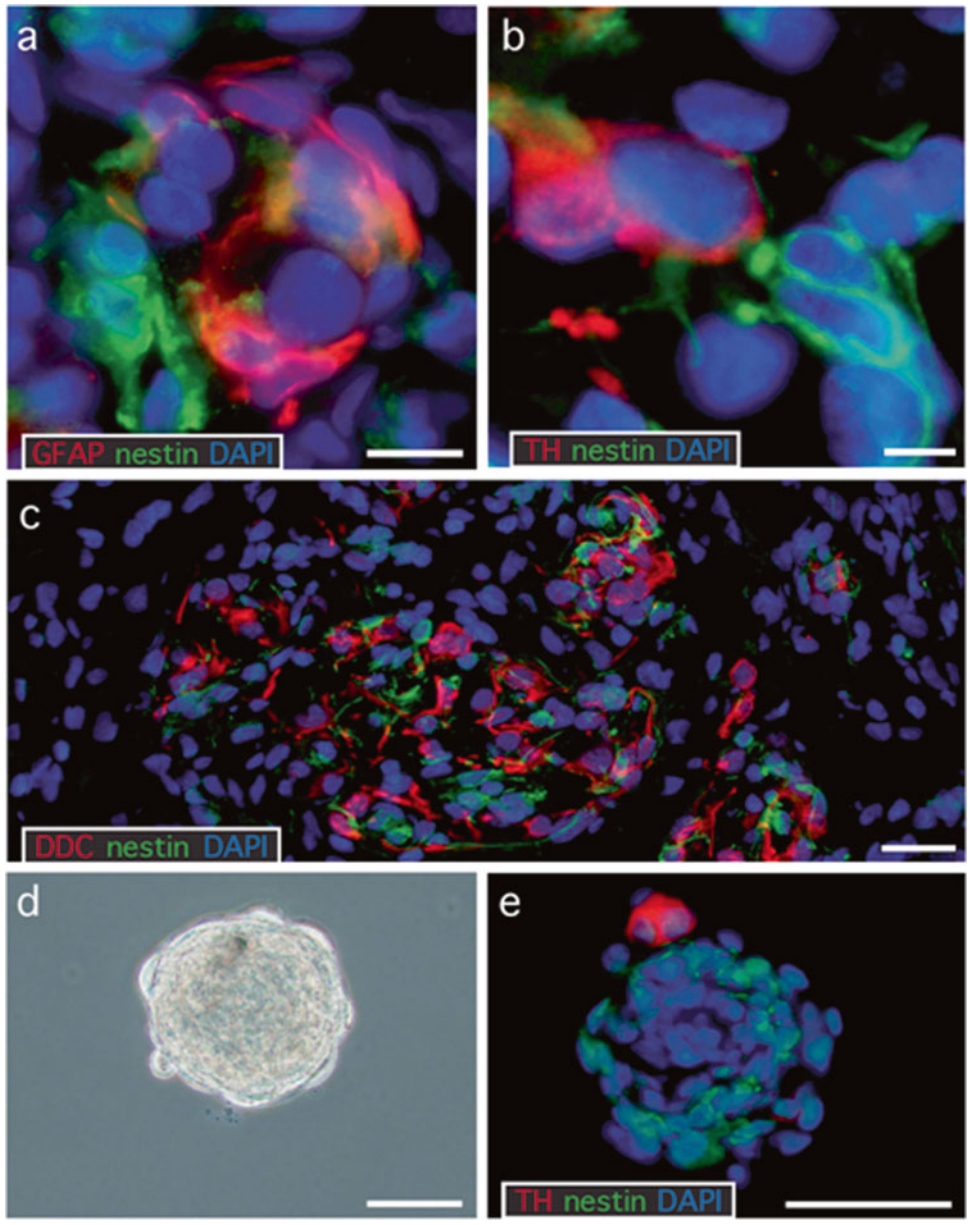


**Fig. 16.5** Human carotid body stem cell niche. (**a**) Fluorescence immunohistochemistry with antibodies against two stem cell markers, GFAP and nestin, in a thin section of the human carotid body. Scale bar: 10 μm. (**b**) Fluorescence immunohistochemistry with antibodies against TH, a glomus cell marker, and against nestin, a stem cell marker, illustrating the presence of neural progenitor cells around a CB glomerulus. Scale bar: 5 μm. (**c**) fluorescence immunohistochemistry image at low magnification with antibodies against DDC, a glomus cell marker, and against nestin. Note the proximity between progenitor cells and glomus cells within the CB glomeruli. Scale bar: 20 μm. (**d**) Bright-field image of a typical neurosphere obtained in non-adherent culture after growth of human carotid body stem cells. Scale bar: 100 μm. (**e**) Fluorescence immunohistochemistry with antibodies against TH and nestin in thin sections of human carotid body neurospheres, illustrating the presence of nestin + neural progenitor cells within the core, and blebs of TH+ glomus cells on the surface of neurospheres. Scale bars: 50 μm (Modified from Ortega-Saenz et al. 2013)

currently being formally investigated as a potential novel approach in the treatment of neurogenic hypertension in humans (McBryde et al. 2013).

**Funding** This research was supported by the Botín Foundation and Axontherapix. Support was also received through grants from the 'Consejería de Salud de la Junta Andalucía' and the Spanish Ministries of Economy and Innovation, and Health (SAF, FIS, CIBERNED and TERCEL programmes).

**Acknowledgements** We wish to express our gratitude to Prof. Antonio Ordoñez as well as the members of the Coordination of Transplants Unit and the Neurosurgery Department of HUVR for their collaboration in the dissection of the vascular segments used in this study.

## References

Alvarez-Buylla R, de Alvarez-Buylla ER (1988) Carotid sinus receptors participate in glucose homeostasis. Respir Physiol 72(3):347–359

Arias-Stella J, Valcarcel J (1976) Chief cell hyperplasia in the human carotid body at high altitudes; physiologic and pathologic significance. Hum Pathol 7(4):361–373

Arjona V, Minguez-Castellanos A, Montoro RJ, Ortega A, Escamilla F, Toledo-Aral JJ, Pardal R, Mendez-Ferrer S, Martin JM, Perez M, Katati MJ, Valencia E, Garcia T, Lopez-Barneo J (2003) Autotransplantation of human carotid body cell aggregates for treatment of Parkinson's disease. Neurosurgery 53(2):321–328; discussion 328-330

Bin-Jaliah I, Maskell PD, Kumar P (2004) Indirect sensing of insulin-induced hypoglycaemia by the carotid body in the rat. J Physiol 556(Pt 1):255–266

Buckler K, Honore E (2004) Molecular strategies for studying oxygen-sensitive K+ channels. Methods Enzymol 381:233–256

Chao CC, Lee EH (1999) Neuroprotective mechanism of glial cell line-derived neurotrophic factor on dopamine neurons: role of antioxidation. Neuropharmacology 38(6):913–916

Chen J, He L, Dinger B, Stensaas L, Fidone S (2002) Role of endothelin and endothelin A-type receptor in adaptation of the carotid body to chronic hypoxia. Am J Physiol Lung Cell Mol Physiol 282(6):L1314–L1323

Chen J, He L, Liu X, Dinger B, Stensaas L, Fidone S (2007) Effect of the endothelin receptor antagonist bosentan on chronic hypoxia-induced morphological and physiological changes in rat carotid body. Am J Physiol Lung Cell Mol Physiol 292(5):L1257–L1262

Cheng H, Fu YS, Guo JW (2004) Ability of GDNF to diminish free radical production leads to protection against kainate-induced excitotoxicity in hippocampus. Hippocampus 14(1):77–86

Conde SV, Peers C (2013) Carotid body chemotransduction gets the human touch. J Physiol 591(Pt 24):6131–6132

Conde SV, Obeso A, Gonzalez C (2007) Low glucose effects on rat carotid body chemoreceptor cells' secretory responses and action potential frequency in the carotid sinus nerve. J Physiol 585(Pt 3):721–730

Cramer JA, Wiggins RH, Fudim M, Engelman ZJ, Sobotka PA, Shah LM (2014) Carotid body size on CTA: correlation with comorbidities. Clin Radiol 69(1):e33–e36

Di Giulio C, Zara S, Cataldi A, Porzionato A, Pokorski M, De Caro R (2012) Human carotid body HIF and NGB expression during human development and aging. Adv Exp Med Biol 758:265–271

Erickson JT, Brosenitsch TA, Katz DM (2001) Brain-derived neurotrophic factor and glial cell line-derived neurotrophic factor are required simultaneously for survival of dopaminergic primary sensory neurons in vivo. J Neurosci 21(2):581–589

Espejo EF, Montoro RJ, Armengol JA, Lopez-Barneo J (1998) Cellular and functional recovery of Parkinsonian rats after intrastriatal transplantation of carotid body cell aggregates. Neuron 20(2):197–206

Fagerlund MJ, Kahlin J, Ebberyd A, Schulte G, Mkrtchian S, Eriksson LI (2010) The human carotid body: expression of oxygen sensing and signaling genes of relevance for anesthesia. Anesthesiology 113(6):1270–1279

Fitzgerald RS, Shirahata M, Chang I, Kostuk E (2009) The impact of hypoxia and low glucose on the release of acetylcholine and ATP from the incubated cat carotid body. Brain Res 1270:39–44

Gallego-Martin T, Fernandez-Martinez S, Rigual R, Obeso A, Gonzalez C (2012) Effects of low glucose on carotid body chemoreceptor cell activity studied in cultures of intact organs and in dissociated cells. Am J Physiol Cell Physiol 302(8):C1128–C1140

Garcia-Fernandez M, Ortega-Saenz P, Castellano A, Lopez-Barneo J (2007) Mechanisms of low-glucose sensitivity in carotid body glomus cells. Diabetes 56(12):2893–2900

Heath D, Edwards C, Harris P (1970) Post-mortem size and structure of the human carotid body. Thorax 25(2):129–140

Hidalgo-Figueroa M, Bonilla S, Gutierrez F, Pascual A, Lopez-Barneo J (2012) GDNF is predominantly expressed in the PV+ neostriatal interneuronal ensemble in normal mouse and after injury of the nigrostriatal pathway. J Neurosci 32(3):864–872

Iturriaga R (2013) Intermittent hypoxia: endothelin-1 and hypoxic carotid body chemosensory potentiation. Exp Physiol 98(11):1550–1551

Izal-Azcarate A, Belzunegui S, San Sebastian W, Garrido-Gil P, Vazquez-Claverie M, Lopez B, Marcilla I, Luquin MA (2008) Immunohistochemical characterization of the rat carotid body. Respir Physiol Neurobiol 161(1):95–99

Kahlin J, Mkrtchian S, Ebberyd A, Hammarstedt-Nordenvall L, Nordlander B, Yoshitake T, Kehr J,

Prabhakar N, Poellinger L, Fagerlund MJ, Eriksson LI (2014) The human carotid body releases acetylcholine, ATP and cytokines during hypoxia. Exp Physiol 99(8):1089–1098

Kokovay E, Temple S (2007) Taking neural crest stem cells to new heights. Cell 131(2):234–236

Koyama Y, Coker RH, Stone EE, Lacy DB, Jabbour K, Williams PE, Wasserman DH (2000) Evidence that carotid bodies play an important role in glucoregulation in vivo. Diabetes 49(9):1434–1442

Koyama Y, Coker RH, Denny JC, Lacy DB, Jabbour K, Williams PE, Wasserman DH (2001) Role of carotid bodies in control of the neuroendocrine response to exercise. Am J Physiol Endocrinol Metab 281(4):E742–E748

Kroll SL, Czyzyk-Krzeska MF (1998) Role of H2O2 and heme-containing O2 sensors in hypoxic regulation of tyrosine hydroxylase gene expression. Am J Physiol 274(1 Pt 1):C167–C174

Kumar P, Prabhakar NR (2012) Peripheral chemoreceptors: function and plasticity of the carotid body. Compr Physiol 2(1):78

Lazarov NE, Reindl S, Fischer F, Gratzl M (2009) Histaminergic and dopaminergic traits in the human carotid body. Respir Physiol Neurobiol 165(2-3):131–136

Leitner ML, Wang LH, Osborne PA, Golden JP, Milbrandt J, Johnson EM Jr (2005) Expression and function of GDNF family ligands and receptors in the carotid body. Exp Neurol 191(Suppl 1):S68–S79

Lopez-Barneo J (2003) Oxygen and glucose sensing by carotid body glomus cells. Curr Opin Neurobiol 13(4):493–499

Lopez-Barneo J, Pardal R, Ortega-Saenz P (2001) Cellular mechanism of oxygen sensing. Annu Rev Plant Physiol Plant Mol Biol 63:259–287

Lopez-Barneo J, Ortega-Saenz P, Pardal R, Pascual A, Piruat JI (2008) Carotid body oxygen sensing. Eur Respir J 32(5):1386–1398

Lopez-Barneo J, Pardal R, Ortega-Saenz P, Duran R, Villadiego J, Toledo-Aral JJ (2009) The neurogenic niche in the carotid body and its applicability to antiparkinsonian cell therapy. J Neural Transm 116(8):975–982

Luquin MR, Montoro RJ, Guillen J, Saldise L, Insausti R, Del Rio J, Lopez-Barneo J (1999) Recovery of chronic parkinsonian monkeys by autotransplants of carotid body cell aggregates into putamen. Neuron 22(4):743–750

McBryde FD, Abdala AP, Hendy EB, Pijacka W, Marvar P, Moraes DJ, Sobotka PA, Paton JF (2013) The carotid body as a putative therapeutic target for the treatment of neurogenic hypertension. Nat Commun 4:2395

McGregor KH, Gil J, Lahiri S (1984) A morphometric study of the carotid body in chronically hypoxic rats. J Appl Physiol 57(5):1430–1438

Minguez-Castellanos A, Escamilla-Sevilla F, Hotton GR, Toledo-Aral JJ, Ortega-Moreno A, Mendez-Ferrer S, Martin-Linares JM, Katati MJ, Mir P, Villadiego J, Meersmans M, Perez-Garcia M, Brooks DJ, Arjona V, Lopez-Barneo J (2007) Carotid body autotransplantation in Parkinson disease: a clinical and positron emission tomography study. J Neurol Neurosurg Psychiatry 78(8):825–831

Mkrtchian S, Kahlin J, Ebberyd A, Gonzalez C, Sanchez D, Balbir A, Kostuk EW, Shirahata M, Fagerlund MJ, Eriksson LI (2012) The human carotid body transcriptome with focus on oxygen sensing and inflammation–a comparative analysis. J Physiol 590(Pt 16):3807–3819

Munoz-Manchado AB, Villadiego J, Suarez-Luna N, Bermejo-Navas A, Garrido-Gil P, Labandeira-Garcia JL, Echevarria M, Lopez-Barneo J, Toledo-Aral JJ (2013) Neuroprotective and reparative effects of carotid body grafts in a chronic MPTP model of Parkinson's disease. Neurobiol Aging 34(3):902–915

Nair S, Gupta A, Fudim M, Robinson C, Ravi V, Hurtado-Rua S, Engelman Z, Lee KS, Phillips CD, Sista AK (2013) CT angiography in the detection of carotid body enlargement in patients with hypertension and heart failure. Neuroradiology 55(11):1319–1322

Narkiewicz K, van de Borne PJ, Montano N, Dyken ME, Phillips BG, Somers VK (1998) Contribution of tonic chemoreflex activation to sympathetic activity and blood pressure in patients with obstructive sleep apnea. Circulation 97(10):943–945

Ortega-Saenz P, Garcia-Fernandez M, Pardal R, Alvarez E, Lopez-Barneo J (2003) Studies on glomus cell sensitivity to hypoxia in carotid body slices. Adv Exp Med Biol 536:65–73

Ortega-Saenz P, Pascual A, Gomez-Diaz R, Lopez-Barneo J (2006) Acute oxygen sensing in heme oxygenase-2 null mice. J Gen Physiol 128(4):405–411

Ortega-Saenz P, Levitsky KL, Marcos-Almaraz MT, Bonilla-Henao V, Pascual A, Lopez-Barneo J (2010) Carotid body chemosensory responses in mice deficient of TASK channels. J Gen Physiol 135(4):379–392

Ortega-Saenz P, Pardal R, Levitsky K, Villadiego J, Munoz-Manchado AB, Duran R, Bonilla-Henao V, Arias-Mayenco I, Sobrino V, Ordonez A, Oliver M, Toledo-Aral JJ, Lopez-Barneo J (2013) Cellular properties and chemosensory responses of the human carotid body. J Physiol 591(Pt 24):6157–6173

Pardal R, Lopez-Barneo J (2002) Low glucose-sensing cells in the carotid body. Nat Neurosci 5(3):197–198

Pardal R, Ludewig U, Garcia-Hirschfeld J, Lopez-Barneo J (2000) Secretory responses of intact glomus cells in thin slices of rat carotid body to hypoxia and tetraethylammonium. Proc Natl Acad Sci U S A 97(5):2361–2366

Pardal R, Ortega-Saenz P, Duran R, Lopez-Barneo J (2007) Glia-like stem cells sustain physiologic neurogenesis in the adult mammalian carotid body. Cell 131(2):364–377

Pascual A, Hidalgo-Figueroa M, Piruat JI, Pintado CO, Gomez-Diaz R, Lopez-Barneo J (2008) Absolute requirement of GDNF for adult catecholaminergic neuron survival. Nat Neurosci 11(7):755–761

Paton FR, Sobotka A, Fudim M, Engelman J, Hart CJ, McBryde D, Abdala P, Marina N, Gourine AV, Lobo M, Patel N, Burchell A, Ratcliffe L, Nightingale A (2013) The carotid body as a therapeutic target for the treatment of sympathetically mediated diseases. Hypertension 61:8

Piruat JI, Pintado CO, Ortega-Saenz P, Roche M, Lopez-Barneo J (2004) The mitochondrial SDHD gene is required for early embryogenesis, and its partial deficiency results in persistent carotid body glomus cell activation with full responsiveness to hypoxia. Mol Cell Biol 24(24):10933–10940

Platero-Luengo A, Gonzalez-Granero S, Duran R, Diaz-Castro B, Piruat JI, Garcia-Verdugo JM, Pardal R, Lopez-Barneo J (2014) An O2-sensitive glomus cell-stem cell synapse induces carotid body growth in chronic hypoxia. Cell 156(1-2):291–303

Pokorski M, Walski M, Dymecka A, Marczak M (2004) The aging carotid body. J Physiol Pharmacol 55(Suppl 3):107–113

Porzionato A, Macchi V, Parenti A, De Caro R (2008) Trophic factors in the carotid body. Int Rev Cell Mol Biol 269:1–58

Prabhakar NR, Semenza GL (2012) Adaptive and maladaptive cardiorespiratory responses to continuous and intermittent hypoxia mediated by hypoxia-inducible factors 1 and 2. Physiol Rev 92(3): 967–1003

Ribeiro MJ, Sacramento JF, Gonzalez C, Guarino MP, Monteiro EC, Conde SV (2013) Carotid body denervation prevents the development of insulin resistance and hypertension induced by hypercaloric diets. Diabetes 62(8):2905–2916

Saavedra A, Baltazar G, Duarte EP (2008) Driving GDNF expression: the green and the red traffic lights. Prog Neurobiol 86(3):186–215

Schultz HD, Marcus NJ, Del Rio R (2013) Role of the carotid body in the pathophysiology of heart failure. Curr Hypertens Rep 15(4):356–362

Shamblin WR, ReMine WH, Sheps SG, Harrison EG Jr (1971) Carotid body tumor (chemodectoma). Clinicopathologic analysis of ninety cases. Am J Surg 122(6):732–739

Smith MP, Cass WA (2007) GDNF reduces oxidative stress in a 6-hydroxydopamine model of Parkinson's disease. Neurosci Lett 412(3):259–263

Stea A, Jackson A, Macintyre L, Nurse CA (1995) Long-term modulation of inward currents in O2 chemoreceptors by chronic hypoxia and cyclic AMP in vitro. J Neurosci 15(3 Pt 2):2192–2202

Teppema LJ, Dahan A (2010) The ventilatory response to hypoxia in mammals: mechanisms, measurement, and analysis. Physiol Rev 90(2):675–754

Timmers HJ, Karemaker JM, Wieling W, Marres HA, Folgering HT, Lenders JW (2003) Baroreflex and chemoreflex function after bilateral carotid body tumor resection. J Hypertens 21(3):591–599

Toledo-Aral JJ, Mendez-Ferrer S, Pardal R, Echevarria M, Lopez-Barneo J (2003) Trophic restoration of the nigrostriatal dopaminergic pathway in long-term carotid body-grafted parkinsonian rats. J Neurosci 23(1):141–148

Urena J, Fernandez-Chacon R, Benot AR, Alvarez de Toledo GA, Lopez-Barneo J (1994) Hypoxia induces voltage-dependent Ca2+ entry and quantal dopamine secretion in carotid body glomus cells. Proc Natl Acad Sci U S A 91(21):10208–10211

Villadiego J, Mendez-Ferrer S, Valdes-Sanchez T, Silos-Santiago I, Farinas I, Lopez-Barneo J, Toledo-Aral JJ (2005) Selective glial cell line-derived neurotrophic factor production in adult dopaminergic carotid body cells in situ and after intrastriatal transplantation. J Neurosci 25(16):4091–4098

Wang ZY, Olson EB Jr, Bjorling DE, Mitchell GS, Bisgard GE (2008) Sustained hypoxia-induced proliferation of carotid body type I cells in rats. J Appl Physiol (1985) 104(3):803–808

Wehrwein EA, Basu R, Basu A, Curry TB, Rizza RA, Joyner MJ (2010) Hyperoxia blunts counterregulation during hypoglycaemia in humans: possible role for the carotid bodies? J Physiol 588(Pt 22):4593–4601

Weir EK, Lopez-Barneo J, Buckler KJ, Archer SL (2005) Acute oxygen-sensing mechanisms. N Engl J Med 353(19):2042–2055

Zhang M, Zhong H, Vollmer C, Nurse CA (2000) Co-release of ATP and ACh mediates hypoxic signalling at rat carotid body chemoreceptors. J Physiol 525(Pt 1):143–158

Zhang M, Buttigieg J, Nurse CA (2007) Neurotransmitter mechanisms mediating low-glucose signalling in cocultures and fresh tissue slices of rat carotid body. J Physiol 578(Pt 3):735–750

# Is the Carotid Body a Metabolic Monitor?

17

M. Shirahata, W.-Y. Tang, M.-K. Shin, and V.Y. Polotsky

**Abstract**

The carotid body is a multi-modal sensor and it has been debated if it senses low glucose. We have hypothesized that the carotid body is modified by some metabolic factors other than glucose and contributes to whole body glucose metabolism. This study examined the roles of insulin, leptin and transient receptor potential (TRP) channels on carotid sinus nerve (CSN) chemoreceptor discharge. In agreement with other studies, CSN activity was not modified by low glucose. Insulin did not affect the CSN hypoxic response. Leptin significantly augmented the CSN response to hypoxia and nonspecific Trp channel blockers (SKF96365, 2-APB) reversed the effect of leptin. Gene expression analysis showed high expression of Trpm3, 6, and 7 channels in the carotid body and petrosal ganglion. The results suggest that the adult mouse carotid body does not sense glucose levels directly. The carotid body may contribute to neural control of glucose metabolism via leptin receptor-mediated TRP channel activation.

**Keywords**

CSN activity • Glucose • Insulin • Leptin • TRP channel

## 17.1 Introduction

It is well established that the carotid body plays a key role in physiological responses to hypoxia and hypercapnea in many species and different preparations. Further, function of the carotid body is modified by other physiological stimuli (Gonzalez et al. 1994). A pioneer work by Alvarez-Buylla and Alvarez-Buylla (1988) has opened the debates if the carotid body senses glucose concentration or regulates glucose metabolism. Regarding glucose sensing, conflicting

M. Shirahata (✉) • W.-Y. Tang
Department of Environmental Health Sciences, Johns Hopkins University, Baltimore, MD, USA
e-mail: mshiraha@jhmi.edu

M.-K. Shin • V.Y. Polotsky
Department of Medicine, Johns Hopkins University, Baltimore, MD, USA



C. Peers et al. (eds.), *Arterial Chemoreceptors in Physiology and Pathophysiology*, Advances in Experimental Medicine and Biology 860, DOI 10.1007/978-3-319-18440-1_17

data have been presented and consensus has not been reached. In general, *in vitro* culture preparations showed glomus cell's sensitivity to low glucose. For example, catecholamine release from cultured carotid body slices increased in response to low glucose (Pardal and López-Barneo 2002). Afferent neural discharge in co-culture preparation of petrosal neurons and glomus cells increased during low glucose superfusion (Zhang et al. 2007). On the other hand, glucose sensitivity of the carotid body has not been consistently shown in acute preparations. Chemoreceptor discharge was not increased with low glucose (Bin-Jaliah et al. 2004; Conde et al. 2007), although the effect of cyanide on chemoreceptor discharge was enhanced by low glucose (Alvarez-Buylla and Alvarez-Buylla 1988). Moreover, phenotypic changes of glomus cells during culture have been suggested (Gallego-Martin et al. 2012). Nevertheless, several experimental data suggest that the carotid body is involved in whole body glucose metabolism: experimentally induced perturbation of glucose metabolism was blocked by carotid body afferent denervation (Alvarez-Buylla and Alvarez-Buylla 1988; Koyama et al. 2000; Shin et al. 2014; Wehrwein et al. 2010). Hence, we have hypothesized that the carotid body is modified by some metabolic factors and contributes to whole body glucose metabolism. In this study we focused the roles of insulin, leptin and Trp channels on CSN chemoreceptor discharge.

## 17.2 Methods

Mice (DBA/2 J, C57BL/6 J) were purchased from Jackson Laboratory, housed and bred in the animal facility of the Johns Hopkins Bloomberg School of Public Health. The experimental protocols were approved by the Animal Care and Use Committee of the Johns Hopkins University.

### 17.2.1 Measurements of CSN Activity

For assessing CSN chemoreceptor activity, the carotid body bifurcation with CSN was obtained from a deeply anesthetized mouse at ~4–6 weeks of age. The tissue was continuously superfused with Krebs solution (in mM: 120 NaCl, 4.7 KCl, 1.2, $CaCl_2$ 1.8 mM, Mg $SO_4 \cdot 7H_2O$, 1.2 $Na_2HPO_4$, 22 $NaHCO_3$, and 11.1 Glucose) bubbled with 95 % $O_2$/5 % $CO_2$ or 95 % $N_2$/5 % $CO_2$ (hypoxic challenge) at 35–37 °C. Extra tissues were removed to expose the carotid body and the CSN. The central cut end of CSN was sucked in a glass suction electrode. Signals were collected and analyzed with an AcqKnowledge software (BioPac Systems, Inc.). CSN activity was expressed as impulses/s. At the end of each experiment the nerve was dislodged from the electrode, the electrode was refilled with Krebs solution and the activity at this point was considered as the noise level and subtracted from each measurement. Statistical analysis was performed with GraphPad Prism 4 using repeated one-way ANOVA. P value less than 0.05 was considered significant.

### 17.2.2 Gene Expression Analysis

Carotid bodies, petrosal ganglia, superior cervical ganglia (SCG), and brainstem were harvested from deeply anesthetized mice in TRIzol solution (Invitrogen), and frozen at −80 °C until use. Total RNA was isolated and reverse transcribed to cDNA with iScript Reverse Transcriptase (BIO-RAD, Hercules, CA). mRNA levels of the genes were quantified by SYBR Green-based real-time PCR using SsoAdvanced Universal SYBR® Green Supermix (BIO-RAD). The 2-ΔΔCt method was used to calculate the relative expression level of transcripts normalized to Rpl19.

## 17.3 Results

### 17.3.1 CSN Chemoreceptor Activity

When Krebs was switched to hyperoxia to hypoxia, the chamber $PO_2$ gradually decreased. The nadir was ~40 mmHg. CSN activity in mice increased along with the decrease in $PO_2$ (Fig. 17.1, left). After the basal hypoxic response was recorded, the superfusate was switched to low glucose (1 mM; substituted with 10 mM sucrose) for 5 min, which did not change the CSN activity. The CSN response to hypoxia during low glucose was not enhanced compared to that of high glucose (11 mM). The results

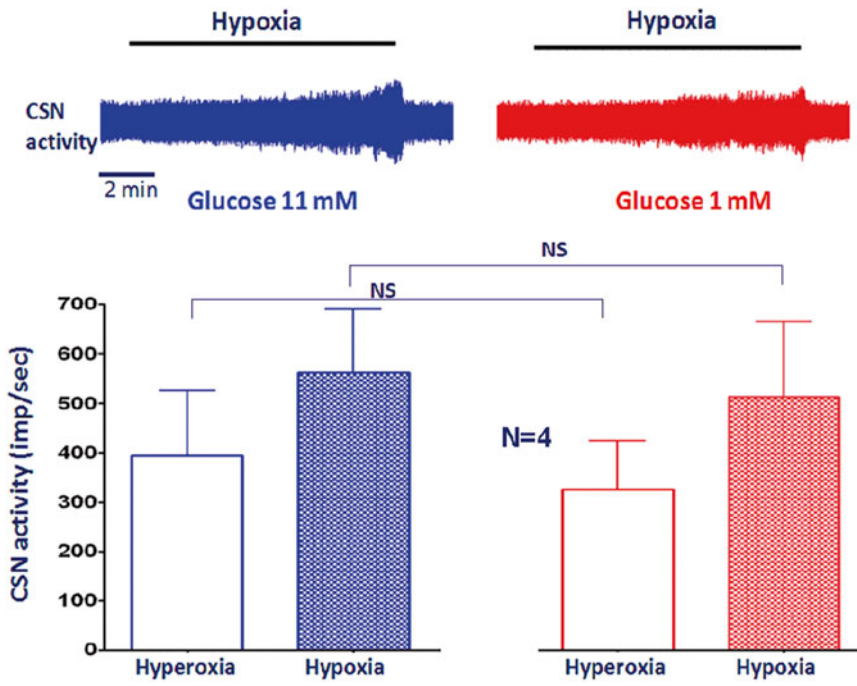


**Fig. 17.1** Hypoxia significantly increased CSN activity. Low glucose did not significantly influence the basal activity or the carotid body response to hypoxia

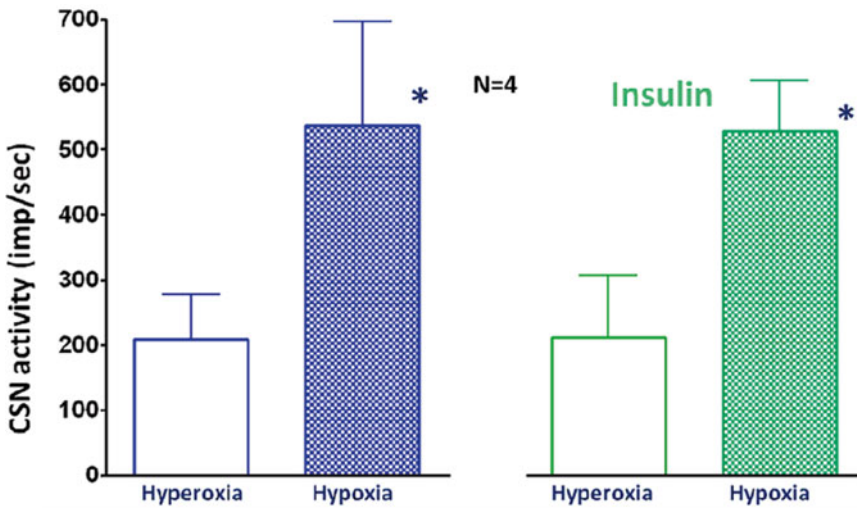


**Fig. 17.2** Hypoxia significantly increased CSN activity, but insulin did not influence the basal activity nor the carotid body response to hypoxia

agreed with other studies in acute CSN recording (Bin-Jaliah et al. 2004; Conde et al. 2007),

Insulin is a key hormone in whole body glucose metabolism. Further, insulin was used to clamp blood glucose levels for studying the role of the carotid body in glucose regulation (Koyama et al. 2000; Wehrwein et al. 2010). Here, we examined if insulin (5 μg/mL) influenced CSN response to hypoxia. The data show that insulin did not have significant influence on the carotid chemoreceptor hypoxic response (Fig. 17.2).

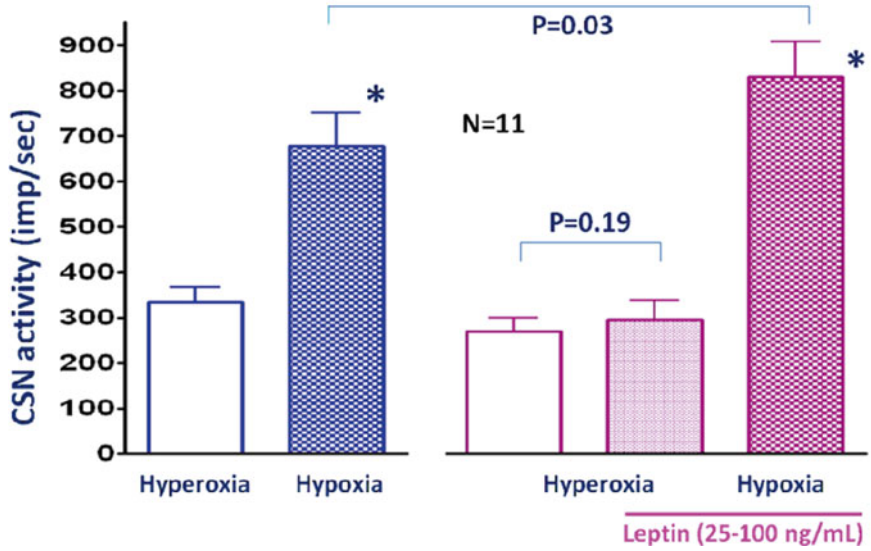


**Fig. 17.3** Leptin perfusion for 5 min did not change CSN activity during hyperoxia. However hypoxic response was significantly enhanced

In a previous study we found that leptin deficiency mice have blunted hypoxic ventilatory response (Tankersley et al. 2013). The presence of leptin receptors in the rat and human carotid body have been shown by Porzionato et al. (2011). In agreement with their work, our data showed high level of leptin receptor gene expression in the mouse carotid body (Balbir et al. 2007). Physiological roles of leptin and its receptors in carotid body function are not known. It is possible that leptin has a stimulatory effect on the carotid body. After obtaining the baseline hypoxic response, leptin (25–100 ng/mL) was added to the Krebs. After 5 min perfusion with leptin, hypoxic challenge was repeated. Leptin significantly enhanced the hypoxic chemoreceptor response (Fig. 17.3).

It has been shown that leptin excites proopiomelatonin neurons via activation of TrpC channels (Qiu et al. 2010). Therefore, we further examined if the effect of leptin on the hypoxic response of CSN is mediated via Trp channels. During hypoxic challenge with leptin, a TRP channel blocker (SKF96365 10 μM or 2-APB 10 μM) was added to the superfusate. The results show that TRP channel blockers inhibited the enhanced hypoxic response mediated by leptin (Fig. 17.4).

### 17.3.2 Gene Expression of TRP Channels

TRP channels are a family of non-selective cation channels. At least 33 subunit genes are encoded and the channels are divided into 7 subfamilies. Among them we examined the mRNA levels of 9 genes from 3 subfamilies (TrpC1, TrpC5, TrpC6, Trpm2, Trpm3, Trpm6, Trpm7, Trpv1, and Trpv2). Compared to the brainstem or the superior cervical ganglia, the carotid body and petrosal ganglia expressed more Trpm type channels (3, 6 and 7; Fig. 17.5). The expression of other channels examined was comparable among tissues (data not presented).

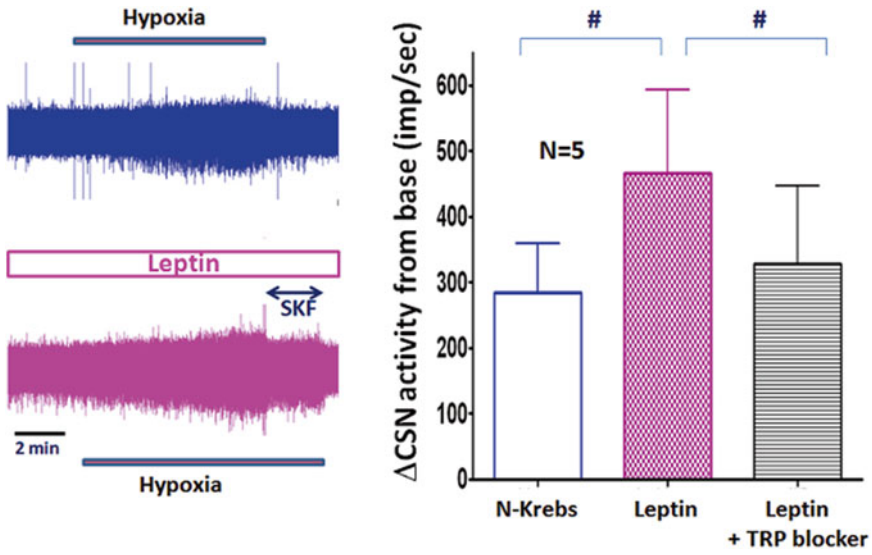


**Fig. 17.4** The raw traces of CSN activity (*top*, control; *bottom*, leptin) show leptin enhanced hypoxic response and non-specific TRP channel blocker (*SKF*) dampened the activity. In the summary graph (*right*) the data with SKF and 2-APB were pooled

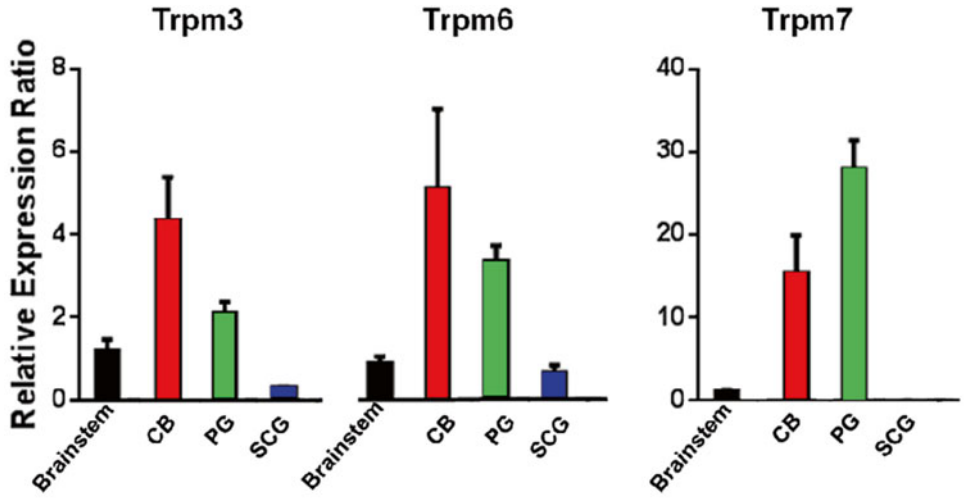


**Fig. 17.5** mRNA levels of Trpm3, Trpm6 and Trpm7 genes in the brainstem, carotid body (*CB*), Petrosal ganglion (*PG*) and superior cervical ganglion (*SCG*). N = 4, error bars: SD

## 17.4 Discussion

The carotid body is a multi-modal sensor. Several recent studies suggest that it senses low glucose and/or participate in regulating metabolism (by Alvarez-Buylla and Alvarez-Buylla 1988; Koyama et al. 2000; Pardal and López-Barneo 2002; Shin et al. 2014; Wehrwein et al. 2010; Zhang et al. 2007). Considering the well established sensitivity to $O_2$ and $CO_2$, and the location of the carotid body, it is tempting to assume that the carotid body is monitoring metabolic states in

the blood that goes to the brain. However to prove that the carotid body is a glucose or metabolic sensor, we need to consider several critical conditions (e.g., sensitivity, low threshold, increase of output etc.). In our model glucose does not influence the carotid chemosensory activity. This result is consistent with other acute studies (Bin-Jaliah et al. 2004; Conde et al. 2007). Although cultured models show glucose sensitivity of glomus cells (Pardal and López-Barneo 2002; Zhang et al. 2007), phenotypic changes in glucose sensitivity during culture has been indicated (Gallego-Martin et al. 2012). Collectively, it seems that the carotid body, if not cultured, does not sense glucose levels directly.

It appears, however, that the carotid body plays a unique role in regulation of whole body glucose metabolism. Stimulation of the carotid body by cyanide increased blood glucose concentration and hepatic glucose output which were abolished by carotid sinus nerve denervation (Alvarez-Buylla and Alvarez-Buylla 1988). Experimental hypoglycemia released several metabolic hormones and enhanced endogenous glucose output, but the carotid body denervation or hyperoxia attenuated these responses (Koyama et al. 2000; Wehrwein et al. 2010). Recently we found that the carotid sinus denervation prevented intermittent hypoxia-induced hyperglycemia (Shin et al. 2014). Thus, the carotid body may participate in the pathogenesis of metabolic diseases.

The current study, together with our previous data showing high expression of leptin receptors in the mouse carotid body (Balbir et al. 2007), suggests that leptin activates leptin receptors in the carotid body and/or nerve endings and enhances CSN response to hypoxia. The results agree with our previous work, showing that leptin deficiency mice have blunted hypoxic ventilatory response (Tankersley et al. 2013). Furthermore, leptin-induced enhancement of hypoxic chemoreceptor response was blocked by TRP channel blockers. Gene expression analysis showed uniquely high expression of Trpm 3, 6, and 7 channels in the carotid body and petrosal ganglion. Because of a lack of specific blockers for these channels, their physiological role in carotid body hypoxic response is not clear yet. Future studies are required to clarify the contribution of leptin and TRP channels to carotid body function.

In conclusion, the carotid body may contribute to neural control of glucose metabolism via leptin receptor-mediated TRP channel activation.

**Acknowledgements** This work was funded, in part, by HL081345, ES016817, HL080105, and AHA 12POST118200001.

## References

Alvarez-Buylla R, Alvarez-Buylla ER (1988) Carotid sinus receptors participate in glucose homeostasis. Respir Physiol 72:347–360

Balbir A, Lee H, Okumura M, Biswal S, Fitzgerald RS, Shirahata M (2007) A search for genes that may confer divergent morphology and function in the carotid body between two strains of mice. Am J Physiol Lung Cell Mol Physiol 292:L704–L715

Bin-Jaliah I, Maskell PD, Kumar P (2004) Indirect sensing of insulin-induced hypoglycaemia by the carotid body in the rat. J Physiol 556:255–266

Conde SV, Obeso A, Gonzalez C (2007) Low glucose effects on rat carotid body chemoreceptor cells' secretory responses and action potential frequency in the carotid sinus nerve. J Physiol 585:721–730

Gallego-Martin T, Fernandez-Martinez S, Rigual R, Obeso A, Gonzalez C (2012) Effects of low glucose on carotid body chemoreceptor cell activity studied in cultures of intact organs and in dissociated cells. Am J Physiol Cell Physiol 302:C1128–C1140

Gonzalez C, Almaraz L, Obeso A, Rigual R (1994) Carotid body chemoreceptors: from natural stimuli to sensory discharges. Physiol Rev 74:829–898

Koyama Y, Coker RH, Stone EE, Lacy DB, Jabbour K, Williams PE, Wasserman DH (2000) Evidence that carotid bodies play an important role in glucoregulation in vivo. Diabetes 49:1434–1442

Pardal R, López-Barneo J (2002) Low glucose-sensing cells in the carotid body. Nat Neurosci 5:197–198

Porzionato A, Rucinski A, Macchi V, Stecco C, Castagliuoloc I, Malendowicz LK, De Caro R (2011) Expression of leptin and leptin receptor isoforms in the rat and human carotid body. Brain Res 1385:56–67

Qiu J, Fang Y, Rønnekleiv OK, Kelly MJ (2010) Leptin excites POMC neurons via activation of TRPC channels. J Neurosci 30:1560–1565

Shin MK, Yao Q, Jun JC, Bevans-Fonti S, Yoo DY, Han W, Mesarwi O, Richardson R, Fu YY, Pasricha PJ, Schwartz AR, Shirahata M, Polotsky VY (2014) Carotid body denervation prevents fasting hyperglycemia during chronic intermittent hypoxia. J Appl Physiol 117:765–776

Tankersley CG, Tang W-Y, Wang X, Pardo C, Bierman A, Shirahata M (2013) Effect of leptin on hypoxic ventilator regulation. ATS international conference A5763

Wehrwein EA, Basu R, Basu A, Curry TB, Rizza RA, Joyner MJ (2010) Hyperoxia blunts counterregulation during hypoglycaemia in humans: possible role for the carotid bodies? J Physiol 588:4593–4601

Zhang M, Buttigieg J, Nurse CA (2007) Neurotransmitter mechanisms mediating low-glucose signalling in cocultures and fresh tissue slices of rat carotid body. J Physiol 578:735–750

# 18 Lipopolysaccharide-Induced Ionized Hypocalcemia and Acute Kidney Injury in Carotid Chemo/Baro-Denervated Rats

R. Fernández, P. Cortés, R. Del Rio, C. Acuña-Castillo, and E.P. Reyes

**Abstract**

The acute kidney injury (AKI) observed during sepsis is due to an uncontrolled release of inflammatory mediators. Septic patients develop electrolytic disturbances and one of the most important is ionized hypocalcemia. AKI adversely affects the function of other organs and hypocalcemia is associated with cardiovascular and respiratory dysfunctions. Since carotid body chemoreceptors modulate the systemic inflammatory response during sepsis syndromes, we used pentobarbitone-anesthetized male Sprague–Dawley rats in control condition (SHAM surgery) and after bilateral carotid neurotomy (carotid chemo/baro-denervated, BCN). We evaluate serum creatinine (CRE), serum neutrophil gelatinase-associated lipocaline (NGAL), ionized calcium (iCa) and cardiac Troponin I (cTnI) 90 min after the IP administration of 15 mg/kg lipopolysaccharide (LPS) or saline. In the SHAM group, LPS failed to induce significant changes CRE, NGAL, or iCa, and increased cTnI. Conversely, in the BCN group LPS increased CRE and NGAL, decreased iCa, and enhanced the increase of cTnI. Our results suggest that carotid chemo/baro-receptors might contribute to the regulation of both renal function and calcemia during sepsis. In addition, results imply that the carotid chemo-baroreceptors serve as an immunosensory organ.

R. Fernández (✉) • P. Cortés
Facultad de Ciencias Biológicas y Facultad de Medicina, Universidad Andrés Bello, Santiago, Chile
e-mail: rhfdez@gmail.com; rfernandez@unab.cl

R. Del Rio
Laboratory of Cardiorespiratory Control, Universidad Autónoma de Chile, Santiago, Chile

C. Acuña-Castillo
Facultad de Química y Biología, Universidad de Santiago de Chile, Santiago, Chile

E.P. Reyes
Centro de Fisiología Celular e Integrativa, Facultad de Medicina, Clínica Alemana-Universidad del Desarrollo, Santiago, Chile

Dirección de Investigación, Universidad Autónoma de Chile, Santiago, Chile



C. Peers et al. (eds.), *Arterial Chemoreceptors in Physiology and Pathophysiology*, Advances in Experimental Medicine and Biology 860, DOI 10.1007/978-3-319-18440-1_18

**Keywords**
Carotid body • Sepsis • Acute kidney injury • Ionized hypocalcemia • Cardiac Troponin I

## 18.1 Introduction

Sepsis is a systemic inflammatory response syndrome that occurs during infection (Bone et al. 2009). As the disease evolves, patients develop organic dysfunction – or failure – of organs different from the one originally affected, leading to a progressive deterioration of the organic functions that can be fatal (Riedemann et al. 2003). During sepsis, inflammatory mediators derived from pathogens and/or activated immune cells, such as lipopolysaccharide (LPS) or cytokines, can spread to the kidneys, filtrate to the Bowman's capsule and the tubular lumen, causing acute kidney injury (AKI) (Gomez et al. 2014). Almost half of the patients with sepsis develop AKI, and of those with concomitant sepsis and AKI, almost 70 % die (Bagshaw et al. 2007; Leelahavanichkul et al. 2008; Lopes et al. 2010).

One of the most clinically important electrolytic disturbances among ICU patients is ionized hypocalcemia. Not only it is associated with a "more severe organ dysfunction" – *e.g.* cardiac failure (Aguilera and Vaughan 2000)–, it is more frequent among non-survivors (Dias et al. 2013). The hypocalcemia is due to a sepsis-induced parathyroid hormone insensitivity and to the tubular injury due the presence of inflammatory mediators and concomitant 1α-hydroxylase deficiency (*i.e.* diminished calcitriol) (Huang et al. 2009; Nguyen et al. 2013; Gomez et al. 2014).

The carotid body (CB) is part of the afferent limb of the neural reflex control of inflammation (reviewed by Fernandez and Acuna-Castillo 2012). CB glomus cells express functional LPS canonical (TLR4) receptors (Fernandez et al. 2011). They also have an immunosensory pathway that may explain the changes in chemosensory discharge in the carotid/sinus nerve (Shu et al. 2007; Fernandez et al. 2008; Fan et al. 2009). Furthermore, the LPS-induced activation of neurons at the *nucleus tractus solitarii* level is suppressed in chemo-baro denervated rats (Reyes et al. 2012).

Taking into consideration all of the above, we suggest that the complete suppression of carotid body chemosensory activity during sepsis favors the onset of AKI and electrolytes disturbances, facilitating organ dysfunction.

## 18.2 Materials and Methods

Young (5 weeks) male Sprague-Dawley rats (110 ± 20 g) anesthetized intraperitoneally (IP) with sodium pentobarbitone 60 mg/kg, were placed in supine position over a heated pad maintained at 37.0 ± 0.1 °C. The animals breathed spontaneously throughout the experiment. Experimental protocols were approved by the Commission of Bioethics and Biosafety of the Universidad Andres Bello.

The animals were separated into four groups: Two groups with sham surgical intervention (*i.e.* with intact carotid/sinus nerves, SHAM), first one treated IP with saline (0.9 % NaCl) (SHAM-saline, n = 8) and the second treated with 15 mg/kg lipopolysaccharide (LPS, from *Escherichia coli* serotype 0127:B8. L3129 Sigma-Aldrich Corp, USA) (SHAM-LPS, n = 9). Likewise, two groups with bilateral carotid neurotomy (BCN) were treated IP with either saline (BCN-saline, n = 9) or with 15 mg/kg LPS (BCN-LPS, n = 8). The systolic blood pressure ($P_S$), Einthoven's lead II ECG signal and tidal volume ($V_T$) were recorded before surgery and up to 90 min after saline or LPS treatment (usually administered 15 min after simulated or effective neurotomy), with a PowerLab® 8/30 (AD Instruments, Castle Hill, Australia) and displayed through Chart® software (AD Instruments). Additionally, instantaneous cardiac and respiratory frequency ($f_H$ and $f_R$), were derived from ECG and $V_T$, respectively.

Ninety minutes after saline or LPS administration, blood extracted -by cardiac puncture- into lithium-heparin–containing tubes was immediately centrifuged at 5,000 rpm for 10 min at 4 °C. We measured plasma electrolytes ($Na^+$, $K^+$, $Cl^-$, and ionized calcium (iCa)), albumin, total proteins, and cardiac troponin I (cTnI) with an iSTAT system (Abbott Laboratories, IL, USA). Using a commercial ELISA kit (Bioporto Diagnostics, Denmark) we measured Neutrophil Gelatinase-Associated Lipocaline (NGAL), a specific marker of tubular damage known to be increased during AKI (Soto et al. 2013). Renal function was assessed measuring plasma levels of creatinine (CRE) and blood urea nitrogen (BUN) with a Piccolo Xpress Chemistry Analyzer (Abaxis, CA, USA) according to the manufacturers' instructions.

Data are expressed as mean ± standard error of the mean (SEM). Plasma measurements were compared by Kruskall-Wallis ANOVA followed by the Dunn post-test. $P < 0.05$ was considered significant. The statistical analysis and graphs were completed using GraphPad Prism v6.0 (GraphPad Software Inc., CA, USA).

## 18.3 Results

### 18.3.1 Cardiorespiratory Changes After IP Administration of LPS

Basal ventilation, $f_H$ and $P_S$ were all uniform and not significantly different in any group. Neither SHAM nor BCN surgeries modified the basal values of the recorded parameters. Similarly, saline administration did not modify either basal or post-surgical ventilatory parameters. LPS administration increase $f_R$ in the SHAM group but, conversely, reduces $f_R$ after BCN. Thus, LPS-induced tachypnea is suppressed by BCN. Saline administration modified neither $f_H$ nor $P_S$. In contrast, LPS significantly reduced $P_S$ in SHAM and BCN rats and it evoked tachycardia in both, SHAM and BCN rats, more prominently in the latest. Full data were published elsewhere (Nardocci et al. 2015).

### 18.3.2 LPS-Induced AKI and Ionized Hypocalcemia

BUN and CRE levels did not change 90 min after LPS administration to the SHAM animals (SHAM-LPS). Saline administration to both SHAM-saline and BCN-saline rats did not modify any of the measured plasma markers. LPS administration after BCN (BCN-LPS) evoked remarkable increases in CRE. In mg/dL, SHAM-saline, 0.66 ± 0.05; SHAM-LPS, 0.61 ± 0.05; BCN-saline, 0.60 ± 0.05; BCN-LPS, 0.98 ± 0.04*. (*, $p < 0.05$ vs. SHAM-saline, SHAM-LPS, and BCN-saline Kruskal-Wallis ANOVA, Dunn's post-test). BUN to CRE ratio (BUN/CRE) is a first approach to elucidate kidney injury. The decreased BUN/CRE in BCN-LPS rats (Fig. 18.1a) suggests an (intra)renal disease. BCN prior to LPS significantly increases plasma NGAL, compared with SHAM-saline, SHAM-LPS and BCN-saline (Fig. 18.1b).

In both SHAM and BCN animals, neither saline nor LPS modified plasma levels of $Na^+$, $K^+$, or $Cl^-$ (not shown). LPS administration after BCN evoked a dramatic decrease in iCa (Fig. 18.1c), but with no significant changes in either plasma albumin or total plasma proteins (Fig. 18.1d).

### 18.3.3 ECG Changes and Cardiac Markers in Septic Rats

Cardiac biomarkers and ECG recordings are valuable for diagnosing sepsis but also to evaluate the progression of the syndrome. Increased cardiac Troponin I (cTnI) levels is an important prognostic indicator in septic patients. Congruently, LPS increased cTnI in SHAM animals (SHAM-LPS) (Fig. 18.2). 90 min after LPS administration BCN rats showed a 6-fold increase in cTnI compared to SHAM-LPS. Increased cTnI levels are consistent with ECG changes observed in SHAM-LPS rats, *i.e.* increase of the corrected QT interval (QTc), augmented ST height and T amplitude and decreased RR interval (RRI) with left cardiac axis deviation from 57° (SHAM-saline) to 53° (SHAM-LPS). In BCN rats, LPS

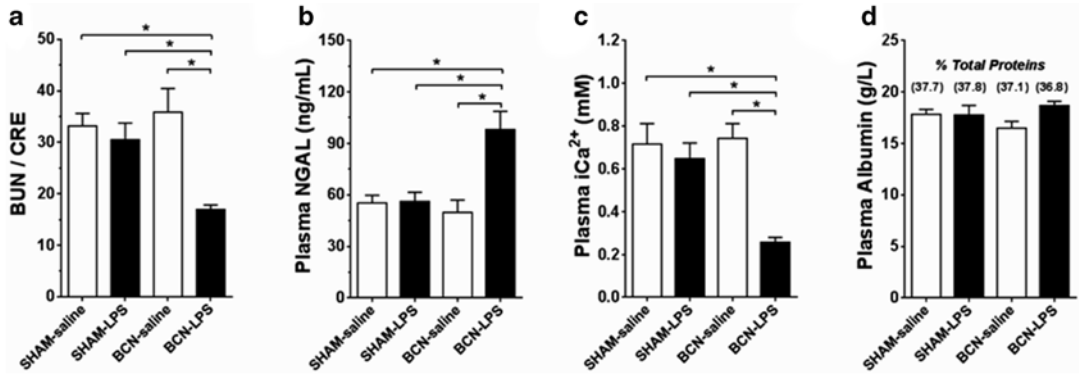


**Fig. 18.1** Plasma markers of kidney damage, ionized calcium, and albumin 90 min after the IP treatment with saline or 15 mg/kg LPS in either SHAM or BCN rats. (**a**) BUN to CRE ratio; (**b**) NGAL; (**c**) iCa; (**d**) Albumin. Values, Means ± SEM. *$p < 0.05$, assessed by the Kruskal-Wallis ANOVA and Dunn's post-test. n = 7–8. In (**d**), values between parentheses are the percentage of albumin over total plasma proteins

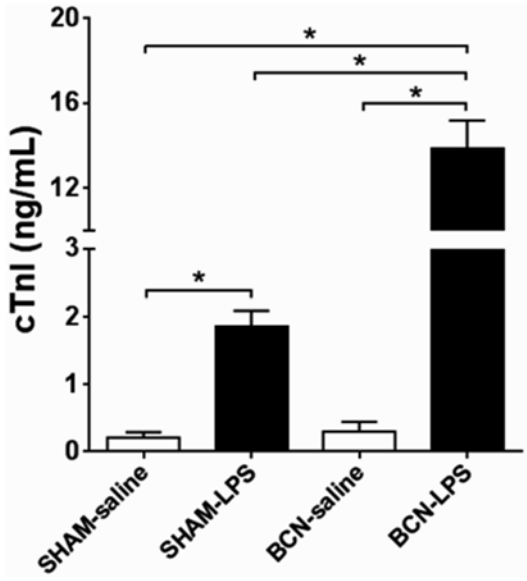


**Fig. 18.2** Plasma cardiac Troponin I (cTnI) 90 min after the IP treatment with saline or 15 mg/kg LPS in either SHAM or BCN rats. Values, Mean ± SEM. *$p < 0.05$, assessed by the Kruskal-Wallis ANOVA and Dunn's post-test. n = 7–8

administration evoked a more pronounced increase in QTc, ST elevation and T amplitude, and a greater decrease in RRI, added to a decrease in both, R amplitude and QRS interval. Left cardiac axis deviation was also increased, from 55° (BCN-saline) to 35° (BCN-LPS).

## 18.4 Discussion

The immune system is connected with and regulated by the central nervous system. The inflammatory reflex comprises (afferent) sensory neurons activated by products of infection or inflammation (*e.g.* LPS, TNF-α). These neurons project to brainstem nuclei, providing a neuronal substrate for efferent activation of cardiorespiratory reflexes and immunomodulatory mechanisms, *i.e.* the hypothalamic–pituitary–adrenal axis, sympathetic activation, the cholinergic anti-inflammatory reflex and the local release of physiological neuromodulators. The carotid body (CB) is part of the afferent limb of the neural reflex control of inflammation (Fernandez et al. 2008, 2011; Zapata et al. 2011; Reyes et al. 2012). Thus, the complete absence of immunosensory inputs after bilateral carotid/sinus neurotomy (BCN) could favor the progression from sepsis to multiple organ dysfunction and death.

As previously reported, BCN modifies cardiorespiratory responses to sepsis (Fernandez et al. 2008), suggesting that systemic responses to sepsis originate, at least in part, in the CB. Plasma markers of kidney function, indicates that LPS administration after BCN increases renal damage, assessed by CRE, BUN-to-CRE ratio and NGAL measurements. Despite its use as renal function marker, we did not find significant

changes in BUN, probably because (i) there are extra-renal factors that modifies urea (*e.g.* tissue proteins, diet, drugs, effective circulating blood volume) and (ii) urinary excretion of urea is directly proportional to urine flow, and both parameters are altered in sepsis syndrome.

Increased CRE found in BCN-LPS rats could be associated to renal dysfunction, because the only extra-renal factor that can affect CRE plasma level is muscle mass. BUN-to-CRE ratio is a valuable index to determine intrinsic or extrinsic renal disease. Decreased BUN/CRE, as we found in BCN-LPS rats, is associated with renal disease (Baum et al. 1975). In addition, LPS administration after BCN increases plasma NGAL, an accurate biomarker predictor of AKI (Soto et al. 2013). Therefore, the suppression of carotid body immunosensory inputs favors LPS-induced AKI. Although -as a consequence of renal injury- we found decreased plasmatic ionized calcium, we did not find significant changes in $Na^+$, $K^+$, $Cl^-$, plasma albumin or total plasma proteins.

Finally, since ionized hypocalcemia is associated with a more severe organ dysfunction. Cardiac dysfunction *per se* is evident in up to 44 % of critically ill septic patients (Singh and Evans 2006), with the etiological agents suspected to be coronary artery disease, hypotension, the direct deleterious effects of infectious and depressant circulating factors (*e.g.* pro-inflammatory mediators). LPS administration to SHAM animals increases plasma levels of cardiac TnI. BCN prior to LPS administration boosted plasma cTnI levels, suggesting an increased cardiac damage. In septic patients, increased cTnI levels serve as an important prognostic indicator (Mehta et al. 2004; Maeder et al. 2006). Additionally, several ECG abnormalities were reported in septic patients, such as reduction of QRS amplitude, increased QTc interval (Rich et al. 2002), and ST-segment elevation (Martinez et al. 2009). Interestingly, we found that ECG abnormalities are increased in BCN-LPS rats.

The administration of LPS and the absence of carotid chemo/barosensory functions favor the development of acute kidney injury, ionized hypocalcemia and heart damage. We propose that carotid chemo/baro-receptors play a protective role during sepsis syndromes.

**Acknowledgments** Supported by FONDECYT 1120976 and UNAB DI-354-13/R (to RF), and UDD CI 23400098 (to EPR).

## References

Aguilera IM, Vaughan RS (2000) Calcium and the anaesthetist. Anaesthesia 55:779–790

Bagshaw SM, Uchino S, Bellomo R et al (2007) Septic acute kidney injury in critically ill patients: clinical characteristics and outcomes. Clin J Am Soc Nephrol 2:431–439

Baum N, Dichoso CC, Carlton CE (1975) Blood urea nitrogen and serum creatinine. Physiology and interpretations. Urology 5:583–588

Bone RC, Balk RA, Cerra FB et al (2009) Definitions for sepsis and organ failure and guidelines for the use of innovative therapies in sepsis. The ACCP/SCCM Consensus Conference Committee, American College of Chest Physicians/Society of Critical Care Medicine. 1992. Chest 136, e28

Dias CR, Leite HP, Nogueira PC et al (2013) Ionized hypocalcemia is an early event and is associated with organ dysfunction in children admitted to the intensive care unit. J Crit Care 28:810–815

Fan J, Zhang B, Shu HF et al (2009) Interleukin-6 increases intracellular Ca2+ concentration and induces catecholamine secretion in rat carotid body glomus cells. J Neurosci Res 87:2757–2762

Fernandez R, Acuna-Castillo C (2012) Neural reflex control of inflammation during sepsis syndromes. In: Azedevo L (ed) Sepsis – an ongoing and significant challenge. InTech, Rijeka, pp 133–156

Fernandez R, Gonzalez S, Rey S et al (2008) Lipopolysaccharide-induced carotid body inflammation in cats: functional manifestations, histopathology and involvement of tumour necrosis factor-alpha. Exp Physiol 93:892–907

Fernandez R, Nardocci G, Simon F et al (2011) Lipopolysaccharide signaling in the carotid chemoreceptor pathway of rats with sepsis syndrome. Respir Physiol Neurobiol 175:336–348

Gomez H, Ince C, De Backer D et al (2014) A unified theory of sepsis-induced acute kidney injury: inflammation, microcirculatory dysfunction, bioenergetics, and the tubular cell adaptation to injury. Shock 41:3–11

Huang CQ, Ma GZ, Tao MD et al (2009) The relationship among renal injury, changed activity of renal 1-alpha hydroxylase and bone loss in elderly rats with insulin resistance or type 2 diabetes mellitus. J Endocrinol Invest 32:196–201

Leelahavanichkul A, Yasuda H, Doi K et al (2008) Methyl-2-acetamidoacrylate, an ethyl pyruvate analog, decreases sepsis-induced acute kidney injury in mice. Am J Physiol Renal Physiol 295:F1825–F1835

Lopes JA, Fernandes P, Jorge S et al (2010) Long-term risk of mortality after acute kidney injury in patients with sepsis: a contemporary analysis. BMC Nephrol 11:9

Maeder M, Fehr T, Rickli H et al (2006) Sepsis-associated myocardial dysfunction: diagnostic and prognostic impact of cardiac troponins and natriuretic peptides. Chest 129:1349–1366

Martinez JD, Babu RV, Sharma G (2009) Escherichia coli septic shock masquerading as ST-segment elevation myocardial infarction. Postgrad Med 121:102–105

Mehta NJ, Khan IA, Gupta V et al (2004) Cardiac troponin I predicts myocardial dysfunction and adverse outcome in septic shock. Int J Cardiol 95:13–17

Nardocci G, Martin A, Abarzua S et al (2015) Sepsis progression to multiple organ dysfunction in carotid chemo/baro-denervated rats treated with lipopolysaccharide. J Neuroimmunol 278:44–52

Nguyen HB, Eshete B, Lau KH et al (2013) Serum 1,25-dihydroxyvitamin D: an outcome prognosticator in human sepsis. PLoS One 8, e64348

Reyes EP, Abarzua S, Martin A et al (2012) LPS-induced c-Fos activation in NTS neurons and plasmatic cortisol increases in septic rats are suppressed by bilateral carotid chemodenervation. Adv Exp Med Biol 758:185–190

Rich MM, McGarvey ML, Teener JW et al (2002) ECG changes during septic shock. Cardiology 97:187–196

Riedemann NC, Guo RF, Ward PA (2003) The enigma of sepsis. J Clin Invest 112:460–467

Shu HF, Wang BR, Wang SR et al (2007) IL-1beta inhibits IK and increases [Ca2+]i in the carotid body glomus cells and increases carotid sinus nerve firings in the rat. Eur J Neurosci 25:3638–3647

Singh S, Evans TW (2006) Organ dysfunction during sepsis. Intensive Care Med 32:349–360

Soto K, Papoila AL, Coelho S et al (2013) Plasma NGAL for the diagnosis of AKI in patients admitted from the emergency department setting. Clin J Am Soc Nephrol 8:2053–2063

Zapata P, Larrain C, Reyes P et al (2011) Immunosensory signalling by carotid body chemoreceptors. Respir Physiol Neurobiol 178:370–374

# 19 Role of the Carotid Body Chemoreflex in the Pathophysiology of Heart Failure: A Perspective from Animal Studies

Harold D. Schultz, Noah J. Marcus, and Rodrigo Del Rio

**Abstract**

The treatment and management of chronic heart failure (CHF) remains an important focus for new and more effective clinical strategies. This important goal, however, is dependent upon advancing our understanding of the underlying pathophysiology. In CHF, sympathetic overactivity plays an important role in the development and progression of the cardiac and renal dysfunction and is often associated with breathing dysregulation, which in turn likely mediates or aggravates the autonomic imbalance. In this review we will summarize evidence that in CHF, the elevation in sympathetic activity and breathing instability that ultimately lead to cardiac and renal failure are driven, at least in part, by maladaptive activation of the carotid body (CB) chemoreflex. This maladaptive change derives from a tonic increase in CB afferent activity. We will focus our discussion on an understanding of mechanisms that alter CB afferent activity in CHF and its consequence on reflex control of autonomic, respiratory, renal, and cardiac function in animal models of CHF. We will also discuss the potential translational impact of targeting the CB in the treatment of CHF in humans, with relevance to other cardio-respiratory diseases.

**Keywords**

Heart failure • Carotid body • Sympathetic nerve activity • Breathing • Oxidative stress • Nitric oxide • Blood flow • KLF2

H.D. Schultz, Ph.D. (✉) • N.J. Marcus
Department of Cellular and Integrative Physiology,
University of Nebraska Medical Center,
Omaha, NE 68198, USA
e-mail: hschultz@unmc.edu

R. Del Rio
Department of Cellular and Integrative Physiology,
University of Nebraska Medical Center,
Omaha, NE 68198, USA

Laboratory of Cardiorespiratory Control, Universidad Autónoma de Chile, Santiago, Chile



C. Peers et al. (eds.), *Arterial Chemoreceptors in Physiology and Pathophysiology*,
Advances in Experimental Medicine and Biology 860, DOI 10.1007/978-3-319-18440-1_19

## 19.1 Introduction

It is well understood that peripheral chemoreceptors normally play an important role in oxygen and carbon dioxide homeostasis for the body. These specialized oxygen-sensitive glomus (type I) cells reside in minute glomus tissue or bodies found at the level of the carotid sinus and aortic arch. Type I cells are stimulated by a reduction in arterial $PO_2$ and/or increase in arterial $PCO_2$, and send neural input to the brainstem to reflexively increase ventilation to avert the developing hypoxemia/hypercapnia. The peripheral chemoreflex also activates sympathetic outflow to resistance vessels to avert the direct vasodilatory effects of hypoxemia/hypercapnia, and thus maintain arterial pressure to assure adequate blood flow and gas exchange to essential organs, particularly the heart and brain. Although the relative functional role of carotid vs. aortic chemoreceptor bodies in the control of ventilation and sympathetic outflow remains somewhat of an enigma, the carotid body (CB) has been shown to be of major importance in this regard in most mammalian species.

It is now recognized that the CB can become maladaptive in certain disease states. In particular, CHF patients (Ponikowski et al. 2001; Niewinski 2014) and animal models (Schultz et al. 2013) exhibit increased CB chemoreflex drive that contributes to sympathetic outflow and ventilation under both normoxic and hypoxic conditions. This maladaptation carries important clinical relevance because tonic overactivation of sympathetic neural outflow, particularly to the heart and kidneys, exacerbates the progression of the cardiac failure (Esler 2010). CHF is also characterized by the development of breathing instability with oscillatory (Cheyne-Stokes) or irregular breathing and central apneas that further negatively impact autonomic and metabolic homeostasis (Brack et al. 2012). Moreover, the high CB chemoreflex sensitivity is correlated with poor prognosis in patients with CHF (Ponikowski et al. 2001; Niewinski 2014) and has been shown to contribute to the pathophysiology and mortality in animal models of CHF (Del Rio et al. 2013a; Marcus et al. 2014a).

## 19.2 Tonic Activation of the Carotid Body in CHF

A potential role of the CB chemoreflex in the pathophysiological changes in CHF has been underappreciated because most stable CHF patients do not exhibit overt hypoxemia, at least to the degree that would substantially activate the peripheral chemoreflex chronically. However, integral to understanding the maladaptive role of CB in CHF is the observation we made several years ago that basal CB afferent discharge driven by the type I cells is markedly elevated at rest under normoxia conditions in CHF animals to levels that would otherwise represent significant hypoxemia in a normal state (Sun et al. 1999a). This finding originally documented in tachycardia pacing-induced CHF in rabbits (Sun et al. 1999a), has since been verified in myocardial infarct-induced CHF in rats (Del Rio et al. 2013b), and genetic cardiomyopathic CHF in mice (Wang et al. 2012). This tonic afferent input to the brainstem results in a tonic reflex drive that contributes to sympathetic hyperactivity and hyperventilation with the associated breathing instability that are characteristic of CHF, even under a normal arterial $PO_2$ condition. This concept is borne out by studies showing that inhibition of CB chemoreceptor activity by hyperoxia or CB ablation reduced sympathetic outflow (Xing et al. 2014; Marcus et al. 2014a; Del Rio et al. 2013a) and reduced hyperventilation and oscillatory breathing (Marcus et al. 2014a; Del Rio et al. 2013a) in animal models of CHF. These changes were followed by improvement in cardiac function and prolonged survival (Del Rio et al. 2013a; Marcus et al. 2014a).

In the following sections we will summarize, local tissue, humoral, hemodynamic, ventilatory, and neural changes that occur in the development of CHF that may collectively play important roles in the sensitization of CB chemoreceptors to drive increased CB reflex function in CHF

independent of oxygen status. These factors act to further exacerbate chemoreflex activation during periods in which periodic hypoxemia does occur. In addition, because these changes in CB afferent function have been shown in at least three different models of cardiac failure (cardiac pacing, coronary ligation, genetic cardiomyopathy) in several different species, the factors responsible for enhanced CB function do not appear to be related specifically to the etologies of cardiomyopathy, but rather, the homeostatic imbalance to the body created by the reduced pumping ability of the heart .

### 19.2.1 Local Tissue and Humoral Factors

The precise cellular/molecular mechanisms responsible for tonic activation of the CB afferent activity in CHF are still not well understood. Although tonic neural discharge is increased in the second order chemoreceptor afferent neurons in the petrosal ganglion that carry CB input to the central nervous system (Sun et al. 1999a; Del Rio et al. 2013b), very little is known about the effects of CHF on the intrinsic excitability of these afferent neurons; however, a number of potential factors have been identified that enhance CB glomus cell excitability in the CHF state. Our studies have demonstrated that superoxide anion ($O_2^{-\bullet}$) and nitric oxide (NO) play an important role in the observed increases in CB glomus cell excitability in CHF (Fig. 19.1).

Oxidative stress has been shown to play an important role in activating the CB in CHF (Schultz et al. 2013). A number of redox changes within the CB are likely to play important roles in increasing oxidative stress. Both circulating and local tissue levels of the pro-oxidant angiotensin II (Ang II) peptide are elevated in CHF (Li et al. 2006). Ang II enhances the excitability of the CB glomus cells via the AT1 receptor (AT1R) and activates NADPH oxidase (NADPHox) to enhance $O_2^{\bullet-}$ production in the CB (Li et al. 2007). AT1R and NADPHox protein and $O_2^{\bullet-}$ production are upregulated in the CB in CHF (Li et al. 2007). Ang II-$O_2^{\bullet-}$ enhances the sensitivity of the CB, at least in part, by inhibiting oxygen sensitive potassium channels ($I_K$) in CB glomus cells (Fig. 19.1) (Li and Schultz 2006). It is also very likely that the Ang II-$O_2^{\bullet-}$ pathway enhances the sensitivity or expression of voltage gated $Ca^{2+}$ channels, which mediate depolarization and release of neurotransmitters from the glomus cells, and suppression of background $K^+$ channels responsible for maintenance of the resting membrane potential in glomus cells. A potential role for changes in the sensitivity or expression of acid sensing ion channel 3 also could be postulated (Lu et al. 2013). In addition, other pro-oxidant pathways may play a contributory role in the sensitization of the CB in CHF but have not been closely analyzed. For example, endothelin (Iturriaga 2013; Peng et al. 2013) and inflammatory cytokines (Iturriaga et al. 2014; Lam et al. 2012) can stimulate ROS production to sensitize the CB and are elevated in CHF.

The relative contribution of humoral vs. local tissue origin of pro-oxidant mediators in the sensitization of the CB in CHF is not clear. The circulating renin-angiotensin system (RAS) is activated in CHF due to renal hypoperfusion, and thus could serve as an important source for Ang II effects on the CB. However, local production of Ang II and other Ang metabolites in the CB can serve as a direct link to modulation of CB function in disease states (Leung et al. 2003). The fact that CB neural activity remains elevated after isolation from the circulation in CHF animals and remains responsive to angiotensin blockers supports an important role of the local Ang system in the CB in CHF (Li and Schultz 2006). CB hyper-responsiveness in the isolated state also discounts the relative importance of many other humoral factors that are known to be elevated in CHF. Nevertheless, an important additional influence from circulating Ang II and other pro-oxidant or neuro-modulatory mediators should not be discounted and deserves further study.

Contributing to local oxidative stress in the CB, expression of both copper/zinc superoxide dismutase (CuZnSOD) and manganese SOD (MnSOD), endogenous intracellular scavengers of

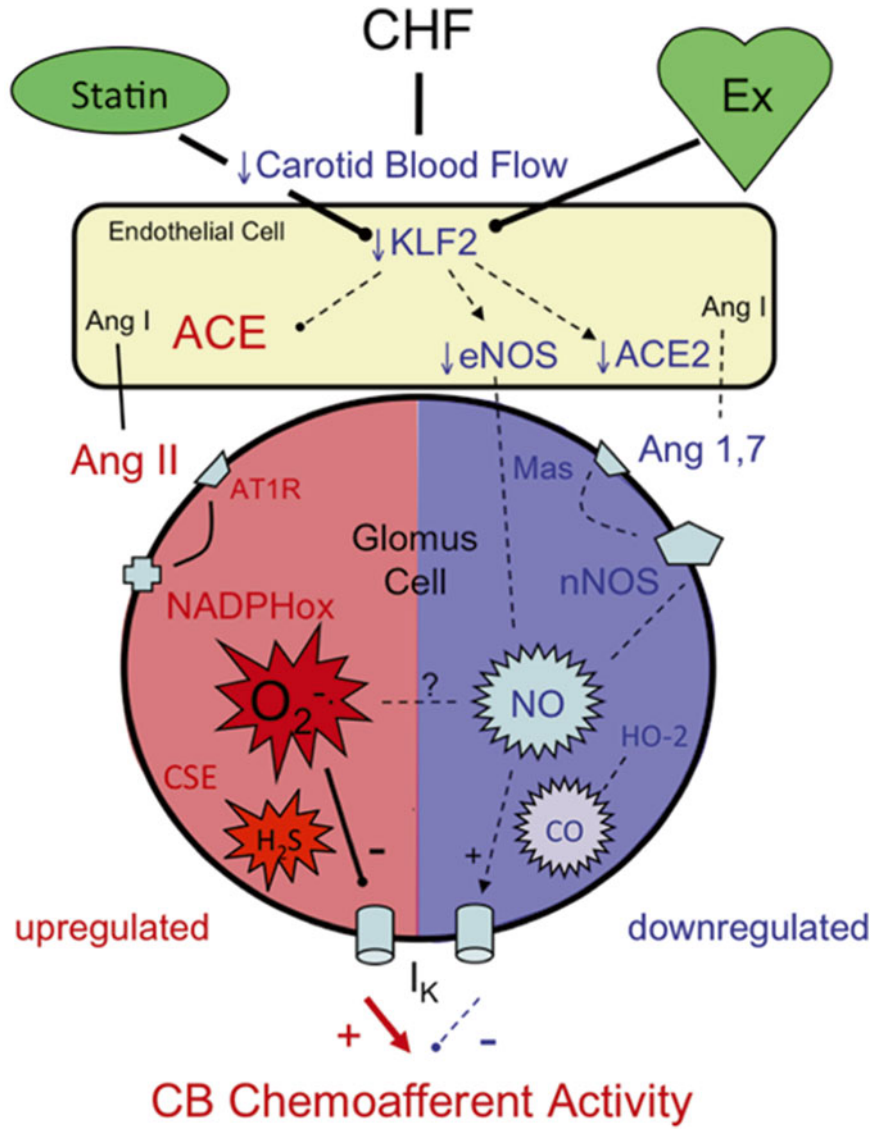


**Fig. 19.1** Known and proposed cellular pathways contributing to enhanced carotid body (CB) chemoreceptor activity in chronic heart failure (CHF). The reactive oxygen species super oxide anion ($O_2^{-\bullet}$) is upregulated by angiotensin (*Ang*) II signaling to inhibit hyperpolaring potassium channel currents ($I_K$) and increase the excitability of glomus cells; whereas an opposing inhibitory influence of nitric oxide (*NO*) on excitability is downregulated. These changes result from a decrease in blood flow in the CB to reduce transcription factor Kruppel-like factor 2 (*KLF2*) resulting in upregulation of angiotensin converting enzyme (*ACE*) and suppression of endothelial (*e*) and neural (*n*) nitric oxide synthase (*NOS*) to alter Ang and NO metabolism. Statins (Simvastatin) and exercise (*Ex*) (*green*) may act to prevent suppression of KLF2 in CHF. Details and other abbreviations discussed in the text (Modified from Schultz and Marcus 2012 by permission from the publisher)

$O_2^{\bullet-}$, is suppressed in glomus cells of the CB in CHF (Ding et al. 2010, 2009). These changes serve to amplify the Ang II-$O_2^{\bullet-}$ activation of CB chemoreceptor activity (Fig. 19.1). Gene transfer to restore expression of either of the SOD isoforms in the CB reverses the enhanced CB chemoreceptor and chemoreflex activation (Ding et al. 2009, 2010) implicating a dual role of both cytosolic and

mitochondrial $O_2^{\bullet-}$ in the Ang II-NOX signaling cascade within CB glomus cells.

Other angiotensin metabolites also may play a role in modulating CB function in CHF. Ang-(1–7) counteracts the neural actions of Ang II (Fig. 19.1). Ang-(1-7) enhances $I_K$ in catecholaminergic neurons, including glomus cells, via Mas receptor (Mas) activation of neural nitric oxide synthase (nNOS) and NO production: an effect that opposes the inhibitory effect of Ang II-$O_2^{\bullet-}$ on these channels (Yang et al. 2011). However, basal NO production and nNOS/eNOS expression within the CB are depressed in CHF (Ding et al. 2008). Thus, the tonic inhibitory effect of NO on the activity of CB chemoreceptors (Schultz et al. 2012) is virtually absent in CHF animals. Downregulation of the inhibitory effects of Ang (1-7) and NO within the CB thus work synergistically with pro-oxidant effects to create tonic activation of CB chemoreceptor discharge even under normoxic conditions in CHF (Fig. 19.1).

In addition to NO, the gas transmitters carbon monoxide (CO) and hydrogen sulfide ($H_2S$) also influence CB chemoreceptor sensitivity (Figs. 19.1 and 19.2) (Prabhakar 2012). CO is constitutively regulated by heme-oxygenase-2 (HO-2) in the CB, and HO-2 protein expression is markedly decreased in the CB in CHF animals (Ding et al. 2008). CO, similar to NO, restrains hypoxic sensitivity of the CB (Ding et al. 2008), and downregulation of the CO and NO pathways in the CB have cumulative effects to enhance peripheral chemoreflex function in pacing-induced CHF rabbits (Ding et al. 2008).

$H_2S$ derived from cystathionine γ-lyase (CSE) also contributes to the CB chemosensory response to hypoxia (Prabhakar 2012). CSE expression is maintained in the CB during CHF and CSE inhibition reduces CB activity, suggesting that $H_2S$ contributes to the maintenance of exaggerated CB afferent responsiveness in CHF (Del Rio et al. 2013b). Furthermore, due to an inhibitory influence of CO on CSE activity, $H_2S$ production in the CB is linked to HO-2 (Prabhakar 2012). Since HO-2 is downregulated in the CB in CHF (Ding et al. 2008), CSE activity would be promoted to enhance $H_2S$-mediated activation of CB chemoreceptor afferent activity as observed in the CHF rats (Fig. 19.2) (Del Rio et al. 2013b).

### 19.2.2 Hemodynamic Factors

The hallmark of systolic CHF is a marked reduction in cardiac output due to impairment of left ventricular function. Although acute changes in systemic hemodynamics are known to have little effect on chemoreceptor activity, chronic changes in blood flow could impact CB function by sufficiently reducing oxygen delivery, or as we hypothesize, via alterations in endothelial function and signaling pathways.

A chronic reduction in blood flow to the CB, sustained over 3 weeks with adjustable cuff occluders on the carotid arteries in rabbits, increased AT1R expression and decreased nNOS expression in the CB and induced an increase in CB afferent activity that collectively were similar to changes observed in CHF rabbits over a similar time course (Fig. 19.3) (Ding et al. 2011). However, the link between reduced CB flow and these altered signaling pathways in the CB was not identified. It is unlikely that the increased CB activity resulted from ischemic hypoxia because the change was found to occur gradually over the course of the 3-week interval, with little effect within the first day. The transcriptional regulation of angiotensin converting enzyme (ACE) and eNOS expression in vascular endothelial cells is influenced by changes in blood flow via altered shear stress (Dekker et al. 2005; Miyakawa et al. 2004). Thus, an endothelial response to changes in blood flow in the CB may play an important role in regulating Ang metabolism and NO effects on CB chemoreceptor function in CHF (Fig. 19.1). However, it is uncertain whether the changes in CB protein expression seen with partial carotid occlusion may be driven by a reduction in brainstem perfusion, which could increase circulating hormones such as Ang II.

Kruppel-like factor 2 (KLF2) is a mechanically activated transcription factor that is important in the transduction of shear-stress effects on endothelial function (Dekker et al. 2005). KLF2 represses transcription of ACE and induces

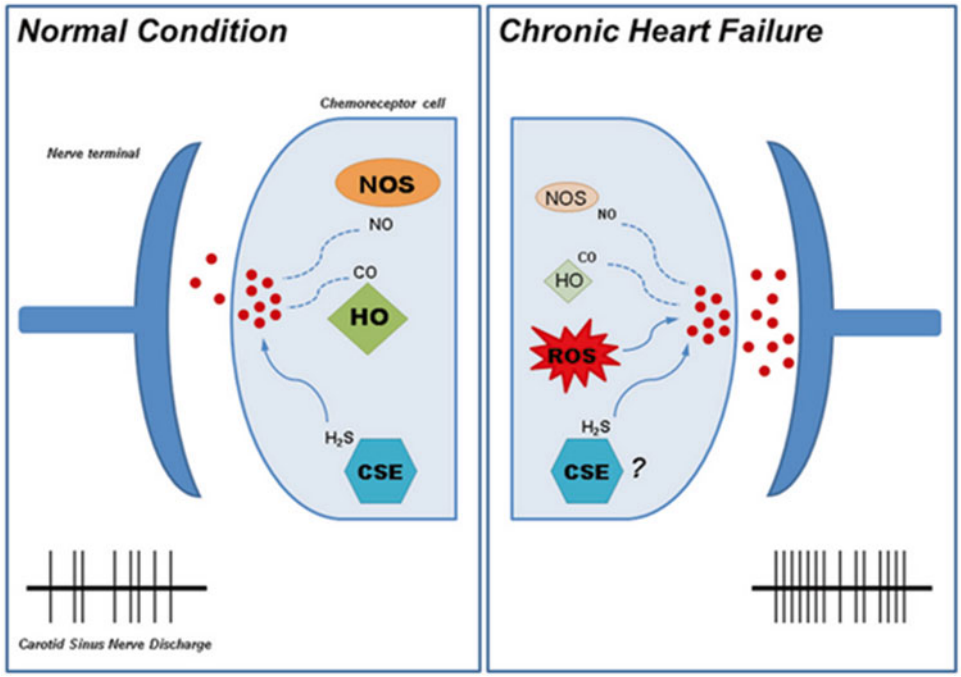


**Fig. 19.2** The contribution of gas neuromodulators to CB chemosensory function in CHF. In normal normoxic conditions, both NO and CO exert inhibitory effects (*dashed lines*) on CB chemoreceptor (glomus) cell excitability, which in turn tempers the release of excitatory neurotransmitters at post-synaptic petrosal ganglion nerve endings to limit afferent neural discharge. By contrast, $H_2S$ exerts an excitatory effect (*solid line*), which is manifested during hypoxia. In CHF, chronic downregulation of NO and CO production disinhibits excitatory influences on chemoreceptor excitability to elevate carotid body afferent discharge under both normoxic and hypoxic conditions. Effects mediated by reactive oxygen species (*ROS*) are shown in Fig. 19.1. *NOS* nitric oxide synthase, *HO* heme-oxygenase 2, *CSE* cystathionine γ-lyase (From Schultz et al. 2012 by permission from the publisher)

transcription of eNOS in endothelial cells (Fig. 19.1) (Dekker et al. 2005) as well as activating expression of transcription factors that regulate expression of anti-oxidant and oxidant enzymes (Nrf2 and NFkB respectively).

KLF2 expression is decreased in the CB in CHF (Fig. 19.4) (Haack et al. 2014), and adenoviral gene transfer of KLF2 to the CB normalizes the hypoxic ventilatory response and decreases the incidence of periodic breathing in CHF (Schultz and Marcus 2012). These findings suggest that KLF2 plays a fundamental role in the alteration in CB function that occurs with a reduction in CB blood flow in CHF. Further studies will be needed to confirm whether these functional effects of KLF2 are linked to normalization of oxidative and nitrosative redox pathways in the CB as discussed above.

### 19.2.3 Neural Factors

In addition to effects of reduced cardiac output, reflex activation of sympathetic nerve activity to the CB in CHF may affect glomus cell excitability or contribute to reduced CB blood flow via local vasoconstriction. Early studies found that the cervical sympathetic nerve stimulation had no direct effect on CB glomus cells or CB nerve activity that were independent of changes in blood flow (Eyzaguirre and Lewin 1961; McCloskey 1975) and that norepinephrine effects are usually inhibitory or biphasic (Prabhakar 1994). However, a recent study has shown that activation of cervical sympathetic nerves by hypoxia increases intracellular $Ca^{2+}$ responses in vascular smooth muscle cells and pericytes in the CB of rats (Yokoyama

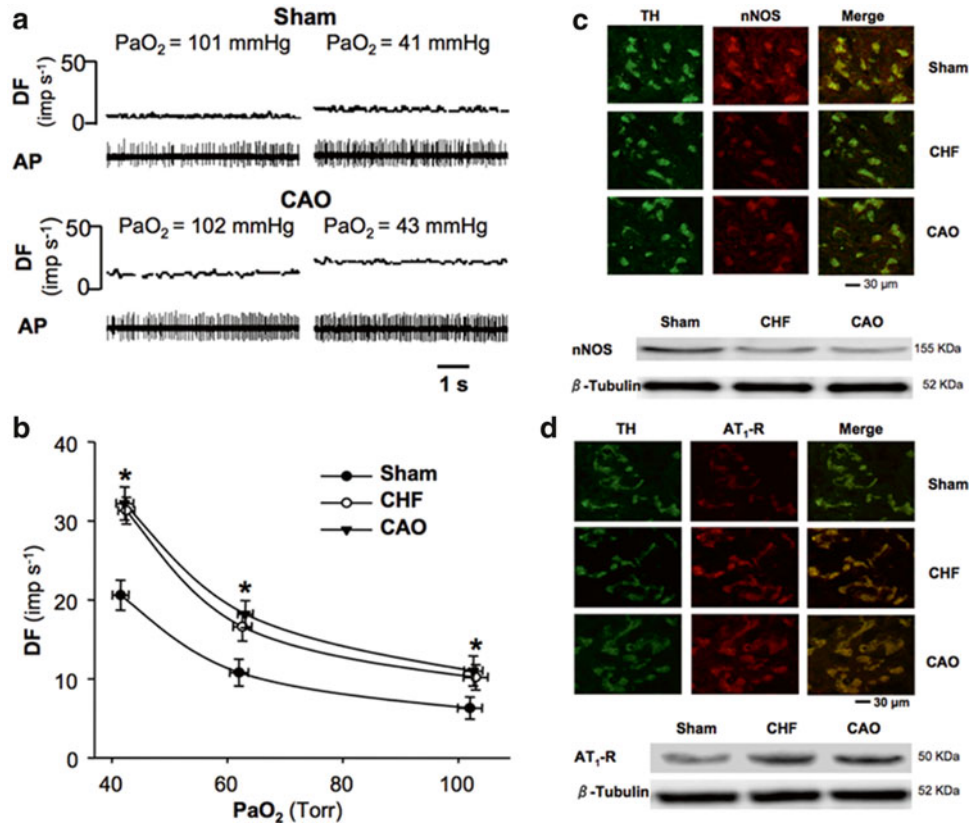


**Fig. 19.3** Chemoreceptor activity and the expression of nNOS and AT1R in the CB from rabbits with sham CHF surgery, CHF, or chronically reduced CB blood flow due to partial carotid artery occlusion (CAO). (**a**) Representative recording of CB chemoreceptor afferent discharge frequency (*DF*) in normoxic and hypoxic states. (**b**) CB chemoreceptor response to hypoxia. Note increased basal discharge in CHF and CAO states at normoxia. (**c**) Immunofluorescent and immunoblot images of nNOS protein in the CB of sham, CHF and CAO rabbits. (**d**) Immunofluorescent and immunoblot images of AT1R protein in the CB of sham, CHF and CAO rabbits. *AP*, action potential. $PaO_2$, arterial oxygen partial pressure. *TH* tyrosine hydroxylase staining of CB glomus cell clusters. *P<0.05 CHF and CAO compared with sham group (Modified from Ding et al. 2011 by permission from the publisher)

et al. 2015). Thus the CB-mediated sympathetic activation could serve to further reduce CB blood flow in CHF and contribute to the enhanced chemosensitivity by way of hemodynamic mechanisms discussed above. This idea has not been rigorously tested, but in preliminary experiments, we have found little effect of acute adrenergic blockade on CB function in CHF animals (unpublished). Additionally, the isolated CB from CHF animals (with sympathetic innervation interrupted) exhibits elevated basal discharge and hypersensitivity to hypoxia (Sun et al. 1999a; Del Rio et al. 2013b; Wang et al. 2012). Nevertheless, the contribution of sympathetic innervation of the CB in CHF needs to be better illuminated.

### 19.2.4 Ventilatory Factors

Cheyne-Stokes or oscillatory breathing (OB) and central apneas associated with CHF may produce intermittent hypoxia and contribute to sensitization of the CB in CHF in a manner similar to that observed in animals exposed to chronic intermittent hypoxia as a model of sleep apnea (Fung et al. 2014). The role of intermittent hypoxia on CB function in CHF has not been

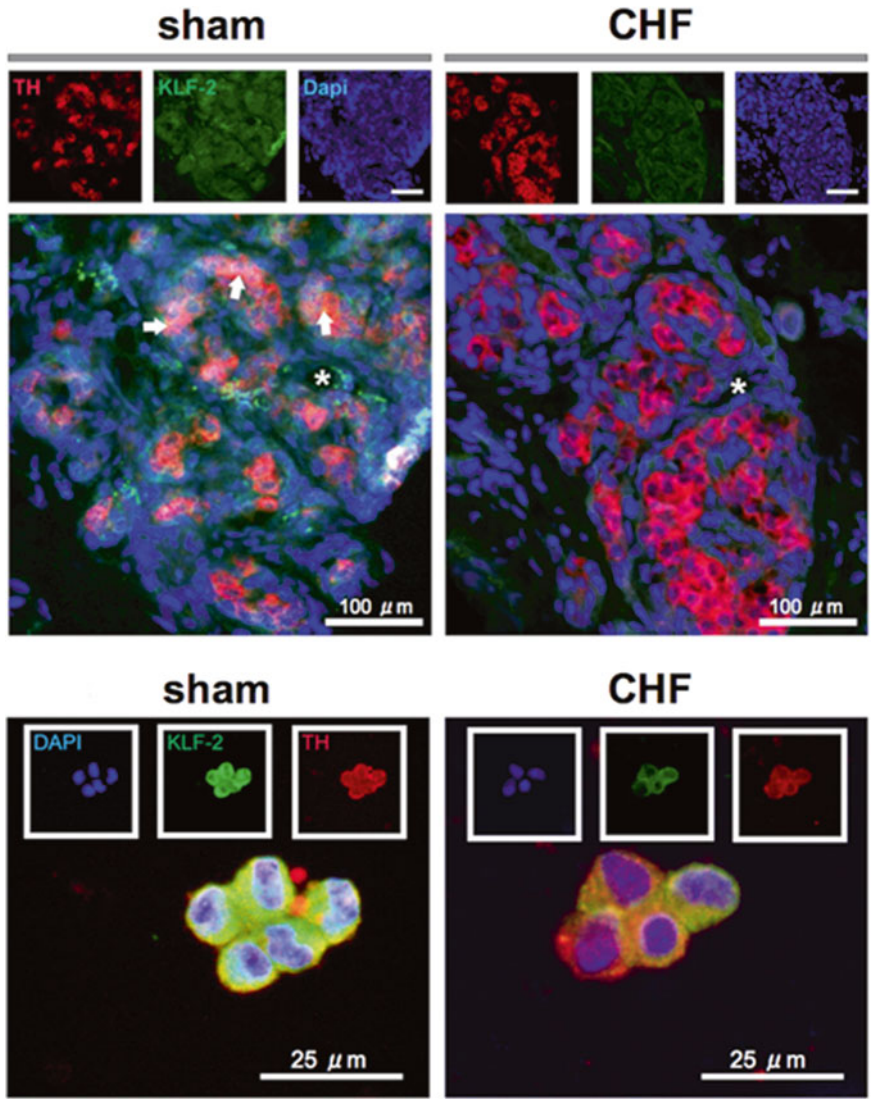


**Fig. 19.4** Immunolocalization of Kruppel-like factor 2 (KLF2) in the CB of CHF rats. Representative images from CBs from a Sham and CHF rats. Upper panels: KLF2 staining was localized to tyrosine hydroxylase (*TH*) positive glomus cells (*arrow*) and blood vessels (*asterisk*) in the CB. KLF2 immunostaining was decreased in the CBs from CHF rats. Lower panels: Similar staining from isolated glomus cell clusters (Modified from Haack et al. 2014 by permission form the publisher)

adequately addressed and remains speculative. In animal models of CHF, however, breathing instability is not a pre-existing condition in the development of heart failure, and in fact CB hyperactivity itself is required to drive the OB and apneas since they are abolished by CB ablation (see Sect. 19.3.2) (Marcus et al. 2014a; Del Rio et al. 2013a). Thus, at least in the animal models, it is difficult to envision destabilized breathing as a primary contributing factor to CB hyperactivity. Nevertheless, in patients, the sleep apnea associated with comorbid conditions that often precede or precipitate CHF such as metabolic syndrome, obesity, and hypertension could

contribute importantly to CB activation. Certainly chronic intermittent hypoxia from destabilized breathing in all etiologies of CHF could serve as a positive feedback (feed forward) mechanism to accelerate, enhance, and sustain CB activation.

### 19.2.5 Temporal Sequence of Events

The temporal sequence of events that transforms CB excitability from normal to tonically activated state in CHF suggests a progressive process over days to weeks. CB chemoreflex sensitivity progressively increases over the course of 3–4 weeks of pacing in CHF rabbits (Schultz et al. 2007). This change correlates with the progressive decrease in left ventricular function over the pacing interval, and was mimicked by a progressive reduction in carotid body blood flow over the same time frame using carotid occluders (Ding et al. 2011). A similar correlation was seen after myocardial infarct in rats where CB afferent and chemoreflex function increased in concert with progressive loss of ventricular function over the course of days to weeks (Del Rio et al. 2013a). These correlations would suggest that a reduction in carotid blood flow to reduce KLF2 expression in the CB is a major event (Fig. 19.1) in initiating changes in downstream cascade of signaling pathways described above.

Similarly, the functional consequences of CB hyperactivity during the progression of CHF are tonically driven by the changes in afferent function. Ablation of the CBs at later stages of CHF results in a rapid reduction in renal sympathetic nerve activity and cardiac arrhythmias, and increased breathing stability and autonomic balance within the time frame of recovery from the surgery in CHF animals (Marcus et al. 2014a). These autonomic changes preceded the improvement in cardiac function that subsequently occurred over the course of several days. When the CB ablation was performed early after myocardial infarct, deterioration of cardiac function was obtunded over subsequent weeks and survival increased (Del Rio et al. 2013a).

## 19.3 Functional Consequences of CB Activation in CHF

### 19.3.1 Autonomic Imbalance

Activation of the sympathetic nervous system and inhibition of the parasympathetic system contribute to the progressive decline in left ventricular function in CHF (Florea and Cohn 2014; Kishi 2012). Beat-to-beat heart rate variability (HRV) can serve as a noninvasive marker of autonomic input to the heart. HRV is markedly reduced in patients with CHF, reflecting a relative increase in sympathetic activity and decrease in parasympathetic activity to the heart. The reduction in HRV is related to the severity of CHF and its prognosis (Lombardi and Mortara 1998). Recent studies have shown that the CB plays an important role in reducing HRV in CHF (Niewinski et al. 2013; Del Rio et al. 2013a; Marcus et al. 2014a; Wang et al. 2012). CHF rats (Del Rio et al. 2013a) and rabbits (Marcus et al. 2014a) displayed marked shifts in the HRV index towards augmented sympathetic tone as evidenced by a decrease in total spectral power of HRV and an increase in the ratio of the spectral powers of the low to high frequency components of the HRV. HRV indices were normalized in these same animals following ablation of the CBs. In a more recent study using direct recordings of cardiac sympathetic nerve activity in CHF sheep, inhibition of the CB with hyperoxia reduced the CHF-induced elevation in cardiac sympathetic nerve activity (Xing et al. 2014). These studies demonstrate that neural input from the CB contributes to the cardiac autonomic imbalance and cardiac sympathetic activation seen in CHF.

Other indices of altered autonomic balance are also seen in CHF. These indices include reduced baroreflex sensitivity, increased sympathetic nerve activity to other organs, increased plasma catecholamines, and increased blood pressure variability (Florea and Cohn 2014). Similar to effects on HRV, CB ablation normalized baroreflex sensitivity, the activity of presympathetic neurons in the RVLM, resting renal sympathetic neural activity (RSNA), and blood

pressure variability in CHF animals (Del Rio et al. 2013a; Marcus et al. 2014a). Thus, input from the CB appears to have a global impact on sympathetic activation in CHF.

### 19.3.2 Breathing Instability

The hyperventilatory state induced by CB overactivity in CHF contributes to breathing instability, OB and increased incidence of central apneas. Studies in humans have provided good evidence that there is an important relationship between OB breathing patterns and changes in CB chemoreflex sensitivity in CHF (Ponikowski and Banasiak 2001). The incidence of OB progressively increases with enhancement of the CB chemoreflex in CHF patients (Giannoni et al. 2008). Other studies have shown that inhibition of CB chemoreceptors reduces OB patterns and the incidence of central apneas in CHF patients (Fontana et al. 2011; Ponikowski et al. 1999). In accordance with these findings, we have shown that CB ablation in either rabbit or rat models of CHF decreases resting ventilation, apneas and respiratory variability (Del Rio et al. 2013a; Marcus and Schultz 2001; Marcus et al. 2014a), confirming that the CB chemoreceptors contribute to the breathing instability associated with CHF. In other studies, pharmacologic attenuation of CB chemoreceptor activity with Simvastatin to reduce KLF2 expression (Haack et al. 2014) or an inhibitor of hydrogen sulfide production (Del Rio et al. 2013b) had similar efficacy in reducing apnea/hypopnea frequency and respiratory variability. These studies suggest that an elevated ventilatory loop gain mediated by the tonically activated CB chemoreflex contributes to breathing instability in CHF.

### 19.3.3 Respiratory-Sympathetic Coupling

It is well known that sympathetic discharge is actively modulated by respiration (Adrian et al. 1932; Haselton and Guyenet 1989) and that enhanced respiratory-sympathetic coupling coincides with enhanced sympathetic drive in animal models of hypertension (Simms et al. 2009; Toney et al. 2010). Alterations in this 'coupling' relationship between central control of respiratory and sympathetic neural drive may underlie the association of altered respiratory patterns and increased sympathetic outflow in CHF. Similar to the phenomenon seen in animals exposed to chronic intermittent hypoxia (Zoccal and Machado 2011), renal sympathetic activity is more tightly entrained to the respiratory pattern in CHF rabbits (Marcus et al. 2014a), and this enhanced entrainment is abrogated after CB ablation. Thus, OB patterns in CHF have the potential to drive increased tonic sympathetic outflow as a result of the increased sympathetic-respiratory coupling driven by the CB (Fig. 19.5). Indeed, the beneficial effects of CB ablation on autonomic function in CHF may be due in part to its effect to rapidly restore normal breathing patterns in CHF animals (Del Rio et al. 2013a). Thus the ventilatory destabilization in association with enhanced respiratory-sympathetic coupling mediated by CB hyper reactivity may serve to aggravate autonomic imbalance and its impact on deterioration of cardiac and renal function.

### 19.3.4 Cardiac Function

Ventricular remodelling and arrhythmogenesis are major contributory factors to progressive cardiac dysfunction and the progression of CHF. These changes in electrical and structural stability of the heart are precipitated in large part by the changes in autonomic balance to the heart in CHF (Lymperopoulos et al. 2013; Fu et al. 2012) as well as humoral and hemodynamic factors (Johnson 2014).

Our findings that increased arrhythmia incidence and decreased HRV in CHF rabbits (Marcus et al. 2014a) and rats (Del Rio et al. 2013a) were concomitantly reversed with CB ablation expands on the previously observed correlation between enhanced chemoreflex sensitivity and arrhythmia incidence in a mouse model of CHF (Wang et al. 2012). These studies provide compelling evidence that CB chemoreceptors by

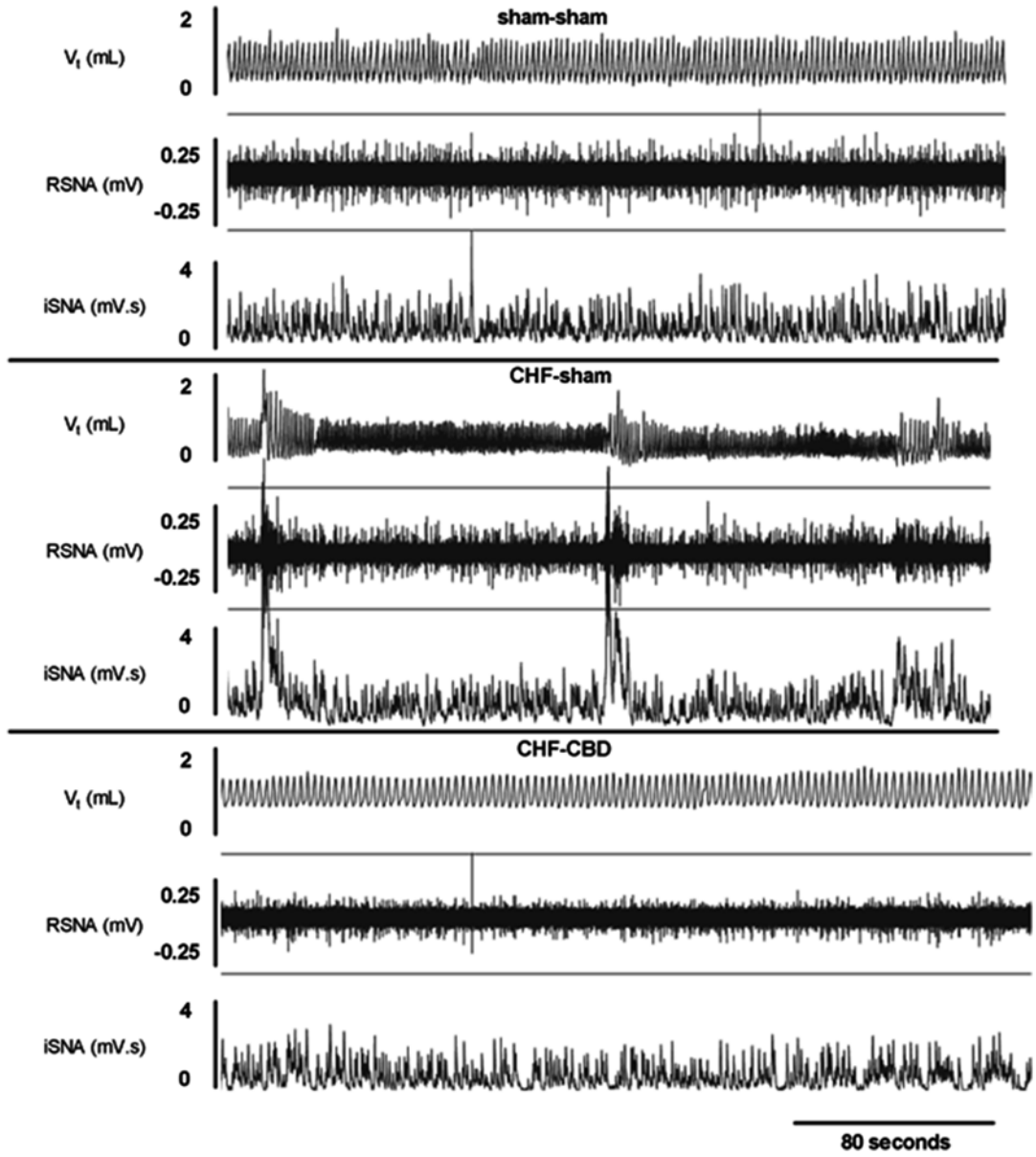


**Fig. 19.5** Effect of CB ablation (CBD) on oscillations in breathing and RSNA in CHF. Representative recordings of tidal volume ($V_t$), renal sympathetic nerve activity (*RSNA*), and integrated RSNA (*iSNA*) in sham-sham, CHF-sham, and CHF-CBD rabbits. Qualitatively these tracings illustrate the concomitant oscillations in breathing and RSNA (respiratory-sympathetic coupling) that occur in CHF, and the effect of CBD to normalize these oscillations (From Marcus et al. 2014a with permission from the publisher). See Marcus et al. (2014a) for further confirmation of respiratory-sympathetic coupling using coherence analysis

way of effects on cardiac autonomic balance contribute to cardiac arrhythmias in CHF.

Increasing end systolic left ventricular (LV) volume predicts adverse cardiovascular outcomes in patients with LV systolic dysfunction (White et al. 1987) and has better predictive value of long-term survival in patients with LV dysfunction than ejection fraction or end diastolic volume.

Progressive increases in LV end systolic volume as well as decrements in ejection fraction and fractional shortening typically occur over the course of development of CHF by rapid pacing in rabbits (Sun et al. 1999b; Marcus et al. 2014a) and coronary ligation in rats (Del Rio et al. 2013a). Carotid body ablation curbed the decreases in ejection fraction and fractional shortening and, more importantly, reversed the increases in systolic and diastolic ventricular volumes with chronic pacing in rabbits (Marcus et al. 2014a). These improvements in cardiac function were shown to occur gradually over a course of a week that followed the immediate improvements in autonomic balance and respiratory stability after CB ablation. Thus the negative impact of excessive tonic CB activity on cardiac function in CHF likely represents a multifactorial process that involves not only immediate impairment of autonomic control of cardiac contractile and electrical stability but also more long-term or gradual effects on the heart that involve neurohumoral influences on intrinsic cardiac myocyte structure/function, and cardiac mechanics by way of altered hemodynamics and volume homeostasis.

Cardiac remodelling and fibrosis present a gradual process that contributes to the development of arrhythmias and impaired left ventricular contractile function in CHF (Cohn et al. 2000). To demonstrate the potential impact of the CB on these more gradual structural impairments in the LV, we performed CB ablation two weeks after coronary infarct in rats, during the early stages of cardiac remodelling and then assessed collagen deposition in the functional LV wall fourteen weeks later. The non-infarcted areas of the LV displayed significantly less tissue remodelling evidenced by decreased collagen deposition (Del Rio et al. 2013a). Furthermore, early CB ablation reduced arrhythmias and delayed the progressive deterioration of left ventricular ejection fraction. Thus, chronic CB activation contributes to cardiac remodelling and fibrosis in CHF, but the mechanisms remain to be elucidated. The tonic cardiac autonomic imbalance (sympathetic activation) is likely a major contributing factor (Florea and Cohn 2014; Roy et al. 2014), but one can envision a role for renal sympathetic enhancement of circulating Ang II (Anavekar and Solomon 2005), sympathetic activation of inflammatory cytokines (Edgley et al. 2012; Colombo et al. 2012) as well as sympathetic effects on volume homeostasis influencing cardiac preload and mechanical stress factors (Jonsson et al. 2014).

### 19.3.5 Renal function

In CHF patients, renal dysfunction is common and is associated with poor prognosis (Bock and Gottlieb 2010). Under normal circumstances, CB chemoreflex activation elicits a reduction in renal blood flow and glomerular filtration rate that is mediated by renal sympathetic nerves (Karim et al. 1987). In CHF, tonic elevations in renal sympathetic nerve activity (RSNA) mediate sustained reductions in renal blood flow and alterations in angiotensin signaling (Clayton et al. 2011) that can exacerbate renal ischemia and injury. Our preliminary findings indicate that in CHF rabbits and rats, resting renal blood flow is markedly reduced and the reduction in renal blood flow to CB chemoreflex activation is markedly accentuated in CHF animals. Carotid body ablation in CHF animals reduced resting RSNA, increased renal blood flow, and decreased markers of renal injury and fibrosis (Fig. 19.6) (Marcus et al. 2014b), as well as the reducing disordered breathing and improving in cardiac function mentioned previously (Marcus et al. 2014a). In addition to the influence of the CB chemoreflex on resting RSNA, additional surges in RSNA may be superimposed by oscillatory breathing and enhanced respiratory-sympathetic coupling to produce repetitive bouts of renal vasoconstriction and impaired blood flow. These findings suggest that tonic CB chemoreflex activation in CHF may contribute to renal pathology in part by its influence on sympathetic outflow to the kidneys (Marcus et al. 2014a).

Renal dysfunction in CHF is particularly ominous because it can precipitate a further decline in cardiac function by way of volume retention

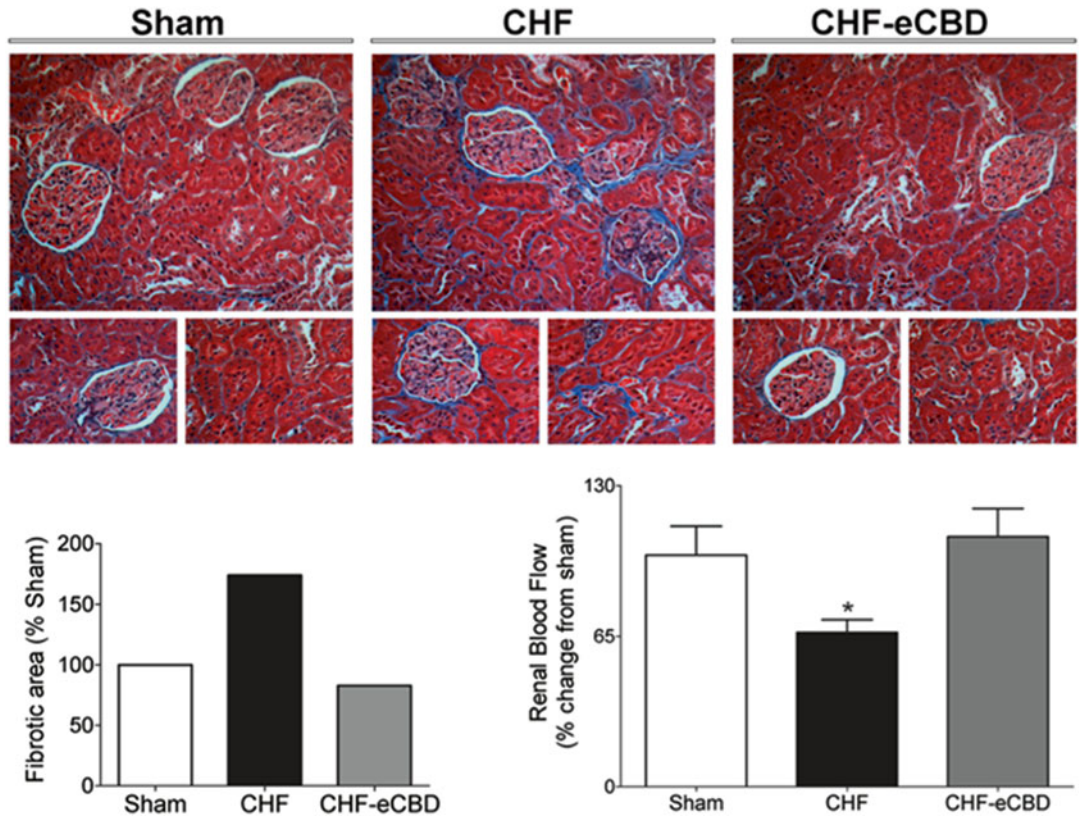


**Fig. 19.6** Effect of CB ablation (CBD) on renal fibrosis and renal blood flow (RBF) in CHF. (**a**) Transverse sections of kidneys taken from sham, CHF, and CHF-eCBD rats 16 weeks after coronary ligation. CB ablation was performed early (eCBD) at 2 weeks after coronary ligation. Collagen deposition is indicated by blue staining, (**b**) Mean data for fibrotic area. (**c**) RBF (Doppler) measured under isoflurane anesthesia 16 weeks after CAL surgery. *$p<0.05$ vs. sham

and increased cardiac preload, initiating a downward spiral of deteriorating cardiac and renal function, known as cardiorenal syndrome. The etiology of cardiorenal syndrome is diverse, but it is aggravated by excessive sympathetic activation of the heart and kidneys causing increases in sodium and water retention and activation of the renin-angiotensin system, renal ischemia secondary to reductions in renal perfusion, and neurohormonal impairment of cardiac function (Bock and Gottlieb 2010). Tonic chemoreflex activation in CHF may contribute to cardiorenal syndrome by increasing sympathetic stimulation of the heart (Fig. 19.7) (Xing et al. 2014; Del Rio et al. 2013a; Marcus et al. 2014a) and kidneys (Sun et al. 1999b; Marcus et al. 2014a).

## 19.4 Translational Impact of CB Hyperactivity in CHF

A case report published recently showed that unilateral CB ablation in a CHF patient resulted in modest improvements in autonomic function, cardiac function, and exercise tolerance, and reduced resting ventilation (Niewinski et al. 2013). This case report supports findings from animal models and confirms the potential of CB ablation or other forms of CB modulation as a therapeutic option in CHF patients. In another recent study involving a group of six CHF patients, bilateral CB ablation markedly reduced the ventilatory and hypertensive blood pressure responses to hypoxia, the

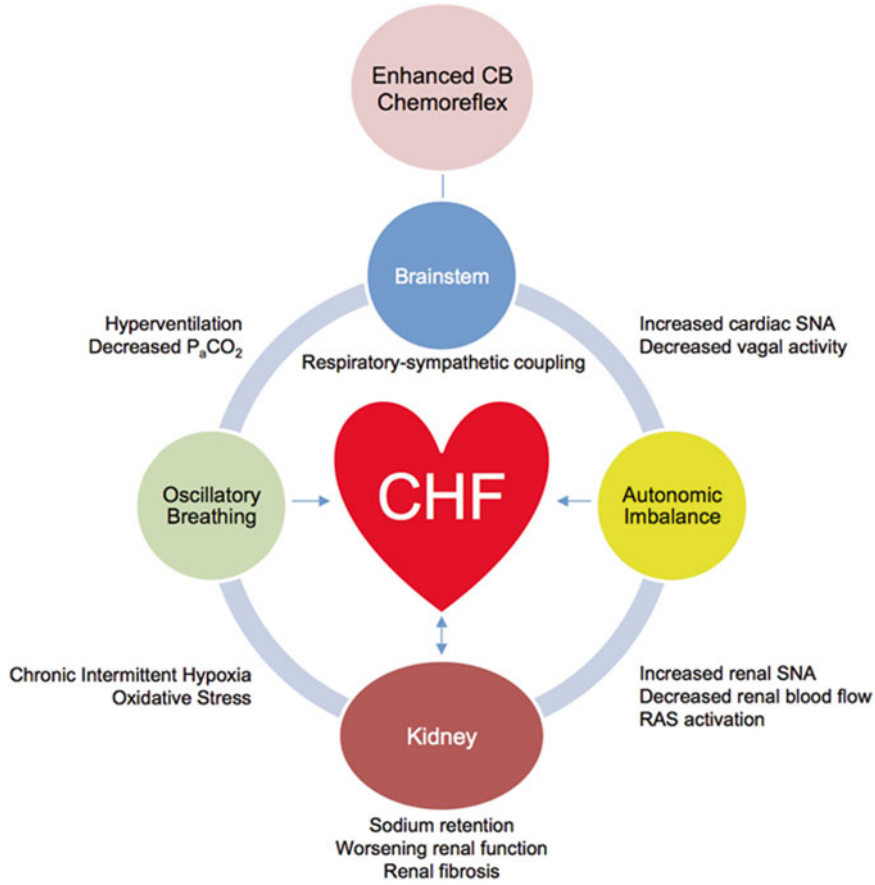


**Fig. 19.7** Role of Carotid Body Chemoreceptors in Cardiac and Renal Dysfunction in CHF. Enhanced tonic afferent activity from carotid body (*CB*) chemoreceptors drives neuronal activity in brainstem centers that integrate peripheral afferents and control respiratory and sympathetic neural outflow. Hyperventilation due to the enhanced CB chemoreflex activation precipitates oscillatory breathing, which exacerbates sympathetic nerve activity (*SNA*) through respiratory-sympathetic coupling, in addition to exposing the heart and kidneys to intermittent hypoxia and oxidative stress. The CB-mediated enhanced respiratory-sympathetic coupling results in increased sympathetic and decreased vagal efferent outflow to the heart, which over time worsens cardiac function and development of fibrosis. Similarly, CB-mediated increases in renal SNA cause reductions in renal perfusion and activation of the renin-angiotensin system, which over time lead to worsening renal function and development of fibrosis. The combined deleterious effects of CB-mediated respiratory-sympathetic coupling on the heart and kidney advance the cardiorenal syndrome (From Marcus et al. 2014c with permission from the publisher)

latter suggesting a reduction in sympathetic tone (Niewinski et al. 2014). Interestingly, CB ablation did not reduce the tachycardia to hypoxia. These results support a role of the CB in the sympathetic activation in CHF patients, but may call into the question the direct role of the CB chemoreflex on sympathetic activation of the heart in humans. Further studies are needed to determine whether there is a differential role of CB and aortic chemoreceptors on other measures of cardiac function in CHF humans.

Of major clinical relevance, it is still not known whether CB ablation reduces morbidity and increases survival or quality of life in CHF patients. As discussed herein, CB ablation improves autonomic balance, breathing stability, and cardiac and renal function in animal models of CHF. Importantly, these improvements correlate with an increased survival rate (Del Rio et al. 2013a). The mechanisms by which removal of the CB increases survival remain to be elucidated but it is likely to involve improved autonomic

control of hemodynamics, cardiac and renal function, and improved control of breathing, Although CB ablation has proven to be efficacious in animal models with no evidence of adverse effects, the potential adverse implications of CB removal in patients with marked hypoxemia or tenuous cardio-respiratory status must be realized. Finding approaches that can reduce excessive tonic CB activity without eliminating its normal protective responses to hypoxia are likely to be a preferred clinical treatment strategy in humans.

A number of pharmacological and genetic approaches have been shown to reduce CB afferent activity in CHF animals and reduce sympathetic nerve activity and improve breathing stability. These methods include NO and CO donors (Ding et al. 2008), anti-oxidants (Li et al. 2007), overexpression of nNOS, Mn-SOD or Cu/Zn-SOD in the CB (Ding et al. 2009, 2010; Li et al. 2005), inhibition of CSE (Del Rio et al. 2013b). However, the long-term efficacy of most of these approaches, singly or in combination, to improve functional status and survival in CHF animals has not been assessed. Potential adverse effects and feasibility of these approaches in humans also have to be considered.

ACE inhibitors and AT1R blockers (ARBs) are routinely used to treat CHF with variable success, and AT1R antagonists reduce CB afferent activity in CHF animals (Li et al. 2006). But, there has been no effort to relate the clinical efficacy of these drugs to effects on chemoreflex function in humans. In fact, the routine use of angiotensin inhibitors in CHF patients participating in clinical studies may be a contributing factor to the variable degrees of CB chemoreflex sensitivity observed in these studies (Chua et al. 1997).

Oxygen supplementation may be an effective approach for some patients. Hyperoxia inhibits CB chemoreceptor discharge and reduces sympathetic nerve activity in CHF animals (Xing et al. 2014; Sun et al. 1999b) and in humans (Querido et al. 2010; Stickland et al. 2008; Ponikowski et al. 1997; Sinski et al. 2014). However, potential hemodynamic consequences of hyperoxia in CHF patients (Mak et al. 2001; Branson and Johannigman 2013), and tissue injury from excessive oxygen exposure can present potential risks to the patient.

In searching for efficacious treatments for CHF patients without undesirable side effects, it should be noted that moderate regular exercise has been shown to improve the functional status of CHF patients (Downing and Balady 2011) that includes normalization of sympatho-vagal balance. The beneficial effects of exercise may be due, at least in part, to improved CB function (Fig. 19.1). Regular exercise is effective in normalizing CB chemoreflex function in CHF rabbits via enhancing NO bioavailability and reducing Ang II- $O_2^{\bullet-}$ influences on the CB (Li et al. 2008). These changes may be due to the effects of exercise to increase blood flow and improve endothelial function and KLF2 expression in the CB.

Clinically, statin treatment has been shown to lower resting sympathetic nerve activity in CHF patients (Deo et al. 2012). Furthermore, simvastatin has been shown to reduce the incidence of arrhythmias and oscillatory breathing and reduce CB chemoreflex sensitivity in CHF rats (Haack et al. 2014). These improvements corresponded with an increase in KLF2 and eNOS expression and a decrease in AT1R expression in the CB. These data suggest that oral simvastatin treatment may be another therapeutic strategy in patients with high chemoreflex sensitivity (Fig. 19.1).

## 19.5 Conclusions

Herein we provide evidence from animal studies to support potential mechanisms by which the CB chemoreceptors become tonically activated in CHF and to underscore a critical role for the CB chemoreceptors in the etiology of several important pathophysiological aspects of CHF. CB chemoreceptors are a major driving force in the development of autonomic dysfunction and breathing abnormalities in CHF. Ablation of the CB chemoreceptors is sufficient to improve these parameters and leads to improved cardiac and renal function and survival. The mechanisms by which the CB chemoreflex exacerbates cardiac

deterioration and morbidity in CHF remain to be better elucidated, but disordered breathing, enhanced respiratory-sympathetic coupling, tonic and episodic increases in cardiac and renal SNA, and reductions in renal function likely play an important role (Marcus et al. 2014c).

Ultimately, the goal is to normalize CB function in humans to allow improvement in functional status to the same degree and success as seen by CB ablation in animal models of CHF. However, the cure may be as complex as the cause in the search for effective methods that work in all patients. Nevertheless, a better understanding of the physiological and molecular mechanisms responsible for CB hyperactivity in CHF will contribute to the development of effective therapeutic approaches.

**Funding** HDS is supported by a Program Project Grant from the Heart, Lung and Blood Institute of NIH (PO1-HL62222).

NJM is supported by a Ruth L. Kirschstein National Research Service Award (NRSA) from NIH (5F32HL108592)

RDR is supported by Fondo de Desarrollo Cientifico y Tecnologico (Fondecyt #1140275)

**Conflicting Interests** The authors have no conflicts of interest to disclose.

## References

Adrian ED, Bronk DW, Phillips G (1932) Discharges in mammalian sympathetic nerves. J Physiol 74(2):115–133

Anavekar NS, Solomon SD (2005) Angiotensin II receptor blockade and ventricular remodelling. J Renin Angiotensin Aldosterone Syst 6(1):43–48. doi:10.3317/jraas.2005.006

Bock JS, Gottlieb SS (2010) Cardiorenal syndrome: new perspectives. Circulation 121(23):2592–2600. doi:10.1161/CIRCULATIONAHA.109.886473

Brack T, Randerath W, Bloch KE (2012) Cheyne-Stokes respiration in patients with heart failure: prevalence, causes, consequences and treatments. Respiration 83(2):165–176. doi:10.1159/000331457

Branson RD, Johannigman JA (2013) Pre-hospital oxygen therapy. Respir Care 58(1):86–97. doi:10.4187/respcare.02251

Chua TP, Ponikowski P, Webb-Peploe K, Harrington D, Anker SD, Piepoli M, Coats AJ (1997) Clinical characteristics of chronic heart failure patients with an augmented peripheral chemoreflex. Eur Heart J 18(3):480–486

Clayton SC, Haack KK, Zucker IH (2011) Renal denervation modulates angiotensin receptor expression in the renal cortex of rabbits with chronic heart failure. Am J Physiol Renal Physiol 300(1):F31–F39. doi:10.1152/ajprenal.00088.2010

Cohn JN, Ferrari R, Sharpe N (2000) Cardiac remodeling–concepts and clinical implications: a consensus paper from an international forum on cardiac remodeling. Behalf of an International Forum on Cardiac Remodeling. J Am Coll Cardiol 35(3):569–582

Colombo PC, Ganda A, Lin J, Onat D, Harxhi A, Iyasere JE, Uriel N, Cotter G (2012) Inflammatory activation: cardiac, renal, and cardio-renal interactions in patients with the cardiorenal syndrome. Heart Fail Rev 17(2):177–190. doi:10.1007/s10741-011-9261-3

Dekker RJ, van Thienen JV, Rohlena J, de Jager SC, Elderkamp YW, Seppen J, de Vries CJ, Biessen EA, van Berkel TJ, Pannekoek H, Horrevoets AJ (2005) Endothelial KLF2 links local arterial shear stress levels to the expression of vascular tone-regulating genes. Am J Pathol 167(2):609–618. doi:10.1016/S0002-9440(10)63002-7

Del Rio R, Marcus NJ, Schultz HD (2013a) Carotid chemoreceptor ablation improves survival in heart failure: rescuing autonomic control of cardiorespiratory function. J Am Coll Cardiol 62(25):2422–2430. doi:10.1016/j.jacc.2013.07.079

Del Rio R, Marcus NJ, Schultz HD (2013b) Inhibition of hydrogen sulfide restores normal breathing stability and improves autonomic control during experimental heart failure. J Appl Physiol (1985) 114(9):1141–1150. doi:10.1152/japplphysiol.01503.2012

Deo SH, Fisher JP, Vianna LC, Kim A, Chockalingam A, Zimmerman MC, Zucker IH, Fadel PJ (2012) Statin therapy lowers muscle sympathetic nerve activity and oxidative stress in patients with heart failure. Am J Physiol Heart Circ Physiol 303(3):H377–H385. doi:10.1152/ajpheart.00289.2012

Ding Y, Li YL, Schultz HD (2008) Downregulation of carbon monoxide as well as nitric oxide contributes to peripheral chemoreflex hypersensitivity in heart failure rabbits. J Appl Physiol (1985) 105(1):14–23. doi:10.1152/japplphysiol.01345.2007

Ding Y, Li YL, Zimmerman MC, Davisson RL, Schultz HD (2009) Role of CuZn superoxide dismutase on carotid body function in heart failure rabbits. Cardiovasc Res 81(4):678–685. doi:10.1093/cvr/cvn350

Ding Y, Li YL, Zimmerman MC, Schultz HD (2010) Elevated mitochondrial superoxide contributes to enhanced chemoreflex in heart failure rabbits. Am J Physiol Regul Integr Comp Physiol 298(2):R303–R311. doi:10.1152/ajpregu.00629.2009

Ding Y, Li YL, Schultz HD (2011) Role of blood flow in carotid body chemoreflex function in heart failure. J Physiol 589(Pt 1):245–258. doi:10.1113/jphysiol.2010.200584

Downing J, Balady GJ (2011) The role of exercise training in heart failure. J Am Coll Cardiol 58(6):561–569. doi:10.1016/j.jacc.2011.04.020

Edgley AJ, Krum H, Kelly DJ (2012) Targeting fibrosis for the treatment of heart failure: a role for transforming growth factor-beta. Cardiovasc Ther 30(1):e30–e40. doi:10.1111/j.1755-5922.2010.00228.x

Esler M (2010) The 2009 Carl Ludwig Lecture: Pathophysiology of the human sympathetic nervous system in cardiovascular diseases: the transition from mechanisms to medical management. J Appl Physiol (1985) 108(2):227–237. doi:10.1152/japplphysiol.00832.2009

Eyzaguirre C, Lewin J (1961) The effect of sympathetic stimulation on carotid nerve activity. J Physiol 159:251–267

Florea VG, Cohn JN (2014) The autonomic nervous system and heart failure. Circ Res 114(11):1815–1826. doi:10.1161/CIRCRESAHA.114.302589

Fontana M, Emdin M, Giannoni A, Iudice G, Baruah R, Passino C (2011) Effect of acetazolamide on chemosensitivity, Cheyne-Stokes respiration, and response to effort in patients with heart failure. Am J Cardiol 107(11):1675–1680. doi:10.1016/j.amjcard.2011.01.060

Fu Y, Xiao H, Zhang Y (2012) Beta-adrenoceptor signaling pathways mediate cardiac pathological remodeling. Front Biosci (Elite Ed) 4:1625–1637

Fung ML, Tipoe GL, Leung PS (2014) Mechanisms of maladaptive responses of peripheral chemoreceptors to intermittent hypoxia in sleep-disordered breathing. Sheng Li Xue Bao 66(1):23–29

Giannoni A, Emdin M, Poletti R, Bramanti F, Prontera C, Piepoli M, Passino C (2008) Clinical significance of chemosensitivity in chronic heart failure: influence on neurohormonal derangement, Cheyne-Stokes respiration and arrhythmias. Clin Sci (Lond) 114(7):489–497. doi:10.1042/CS20070292

Haack KK, Marcus NJ, Del Rio R, Zucker IH, Schultz HD (2014) Simvastatin treatment attenuates increased respiratory variability and apnea/hypopnea index in rats with chronic heart failure. Hypertension 63(5):1041–1049. doi:10.1161/HYPERTENSIONAHA.113.02535

Haselton JR, Guyenet PG (1989) Central respiratory modulation of medullary sympathoexcitatory neurons in rat. Am J Physiol 256(3 Pt 2):R739–R750

Iturriaga R (2013) Intermittent hypoxia: endothelin-1 and hypoxic carotid body chemosensory potentiation. Exp Physiol 98(11):1550–1551. doi:10.1113/expphysiol.2013.075820

Iturriaga R, Moya EA, Rio RD (2014) Inflammation and oxidative stress during intermittent hypoxia: the impact on chemoreception. Exp Physiol. doi:10.1113/expphysiol.2014.079525

Johnson FL (2014) Pathophysiology and etiology of heart failure. Cardiol Clin 32(1):9–19. doi:10.1016/j.ccl.2013.09.015, vii

Jonsson S, Agic MB, Narfstrom F, Melville JM, Hultstrom M (2014) Renal neurohormonal regulation in heart failure decompensation. Am J Physiol Regul Integr Comp Physiol 307(5):R493–R497. doi:10.1152/ajpregu.00178.2014

Karim F, Poucher SM, Summerill RA (1987) The effects of stimulating carotid chemoreceptors on renal haemodynamics and function in dogs. J Physiol 392:451–462

Kishi T (2012) Heart failure as an autonomic nervous system dysfunction. J Cardiol 59(2):117–122. doi:10.1016/j.jjcc.2011.12.006

Lam SY, Liu Y, Ng KM, Lau CF, Liong EC, Tipoe GL, Fung ML (2012) Chronic intermittent hypoxia induces local inflammation of the rat carotid body via functional upregulation of proinflammatory cytokine pathways. Histochem Cell Biol 137(3):303–317. doi:10.1007/s00418-011-0900-5

Leung PS, Fung ML, Tam MS (2003) Renin-angiotensin system in the carotid body. Int J Biochem Cell Biol 35(6):847–854

Li YL, Schultz HD (2006) Enhanced sensitivity of Kv channels to hypoxia in the rabbit carotid body in heart failure: role of angiotensin II. J Physiol 575(Pt 1):215–227. doi:10.1113/jphysiol.2006.110700

Li YL, Li YF, Liu D, Cornish KG, Patel KP, Zucker IH, Channon KM, Schultz HD (2005) Gene transfer of neuronal nitric oxide synthase to carotid body reverses enhanced chemoreceptor function in heart failure rabbits. Circ Res 97(3):260–267. doi:10.1161/01.RES.0000175722.21555.55

Li YL, Xia XH, Zheng H, Gao L, Li YF, Liu D, Patel KP, Wang W, Schultz HD (2006) Angiotensin II enhances carotid body chemoreflex control of sympathetic outflow in chronic heart failure rabbits. Cardiovasc Res 71(1):129–138. doi:10.1016/j.cardiores.2006.03.017

Li YL, Gao L, Zucker IH, Schultz HD (2007) NADPH oxidase-derived superoxide anion mediates angiotensin II-enhanced carotid body chemoreceptor sensitivity in heart failure rabbits. Cardiovasc Res 75(3):546–554. doi:10.1016/j.cardiores.2007.04.006

Li YL, Ding Y, Agnew C, Schultz HD (2008) Exercise training improves peripheral chemoreflex function in heart failure rabbits. J Appl Physiol (1985) 105(3):782–790. doi:10.1152/japplphysiol.90533.2008

Lombardi F, Mortara A (1998) Heart rate variability and cardiac failure. Heart 80(3):213–214

Lu Y, Whiteis CA, Sluka KA, Chapleau MW, Abboud FM (2013) Responses of glomus cells to hypoxia and acidosis are uncoupled, reciprocal and linked to ASIC3 expression: selectivity of chemosensory transduction. J Physiol 591(Pt 4):919–932. doi:10.1113/jphysiol.2012.247189

Lymperopoulos A, Rengo G, Koch WJ (2013) Adrenergic nervous system in heart failure: pathophysiology and therapy. Circ Res 113(6):739–753. doi:10.1161/CIRCRESAHA.113.300308

Mak S, Azevedo ER, Liu PP, Newton GE (2001) Effect of hyperoxia on left ventricular function and filling pressures in patients with and without congestive heart failure. Chest 120(2):467–473

Marcus NJ, Schultz HD (2001) Role of carotid body chemoreflex function in the development of Cheyne-Stokes respiration during progression of congestive heart failure. FASEB J 25:841.847

Marcus NJ, Del Rio R, Schultz EP, Xia XH, Schultz HD (2014a) Carotid body denervation improves autonomic and cardiac function and attenuates disordered breathing in congestive heart failure. J Physiol 592(Pt 2):391–408. doi:10.1113/jphysiol.2013.266221

Marcus NJ, Del Rio R, Schultz HD (2014b) Carotid body denervation reduces renal sympathetic nerve activity and fibrosis, and increases renal blood flow in congestive heart failure. FASEB J 28:875.814

Marcus NJ, Del Rio R, Schultz HD (2014c) Central role of carotid body chemoreceptors in disordered breathing and cardiorenal dysfunction in chronic heart failure. Front Physiol 5:438. doi:10.3389/fphys.2014.00438

McCloskey DI (1975) Mechanisms of autonomic control of carotid chemoreceptor activity. Respir Physiol 25(1):53–61

Miyakawa AA, de Lourdes JM, Krieger JE (2004) Identification of two novel shear stress responsive elements in rat angiotensin I converting enzyme promoter. Physiol Genomics 17(2):107–113. doi:10.1152/physiolgenomics.00169.2003

Niewinski P (2014) Pathophysiology and potential clinical applications for testing of peripheral chemosensitivity in heart failure. Curr Heart Fail Rep 11(2):126–133. doi:10.1007/s11897-014-0188-6

Niewinski P, Janczak D, Rucinski A, Jazwiec P, Sobotka PA, Engelman ZJ, Fudim M, Tubek S, Jankowska EA, Banasiak W, Hart EC, Paton JF, Ponikowski P (2013) Carotid body removal for treatment of chronic systolic heart failure. Int J Cardiol 168(3):2506–2509. doi:10.1016/j.ijcard.2013.03.011

Niewinski P, Janczak D, Rucinski A, Tubek S, Engelman ZJ, Jazwiec P, Banasiak W, Sobotka PA, Hart EC, Paton JF, Ponikowski P (2014) Dissociation between blood pressure and heart rate response to hypoxia after bilateral carotid body removal in men with systolic heart failure. Exp Physiol 99(3):552–561. doi:10.1113/expphysiol.2013.075580

Peng YJ, Nanduri J, Raghuraman G, Wang N, Kumar GK, Prabhakar NR (2013) Role of oxidative stress-induced endothelin-converting enzyme activity in the alteration of carotid body function by chronic intermittent hypoxia. Exp Physiol 98(11):1620–1630. doi:10.1113/expphysiol.2013.073700

Ponikowski P, Banasiak W (2001) Chemosensitivity in chronic heart failure. Heart Fail Monit 1(4):126–131

Ponikowski P, Chua TP, Piepoli M, Ondusova D, Webb-Peploe K, Harrington D, Anker SD, Volterrani M, Colombo R, Mazzuero G, Giordano A, Coats AJ (1997) Augmented peripheral chemosensitivity as a potential input to baroreflex impairment and autonomic imbalance in chronic heart failure. Circulation 96(8):2586–2594

Ponikowski P, Anker SD, Chua TP, Francis D, Banasiak W, Poole-Wilson PA, Coats AJ, Piepoli M (1999) Oscillatory breathing patterns during wakefulness in patients with chronic heart failure: clinical implications and role of augmented peripheral chemosensitivity. Circulation 100(24):2418–2424

Ponikowski P, Chua TP, Anker SD, Francis DP, Doehner W, Banasiak W, Poole-Wilson PA, Piepoli MF, Coats AJ (2001) Peripheral chemoreceptor hypersensitivity: an ominous sign in patients with chronic heart failure. Circulation 104(5):544–549

Prabhakar NR (1994) Neurotransmitters in the carotid body. Adv Exp Med Biol 360:57–69

Prabhakar NR (2012) Carbon monoxide (CO) and hydrogen sulfide (H(2)S) in hypoxic sensing by the carotid body. Respir Physiol Neurobiol 184(2):165–169. doi:10.1016/j.resp.2012.05.022

Querido JS, Kennedy PM, Sheel AW (2010) Hyperoxia attenuates muscle sympathetic nerve activity following isocapnic hypoxia in humans. J Appl Physiol (1985) 108(4):906–912. doi:10.1152/japplphysiol.01228.2009

Roy A, Guatimosim S, Prado VF, Gros R, Prado MA (2014) Cholinergic activity as a new target in diseases of the heart. Mol Med. doi:10.2119/molmed.2014.00125

Schultz HD, Marcus NJ (2012) Heart failure and carotid body chemoreception. Adv Exp Med Biol 758:387–395. doi:10.1007/978-94-007-4584-1_52

Schultz HD, Li YL, Ding Y (2007) Arterial chemoreceptors and sympathetic nerve activity: implications for hypertension and heart failure. Hypertension 50(1):6–13. doi:10.1161/HYPERTENSIONAHA.106.076083

Schultz HD, Del Rio R, Ding Y, Marcus NJ (2012) Role of neurotransmitter gases in the control of the carotid body in heart failure. Respir Physiol Neurobiol 184(2):197–203. doi:10.1016/j.resp.2012.07.010

Schultz HD, Marcus NJ, Del Rio R (2013) Role of the carotid body in the pathophysiology of heart failure. Curr Hypertens Rep 15(4):356–362. doi:10.1007/s11906-013-0368-x

Simms AE, Paton JF, Pickering AE, Allen AM (2009) Amplified respiratory-sympathetic coupling in the spontaneously hypertensive rat: does it contribute to hypertension? J Physiol 587(Pt 3):597–610. doi:10.1113/jphysiol.2008.165902

Sinski M, Lewandowski J, Przybylski J, Zalewski P, Symonides B, Abramczyk P, Gaciong Z (2014) Deactivation of carotid body chemoreceptors by hyperoxia decreases blood pressure in hypertensive patients. Hypertens Res 37(9):858–862. doi:10.1038/hr.2014.91

Stickland MK, Morgan BJ, Dempsey JA (2008) Carotid chemoreceptor modulation of sympathetic vasoconstrictor outflow during exercise in healthy humans. J Physiol 586(6):1743–1754. doi:10.1113/jphysiol.2007.147421

Sun SY, Wang W, Zucker IH, Schultz HD (1999a) Enhanced activity of carotid body chemoreceptors in

rabbits with heart failure: role of nitric oxide. J Appl Physiol (1985) 86(4):1273–1282

Sun SY, Wang W, Zucker IH, Schultz HD (1999b) Enhanced peripheral chemoreflex function in conscious rabbits with pacing-induced heart failure. J Appl Physiol (1985) 86(4):1264–1272

Toney GM, Pedrino GR, Fink GD, Osborn JW (2010) Does enhanced respiratory-sympathetic coupling contribute to peripheral neural mechanisms of angiotensin II-salt hypertension? Exp Physiol 95(5):587–594. doi:10.1113/expphysiol.2009.047399

Wang T, Lang GD, Moreno-Vinasco L, Huang Y, Goonewardena SN, Peng YJ, Svensson EC, Natarajan V, Lang RM, Linares JD, Breysse PN, Geyh AS, Samet JM, Lussier YA, Dudley S, Prabhakar NR, Garcia JG (2012) Particulate matter induces cardiac arrhythmias via dysregulation of carotid body sensitivity and cardiac sodium channels. Am J Respir Cell Mol Biol 46(4):524–531. doi:10.1165/rcmb.2011-0213OC

White HD, Norris RM, Brown MA, Brandt PW, Whitlock RM, Wild CJ (1987) Left ventricular end-systolic volume as the major determinant of survival after recovery from myocardial infarction. Circulation 76(1):44–51

Xing DT, May CN, Booth LC, Ramchandra R (2014) Tonic arterial chemoreceptor activity contributes to cardiac sympathetic activation in mild ovine heart failure. Exp Physiol 99(8):1031–1041. doi:10.1113/expphysiol.2014.079491

Yang RF, Yin JX, Li YL, Zimmerman MC, Schultz HD (2011) Angiotensin-(1-7) increases neuronal potassium current via a nitric oxide-dependent mechanism. Am J Physiol Cell Physiol 300(1):C58–C64. doi:10.1152/ajpcell.00369.2010

Yokoyama T, Nakamuta N, Kusakabe T, Yamamoto Y (2015) Sympathetic regulation of vascular tone via noradrenaline and serotonin in the rat carotid body as revealed by intracellular calcium imaging. Brain Res 1596:126–135. doi:10.1016/j.brainres.2014.11.037

Zoccal DB, Machado BH (2011) Coupling between respiratory and sympathetic activities as a novel mechanism underpinning neurogenic hypertension. Curr Hypertens Rep 13(3):229–236. doi:10.1007/s11906-011-0198-7

# A Short-Term Fasting in Neonates Induces Breathing Instability and Epigenetic Modification in the Carotid Body

20

Machiko Shirahata, Wan-Yee Tang, and Eric W. Kostuk

**Abstract**

The respiratory control system is not fully developed in newborn, and data suggest that adequate nutrition is important for the development of the respiratory control system. Infants need to be fed every 2–4 h to maintain appropriate energy levels, but a skip of feeding can occur due to social economical reasons or mild sickness of infants. Here, we asked questions if a short-term fasting (1) alters carotid body (CB) chemoreceptor activity and integrated function of the respiratory control system; (2) causes epigenetic modification within the respiratory control system. Mouse pups (<P14) were fasted for 3–6 h. Breathing became irregular and slow. The number and duration of apnea increased. Ventilatory response to hypoxia was also depressed even after the pups were returned to own dams. These effects were more prominent when the pups were younger and fasting time was longer. The hypoxic response of the carotid sinus nerve activity appeared to be depressed after fasting. Moreover, fasting increased global 5mC and 5-hmC content in DNA isolated from the CB but not DNA in the superior cervical ganglion (SCG). Methylation specific PCR (MSPCR) revealed that fasting increased methylation of leptin and socs3 genes. The results suggest fasting inhibits CB activity leading to hypoventilation, and low glucose does not compensate the low CB activity. Epigenetic effect on CB function/activity may be related to the prolonged effect of fasting on ventilation.

**Keywords**

Carotid body • Epigenetics • Fasting • Hypoxia • Mouse • Respiratory control

M. Shirahata (✉) • W.-Y. Tang • E.W. Kostuk
Department of Environmental Health Sciences, Johns Hopkins University, Baltimore, MD, USA
e-mail: mshiraha@jhmi.edu; Wtang10@jhu.edu



C. Peers et al. (eds.), *Arterial Chemoreceptors in Physiology and Pathophysiology*, Advances in Experimental Medicine and Biology 860, DOI 10.1007/978-3-319-18440-1_20

## 20.1 Introduction

The respiratory control system is not fully developed in newborn, and thus, breathing instability including apnea and periodic breathing are often observed in infants and are considered as "normal" (Edwards et al. 2013). However, severe respiratory depression or arrest may occur under certain genetic and environmental disposition. Well-known examples are mutations of PHOX2B, which cause congenital central hypoventilation syndrome (Gaultier et al. 2005). As to environmental factors, maternal nicotine exposure and inflammation reduce ventilation and increases apnea frequencies (Gauda et al. 2013). Recently, an importance of perinatal nutrition for the development of breathing control system has been highlighted (de Brito Alves et al. 2014; Penatti et al. 2011). Maternal deficiency of tryptophan (a precursor for serotonin) during perinatal period alters cardiopulmonary regulation in rat pups. This may have an important implication in the etiology of sudden infant death syndrome which has strong association with abnormal serotonergic mechanisms in the brain stem (Kinney et al. 2009) and social economic status (Spencer and Logan 2004). In addition, we have recently observed that increased apneas and periodic breathing in under-nourished mice at P14 (Fig. 20.1). In this study we focused on the relationship between breathing instability and nutritional states of infants, in particular short-term fasting. Although infants are usually fed every 2–4 h, a skip of feeding can occur due to social economical reasons or mild sickness of infants. We have hypothesized that a short-term fasting, when applied during a developmental window, inhibits CB chemoreceptor activity and integrated function of respiratory neural network. Epigenetic modification of gene expression via DNA methylation may contribute to the prolonged effect of fasting on the respiratory regulatory system.

## 20.2 Methods

Mice (DBA/2 J, A/J) were housed and bred in the animal facility of the Johns Hopkins Bloomberg School of Public Health (Baltimore, MD). Pups

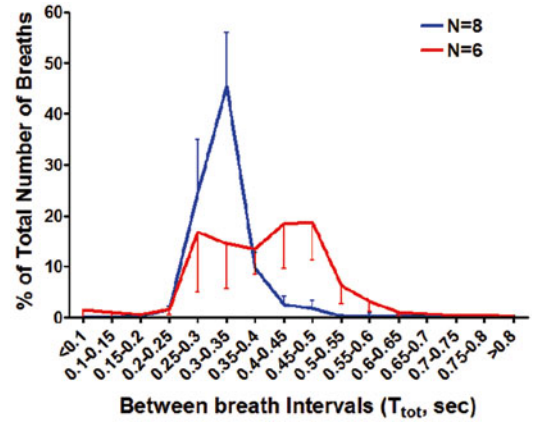


**Fig. 20.1** Regular breathing was established by P14 in well nourished mice (*blue*; body weight 8.30 ± 0.32 g) showing a narrow distribution of the between breath intervals with a sharp peak. However, irregular and slower breathing continued in under-nourished mice (*red*; body weight 4.39 ± 0.39). Data are mean ± SE. Ventilation was measured with a whole body plethysmography when the mice were considered asleep. The surface temperature of the mice was not different between the groups (~37 °C)

(P6-14) were fasted for 3–6 h, while they were housed in a warm chamber or with an experienced but non-lactating female mouse. The experimental protocols were approved by the Animal Care and Use Committee of the Johns Hopkins University.

### 20.2.1 Measurements of Ventilation and Carotid Sinus Nerve (CSN) Activity

Ventilation was measured using continuous-flow whole body plethysmography before and after fasting. A heating lamp was placed above to maintain chamber temperature (30–33 °C). When a pup was settled in the chamber and judged asleep (Balbir et al. 2008), $FIO_2$ was altered randomly (21 %, 15 %, or 100 %). Chamber pressure, oxygen tension and movements of the pup were recorded for 3 minutes at each $FIO_2$. For assessing CSN chemoreceptor activity, the CB with CSN was obtained from a deeply anesthetized mouse at ~4 weeks of age which experienced 6 h fasting at P6. The tissue was continuously superfused with Krebs solution (in mM): 120 NaCl, 4.7 KCl, 1.2, $CaCl_2$

1.8 mM, Mg $SO_4 \cdot 7H_2O$, 1.2 $Na_2HPO_4$, 22 $NaHCO_3$, and 11.1 Glucose bubbled with 95 % $O_2$/5 % $CO_2$ or 95 % $N_2$/5 % $CO_2$ (hypoxic challenge) at 35–37 °C. CSN was exposed and the activity was recorded using a suction electrode. Signals were collected and analyzed with a digital recording software (AcqKnowledge: BioPac Systems, Inc.).

### 20.2.2 Assessment of Epigenetic Changes

After 6 h fasting the CBs and SCG were harvested from anesthetized pups. Genomic DNA was isolated for DNA methylation and hydroxymethylation analysis. DNA methylation is the covalent addition of a methyl group from S-adenosyl-L-methionine (SAM) to a 5-carbon of cytosine residue in a CpG site, a formation of 5-methylcytosine (5-mC). Existence of 5-mC prevents binding of transcription activators at their recognized region, leading to decreased gene transcription. On the other hand, oxidation of 5-mC to 5-hydroxymethylcytosine (5-hmC) is suggested to play an important role in induction of gene transcription (Dao et al. 2014). Both 5-mC and 5-hmC levels in CB and SCG DNA were measured using capture and detection antibodies followed by colorimetric quantification (ELISA kit from Zymo Research, CA). We further assessed the promoter methylation of *lep*, *lepr* and *socs3* genes in the CB with quantitative methylation specific PCR. Control DNAs (fully methylated and fully unmethylated, Zymo Research, CA) were mixed in various concentrations and served as quantification standards (0, 20, 40, 60, and 100 % methylated DNA) when determining methylation degrees (%) of samples from real-time PCR.

## 20.3 Results

### 20.3.1 Breathing

As expected, untreated pups at P6 showed irregular breathing (Fig. 20.2a left), which is represented with broad distributions of between breath intervals (Fig. 20.2b). When exposed to mild hypoxia (15 % $O_2$), the irregularity was lessened with increased respiratory frequency. After 6-h fasting, breathing became slower and more irregular (Fig. 20.2a right). The number and duration of apneas increased. Ventilatory response to hypoxia was present, but depressed with persistent prolonged apneas. These effects of fasting on ventilation were milder when fasting time was shorter (Fig. 20.2c).

Pups had mild loss of body weight. Blood glucose levels were lowered. These effects were also dependent on the duration of fasting (Table 20.1). It is noteworthy to mention that breathing was slower after fasting even though blood glucose level was lower.

After the pups returned to own dams, they regained the weight within 12 h, but the depressed ventilation did not recover (Fig. 20.3).

### 20.3.2 CSN Chemoreceptor Activity

Although CSN chemoreceptor activity best represents integrated carotid body function, the size of a mouse pup hampers direct assessment of CSN activity in neonatal mice. We recorded CSN chemoreceptor activity in vitro after ~3 weeks from the fasting challenge. Compared to the control mice (no fasting) the hypoxic response of CSN activity appeared to be depressed in animals experienced with 6 h fasting at P6 ($p = 0.057$, unpaired t-test) (Fig. 20.4).

### 20.3.3 Epigenetic Modifications

We examined if the results shown above, long-lasting effects of a short-term fasting on the CB, are associated with epigenetic modifications in the CB. We first tested if fasting caused specific epigenetic changes in the CB. We found that fasting increased global 5mC and 5-hmC content in DNA isolated from the CB but not DNA in the superior cervical ganglion (SCG).

Since leptin augments the CSN chemoreceptor response to hypoxia in mice (data not shown),

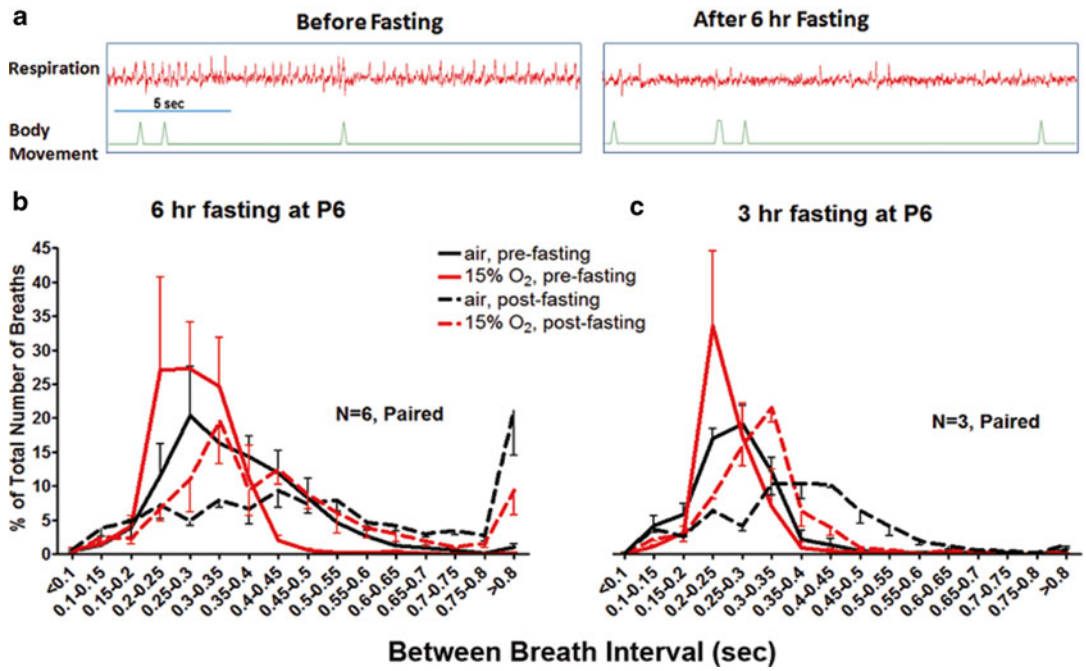


**Fig. 20.2** (**a**) Representative respiratory recordings obtained from a DBA/2 J mouse (P6) during air breathing. Body movement was used as an indicator of brain states. Upward sharp deflections depicted twitches and no coordinated movements were observed. The mouse was asleep in both recording conditions. After 6 hr fasting, prolonged apneas were seen. (**b**) Summary from 6 animals (mean ± SE) shows that fasting (6 h) caused a significant increase in apnea numbers during air breathing. Hypoxic response was depressed and apneas were still apparent. (**c**) 3-h fasting induced irregular and slower breathing, but prolonged apneas were infrequent

**Table 20.1** Effects of fasting on body weight and blood glucose

| Duration of fasting | Body weight loss (% of pre-fast) | Blood glucose (mg/dL) |
|---|---|---|
| 6 h | 2.21 ± 0.38 (N = 5) | 59.6 ± 2.9 (N = 9) |
| 3 h | 1.05 (N = 3) | 82.8 ± 2.3 (N = 10) |

we further tested if fasting alters epigenetic modification of leptin signaling genes. Methylation specific PCR (MSPCR) revealed that fasting increased methylation of *leptin* and *socs3* genes.

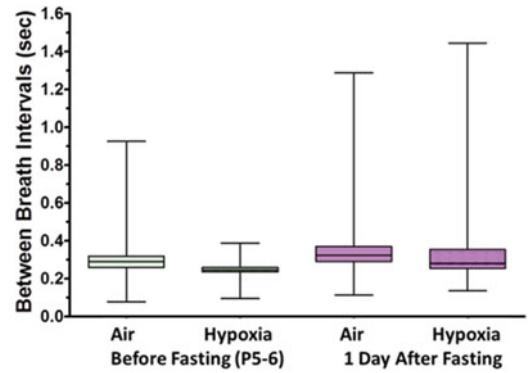


**Fig. 20.3** Breathing was recorded from 4 pups before and 1 day after fasting (6 h). Box-whisker-plots show that median values of between breath intervals are larger and distributions are wider 1 day after fasting compared to the values before fasting. The distributions are statistically different

## 20.4 Discussion

This study has demonstrated that a short-term fasting in P6 mice caused severe ventilatory depression. Depressed hypoxic response suggests that fasting impairs CB function and/or its integrated respiratory neural network. During fasting, stored energy sources such as glycogen, triglyceride and protein are converted to glucose,

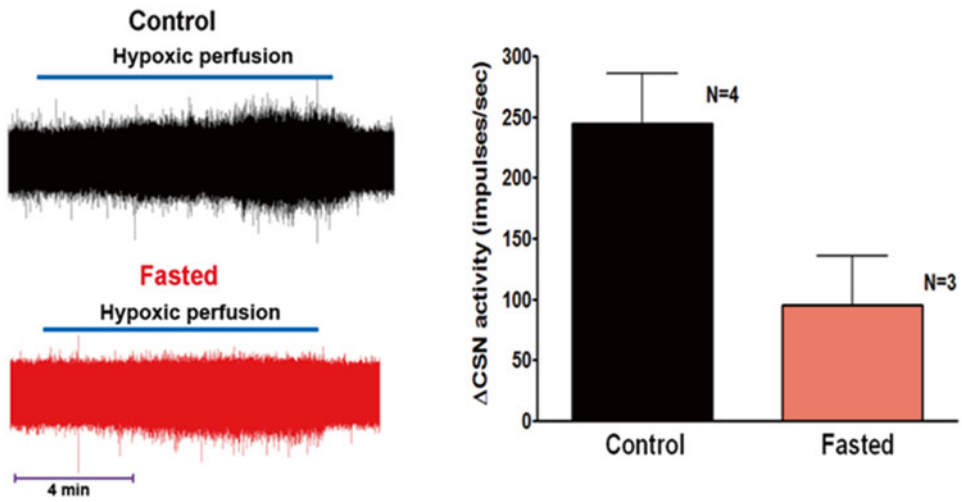


**Fig. 20.4** *Left panel:* Raw traces of CSN chemoreceptor activity in control (non-fasted) and fasted (at P6) mice. *Right Panel:* Increases in CSN activity from the baseline in response to reduced $PO_2$ in the chamber (~40 mmHg). Mean ± SE. P = 0.057

fatty acids and ketones (fasting systems). However, in infants the energy stores are not plentiful and fasting systems are not totally effective (Hoe 2008). Thus, infant easily become hypoglycemic upon fasting. In our study the glucose levels were lowered in association with the duration of fasting (Table 20.1). An intriguing question is if the lowered glucose levels affect CB function. Previous studies suggest an involvement of the CB in glucose metabolism (Alvarez-Buylla and Alvarez-Buylla 1988; Koyama et al. 2000), but the direct effect of glucose on CB, if any, could be stimulation (Pardal and López-Barneo 2002; Zhang et al. 2007), not depression as observed in the current study. Also, direct effects of glucose on the CB are still debated (Bin-Jaliah et al. 2004; Gallego-Martin et al. 2012). Further, ventilatory depression was not immediately resolved after resuming the feeding. The depression of breathing and hypoxic response continued even 1D after fasting. Thus, low glucose does not seem to be a major factor for ventilatory depression caused by 3–6 h fasting.

Although the underlying mechanisms for fasting-induced ventilatory depression were not apparent from this study, it is worth to discuss epigenetic modifications occurred in the CB 6 h after fasting. Epigenetic modifications produce an array of unique phenotypes that control cell/organ differentiation and development. Epigenetic changes are implicated in many aspects of cell biology including inheritance of genes from parents, aging, and most recently, chronic diseases. Moreover, there is emerging evidence explaining "Barker's hypothesis of fetal reprogramming" by demonstrating how epigenetic changes of genes resulting from early environmental exposures contribute to the fetal origin of the childhood/lifetime disease (Reviews in Tang and Ho 2007; Dao et al. 2014). Our data showed that increase in global 5mC and 5-hmC content in CB DNA but not SCG DNA from mice with fasting (Fig. 20.5). These preliminary observations suggested that fasting induces epigenetic changes in the CB genome via DNA methylation and/or hydroxymethylation. Further gene specific analysis showed that leptin gene and its downstream gene socs3 were epigenetically modified via promoter methylation (Fig. 20.6). Future studies may highlight that these modifications are associated with prolonged depression of CB and its network function.

Maternal or prenatal nutrition have been shown to affect ventilatory control systems and could become background etiology of sudden infant death syndrome (Penatti et al. 2011).

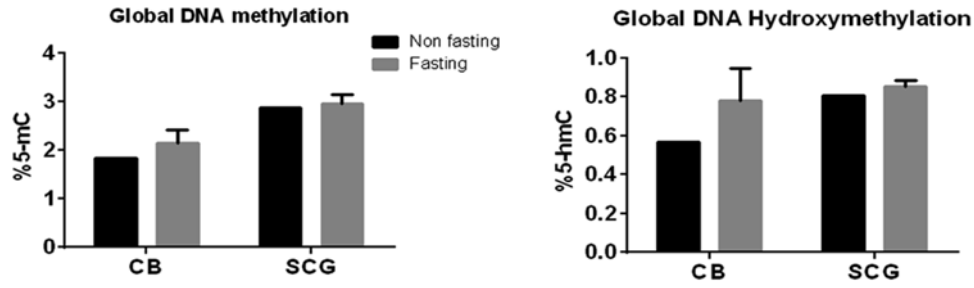


**Fig. 20.5** After 6 h of fasting at P6, the CB showed higher global methylation and hydromethylation compared to control. Mean ± SE

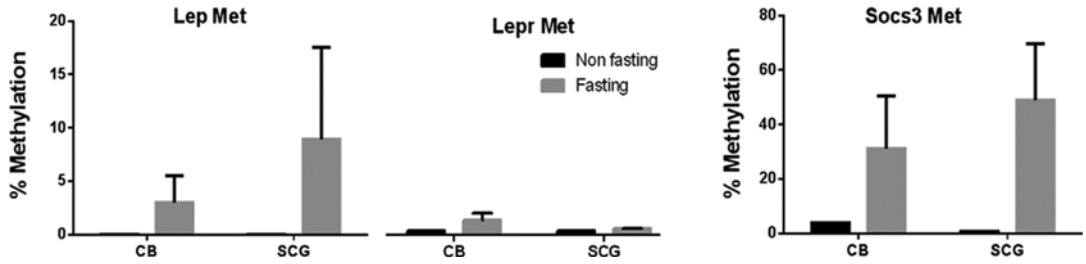


**Fig. 20.6** Methylation of leptin, leptin receptor and Socs3 genes in the CB and SCG assessed by quantitative MSPCR. Real-time PCR was done on bisulfite-treated DNA samples using primers specific for methylated DNA. Fasting animal showed increased methylation of lep and socs3. Mean ± SE

Considering that mild sickness and social economical background are risk factors for SIDS (Spencer and Logan 2004), the current study may have an important clinical implication. A skip of feeding can occur due to social economical reasons or mild sickness of infants. Our data suggest that even if fasting is short period and transient, if it occurs within a developmental window, it may cause prolonged ventilatory depression in infants.

**Acknowledgements** This work was funded, in part, by HL081345 and ES016817.

## References

Alvarez-Buylla A-B (1988) Carotid sinus receptors participate in glucose homeostasis. Respir Physiol 72:347–360

Balbir A, Lande B, Fitzgerald RS, Polotsky V, Mitzner W, Shirahata M (2008) Behavioral and respiratory characteristics during sleep in neonatal DBA/2J and A/J mice. Brain Res 1241:84–91

Bin-Jaliah I, Maskell PD, Kumar P (2004) Indirect sensing of insulin-induced hypoglycaemia by the carotid body in the rat. J Physiol 556:255–266

Dao T, Cheng RY, Revelo MP, Mitzner W, Tang W (2014) Hydroxymethylation as a novel environmental biosensor. Curr Environ Health Rep 1:1–10

de Brito Alves JL, Nogueira VO, de Oliveira GB, da Silva GS, Wanderley AG, Leandro CG, Costa-Silva JH (2014) Short- and long-term effects of a maternal low-protein diet on ventilation, $O_2$/$CO_2$ chemoreception and arterial blood pressure in male rat offspring. Br J Nutr 111:606–615

Edwards BA, Sands SA, Berger PJ (2013) Postnatal maturation of breathing stability and loop gain: the role of carotid chemoreceptor development. Respir Physiol Neurobiol 185:144–155

Gallego-Martin T, Fernandez-Martinez S, Rigual R, Obeso A, Gonzalez C (2012) Effects of low glucose on carotid body chemoreceptor cell activity studied in cultures of intact organs and in dissociated cells. Am J Physiol Cell Physiol 302:C1128–C1140

Gauda EB, Shirahata M, Mason A, Pichard LE, Kostuk EW, Chavez-Valdez R (2013) Inflammation in the carotid body during development and its contribution to apnea of prematurity. Respir Physiol Neurobiol 185:120–131

Gaultier C, Trang H, Dauger S, Gallego J (2005) Pediatric disorders with autonomic dysfunction: what role for PHOX2B? Pediatr Res 58:1–6

Hoe FM (2008) Hypoglycemia in infants and children. Adv Pediatr 55:367–384

Kinney HC, Richerson GB, Dymecki SM, Darnall RA, Nattie EE (2009) The brainstem and serotonin in the sudden infant death syndrome. Annu Rev Pathol 4:517–550

Koyama Y, Coker RH, Stone EE, Lacy DB, Jabbour K, Williams PE, Wasserman DH (2000) Evidence that carotid bodies play an important role in glucoregulation in vivo. Diabetes 49:1434–1442

Pardal R, López-Barneo J (2002) Low glucose-sensing cells in the carotid body. Nat Neurosci 5:197–198

Penatti EM, Barina AE, Raju S, Li A, Kinney HC, Commons KG, Nattie EE (2011) Maternal dietary tryptophan deficiency alters cardiorespiratory control in rat pups. J Appl Physiol 110:318–328

Spencer N, Logan S (2004) Sudden unexpected death in infancy and socioeconomic status: a systematic review. J Epidemiol Community Health 58:366–373

Tang W-Y, Ho S-M (2007) Epigenetic reprogramming and imprinting in origins of disease. Rev Endocr Metab Disord 8:173–182

Zhang M, Buttigieg J, Nurse CA (2007) Neurotransmitter mechanisms mediating low-glucose signalling in cocultures and fresh tissue slices of rat carotid body. J Physiol 578:735–750

# Carotid Body Chemoreflex Mediates Intermittent Hypoxia-Induced Oxidative Stress in the Adrenal Medulla

21

Ganesh K. Kumar, Ying-Jie Peng, Jayasri Nanduri, and Nanduri R. Prabhakar

**Abstract**

Intermittent hypoxia (IH) increases reactive oxygen species generation resulting in oxidative stress in the adrenal medulla (AM), a major end-organ of the sympathetic nervous system which facilitates catecholamine secretion by hypoxia. Here, we show that carotid body chemoreflex contributes to IH-induced oxidative stress in the AM. Carotid bodies were ablated by cryo-coagulation of glomus cells, the putative $O_2$ sensing cells. Carotid body ablated (CBA) and control rats were exposed to IH and the redox state of the AM was assessed biochemically. We found that IH raised reactive oxygen species levels along with an increase in NADPH oxidase (Nox), a pro-oxidant enzyme and a decrease in superoxide dismutase-2 (SOD2), an anti-oxidant enzyme. Further, IH increased hypoxia-inducible factor (HIF)-1α, whereas decreased HIF-2α, the transcriptional regulator of Nox and SOD-2, respectively. These IH-induced changes in the AM were absent in CBA rats. Moreover, IH increased splanchnic nerve activity and facilitated hypoxia-evoked catecholamine efflux from the AM and CBA prevented these effects. These findings suggest that IH-induced oxidative stress and catecholamine efflux in the AM occurs via carotid body chemoreflex involving HIF α isoform mediated imbalance in pro-, and anti-oxidant enzymes.

G.K. Kumar (✉) • Y.-J. Peng
Institute for Integrative Physiology & Center for Systems Biology for O2 Sensing, The University of Chicago, Chicago, IL 60637, USA
e-mail: gkumar@bsd.uchicago.edu

J. Nanduri
Biological Science Division, Institute for Integrative Physiology, 5841 S. Maryland Avenue, MC 5068, Room N-711, University of Chicago, Chicago, IL 60637, USA
e-mail: jnanduri@uchicago.edu

N.R. Prabhakar
Biological Science Division, Institute for Integrative Physiology and Center for Systems Biology of O(2) Sensing, University of Chicago, Chicago, IL USA
e-mail: nanduri@uchicago.edu



C. Peers et al. (eds.), *Arterial Chemoreceptors in Physiology and Pathophysiology*, Advances in Experimental Medicine and Biology 860, DOI 10.1007/978-3-319-18440-1_21

**Keywords**
Reactive oxygen species • Sleep disordered breathing • Hypoxia-inducible factors • Carotid body ablation • Pro-oxidant and anti-oxidant

## 21.1 Introduction

Sleep disordered breathing (SDB), a highly prevalent health problem in adult men and infants born prematurely, is associated with intermittent hypoxia (IH). Humans with SDB are prone to develop cardiovascular abnormalities including hypertension. Studies in rodents exposed to IH showed that reactive oxygen species (ROS) generation is increased in peripheral and central nervous tissues and pretreatment with anti-oxidant prevented not only the elevation in ROS but also the cardiovascular abnormalities evoked by IH (*for references see* Prabhakar et al. 2007). Since ROS emerges as a critical mediator of IH-induced patho-physiology, it is of considerable importance to determine whether ROS generation is due to a direct effect of IH on various tissues or is mediated by an indirect mechanism. The $pO_2$ of most tissues under basal, normoxic condition is in the range of 30–60 mmHg (Carreau et al. 2011) which is much lower than the arterial $pO_2$ of ~100 mmHg. In each cycle of IH, the arterial $O_2$ saturation of rats decreases from 97 to 80 % (Peng et al. 2014). Consequently, most tissues may not be able to sense this modest level of hypoxia during IH. On the other hand, carotid bodies, due to their very high blood flow and exquisite sensitivity to hypoxia, are capable of sensing and responding to modest changes in $pO_2$ during each cycle of IH and the resulting augmented chemoreflex may, in turn, transmit the changes in $pO_2$ to other tissues. These considerations led us to *hypothesize* that activation of carotid body chemoreflex contributes to IH-induced ROS generation in various tissues. In a recent study, we tested this hypothesis by examining ROS generation in the adrenal medulla (AM), an end-organ of the sympathetic nervous system activated by the carotid body chemoreflex (Peng et al. 2014).

## 21.2 Methods

### 21.2.1 Animals

Experimental protocols were approved by the Institutional Animal Care and Use Committee of the University of Chicago. Experiments were performed on adult, male Sprague-Dawley rats. At the termination of the experiment, rats were killed with an overdose of anesthesia. Carotid body ablation (CBA) was performed bilaterally using cryocoagulation with liquid nitrogen as described previously (Verna et al. 1975). Sham-operated rats served as controls.

### 21.2.2 Exposure to IH

Control (sham-operated) and CBA rats were allowed to recover from surgery for 1 week. Rats were exposed to alternating cycles of hypoxia (5 % $O_2$ for 15 s) and normoxia (21 % $O_2$ for 5 min) between 09.00 and 17.00 h for 10 days. Rats exposed to alternating cycles of normoxia served as controls.

### 21.2.3 Measurements of ROS, NADPH Oxidase (Nox) and Superoxide Dismutase (SOD)

The cytosolic and mitochondrial aconitase activities were measured as an index of ROS generation as described (Peng et al. 2014). Enzyme activities of Nox and SOD were determined in the membrane and mitochondrial fractions as described (Peng et al. 2014).

### 21.2.4 Western Blot Analysis of Hypoxia-Inducible Factor (HIF) α Isoforms

The expression of HIF-1α and HIF-2α proteins was analyzed by immunoblot analysis as described (Peng et al. 2014).

### 21.2.5 Splanchnic Nerve Activity

The branch of the left splanchnic nerve was isolated and cut above the coeliac ganglion. The central cut ends of the nerves were placed on bipolar platinum-iridium electrode for recording electrical activity as described (Peng et al. 2014).

### 21.2.6 Data Analysis

All data are presented as means ± SEM. Statistical significance was assessed by one-way ANOVA followed by unpaired t-test. *P* value less than 0.05 was considered significant.

## 21.3 Results and Discussion

### 21.3.1 Effect of CBA on ROS Generation by IH

The activity of aconitase, an enzyme in the tricarboxylic acid cycle, is sensitive to and inhibited by ROS (Gardner 2002). The enzyme occurs both in the cytosol and in the mitochondria and measuring the inhibition of aconitase activity in both fractions will provide a measure of ROS generation. As shown in Table 21.1, IH decreased aconitase activity by 60 % and 50 % in the cytosolic and mitochondrial fractions of the AM, respectively. IH-induced decrease in aconitase activity was absent in CBA treated rats suggesting that oxidative stress in the AM of IH treated rats is mediated by the carotid body chemoreflex.

**Table 21.1** Effect of Carotid Body Ablation (CBA) on IH-induced oxidative stress in the rat adrenal medulla

| Samples[a] | Aconitase ($nmol.min^{-1}.mg^{-1}$) | |
|---|---|---|
| | Cytosol | Mitochondria |
| Control | 6.6 ± 0.4 | 4.1 ± 0.5 |
| IH-treated | 2.6 ± 0.3 | 2.1 ± 0.2 |
| CBA + IH-treated | 5.5 ± 0.7 | 3.5 ± 0.4 |

[a]n = 6–7 rats per group

### 21.3.2 Effect of CBA on IH-Induced Changes in Nox and SOD

The cellular level of ROS is tightly regulated by the balance between the activities of the pro-, and anti-oxidant enzymes. NADPH oxidase (Nox) and superoxide dismutase-2 (SOD-2) are the major pro-, and anti-oxidant enzymes, respectively. Therefore, we determined whether carotid body chemoreflex contributes to IH-induced changes in the mRNA levels and enzyme activities of Nox and SOD-2. IH increased mRNA levels of Nox2 by ~2.5-fold with a concomitant increase in Nox activity in the AM (Table 21.2). On the other hand, mRNA levels of SOD-2 decreased by ~50 % and SOD activity was significantly lower in IH-treated AM than in controls (~50 %; $p < 0.01$; Table 21.2). IH-induced changes in Nox and SOD in the AM were absent in CBA rats.

### 21.3.3 Effect of CBA on IH-Induced Changes in HIF-α Isoform Expression

HIF-1α is known to regulate gene expression of pro-oxidant enzymes including Nox whereas that of anti-oxidant enzymes such as SOD is under

**Table 21.2** Effect of Carotid Body Ablation (CBA) on IH-induced alteration in Nox and SOD-2 activities

| Samples[a] | Nox activity ($nmol.min^{-1}.mg^{-1}$) | SOD-2 activity (% of Control) |
|---|---|---|
| Control | 0.42 ± 0.02 | 100 |
| IH-treated | 1.13 ± 0.04 | 50 ± 2 |
| CBA + IH-treated | 0.46 ± 0.02 | 98 ± 4 |

[a]n = 6–7 rats per group

**Table 21.3** Effect of Carotid Body Ablation (CBA) on IH-induced alteration in HIF-α Isoform expression

| Samples[a] | HIF-1α protein (% of control) | HIF-2α protein (% of control) |
|---|---|---|
| Control | 100 | 100 |
| IH-treated | 320 ± 5 | 52 ± 4 |
| CBA + IH-treated | 98 ± 2 | 97 ± 3 |

[a]n = 6–7 rats per group

**Table 21.4** Effect of CBA on IH-induced augmented catecholamine efflux by hypoxia in the AM

| Samples[a] | Norepinephrine (ng/100 ml) | Epinephrine (ng/100 ml) |
|---|---|---|
| Control | 20 ± 4 | 88 ± 6 |
| IH-treated | 75 ± 3 | 190 ± 7 |
| CBA + IH-treated | 22 ± 2 | 105 ± 2 |

[a]n = 6–7 rats per group

the control of HIF-2α. Therefore, we determined whether carotid body chemoreflex via altering HIF-α isoform expression in the adrenal medulla contributes to IH-induced changes in Nox2 and SOD-2 mRNA levels. In IH-treated AM, HIF-1α protein expression is significantly higher whereas that of HIF-2α is lower than normoxia-treated control AM (Table 21.3). However, in CBA rats, IH-induced changes in HIF-*α* isoform expression were absent.

### 21.3.4 Effect of CBA on IH-Induced Changes in Adrenal Sympathetic Nerve Activity

A branch of the splanchnic nerve provides the sympathetic input to the AM. We tested whether carotid body chemoreflex mediates the increased sympathetic flow to the AM in IH treated rats. Sham-operated and IH exposed rats exhibit elevated adrenal sympathetic nerve activity both during normoxia and hypoxia and these IH-induced effects were absent in CBA rats.

### 21.3.5 Effect of CBA on IH-Induced Functional Changes in the Adrenal Medulla

Previous studies have shown that IH facilitated hypoxia-evoked catecholamine (CA) efflux from the adrenal medulla in a ROS-dependent manner (Kumar et al. 2006; Kuri et al. 2007). Since CBA prevented IH-induced generation of ROS, we tested whether carotid body chemoreflex mediates IH-induced augmented CA efflux in the AM. Consistent with our previous reports, hypoxia markedly enhanced both norepinephrine and epinephrine efflux from AM slices in IH exposed, sham-operated rats and IH-induced augmented CA efflux by hypoxia was absent in CBA rats (Table 21.4).

Our results demonstrated that IH-induced increase in ROS in the AM, an end-organ of the sympathetic nervous system is primarily mediated by the chemoreflex arising from the carotid body but not due to a direct effect of hypoxia. At first, IH activates the carotid body and the ensuing chemoreflex induces an imbalance between HIF-1α and HIF-2α that transcriptionally regulate Nox, a pro-oxidant and SOD, an anti-oxidant leading to increased generation of ROS. The carotid body chemoreflex-mediated oxidative stress in the AM facilitates enhanced CA efflux which may contribute to hypertension associated with apneas.

**Acknowledgement** This research was supported by grant P01-HL-90554 from the National Institute of Health, Heart, Lung and Blood Institute.

## References

Carreau A, El Hafny-Rahbi B, Matejuk A et al (2011) Why is the partial oxygen pressure of human tissues a crucial parameter? Small molecules and hypoxia. J Cell Mol Med 15:1239–1253

Gardner PR (2002) Aconitase sensitive target and measure of superoxide. Methods Enzymol 349:9–23

Kumar GK, Rai V, Sharma SD et al (2006) Chronic intermittent hypoxia induces hypoxia-evoked catecholamine efflux in adult rat adrenal medulla via oxidative stress. J Physiol 575:229–239

Kuri BA, Khan SA, Chan SA et al (2007) Increased secretory capacity of mouse adrenal chromaffin cells by

chronic intermittent hypoxia: involvement of protein kinase C. J Physiol 584:313–319

Peng YJ, Yuan G, Khan S et al (2014) Regulation of hypoxia-inducible factor-α isoforms and redox state by carotid body neural activity in rats. J Physiol 592:3841–3858

Prabhakar NR, Kumar GK, Nanduri J et al (2007) ROS signaling in systemic and cellular responses to chronic intermittent hypoxia. Antioxid Redox Signal 9:1397–1403

Verna A, Roumy M, Leitner LM (1975) Loss of chemoreceptive properties of the rabbit carotid body after destruction of the glomus cells. Brain Res 100:13–23

# 22 The Association Between Antihypertensive Medication and Blood Pressure Control in Patients with Obstructive Sleep Apnea

Lucília N. Diogo, Paula Pinto, Cristina Bárbara, Ana L. Papoila, and Emília C. Monteiro

**Abstract**

Obstructive sleep apnea and hypertension are closely related diseases. The lowering effect of continuous positive airway pressure (CPAP) on blood pressure (BP) control is modest and concomitant antihypertensive therapy is still required. However, the best antihypertensive regimen for BP control in patients with OSA remains unknown. We aimed to investigate a hypothetical association between ongoing antihypertensive medication and BP control rates in patients with OSA. We conducted a prospective observational study in a cohort of 205 patients with OSA and hypertension who underwent a sleep study and 24-h ambulatory blood pressure monitoring (ABPM). Ongoing antihypertensive medication profile was recorded. Logistic regression models were used to investigate the association between antihypertensive regimen and BP control, before (n = 205) and, when applicable, after CPAP adaptation (n = 90). One hundred and fifty-five patients (155/205) were being treated with 31 different antihypertensive regimens. At baseline, the antihypertensive regimens and the number of antihypertensive drugs were not associated with BP control (p = 0.847; p = 0.991). After CPAP adaptation, a decrease in

L.N. Diogo, Pharm.D., M.Sc. (✉) • E.C. Monteiro
Centro de Estudos de Doenças Crónicas, CEDOC,
NOVA Medical School/Faculdade de Ciências
Médicas, Universidade Nova de Lisboa,
Campo dos Mártires da Pátria, 130,
1169-056 Lisbon, Portugal
e-mail: lucilia.diogo@fcm.unl.pt

P. Pinto • C. Bárbara
Serviço de Pneumologia II, Centro Hospitalar Lisboa
Norte (CHLN)-Hospital Pulido Valente,
1600-190 Lisbon, Portugal

A.L. Papoila
Centro de Estudos de Doenças Crónicas, CEDOC,
NOVA Medical School/Faculdade de Ciências
Médicas, Universidade Nova de Lisboa,
Campo dos Mártires da Pátria, 130,
1169-056 Lisbon, Portugal

CEAUL, 1749-016 Lisbon, Portugal



C. Peers et al. (eds.), *Arterial Chemoreceptors in Physiology and Pathophysiology*,
Advances in Experimental Medicine and Biology 860, DOI 10.1007/978-3-319-18440-1_22

median night-time systolic and diastolic BP was observed (p=0.001; p=0.006). Nevertheless, the lack of association between antihypertensive regimens and the number of antihypertensive drugs and BP control remained (p=0.864; p=0.800). Our findings confirm that although CPAP improves nocturnal BP, this improvement is not sufficient to control blood pressure for 24 h. This study shows, for the first time, that in patients with OSA, there is no association between BP control and both the antihypertensive regimen and the number of antihypertensive drugs.

**Keywords**

Ambulatory blood pressure monitoring • Antihypertensive drugs • Blood pressure • Continuous positive airway pressure • Hypertension and obstructive sleep apnea

## 22.1 Introduction

Obstructive sleep apnea is a highly prevalent sleep-related breathing disorder, briefly characterized by repetitive episodes of airflow cessation (apnea) or airflow reduction (hypopnea) in the upper airways during sleep. The link between OSA and hypertension is well established (Baguet et al. 2009). Sympathetic nervous system stimulation mediated mainly by activation of carotid body chemoreflexes and/or asphyxia is a relevant underlying mechanism of hypertension-related OSA. However, the best therapeutic targets for the control of BP in these patients have not been established. Continuous Positive Airway Pressure (CPAP) is considered the gold standard for the treatment of symptomatic OSA patients. However, the effectiveness of CPAP on blood pressure (BP) control is still controversial and CPAP alone seems to be insufficient to sustain BP control; therefore, the use of antihypertensive drugs (AHD) is unavoidable. Data on antihypertensive drug regimens in patients with OSA are scarce; the effects of antihypertensive agents on OSA patients are not consistent, and there are limited data on whether a specific AHD regimen has any positive effect on the control of BP in OSA patients (Diogo and Monteiro 2014). The main goal of this prospective cohort study was to determine the association between ongoing antihypertensive (AH) regimens and BP control patients with OSA, before and after CPAP adaptation.

## 22.2 Methods

Patients clinically suspected of having OSA, aged above 18 years, who were attending their first visit at the Centro Hospitalar Lisboa Norte (CHLN), EPE Sleep Unit were assessed for eligibility (Fig. 22.1).

All patients were fully informed about the study and gave written consent in accordance with the Declaration of Helsinki. The study protocol was previously approved by CHLN, EPE's Ethics Committee.

Diagnosis of OSA was established by overnight polysomnography. OSA was categorised according to current AHI (apnea-hypopnea index) cut-offs of <5 (non-diagnostic), 5≥ and <15 (mild), 15≥ and <30 (moderate) and ≥30 (severe). All patients underwent 24-h ambulatory blood pressure monitoring (ABPM). A dipping profile was defined as a reduction in the average systolic and diastolic BP at night that was higher than 10 % compared to daytime values. Uncontrolled BP was defined according to ESC and ESH guidelines (Mancia et al. 2013). Patients also completed a data collection form that included ongoing medication profile registration ("Brown-bag" medication review). Figure 22.2 summarizes the study protocol.

The main outcome variables were BP control rates (controlled and uncontrolled) in patients undergoing antihypertensive medication. We analysed the use of AHD by regimen:

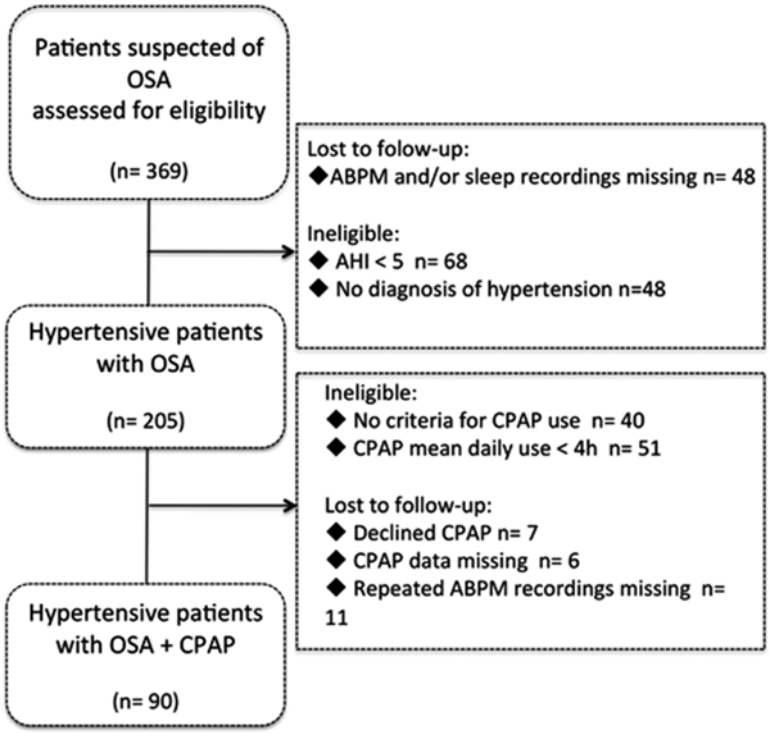


**Fig. 22.1** Patient eligibility and follow-up. Of the 369 patients consecutively included, 68 were patients with no diagnosis of OSA and 48 with no diagnosis of hypertension. The ABPM and/or sleep recordings were missing for 48 patients due to technical problems or because they did not attend the ABPM (n = 41) or sleep study (n = 7). Forty had no indication for CPAP therapy. One hundred and sixty-five were scheduled for CPAP adaptation; however, 7 refused CPAP, CPAP data were missing in 6 patients and 51 had no compliance. Of the 369, only the data from 90 patients were used to investigate the association between ongoing AH regimen and blood pressure control rates after CPAP adaptation. **AHI** indicates: Apnea-Hypopnea Index; **ABPM:** Ambulatory Blood Pressure Monitoring; **CPAP:** Continuous Positive Airway Pressure; **OSA**: obstructive sleep apnea

1-with angiotensin-converting enzyme inhibitors (ACEi); 2-with angiotensin II receptor blockers (ARAs); 3-with β-blockers; and 4-others (including diuretics and calcium channel blockers), and the number of antihypertensive drugs (1-one, monotherapy; 2-two or more, polytherapy) included in each patient regimen. In all patients, antihypertensive drugs were taken for at least 6 months without changing the medication profile until the end of the follow-up. CPAP titration was performed using self-adjusting CPAP devices (autoCPAP) and CPAP adherence was assessed from the device counter. Logistic regression models were used to investigate the association between antihypertensive regimen and frequency of controlled and uncontrolled BP before and after CPAP adaptation in patients with OSA. Statistical analysis was performed using the IBM SPSS Statistics (IBM SPSS Statistics for Windows, Version 21.0. Armonk, NY). Results were considered significant when $\alpha = 0.05$.

## 22.3 Results

Median apnea-hypopnea index was 20.0/h ($P_{25} = 10.2$/h, $P_{75} = 32.6$/h) and concerning OSA severity, 39.0 % (80/205), 30.2 % (62/205) and 30.7 % (63/205) of the patients presented mild, moderate and severe OSA, respectively. Table 22.1 shows key patient characteristics summarized according to BP control. ABPM data, attained at baseline, are described in Table 22.2.

Of the 205 hypertensive OSA patients, 155 were being treated with antihypertensive medication. The antihypertensive medication profile

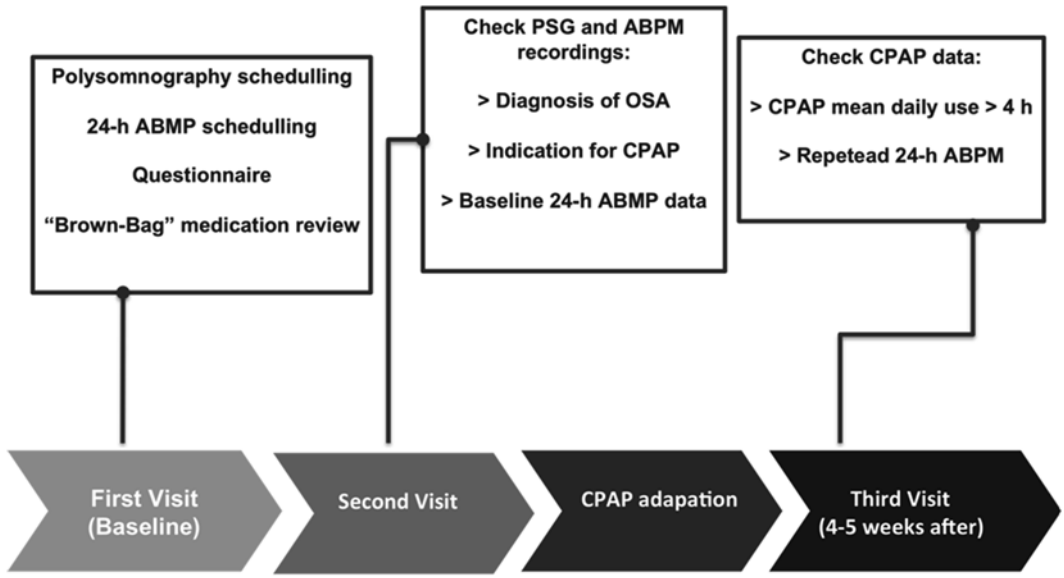


**Fig. 22.2** Schematic representation of study protocol. At baseline, patients underwent overnight polysomnography, 24-h ABPM and completed a questionnaire that included ongoing antihypertensive medication profile registration. Patients with OSA diagnosis and indication for CPAP treatment were scheduled for CPAP adaptation. 4–5 weeks after CPAP adaptation, the device data were checked and patients with at least 4 hour-mean daily CPAP use and data for baseline ABPM underwent repeated 24-h ABPM (n = 90). **ABPM** indicates: Ambulatory Blood Pressure Monitoring**; CPAP:** Continuous Positive Airway Pressure; **OSA:** Obstructive Sleep Apnea

**Table 22.1** Hypertensive OSA patient characteristics at baseline

| Variable | All patients (n = 205) | Controlled (n = 60) | Uncontrolled (n = 145) | *p* |
|---|---|---|---|---|
| Age, years | 59.0 (11.6) | 62.2 (10.4) | 57.7 (11.8) | 0.012$^{\Psi}$ |
| Gender, male (%) | 149 (72.7) | 40.0 (66.7) | 109 (75.2) | 0.214$^{\&}$ |
| Race, Caucasian (%) | 196 (95.6) | 60 (100.0) | 136 (93.8) | 0.061$^{*}$ |
| BMI, kg/m$^2$ | 31.0 (5.0) | 31.5 (6.2) | 30.8 (4.5) | 0.420$^{\#}$ |
| Neck circumference, cm | 42.2 (3.8) | 42.1 (4.1) | 42.2 (3.8) | 0.822$^{\Psi}$ |
| Waist circumference, cm | 109.6 (12.1) | 110.1 (13.5) | 109.4 (11.5) | 0.727$^{\Psi}$ |
| **Smoking habits** | | | | 0.305$^{\&}$ |
| Non-smokers (%) | 111 (54.1) | 31 (51.7) | 80 (55.2) | |
| Former smokers (%) | 76 (37.1) | 26 (43.3) | 50 (34.5) | |
| Current smokers (%) | 18 (8.8) | 3 (5.0) | 15 (10.3) | |
| Number of comorbidities >2 (%)$^{\Phi}$ | 114 (55.6) | 39 (65.0) | 75 (51.7) | 0.082$^{\&}$ |
| Self-reported hypertension (%) | 159 (77.6) | 59 (98.3) | 100 (69.0) | <0.001$^{\&}$ |

Data are presented as mean (SD: standard deviation), median (interquartile range: $P_{25}$, $P_{75}$) or number (%)
*OSA* obstructive sleep apnea, *BMI* body mass index, *AH* antihypertensive drugs, *AHI* apnea-hypopnea index
$^{\Phi}$including self-reported hypertension, $^{\Psi}$Student's t-test, $^{\#}$Welch's t test, $^{\&}$Chi-squared test, $^{*}$Fisher's exact test

found in controlled and uncontrolled groups, respectively, was: 19 (31.7 %) and 30 (20.7 %) patients treated with monotherapy and 41 (68.3 %) and 65 (44.8 %) patients treated with regimens that included two or more antihypertensive drugs. Thirty-one different antihypertensive regimens were found for hypertensive OSA patients. The most prevalent are shown in Table 22.3.

We performed a univariate analysis to investigate the association between AH regimen and better BP control. No association was found

**Table 22.2** ABPM data at baseline

| Variable | All patients (n = 205) | Controlled (n = 60) | Uncontrolled (n = 145) | *p* |
|---|---|---|---|---|
| **24-h ABPM** (mmHg): | | | | |
| Mean 24-h BP | 94.0 (86.0, 98.0) | 83.0 (80.0, 85.8) | 96.0 (93.0, 101.0) | <0.001[Ψ] |
| Daytime systolic BP | 129.0 (121.0, 139.0) | 119.5 (111.3, 124.0) | 135.0 (127.5, 144.0) | <0.001[Ψ] |
| Daytime diastolic BP | 79.0 (72.0, 85.0) | 71.5 (67.0, 75.0) | 83.0 (78.0, 88.0) | <0.001[Ψ] |
| Night-time systolic BP | 118.0 (107.5, 128.0) | 105.5 (97.3, 109.0) | 124.0 (115.5, 131.5) | <0.001[Ψ] |
| Night-time diastolic BP | 69.0 (62.0, 75.0) | 61.0 (57.0, 64.0) | 72.0 (67.0, 77.0) | <0.001[Ψ] |
| **24 h-BP profile:** | | | | |
| Non-dipper systolic (%) | 108 (52.7) | 21 (35.0) | 87 (60.0) | 0.001[&] |
| Non-dipper diastolic (%) | 79 (38.5) | 12 (20.0) | 67 (46.2) | <0.001[&] |

Data are presented as median (interquartile range: $P_{25}$, $P_{75}$) or number (%)
*OSA* obstructive sleep apnea, *ABPM* ambulatory blood pressure monitoring, *BP* blood pressure, *HT* hypertension
[Ψ]Mann-Whitney test, [&]Chi-squared test

**Table 22.3** Antihypertensive regimens in patients with OSA

| Antihypertensive regimen | Hypertensive OSA patients n = 155 |
|---|---|
| Combination of ARBs + diuretics | 28 (18.1) |
| Monotherapy with ACEi | 21 (13.5) |
| Monotherapy with ARBs | 14 (9.0) |
| Combination of ACEi + diuretics | 10 (6.5) |
| Combination of CCB + diuretics + ARBs | 8 (5.2) |
| Combination of ARBs + CCB | 8 (5.2) |
| Monotherapy with CCB | 7 (4.5) |

Data are presented as number (%)
*OSA* obstructive sleep apnea, *AH* antihypertensive drugs, *ACEi* angiotensin-converting enzyme inhibitors, *ARBs* angiotensin II receptor blockers, *CCB* calcium channel blockers

between the number of antihypertensive drugs and the antihypertensive regimens and BP control (p = 0.991 and p = 0.847, respectively) (Table 22.4).

In addition to AH regimens, and number of AHD age (p = 0.012), gender (p = 0.214), BMI (p = 0.420), neck circumference (p = 0.822), waist circumference (p = 0.727), smoking habits (p = 0.305), number of comorbidities (p = 0.082) and OSA severity (p = 0.325) were variables included in the analysis. Age and the number of comorbidities were selected for the multivariable analysis. However, none of these variables remained in the multivariable model.

Ninety patients were eligible to investigate the association between ongoing AH regimen and hypertension control rates after CPAP adaptation (Fig. 22.1). Regarding ABPM data measured at baseline and after CPAP adaptation (Table 22.5), no significant differences were found between daytime systolic and diastolic BP.

As expected, a decrease in median night-time systolic (median = 4.5 mmHg) and diastolic BP (median = 3.5 mmHg) was observed (p = 0.001 and p = 0.006) after CPAP adaptation. Nevertheless, this decrease in night-time BP was not enough to allow reclassification from uncontrolled to controlled BP in a substantial number of patients being treated with AHD (p = 0.332). In fact, of the 46/74 (62.2 %) uncontrolled patients at baseline, only 11/74 (14.9 %) became controlled after CPAP adaptation.

After CPAP, the lack of association between antihypertensive regimens and the number of antihypertensive drugs and BP control remained (p = 0.864 and p = 0.800) (Table 22.4).

## 22.4 Discussion

To the best of our knowledge, this is the first study that has described the association between antihypertensive regimen and BP control rates in patients with OSA.

In general, our sample matches a typical population of OSA patients. Actually, the high prevalence of new diagnoses of OSA, indicating that patients are being referred appropriately as well as the distribution of OSA severity found in

**Table 22.4** Association between anti-hypertensive regimens/ number of anti-hypertensive drugs and BP Control at baseline and after CPAP adaptation

| | Before CPAP | | | After CPAP | | |
|---|---|---|---|---|---|---|
| Variable | Controlled (n=60) | Uncontrolled (n=95) | p | Controlled (n=33) | Uncontrolled (n=41) | p |
| **Number of AH** | | | 0.991[&] | | | 0.800[&] |
| One | 19/49 (38.8) | 30/49 (61.2) | | 9/22 (40.9) | 13/22 (59.1) | |
| Two or more | 41/106 (38.7) | 65/106 (61.3) | | 24/52 (46.2) | 28/52 (53.8) | |
| **AH regimens** | | | 0.847[&] | | | 0.864[*] |
| With ACEi | 16/39 (41.0) | 23/39 (59.0) | | 8/21 (38.1) | 13/21 (61.9) | |
| With ARBs | 24/58 (41.4) | 34/58 (58.6) | | 11/25 (44.0) | 14/25 (56.0) | |
| With BB | 5/13 (38.5) | 8/13 (61.5) | | 1/2 (50.0) | 1/2 (50.0) | |
| Others | 15/45 (33.3) | 30/45 (66.7) | | 13/26 (50.0) | 13/26 (50.0) | |

Data are presented as number (%)
*CPAP* continuous positive airway pressure, *AH* antihypertensive drugs, *ACEi* angiotensin-converting enzyme inhibitors, *ARBs* angiotensin II receptor blockers, *BB* beta-blockers
[&]Chi-squared test, [*]Fisher's exact test

**Table 22.5** ABPM data at baseline and after CPAP adaptation of patients with OSA, hypertension and CPAP mean daily use ≥4 h (n=90)

| Variable | Baseline | After CPAP adaptation | *p* [Ψ] |
|---|---|---|---|
| Daytime systolic BP | 128.5 (121.5, 138.0) | 127.5 (119.0, 135.0) | 0.156[#] |
| Daytime diastolic BP | 79.0 (70.8, 84.0) | 76.5 (71.0, 83.0) | 0.132[Ψ] |
| Night-time systolic BP | 118.5 (107.0, 129.0) | 114.0 (106.8, 123.5) | 0.001[#] |
| Night-time diastolic BP | 69.0 (61.0, 74.0) | 65.5 (60.0, 72.0) | 0.006[Ψ] |

Data are presented as median (interquartile range: $P_{25}$, $P_{75}$)
*CPAP* continuous positive airway pressure, *ABPM* ambulatory blood pressure monitoring, *BP* blood pressure
[Ψ]Wilcoxon test, [#]Sign Test

CHLN sleep consultation, is similar to those reported by other authors (Lavie et al. 2000). The prevalence of hypertension among patients with OSA is estimated to be around 50 % (Calhoun 2010). Our patients with OSA had a higher prevalence of hypertension probably due to the use of ABPM. Using ABPM with 24 h monitoring, we detected a non-dipper systolic profile in our OSA patients, an observation that has been previously reported by Davies et al, (Davies et al. 2000). Moreover, the high prevalence of uncontrolled BP (70.7 %; 145/205) and underdiagnosed hypertension (24.4 %; 50/205) among these patients has been reported by others (Baguet et al. 2009; Börgel et al. 2004).

The high number of different AH regimens (n=31) and the number of patients (n=106) with regimens that included two or more AH drugs suggest that controlling BP in these patients can be difficult and that consensus and guidelines based on evidence are needed to help guide therapy. Despite the large number of studies involving OSA patients, only a few have investigated the efficacy of different AHD and, in general, most are individual drug studies. Most these studies were designed to determine the efficacy of the drug being studied on reducing BP. What is absent from these studies is whether the BP-lowering effect leads to an augmentation of the number of controlled hypertensive patients in the study population; see Diogo & Monteiro for review (Diogo and Monteiro 2014). Briefly, individual drug studies find that the blockade of β1-adrenergic receptors (e.g., atenolol and nebivolol) and the renin-angiotensin-aldosterone (RAA) pathway, including both ACEi and angiotensin AT1 receptor antagonists, might be helpful. Spironolactone (a mineralocorticoid receptor antagonist) blocks aldosterone levels and may be efficacious in treating patients with resistant HT (Ziegler et al. 2011; Gaddam et al. 2010), and

patients with severe OSA (Oliveras and Schmieder 2013), a population who often have elevated aldosterone levels (Ziegler et al. 2011). Volume overload appears to contribute to the development of OSA (Friedman et al. 2010); however, diuretics, namely thiazide, have not been effective AH agents in OSA patients who do not have fluid retention (Ziegler et al. 2011). Calcium channel blockers, although effective in lowering BP, may negatively impacting sleep duration in HT patients with OSA , specifically lowering sleep time and sleep efficiency as described by Nerbass et al. (2011). In our study population, the most commonly prescribed AHD were diuretics and RAA blockers. However, the number of OSA patients using these AHD with uncontrolled BP was particularly high. In fact, 61.2 % (30/49) and 61.3 % (65/106) of patients being treated with monotherapy and polytherapy regimens, respectively, had blood pressures that remained uncontrolled. In our population, increasing the number of AHD was not effective in controlling hypertension in patients with OSA, and we found no associations between AH regimens and number of AHD and BP control before or after CPAP application.

We included only patients who were adherent with CPAP therapy for at least 4 h per night on average, as this is a threshold that is often used to define minimum acceptable CPAP use. This level of CPAP use has been reported by others to decrease the incidence of hypertension in patients with OSA (Barbé et al. 2012). Therefore, it would be expected that the combined effect of CPAP and AHD on BP control would be more pronounced than the isolated effect of AHD. However, the lack of association between AH regimens and BP control remained after CPAP adaptation, which suggests CPAP contributes minimally to controlling BP in these patients. Our findings are consistent with those of others (for a review see Diogo and Monteiro 2014). Börgel et al. (2004) showed that the absence of AHD is an independent predictor of the lowering effect of CPAP therapy on systolic and diastolic BP. Furthermore, Dernaika et al. reported that the effects of CPAP therapy on BP regulation appear to be less evident in hypertensive patients simultaneously treated with AHD (Dernaika et al. 2009). In our patient population, 8 of the 16 patients who were not on AH medication, after CPAP adaptation their blood pressure became controlled. Both results suggest that an earlier diagnosis of hypertension related to OSA and treatment with CPAP may be more effective than an AHD regimen in this population.

The effect of CPAP on lowering BP was greater for nocturnal BP, specifically nocturnal SBP. Importantly, this CPAP lowering effect on nocturnal blood pressure was not sufficient to reclassify patients from having blood pressures that were uncontrolled to controlled. CPAP prevents the bursts of sympathetic activity at the end of each respiratory event (Somers et al. 1995); although we did not directly measure sympathetic activity in our patients, the hypothetical reduction in sympathetic activity was not associated with an appreciable decrease in diurnal BP.

Perhaps it is more important to study the combined effect of CPAP and AH medication than either one alone in patients with OSA. Pépin et al. (2010) designed a study to assess the respective efficacy of CPAP and valsartan (ARBs) in reducing BP hypertensive patients with OSA who had never been treated for either condition. They speculated that the combined effect of both therapies on BP control might be additive in patients in whom hypertension is still uncontrolled by specific AH drugs. However, they did not quantify the combined effect of CPAP and valsartan. They found that valsartan induced a four-fold greater decrease in mean 24 h BP than CPAP alone (Pépin et al. 2010).

Our study has several limitations. First, it is an observational study, and thus, we are unable to determine whether the severity of hypertension before treatment was a confounding factor in the evaluation of the efficacy of AH regimens. Second, our sample size is small and the patients were treated at a single center. However, our center could be considered representative of the general OSA population because we found similar patient characteristics to those described in

the literature. Third, the significant variability in AHD regimen found in the present work together with the small sample size, does not allow us to identify the best AHD regimen for these patients. Fourth, we used the "Brown-Bag" medication review in order to record patients ongoing medication profile; data regarding adherence to AH drug treatment (before and after inclusion) were checked only based on self-reported adherence and were not confirmed by a "pill-count" method or other adherence measures. Despite these potential limitations, our results highlight the urgent need for innovative AHD therapies to treat patients with OSA who have hypertension.

## 22.5 Conclusions

In conclusion, we found that none of the currently available antihypertensive drugs, either alone or in combination, are sufficient enough to control BP in these patients, either before or after CPAP adaptation. BP control is independent of both the antihypertensive regimen and the number of antihypertensive drugs, and increasing the number of AHD does not improve efficacy in controlling BP in patients with OSA. Our results confirm that CPAP improves 24 h-BP profile is insufficient to effectively treat hypertension in patients with OSA. Moreover, the observation that CPAP alone can treat hypertension in patients with OSA who had not been previously treated with AHD suggest that an earlier diagnosis of hypertension related to OSA is important and CPAP therapy is key; CPAP may be more effective treatment than AHD regimens in this population since current AHD regimens are useful to prevent but not able to completely revert hypertension after it develops in patients with OSA.

**Acknowledgments** LND is supported by the Portuguese Fundação para a Ciência e a Tecnologia (FCT) fellowships (SFRH/BD/48335/2008; PTDC/SAU-TOX/112264/2009) and CEDOC (Chronic Diseases Research Centre, Lisbon, Portugal).

## References

Baguet JP, Barone-Rochette G, Pépin JL (2009) Hypertension and obstructive sleep apnea syndrome: current perspectives. J Hum Hypertens 23:431. doi:10.1038/jhh.2008.147

Barbé F et al (2012) Effect of continuous positive airway pressure on the incidence of hypertension and cardiovascular events in non-sleepy patients with obstructive sleep apnea: a randomized controlled trial. JAMA 307:2161–2168. doi:10.1001/jama.2012.4366

Börgel J, Sanner BM, Keskin F, Bittlinsky A, Bartels NK, Büchner N, Huesing A, Rump LC, Mügge A (2004) Obstructive sleep apnea and blood pressure. Interaction between the blood pressure-lowering effects of positive airway pressure therapy and antihypertensive drugs. Am J Hypertens 17:1081–1087

Calhoun DA (2010) Obstructive sleep apnea and hypertension. Curr Hypertens Rep 12:189–195. doi:10.1007/s11906-010-0112-8

Davies CW, Crosby JH, Mullins RL, Barbour C, Davies RJ, Stradling JR (2000) Case-control study of 24 hour ambulatory blood pressure in patients with obstructive sleep apnea and normal matched control subjects. Thorax 55:736–740

Dernaika TA, Kinasewitz GT, Tawk MM (2009) Effects of nocturnal continuous positive airway pressure therapy in patients with resistant hypertension and obstructive sleep apnea. J Clin Sleep Med 5:103–107

Diogo LN, Monteiro EC (2014) The efficacy of antihypertensive drugs in chronic intermittent hypoxia conditions. Front Physiol 5:361. doi:10.3389/fphys.2014.00361

Friedman O, Bradley TD, Chan CT, Parkes R, Logan AG (2010) Relationship between overnight rostral fluid shift and obstructive sleep apnea in drug-resistant hypertension. Hypertension 56:1077–1082

Gaddam K, Pimenta E, Thomas SJ, Cofield SS, Oparil S, Harding SM et al (2010) Spironolactone reduces severity of obstructive sleep apnoea in patients with resistant hypertension: a preliminary report. J Hum Hypertens 8:532–537. doi:10.1038/jhh.2009.96

Lavie P, Herer P, Hoffstein V (2000) Obstructive sleep apnea syndrome as a risk factor for hypertension: population study. BMJ 320:479–482

Mancia G et al (2013) 2013 ESH/ESC guidelines for the management of arterial hypertension: the task force for the management of arterial hypertension of the European Society of Hypertension (ESH) and of the European Society of Cardiology (ESC). Eur Heart J 2013(34):2159–2219. doi:10.1097/HJH.0b013e328364ca4c

Nerbass FB, Pedrosa RP, Genta PR, Drager LF, Lorenzi-Filho G (2011) Calcium channel blockers are independently associated with short sleep duration in hypertensive patients with obstructive sleep apnea. J Hypertens 29:1236–1241. doi:10.1097/HJH.0b013e3283462e8b

Oliveras A, Schmieder RE (2013) Clinical situations associated with difficult-to-control hypertension. J Hypertens 31(Suppl 1):S3–S8. doi:10.1097/HJH.0b013e32835d2af0

Pépin JL, Tamisier R, Barone-Rochette G, Launois SH, Lévy P, Baguet JP (2010) Comparison of continuous positive airway pressure and valsartan in hypertensive patients with sleep apnea. Am J Respir Crit Care Med 182:954–960. doi:10.1164/rccm.200912-1803OC

Somers VK, Dyken ME, Clary MP, Abboud FM (1995) Sympathetic neural mechanisms in obstructive sleep apnea. J Clin Invest 96:1897–1904

Ziegler MG, Milic M, Sun P (2011) Antihypertensive therapy for patients with obstructive sleep apnea. Curr Opin Nephrol Hypertens 20:50–55. doi:10.1097/MNH.0b013e3283402eb

# 23 An Overview on the Respiratory Stimulant Effects of Caffeine and Progesterone on Response to Hypoxia and Apnea Frequency in Developing Rats

Aida Bairam, NaggaPraveena Uppari, Sébastien Mubayed, and Vincent Joseph

**Abstract**

The respiratory stimulant caffeine is the most frequently used xanthine (theophylline or aminophylline) for the treatment of apnea in premature infants. It decreases but does not eliminate apnea. In most cases such decreases is insufficient to prevent the use of artificial ventilation. Progesterone is a respiratory stimulant in adult mammals including human, and it decreases sleep apnea in menopausal women. Whether progesterone as an adjunct to caffeine therapy could be effective in further reducing the frequency of apnea in premature infants is not known because its respiratory effect in newborns has not been well studied. Using rat pups at different postnatal ages, we first determined whether the respiratory stimulant effects of acute caffeine (10 mg/kg, i.p.) or progesterone (4 mg/kg i.p.) are age dependent. These studies showed that caffeine enhances the ventilatory response to hypoxia in 1 and 4 days-old rats while it decreases apnea frequency in 12-days-old. In contrast, progesterone enhances the ventilatory response to hypoxia in less than 7-days-old but decreases apnea in 1-day-old rats. Preliminary experiments show that administration of progesterone (4 mg/kg i.p.) to newborn rats that are chronically treated with caffeine (mimicking its clinical uses – 7.5 mg/kg once/day by gavage)

A. Bairam, M.D., Ph.D. (✉)
Pediatric Department, Laval University, Research Center of Centre Hospitalier, Universitaire de Quebec, Quebec City, QC, Canada

Centre de recherche du CHUQ, HSFA,
10, rue de l'Espinay, Québec G1L 3L5, QC, Canada
e-mail: Aida.bairam@crsfa.ulaval.ca

N. Uppari • S. Mubayed • V. Joseph
Pediatric Department, Laval University, Research Center of Centre Hospitalier, Universitaire de Quebec, Quebec City, QC, Canada


C. Peers et al. (eds.), *Arterial Chemoreceptors in Physiology and Pathophysiology*,
Advances in Experimental Medicine and Biology 860, DOI 10.1007/978-3-319-18440-1_23

enhances the respiratory stimulant effects of caffeine. Surprisingly, acute injection of progesterone enhances apnea frequency and reduces hypoxic ventilatory response in 12-day-old rats.

**Keywords**
Caffeine • Progesterone • Newborn • Rats • Breathing • Apnea

## 23.1 Introduction

The respiratory control system undergoes considerable maturation before and after birth. The important correlate of an immature system, particularly in babies born before term, is respiratory irregularities and apneas (Darnall et al. 2006; Greer 2012). These events, regardless of gestational age, are often associated with increasing hospitalization and long-term neurocognitive morbidity (Janvier et al. 2004; Eichenwald et al. 2011). Although apneas reflect more the "physiological" rather than "pathological" immaturity of the mechanisms regulating breathing, they are systematically treated.

The respiratory stimulants represent the best option, and caffeine (a methylxanthine derivative) is currently the main therapy worldwide. Nevertheless, a substantial percentage of apneas persist despite therapeutic plasma levels of caffeine are achieved (Darnall et al. 2006; Schoen et al. 2014) and the treatment of apnea often necessitates aggressive therapy such as mechanical ventilation, particularly in very preterm neonates (<28 weeks of gestation). It has been suggested that progesterone may be used as an alternative or adjunct to caffeine, but proper investigations of its relative efficacy alone or in combination with caffeine are still lacking (Finer et al. 2006; Mathew 2011). Keeping in mind the important changes that take place within the central (*brainstem respiratory center*) and peripheral (*carotid body chemoreceptors*) component of the respiratory control system during early life (Darnall et al. 2006; Edwards et al. 2013; MacFarlane et al. 2013), in the following overview we will emphasis on data obtained from our laboratory using newborn rats as an animal model.

We will first describe investigations obtained with caffeine or progesterone and then with a simultaneous administration of both on basal ventilation, the hypoxic ventilatory response (HVR) and apnea frequency in Sprague-Dawley rats at postnatal age ranged from 1 to 12 days old (P1–P12). All rats used in the experiments were born and bred in our animal care facilities at research center of Saint François d'Assise Hospital. The dam was used only once while male rats were used twice for mating. At birth, litters were culled to 12 pups with an equal male/female ratio (whenever possible). Each group (age and treatment) was composed of rats from at least 8 litters to further widen genetic distribution and minimize litter-specific effects. Moreover, pups from one litter were randomly distributed between the various experimental groups. In order to minimize sex-specific effects, for experiments using animals less than or equal to 7 days of age both male and female rat pups were used, for experiments using animals at 12 days of age only male rats were used. Each rat was used only once but was returned to his mother to be sacrificed (mother and litters) at 12th postnatal day (i.e. the end of experiment). For the respiratory recordings (see details in Lefter et al. 2007; Julien et al. 2008, 2010, 2011; Bairam et al. 2013a), the rat was allowed to habituate to the plethysmograph for 10 min, after which time the animal was administered the experimental drug or saline by i.p. injection (see details in each section) and then returned to the plethysmography. Recording began once respiration stabilized with the animal breathing room air (basal, 21 % $O_2$, 10 min) followed by hypoxia (12 % O2, 20 min). This exposure paradigm allowed for the dynamic HVR: initial (early) and the steady-state (late) phases to be recorded.

One-way or two-way ANOVA followed by post-hoc tests were used when appropriate. A p-value <0.05 is considered significant.

## 23.2 The HVR in Newborn

Central and peripheral chemoreceptors sense $O_2$ level in the blood. As a result, low arterial content of $O_2$ increases the excitatory inputs to central respiratory neural networks. These sensory signals then initiate a proper increase of respiration to augment pulmonary gas exchange, a reflex that undergoes significant changes during the postnatal period in newborn mammals. For instance, it exhibits a biphasic pattern, i.e. an initial increase in ventilation resulting from stimulation of peripheral chemoreceptors (primarily located in the carotid bodies), followed by a decline, sometimes to a level below pre-hypoxic values. The respiratory depression that takes place during the late phase of hypoxia likely originates centrally where inhibitory mechanisms can override the excitatory inputs from peripheral chemoreceptors. The central mechanisms include changes in metabolism, local perfusion, and in the production of inhibitory transmitters (e.g. GABA and adenosine) (Darnall et al. 2006; Greer 2012; Edwards et al. 2013). Both phases develop toward the adult pattern where the increase in ventilation is sustained throughout the hypoxic episode. The HVR is regularly used as a tool to describe the magnitude of maturation of the respiratory control system. Because hypoxemic episodes are frequently observed during apneas, the preterm infants are exposed to chronic intermittent hypoxia that consequently disrupts the HVR and may contribute to enhance the occurrence of apnea (Martin et al. 2012; Rhein et al. 2014). Chronic exposure to intermittent hypoxia rather hypercapnia disrupts the central and peripheral respiratory reflexes (Julien et al. 2008; Mayer et al. 2013). On the other hand, exposure to intermittent hypoxia may induce an increase in normoxic ventilation termed as "ventilatory long term facilitation" (vLTF) (Julien et al. 2008; Martin et al. 2012). vLTF is a prominent and intriguing property of the respiratory control system defined as a sustained increase in minute ventilation following repeated but brief hypoxic exposures. vLTF may be an endogenous protective mechanisms that prevents recurrent apneas in newborns.

## 23.3 Rationale for Using Respiratory Stimulants to Treat Apnea in Newborns

### 23.3.1 Caffeine

An adenosine A1 and A2 receptor antagonist, is the drug of choice for treating neonates with apnea. The inhibitory effects of adenosine on respiration are well described in newborn subjects. By blocking adenosine, caffeine increases central respiratory drive and suppresses the late phase of the HVR in various animal species and in preterm infants (Darnall et al. 2006; Mathew 2011; Dobson et al. 2014; Schoen et al. 2014). These effects are generally related to an improvement of sensitivity and/or responsiveness to decrease in arterial $O_2$ and increase in $CO_2$ in newborn mammals. However, expression and (probably) functionality of adenosine A1 and A2 receptors change substantially during development (Montandon et al. 2008; Bairam et al. 2013b). In the rat central nervous system, including the brainstem, these receptors appear early in the embryonic brain, and their levels increase gradually in an age- and region-specific manner to reach adult levels by P14. In the carotid body, although both receptor types are detected in adult rats; only A2 receptor mRNA levels undergo progressive down-regulation with age, reaching values similar to those found in adults by P14. So far, the developmental expression pattern of A1 receptor and its physiological role in chemoreceptor activity are still poorly known. Interestingly, while activation of brainstem A1 and A2 receptors inhibits respiration, activation of A2 receptors in the carotid body appears to increase chemoreceptor activity in adult rats (Montandon et al. 2008; Bairam et al. 2013b). Considering the important developmental changes for adenosine receptor expression in the respiratory control system, suboptimal efficacy of caffeine might be

related to age. Although the efficacy of caffeine for the treatment of apnea is not disputed, no data exist that examines the effect of gestational or postnatal age as an essential variable affecting efficacy of caffeine on apnea frequency in premature infants. Using *in vitro* models, specifically brainstem slices from newborn rats or mice (aged P0–P4), methylxanthines (theophylline, aminophylline, caffeine) enhance respiratory rhythm generation in an age-dependent manner (Kawai et al. 1995; Mironov et al. 1999).

#### 23.3.1.1 Respiratory Effects of Caffeine Are Age-Dependent in Developing Rats

We first performed experiments to determine the dose response curve of caffeine on ventilation (0, 5, 10 and 20 mg/kg, i.p. Fig. 23.1; 5 rats per dose). Caffeine at 10 mg/kg enhances basal ventilation in P12 but not in P4 rats, but also increases $O_2$ consumption to a similar extent, so that the ratio of minute ventilation/oxygen consumption is not increased. Because the breathing and metabolic variables were similar between animals who received 10 and 20 mg/kg of caffeine, in subsequent experiments, P4 and P12 rats (about 12 rats per group age) were given 10 mg/kg of caffeine. Caffeine decreases apnea frequency during basal ventilation in P12 but not in P4 rats; while it enhances the HVR in P4 but not P12 rats, it has no significant effect on apnea frequency during hypoxia in both ages (Bairam et al. 2013b). Because it is recommended that caffeine be used within a few days after birth to reduce the need for mechanical ventilation and the occurrence of bronchopulmonary dysplasia (Davis et al. 2010; Dobson et al. 2014; Taha et al. 2014), an additional experimental group of rats at P1 were used. We recently published our findings obtained in animals at P4 and P12 rats (Bairam et al. 2013b) but have also presented the data in (Figs. 23.2 and 23.3). Caffeine enhances basal ventilation in P1 rats similar to P12 rats (Fig. 23.2) while it significantly decreases apnea frequency in P12 rats (Fig. 23.2). However, caffeine increases minute ventilation during the late phase of HVR (Fig. 23.3) with no significant effects on apnea (data not shown) during hypoxia in P4 and P12 rats (Bairam et al. 2013b). A positive correlation between the decrease in apnea frequency and the increase in basal minute ventilation with caffeine was only observed in P12 rats (p values

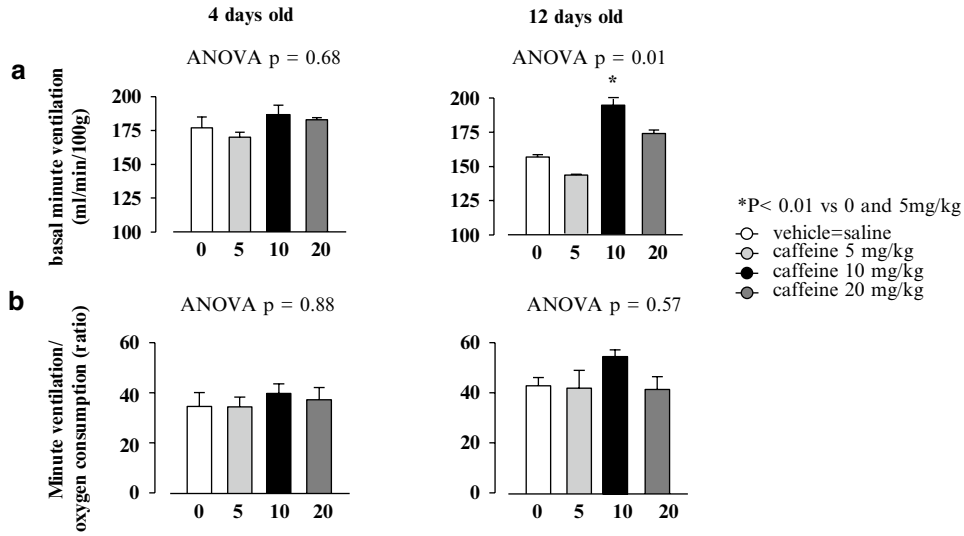


**Fig. 23.1** Dose-response curve of caffeine under basal condition (normoxia = 21 % $O_2$). The dose of 10 mg/kg (i.e. 20 mg/kg caffeine citrate, similar to its clinical use) significantly increases basal ventilation in 12- but not in 4-day-old rats, but does not change the oxygen consumption ratio ($\dot{V}_E / \dot{V}_{O_2}$ : B) in either age. n = 5 rats for each dose. Data are mean ± SEM

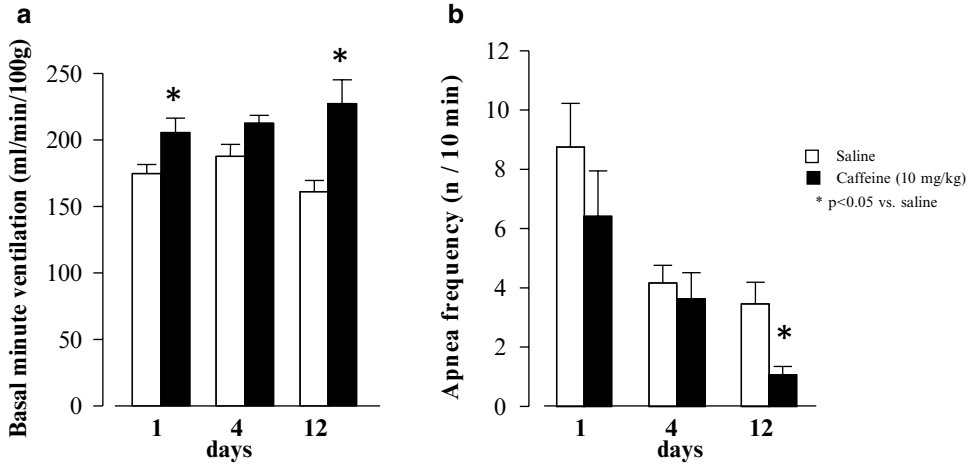


**Fig. 23.2** Effects of caffeine on basal ventilation (normoxia) and apnea frequency in developing rats. Caffeine increases basal ventilation in 1 and 12 days-old rats but significantly decreases apnea frequency in 12-days-old rats. n = 8–12 rats for each group and age. Data are mean ± SEM

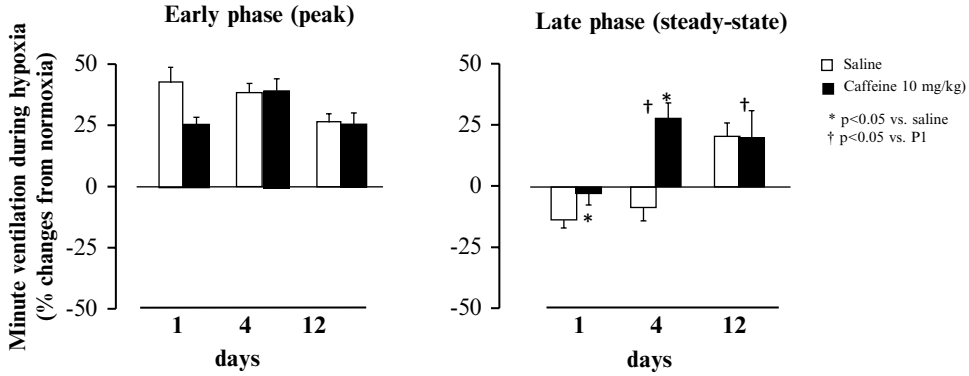


**Fig. 23.3** Effects of caffeine on hypoxic ventilatory response (12 % $O_2$) in developing rats. Caffeine has no effect on the early phase of the ventilatory response to hypoxia but decreases the inhibition of ventilation during the steady state response to hypoxia in 1- and 4-days old rats. n = 8–12 rats for each group and age. Data are mean ± SEM

are respectively 0.47, 0.56, and 0.04 for P1, P4 and P12). The discrepancy in the effects of caffeine on basal ventilation, HVR and apnea frequency suggest to us that caffeine reduces apnea by increasing central respiratory drive rather than by increasing HVR (Julien et al. 2010; Bairam et al. 2013b). Indeed, other mechanisms than those involved in the regulation of breathing during development are involved in decreasing apnea frequency with caffeine. These mechanisms may be related to an enhancement of diaphragmatic muscle activity (Heyman et al. 1991; Kassim et al. 2009) and/or to an improvement in pulmonary mechanics following caffeine administration (Davis et al. 1989; Yoder et al. 2005).

#### 23.3.1.2 Respiratory Effects of Caffeine in Newborns Rats Exposed to Chronic Intermittent Hypoxia

Similar to what is observed in preterm neonates with apnea (Al-Matary et al. 2004; Nock

et al. 2004), exposure to intermittent hypoxia in newborn rats increases the response of peripheral chemoreceptors to hypoxia (Peng et al. 2004; Julien et al. 2008; Mayer et al. 2013). Interestingly, we showed that rat pups raised under chronic intermittent hypoxia (5 % $O_2$/100 s every 10 min; 6 cycles/h followed by 1 h at 21 % $O_2$, 24 h/day) during the first 10 days of life (i.e. the sensitive period for respiratory control development in rats) have an increased hypoxic responsiveness and apnea frequency when exposed to a series of 10 brief hypoxic episodes (Julien et al. 2008). In addition to sensitizing the carotid body to acute hypoxic exposure, chronic intermittent hypoxia abolishes vLTF. Because apnea frequency in human preterm increases during the first days of birth, we studied the effects of caffeine on vLTF in 12 days old rats that were exposed to intermittent hypoxia between postnatal days 3–12. In these rats we observed that a single caffeine injection at 10 mg/kg enhances the expression of the vLTF, decreases apnea frequency, but has no significant effect on the HVR in comparison to saline injected rats (Julien et al. 2010). These observations suggest to us that the therapeutic effect of caffeine in newborn infants is linked to its stimulatory effect on vLTF. Indeed, in P12 rats exposed to both chronic neonatal intermittent hypoxia and caffeine (7.5 mg/kg/day given by gavage from P3–P12), basal ventilation is enhanced and apnea frequency is reduced compared to the response observed in water given rats (control) exposed to intermittent hypoxia (Julien et al. 2011). Because early therapeutic use of caffeine in neonates within several days of life (Schoen et al. 2014; Taha et al. 2014) is recommended, it would be interesting to assess whether the above-mentioned effects of caffeine on intermittent hypoxia are age dependent.

In summary, similar to what has been observed in newborn infants, we show that in newborn rats caffeine decreases (but does not abolish) apnea, and this effect is age dependent. Furthermore, the efficacy of caffeine on apnea frequency, whether administered acutely or chronically, is independent of its effect on HVR but related to an increase in central respiratory drive.

### 23.3.2 Progesterone

Progesterone acting both on peripheral and central chemoreceptors is a potent respiratory stimulant in adult humans and animals (Behan and Wenninger 2008). For instance, in adult humans progesterone (1) increases ventilation in pregnant women, (2) reduces the $CO_2$ retention in patients with obstructive pulmonary diseases, and (3) decreases sleep disordered breathing in adult men and post-menopausal women (Saaresranta and Polo 2003; Shahar et al. 2003; Behan and Wenninger 2008). Progesterone acts on two types of receptors, membrane and nuclear receptors (Behan and Wenninger 2008 – see also chapter by R. Boukari in the present volume). So far, most of our knowledge regarding the effects of progesterone on respiration establishes an important role for the nuclear receptors, which are expressed within the central nervous system, brainstem respiratory nuclei, and carotid body (Haywood et al. 1999; Behan and Thomas 2005; Joseph et al. 2006).

In the newborn, exogenous progesterone may be efficacious in preventing osteoporosis in premature infants (Trotter et al. 1999a). In infants with congenital hypoventilation syndrome, medroxyprogesterone acetate (2–4 mg/kg/day) increases ventilation and promoted weaning from mechanical ventilation (Milerad et al. 1985); these observations are limited to few case reports. Hence, in sharp contrast to caffeine, studies determining the efficacy of progesterone as a respiratory stimulant in human neonates have not been done. Experiments in newborn rats outlined below were designed to address this gap in knowledge.

#### 23.3.2.1 Respiratory Effects of Progesterone Are Age-Dependent in Developing Rats

Newborn mammals are exposed to high levels of progesterone at birth and during the early days of life (Rhoda et al. 1984; Trotter et al. 1999b). The most important source of progesterone is the placenta, but the adrenals and the brain also synthetize progesterone after birth

(Rhoda et al. 1984). In 10 days old rats chronically exposed to progesterone via the lactating mothers supplemented by an osmotic mini-pump HVR was enhanced and apnea frequency was reduced in both normoxia and hypoxia (Lefter et al. 2007). To address whether acute progesterone administration might have similar effects, and if these effects are age specific, experiments were also performed in rat pups at P1, P4, P7, and P12 (Bairam et al. 2013a). Progesterone (4 mg/kg, i.p.) has no effect on basal ventilation at all ages but reduces apnea frequency in P1 rats. In response to hypoxia, progesterone enhances the HVR in rats younger than 7 days of life but reduces apnea frequency only in P1 rats. Furthermore, deletion of the nuclear progesterone receptors (PR) in KO mice reduces HVR at 1 and 10 days of age (not P4) as compared to wild type mice, likely indicating an influence of progesterone synthesis in the brain around birth and P10 (Potvin et al. 2014).

#### 23.3.2.2 Respiratory Effects of Progesterone in Newborns Rats Exposed to Chronic Intermittent Hypoxia

In menopausal women with sleep disordered breathing, administration of progesterone significantly decreases apnea frequency and the apnea-hypopnea index (Saaresranta and Polo 2003; Shahar et al. 2003); a similar effect is observed in men treated with progesterone (Saaresranta and Polo 2003). In a preliminary study, we evaluated the effects of 4 mg/kg of progesterone in P12 rats exposed to intermittent hypoxia from P3 to P12 (see 3.1.2). In contrast to the effect of caffeine, progesterone had no effect on vLTF. But, it did

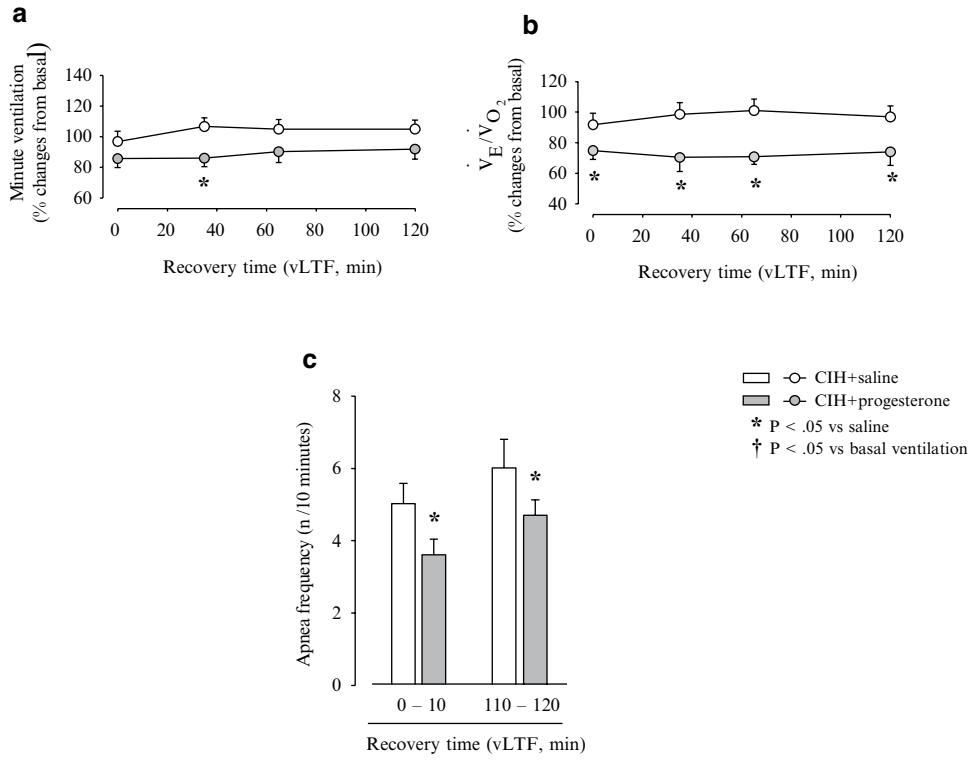


**Fig. 23.4** Effects of progesterone on basal ventilation (normoxia) and apnea frequency during the recovery period (ventilatory long-term facilitation, vLTF). (**a**) Minute ventilation; (**b**) $O_2$ exchange ratio ($\dot{V}_E/\dot{V}_{O_2}$); and, (**c**) apnea frequency. Measures were performed in 12-day-old male rats previously exposed to chronic intermittent hypoxia (CIH) from 3–12 days of life and subjected to 10 brief hypoxic cycles before recording the vLTF. Data are presented as a percentage changes from the basal ventilation recorded before exposure to the 10 brief hypoxic cycles. Progesterone slightly decreases minute ventilation, $\dot{V}_E/\dot{V}_{O_2}$, and apnea frequency. n = 11 rats for each group. Data are mean ± SEM

decrease apnea frequency (Fig. 23.4). These preliminary findings suggest to us that progesterone modifies ventilation in response to chronic intermittent hypoxia in newborn rats.

In summary, while there remains a paucity of data on the role of progesterone on control of breathing during development, our data strongly supports the hypothesis that circulating as well as neuronal progesterone (nuclear Progesterone Receptor Nock-Out mice, PRKO model) regulate breathing, and that this effect is at least partially mediated by the nuclear progesterone receptors. The effects of chronic vs. acute administration of progesterone on breathing appear to be different, and the potential contributions of membrane progesterone receptors in modulating breathing during development are still unknown.

### 23.3.3 Caffeine and Progesterone

Because caffeine is routinely used for the treatment of apnea, we determined the effects of progesterone on the background of a chronic treatment with caffeine. We first tested if progesterone might enhance the effects of caffeine on apnea frequency and HVR. We used our model of chronic caffeine administration (7.5 mg/kg) by daily gavage between postnatal days 3–12 (Montandon et al. 2008; Julien et al. 2011). At P12 we recorded respiration following a single intraperitoneal injection of either saline or progesterone (4 mg/kg). Respiratory variables were recorded under normoxia (10 min) 30 min after the injection, and in response to moderate hypoxia (12 % $O_2$, 20 min). We assessed the frequency of apneas and minute ventilation under normoxia and during the last 10 min of hypoxia. In normoxia, progesterone had no effect on minute ventilation but surprisingly increased apnea frequency (Fig. 23.5). During hypoxia, progesterone reduced minute ventilation, but had no effect on apnea frequency. These results do not support our initial hypothesis. Since chronic caffeine exposure increases GABAA receptors (Picard et al. 2008), we speculate that allopregnanolone (a metabolite of progesterone) depresses respiration via GABAA receptor activation (Ren and Greer 2006a, b). If our findings are relevant to the human infant, the addition of progesterone to caffeine for the treatment of apnea in newborn is likely not to be effective in reducing apnea frequency.

## 23.4 Conclusion

Persistent apnea in human infants increases morbidity and length of hospitalization. Our data obtained from newborn rats support the hypothesis

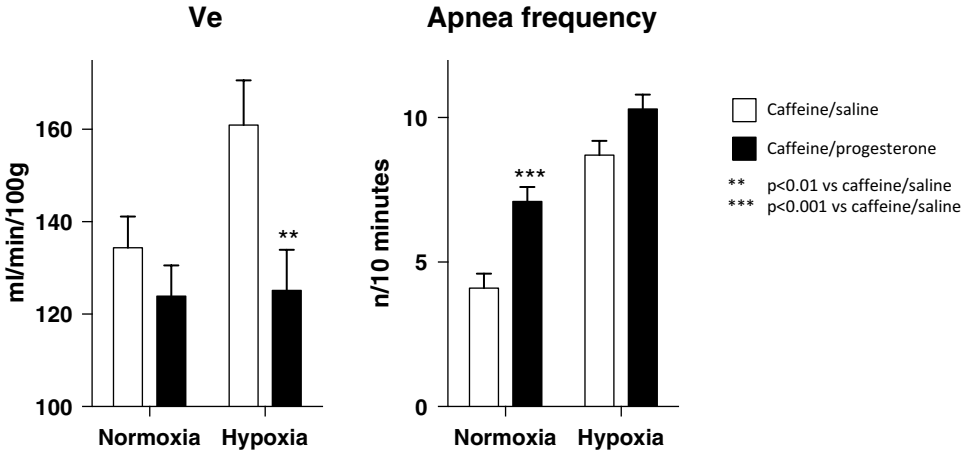


**Fig. 23.5** Effects of progesterone on the hypoxic ventilatory response and apnea frequency in 12-days-old rats that received caffeine between postnatal days 3–12 (7.5 mg/kg/day by gavage). Compared to rats injected with saline, progesterone (4 mg/kg, i.p.) decreases minute ventilation during the late phase of the hypoxic exposure (10–20 min) and increases apnea frequency during normoxia. n = 15 rats for each group. Data are mean ± SEM

that progesterone is a respiratory stimulant that regulates the HVR and apnea frequency in an age-dependent manner. However, these respiratory effects of progesterone vary with the experimental conditions (acute and chronic exposure), and are disrupted in rats treated with caffeine. In future experiments, we will determine how progesterone and caffeine interact, and the differential effects of acute vs. chronic progesterone administration on respiration in newborns.

**Acknowledgements** Studies founded by a grant from the Canadian Institute for Health Research to Aida Bairam (MOP-119272).

## References

Al-Matary A, Kutbi I, Qurashi M et al (2004) Increased peripheral chemoreceptor activity may be critical in destabilizing breathing in neonates. Semin Perinatol 28(4):264–272

Bairam A, Lumbroso D, Joseph V (2013a) Effect of progesterone on respiratory response to moderate hypoxia and apnea frequency in developing rats. Respir Physiol Neurobiol 185(3):515–525

Bairam A, Niane LM, Joseph V (2013b) Role of ATP and adenosine on carotid body function during development. Respir Physiol Neurobiol 185(1):57–66

Behan M, Thomas CF (2005) Sex hormone receptors are expressed in identified respiratory motoneurons in male and female rats. Neuroscience 130(3):725–734

Behan M, Wenninger JM (2008) Sex steroidal hormones and respiratory control. Respir Physiol Neurobiol 164(1–2):213–221

Darnall RA, Ariagno RL, Kinney HC (2006) The late preterm infant and the control of breathing, sleep, and brainstem development: a review. Clin Perinatol 33(4):883–914

Davis JM, Bhutani VK, Stefano JL et al (1989) Changes in pulmonary mechanics following caffeine administration in infants with bronchopulmonary dysplasia. Pediatr Pulmonol 6(1):49–52

Davis PG, Schmidt B, Roberts RS et al (2010) Caffeine for Apnea of Prematurity trial: benefits may vary in subgroups. J Pediatr 156(3):382–387

Dobson NR, Patel RM, Smith PB et al (2014) Trends in caffeine use and association between clinical outcomes and timing of therapy in very low birth weight infants. J Pediatr 164(5):992–998

Edwards BA, Sands SA, Berger PJ (2013) Postnatal maturation of breathing stability and loop gain: the role of carotid chemoreceptor development. Respir Physiol Neurobiol 185(1):144–155

Eichenwald EC, Zupancic JA, Mao WY et al (2011) Variation in diagnosis of apnea in moderately preterm infants predicts length of stay. Pediatrics 127(1):53–58

Finer NN, Higgins R, Kattwinkel J et al (2006) Summary proceedings from the apnea-of-prematurity group. Pediatrics 117(3 Pt 2):S47–S51

Greer JJ (2012) Control of breathing activity in the fetus and newborn. Compr Physiol 2(3):1873–1888

Haywood SA, Simonian SX, van der Beek EM et al (1999) Fluctuating estrogen and progesterone receptor expression in brainstem norepinephrine neurons through the rat estrous cycle. Endocrinology 140(7):3255–3263

Heyman E, Ohlsson A, Heyman Z et al (1991) The effect of aminophylline on the excursions of the diaphragm in preterm neonates. A randomized double blind controlled study. Acta Paediatr Scand 80(3):308–315

Janvier A, Khairy M, Kokkotis A et al (2004) Apnea is associated with neurodevelopmental impairment in very low birth weight infants. J Perinatol 24(12):763–768

Joseph V, Doan VD, Morency CE et al (2006) Expression of sex-steroid receptors and steroidogenic enzymes in the carotid body of adult and newborn male rats. Brain Res 1073–1074:71–82

Julien C, Bairam A, Joseph V (2008) Chronic intermittent hypoxia reduces ventilatory long-term facilitation and enhances apnea frequency in newborn rats. Am J Physiol Regul Integr Comp Physiol 294(4):R1356–R1366

Julien CA, Joseph V, Bairam A (2010) Caffeine reduces apnea frequency and enhances ventilatory long-term facilitation in rat pups raised in chronic intermittent hypoxia. Pediatr Res 68(2):105–111

Julien CA, Joseph V, Bairam A (2011) Alteration of carotid body chemoreflexes after neonatal intermittent hypoxia and caffeine treatment in rat pups. Respir Physiol Neurobiol 177(3):301–312

Kassim Z, Greenough A, Rafferty GF (2009) Effect of caffeine on respiratory muscle strength and lung function in prematurely born, ventilated infants. Eur J Pediatr 168(12):1491–1495

Kawai A, Okada Y, Muckenhoff K et al (1995) Theophylline and hypoxic ventilatory response in the rat isolated brainstem-spinal cord. Respir Physiol 100(1):25–32

Lefter R, Morency CE, Joseph V (2007) Progesterone increases hypoxic ventilatory response and reduces apneas in newborn rats. Respir Physiol Neurobiol 156(1):9–16

MacFarlane PM, Ribeiro AP, Martin RJ (2013) Carotid chemoreceptor development and neonatal apnea. Respir Physiol Neurobiol 185(1):170–176

Martin RJ, Di Fiore JM, Macfarlane PM et al (2012) Physiologic basis for intermittent hypoxic episodes in preterm infants. Adv Exp Med Biol 758:351–358

Mathew OP (2011) Apnea of prematurity: pathogenesis and management strategies. J Perinatol 31(5):302–310

Mayer CA, Ao J, Di Fiore JM et al (2013) Impaired hypoxic ventilatory response following neonatal sustained and subsequent chronic intermittent hypoxia in rats. Respir Physiol Neurobiol 187(2):167–175

Milerad J, Lagercrantz H, Lofgren O (1985) Alveolar hypoventilation treated with medroxyprogesterone. Arch Dis Child 60(2):150–155

Mironov SL, Langohr K, Richter DW (1999) A1 adenosine receptors modulate respiratory activity of the neonatal mouse via the cAMP-mediated signaling pathway. J Neurophysiol 81(1):247–255

Montandon G, Kinkead R, Bairam A (2008) Adenosinergic modulation of respiratory activity: developmental plasticity induced by perinatal caffeine administration. Respir Physiol Neurobiol 164(1–2):87–95

Nock ML, Difiore JM, Arko MK et al (2004) Relationship of the ventilatory response to hypoxia with neonatal apnea in preterm infants. J Pediatr 144(3):291–295

Peng YJ, Rennison J, Prabhakar NR (2004) Intermittent hypoxia augments carotid body and ventilatory response to hypoxia in neonatal rat pups. J Appl Physiol 97(5):2020–2025

Picard N, Guenin S, Larnicol N et al (2008) Maternal caffeine ingestion during gestation and lactation influences respiratory adaptation to acute alveolar hypoxia in newborn rats and adenosine A2A and GABA A receptor mRNA transcription. Neuroscience 156(3):630–639

Potvin C, Rossignol O, Uppari N et al (2014) Reduced hypoxic ventilatory response in newborn mice knocked-out for the progesterone receptor. Exp Physiol 99(11):1523–1537

Ren J, Greer JJ (2006a) Modulation of respiratory rhythmogenesis by chloride-mediated conductances during the perinatal period. J Neurosci 26(14):3721–3730

Ren J, Greer JJ (2006b) Neurosteroid modulation of respiratory rhythm in rats during the perinatal period. J Physiol 574(Pt 2):535–546

Rhein LM, Dobson NR, Darnall RA et al (2014) Effects of caffeine on intermittent hypoxia in infants born prematurely: a randomized clinical trial. JAMA Pediatr 168(3):250–257

Rhoda J, Corbier P, Roffi J (1984) Gonadal steroid concentrations in serum and hypothalamus of the rat at birth: aromatization of testosterone to 17 beta-estradiol. Endocrinology 114(5):1754–1760

Saaresranta T, Polo O (2003) Sleep-disordered breathing and hormones. Eur Respir J 22(1):161–172

Schoen K, Yu T, Stockmann C et al (2014) Use of methylxanthine therapies for the treatment and prevention of apnea of prematurity. Paediatr Drugs 16(2):169–177

Shahar E, Redline S, Young T et al (2003) Hormone replacement therapy and sleep-disordered breathing. Am J Respir Crit Care Med 167(9):1186–1192

Taha D, Kirkby S, Nawab U et al (2014) Early caffeine therapy for prevention of bronchopulmonary dysplasia in preterm infants. J Matern Fetal Neonatal Med 27(16):1698–1702

Trotter A, Maier L, Grill HJ et al (1999a) Effects of postnatal estradiol and progesterone replacement in extremely preterm infants. J Clin Endocrinol Metab 84(12):4531–4535

Trotter A, Maier L, Grill HJ et al (1999b) 17Beta-estradiol and progesterone supplementation in extremely low-birth-weight infants. Pediatr Res 45(4 Pt 1):489–493

Yoder B, Thomson M, Coalson J (2005) Lung function in immature baboons with respiratory distress syndrome receiving early caffeine therapy: a pilot study. Acta Paediatr 94(1):92–98

# 24 Hyperbaric Oxygen Therapy Improves Glucose Homeostasis in Type 2 Diabetes Patients: A Likely Involvement of the Carotid Bodies

P. Vera-Cruz, F. Guerreiro, M.J. Ribeiro, M.P. Guarino, and S.V. Conde

**Abstract**

The carotid bodies (CBs) are peripheral chemoreceptors that respond to hypoxia increasing minute ventilation and activating the sympathetic nervous system. Besides its role in ventilation we recently described that CB regulate peripheral insulin sensitivity. Knowing that the CB is functionally blocked by hyperoxia and that hyperbaric oxygen therapy (HBOT) improves fasting blood glucose in diabetes patients, we have investigated the effect of HBOT on glucose tolerance in type 2 diabetes patients. Volunteers with indication for HBOT were recruited at the Subaquatic and Hyperbaric Medicine Center of Portuguese Navy and divided into two groups: type 2 diabetes patients and controls. Groups were submitted to 20 sessions of HBOT. OGTT were done before the first and after the last HBOT session. Sixteen diabetic patients and 16 control individual were

P. Vera-Cruz
CEDOC, Centro de Estudos Doenças Crónicas, Nova Medical School, Faculdade de Ciências Médicas, Universidade Nova de Lisboa,
Campo Mártires da Pátria, 130, 1169-056 Lisbon, Portugal

CINAV, Naval Research Centre, Lisbon, Portugal

F. Guerreiro
Subaquatic and Hyperbaric Medicine Centre of the Portuguese Navy, Lisbon, Portugal

M.J. Ribeiro • S.V. Conde (✉)
CEDOC, Centro de Estudos Doenças Crónicas, Nova Medical School, Faculdade de Ciências Médicas, Universidade Nova de Lisboa,
Campo Mártires da Pátria, 130,
1169-056 Lisbon, Portugal
e-mail: silvia.conde@fcm.unl.pt

M.P. Guarino
CEDOC, Centro de Estudos Doenças Crónicas, Nova Medical School, Faculdade de Ciências Médicas, Universidade Nova de Lisboa,
Campo Mártires da Pátria, 130, 1169-056 Lisbon, Portugal

School of Health Sciences; Health Research Unit – UIS, Polytechnic Institute of Leiria, Leiria, Portugal



C. Peers et al. (eds.), *Arterial Chemoreceptors in Physiology and Pathophysiology*,
Advances in Experimental Medicine and Biology 860, DOI 10.1007/978-3-319-18440-1_24

included. Fasting glycemia was143.5 ± 12.62 mg/dl in diabetic patients and 92.06 ± 2.99 mg/dl in controls. In diabetic patients glycemia post-OGTT was 280.25 ± 22.29 mg/dl before the first HBOT session. After 20 sessions, fasting and 2 h post-OGTT glycemia decreased significantly. In control group HBOT did not modify fasting glycemia and post-OGTT glycemia. Our results showed that HBOT ameliorates glucose tolerance in diabetic patients and suggest that HBOT could be used as a therapeutic intervention for type 2 diabetes.

**Keywords**
Glucose tolerance • Hyperbaric oxygen therapy • Type 2 diabetes

## 24.1 Introduction

Metabolic diseases, like type 2 diabetes, obesity and the metabolic syndrome, affect millions of individuals globally, contributing to significant morbidity and mortality worldwide. This represents an alarming health problem with severe economical and social repercussions, being urgent to identify prevention strategies and treatment interventions that would help to stem this epidemic.

Hyperbaric oxygen therapy (HBOT) is a well-established treatment for decompression sickness and other conditions like carbon monoxide intoxication, infections, arterial gas embolism, radio-induced lesions and delayed wound healing as a result of diabetes or arteriosclerosis. In a hyperbaric chamber, patients breathe pure oxygen (100 %) and the air pressure is raised up to two and a half times higher than at the sea level air pressure allowing lungs to gather more oxygen than would be possible breathing pure oxygen at sea level air pressure (Al-Waili et al. 2006).

The maximum duration and working pressure in routine sessions of HBOT are 90 min at 2.5 atmospheres, in order to prevent the occurrence of toxic neurological and respiratory effects of hyperoxia (Al-Waili et al. 2006).. The benefits of HBOT are well documented in diabetic patients with foot ulcers (Desola et al. 1998). Additionally, there is some evidence that HBOT improves fasting glycemia by 20 % in type 2 diabetes patients (Desola et al. 1998; Ekanayake and Doolette 2001; Karadurmus et al. 2010; Wilkinson et al. 2012) and that lowers C-reactive protein and insulin resistance in diabetic patients (Ekanayake and Doolette 2001; Chateau-Degat and Belley 2012) without changing insulin levels (Desola et al. 1998). Moreover, it has been seen that HBOT significantly decreases systolic blood pressure, both in type 2 diabetes and in hypertensive patients (Peleg et al. 2013). In contrast, severe side effects of HBOT such as oxidative stress and oxygen toxicity have also been described, leading inclusively to cytotoxic effects in the beta cell and hyperglycemia (Matsunami et al. 2008).

One of the reasons that can account for these contradictory effects is the duration of HBOT protocol: while some authors have performed an acute HBOT protocol (Desola et al. 1998; Peleg et al. 2013), others submit patients to 90 min HBOT sessions during 2 weeks (Wilkinson et al. 2012) or 2 h during 5 weeks (Chateau-Degat and Belley 2012). Also, the majority of these studies included a very small number of type 2 diabetes patients and some of them reported that the decrease in blood glucose is not related with HBOT.

Recently we described that the carotid bodies (CB), peripheral chemoreceptors that classically respond to hypoxia, are involved in the development of insulin resistance and hypertension associated with the consumption of hypercaloric diets and sedentary lifestyles (Ribeiro et al. 2013). We have observed that CB activity was increased in animal models of metabolic syndrome and type 2 diabetes and that the abolishment of CB activity

through the resection of its sensitive nerve, the carotid sinus nerve, prevents the development of insulin resistance and hypertension induced by hypercaloric diets (Ribeiro et al. 2013). Knowing that CB activity is functionally blocked by hyperoxia herein we investigated the effect of HBOT on glucose tolerance in type 2 diabetes patients.

## 24.2 Methods

Volunteers with indication for HBOT were recruited at the Subaquatic and Hyperbaric Medicine Center of the Portuguese Navy. Written informed consent was obtained from all individuals and the study was approved by the Ethical Committee of the Portuguese Navy Hospital. Volunteers were divided into two groups: type 2 diabetes patients and control. Inclusion criteria for the group with diabetes mellitus were those defined by the American Diabetes. Association in 2010: HbA1C ≥6.5 % or FPG ≥126 mg/dl or 2-h plasma ≥200 mg/dl during an OGTT or in a patient with classic symptoms of hyperglycemia or hyperglycemic crisis, a random plasma glucose ≥200 mg/dl. Exclusion criteria were respiratory disease, renal disease and psychiatric illness previously identified. Indications for HBOT included sudden deafness, radio-induced cystitis and diabetic foot ulcers for the type 2 diabetes group. No medications were changed during the study.

Anthropometric data, like weight, height and abdominal perimeter were collected from all volunteers. All patients performed a daily HBOT sessions protocol, five times a week for a total of 20 sessions. Each session lasted for 100 min, comprising two periods of 35 min breathing 100 % oxygen at 2.5 absolute atmospheres separate by a 5 min air break interval or 70 min, plus 25 min for compression and decompression. Patients were submitted to an Oral Glucose Tolerance Test (OGTT) in two different time points: before initiating the HBOT protocol and after completing 20 HBOT sessions. The OGTT consisted in the administration of a beverage with orange flavour containing 75 g glucose (Top Star 75, Toplabs, Portugal) and the measurement of blood glucose immediately before and two hours after ingestion.

Data were presented as mean values with their standard errors, unless stated otherwise. Normally distributed variables were analysed using unpaired Student's t-test while non-normally distributed variables were compared using the Mann-Whitney U-test. Differences were considered significant at $P<0.05$. The significance of the differences between the mean values was calculated by two-way ANOVA with Bonferroni multiple comparison test. GraphPad Prism version 4 (GraphPad Software Inc., San Diego, CA, USA) was used to perform statistical analysis.

## 24.3 Results

The study was conducted in 32 patients (Table 24.1): 16 controls (non-type 2 diabetes patients – control group) and 16 type 2 diabetes patients (study group). Demographic and baseline patient characteristics are presented in Table 24.1. Body mass index were not different between the control and study group, however individuals with type 2 diabetes had a higher abdominal perimeter ($p<0.01$). As depicted in Table 24.1, fasting plasma glucose was significantly higher in type 2 diabetes patients than in controls (controls = 92.15 ± 3.68 mg/dl, diabetes = 143.5 ± 12.62 mg/dl). HBOT did not change fasting glucose levels in control subjects, but it decreased these levels to 119.1 ± 4.80 mg/dl in type 2 diabetes patients, however without reaching statistical significance ($p=0.089$) (Fig. 24.1). Additionally, in control subjects, plasma glucose

**Table 24.1** Comparison between demographic and baseline variables in controls and type 2 diabetes patients

| Parameters | Non-type-2-diabetes | Type 2 diabetes | p-value |
|---|---|---|---|
| n | 16 | 16 | |
| Male | 11 | 15 | |
| Age (years) | 58 (52,64) | 64 (58,69) | NS |
| Body mass index (kg $m^{-2}$) | 25 (23,28) | 26 (24,28) | NS |
| Abdominal perimeter (cm) | 91 (83,98) | 110 (96,124) | <0.01 |
| Fasting glucose levels (mg/dl) | 92.15 ± 3.68 | 143.5 ± 12.62 | <0.001 |

Data are expressed has mean (95%CI) or as mean ± SEM. NS, nonsignificant (P > 0.05); n, number of patients

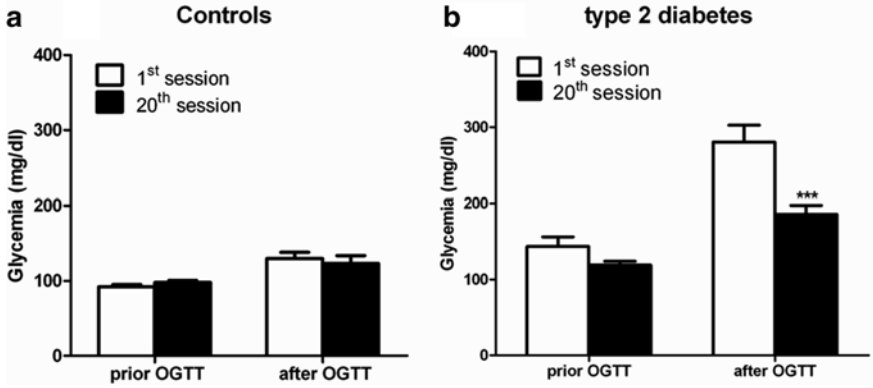


**Fig. 24.1** Effect of 20 sessions of hyperbaric oxygen therapy in glucose tolerance in controls and type 2 diabetes patients. Glucose tolerance was assessed through an oral glucose tolerance test (OGTT), which consisted in the oral administration of a glucose drink containing 75 g glucose and measurement of blood glucose before and 2 h after ingestion. All patients performed a hyperbaric oxygen protocol of 100 % oxygen at 2.5 absolute atmospheres for 60 min five times a week for a total of 20 sessions. Data are means ± S.E.M. ***$p < 0.001$ compared with values in the 1st hyperbaric oxygen therapy session (two-way ANOVA with Bonferroni multicomparison test)

levels measured 2 h after an OGTT were not different at the 1st and 20th session of hyperbaric oxygen therapy (Fig. 24.1a).

In contrast, glycemia measured 2 h after the ingestion of 75 g of glucose significantly decreased from 280.25 ± 22.29 mg/dl to 185.78 ± 11.70 mg/dl after 20 sessions of HBOT in type 2 diabetes patients (Fig. 24.1b).

## 24.4 Discussion

Our study indicates that hyperbaric oxygen therapy (HBOT) ameliorates glucose tolerance in type 2 diabetes patients. The effect of HBOT in glucose tolerance is powerful as it accompanies the previously described hypoglycaemic effect of this intervention in fasting plasma glucose. Additionally we show that HBOT did not alter glucose homeostasis in control subjects.

In the last decade several studies have demonstrated that HBOT improves fasting plasma glucose (Desola et al. 1998; Ekanayake and Doolette 2001; Karadurmus et al. 2010; Wilkinson et al. 2012) and insulin sensitivity in type 2 diabetes patients (Ekanayake and Doolette 2001; Chateau-Degat and Belley 2012), however without modifying HbA1c (Chateau-Degat and Belley 2012), Herein we showed that 20 sessions of HBOT decreased fasting glucose levels by 21 %, being this value in agreement with the literature (Desola et al. 1998; Ekanayake and Doolette 2001; Karadurmus et al. 2010; Wilkinson et al. 2012). Additionally we also show, for the first time, that HBOT ameliorates glucose tolerance in type 2 diabetic patients by 34 %, meaning that HBOT was capable of improving the ability of the body to stimulate glucose metabolism, either by increasing glucose uptake or glucose oxidation in the post-prandial state. Although glucose tolerance and insulin sensitivity are not the same, they are positively correlated and this improvement in glucose tolerance is probably due to an increase in insulin sensitivity, since it was already observed that HBOT does not change insulin secretion (Desola et al. 1998). Herein we did not observe any effect of HBOT either in fasting glucose levels or in glucose tolerance in control subjects. However, our results disagree with the previous findings of Peleg et al. (2013) and Wilkinson et al. (2012) in which a decrease in fasting glucose levels and in HbA1c in control subjects was observed.

In the present manuscript the mechanisms underlying the effect of HBOT in glucose tolerance in type 2 diabetes patients were not tested, although it was previously shown in diabetic rats that exposure to HBOT improves glucose and

lipid oxidative metabolism in skeletal muscle (Fujita et al. 2012). Another plausible mechanism of action for HBOT on glucose tolerance is the inhibition of the carotid body (CB) chemoreceptors. It is known that hyperoxia blunts the peripheral chemoreceptor activity (Fidone and Gonzalez 1986) and we have recently described that the CB is a powerful glucose and insulin sensor and that surgical ablation of its sensitive nerve prevents the development of diet-induced metabolic diseases (Ribeiro et al. 2013). Therefore we postulate that the functional inhibition of CB chemoreceptor activity obtained by exposure to HBOT accounts for the improvement in glucose tolerance observed in type 2 diabetes patients. Hyperoxia is commonly used to acutely block the CB chemoreceptors and in fact it was recently seen that deactivation of CB chemoreceptors by hyperoxia decreases blood pressure in hypertensive patients (Sinski et al. 2014).

We can conclude that HBOT improves both fasting glycemia and glucose tolerance in type 2 diabetes patients suggesting a novel application for this technology as a therapeutic intervention for controlling post-prandial glucose excursions in type 2 diabetes.

## References

Al-Waili NS, Butler GJ, Beale J, Abdullah MS, Finkelstein M, Merrow M, Rivera R, Petrillo R, Carrey Z, Lee B, Allen M (2006) Influences of hyperbaric oxygen on blood pressure, heart rate and blood glucose levels in patients with diabetes mellitus and hypertension. Arch Med Res 37:991–997

Chateau-Degat ML, Belley R (2012) Hyperbaric oxygen therapy decreases blood pressure in patients with chronic wounds. Undersea Hyperb Med 39:881–889

Desola J, Crespo A, Garcia A, Salinas A, Sala J, Sánchez U (1998) Indicaciones y contraindicaciones de la oxigenoterapia hiperbárica. JANO/Medicina LIV(1260):5–11

Ekanayake L, Doolette DJ (2001) Effects of hyperbaric oxygen treatment on blood sugar levels and insulin levels in diabetics. SPUMS 31:16–20

Fidone SJ, Gonzalez C (1986) Initiation and control of chemoreceptor activity in the carotid body. In: Cherniack NS, Widdicombe JG (eds) Handbook of physiology, Section 3, The respiratory system, vol II, Control of breathing, Part 1. American Physiological Society, Bethesda, pp 247–312

Fujita N, Nagatomo F, Murakami S, Kondo H, Ishihara A, Fujino H (2012) Effects of hyperbaric oxygen on metabolic capacity of the skeletal muscle in type 2 diabetic rats with obesity. ScientificWorldJournal 637978

Karadurmus N, Sahin M, Tasci C, Naharci I, Ozturk C, Ilbasmis S, Dulkadir Z, Sen A, Saglam K (2010) Potential benefits of hyperbaric oxygen therapy on atherosclerosis and glycemic control in patients with diabetic foot. Endokrynol Pol 61:275–279

Matsunami T, Sato Y, Morishima T, Mano Y, Yukawa M (2008) Enhancement of glucose toxicity by hyperbaric oxygen exposure in diabetic rats. J Exp Med 216:127–132

Peleg RK, Fishlev G, Bechor Y, Bergan J, Friedman M, Koren S, Tirosh A, Efrati S (2013) Effects of hyperbaric oxygen on blood glucose levels in patients with diabetes mellitus, stroke or traumatic injury and healthy volunteers: a prospective, crossover, controlled trial. Diving Hyperb Med 43:218–221

Ribeiro MJ, Sacramento JF, Gonzalez C, Guarino MP, Monteiro EC, Conde SV (2013) Carotid body denervation prevents the development of insulin resistance and hypertension induced by hypercaloric diets. Diabetes 62:2905–2916

Sinski M, Lewandowski J, Przybylski J, Zalewski P, Symonides B, Abramczyk P, Gaciong Z (2014) Deactivation of carotid body chemoreceptors by hyperoxia decreases blood pressure in hypertensive patients. Hypertens Res 37:858–862

Wilkinson D, Chapman IM, Heilbronn LK (2012) Hyperbaric oxygen therapy improves peripheral insulin sensitivity in humans. Diabet Med 29:986–989

# Possible Role of TRP Channels in Rat Glomus Cells

25

Insook Kim, Lasha Fite, David F. Donnelly, Jung H. Kim, and John L. Carroll

**Abstract**

Carotid body (CB) glomus cells depolarize in response to hypoxia, causing a $[Ca^{2+}]_i$ increase, at least in part, through activation of voltage-dependent channels. Recently, Turner et al. (2013) showed that mouse glomus cells with knockout of TASK1/3$^{-/-}$ channels have near-normal $[Ca^{2+}]_i$ response to hypoxia. Thus, we postulated that TRP channels may provide an alternate calcium influx pathway which may be blocked by the TRP channel antagonist, 2-APB (2-aminoethoxydiphenylborane). We confirmed that 2-APB inhibited the afferent nerve response to hypoxia, as previously reported (Lahiri S, Patel G, Baby S, Roy A (2009) 2-APB mediated effects on hypoxic calcium influx in rat carotid body glomus cells. FASEB 2009, Abstract, LB157; Kumar P, Pearson S, Gu Y (2006) A role for TRP channels in carotid body chemotransduction? FASEB J 20:A12–29). To examine the mechanism for this inhibition, we examined dissociated rat CB glomus cells for $[Ca^{2+}]_i$ responses to hypoxia, anoxia (with sodium dithionite), 20 mM $K^+$, NaSH, NaCN, and FCCP in absence/presence of 2-APB (100 μM). Also the effect of 2-APB on hypoxia and/or anoxia were investigated on NADH and mitochondria (MT) membrane potential. Our findings are as follows: (1) 2-APB significantly blocked the $[Ca^{2+}]_i$ increase in response to hypoxia and anoxia, but not the responses to 20 mM $K^+$. (2) The $[Ca^{2+}]_i$ responses NaSH, NaCN, and FCCP were significantly blocked by 2-APB. (3) Hypoxia-induced increases in NADH/$NAD^+$ and MT membrane depo-

I. Kim (✉) • L. Fite • J.L. Carroll
Pediatrics, University of Arkansas for Medical Sciences, Little Rock, AR, USA
e-mail: kiminsook@uams.edu; jlfite@uams.edu; CarrollJohnL@uams.edu

D.F. Donnelly
Pediatrics, Yale University School of Medicine, New Haven, CT, USA
e-mail: david.donnelly@yale.edu

J.H. Kim
System Engineering, University of Arkansas, Little Rock, AR, USA
e-mail: jhkim@ualr.edu



C. Peers et al. (eds.), *Arterial Chemoreceptors in Physiology and Pathophysiology*, Advances in Experimental Medicine and Biology 860, DOI 10.1007/978-3-319-18440-1_25

larization were not effected by 2-APB. Thus TRP channels may provide an important pathway for calcium influx in glomus cells in response to hypoxia.

**Keywords**
Carotid body • Glomus cells • TRP channels • 2-APB • $[Ca^{2+}]_i$ • NADH/$NAD^+$ • Mitochondria (MT) membrane potential

## 25.1 Introduction

Carotid body glomus cells respond to acute hypoxia by cell membrane depolarization and an increase in intracellular calcium ($[Ca^{2+}]_i$) mediated by voltage gated calcium channels and partially by $Ca^{2+}$ release from store-operated $Ca^{2+}$ channels (Lahiri et al. 1996). Much experimental work supported the postulate that the depolarization is mediated by hypoxia-induced closure of 'leak' $K^+$ channels, subsequently identified as belonging to the TASK1/TASK3 family of leak channels (Kim et al. 2009; Williams and Buckler 2004). However, glomus cells from genetically modified mice lacking both TASK1 and TASK3 exhibit a near-normal hypoxia-induced increase in intracellular calcium and a normal hypoxia-induced catecholamine release (Turner and Buckler 2013). These findings suggest that other calcium influx pathways may play a critical role in mediating calcium influx into these cells during hypoxia.

This pathway may potentially be mediated by TRP channels. Transient receptor potential (TRP) channels are relatively non-selective ion channels enabling the exchange of cations and enable the intracellular rise in $Na^+$ and/or $Ca^{2+}$ concentration to broad range of stimuli and ultimately cell membrane depolarization. Immunocytochemical staining demonstrated that rat glomus cells express six members of the TRPC family of channels (Buniel et al. 2003), and previous work has indicated that inhibition of TRP channels reduces the hypoxia-induced increase in chemoreceptor afferent activity (Lahiri et al. 2009; Kumar et al. 2006). Our present work examined the effect of TRP channel blockade on the hypoxia-induced increase in glomus cell $[Ca^{2+}]_i$ and the potential effects of TRP channel blockade on mitochondrial function, as mitochondria appear to be the sensing site for hypoxia.

## 25.2 Methods

### 25.2.1 Animal Model

The use of animals in this study was approved by the Animal Care and Use Committee of the University of Arkansas for Medical Sciences. Experiments were conducted on Sprague-Dawley rat pups of both sexes. Carotid bodies were harvested from rats aged 14–18 days functionally mature.

### 25.2.2 Carotid Body Cell Isolation

Rat pups were anesthetized with isoflurane, decapitated, and the heads placed in ice-cold buffered saline solution (BSS). Whole CBs were dissected out and placed in ice-cold low $Ca^{2+}$/$Mg^{2+}$ BSS. Isolated CBs were dissociated with enzyme cocktail containing trypsin and collagenase by incubating at 37 °C for 20–25 min. Dissociated CB cells were placed on poly-D-lysine coated glass coverslips and incubated (>3 h) in CB growth medium at 37 °C until use. Glomus cells were identified by positive binding to fluorescent-labeled peanut agglutinin (Kim et al. 2009).

### 25.2.3 Intracellular Calcium Measurement

Intracellular $Ca^{2+}$ ($[Ca^{2+}]_i$) concentration was measured using the fura-2. Plated CB cells were loaded with fura-2 AM (Molecular Probes) for 30 min at 37 °C in 21% $O_2$/5% $CO_2$. Fura-2 fluorescent emission was measured at 510 nm in response to alternating excitation at 340 and 380 nm. Images were acquired and stored using a NIKON TE300 microscope and CCD (CoolSNAP HQ2) camera under computer control (Metafluor). For $[Ca^{2+}]_i$, the background light levels were subtracted from each image before measurement of fluorescence intensity. $[Ca^{2+}]_i$ was determined using the 340/380 fluorescence ratio as described previously (Wasicko et al. 1999). Calibration was performed using cell-free solutions.

### 25.2.4 Autofluorescence (NADH) Measurement

NADH is autofluorescent while the oxidized form $NAD^+$ is not autofluorescent. Thus, the relative NADH/$NAD^+$ may be measured without using any fluorophore dyes (Duchen and Biscoe 1992a). Autofluorescence was measured by using 360 nm excitation and 460 m emission filters. Images were acquired and stored using a Nikon TE300 inverted microscope with oil-emersion objective and using cooled CCD camera under computer control (Metafluor).

### 25.2.5 Mitochondria Membrane Potential ($\Delta\psi_m$)

Mitochondria membrane potential ($\Delta\psi_m$) was monitored by using rhodamine 123 (Rhod123) Cells were incubated with 10 μg/ml Rhod123 in the culture medium for 30 min at RT (Duchen and Biscoe 1992b). Rhod123 fluorescence was excited at 490 nm and measured at 525 nm. Images were acquired and stored using a Nikon TE300 inverted microscope with oil-emersion objective and using cooled CCD camera under computer control (NIS Element).

## 25.3 Results

### 25.3.1 Effect of 2-APB on the CB Glomus Cell $[Ca^{2+}]_i$ Response

The hypoxia induced increase of calcium in glomus cells were measured in the absence and presence of 2-APB (100 μM), a broad spectrum TRP channel blocker. 2-APB significantly reduced the $[Ca^{2+}]_i$ response to hypoxia (0 % $O_2$) and anoxia (0 % $O_2$ with dithionite) after CB glomus cells were pre-treated with 2-APB for 5 min prior to exposure to hypoxia and anoxia (Fig. 25.1a and b). On the other hand, 2-APB did not inhibit the calcium response to 20 mM KCl, demonstrating the drug did not block voltage-gated calcium channel or the ability of the cell to depolarize. Other chemoreceptor stimuli, notably mitochondrial poisons NaCN (100 μM), FCCP (1 μM), and recently-proposed transmitter $H_2S$ (100 μM NaSH), also increased glomus cell calcium levels which was significantly blocked by application of 2-APB (Fig. 25.1c, d, and e).

### 25.3.2 Effect of 2-APB on Mitochondria Response to Hypoxia

Mitochondria appear to be the sensing site for hypoxia in the carotid body, since their mitochondria depolarize and redox states increase at oxygen levels consistent the increase in intracellular calcium. In order to observe the effect of 2-APB (100 μM) on increased mitochondria (MT) response to hypoxia (0 % $O_2$), cells were pre-treated with 2-APB for 5 min prior to exposure to hypoxia in presence of 2-APB (100 μM). For the MT response, autofluorescence derived from mitochondrial NADH was measured and the changes of MT membrane potential ($\Delta\psi_m$) were measured by monitoring Rhod123 fluorescence intensity. As positive controls for autofluorescence and Rhod123 fluorescence, the stimulants of MT, NaCN (100 μM) and FCCP (0.5 μM), were tested at the end of each experiment respectively (Wyatt and Buckler 2004). Neither the

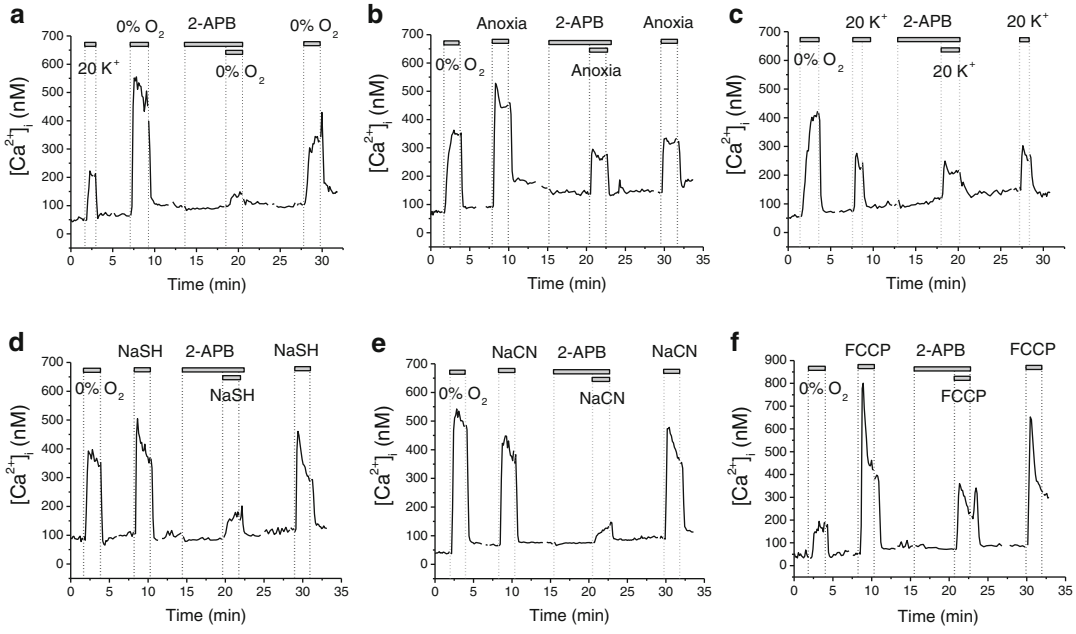


**Fig. 25.1** The Effects of 2-APB on $[Ca^{2+}]_i$ Response to hypoxia (0 % $O_2$) (**a**), anoxia (**b**), 20 mM KCl (**c**), NaSH (100 μM) (**d**), NaCN (100 μM) (**e**), and FCCP (1 μM) (**f**) after 5 min 2-APB preconditioning. These are representative averaged traces

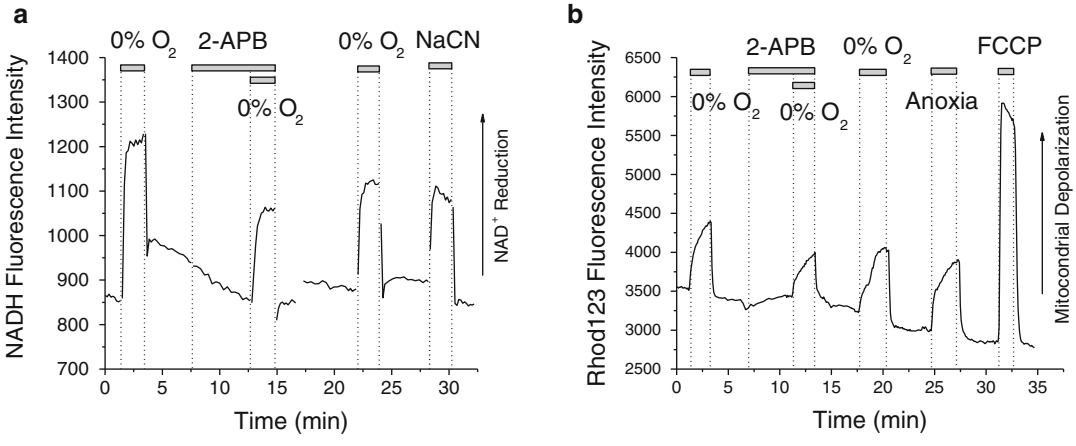


**Fig. 25.2** The Effects of 2-APB (100 μM) on hypoxia (0 % $O_2$)-induced NADH fluorescence (**a**) and Rhod123 fluorescence (**b**) intensity after 5 min 2-APB preconditioning. NaCN (100 μM) and FCCP (0.5 μM) were used as positive control. These are representative averaged traces

increased autofluorescence intensity (NADH/$NAD^+$ ratio) (Fig. 25.2a) nor the increased Rhod123 fluorescence (Fig. 25.2b) intensity induced by hypoxia and anoxia were significantly effected by 2-APB (100 μM).

## 25.4 Discussion

The main implication from our ongoing studies is that TRP channels may provide an important pathway for the influx of calcium into glomus

cells during hypoxia. We demonstrate that blockade of TRP channels with 2-APB, broad spectrum blocker, greatly impairs the hypoxia or anoxia-induced increase in calcium in these cells. This demonstration is consistent with previous work which demonstrated an impairment of the afferent nerve response to hypoxia by 2-APB (Lahiri et al. 2009; Kumar et al. 2006).

TRP channels represent a wide spectrum of channels which are generally selective to cations. They are implicated in playing an important role in some oxygen sensing tissue. For instance, TRPC6 plays a role in mediating hypoxic pulmonary constriction (Malczyk et al. 2013; Weissmann et al. 2006). Immunocytochemical studies demonstrate that the carotid body expresses multiple subtypes of TRP channels, which includes six of seven subtypes of the TRP C family (Buniel et al. 2003), including TRPC6.

The need to look for alternate calcium influx pathways stems from recent results using genetically engineered mice. Over the past 10 years, a strong hypothesis for the mechanism of hypoxia-induced increase in calcium has been the closure of a 'leak' $K^+$ channel by hypoxia. Subsequent works by us and others have identified the leak channel to be a heterodimer of TASK1 and TASK3 with a limited expression of homodimer of TASK 1 and TASK3 (Kim et al. 2009; Williams and Buckler 2004). This identity was recently confirmed by Turner who demonstrated a near lack of leak channel activity in glomus cells harvested from mice lacking both TASK1 and TASK3 (Turner and Buckler 2013). Surprisingly, glomus cells of these mice showed near-normal calcium responses to hypoxia. While this may have been due to a compensatory expression of other leak channels, cell attached recording failed to detect other leak channel activity, suggesting that another transduction pathway is present and fully capable of accounting for the glomus cell $[Ca^{2+}]_i$ response to hypoxia.

Our ongoing experiments demonstrate that TRP channels may be an essential element of this pathway since the calcium response to hypoxia and anoxia was greatly inhibited by 2-APB. Similarly, the calcium influx caused by mitochondrial poisons, FCCP and cyanide is also inhibited by 2-APB. We also tested the effect of 2-APB on the response to $H_2S$. $H_2S$ has been postulated to be generated in glomus cells and the generation rate to be increased by hypoxia. Exogenous $H_2S$ is excitatory to afferent nerve activity and knockout of enzymes which generate $H_2S$ reduces the afferent nerve response to hypoxia (Makarenko et al. 2012; Prabhakar 2012). Thus, $H_2S$ has been postulated to be an important or essential transmitter or mediator of the hypoxia response. However, this has been called into question as many of the actions of $H_2S$ may be accounted for by its inhibition of mitochondrial function. In any case, we demonstrate that $H_2S$ increases the level of intracellular calcium in glomus cells and this increase is significantly inhibited by 2-APB.

Although 2-APB inhibited calcium influx caused by a multiple of stimuli, it had little effect on mitochondrial function. Neither mitochondrial membrane potential nor cellular redox state ($NADH/NAD^+$ ratio) was directly affected by 2-APB treatment. Since mitochondria appear to be the site of oxygen sensing, these results suggest that mitochondria are not directly effected by 2-APB or indirectly effected by metabolic changes. For instance, if 2-APB reduced cellular respiration, $NADH/NAD^+$ would be expected to increase, as was observed during metabolic inhibition with cyanide.

In conclusion, our results indicate an important and perhaps critical role of TRP channels in mediating the carotid body response to hypoxia. It opens the door to multiple questions such as the family and subfamily of channel involved in the transduction process. This identification would be facilitated by the development of drugs which target subfamilies of TRP channels, but, at present, these are generally unavailable. In addition, the mechanism of channel modulation through changes in mitochondrial state or respiration is unexplored, but should be a worthwhile direction in our future studies.

**Acknowledgements** This study was supported by Dr. Carroll FY13 SAF Bridging fund and ABI Project fund from ACHRI.

## References


Buniel MC, Schilling WP, Kunze DL (2003) Distribution of transient receptor potential channels in the rat carotid chemosensory pathway. J Comp Neurol 464:404–413

Duchen MR, Biscoe TJ (1992a) Mitochondrial function in type I cells isolated from rabbit arterial chemoreceptors. J Physiol 450:13–31

Duchen MR, Biscoe TJ (1992b) Relative mitochondrial membrane potential and $[Ca^{2+}]_i$ in type I cells isolated from the rabbit carotid body. J Physiol 450:33–61

Kim D, Cavanaugh EJ, Kim I, Carroll JL (2009) Heteromeric TASK-1/TASK-3 is the major oxygen-sensitive background $K^+$ channel in rat carotid body glomus cells. J Physiol 587:2963–2975

Kumar P, Pearson S, Gu Y (2006) A role for TRP channels in carotid body chemotransduction? FASEB J 20:A12–29

Lahiri S, Patel G, Baby S, Roy A (2009) 2-APB mediated effects on hypoxic calcium influx in rat carotid body glomus cells. FASEB 2009, Abstract, LB157

Lahiri S, Osanai S, Buerk DG, Mokashi A, Chugh DK (1996) Thapsigargin enhances carotid body chemosensory discharge in response to hypoxia in zero $[Ca^{2+}]e$: evidence for intracellular $Ca^{2+}$ release. Brain Res 709(1):141–144

Makarenko VV, Nanduri J, Raghuraman G, Fox AP, Gadalla MM, Kumar GK, Snyder SH, Prabhakar NR (2012) Endogenous $H_2S$ is required for hypoxic sensing by carotid body glomus cells. Am J Physiol Cell Physiol 303:C916–C923

Malczyk M, Veith C, Fuchs B, Hofmann K, Storch U, Schermuly RT, Witzenrath M, Ahlbrecht K, Fecher-Trost C, Flockerzi V et al (2013) Classical transient receptor potential channel 1 in hypoxia-induced pulmonary hypertension. Am J Respir Crit Care Med 188:1451–1459

Prabhakar NR (2012) Endogenous $H_2S$ is required for hypoxic sensing by carotid body glomus cells. Am J Physiol Cell Physiol 303:C916–C923

Turner PJ, Buckler KJ (2013) Oxygen and mitochondrial inhibitors modulate both monomeric and heteromeric TASK-1 and TASK-3 channels in mouse carotid body type-1 cells. J Physiol 591:5977–5998

Wasicko MJ, Sterni LM, Bamford OS, Montrose MH, Carroll JL (1999) Resetting and postnatal maturation of oxygen chemosensitivity in rat carotid chemoreceptor cells. J Physiol 514(Pt 2):493–503

Weissmann N, Dietrich A, Fuchs B, Kalwa H, Ay M, Dumitrascu R, Olschewski A, Storch U, Mederos y Schnitzler M, Ghofrani HA (2006) Classical transient receptor potential channel 6 (TRPC6) is essential for hypoxic pulmonary vasoconstriction and alveolar gas exchange. Proc Natl Acad Sci U S A 103:19093–19098

Williams BA, Buckler KJ (2004) Biophysical properties and metabolic regulation of a TASK- like potassium channel in rat carotid body type-1 cells. Am J Physiol Lung Cell Mol Physiol 286 (1):L221–L230

Wyatt CN, Buckler KJ (2004) The effect of mitochondrial inhibitors on membrane currents in isolated neonatal rat carotid body type I cells. J Physiol 556:175–191

# Nitric Oxide Deficit Is Part of the Maladaptive Paracrine-Autocrine Response of the Carotid Body to Intermittent Hypoxia in Sleep Apnea

26

M.L. Fung

**Abstract**

The carotid body functions to maintain the blood gas homeostasis, whereas anomalous carotid chemoreceptor activities could be pathogenic in patients with sleep apnea. Recent findings suggest an upregulation of renin-angiotensin system (Lam SY, Liu Y, Ng KM et al. Exp Physiol 99:220–231, 2014), which could lead to inflammation in the carotid body during intermittent hypoxia (Lam SY, Liu Y, Ng KM et al. Histochem Cell Biol 137:303–317, 2012). In addition, the level of nitric oxide detected in the carotid body was significantly decreased following intermittent hypoxia for days. These locally regulated mechanisms are proposed to be a significant part of the hypoxia-mediated maladaptive changes of the carotid body, which could play a role in the pathophysiological cascade of sleep apnea in patients with an overactivity of the chemoreflex.

**Keywords**

Chemoreceptor • NO synthase • Obstructive sleep apnea

## 26.1 Introduction

The carotid body plays significant roles in the maintenance of the blood gases and pH homeostasis. Thus hypoxia increases the chemoreceptor discharge in the carotid body which stimulates the brainstem respiratory activities leading to a reflexive increase in respiratory rate. In addition, the carotid body plays important roles in cardiorespiratory changes in chronic and intermittent hypoxia (Gonzalez et al. 1994; Prabhakar et al. 2001). The hypoxic response of the carotid body is modulated by nitric oxide (NO), locally produced by NO synthase (NOS) located in nerve endings and vascular endothelium in the carotid body (Moya et al. 2012; Nurse 2014). Hence, NOS inhibition enhances the hypoxic response of the carotid body despite minimal effects on the resting activity (Chugh et al. 1994; Wang et al. 1994). We have shown an increase in endogenous NO level in the rat carotid body in acute hypoxia,

M.L. Fung (✉)
Department of Physiology, The University of Hong Kong, Pokfulam, Hong Kong, China
e-mail: fungml@hku.hk



C. Peers et al. (eds.), *Arterial Chemoreceptors in Physiology and Pathophysiology*,
Advances in Experimental Medicine and Biology 860, DOI 10.1007/978-3-319-18440-1_26

which is physiologically important to the inhibition of carotid chemoreceptor activity for a negative feedback control of the activity in hypoxia (Fung et al. 2001; Ye et al 2002). Reports have shown a significant decreased expression of the endothelial NOS (Del Rio et al. 2011) and neuronal NOS (Marcus et al. 2010) in the rat carotid body during weeks of intermittent hypoxia, suggesting that a role of NO in the augmented chemoreceptor activity. At present, there is a paucity of information on the endogenous NO release in the carotid body following chronic intermittent hypoxia. It was hypothesized that intermittent hypoxia induces a decrease in the endogenous NO produced by the rat carotid body.

## 26.2 Methods

The experimental protocol for this study was approved by the Committee on the Use of Live Animals in Teaching and Research of the University of Hong Kong. Male Sprague-Dawley rats (28-day-old, 70 g) were divided into normoxic (Nx) and intermittent hypoxic (IH) groups. The rat cages were kept in acrylic chambers under normobaric conditions and the rats had free access to water and chow. The Nx controls were kept in room air with maintenance matching the hypoxic group (Lam et al. 2012, 2014). For the IH group, the fractional amount of oxygen levels inside the chamber was altered between 21 and 5 ± 0.5 % per min, 60 cycles/h, 8 h per day diurnally. As a result, the inspired oxygen level fell to 4–5 % (nadir arterial oxygen saturation 70 %) for about 15 s/min, which mimicks the recurrent episodic hypoxemia in OSA patients (Fletcher 2001). Following deep anesthesia, the rat was decapitated and the carotid bifurcation was excised rapidly. The carotid body was carefully dissected free from the bifurcation in chilled rat Ringer's solution oxygenated with 95 % $O_2$ and 5 % $CO_2$. The carotid body was then incubated in a tissue bath with collagenase (0.06 %) and protease (0.02 %) in oxygenated Ringer's for 30 min at 35 ± 1 °C. The carotid body was then held in the recording chamber at 35 ± 1 °C, and superfused with oxygenated Ringer's solution at a flow rate of 2 ml/min.

The fabrication and calibration of the NO electrode has been described in previous reports (Fung et al. 2001; Ye et al 2002). Electrochemical experiments were performed on a CHI 660A Electrochemical Analyzer (CH Instruments, USA). The NO electrode was calibrated and the current was measured at a voltage of 0.85 V. The electrode and carotid body were equilibrated in the perfusate for 15–30 min. The tip of the NO electrode was gently inserted into the carotid body under visual guidance with a dissecting microscope. Following current recording in the resting condition for 10–15 min, the endogenous NO production was blocked by non-selective NO synthase (NOS) inhibitor $N^G$-Monomethyl-*L-arginine* acetate (LNMMA). For the drug treatment, LNMMA (100 uM) was added freshly to the Ringer's solution for the perfusion. Acute hypoxia was induced for 5 min followed by recovery for 20–30 min. Acute hypoxia was induced by switching the perfusate to Ringer's solution gassed with 95 % $N_2$ and 5 % $CO_2$. The rat Ringer's solution contained (mM): NaC1 125, KC1 3.1, $NaHCO_3$ 26, $NaH_2PO_4$ 1.25, $MgSO_4$ 1.3, $CaCl_2$ 2.4, D-Dextrose 10, pH at 7.35.

For the post-analysis of NO release, the resting and peak values of the current were subtracted and calibrated in NO concentration (nanomoles) according to the current response curve of the NO electrode. Values were presented as mean+/−SE. Means were compared with Student *t*-test or the non-parametric Wilcoxon signed-rank test. ANOVA with a post-hoc test (Dunnett's *t*-test) was used for multiple comparisons of values in studies among groups. Differences were considered significant at $P < 0.05$.

## 26.3 Results

In the presence of NOS inhibition by LNMMA (100 uM), the NO level was decreased by about 80 nM in the normoxic control but was significantly decreased by about 40 nM in the hypoxic groups (IH3, IH7, IH10 under intermittent hypoxia, respectively for 3, 7, 10 days) (Fig. 26.1). The decrease in the LNMMA-

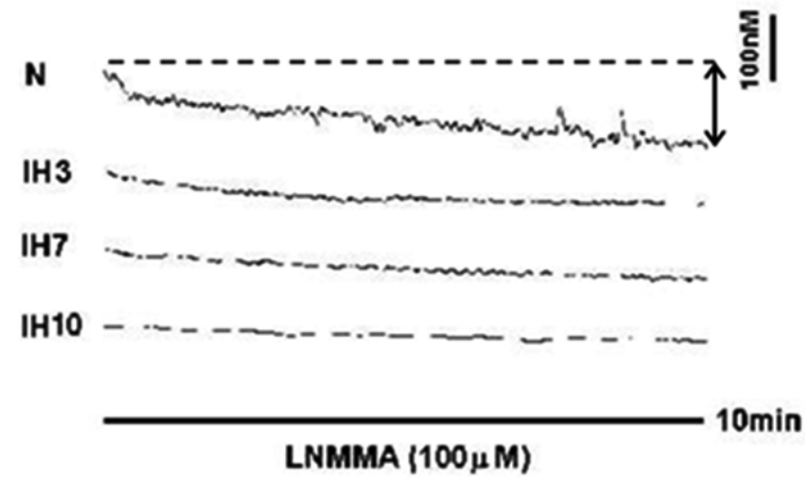


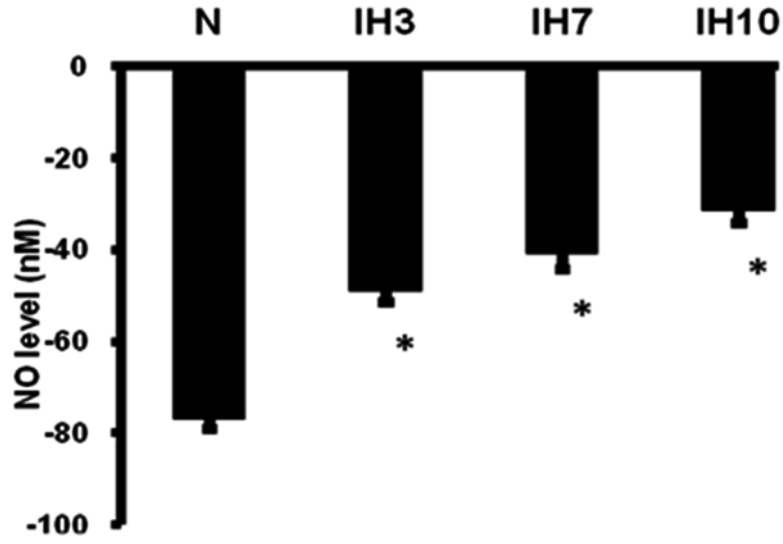


**Fig. 26.1** Current tracings of the NO level recorded from the rat carotid body from the normoxic (*N*) and hypoxic (*IH*) rats. Please note the downward shift of the tracings caused by an inhibition of NO synthase with LNMMA (*bold line*). A virtual baseline (*dash line*) was set for measuring the amount of current changes (*vertical bar with arrows*). The data are expressed as means plus S.E. (n = 6 for each group, * $p < 0.05$)

inhibited NO level was time-dependent to the days of hypoxic treatment (Fig. 26.1). In addition, the NO level elevated by acute hypoxia was about 180 nM in the normoxic control but was significantly lowered to 80 nM in the hypoxic groups (Fig. 26.2).

## 26.4 Discussion

The main finding is a significant decrease in the NO level detected in the rat carotid body following days of an intermittent hypoxic condition simulating a severe condition of obstructive sleep

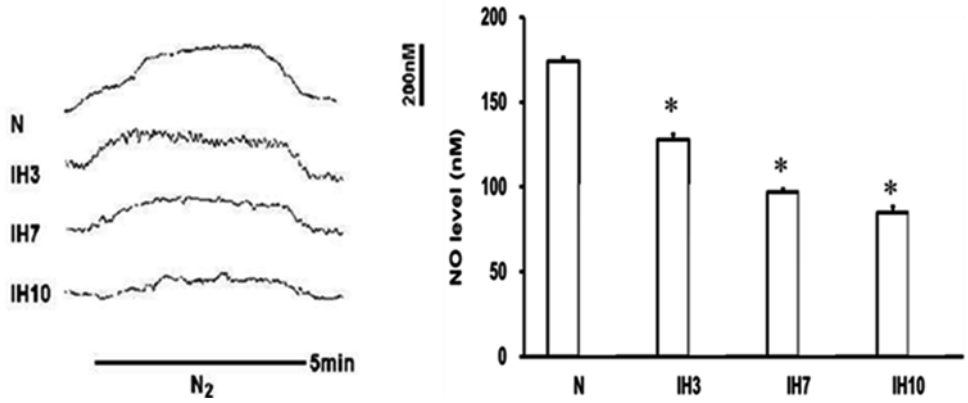


**Fig. 26.2** Current tracings of the NO level recorded from the rat carotid body from the normoxic (*N*) and hypoxic (*IH*) rats. The tracings were upwardly shifted in acute hypoxia ($N_2$, *bold line*). The elevated NO level was significantly less (n = 10 for each group, * $p < 0.05$) in the IH groups

apnea in patients with an apnea-hypoapnea index of 60. The observation is consistent with previous findings showing a significant decreased expression of the endothelial NOS (Del Rio et al. 2011) and neuronal NOS (Marcus et al. 2010) in the rat carotid body during weeks of intermittent hypoxia. The current recording by NO electrode is sensitive to NOS inhibition, supporting that the local NO production is specific to the NOS in the carotid body (Fung et al. 2001; Ye et al 2002). Taken together, evidence indicates a decreased NO bioavailability in the carotid body, which may play a pathogenic role in the overactivity of the chemoreceptor and chemoreflex activities in patients with sleep apnea.

The endogenous NO production is dependent on multiple sources, which could modulate the chemoreceptor activity. Activation of P2X receptors in the glossopharyngeal efferent fibres could lead to an inhibition of chemoreceptor activities via an NO mechanism (Campanucci et al. 2006; Nurse 2014). Altered autonomic efferent activities may be associated with a decrease in the nNOS-containing fibers for the NO release in the carotid body. In addition, calcium influx during hypoxia might activate the NO production in the glomic tissues but the precise mechanism if any alterations remain unclear. Also, vascular release of the NO from the endothelial cells is probably an alternative source, although it is not clear the extracellular ATP levels and the contribution of the endothelial P2X receptors to the NO elevation under hypoxic conditions. As a result of a decrease in the constitutive and hypoxia-induced production of NO in the carotid body, this could cause a disinhibition of the chemoreceptor activity, leading to an augmented activity under resting and hypoxic conditions. Thus, NO deficit could be a part of altered locally regulated mechanisms underlying the hypoxia-mediated maladaptive changes of the carotid body, which could play a role in the pathophysiological cascade of sleep apnea in patients with an overactivity of the chemoreflex.

**Acknowledgements** I thank Ms Meifang Li and Mr Y. M. Lo for their technical assistance. Studies were supported by grants from the Research Grants Council, Hong Kong (Grant No. HKU 766110 M, HKU 7510/06 M) and internal funding and conference grant from the University Research Committee, The University of Hong Kong.

## References

Campanucci VA, Zhang M, Vollmer C, Nurse CA (2006) Expression of multiple P2X receptors by glossopharyngeal neurons projecting to rat carotid body O2-chemoreceptors: role in nitric oxide-mediated efferent inhibition. J Neurosci 26:9482–9493

Chugh DK, Katayama M, Mokashi A, Bebout DE, Ray DK, Lahiri S (1994) Nitric oxide-related inhibition of carotid chemosensory nerve activity in the cat. Respir Physiol 97:147–156

Del Rio R, Moya EA, Iturriaga R (2011) Differential expression of pro-inflammatory cytokines, endothelin-1 and nitric oxide synthases in the rat carotid body exposed to intermittent hypoxia. Brain Res 1395:74–85

Fletcher EC (2001) Invited review: Physiological consequences of intermittent hypoxia: systemic blood pressure. J Appl Physiol 90:1600–1605

Fung ML, Ye JS, Fung PC (2001) Acute hypoxia elevates nitric oxide generation in rat carotid body in vitro. Pflugers Arch 442:903–909

Gonzalez C, Almaraz L, Obeso A, Rigual R (1994) Carotid body chemoreceptors: from natural stimuli to sensory discharges. Physiol Rev 74:829–898

Lam SY, Liu Y, Ng KM et al (2012) Chronic intermittent hypoxia induces local inflammation of the rat carotid body via functional upregulation of proinflammatory cytokine pathways. Histochem Cell Biol 137:303–317

Lam SY, Liu Y, Ng KM et al (2014) Up-regulation of a local renin-angiotensin system in the carotid body during chronic intermittent hypoxia. Exp Physiol 99:220–231

Marcus NJ, Li YL, Bird CE, Schultz HD, Morgan BJ (2010) Chronic intermittent hypoxia augments chemoreflex control of sympathetic activity: role of the angiotensin II type 1 receptor. Respir Physiol Neurobiol 171(1):36–45

Moya EA, Alcayaga J, Iturriaga R (2012) NO modulation of carotid body chemoreception in health and disease. Respir Physiol Neurobiol 184(2):158–164

Nurse CA (2014) Synaptic and paracrine mechanisms at carotid body arterial chemoreceptors. J Physiol 592(16):3419–3426

Prabhakar NR, Fields RD, Baker T, Fletcher EC (2001) Intermittent hypoxia: cell to system. Am J Physiol Lung Cell Mol Physiol 281:L524–L528

Wang ZZ, Stensaas LJ, Bredt DS, Dinger B, Fidone SJ (1994) Localization and actions of nitric oxide in the cat carotid body. Neuroscience 60:275–286

Ye JS, Tipoe GL, Fung PC, Fung ML (2002) Augmentation of hypoxia-induced nitric oxide generation in the rat carotid body adapted to chronic hypoxia: an involvement of constitutive and inducible nitric oxide synthases. Pflugers Arch 444:178–185

# Respiratory Control in the *mdx* Mouse Model of Duchenne Muscular Dystrophy

27

David P. Burns, Deirdre Edge, Dervla O'Malley, and Ken D. O'Halloran

**Abstract**

Duchenne muscular dystrophy (DMD) is a genetic disease caused by defects in the dystrophin gene resulting in loss of the structural protein dystrophin. Patients have reduced diaphragm functional capacity due to progressive muscle weakness. Respiratory morbidity in DMD is further characterised by hypoxaemic periods due to hypoventilation. DMD patients die prematurely due to respiratory and cardiac failure. In this study, we examined respiratory function in young adult male *mdx* (dystrophin deficient) mice (C57BL/10ScSn-Dmd$^{mdx}$/J; n = 10) and in wild-type controls (WT; C57BL/10ScSnJ; n = 11). Breathing was assessed in unrestrained, unanaesthetised animals by whole-body plethysmography. Ventilatory parameters were recorded during air breathing and during exposure to acute hypoxia ($F_iO_2 = 0.1$, 20 min). Data for the two groups of animals were compared using Student's *t* tests. During normoxic breathing, *mdx* mice had reduced breathing frequency ($p = 0.011$), tidal volume ($p = 0.093$) and minute ventilation ($p = 0.033$) compared to WT. Hypoxia increased minute ventilation in WT and *mdx* animals. *Mdx* mice had a significantly increased ventilatory response to hypoxia which manifest as an elevated % change from baseline for minute ventilation ($p = 0.0015$) compared to WT. We conclude that *mdx* mice have impaired normoxic ventilation suggestive of hypoventilation. Furthermore, *mdx* mice have an enhanced hypoxic ventilatory response compared to WT animals which we speculate may be secondary to chronic hypoxaemia. Our results indicate that a significant respiratory phenotype is evident as early as 8 weeks in the *mdx* mouse model of DMD.

D.P. Burns (✉) • D. Edge • D. O'Malley
K.D. O'Halloran
Department of Physiology, School of Medicine,
University College Cork, Cork, Ireland
e-mail: david.burns@umail.ucc.ie



C. Peers et al. (eds.), *Arterial Chemoreceptors in Physiology and Pathophysiology*,
Advances in Experimental Medicine and Biology 860, DOI 10.1007/978-3-319-18440-1_27

**Keywords**
Duchenne muscular dystrophy • *mdx* • Control of breathing • Plethysmography • Hypoxic ventilatory response • Neuromuscular disease

## 27.1 Introduction

Duchenne muscular dystrophy (DMD) is a fatal X-chromosome linked recessive disorder resulting in deletion or genetic rearrangement of the dystrophin gene. Patients lack the protein dystrophin (427kD) which has a major structural role in muscle. Dystrophin forms part of the dystrophin-glycoprotein complex which acts by linking the internal cytoskeleton to the extracellular matrix (Nowak and Davies 2004). Absence of dystrophin predisposes the sarcolemma to damage and degeneration by mechanical forces during repeated cycles of muscle contraction and relaxation (Petrof et al. 1993). Dystrophin deficiency in the diaphragm induces a significant decline in pulmonary function with age in humans (Inkley et al. 1974). Patients suffer from diaphragm weakness due to an accumulation of connective and adipose tissue (De Bruin et al. 1997) resulting in reduced mechanical force production (Beck et al. 2006). Patients are known to hypoventilate (Smith et al. 1989b) and obstructive events have been characterised in patients during sleep (Barbé et al. 1994; Hill et al. 1992). These disruptions to breathing lead to recurrent blood gas disturbances, such as hypercapnia and hypoxaemia (Kirk et al. 2000; Smith et al. 1989a), similar to patients suffering from obstructive sleep apnoea (Krieger et al. 1989). Respiratory failure is the leading cause of premature death in DMD. There is currently no cure for the disease. The *mdx* mouse, a model of DMD, has a genetic mutation resulting in the loss of the dystrophin protein (Bulfield et al. 1984). This model has a relatively mild phenotype when compared to the human condition (Nowak and Davies 2004). However, *mdx* mouse diaphragm shows severe muscle dysfunction (Coirault et al. 2003) and fibrosis (Ishizaki et al. 2008) similar to that seen in DMD patients. The *mdx* mouse has been widely used to investigate the pathophysiology of DMD and to test therapeutic interventions. Several groups have performed ventilatory studies in *mdx* mice to describe the respiratory phenotype (Ishizaki et al. 2008; Huang et al. 2011; Gosselin et al. 2003; Gayraud et al. 2007; Mosqueira et al. 2013), however, there are inconsistencies within this work and much remains to be elucidated regarding respiratory control in *mdx* mice. In addition, there is a paucity of information regarding hypoxic ventilatory responses in this animal model. We sought to establish if ventilatory function is compromised in young adult *mdx* mice compared to wild type (WT) controls using whole body plethysmography. We also examined the ventilatory response to an acute hypoxic challenge in WT and *mdx* mice. We hypothesise that dystrophin deficiency adversely affects ventilatory control in young adult *mdx* mice.

## 27.2 Methods

### 27.2.1 Animals

Male and female WT (C57BL/10ScSnJ) and *mdx* (C57BL/10ScSn-Dmd$^{mdx}$/J) mice were obtained from the Jackson Laboratory (Jackson Laboratory, Bar Harbor, ME) and were bred in our institution's animal housing facility. Animals were housed in a temperature- and humidity-controlled facility, operating on a 12 h light: 12 h dark cycle with food and water available *ad libitum*. Young adult (8 weeks old) male WT and *mdx* mice were studied. All procedures were performed under licence from the Irish Government Department of Health and

Children in accordance with National and European guidelines following research ethics committee approval.

### 27.2.2 Whole-Body Plethysmography

Respiratory recordings were performed in unrestrained mice during quiet rest. Animals were introduced into plethysmography chambers (BUXCO Europe Ltd.) and allowed a 60–90 min acclimatisation period with room air passing through the chambers (1 L/min). Following the acclimatisation period, a 10 min baseline recording was performed in normoxia. This was followed by a 20 min hypoxic challenge (10 % $O_2$, balance $N_2$). Following recovery, a 10 min normoxic baseline period was recorded. Typically, two chambers were used in parallel, allowing simultaneous measurement of respiratory parameters in a paired study design. Respiratory parameters including respiratory frequency (*f*), tidal volume ($V_T$), and minute ventilation ($V_E$) were recorded on a breath-by-breath basis for analysis.

### 27.2.3 Data Analysis

All values are shown as mean ± SEM. Both normoxic bouts were pooled to generate one set of baseline data. For the hypoxic challenge, ventilatory measurements were averaged on a minute by minute basis from which we determined the peak ventilatory response to hypoxia. Normalised $V_E$ (ml/min/g body mass) was determined from the *f* (breaths per minute) multiplied by $V_T$ (ml/breath) per g body mass.

## 27.3 Results

### 27.3.1 Body Mass

There was a significant difference in body mass ($p < 0.0001$; Student's *t* test) between age-matched WT (21.1 ± 0.3 g; n = 10) and *mdx* (23.6 ± 0.4 g; n = 11) animals.

### 27.3.2 Baseline Normoxic Ventilation

*Mdx* mice had a significantly lower *f* ($p = 0.011$; Student's *t* test) and $V_E$ ($p = 0.033$) during stable normoxic ventilation compared to WT controls. There were no significant differences in $V_T$ during normoxia in *mdx* compared to WT, although a trend towards a significant reduction in *mdx* was observed ($p = 0.093$) (Fig. 27.1).

### 27.3.3 Hypoxic Ventilatory Response

Exposure to hypoxia increase $V_E$ in WT ($p = 0.061$) and *mdx* ($p = 0.0003$) mice. Examination of the hypoxic ventilatory response (HVR), determined as % change from baseline, revealed that *mdx* mice had a significantly enhanced HVR ($p = 0.002$) in comparison to WT (Fig. 27.2).

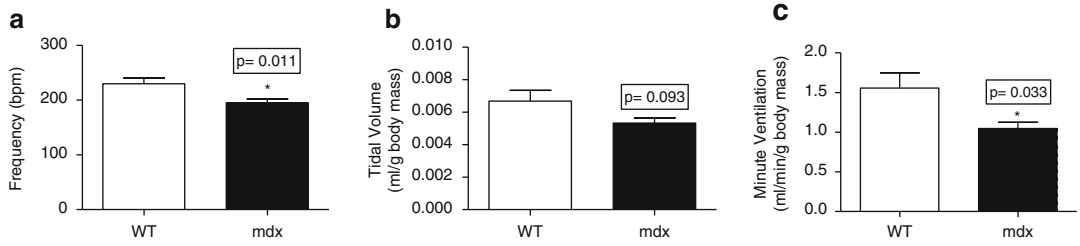


**Fig. 27.1** Values (mean ± SEM) for respiratory frequency (**a**), tidal volume (**b**) and minute ventilation (**c**) in WT (n = 10) and *mdx* (n = 11) mice during normoxic exposure. * denotes significant difference from WT (Student's *t* test)

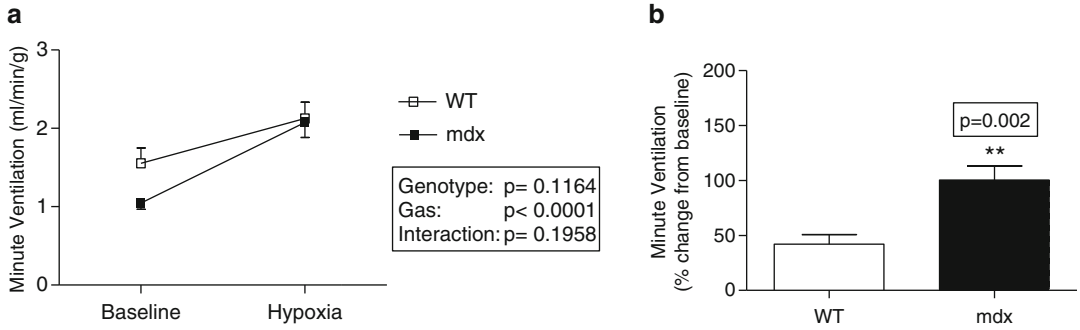


**Fig. 27.2** (**a**) Minute ventilation during normoxic exposure and during the peak response to hypoxia. Data were statistically compared by two-way (genotype x gas) analysis of variance. (**b**) Peak hypoxic ventilatory response expressed as % change from baseline. Values mean ± SEM. ** denotes significant difference from WT (Student's *t* test)

## 27.4 Discussion

To date, reports of respiratory function in the *mdx* mouse have been poorly described, despite respiratory failure being one of the main causes of morbidity in patients with DMD. Several groups have attempted to characterise the respiratory phenotype in the *mdx* mouse model but a lack of standardised procedures amongst research groups have led to a series of apparent discrepancies within the collective data. In this study, we have shown that dystrophin deficiency impairs normoxic ventilation in *mdx* mice compared to WT controls. *Mdx* mice expressed a significantly lower *f* and $V_E$. $V_T$ was also reduced in *mdx* mice but this did not reach statistical significance. Our observations are generally consistent with Mosqueira et al. (2013) who reported significantly reduced *f*, $V_T$ and $V_E$ during normoxic breathing in 6–7 month old *mdx* mice compared to age-matched WT animals. Ishizaki et al. (2008) reported significant reductions in *f* in 2 and 4 month old *mdx* mice. Similarly, Huang et al. (2011) showed significant reductions in *f* and $V_T$ in 3 and 6 month old *mdx* mice. However, in previous studies, *f* values for *mdx* and WT animals are unusually high (345–450 breaths/min) when compared to previously reported data in other inbred strains (Han et al. 2001, 2002). The apparent tachypnoea could be attributed to too short an acclimatisation period for the animals in the plethysmography chambers, and might reflect exploratory behaviour (including sniffing) more so than resting ventilation. It should be noted too that there is a behavioural phenotype in the *mdx* mouse (Manning et al. 2014). Hence, we employed a longer acclimatisation than typically employed in plethysmography studies. Alteration in ventilatory control in *mdx* mice extends to the HVR, where *mdx* mice appear to have an enhanced ventilatory response to acute hypoxic stress. Despite impaired normoxic ventilation in *mdx* mice, we observed that they could match the ventilatory capacity of WT animals upon exposure to hypoxia. This is interesting in that it suggests that, at 8 weeks at least, they retain the capacity for enhanced mechanical ventilation of the lungs capable of reaching ventilatory values equivalent to WT animals. In contrast to our finding, Mosqueira et al. (2013) have reported a blunting of the HVR in 6–7 month old *mdx* mice though it is clear from their data that the absolute change in ventilation upon exposure to hypoxia is greater, not less, in *mdx* animals. This, together with a reduction in baseline ventilation during normoxia is entirely consistent with our observations reported herein in younger *mdx* mice. Of interest, Mosqueira et al. (2013) reported dystrophin deficiency in carotid body (CB) from *mdx* mice by immuno-blotting and gene

expression analysis. The CB is described as the primary peripheral chemoreceptor which is sensitive to changes in arterial oxygen and carbon dioxide tension and pH (Kumar and Prabhakar 2012). The loss of dystrophin from the *mdx* CB may have a role in the observed alterations in HVR in *mdx* mice at 8 weeks and 6–7 months of age which warrants further attention. It should be noted however that we did not measure arterial oxygen saturation or arterial $PO_2$ during gas challenge and as such our finding of enhanced ventilatory responsiveness must be viewed in the context of a response to a standard single-point $FiO_2$ challenge. It is tempting to suggest that the apparent hypoventilation in *mdx* mice – a feature of the human condition – gives rise to hypoxaemia, which could further alter the respiratory phenotype in the *mdx* model (and DMD). We have previously reported hypoxic remodelling in animal models of disease (McMorrow et al. 2011; Carberry et al. 2014; Shortt et al. 2014) and enhanced HVR following acclimatisation to chronic hypoxia is well described in many species including the mouse (Powell et al. 1998; Huey et al. 2000). Thus, we speculate that hypoxia may be an early feature of DMD that in turn influences the respiratory phenotype perhaps establishing a vicious cycle of morbidity. In conclusion, this study supports the hypothesis that dystrophin deficiency impairs normal ventilation in the most widely studied animal model of DMD. This impairment is characterised by hypoventilation and an apparent enhancement of the HVR. Dystrophin deficiency in respiratory muscle and the motor neurones controlling their activity may underpin the ventilatory phenotype. Increasing our understanding of the mechanisms of respiratory morbidity in translational models of DMD is important in the context of management of the disease in patients and the development of new therapeutic interventions.

**Acknowledgements** Supported by the Department of Physiology, University College Cork, Cork, Ireland. DOM and KOH are funded by Muscular Dystrophy Ireland.

## References

Barbé F, Quera-Salva MA, Mccann C, Gajdos P, Raphael JC, De Lattre J, Agustí AG (1994) Sleep-related respiratory disturbances in patients with Duchenne muscular dystrophy. Eur Respir J 7:1403–1408

Beck J, Weinberg J, Hamnegård CH, Spahija J, Olofson J, Grimby G, Sinderby C (2006) Diaphragmatic function in advanced Duchenne muscular dystrophy. Neuromuscul Disord 16:161–167

Bulfield G, Siller WG, Wight PA, Moore KJ (1984) X chromosome-linked muscular dystrophy (mdx) in the mouse. Proc Natl Acad Sci U S A 81:1189–1192

Carberry JC, Mcmorrow C, Bradford A, Jones JF, O'Halloran KD (2014) Effects of sustained hypoxia on sternohyoid and diaphragm muscle during development. Eur Respir J 43:1149–1158

Coirault C, Pignol B, Cooper RN, Butler-Browne G, Chabrier PE, Lecarpentier Y (2003) Severe muscle dysfunction precedes collagen tissue proliferation in mdx mouse diaphragm. J Appl Physiol (1985) 94:1744–1750

De Bruin PF, Ueki J, Bush A, Khan Y, Watson A, Pride NB (1997) Diaphragm thickness and inspiratory strength in patients with Duchenne muscular dystrophy. Thorax 52:472–475

Gayraud J, Matecki S, Hnia K, Mornet D, Prefaut C, Mercier J, Michel A, Ramonatxo M (2007) Ventilation during air breathing and in response to hypercapnia in 5 and 16 month-old mdx and C57 mice. J Muscle Res Cell Motil 28:29–37

Gosselin LE, Barkley JE, Spencer MJ, Mccormick KM, Farkas GA (2003) Ventilatory dysfunction in mdx mice: impact of tumor necrosis factor-alpha deletion. Muscle Nerve 28:336–343

Han F, Subramanian S, Dick TE, Dreshaj IA, Strohl KP (2001) Ventilatory behavior after hypoxia in C57BL/6J and A/J mice. J Appl Physiol (1985) 91:1962–1970

Han F, Subramanian S, Price ER, Nadeau J, Strohl KP (2002) Periodic breathing in the mouse. J Appl Physiol (1985) 92:1133–1140

Hill NS, Redline S, Carskadon MA, Curran FJ, Millman RP (1992) Sleep-disordered breathing in patients with Duchenne muscular dystrophy using negative pressure ventilators. Chest 102:1656–1662

Huang P, Cheng G, Lu H, Aronica M, Ransohoff RM, Zhou L (2011) Impaired respiratory function in mdx and mdx/utrn(+/-) mice. Muscle Nerve 43:263–267

Huey KA, Low MJ, Kelly MA, Juarez R, Szewczak JM, Powell FL (2000) Ventilatory responses to acute and chronic hypoxia in mice: effects of dopamine D(2) receptors. J Appl Physiol (1985) 89:1142–1150

Inkley SR, Oldenburg FC, Vignos PJ (1974) Pulmonary function in Duchenne muscular dystrophy related to stage of disease. Am J Med 56:297–306

Ishizaki M, Suga T, Kimura E, Shiota T, Kawano R, Uchida Y, Uchino K, Yamashita S, Maeda Y, Uchino M (2008) Mdx respiratory impairment following fibrosis of the diaphragm. Neuromuscul Disord 18:342–348

Kirk VG, Flemons WW, Adams C, Rimmer KP, Montgomery MD (2000) Sleep-disordered breathing in Duchenne muscular dystrophy: a preliminary study of the role of portable monitoring. Pediatr Pulmonol 29:135–140

Krieger J, Sforza E, Apprill M, Lampert E, Weitzenblum E, Ratomaharo J (1989) Pulmonary hypertension, hypoxemia, and hypercapnia in obstructive sleep apnea patients. Chest 96:729–737

Kumar P, Prabhakar NR (2012) Peripheral chemoreceptors: function and plasticity of the carotid body. Compr Physiol 2:141–219

Manning J, Kulbida R, Rai P, Jensen L, Bouma J, Singh SP, O'Malley D, Yilmazer-Hanke D (2014) Amitriptyline is efficacious in ameliorating muscle inflammation and depressive symptoms in the mdx mouse model of Duchenne muscular dystrophy. Exp Physiol 99:1370–1386

Mcmorrow C, Fredsted A, Carberry J, O'Connell RA, Bradford A, Jones JF, O'Halloran KD (2011) Chronic hypoxia increases rat diaphragm muscle endurance and sodium-potassium ATPase pump content. Eur Respir J 37:1474–1481

Mosqueira M, Baby SM, Lahiri S, Khurana TS (2013) Ventilatory chemosensory drive is blunted in the mdx mouse model of Duchenne Muscular Dystrophy (DMD). PLoS One 8, e69567

Nowak KJ, Davies KE (2004) Duchenne muscular dystrophy and dystrophin: pathogenesis and opportunities for treatment. EMBO Rep 5:872–876

Petrof BJ, Shrager JB, Stedman HH, Kelly AM, Sweeney HL (1993) Dystrophin protects the sarcolemma from stresses developed during muscle contraction. Proc Natl Acad Sci U S A 90:3710–3714

Powell FL, Milsom WK, Mitchell GS (1998) Time domains of the hypoxic ventilatory response. Respir Physiol 112:123–134

Shortt CM, Fredsted A, Chow HB, Williams R, Skelly JR, Edge D, Bradford A, O'Halloran KD (2014) Reactive oxygen species mediated diaphragm fatigue in a rat model of chronic intermittent hypoxia. Exp Physiol 99:688–700

Smith PE, Edwards RH, Calverley PM (1989a) Oxygen treatment of sleep hypoxaemia in Duchenne muscular dystrophy. Thorax 44:997–1001

Smith PE, Edwards RH, Calverley PM (1989b) Ventilation and breathing pattern during sleep in Duchenne muscular dystrophy. Chest 96:1346–1351

# 28 Mild Chronic Intermittent Hypoxia in Wistar Rats Evokes Significant Cardiovascular Pathophysiology but No Overt Changes in Carotid Body-Mediated Respiratory Responses

Clare J. Ray, Ben Dow, Prem Kumar, and Andrew M. Coney

**Abstract**

Models of chronic intermittent hypoxia (CIH), the main feature of obstructive sleep apnoea (OSA), have demonstrated dysregulation of the cardiovascular and respiratory systems resulting in hypertension, cardiac hypertrophy and alterations in the hypoxic ventilatory response (HVR) due to changes in sympathetic and respiratory control by the carotid body. In the UK, treatment of OSA is only offered to patients with an apnoea-hypopnoea index (AHI) >15, we investigated whether mild CIH produced significant pathophysiological changes, which might inform treatment guidelines.

Rats were exposed to CIH (6 $h^{-1}$, 8 h $day^{-1}$, 5 % $O_2$ nadir) for 2 weeks and then arterial blood pressure (ABP), heart rate (HR) and ventilation were recorded in these and normoxic control rats (N) under Alfaxan anaesthesia, at baseline and in response to Dejours test, graded hypoxia and hypercapnia. Hearts were analysed post-mortem.

CIH induced significant increases in baseline ABP (142 ± 5 vs 122 ± 2 mmHg), HR (448 ± 9 vs 412 ± 5 bpm) and cardiac mass (3.5 ± 0.1 vs 2.7 ± 0.1 g kg body $mass^{-1}$) as a result of a selective left ventricular hypertrophy (1.6 ± 0.1 vs 1.3 ± 0.08 g kg body $mass^{-1}$; FCSA 464 ± 32 $\mu m^2$ vs 314 ± 9 $\mu m^2$). There was no significant difference between N and CIH in baseline respiration or the response to Dejours test, graded hypoxia and hypercapnia.

C.J. Ray (✉) • B. Dow • P. Kumar • A.M. Coney
School of Clinical and Experimental Medicine, College of Medical and Dental Sciences, University of Birmingham, Birmingham B15 2TT, UK
e-mail: c.j.ray@bham.ac.uk; a.m.coney@bham.ac.uk



C. Peers et al. (eds.), *Arterial Chemoreceptors in Physiology and Pathophysiology*, Advances in Experimental Medicine and Biology 860, DOI 10.1007/978-3-319-18440-1_28

These results demonstrate that mild CIH can induce the significant cardiovascular changes associated with OSA without overt changes in respiratory function. Given evidence that CIH changes carotid body sensory activity, a possible explanation for these results is that there is differential integration of chemoreceptor input with respiratory and cardiac sympathetic outputs.

**Keywords**
Chronic intermittent hypoxia • Obstructive sleep apnoea • Carotid body • Hypertension

## 28.1 Introduction

In rats, 35 days of chronic intermittent hypoxia (CIH; 120 $h^{-1}$, 7 h $day^{-1}$) resulted in a significant elevation in blood pressure and left ventricular hypertrophy (Fletcher et al. 1992a), which was prevented by sympathetic denervation (Fletcher et al. 1992b). The hypertension was also prevented by section of the peripheral chemoreceptors (Leke et al. 1997). Likewise, obese patients with OSA had hypertension and elevated sympathetic activity that was reversed with continuous positive airway pressure (CPAP) treatment (Somers et al. 1995). These results suggest a role for the carotid bodies in the development of the hypertension of obstructive sleep apnoea (OSA) since carotid body stimulation increases sympathetic activity.

As well as cardiovascular changes, patients with OSA and several species exposed to CIH show an enhanced hypoxic ventilatory response (HVR) leading to the suggestion that $O_2$ sensing by the carotid body is also altered by CIH (see Kumar and Prabhakar 2012). Indeed, the carotid body sensory response to hypoxia is enhanced by CIH (9 $h^{-1}$, 8 h $day^{-1}$) in rats (Peng and Prabhakar 2004). In cats exposed to CIH (10 $h^{-1}$, 8 h $day^{-1}$) basal carotid body discharge was increased and the HVR enhanced, however, this was without a significant effect on the cardiovascular response to hypoxia (Rey et al. 2004), allowing for the possibility that respiratory and cardiovascular control by the carotid body might be altered differentially and over a different time period.

The National Institute for Health and Care Excellence (NICE 2008) estimates that up to 4 % of middle-aged males and 2 % of middle-aged females in the UK suffer from OSA. Patients with OSA can suffer up to 60 hypoxic episodes an hour, with a diagnosis of mild OSA being made in patients with an apnoea-hypopnoea index (AHI) of 5–14. However, NICE only recommend the use of CPAP treatment in patients with moderate (AHI 15–30) or severe (AHI >30) OSA. Similarly, a range of hypoxic episodes per hour is used in the animal models of CIH used to study OSA (Dematteis et al. 2009). It is clear from these studies, that the CIH paradigm used, can differentially modulate the effects on the cardiovascular and respiratory systems (see Introduction of Gonzalez-Martin et al. 2011). Since patients with mild OSA are not offered CPAP, it is important to establish whether mild CIH causes significant pathophysiological changes and if so should the threshold for OSA treatment be re-evaluated?

The aim of this study was to characterise baseline cardiovascular and respiratory changes that occur with 2-weeks of mild CIH using six hypoxic episodes an hour. We also investigated the role of the carotid body in these changes using Dejours test, assessing the HVR and the response to hypercapnia. We hypothesized that mild CIH would evoke significant changes in carotid body-mediated cardio-respiratory reflex control at rest resulting in hypertension and enhanced carotid body mediated responses to oxygen and carbon dioxide.

## 28.2 Methods

### 28.2.1 Induction of CIH

Twelve 10-week old male Wistar rats (Charles River, Kent, UK), were used in this study. Animals were housed in the Biomedical Services Unit, University of Birmingham and all procedures complied with the Animals (Scientific Procedures) Act, 1986. Animals were split into two groups, a normoxic (N) group (n = 6) and a group exposed to chronic intermittent hypoxia (CIH; n = 6). N rats were housed in groups of 3, in individually ventilated cages (IVCs) for 14 days. CIH rats were also housed in groups of 3 in IVCs for 14 days, except for 8 h a day (~8 am-4 pm) when the cages were placed in a hypoxic chamber and the animals exposed to 6 cycles of hypoxia per hour. The hypoxic cycles, controlled by a Biospherix Oxycycler (NY, USA), consisted of reduction in $O_2$ from 21 % to a nadir of 5 % over 90s, followed by a return to 21 % $O_2$ over the next 90s, with a 7 min period at 21 % $O_2$ before the start of the next cycle. In a study by Lucking et al. (2014) reduction in $O_2$ to 5 % over this time period resulted in a significant reduction in arterial haemoglobin saturation ($S_aO_2$) to ~70 %.

### 28.2.2 Surgical Preparation

After 14 days of N or CIH animals were brought to the laboratory for terminal *in vivo* procedures. Animals were initially anaesthetised with isoflurane (3.5 % in $O_2$, 3.5 L $min^{-1}$) and placed on a thermostatically controlled blanket to maintain body temperature at 37 °C. The jugular vein was cannulated so that anaesthesia could be maintained with the steroid Alfaxan (5 mg $ml^{-1}$ in saline, 1.5–2 ml $h^{-1}$). Depth of anaesthesia was monitored at all times.

The right brachial artery was cannulated to allow measurement of arterial blood pressure (ABP) and online calculation of heart rate (HR), mean arterial pressure (MAP), systolic pressure (SP) and diastolic pressure (DP), and the left to allow the collection of arterial blood samples for measurement of the partial pressure of oxygen ($P_aO_2$), carbon dioxide ($P_aCO_2$) and arterial pH using a GEM 4,000 blood gas analyser (IL, Cheshire, UK). The trachea was cannulated to allow attachment of a spirometer to measure air flux and the calculation of tidal volume ($V_T$), respiratory frequency (*f*) and minute ventilation ($V_E$). Data were collected using a Powerlab (AD Instruments, Oxford, UK) connected to a computer. Rats were allowed ~1 h post-surgery to stabilise; baseline cardiovascular and respiratory variables were analysed before the protocols below to allow comparison between N and CIH.

### 28.2.3 Experimental Protocols

The respiratory response to breathing 100 % $O_2$ for 20s was recorded (Dejours test). This was repeated five times in each animal, allowing ventilation to return to baseline between each stimulus. Responses were analysed by comparing $V_T$, *f* and $V_E$ in the 10s before and in the final 10s of each stimulus. $\Delta V_T$, $\Delta f$, and $\Delta V_E$ were calculated to allow comparison between N and CIH.

The respiratory response to graded hypoxia was recorded over 10 min with the animal breathing each of four levels of hypoxia for 2 min. Hypoxic gases were mixed using a system of rotameters in a gas proportioner frame (CP Instruments, UK). An arterial blood sample was taken before the 10 min protocol and in the final 30s of each stimulus to measure $P_aO_2$. Responses in each group were analysed by comparing $V_T$, *f* and $V_E$ in the 30s before the protocol and in the final 30s of each level of hypoxia and were plotted against $P_aO_2$ measured at these time points.

The respiratory response to one level of hypercapnia was recorded over 5 min; the hypercapnic gas mixture was mixed using the system above. An arterial blood sample was taken before and during the final 30s of the stimulus to measure $P_aCO_2$. Responses were analysed by comparing $V_T$, *f* and $V_E$ in the 30s before the protocol with the final 30s of hypercapnia plotted against $P_aCO_2$. $CO_2$ sensitivity of $V_T$, *f* and $V_E$ was calculated to allow comparison between N and CIH.

### 28.2.4 Heart Tissue Mass and Histology

At the end of the protocols rats were killed and the heart was removed. The whole heart, left (LV), right ventricle (RV) and interventricular septum (IVS) were weighed and tissue mass was expressed as g kg body mass$^{-1}$ to allow N and CIH to be compared. LV + IVS mass to RV mass ratio and LV + IVS expressed as % body mass were calculated to give an indication of LV hypertrophy. The LV was frozen for histological analysis.

10 μm sections of LV (9 sections per heart) were fixed and stained with lectin to allow visualisation of capillaries and muscle fibres to be counted. Three areas (0.12 mm$^2$) of each of the sections were randomly selected and the fibres counted. Mean fibre cross sectional area (FCSA) was calculated for each area and the mean of the 27 areas counted gave the FCSA for each animal allowing comparison between N and CIH.

### 28.2.5 Statistical Analysis

All statistical analyses were performed using aabel 20/20 data vision 3 (Gigawiz, OK, USA). Comparisons within groups were made using Student's paired t-test or ANOVA for repeated measures and between groups using Student's unpaired t-test or factorial ANOVA, as appropriate. $P < 0.05$ was considered significant.

## 28.3 Results

There was no significant difference in body mass between N and CIH animals (361 ± 6 vs 343 ± 9 g). There was also no significant difference between baseline $P_aO_2$, $P_aCO_2$ and arterial pH between N and CIH animals (Table 28.1). CIH caused a significant increase in MAP (142 ± 5 vs 122 ± 2 mmHg), SP (159 ± 6 vs 142 ± 2 mmHg), DP (125 ± 4 vs 103 ± 1 mmHg) and HR (448 ± 9 vs 412 ± 5 bpm; Fig. 28.1, a–e). There was no significant effect of CIH on all baseline respiratory variables (Fig. 28.1, f–h).

**Table 28.1** Baseline arterial blood gases and pH

| | N | CIH |
|---|---|---|
| $P_aO_2$ (mmHg) | 91 ± 1 | 96 ± 3 |
| $P_aCO_2$ (mmHg) | 48 ± 1 | 46 ± 1 |
| pH | 7.37 ± 0.01 | 7.36 ± 0.01 |

Mean ± SEM baseline $P_aO_2$, $P_aCO_2$ and arterial pH in N and CIH animals. There is no significant difference in the blood gases and arterial pH between N and CIH animals (unpaired t-test; n = 6)

In N and CIH animals breathing 100 % $O_2$ (Dejours test), had no effect on $V_T$ but significantly decreased *f* and therefore $V_E$ (Fig. 28.2, columns 1 & 2). However there was no significant difference in the response to Dejours test between N and CIH animals (Fig. 28.2, column 3).

As expected, graded hypoxia significantly decreased $P_aO_2$ and significantly increased the corresponding $V_T$, *f*, and therefore $V_E$ in N and CIH groups. However, there was no difference in this response between N and CIH (Fig. 28.3).

Breathing a hypercapnic gas mixture evoked a significant increase in $P_aCO_2$ and significantly increased the corresponding $V_T$, *f* and $V_E$ in N and CIH animals (Fig. 28.4, columns 1 & 2). CIH had no effect on the $CO_2$ sensitivity of the $V_T$, *f* and $V_E$ responses (Fig. 28.4, column 3).

CIH evoked a significant increase in whole heart (3.5 ± 0.1 vs 2.7 ± 0.1), LV (1.6 ± 0.1 vs 1.3 ± 0.08) and IVS (1.5 ± 0.2 vs 1.0 ± 0.1) tissue mass (g kg body mass$^{-1}$; Fig. 28.5a). There was no change in RV tissue mass. LV + IVS to RV ratio increased from 5.4 ± 0.6 in N to 7.5 ± 0.8 in CIH and LV + IVS expressed as a % of body mass increased from 0.2 ± 0.01 % in N to 0.3 ± 0.01 % in CIH (Fig. 28.5, b & c). Mean FCSA significantly increased from 314 ± 9 μm$^2$ in N to 464 ± 32 μm$^2$ (Fig. 28.5, d & e).

## 28.4 Discussion

In the present study, we have used a model of CIH where the frequency (6 h$^{-1}$) is above the diagnostic but below the treatment threshold of OSA (according to NICE guidelines). These animals showed significant hypertension and tachycardia, an increase in MAP of 20 mmHg and HR

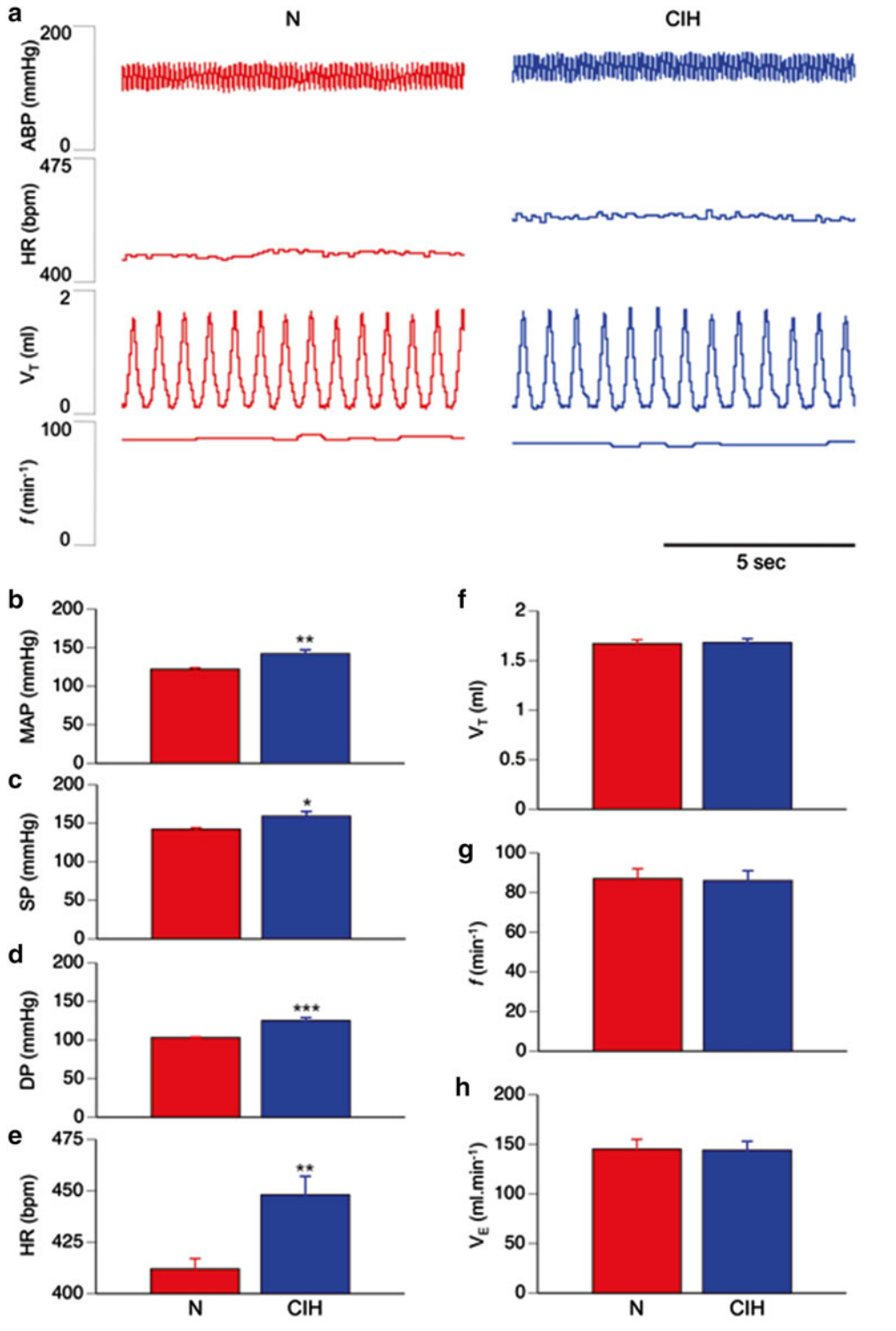


**Fig. 28.1** CIH significantly increases baseline ABP and HR but has no effect on baseline ventilation. (**a**) Example traces showing 10s baseline ABP, HR, $V_T$ and *f* in N and CIH rat. Graphs show mean (+ SEM): MAP (**b**); SP (**c**); DP (**d**); HR (**e**); $V_T$ (**f**); *f* (**g**) and $V_E$ (**h**) in N (*red*) and CIH (*blue*) groups. *, **, *** $P<0.05$, 0.01 and 0.001 respectively vs N, unpaired t-test ($n=6$)

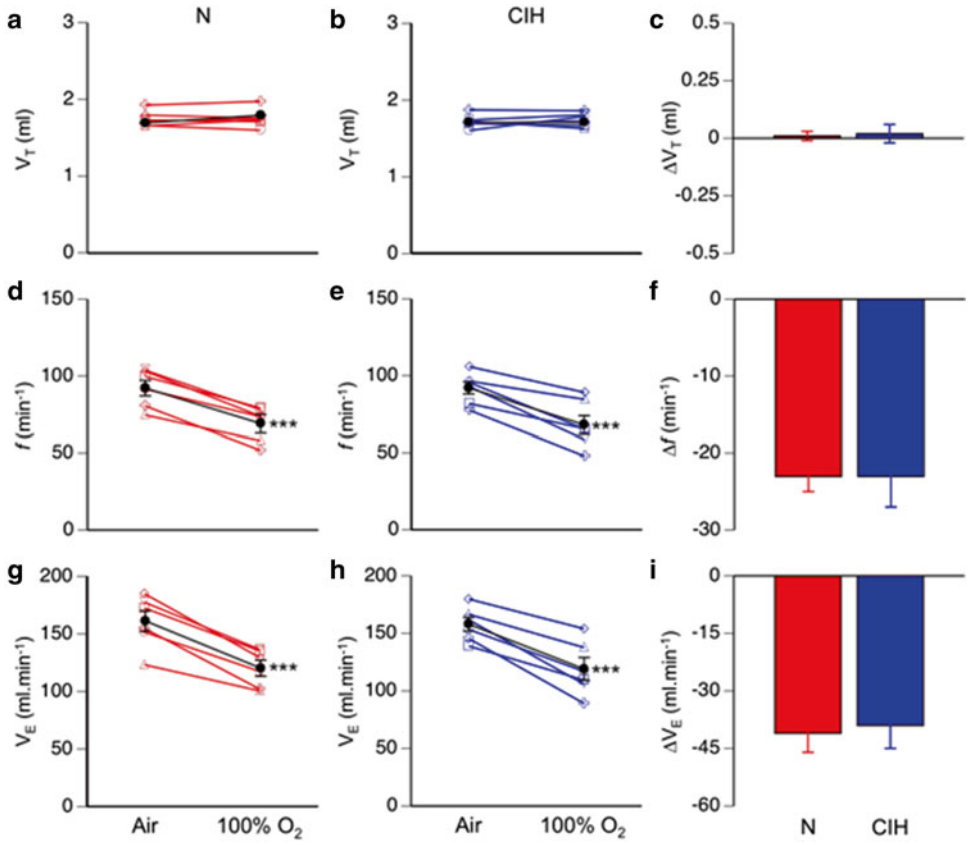


**Fig. 28.2** CIH had no effect on the ventilatory response to breathing 100 % $O_2$ (Dejours test). The graphs in the left (*N*) and centre (*CIH*) columns show $V_T$ (**a & b**), $f$ (**d & e**), and $V_E$ (**g & h**) in each individual animal (*red* symbols N, *blue* symbols CIH) when breathing air and 100 % $O_2$. Mean (±SEM) $V_T$, $f$ and $V_E$ when breathing air and 100 % $O_2$ are shown in black. *** $P<0.001$ vs air, paired *t*-test (n = 6). The graphs in the right column show mean (±SEM) $\Delta V_T$ (**c**), $\Delta f$ (**f**) and $\Delta V_E$ (**i**) evoked by breathing 100 % $O_2$ in N (*red*) and CIH (*blue*) animals. There was no significant difference in the ventilatory response to 100 % $O_2$ between N and CIH animals (unpaired t-test; n = 6)

of 36 bpm, and this resulted in a selective LV hypertrophy and an increase in cardiac myocyte size. These results are consistent with CIH increasing cardiac sympathetic activity as suggested by others (Narkiewicz et al. 1998; Bradley and Floras 2003). Indeed, Lucking et al. (2014) found that in rats exposed to CIH (12 $h^{-1}$, 5 % $O_2$ nadir) for 2 weeks there was no change in lumbar sympathetic control of the vasculature. Having ruled out an increased renal sympathetic activity they concluded that the observed hypertension resulted from an increased cardiac output driven by cardiac sympathetic hyperactivity. It has been suggested that the main stimulus for increased sympathetic activity in CIH is a change in carotid body function but the evidence for this varies depending on the exact CIH protocol and species used.

Whilst our model demonstrated significant cardiovascular changes under baseline conditions, we did not observe any differences in resting ventilation. In order to investigate carotid body function we measured ventilatory responses under various conditions. Exposure to hypercapnia induced increases in ventilation as expected but these were not affected by prior exposure to CIH. These results are consistent with the literature (Kumar and Prabhakar 2012) and are not unexpected since the primary sensing of $CO_2$ levels is through the central chemoreceptors. If our

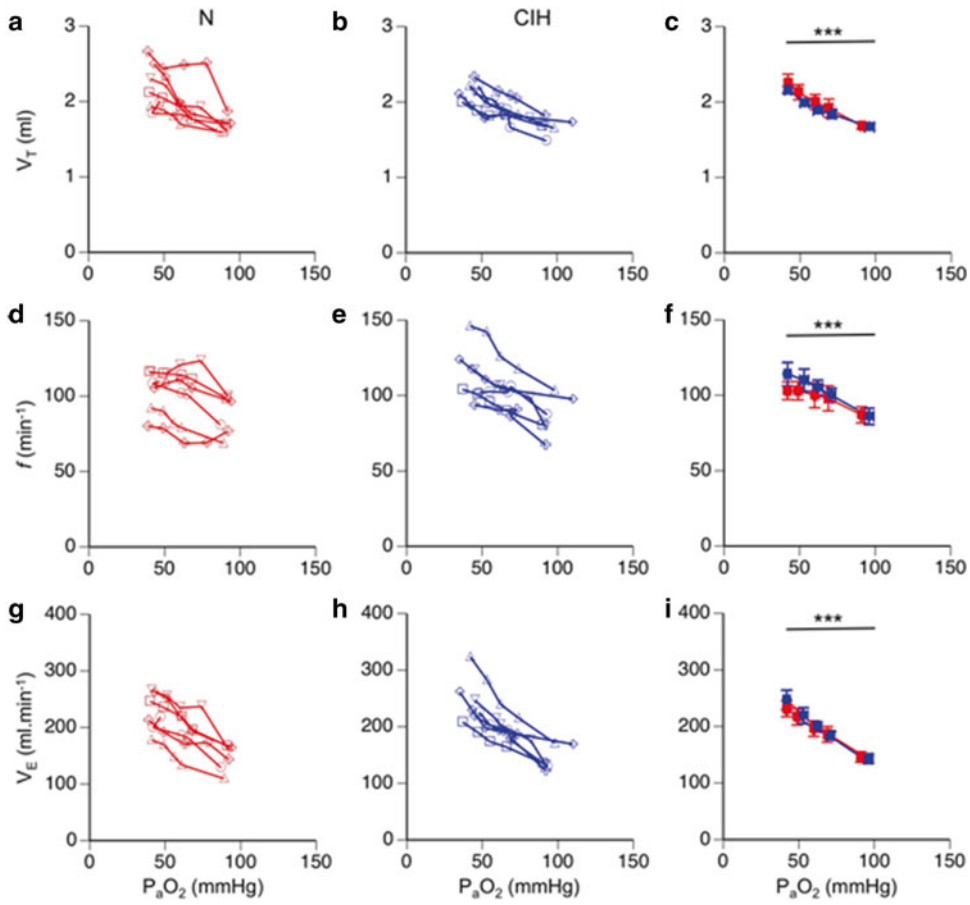


**Fig. 28.3** CIH had no effect on the ventilatory response to graded hypoxia. The graphs in the left (*N*) and centre (*CIH*) columns show $V_T$ (**a & b**), $f$ (**d & e**), and $V_E$ (**g & h**) in each individual animal (*red* symbols N, *blue* symbols CIH) plotted against $P_aO_2$ when breathing air and four graded hypoxic gas mixtures. The graphs in the right column show mean (±SEM) $V_T$ (**c**), $f$ (**f**) and $V_E$ (**i**) for the N (*red*) and CIH (*blue*) groups plotted against mean (±SEM) $P_aO_2$ when breathing air and four graded hypoxic gas mixtures. For the ventilatory response to graded hypoxia, *** $P<0.001$, repeated measures ANOVA (n=6). There was no significant difference in the ventilatory response to graded hypoxia between N and CIH animals (factorial ANOVA; n=6)

CIH protocol had induced changes in carotid body function it might be expected that the response to hyperoxia or hypoxia be altered. All animals responded to hyperoxia and hypoxia, however, we found no difference between N and CIH animals, indicating that CIH had no effect on carotid body-mediated control of ventilation in our model. There is greater disparity in the literature regarding the effects of CIH on ventilatory responses to increases or decreases in $O_2$ levels. Explanations for these inconsistencies may include species/strain differences and/or frequency of CIH and the severity of the hypoxia induced (ie degree of haemoglobin desaturation/change in $P_aO_2$). The latter may contribute to the variation seen in OSA patients, however, consideration may need to be given to all parts of the chemoreflex pathway to understand the source of this variability.

Further complicating our understanding of the role of chemoreceptor function in driving the effects of CIH, is that we observed changes in the cardiovascular system with no changes in the respiratory system. One possibility is that an increased sympathetic activity is unrelated to carotid body function. For example, in patients,

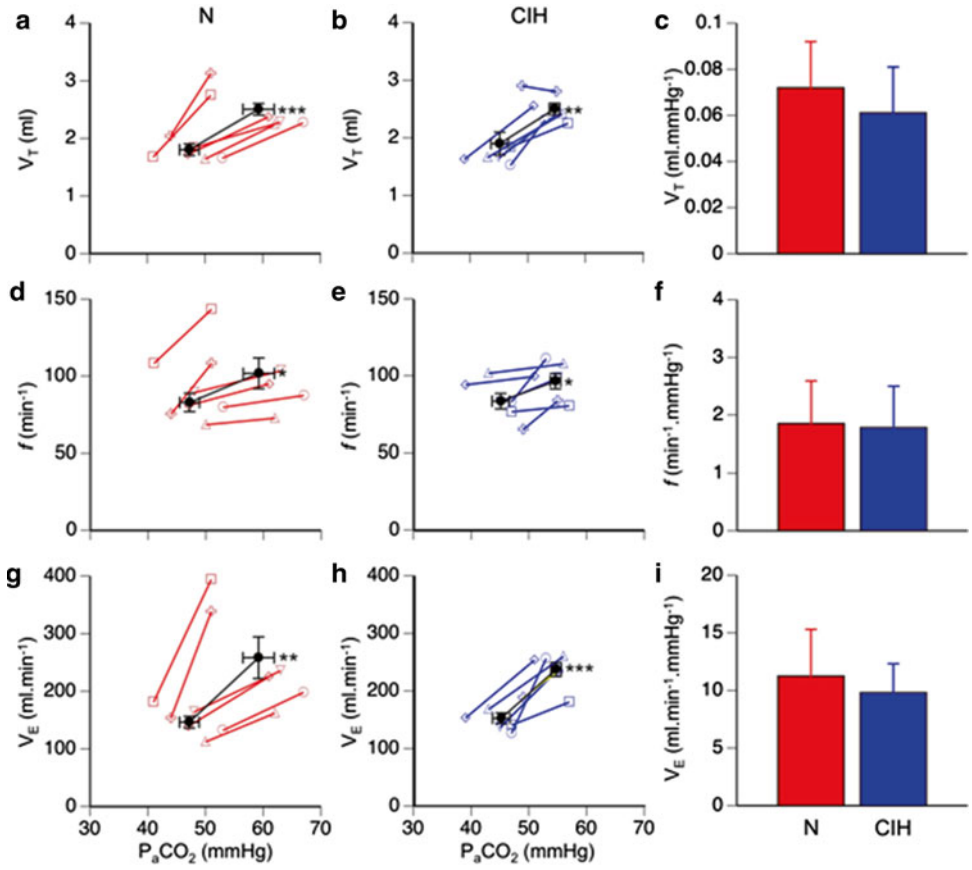


**Fig. 28.4** CIH had no effect on the ventilatory response to hypercapnia. The graphs in the left (*N*) and centre (*CIH*) columns show $V_T$ (**a & b**), $f$ (**d & e**), and $V_E$ (**g & h**) in each individual animal (*red* symbols N, *blue* symbols CIH) plotted against $P_aCO_2$ when breathing air and a hypercapnic gas mixture. Mean (±SEM) $V_T$, $f$ and $V_E$ are plotted against the mean (±SEM) $P_aCO_2$ when breathing air and the hypercapnic gas mixture and are shown in *black*. *, **, *** $P<0.05$, 0.01 and 0.001 respectively vs air, paired *t*-test (n = 6). The graphs in the right column show mean (+SEM) $CO_2$ sensitivity for $V_T$ (**c**), $f$ (**f**), and $V_E$ (**i**) in N (*red*) and CIH (*blue*) animals. There was no significant difference in the $CO_2$ sensitivity of $V_T$, $f$ and $V_E$, between N and CIH animals (unpaired t-test; n = 6)

OSA is associated with obesity and obesity is linked to sympathetic hyperactivity (see Lambert et al. 2010), however in the present study there was no significant difference in body mass between N and CIH. A second possibility is that the chemoreflex pathway itself is altered. These changes can be sensitive to both the severity and the time course of CIH exposure. Carotid body sensory discharge itself might be altered (Peng and Prabhakar 2004) resulting in a different chemoreceptor input into the brainstem. However, integration and modulation of this input can occur differently (see Gonzalez-Martin et al. 2011) in response to the CIH paradigm, and may do so despite carotid body-mediated ventilatory responses per se remaining apparently unaltered. The implication of this would be that output from the ventral respiratory group could remain unchanged, however, the output from the paraventricular nucleus could be increased resulting in higher levels of cardiac sympathetic activity. Evidence has been published showing independent changes in respiratory drive and sympathetic activity in response to acute intermittent hypoxia (Xing and Pilowsky 2010).

In summary, exposure to mild CIH can induce the cardiovascular changes associated

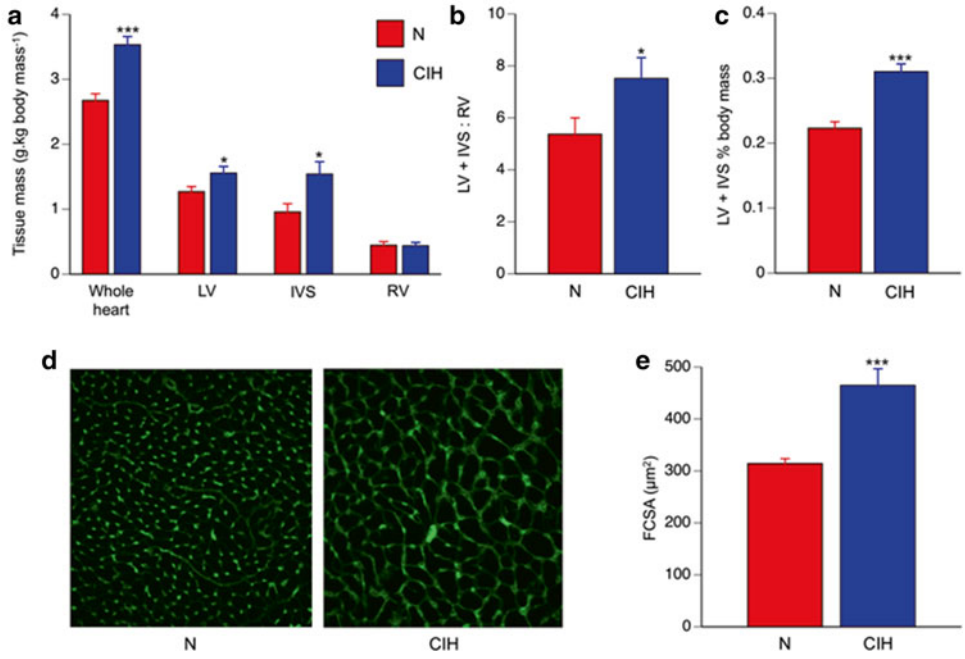


**Fig. 28.5** CIH evoked significant left ventricular hypertrophy. Heart tissue mass (mean + SEM) in N (*red*) and CIH (*blue*) groups is shown in (**a**) as whole heart and split into the LV, IVS and RV. (**b**) and (**c**) show mean (+SEM) of LV + IVS : RV and LV + IVS expressed as % body mass respectively in N (*red*) and CIH (*blue*) groups. *, *** $P<0.05$ and 0.001 respectively vs N (unpaired t-test; n = 6). (**d**), representative micrographs showing a lectin stained section of left ventricle allowing the visualisation of cardiac myocyte fibre size in an N (*left*) and CIH (*right*) animal. Mean (+SEM) FCSA is shown in (**e**) for N (*red*) and CIH (*blue*) groups. The mean value for each animal was obtained by analysing three randomly selected areas of nine sections of each left ventricle in the group. *** $P<0.001$ vs N (unpaired t-test; N = 6; n = 162)

with OSA and these are likely to be caused by increased cardiac sympathetic activity. Further, these cardiovascular changes occurred without overt changes in carotid body-mediated respiratory function, likely as a result of differing integration of chemoreceptor input with respiratory and cardiac sympathetic outputs. Given that in our model low frequency CIH for 2 weeks evoked profound hypertension and significant left ventricular hypertrophy, it raises the question as to whether in OSA patients an AHI >15 should be used alone as the standard threshold for offering CPAP treatment. In addition, it appears that assessing all components of the chemoreflex will be important in determining exactly how alterations in carotid body sensory activity in CIH result in pathophysiological changes in the respiratory and cardiovascular systems.

## References

Bradley TD, Floras JS (2003) Sleep apnea and heart failure: Part I: Obstructive sleep apnea. Circulation 107:1671–1678

Dematteis M, Godin-Ribuot D, Arnaud C et al (2009) Cardiovascular consequences of sleep-disordered breathing: contribution of animal models to understanding human disease. ILAR J 50:262–281

Fletcher EC, Lesske J, Qian W et al (1992a) Repetitive, episodic hypoxia causes diurnal elevation of blood pressure in rats. Hypertension 19:555–561

Fletcher EC, Lesske J, Culman J et al (1992b) Sympathetic denervation blocks blood pressure elevation in episodic hypoxia. Hypertension 20:612–619

Gonzalez-Martin MC, Vega-Agapito MV, Conde SV et al (2011) Carotid body function and ventilatory responses in intermittent hypoxia. Evidence for anomalous brainstem integration of arterial chemoreceptor input. J Cell Physiol 226:1961–1969

Kumar P, Prabhakar NR (2012) Peripheral chemoreceptors: function and plasticity of the carotid body. Compr Physiol 2:141–219

Lambert E, Sari CI, Dawood T et al (2010) Sympathetic nervous system activity is associated with obesity-induced subclinical organ damage in young adults. Hypertension 56:351–358

Leke J, Fletcher EC, Bao G et al (1997) Hypertension cause by chronic intermittent hypoxia – influence of chemoreceptors and sympathetic nervous system. J Hypertens 15:1590–1603

Lucking EF, O'Halloran KD, Jones JFX (2014) Increased cardiac output contributes to the development of chronic intermittent hypoxia induced hypertension. Exp Physiol. doi:10.1113/expphysiol.2014.080556

Narkiewicz K, Montano N, Cogliati C et al (1998) Altered cardiovascular variability in obstructive sleep apnea. Circulation 98:1071–1077

NICE (2008) Continuous positive airway pressure for the treatment of obstructive sleep apnoea/hypopnoea syndrome. www.nice.org.uk/guidance/ta139

Peng Y-J, Prabhakar NR (2004) Effects of two paradigms of chronic intermittent hypoxia on carotid body sensory activity. J Appl Physiol 96:1236–1242

Rey S, Del Rio R, Alcayaga J et al (2004) Chronic intermittent hypoxia enhances cat chemosensory and ventilatory responses to hypoxia. J Physiol 560:577–586

Somers VK, Dyken ME, Clary MP et al (1995) Sympathetic neural mechanisms in obstructive sleep apnea. J Clin Invest 96:1897–1904

Xing T, Pilowsky PM (2010) Acute intermittent hypoxia in rat in vivo elicits a robust increase in tonic sympathetic nerve activity that is independent of respiratory drive. J Physiol 588:3075–3088

# 29 Crucial Role of the Carotid Body Chemoreceptors on the Development of High Arterial Blood Pressure During Chronic Intermittent Hypoxia

Rodrigo Iturriaga, David C. Andrade, and Rodrigo Del Rio

**Abstract**

Exposure to chronic intermittent hypoxia (CIH), the main feature of obstructive sleep apnea, produces autonomic and cardiorespirartory alterations, and leads to systemic hypertension. These alterations are associated with enhanced carotid body (CB) chemosensory and ventilatory hypoxic reflexes and a decrease baroreflex (BRS) efficiency. The aim of this study was to determine the therapeutic effect of CB ablation on the elevated arterial blood pressure, the reduced BRS and the potentiated ventilatory response induced by CIH in conscious rats. Arterial blood pressure (BP) was continuous measured by telemetry in male Sprague-Dawley rats exposed to CIH (5 % $O_2$, 12 times/h, and 8 h/day). After 21 days of CIH, the CBs were selectively cryodestroyed, and rats were kept one more week in CIH. Ventilatory responses to hypoxia were assessed by whole body plethysmography and spontaneous BRS measured by the sequence method. Exposure to CIH produces hypertension, increased the chemoreflex ventilatory hypoxic responses, and decreased BRS. The ablation of the CBs normalized the elevated BP, and the altered ventilatory response and BRS. Present results suggest that the CB play a crucial role in the development of high arterial pressure and autonomic alterations induced by CIH.

**Keywords**

Obstructive sleep apnea • Carotid body • Intermittent hypoxia • Chemoreflex • Baroreflex

R. Iturriaga (✉) • D.C. Andrade
Laboratorio de Neurobiología, Facultad de Ciencias Biológicas, Pontificia Universidad Católica de Chile, Santiago, Chile
e-mail: riturriaga@bio.puc.cl

R. Del Rio
Laboratorio de Control Cardiorrespiratorio. Centro de Investigación Biomédica, Universidad Autónoma de Chile, Santiago, Chile


C. Peers et al. (eds.), *Arterial Chemoreceptors in Physiology and Pathophysiology*, Advances in Experimental Medicine and Biology 860, DOI 10.1007/978-3-319-18440-1_29

## 29.1 Introduction

The obstructive sleep apnea (OSA) syndrome, a worldwide sleep-breathing disorder, is recognized as an independent risk factor for the development of systemic hypertension (Dempsey et al. 2010; Garvey et al. 2009; Somers et al. 2008). Among the disturbances produced by OSA, the chronic intermittent hypoxia (CIH) is considered the main factor for the progression of the hypertension (Dempsey et al. 2010; Iturriaga et al. 2009; Somers et al. 2008). Although the link between OSA and hypertension is well established, the pathophysiological mechanisms responsible for the hypertension are not entirely understood. It has been proposed that CIH produces oxidative stress, inflammation, and sympathetic hyperactivity, which lead to endothelial dysfunction and hypertension (Dempsey et al. 2010; Garvey et al. 2009; Iturriaga et al. 2009). However, a growing body of evidences suggests that the carotid body (CB) plays a pivotal role in the development of the hypertension. Indeed, CIH selectively enhances the CB chemosensory responsiveness to hypoxia (Del Rio el at. 2010, 2011, 2012; Pawar et al. 2009; Peng et al. 2003; Rey et al. 2004), which in turn may increase the sympathetic outflow to the arterial blood vessels (Prabhakar et al. 2005; Iturriaga et al. 2009).

It has been shown that OSA patients exhibit enhanced sympathetic drive (Dempsey et al. 2010; Somers et al. 2008). Similarly, animals exposed to CIH show enhanced sympathetic responses to hypoxia, and develop systemic hypertension (Del Rio et al. 2010; Greenberg et al. 1999; Prabhakar et al. 2005; Rey et al. 2008). The autonomic dysfunction characterized by enhanced sympathetic outflow, a reduction of the efficiency of the cardiac baroreflex sensitivity (BRS) and alterations of heart rate variability has been proposed to play a pivotal role in the development of high arterial blood pressure (Rey et al. 2008; Lai et al. 2006).

We hypothesized that the CIH-induced hypertension is critically dependent on the enhanced CB chemoreflex and the decrease in BRS. To determine the contribution of the CB to the hypertension induced by CIH in conscious rats, we performed selective ablation of the CB in hypertensive rats exposed to CIH. In addition, we measured the spontaneous baroreflex (sBRS) and ventilatory responses to hypoxia.

## 29.2 Methods

### 29.2.1 Animals and Intermittent Hypoxic Exposure

Experiments were performed on male Sprague-Dawley rats (250 g), fed with standard diet *ad libitum* and kept on a 12-h light/dark schedule (07:30–19:30). The protocol was approved by the Bioethical Committee of the Biological Science Faculty of Pontificia Universidad Católica de Chile, Santiago. Unrestrained, freely moving rats housed in individual chambers (12 cm × 35 cm, 2.2 L) were exposed to 5 % inspired $O_2$ for 20 s followed by room air for 280 s; 12 episodes/h; 8 h/day for 21 days. The hypoxic pattern was applied from 08:30 to 16:30 h. A computerize system based on solenoid valves controls the alternating cycles of $N_2$ and room air. In the Sham condition (7 days), rats were exposed to air by air flushing an equal flow of compressed air into chambers. Room temperature was kept at 22–23 °C.

### 29.2.2 Evaluation of Ventilatory Chemoreflex Function

Tidal volume ($V_T$) was determined by unrestrained whole body plethysmography (Fine Pointe, Buxco Research Systems, USA). Resting breathing was recorded for 15 min while the rats breathe room air. Peripheral chemoreceptors were stimulated by allowing the rats to breathe hypoxic gas (10 % and 15 % $O_2$ in balance $N_2$) for 10 min. The frequency of sampling was 1,000 Hz.

### 29.2.3 Arterial Blood Pressure and Spontaneous Baroreflex Sensitivity

We performed arterial blood pressure (BP) measurements in conscious freely moving rats using a radiotelemetry monitoring system (Data Science International, USA). Briefly, rats were anesthetized with 2 % isoflurane in $O_2$, and a skin incision was made to expose the femoral artery. The tip of a pressure transmission catheter was guided into the femoral artery, and the transmitter body was placed into subcutaneous pocket. The sBRS was measured by sequence method (Hemolab Software). Slopes were calculated ratio to ΔR-R/ΔBP with a correlation coefficient r >0.8.

### 29.2.4 Carotid Body Ablation

After 21 days of CIH the rats were anesthetized with 2 % isoflurane in $O_2$ and the CBs were exposed and cryogenically destroyed as previously described (Del Rio et al. 2013). The effectiveness of this maneuver was confirmed by the disappearance of the CB-mediated ventilatory reflex response to NaCN.

### 29.2.5 Statistics Analysis

The data are expressed as means ± SEM. Differences between two groups were assessed by Student T-test comparisons. Differences between more groups were assessed with one-way ANOVA or Kruskal Wallis tests, followed by appropriate posthoc comparisons. The level was set at $p<0.05$ for statistical significance. The tidal volume ($V_T$) at different $O_2$ levels was fitted to the following exponential curve.

$$V_T = \text{bas} + (\text{max} - \text{bas})e^{-k/PO_2} \qquad (29.1)$$

where bas is the ventilatory response to 21 % $O_2$ and max is the ventilatory response to 10 % $O_2$. All statistical analysis was performed using GraphPad Prisma 6.0 (GraphPad Software, Inc., San Diego, CA, USA).

## 29.3 Results

### 29.3.1 Effects of CB ablation on the CIH-Induced Hypertension

The mean arterial pressure increases (~10 mmHg) after 3 days of CIH (Fig. 29.1). To determine the

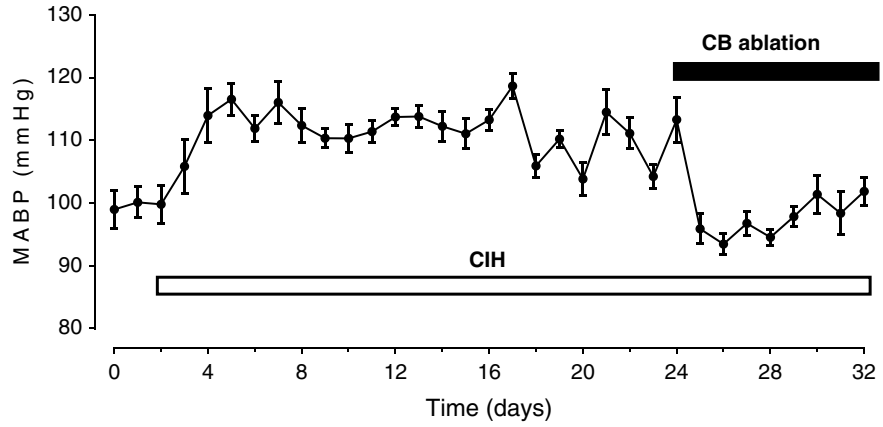


**Fig. 29.1** Effect of bilateral CB ablation on the elevated mean arterial blood pressure (MABP) in rats exposed to chronic intermittent hypoxia (CIH). n= 5

contribution of the CB to the elevated BP, both CBs were destroyed. The maneuver abolished the hypertension even in the presence of the hypoxic stimulus, suggesting that the BP elevation is critically dependent on functional CBs.

### 29.3.2 Effects of CB Ablation on the Enhanced Hypoxic Ventilatory Chemoreflex Response

Figure 29.2 shows the effects of the CB ablation on ventilatory responses ($V_T$) measured in response to 10 % $F_iO_2$ in 4 rats before (Sham condition), after 20 days of intermittent hypoxia (CIH), and following 7 days of the CB ablation in the presence of the hypoxic stimulus (CIH + CBA condition). The bilateral CB ablation reduced both the enhanced normoxic and hypoxic $V_T$ response induced by CIH.

### 29.3.3 Effects of CB Ablation on Spontaneous Baroreflex Changes induced by CIH

We measured sBRS in rats exposed to Sham conditions, after 20 days of CIH, and after 7 days of the CB ablation. CIH reduced the sBRS sensitivity related to the Sham condition (Fig. 29.3). Notably, CB ablation increased the sBRS to

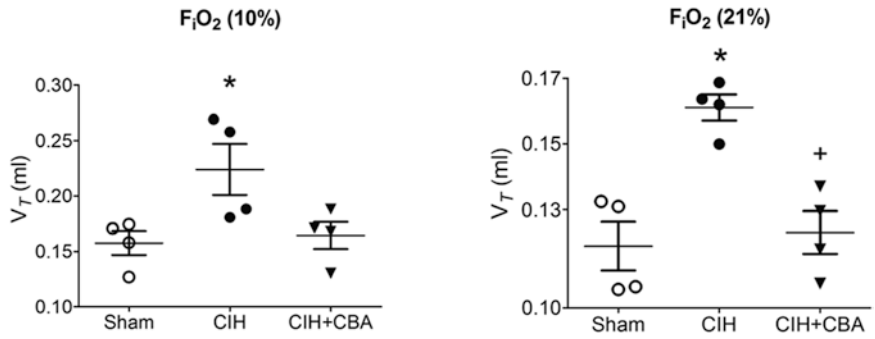


**Fig. 29.2** Tidal volume ($V_T$) measured at 10 % $O_2$ and 21 % $O_2$ in the same rats in Sham condition, following 20 days of intermittent hypoxia (CIH) and after 7 days after the CB ablation (CBA+ CIH). * $p<0.05$ vs. Sham, CIH. n=4

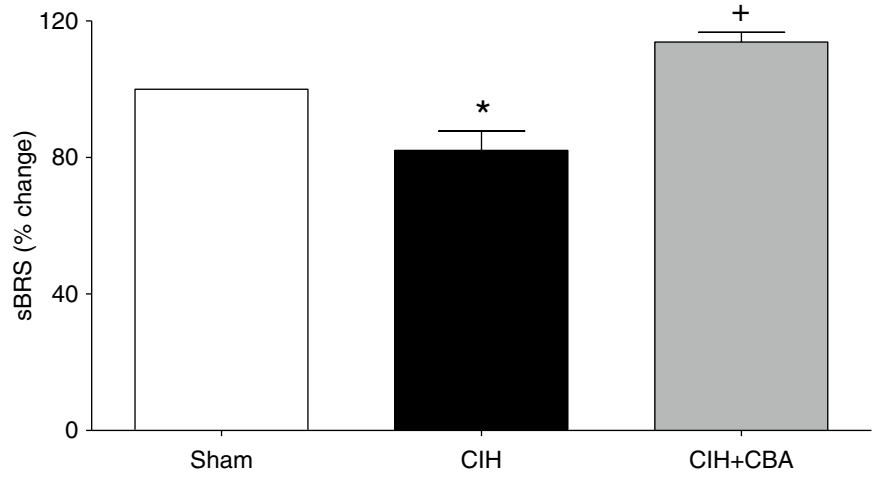


**Fig. 29.3** Spontaneous baroreflex sensitivity (sBRS) in Sham, (CIH) and CIH+CBA conditions. * $p<0.05$ vs. Sham; + $p<0.05$ vs. CIH, n=4

values comparable to the ones obtained in sham conditions.

## 29.4 Discussion

Chronic intermittent hypoxia enhances carotid body (CB) chemosensory and ventilatory responses to hypoxia, and leads to systemic hypertension. These alterations are attributed to oxidative stress since antioxidant treatment prevented the enhanced hypoxic chemosensory and ventilatory responses and the hypertension. (Del Rio et al. 2012, 2011, 2013; Peng et al. 2003; Pawar et al. 2009). We propose that the enhanced CB chemosensory tone plays a crucial role in the maintenance of the hypertension during CIH.

The role played by the CB in the development and progression of the hypertension induced by OSA is an unanswered question. The CB is involved in several sympathetic-mediated diseases and the carotid sinus denervation or the selective CB ablation has been proposed as a feasible clinical treatment for severe and resistant hypertension in humans (Mc Bryde et al. 2013; Paton et al. 2013), and the cardiorespiratory alterations in chronic heart failure (Del Rio et al. 2013). Thus, it is plausible that CB ablation will improve the cardiovascular alterations in OSA. However, there is no available information showing the effects of CB denervation in OSA patients or animals exposed to CIH.

To study the origin of the CIH-induced hypertension and the contribution of the enhanced CB chemosensory response to hypoxia, we performed selective ablation of both CBs in hypertensive rats exposed to CIH. The removal of the CB inputs markedly decreases BP, suggesting that the maintenance of the hypertension following CIH is critically dependent on the intermittent hypoxic stimulation of the CB chemoreceptors, and the resulting sympathetic activation. The effectiveness of this maneuver was confirmed by the absence of a ventilatory reflex response to NaCN. Remarkably, the selective ablation of the CBs restored normal BP values comparable to the ones observed in sham rats. However, we cannot preclude that the relative contribution of the CB to the hypertension will diminish if the CIH stimulus is maintained for 2–3 more weeks, whereas the contribution of the vascular compartment may increase.

In summary, our data using telemetry recordings show that BP increases 3 days after the beginning of CIH, which is consistent with the time required to establish enhanced CB chemosensory responses to hypoxia and oxidative stress in the CB, both of which remained elevated for 21 days of CIH (Del Rio et al. 2010, 2012). The CIH-induced hypertension, which occurs after 3–5 days of exposure, is not related to endothelial dysfunction and/or vascular remodeling since CB ablation totally normalized BP in animals exposed to CIH. It is likely that this fast hypertensive response is caused by a higher sympathetic outflow due to the cyclic hypoxic excitation of the CB. Thus, our results indicate that the CB plays a key role in the progression and maintenance of the CIH-induced hypertension.

**Acknowledgements** This work was supported by grant 1100405 from the National Fund for Scientific and Technological Development of Chile (FONDECYT) and the project Puente 28/2014 of the VRI-PUC.

## References

Del Rio R, Moya EA, Iturriaga R (2010) Carotid body and cardiorespiratory alterations in intermittent hypoxia: the oxidative link. Eur Respir J 36:143–150

Del Rio R, Moya EA, Iturriaga R (2011) Differential expression of pro-inflammatory cytokines, endothelin-1 and nitric oxide synthases in the rat carotid body exposed to intermittent hypoxia. Brain Res 1395:74–85

Del Rio R, Moya EA, Parga MJ, Madrid C, Iturriaga R (2012) Carotid body inflammation and cardiorespiratory alterations in intermittent hypoxia. Eur Respir J 39:1492–1500

Del Rio R, Marcus NJ, Schultz HD (2013) Carotid chemoreceptor ablation improves survival in heart failure: rescuing autonomic control of cardiorespiratory function. J Am Coll Cardiol 62:2422–2430

Dempsey JA, Veasey SC, Morgan BJ, O'Donnell CP (2010) Pathophysiology of sleep apnea. Physiol Rev 90:47–112

Garvey JF, Taylor CT, McNicholas WT (2009) Cardiovascular disease in obstructive sleep apnoea syndrome: the role of intermittent hypoxia and inflammation. Eur Respir J 33:1195–1205

Greenberg HE, Sica A, Batson D, Scharf SM (1999) Chronic intermittent hypoxia increases sympathetic responsiveness to hypoxia and hypercapnia. J Appl Physiol 86:298–305

Iturriaga R, Moya EA, Del Rio R (2009) Carotid body potentiation induced by intermittent hypoxia: implications for cardiorespiratory changes induced by sleep apnoea. Clin Exp Pharmacol Physiol 36:1197–1204

Lai CJ, Yang CC, Hsu YY, Lin YN, Kuo TB (2006) Enhanced sympathetic outflow and decreased baroreflex sensitivity are associated with intermittent hypoxia-induced systemic hypertension in conscious rats. J Appl Physiol 100:1974–1982

Mcbryde FD, Abdala AP, Hendy EB, Pijacka W, Marvar P, Moraes DJA, Sobotka PA, Paton JFR (2013) The carotid body as a putative therapeutic target for the treatment of neurogenic hypertension. Nat Commun 4:2395

Paton JFR, Sobotka PA, Fudim M, Engelman ZJ, Hart ECJ, Mcbryde FD, Abdala AP, Marina N, Gourine AV, Lobo M, Patel N, Burchell A, Ratcliffe L, Nightingale A (2013) The carotid body as a therapeutic target for the treatment of sympathetically mediated diseases. Hypertension 61:5–13

Pawar A, Nanduri J, Yuan G, Khan SA, Wang N, Kumar GK, Prabhakar NR (2009) Reactive oxygen species-dependent endothelin signaling is required for augmented hypoxic sensory response of the neonatal carotid body by intermittent hypoxia. Am J Physiol Regul Integr Comp Physiol 296:R735–R742

Peng YJ, Overholt JL, Kline D, Kumar GK, Prabhakar NR (2003) Induction of sensory long-term facilitation in the carotid body by intermittent hypoxia: implications for recurrent apneas. Proc Natl Acad Sci U S A 100:10073–10078

Prabhakar NR, Peng YJ, Jacono FJ, Kumar GK, Dick TE (2005) Cardiovascular alterations by chronic intermittent hypoxia: importance of carotid body chemoreflexes. Clin Exp Pharmacol Physiol 32:447–449

Rey S, Del Rio R, Alcayaga J, Iturriaga R (2004) Chronic intermittent hypoxia enhances cat chemosensory and ventilatory responses to hypoxia. J Physiol 560:577–586

Rey S, Tarvainen MP, Karjalainen PA, Iturriaga R (2008) Dynamic time-varying analysis of heart rate and blood pressure variability in cats exposed to short-term chronic intermittent hypoxia. Am J Physiol Regul Integr Comp Physiol 295:R28–R37

Somers VK, White DP, Amin R, Abraham WT, Costa F, Culebras A, Daniels S, Floras JS, Hunt CE, Olson LJ, Pickering TG, Russell R, Woo M, Young T (2008) Sleep apnea and cardiovascular disease. J Am Coll Cardiol 52:686–717

# Relative Contribution of Nuclear and Membrane Progesterone Receptors in Respiratory Control

30

Ryma Boukari, François Marcouiller, and Vincent Joseph

**Abstract**

Progesterone is a steroid hormone whose physiological effects can affect various systems, including reproductive, immune and cardiorespiratory systems. In fact, there are growing evidences proving that progesterone is potent respiratory stimulant with therapeutic value for sleep-disordered breathing. However there is no clear understanding of how progesterone mediates its stimulant respiratory effects and alleviates apnea. Mechanistically, it was demonstrated that this hormone elicits some of its respiratory effect via the classical mechanism of the nuclear progesterone receptor (nPR), a transcription factor belonging to the super family of steroid hormone receptors. Moreover, experimental results indicate that activation of alternative non-genomic (i.e. non-nuclear) signaling pathways such as the membrane progesterone receptors (mPR) could have a key role in the regulation of the respiratory control system. We provide preliminary results suggesting an important role of mPRβ on respiratory control and ventilatory response to hypoxia in adult female mice.

**Keywords**

Breathing disorders • Hypoxic ventilatory response • Sex-steroids • Hormonal treatment

## 30.1 Introduction

Breathing disorders such as obstructive sleep apnea, sudden infant death, and Rett syndromes show several sex differences in their prevalence, indicating that sex is primordial determinant of respiratory health and lending weight to the link of gonadal steroid hormones in respiratory

R. Boukari • F. Marcouiller • V. Joseph (✉)
Centre de recherche du CHU de Québec, Québec, QC, Canada

Department of Pediatrics, Université Laval, Québec, QC, Canada
e-mail: vincent.joseph@fmed.ulaval.ca



C. Peers et al. (eds.), *Arterial Chemoreceptors in Physiology and Pathophysiology*,
Advances in Experimental Medicine and Biology 860, DOI 10.1007/978-3-319-18440-1_30

control (Kapsimalis and Kryger 2002; Chahrour and Zoghbi 2007). Progesterone is a steroid synthetized primarily in the gonads, the adrenal glands and in the placenta, but progesterone is also synthetized de novo in the central and peripheral nervous system, and can thus be classified as a neurosteroid (Birzniece et al. 2006). Progesterone is well- known as a powerful respiratory stimulant with a potential therapeutic value for the treatment of apnea in adults (Shahar et al. 2003), and it has been suggested that it could also be used for the treatment of apnea in preterm neonates (Finer et al. 2006). However, progesterone is not clinically approved for respiratory disordered breathing, because experimental data are still scarce, and there is no clear mechanical studies explaining how progesterone influences the control of breathing and alleviates apnea. Here, we will briefly focus on progesterone receptors, to highlight that we lack critical knowledge on their relative contributions in the regulation of the respiratory control system. However, our preliminary results clearly indicate that these receptors could play an important role in regulation of breathing.

## 30.2 Respiratory Effects of Progesterone

Progesterone is a potent respiratory stimulant, (Dempsey et al. 1986). Medroxyprogesterone, an analogue of progesterone, increases minute ventilation and responsiveness to hypercapnia or hypoxia (Skatrud et al. 1978; Zwillich et al. 1978). In addition, menopause is a risk factor for sleep apnea, and hormone replacement with progesterone reduces sleep disordered breathing in post-menopausal women (Shahar et al. 2003). Furthermore, progesterone reduces the occurrence of apnea in newborn and adult rats (Yamazaki et al. 2005; Lefter et al. 2007). Progesterone acts at different levels of the respiratory control system, including areas in central nervous system (Bayliss et al. 1987) and in peripheral chemoreceptors (Hannhart et al. 1990; Joseph et al. 2012). The direct application of progesterone on the dorsal surface of the medulla, at the level of the Nucleus Tractus Solitarius (NTS), increases phrenic nerve activity (Bayliss et al. 1987), and the effects of progesterone on respiratory activity requires intact hypothalamic structures (Bayliss et al. 1990).

## 30.3 Molecular Mechanisms by Which Progesterone Stimulates Breathing

Progesterone exerts it biological effects by genomic and non-genomic mechanisms (Fig. 30.1). We recently reported that progesterone uses non-genomic mechanisms to increase $VO_2$ and $VCO_2$ (Marcouiller et al. 2014), most likely through the truncated form of the nuclear progesterone receptor (nPR) located on the external membrane of the mitochondria (Dai et al. 2013). Moreover, allopregnanolone, a neuroactive metabolite of progesterone, affects breathing in newborn rats and arterial baroreflex responses in adults (Ren and Greer 2006; Heesch 2011). Despite the multiple potential pathways by which progesterone acts, little is known about the role of these pathways in regulating respiration.

### 30.3.1 Genomic Mechanisms

The nuclear progesterone receptor (nPR) belongs to the superfamily of the steroid hormone receptors. In the classical model of nPR activation, progesterone, a lipophilic molecule, diffuses through the cellular and nuclear membranes to bind to a nPR. When bound by progesterone, nPR undergoes conformational changes, dissociates from chaperone proteins, dimerizes, and directly interacts with specific response elements in the promoter regions of target genes through its DNA-binding domain (Mani 2006). The nPR gene (located on chromosome 11 in humans) encodes a single mRNA that, through alternative splicing, generates two major PR isoforms (nPR-A and nPR-B). These isoforms regulate

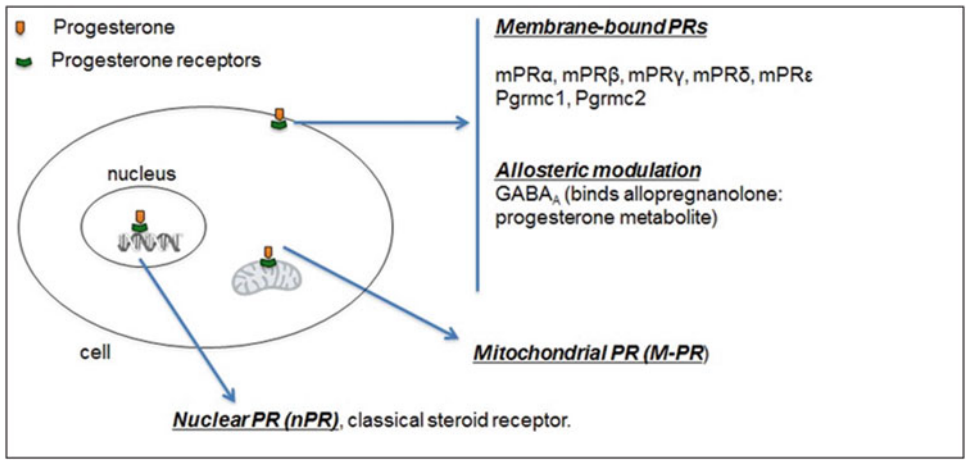


**Fig. 30.1** Potential mechanisms of action by which progesterone might produce its respiratory effects. Progesterone, either from systemic circulation or produced locally in the neuronal system, can bind and signal throughout the classical nuclear receptor, membrane progesterone receptor (mPRα to mPRξ), and the Progesterone receptor membrane component (Pgrmc) 1 and 2. In addition, allopregnanolone, a metabolite of progesterone, can bind GABA$_A$ receptor

the expression of different target genes and, therefore, different functions in cells (Mani 2006; Camacho-Arroyo et al. 2007; González-Flores et al. 2011). Several other isoforms have been identified. Because some of these isoforms have a defective DNA-binding domain and lack the nuclear localization signal, they are expected to be localized in the cytosol or on cell membranes, rather than in the nucleus, and activate the mitogen-activated protein kinase (MAPK) signaling cascade (Maller 2003; Brinton et al. 2008).

In the central nervous system, nPR is localized in the preoptic, paraventricular, ventromedial, dorsomedial, and arcuate hypothalamic nuclei and more importantly, in brainstem areas involved in respiratory control, such as the NTS (the major site of peripheral chemoreceptors integration in the brainstem), the motor nuclei of the Xth and XIIth cranial nerves, and the locus coeruleus (Romeo et al. 2005; Helena et al. 2006; Brinton et al. 2008). In the peripheral nervous system, nPR immunostaining is localized in cells in the carotid bodies of adults, newborn and fetal rats (Joseph et al. 2006). Thus, localization of nPR in these areas of the peripheral and central nervous system are highly suggestive that nPR are involved in respiratory control. Indeed, intraperitoneal injection of progesterone decreases the frequency of apneic episodes recorded during sleep (identified by behavioral criteria) by 50 % in 14-week-old male rats and by almost 80 % in 26- week-old rats. This effect is abolished when mifepristone, an nPR antagonist, is injected 1.5 h before progesterone injection (Yamazaki et al. 2005). Moreover, in anesthetized cats, i.v. progesterone administration enhances phrenic nerve activity, this effect is not elicited by other steroids, and is blocked by pre-treatment with mifepristone suggesting that it is mediated by nPR. Progesterone also enhances the peripheral chemoreceptor response to hypoxia (Hannhart et al. 1990) and enhances ventilatory activity by decreasing the synthesis of dopamine, an inhibitory neurotransmitter in peripheral chemoreceptors (Joseph et al. 2002); nPR-A signaling regulates the expression of tyrosine hydroxylase, the rate-limiting enzyme in dopamine synthesis (González-Flores et al. 2011). Our recent data suggest that nPR is an important modulator of respiratory control during sleep and in chemoreflex sensitivity. Specifically, adult female mice in which nPR is deleted (PRKO mice) have a

higher frequency of sighs and post-sigh apneas during non-REM sleep and reduced responses to hypercapnia after chronic treatment with administration of progesterone (Marcouiller et al. 2014)

### 30.3.2 Non-genomic Mechanisms

Activation of the nuclear progesterone receptor is expected to induce measurable physiological responses coinciding with *de novo* protein synthesis (within 30–45 min). However, steroid-induced effects may occur rapidly (within 2–3 min); these effects are likely initiated by cell surface receptors (Revelli et al. 1998). Based on these data, the search for membrane progesterone receptors (mPR) has been of great interest, culminating in the discovery of a gene and a corresponding protein with the characteristics of a fully functional mPR in sea trout ovaries (Zhu et al. 2003b). Structural and phylogenetic analyses have revealed the presence of similar genes in other species, including humans and mice (Zhu et al. 2003a), and three distinct mPR genes (mPRα, mPRβ, and mPR$\gamma$) have been originally identified. The family of mPR include five different members (mPRα, mPRβ, mPR$\gamma$, mPRδ and mPRξ) (Singh et al. 2013), which belong to the progestin and adipoQ receptor (PAQR) family. mPR proteins are located in the plasma membrane and have seven transmembrane domains with extracellular and intracellular terminals that respectively confer selective progesterone binding and activation of intracellular Gi proteins. When bound by progesterone, mPRα inhibits cAMP production to activate MAPK, which in turns activates the extracellular signal-regulated kinase (Erk1 and Erk2) signaling pathway. mPRα is predominantly expressed in reproductive tissues, mPRβ in the brain, and mPR$\gamma$ in the kidneys (Zhu et al. 2003b). In mice, mPRα and mPRβ proteins and mRNA are expressed in the spinal cord with a distinct staining pattern that likely underlies the important trophic and protective effects of progesterone at this level (Labombarda et al. 2010). In rats, the mRNAs for mPRα and mPRβ are expressed in the cortex and thalamic nuclei (Intlekofer and Petersen 2011).

The pioneer study conducted by Pascual et al. (2002) showed that progesterone is able to restore the decreased transmission of afferent signals in the NTS during hypoxia, which could explain the stimulatory effect of progesterone in response to this stimulus. Because these effects required between 2 and 3 min to occur, it was suggested that a non-genomic mechanism of action was involved (Pascual et al. 2002). Based on these preliminary data, we sought to determine the expression of mPRβ and mPRα in the brainstem of adult female mice by immunohistochemistry (see (Labombarda et al. 2010), and found staining in the NTS, and the motor nuclei of the Xth and XIIth cranial nerves (Fig. 30.2). We have tested the functional role of mPRβ in adult female mice that were treated for 14 days with an intracerebro-ventricular infusion of a specific siRNA against mPRβ (0.04 mg/day; Stealth Select RNAi™, Life Technologies, Burlington, ON, Canada) in the IVth ventricle, to abolish its expression in central areas of respiratory control. Preliminary results indicate that the deletion of mPRβ induces a depression of the ventilatory response to hypoxia as shown in Fig. 30.3. Interestingly, while hypoxic exposure induced a rapid increase of respiratory frequency in control mice, we observed a mean delay of $4.5 \pm 1.1$ min before any observable response occurred in mice treated with the siRNA against mPRβ. The efficiency of the knock-down of mPRβ has been verified by immunohistochemistry, showing a wide-spread absence of staining in the brainstem (not shown). These preliminary results support a key role for mPRβ, in respiratory control in adult mice.

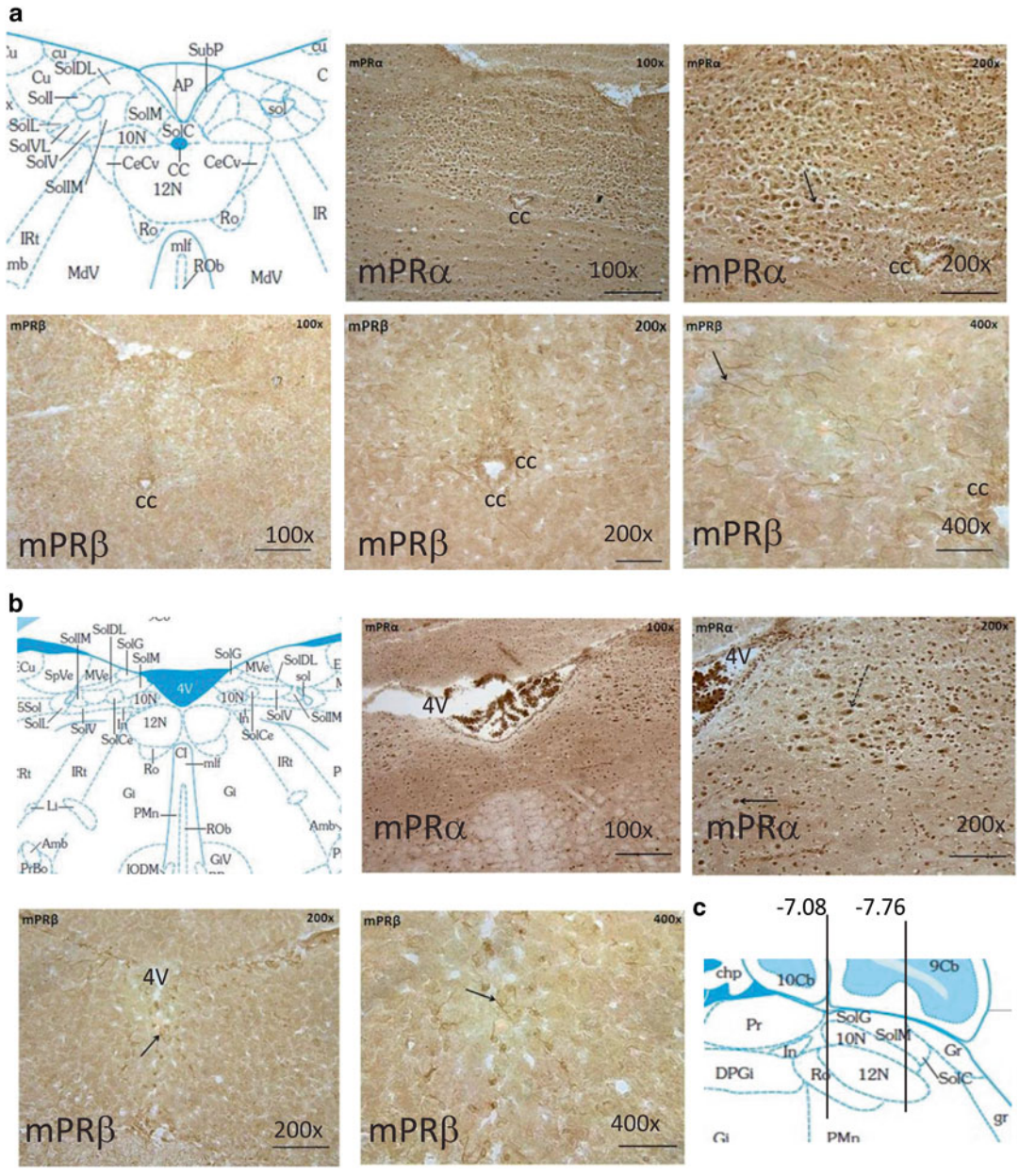


**Fig. 30.2** Immunohistochemistry for mPRα and mPRβ in the dorsal region of the adult mouse brainstem. (**a**) Neuroanatomical drawing at bregma – 7.76 mm (from Franklin and Paxinos) and corresponding staining at this level (100, 200, or 400×). (**b**) Neuroanatomical drawing at bregma – 7.08 mm and corresponding staining (100, 200, or 400×). Note the staining for mPRα in cell bodies on the NTS (SolM, SolC) and XIIthMN (12 N) at both bregma levels, and for mPRβ on neurites in the NTS. (**c**) Sagittal view (lateral 0.12 mm) of the brainstem; coronal planes at bregma −7.76 and −7.08 mm. CC: central canal, SolM, SolC, SolG, SolDL, SollM, SolV,… subdivision of the NTS. 12 N: hypoglos-sal nucleus, 10 N: vagal nucleus. Scale bar at 100× = 100 μm; at 200× = 50 μm

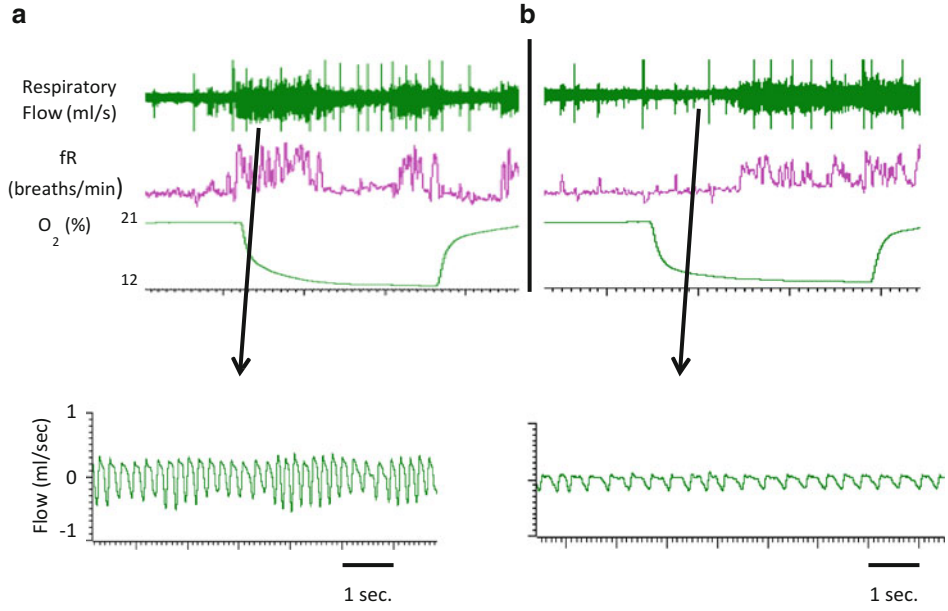


**Fig. 30.3** Example of respiratory recordings (Flow – ml/s, and frequency: fR – breaths/min) under normoxia and in response to hypoxia in control adult female mice (**a**) and after infusion of a specific siRNA against mPRβ (**b**). Note the delay of the response in the treated mice. The lower traces show for each animal a typical breathing pattern during the onset of hypoxic exposure (time scale: 1 s)

## 30.4 Conclusion

With growing awareness of the potent respiratory effects of progesterone, further experiments are required to elucidate its mechanisms of action with the perspective to develop novel pharmacological approaches for the treatment of respiratory disordered due to unstable respiratory control system. Specific knockdown of PR in-¯vivo with siRNA infusion, or knock-out models appear as promising tools to elucidate the relative contributions of the different members from the large PR family.

**Acknowledgements** Studies founded by a grant from the Canadian Institute for Health Research to VJ (MOP-102715). The authors acknowledge the work of Karim Habbal for immunohistological preparation of brainstem slices.

## References

Bayliss DA, Millhorn DE, Gallman EA et al (1987) Progesterone stimulates respiration through a central nervous system steroid receptor-mediated mechanism in cat. Proc Natl Acad Sci 84(21):7788–7792

Bayliss DA, Cidlowski JA, Millhorn DE (1990) The stimulation of respiration by progesterone in ovariectomized cat is mediated by an estrogen-dependent hypothalamic mechanism requiring gene expression. Endocrinology 126(1):519–527

Birzniece V, Bäckström T, Johansson I-M et al (2006) Neuroactive steroid effects on cognitive functions with a focus on the serotonin and GABA systems. Brain Res Rev 51(2):212–239

Brinton RD, Thompson RF, Foy MR et al (2008) Progesterone receptors: form and function in brain. Front Neuroendocrinol 29(2):313–339

Camacho-Arroyo I, Gonzalez-Arenas A, Gonzalez-Moran G (2007) Ontogenic variations in the content and distribution of progesterone receptor isoforms in the

reproductive tract and brain of chicks. Comp Biochem Physiol A Mol Integr Physiol 146(4):644–652
Chahrour M, Zoghbi HY (2007) The story of Rett syndrome: from clinic to neurobiology. Neuron 56(3):422–437
Dai Q, Shah AA, Garde RV et al (2013) A truncated progesterone receptor (PR-M) localizes to the mitochondrion and controls cellular respiration. Mol Endocrinol 27(5):741–753
Dempsey JA, Olson EB, Skatrud JB (1986) Hormones and neurochemicals in the regulation of breathing. In: Handbook of physiology: the respiratory system. Control of breathing: section 3, vol II, part 1, chapter 7. American Physiological Society, Bethesda, pp 181–221
Finer NN, Higgins R, Kattwinkel J et al (2006) Summary proceedings from the apnea-of-prematurity group. Pediatrics 117(Suppl 1):S47–S51
González-Flores O, Gómora-Arrati P, García-Juárez M et al (2011) Progesterone receptor isoforms differentially regulate the expression of tryptophan and tyrosine hydroxylase and glutamic acid decarboxylase in the rat hypothalamus. Neurochem Int 59(5):671–676
Hannhart B, Pickett CK, Moore LG (1990) Effects of estrogen and progesterone on carotid body neural output responsiveness to hypoxia. J Appl Physiol 68(5):1909–1916
Heesch CM (2011) Neurosteroid modulation of arterial baroreflex function in the rostral ventrolateral medulla. Auton Neurosci 161(1):28–33
Helena CVV, de Oliveira PM, Sanvitto GL et al (2006) Changes in α-estradiol receptor and progesterone receptor expression in the locus coeruleus and preoptic area throughout the rat estrous cycle. J Endocrinol 188(2):155–165
Intlekofer KA, Petersen SL (2011) Distribution of mRNAs encoding classical progestin receptor, progesterone membrane components 1 and 2, serpine mRNA binding protein 1, and progestin and ADIPOQ receptor family members 7 and 8 in rat forebrain. Neuroscience 172:55–65
Joseph V, Soliz J, Soria R et al (2002) Dopaminergic metabolism in carotid bodies and high-altitude acclimatization in female rats. Am J Physiol Regul Integr Comp Physiol 282(3):R765–R773
Joseph V, Doan VD, Morency CE et al (2006) Expression of sex-steroid receptors and steroidogenic enzymes in the carotid body of adult and newborn male rats. Brain Res 1073–1074:71–82
Joseph V, Niane LM, Bairam A (2012) Antagonism of progesterone receptor suppresses carotid body responses to hypoxia and nicotine in rat pups. Neuroscience 207:103–109
Kapsimalis F, Kryger MH (2002) Gender and obstructive sleep apnea syndrome, part 2: mechanisms. Sleep 25(5):499–506
Labombarda F, Meffre D, Delespierre B et al (2010) Membrane progesterone receptors localization in the mouse spinal cord. Neuroscience 166(1):94–106
Lefter R, Morency C-E, Joseph V (2007) Progesterone increases hypoxic ventilatory response and reduces apneas in newborn rats. Respir Physiol Neurobiol 156(1):9–16
Maller JL (2003) Signal transduction. Fishing at the cell surface. Science 300(5619):594–595
Mani SK (2006) Signaling mechanisms in progesterone–neurotransmitter interactions. Neuroscience 138(3):773–781
Marcouiller F, Boukari R, Laouafa S et al (2014) The nuclear progesterone receptor reduces post-sigh apneas during sleep and increases the ventilatory response to hypercapnia in adult female mice. PLoS One 9(6), e100421
Pascual O, Morin-Surun MP, Barna B et al (2002) Progesterone reverses the neuronal responses to hypoxia in rat nucleus tractus solitarius in vitro. J Physiol 544(2):511–520
Ren J, Greer JJ (2006) Neurosteroid modulation of respiratory rhythm in rats during the perinatal period. J Physiol 574(2):535–546
Revelli A, Massobrio M, Tesarik J (1998) Nongenomic actions of steroid hormones in reproductive tissues 1. Endocr Rev 19(1):3–17
Romeo RD, Bellani R, McEwen BS (2005) Stress-induced progesterone secretion and progesterone receptor immunoreactivity in the paraventricular nucleus are modulated by pubertal development in male rats. Stress 8(4):265–271
Shahar E, Redline S, Young T et al (2003) Hormone replacement therapy and sleep-disordered breathing. Am J Respir Crit Care Med 167(9):1186–1192
Singh M, Su C, Ng S (2013) Non-genomic mechanisms of progesterone action in the brain. Front Neurosci 7
Skatrud JB, Dempsey JA, Kaiser DG (1978) Ventilatory response to medroxyprogesterone acetate in normal subjects: time course and mechanism. J Appl Physiol Respir Environ Exerc Physiol 44(6):939–944
Yamazaki H, Haji A, Ohi Y et al (2005) Effects of progesterone on apneic events during behaviorally defined sleep in male rats. Life Sci 78(4):383–388
Zhu Y, Bond J, Thomas P (2003a) Identification, classification, and partial characterization of genes in humans and other vertebrates homologous to a fish membrane progestin receptor. Proc Natl Acad Sci 100(5):2237–2242
Zhu Y, Rice CD, Pang Y et al (2003b) Cloning, expression, and characterization of a membrane progestin receptor and evidence it is an intermediary in meiotic maturation of fish oocytes. Proc Natl Acad Sci 100(5):2231–2236
Zwillich CW, Natalino MR, Sutton FD et al (1978) Effects of progesterone on chemosensitivity in normal men. J Lab Clin Med 92(2):262–269

# 31 Inhibition of Protein Kinases AKT and $ERK_{1/2}$ Reduce the Carotid Body Chemoreceptor Response to Hypoxia in Adult Rats

Pablo Iturri, Vincent Joseph, Gloria Rodrigo, Aida Bairam, and Jorge Soliz

**Abstract**

The carotid body is the main mammalian oxygen-sensing organ regulating ventilation. Despite the carotid body is subjected of extensive anatomical and functional studies, little is yet known about the molecular pathways signaling the neurotransmission and neuromodulation of the chemoreflex activity. As kinases are molecules widely involved in motioning a broad number of neural processes, here we hypothesized that pathways of protein kinase B (AKT) and extracellular signal-regulated kinases ½ (ERK1/2) are implicated in the carotid body response to hypoxia. This hypothesis was tested using the in-vitro carotid body/carotid sinus nerve preparation ("en bloc") from Sprague Dawley adult rats. Preparations were incubated for 60 min in tyrode perfusion solution (control) or containing 1 μM of LY294002 (AKT inhibitor), or 1 μM of UO-126 (ERK1/2 inhibitor). The carotid sinus nerve chemoreceptor discharge rate was recorded under baseline (perfusion solution bubbled with 5 % $CO_2$ balanced in $O_2$) and hypoxic (perfusion solution bubbled with 5 % $CO_2$ balanced in $N_2$) conditions. Compared to control, both inhibitors signifi-

P. Iturri
Department of Pediatrics, Centre de Recherche de l'Hôpital St-François d'Assise (CR-SFA), Faculty of Medicine, Centre Hospitalier Universitaire de Québec (CHUQ), Laval University, 10, rue de l'Espinay, Québec G1L 3L5, QC, Canada

Molecular Biology and Biotechnology Institute, Universidad Mayor de San Andres, La Paz, Bolivia

V. Joseph • J. Soliz, Ph.D. (✉)
Department of Pediatrics, Centre de Recherche de l'Hôpital St-François d'Assise (CR-SFA), Faculty of Medicine, Centre Hospitalier Universitaire de Québec (CHUQ), Laval University, 10, rue de l'Espinay, Québec G1L 3L5, QC, Canada
e-mail: jorge.soliz@crchuq.ulaval.ca

A. Bairam, M.D., Ph.D.
Pediatric Department, Laval University, Research Center of Centre Hospitalier, Universitaire de Quebec, 10, rue de l'Espinay, Quebec City, QC, Canada

Centre de recherche du CHUQ, HSFA, 10, rue de l'Espinay, Québec G1L 3L5, QC, Canada
e-mail: Aida.bairam@crsfa.ulaval.ca

G. Rodrigo
Molecular Biology and Biotechnology Institute, Universidad Mayor de San Andres, La Paz, Bolivia



C. Peers et al. (eds.), *Arterial Chemoreceptors in Physiology and Pathophysiology*, Advances in Experimental Medicine and Biology 860, DOI 10.1007/978-3-319-18440-1_31

cantly decreased the normoxic and hypoxic carotid body chemoreceptor activity. LY294002- reduced carotid sinus nerve discharge rate in hypoxia by about 20 %, while UO-126 reduces the hypoxic response by 45 %. We concluded that both AKT and ERK1/2 pathways are crucial for the carotid body intracellular signaling process in response to hypoxia.

**Keywords**
Carotid body • Hypoxia • Chemoreception • ERK • AKT

## 31.1 Introduction

Carotid bodies are sensory organs whose stimulation by the hypoxemia activates the chemoreflex pathway (Prabhakar and Overholt 2000). The glomus cells (the chemoreceptive elements of carotid bodies) contain $O_2$ sensitive potassium channels whose "open probability" decreases during hypoxia(Lopez-Barneo et al. 2001; Weir et al. 2005). The inhibition of $K^+$ channels (Lopez-Barneo et al. 1988; Ganfornina and Lopez-Barneo 1991) leads to cell depolarization, calcium channels opening and transmembrane calcium influx (Buckler and Vaughan-Jones 1994; Urena et al. 1994). The increase in cytosolic calcium triggers the release of neurotransmitters (Montoro et al. 1996), including catecholamines, adenosine triphosphate (ATP) and acetylcholine (Ach) (Prabhakar and Overholt 2000; Bairam and Carroll 2005), which, in turns increases carotid sinus nerve activity and ventilation in response to hypoxia.

While research in carotid bodies has mainly focused on the mechanisms of oxygen sensing, little is yet known about the pathways signaling the neurotransmission and neuromodulation of the chemoreflex activity. Besides, the pathways of protein kinase B (AKT) and extracellular signal-regulated kinases ½ (ERK1/2), are involved in major processes accomplishing a wide variety of neural tasks, including glucose metabolism (Engelman et al. 2006), cellular apoptosis and survival (Teng et al. 2014), differentiation (Chan et al. 2013), neural proliferation and migration (Dey et al. 2005), neuro-protection (Zhang et al. 2014), neuro-degeneration (Fang et al. 2014), and synaptic signaling (Yoshii and Constantine-Paton 2014. Moreover, AKT and ERK1/2 in brain tissue participate in the modulation of dopaminergic (Beaulieu et al. 2006), muscarinic (Rosenblum et al. 2000), adrenergic (Taraviras et al. 2002), serotonergic (Cowen 2007), GABAergic (Balasubramanian et al. 2004) and adenosinergic (Wiese et al. 2007) neurotransmission. As most of these substances are endogenously synthetized by the carotid body chemoreceptor cells and modulate the activity of glomus cells and carotid sinus nerve, we hypothetized that both ATK and ERK1/2 are involved in the carotid body function. Indeed, recent evidence showed that human carotid body cells are immunopositive for AKT and ERK1/2 and that their phosphorylated forms (pAKT, pERK) are expressed in an age-dependent manner (Porzionato et al. 2010). While the expression and activity of AKT and ERK1/2 and their phosphorylated forms were low at fetal age (mean age of 177 days post-conception), it increases significantly at infancy (mean age of 10 months postnatal), and then remained stable at young (mean age of 38 years) and adult ages (mean age of 72.4 years) (Porzionato et al. 2010). These findings suggest that both molecules are implicated in carotid body function at early ages, but also support our hypothesis that ATK and ERK1/2 pathways contribute to the function of the carotid body in adult animals. Using an *in vitro* recording technique we evaluated the chemoreceptor activity throughout the carotid sinus nerve. Our results showed that AKT and ERK1/2 are molecules involved in the carotid body response to hypoxia, and in consequence, in the carotid body chemoreflex activity regulating ventilation.

## 31.2 Material and Methods

### 31.2.1 Animals

Male Sprague–Dawley adult rats from Charles River distributor (St. Constant, Québec, Canada) were used in this study. After purchasing, rats were maintained in our animal facility for at least 1 week before experimentation. Rats were kept on 12:12-h light–dark cycle with 24-h free access to pellet food and water. Experiments were performed in 30 rats aged between 12 and 16 weeks. The carotid body from one side was used as control the carotid body from the other side was incubated with an AKT inhibitor (LY294002; AKT group) or an ERK1/2 inhibitor (UO-126; ERK group). The success rate for our recordings (carotid bodies with a reversible response to hypoxia) was 65 %. As such, the number of carotid bodies used is: 19 for the control group, 10 for the AKT group, and 10 for the ERK group. All experimental protocols were approved by the local committee of animal care of Laval University and are in concordance with the guidelines of the Canadian Council of Animal Care.

#### 31.2.1.1 Ex Vivo Electrophysiological Recording of the Carotid Sinus Nerve (CSN) Activity

The rats were anesthetised with ketamine/xylacine (0.1 ml/100 g, i.p.), both carotid bifurcations were removed "en bloc". The excised tissue was placed in a petri dish containing ice-cold Tirode solution (in mM: 125 NaCl, 5 KCl, 2 MgSO4, 1.2 NaH2 PO4, 25 NaHCO3, 1.8 CaCl2, 5 sucrose, and 10 glucose, pH 7.4), bubbled with 5 % $CO_2$ balance in $O_2$. In following, the carotid body sinus nerve (CSN) was carefully dissected and cleaned from surrounding connective tissue (Fig. 31.1). We used the standard in vitro recording of the CSN activity, as previously described (Joseph et al. 2012). In brief, the preparation was transferred to a recording chamber, thermostated at 36 °C (TC2Bip temperature controller; Cell Micro-Controls; Norfolk, VA, USA), and superfused at a flow rate of 6 mL/min with Tyrode solution bubbled with 5 % $CO_2$ balance in $O_2$; pH 7.4. The CSN was drawn up into the tip of a glass suction electrode (Model # 573000, A-M Systems Inc., Carlsborg, WA) for monopolar recording of the activity. Sufficient suction was applied to seal the electrode tip against connective tissue encircling the junction of the carotid body and CSN. A reference electrode was gently placed over the carotid body, making contact with its surface, while a grounding electrode is placed in the recording chamber. The neural signal was fed to a differential input head-stage preamplifier, filtered (30–1,500 Hz), and amplified (Neurolog modules NL100AK, NL104A, NL126, NL106). The signal was then processed by an A/D converter (Micro 1401–2 Cambridge

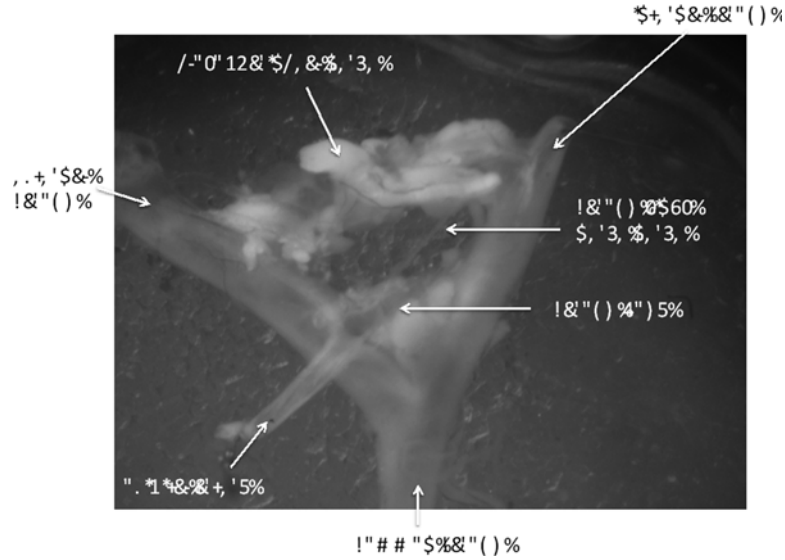


**Fig. 31.1** "En block" dissection of the carotid bifurcation containing the carotid body and the carotid sinus nerve (CSN)

Electronic Design (CED), Cambridge, UK) for display of raw activity and frequency histograms on a computer running the Spike 2 software (CED). Chemoreceptor discharges are discriminated in Spike 2 as action potentials with amplitude of 25 % above baseline noise and which responded to a decrease in superfusate $PO_2$ with a reversible increase in discharge frequency.

### 31.2.2 Experimental Protocol

The impact of AKT and ERK1/2 on the CSN chemoreceptor discharge rate was assessed as follows. Each carotid body preparation was incubated at 36 °C with Tyrode solution only (control), or with Tyrode solution containing either 1 μM LY294002 (AKT inhibitor; Cell Sygnaling, North Carolina, USA), or 1 μM of UO-126 (ERK1/2 inhibitor; Cell Sygnaling, North Carolina, USA). The incubation period lasted 60 min. Once in the recording chamber, the experiment began when a stable CSN discharge rate was observed under baseline condition for at least 10 min (Tyrode solution bubbled with 5 % $CO_2$ balance in $O_2$). Then normoxic recording was maintained for further 5 min before switching to hypoxic conditions (Tyrode solution bubbled with 5 % $CO_2$ balance in $N_2$), which was maintained until stable activity was observed (about a total of 5–7 min). Finally, the preparation was returned to normoxic conditions (recovery: Tyrode solution bubbled with 5 % $CO_2$ balance in $O_2$) for additional 10 min. This last recording was used to assure the viability of the preparation and its ability to recover from hypoxia. Each carotid body preparation was used for a maximum of two complete experiments covering normoxia, hypoxia and recovery. In these cases, the mean of both responses was calculated and this value was considered as one experiment.

### 31.2.3 Data Analysis

Average recording were obtained second-by-second. In following, 150 s were used to calculate the normoxic basal activity under normoxic and recovery conditions, and 250 s (from the "plato" of the response) was used to calculate the activity under hypoxic condition. All statistical analyses were performed using Prism software (version. 6). Finally, a t-student test was used to perform the statistical comparison between the different groups. All results were reported as mean SEM. $P<0.05$ was considered statistically significant.

## 31.3 Results

### 31.3.1 AKT Inhibitor (LY294002) Reduces CSN Activity

LY294002 decreased CSN discharge in normoxia (from $6.4\pm0.1$ to $5.3\pm0.1$ impulses per second ($p<0.0001$, Fig. 31.2d), hypoxia, (from $12.5\pm0.03$ to $10.0\pm0.1$ impulses per second ($p<0.0001$, Fig. 31.2e) and during recovery (from $6.1\pm0.1$ to $4.6\pm0.1$ impulses per second ($p<0.0001$, $n=19$ untreated $n=10$ LY294002 treated carotid body explants, Fig. 31.2f), indicating that LY294002 has the capacity to alter the carotid body response to hypoxia.

### 31.3.2 ERK1/2 Inhibitor (UO-126) Blunts the CSN Activity

UO-126 decreased CSN discharge in normoxia (from $6.4\pm0.1$ *vs.* $5.4\pm0.1$ impulses per second ($p<0.0001$, Fig. 31.3d), the CSN discharge was blunted in hypoxia, (from $12.4\pm0.1$ *vs.* $7.4\pm0.1$ impulses per second ($p<0.0001$, Fig. 31.3e) and decreased during recovery (from $6.6\pm0.1$ *vs.* $6.2\pm0.1$ impulses per second ($p<0.005$, $n=19$ untreated $n=10$ UO-126 treated carotid body explants, Fig. 31.3f). Finally, the inhibitory power of UO-126 on carotid sinus nerve activity in hypoxia was 25 % stronger than LY294002 (Fig. 31.4).

## 31.4 Discussion

This study shows that the inhibition of pathways of protein kinase B (AKT) and the extracellular signal-regulated kinases ½ (ERK1/2) reduces the carotid sinus nerve activity under normoxic,

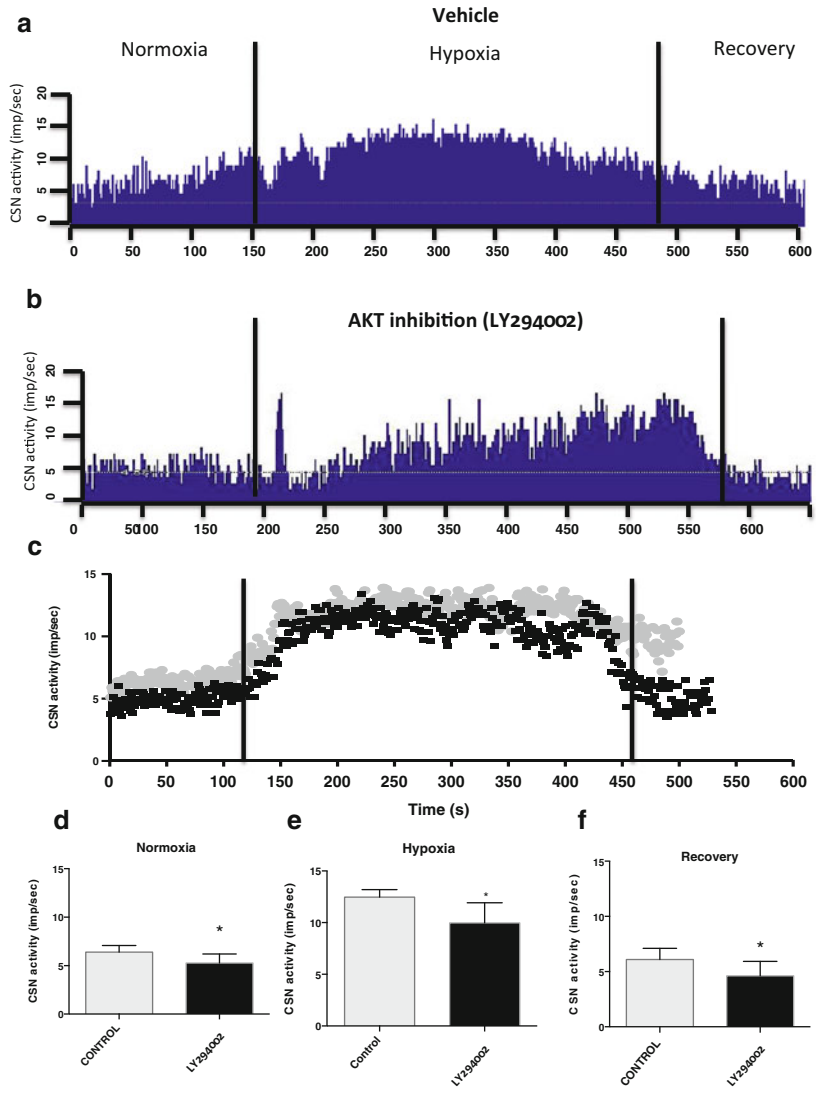


**Fig. 31.2** AKT inhibitor (LY294002) reduces CSN activity. (**a**) Typical recording of CSN activity in vitro preparation of superfused carotid body/CSN under normoxia, hypoxia and normoxia after hypoxia (recovery) (**b**) Recording of CSN activity in vitro preparation of superfused carotid body/CSN under normoxia, hypoxia and normoxia after hypoxia (recovery) under the effect of AKT inhibitor (LY294002). (**c**) Second-by-second normoxic (*left*), hypoxic (*center*) and recovery responses (*right*) of CSN, all results represent the mean (n = 10). (**d**, **e**, **f**) Graph bar representing the statistical difference between control and inhibitor exposed under normoxic, hypoxic and recovery state ($p < 0{,}001$)

hypoxic and recovery conditions. Interestingly however, while AKT inhibition decreased partially the hypoxic activity, ERK1/2 inhibition almost completely hinders it.

Both AKT and ERK½ are two important signaling pathways involved in the integration of extracellular signals that are particularly important for cell survival and proliferation (Dey et al. 2005; Teng et al. 2014). Growth factors, cytokines and many other cellular stimuli trigger the AKT signaling pathway, activating in turn many different substrates involved in various cellular functions, such survival, growth, proliferation, metabolism and migration (reviewed in Engelman

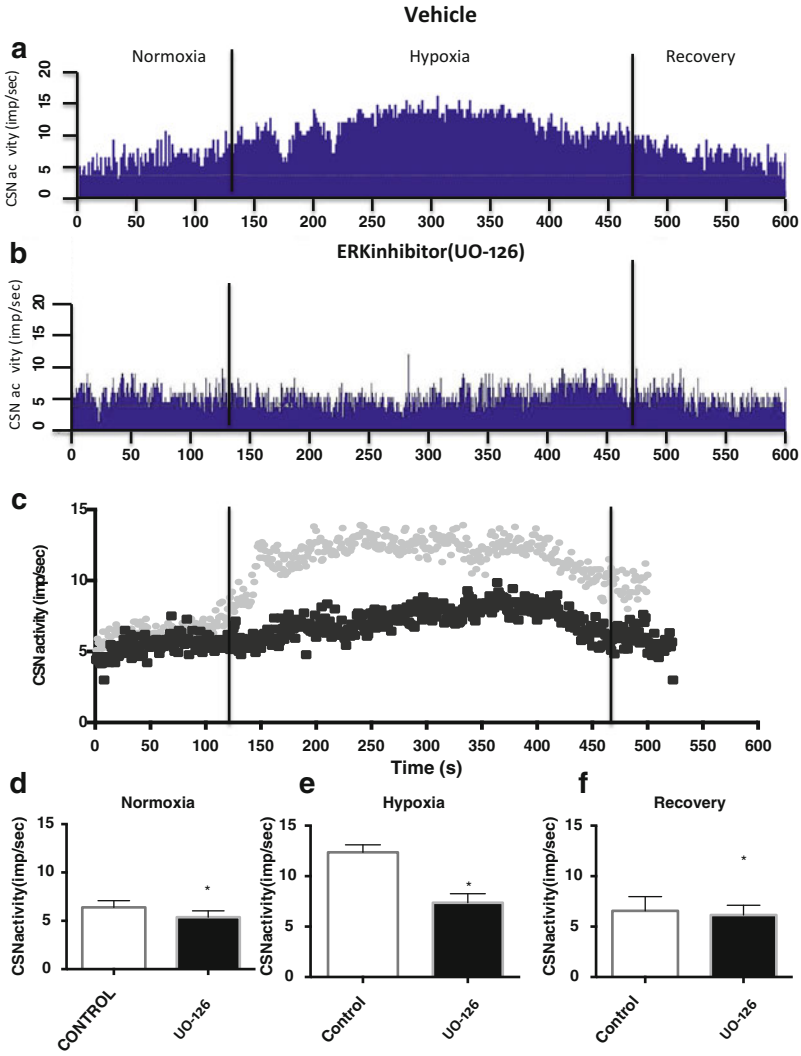


**Fig. 31.3** ERK1/2 inhibitor (UO-126) blunts the CSN activity. (**a**) Typical recording of CSN activity in vitro preparation of superfused carotid body/CSN under normoxia, hypoxia and normoxia after hypoxia (recovery) (**b**) Recording of CSN activity in vitro preparation of superfused carotid body/CSN under nomoxia, hypoxia and normoxia after hypoxia (recovery) under the effect of ERK inhibitor (UO126). (**c**) Second-by-second normoxic (*left*), hypoxic (*center*) and recovery responses (*right*) of CSN, all results represent the mean (n = 10). (**d**, **e**, **f**) Graph bar representing the statistical difference between control and inhibitor exposed under normoxic, hypoxic and recovery state ($p < 0{,}001$)

et al. 2006; Manning and Cantley 2007). In the nervous system, the activation of AKT pathway is required in the synaptic plasticity processes such long-term potentiation and long-term depression (Kelly and Lynch 2000; Sanna et al. 2002; Man et al. 2003; Opazo et al. 2003).

On the other hand, as other members of the serine/threonine protein kinases, ERK1/2 acts linking extracellular signals to nuclear events (Waskiewicz and Cooper 1995; Su and Karin 1996; Nishio et al. 2001), and the implication of ERK1/2 in cell proliferation process is classically known (reviewed in Chambard et al. 2007).

Important for this work is to remind however that dopaminergic (Beaulieu et al. 2006), muscarinic (Rosenblum et al. 2000), adrenergic

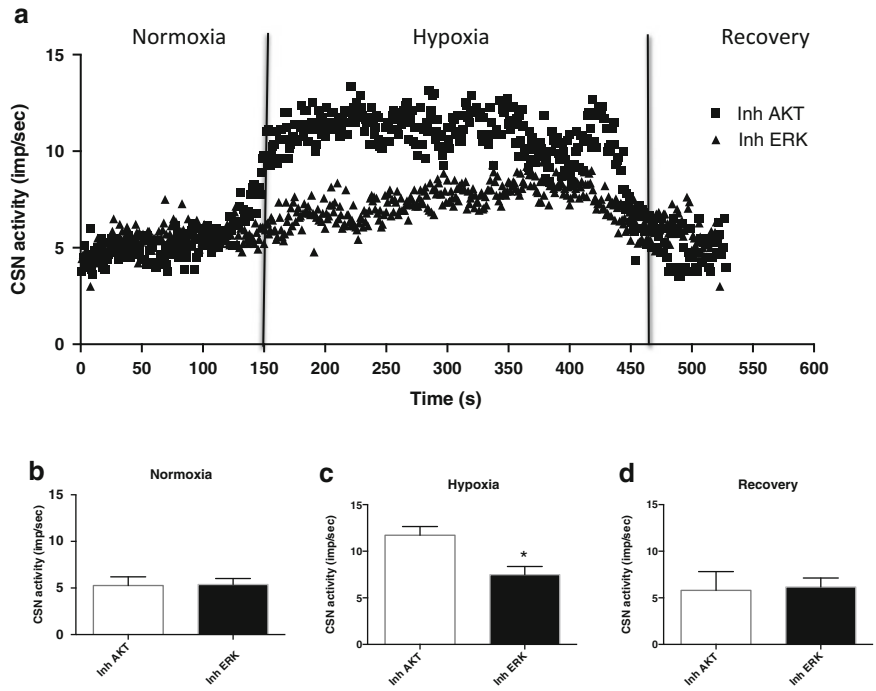


**Fig. 31.4** Comparative inhibition of LY294002 and UO-126. (**a**) Recording of CSN activity in vitro preparation of superfused carotid body/CSN under nomoxia, hypoxia and normoxia after hypoxia (recovery) under the effect of LY294002 and UO-126. (**b**, **c**, **d**) Graph bar representing the statistical difference of both inhibitors. Only hypoxia was statistically significant ($p<0{,}001$)

(Taraviras et al. 2002), serotonergic (Cowen 2007), GABAergic (Balasubramanian et al. 2004) and adenosinergic (Wiese et al. 2007) neurotransmission are processes modulated by AKT and ERK1/2. As these neurotransmitters are produced in the carotid body and regulated under hypoxia, we hypothesized that ATK and ERK1/2 pathways are involved in the regulation of carotid body function. Supporting this hypothesis, a recent study showed that AKT, ERK1/2, and its phosphorylated forms are expressed/activated in the human carotid body, especially at young and adult ages (Porcionato et al. 2010). Indeed, our results show that AKT and ERK1/2 significantly decrease the normoxic hypoxic and recovery CSN discharge. More interestingly, while AKT inhibition reduced the CSN activity partially, the inhibition of ERK1/2 abolished it completely. At the current stage of the knowledge, it is difficult to propose a regulatory mechanism for this process. Nevertheless, there are evidences showing that hypoxia activates AKT and ERK pathways (Lee et al. 2006; Beitner-Johnson et al. 2001; Hirai et al. 2004). As AKT and ERK1/2 regulate the expression of growth factors that in turn modulate the potassium current density (Borowiec et al. 2007), it is tempting to suggest that AKT & ERK1/2 participate in the synthesis and liberation of acetylcholine and ATP, which are the major carotid body neurotransmitters upon hypoxia.

In conclusion, we found that AKT and ERK1/2 signaling pathways, are crucially involved in regulating the CSN chemoreceptor activity (you do not measure any of these transmitters?). suggesting that both are involved the carotid body chemoreflex activity and consequently in the regulation of the ventilatory response to hypoxia.

**Acknowledgements** The authors wish to thank to Melanie Pelletier for her superb assistance and Richard Kinkead for fruitful discussions. J.S. is supported by grants from The Molly Towell Perinatal research Foundation (MTPRF), The Fonds de la Recherche Québec en Santé (FRQ-S: MOP-26974), and The Canadian Institute for Health Research (CIHR: MOP-130258).

## References


Bairam A, Carroll JL (2005) Neurotransmitters in carotid body development. Respir Physiol Neurobiol 149(1–3):217–232

Balasubramanian S, Teissere JA, Raju DV et al (2004) Hetero-oligomerization between GABAA and GABAB receptors regulates GABAB receptor trafficking. J Biol Chem 279(18):18840–18850

Beaulieu JM, Sotnikova TD, Gainetdinov RR et al (2006) Paradoxical striatal cellular signaling responses to psychostimulants in hyperactive mice. J Biol Chem 281(43):32072–32080

Beitner-Johnson D, Rust RT, Hsieh TC, Millhorn DE (2001) Hypoxia activates Akt and induces phosphorylation of GSK-3 in PC12 cells. Cell Signal 13(1):23–27

Borowiec AS, Hague F, Harir N, Guenin S, Guerineau F, Gouilleux F, Roudbaraki M, Lassoued K, Ouadid-Ahidouch H (2007) IGF-1 activates hEAG K(+) channels through an Akt-dependent signaling pathway in breast cancer cells: role in cell proliferation. J Cell Physiol 212(3):690–701

Buckler KJ, Vaughan-Jones RD (1994) Effects of hypoxia on membrane potential and intracellular calcium in rat neonatal carotid body type I cells. J Physiol 476(3):423–428

Chambard JC, Lefloch R, Pouyssegur J, Lenormand P (2007) ERK implication in cell cycle regulation. Biochim Biophys Acta 1773(8):1299–1310

Chan WS, Sideris A, Sutachan JJ et al (2013) Differential regulation of proliferation and neuronal differentiation in adult rat spinal cord neural stem/progenitors by ERK1/2, Akt, and PLCgamma. Front Mol Neurosci 6:23

Cowen DS (2007) Serotonin and neuronal growth factors – a convergence of signaling pathways. J Neurochem 101(5):1161–1171

Dey N, Howell BW, De PK et al (2005) CSK negatively regulates nerve growth factor induced neural differentiation and augments AKT kinase activity. Exp Cell Res 307(1):1–14

Engelman JA, Luo J, Cantley LC (2006) The evolution of phosphatidylinositol 3-kinases as regulators of growth and metabolism. Nat Rev Genet 7(8):606–619

Fang W, Gao G, Zhao H et al (2014) Role of the Akt/GSK-3beta/CRMP-2 pathway in axon degeneration of dopaminergic neurons resulting from MPP+ toxicity. Brain Res 1602:9–19

Ganfornina MD, Lopez-Barneo J (1991) Single K+ channels in membrane patches of arterial chemoreceptor cells are modulated by O2 tension. Proc Natl Acad Sci U S A 88(7):2927–2930

Hirai K, Hayashi T, Chan PH, Zeng J, Yang GY, Basus VJ, James TL, Litt L (2004) P13K inhibition in neonatal rat brain slices during and after hypoxia reduces phospho-Akt and increases cytosolic cytochrome c and apoptosis. Brain Res Mol Brain Res 124(1):51–61

Joseph V, Niane LM, Bairam A (2012) Antagonism of progesterone receptor suppresses carotid body responses to hypoxia and nicotine in rat pups. Neuroscience 207:103–109

Kelly A, Lynch MA (2000) Long-term potentiation in dentate gyrus of the rat is inhibited by the phosphoinositide 3-kinase inhibitor, wortmannin. Neuropharmacology 39(4):643–651

Lee SM, Lee CT, Kim YW, Han SK, Shim YS, Yoo CG (2006) Hypoxia confers protection against apoptosis via PI3K/Akt and ERK pathways in lung cancer cells. Cancer Lett 242(2):231–238

Lopez-Barneo J, Lopez-Lopez JR, Urena J et al (1988) Chemotransduction in the carotid body: K+ current modulated by PO2 in type I chemoreceptor cells. Science 241(4865):580–582

Lopez-Barneo J, Pardal R, Ortega-Saenz P (2001) Cellular mechanism of oxygen sensing. Annu Rev Physiol 63:259–287

Man HY, Wang Q, Lu WY, Ju W, Ahmadian G, Liu L, D'Souza S, Wong TP, Taghibiglou C, Lu J, Becker LE, Pei L, Liu F, Wymann MP, MacDonald JF, Wang YT (2003) Activation of PI3-kinase is required for AMPA receptor insertion during LTP of mEPSCs in cultured hippocampal neurons. Neuron 38(4):611–624

Manning BD, Cantley LC (2007) AKT/PKB signaling: navigating downstream. Cell 129(7):1261–1274

Montoro RJ, Urena J, Fernandez-Chacon R et al (1996) Oxygen sensing by ion channels and chemotransduction in single glomus cells. J Gen Physiol 107(1):133–143

Nishio H, Matsui K, Tsuji H, Tamura A, Suzuki K (2001) Immunolocalization of the mitogen-activated protein kinase signaling pathway in Hassall's corpuscles of the human thymus. Acta Histochem 103(1):89–98

Opazo P, Watabe AM, Grant SG, O'Dell TJ (2003) Phosphatidylinositol 3-kinase regulates the induction of long-term potentiation through extracellular signal-related kinase-independent mechanisms. J Neurosci 23(9):3679–3688

Porzionato A, Macchi V, Parenti A, De Caro R (2010) Extracellular signal-regulated kinase and phosphatidylinositol-3-kinase/AKT signalling pathways in the human carotid body and peripheral ganglia. Acta Histochem 112(4):305–316

Prabhakar NR, Overholt JL (2000) Cellular mechanisms of oxygen sensing at the carotid body: heme proteins and ion channels. Respir Physiol 122(2–3):209–221

Rosenblum K, Futter M, Jones M et al (2000) ERKI/II regulation by the muscarinic acetylcholine receptors in neurons. J Neurosci 20(3):977–985

Sanna PP, Cammalleri M, Berton F, Simpson C, Lutjens R, Bloom FE, Francesconi W (2002) Phosphatidylinositol 3-kinase is required for the expression but not for the induction or the maintenance of long-term potentiation in the hippocampal CA1 region. J Neurosci 22(9):3359–3365

Su B, Karin M (1996) Mitogen-activated protein kinase cascades and regulation of gene expression. Curr Opin Immunol 8(3):402–411

Taraviras S, Olli-Lahdesmaki T, Lymperopoulos A et al (2002) Subtype-specific neuronal differentiation of PC12 cells transfected with alpha2-adrenergic receptors. Eur J Cell Biol 81(6):363–374

Teng L, Kou C, Lu C et al (2014) Involvement of the ERK pathway in the protective effects of glycyrrhizic acid against the MPP+-induced apoptosis of dopaminergic neuronal cells. Int J Mol Med 34(3):742–748

Urena J, Fernandez-Chacon R, Benot AR et al (1994) Hypoxia induces voltage-dependent Ca2+ entry and quantal dopamine secretion in carotid body glomus cells. Proc Natl Acad Sci U S A 91(21):10208–10211

Waskiewicz AJ, Cooper JA (1995) Mitogen and stress response pathways: MAP kinase cascades and phosphatase regulation in mammals and yeast. Curr Opin Cell Biol 7(6):798–805

Weir EK, Lopez-Barneo J, Buckler KJ et al (2005) Acute oxygen-sensing mechanisms. N Engl J Med 353(19):2042–2055

Wiese S, Jablonka S, Holtmann B et al (2007) Adenosine receptor A2A-R contributes to motoneuron survival by transactivating the tyrosine kinase receptor TrkB. Proc Natl Acad Sci U S A 104(43):17210–17215

Yoshii A, Constantine-Paton M (2014) Postsynaptic localization of PSD-95 is regulated by all three pathways downstream of TrkB signaling. Front Synaptic Neurosci 6:6

Zhang X, Zhang Q, Tu J et al (2014) Prosurvival NMDA 2A receptor signaling mediates postconditioning neuroprotection in the hippocampus. Hippocampus 25(3):286–296

# 32 Ecto-5′-Nucleotidase, Adenosine and Transmembrane Adenylyl Cyclase Signalling Regulate Basal Carotid Body Chemoafferent Outflow and Establish the Sensitivity to Hypercapnia

Andrew P. Holmes, Ana Rita Nunes, Martin J. Cann, and Prem Kumar

**Abstract**

Carotid body (CB) stimulation by hypercapnia causes a reflex increase in ventilation and, along with the central chemoreceptors, this prevents a potentially lethal systemic acidosis. Control over the CB chemoafferent output during normocapnia and hypercapnia most likely involves multiple neurotransmitters and neuromodulators including ATP, acetylcholine, dopamine, serotonin and adenosine, but the precise role of each is yet to be fully established. In the present study, recordings of chemoafferent discharge frequency were made from the isolated *in vitro* CB in order to determine the contribution of adenosine, derived specifically from extracellular catabolism of ATP, in mediating basal chemoafferent activity and responses to hypercapnia. Pharmacological inhibition of ecto-5′-nucleotidase (CD73), a key enzyme required for extracellular generation of adenosine from ATP, using α,β-methylene ADP, virtually abolished the basal normocapnic single fibre discharge frequency (superfusate $PO_2 \sim 300$ mmHg, $PCO_2 \sim 40$ mmHg) and diminished the chemoafferent response to hypercapnia ($PCO_2 \sim 80$ mmHg). These effects were mimicked by the blockade of adenosine receptors with 8-(p-sulfophenyl)

A.P. Holmes (✉) • P. Kumar
Level 1 IBR, School of Clinical and Experimental Medicine, University of Birmingham, Edgbaston, Birmingham B15 2TT, UK
e-mail: a.p.holmes@bham.ac.uk

A.R. Nunes
CEDOC, Chronic Diseases Research Center, NOVA Medical School/Faculdade de Ciências Médicas, Universidade Nova de Lisboa, Campo Mártires da Pátria, 130, Lisbon 1169-056, Portugal

M.J. Cann
School of Biological and Biomedical Sciences, Durham University, South Road, Durham DH1 3LE, UK



C. Peers et al. (eds.), *Arterial Chemoreceptors in Physiology and Pathophysiology*, Advances in Experimental Medicine and Biology 860, DOI 10.1007/978-3-319-18440-1_32

theophylline. The excitatory impact of adenosinergic signalling on CB hypercapnic sensitivity is most likely to be conferred through changes in cAMP. Here, inhibition of transmembrane, but not soluble adenylate cyclases, reduced normocapnic single fibre activity and inhibited the elevation evoked by hypercapnia by approximately 50 %. These data therefore identify a functional role for CD73 derived adenosine and transmembrane adenylate cyclases, in modulating the basal chemoafferent discharge frequency and in priming the CB to hypercapnic stimulation.

**Keywords**
Carotid body • Adenosine • Hypercapnia • Ecto-5′-nucleotidase • cAMP

## 32.1 Introduction

The mammalian carotid bodies (CBs) are the primary peripheral chemoreceptors that respond to acute hypoxia, and stimulation drives the reflex hyperventilation that acts to preserve $O_2$ delivery and metabolism in the brain and vital organs (Kumar 2009). However, the importance of the CB in the regulation of breathing is not limited to hypoxia. Continuous chemoafferent input from CB into the central nervous system (CNS) is thought to account for up to 60 % of eupneic ventilation (Blain et al. 2009). Furthermore, the CBs are activated by other blood stimuli including hypercapnia and acidosis, both of which are potentially lethal if not adequately countered.

It was originally proposed that approximately 30–50 % of the reflex ventilatory response to arterial hypercapnia was mediated through direct stimulation of the CB (Heeringa et al. 1979; Rodman et al. 2001), with the remaining contribution arising from chemoreceptors located in the CNS (Nattie 1999). However, a more recent investigation has shown that a complete silencing of the CB chemoafferent output significantly depresses the central $CO_2$ chemoreceptor sensitivity (Blain et al. 2010). Therefore, in addition to direct hypercapnic CB excitation, maintenance of a tonic CB chemoafferent signal into the CNS seems to have an important role in establishing the hypercapnic sensitivity of the central chemoreceptors and further emphasises the importance of the CB in blood $CO_2$ and pH homeostasis.

Control over the CB chemoafferent output in basal conditions and during hypercapnia most likely involves multiple neurotransmitters and neuromodulators including ATP, acetylcholine, dopamine, serotonin and adenosine (Nurse 2010), but the contribution of each is yet to be fully characterised. Despite adenosine being an established neuromodulatory substance in the central nervous system (Cunha 2001), its source and physiological role in the CB remains somewhat unresolved. Up to now the majority of investigations have focused on the action of adenosine in mediating the CB response to acute changes in $O_2$ tension (McQueen and Ribeiro 1986; Conde et al. 2006, 2012) or the adaptations following chronic hypoxia (Livermore and Nurse 2013). However, the physiological importance and source of endogenous adenosine in establishing basal CB chemoafferent activity and responses to hypercapnia is unclear.

Physiologically active concentrations of adenosine, present in the synapse between the CB type I cell and the adjacent chemoafferent neurone, may originate from multiple sources. First, adenosine may be generated via extracellular catabolism of ATP; an excitatory neurotransmitter that is secreted from type I and type II cells (Zhang et al. 2012; Piskuric and Nurse 2013). This conversion requires two key enzymes; ectonucleoside triphosphate diphosphohydrolyase 1 (CD39) and ecto-5′-nucleotidase (CD73) (Bianchi and Spychala 2003). Second, adenosine may be formed in the type I cell and then released into the synapse through the bidirectional equilibrative nucleotide transporter (ENT) (Cass et al. 1998). Measurements of whole organ adenosine suggest a possible contribution of both sources to

the total 'pool' of available adenosine and this may be subject to variation depending on the ambient level of $O_2$ (Conde and Monteiro 2004; Conde et al. 2012). This current study aims to more clearly define the functional importance of endogenous adenosine specifically generated from extracellular catabolism of ATP in modulating the sensory neuronal output of the CB, both under basal conditions and during hypercapnia.

The four G-protein coupled adenosine receptors cloned to data ($A_1$, $A_{2A}$, $A_{2B}$ and $A_3$) all exert their actions through inhibition or excitation of transmembrane adenylyl cyclases (tmACs) and production of cAMP (reviewed in (Ribeiro and Sebastiao 2010)). Thus any functional role of adenosine is likely to be conferred through modifications in cAMP accumulation. We have previously reported that the CB expresses numerous different tmAC mRNA transcripts (Nunes et al. 2013) as well as the soluble AC (sAC) isoform (Nunes et al. 2009). CB cAMP is elevated during hypercapnia (Perez-Garcia et al. 1990) and, in isolated type I cells, cAMP analogues potentiate inward $Ca^{2+}$ current in a manner that is quantitatively similar to hypercapnia (Summers et al. 2002). Here we investigate whether direct targeting of tmAC or sAC impairs the CB chemoafferent outflow in normocapnia and/or hypercapnia.

## 32.2 Methods

### 32.2.1 Ethical Approval

All surgical procedures were performed in accordance with project and personal licences issued under the UK Animals (Scientific Procedures) Act 1986 and were approved by the Biomedical Services Unit at the University of Birmingham.

### 32.2.2 Extracellular Recordings of Single and Few-Fibre Chemoafferent Neurones

The whole carotid bifurcation along with the attached carotid sinus nerve (CSN) and CB were isolated from adult male Wistar rats (50–200 g) under inhalation anaesthesia (2–4 % isoflurane in $O_2$). Following tissue removal, animals were immediately killed by exsanguination. The bifurcations were rapidly transferred into an ice cold bicarbonate buffered extracellular Krebs solution containing, in mM: 115 NaCl, 4.5 KCl, 1.25 $NaH_2PO_4$, 5 $Na_2SO_4$, 1.3 $MgSO_4$, 24 $NaHCO_3$, 2.4 $CaCl_2$, 11 D-glucose, equilibrated with 95 % $O_2$ and 5 % $CO_2$.

Extracellular recordings of single or few-fibre chemoafferent activity were made from the cut end of the CSN, as described previously (Holmes et al. 2014). The chemoafferent derived voltage was recorded using a CED micro1401 and visualised on a PC with Spike2 software (Cambridge Electronic Design, Cambridge, UK). The chemoafferent voltage signal was sampled at 15,000 Hz. Using the in-built wavemark analysis in the Spike2 software, electrical activity originating from a single chemoafferent fibre was determined by its unique 'wavemark' signature based on frequency, shape and amplitude.

### 32.2.3 Experimental Solutions and Drugs

During experimentation, whole CBs were continuously superfused with a standard bicarbonate buffered Krebs solution containing, in mM: 115 NaCl, 4.5 KCl, 1.25 $NaH_2PO_4$, 5 $Na_2SO_4$, 1.3 $MgSO_4$, 24 $NaHCO_3$, 2.4 $CaCl_2$ and 11 D-glucose. All solutions were heated to 37 °C using a water bath (Grant W14; Grant Instruments, Cambridge, UK) and had a pH of 7.4 except during hypercapnic acidosis.

Chemoafferent responses to hypercapnia acidosis were induced by raising the superfusate $PCO_2$ from approximately 40 mmHg (pH 7.4) to 80 mmHg (pH 7.15) at a constant $PO_2$ (300 mmHg), as has been previously reported (Bin-Jaliah et al. 2005). Since the chemoafferent response to hypercapnia is thought to peak initially and then adapt to a lower sustained frequency (Black et al. 1971), measurements of chemoafferent activity were taken from the fifth minute of the hypercapnic stimulus, after a relatively steady state frequency had been achieved. $CO_2$ sensitivity was subsequently calculated as the increase in single fibre discharge frequency

per mmHg increase in superfusate $PCO_2$ ($\Delta$Hz/mmHg $PCO_2$), given that the rise in discharge frequency is linear over this $PCO_2$ range (Biscoe et al. 1970; Fitzgerald and Parks 1971; Pepper et al. 1995; Vidruk et al. 2001).

### 32.2.4 Analysis of Data

Values are expressed as mean ± standard error of mean unless otherwise stated. Statistical analysis was performed using (i) a paired 2-tailed student's t-test or (ii) repeated measures one way Analysis of Variance (ANOVA) with Bonferroni or Dunnett's post hoc analysis where appropriate (Prism v5; GraphPad Software, La Jolle, CA, USA). Significance was taken as $p < 0.05$.

## 32.3 Results

### 32.3.1 Basal Chemoafferent Outflow is Dependent on Ecto-5′-Nucleotidase (CD73) Activity and Adenosinergic Signalling

Basal chemoafferent output from the CB provides the peripheral component of the drive to breathe. Initial experiments sought to determine whether or not adenosine generated from extracellular ATP catabolism has any part in establishing this sensory neuronal activity of the CB. Pharmacological targeting of ecto-5′-nucleotidase (CD73; a key membrane bound enzyme involved in the formation of adenosine from extracellular ATP) using the inhibitor α,β-methylene ADP (AOPCP; 100 μM; Conde and Monteiro 2004) had a striking effect on basal single fibre activity, diminishing the discharge frequency by 91.2 ± 3.8 % (Fig. 32.1a *upper* and b). A similar (93.9 ± 1.9 %) reduction in basal frequency was observed in the presence of the adenosine receptor antagonist 8-(p-sulfophenyl) theophylline (8-SPT, 300 μM; Wyatt et al. 2007) (Fig. 32.1a *middle* and b). The four G-protein coupled adenosine receptors cloned to date ($A_1$, $A_{2A}$, $A_{2B}$ and $A_3$) all exert their actions through inhibition or excitation of transmembrane adenylyl cyclases (tmACs) and modification of cAMP production. In the current investigation, the presence of 9-(Tetrahydro-2-furanyl)-9*H*-purin-6-amine (SQ22536; a tmAC inhibitor; 200 μM, $IC_{50} = 20$ μM; (Rocher et al. 2009)) caused a 70.2 ± 16.0 % decrease in basal single fibre frequency (Fig. 32.1a *lower* and b). This is consistent with the idea that tonic generation of adenosine from ATP modulates basal CB neuronal outflow through production of cAMP.

### 32.3.2 Chemoafferent Responses to Hypercapnia Are Dependent on Ecto-5′-Nucleotidase (CD73) Activity, Adenosinergic Receptor Stimulation and Transmembrane Adenylyl Cyclase Production of cAMP

Experiments were designed to establish or rule out a potential role for endogenous adenosine in mediating the heightened sensory neuronal activity of the CB in hypercapnia. Selective inhibition of CD73 with AOPCP (100 μM) diminished the single fibre discharge frequency recorded in both normocapnic (40 mmHg $PCO_2$) and hypercapnic (80 mmHg $PCO_2$) conditions (Fig. 32.2a, b). Furthermore, AOPCP caused a dramatic (98.0 ± 1.8 %) reduction in CB $CO_2$ sensitivity (Fig. 32.2c). This inhibitory effect was rapidly reversed once the drug was removed from the superfusate as demonstrated in the raw trace example in Fig. 32.2a. Similar observations were made in the presence of 8-SPT (300 μM). 8-SPT significantly attenuated chemoafferent activity in both normocapnia and hypercapnia (Fig. 32.2d) and markedly decreased the CB $CO_2$ sensitivity by 81.5 ± 5.8 % (Fig. 32.2e).

As with the basal discharge, the excitatory impact of adenosinergic signalling on CB hypercapnic sensitivity is most likely to be conferred through activation of tmACs coupled to the adenosine receptors. Here, addition of the tmAC inhibitor SQ22536 (200 μM), produced a rapid reduction in normocapnic single fibre activity and inhibited the elevation evoked by hypercapnia

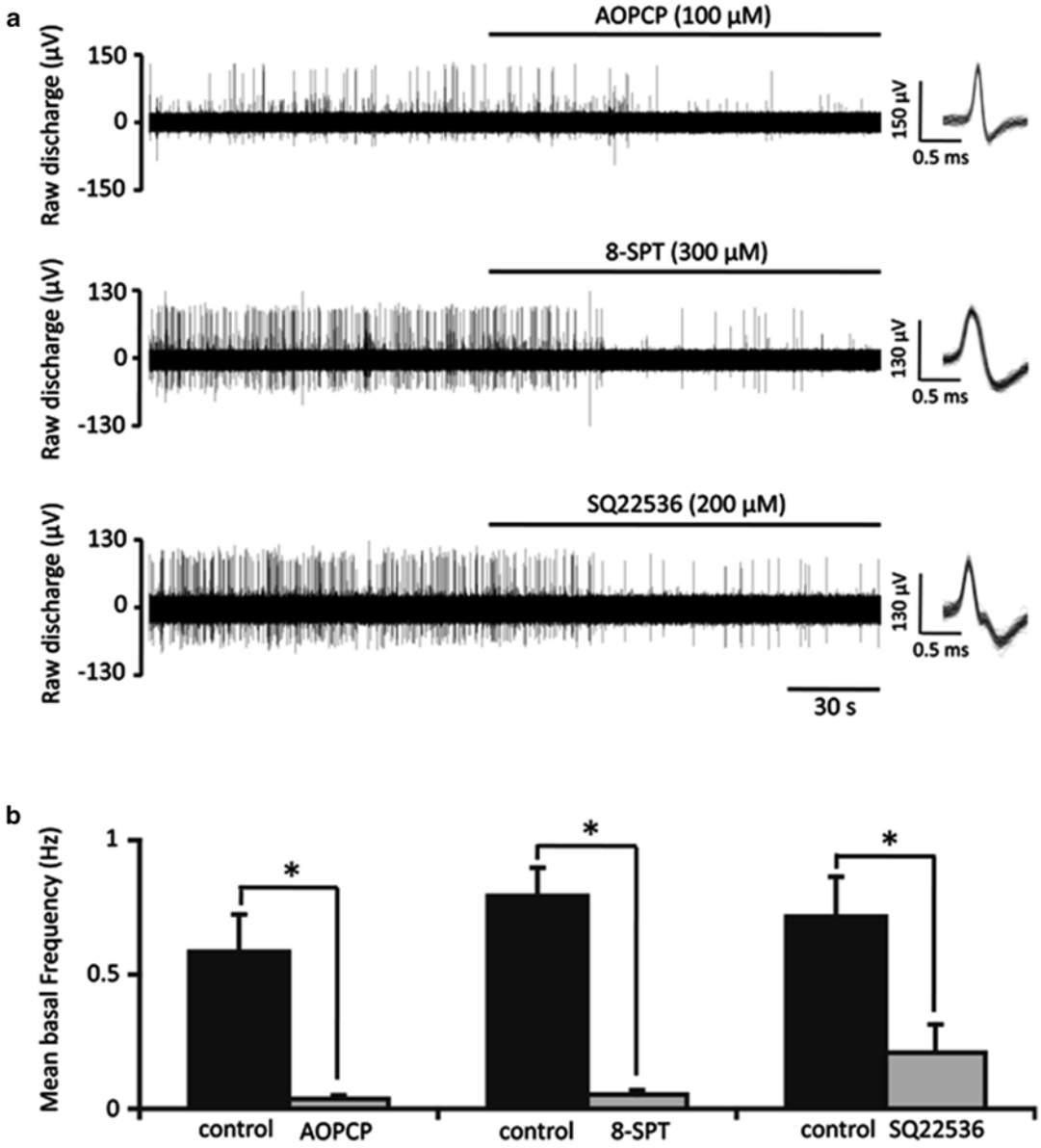


**Fig. 32.1** The basal chemoafferent discharge frequency of the carotid body (*CB*) is critically dependent on ecto-5′-nucleotidase (CD73) mediated formation of adenosine. (**a**) Example raw neuronal traces demonstrating the inhibitory impact of three different compounds on basal chemoafferent outflow: AOPCP (100 μM; inhibitor of CD73), 8-SPT (300 μM; non-selective adenosine receptor antagonist) and SQ22536 (200 μM; inhibitor of transmembrane adenylate cyclases). For each trace, overdrawn action potentials are shown inset to exhibit single fibre discrimination. (**b**) Mean single fibre basal frequencies in the presence and absence of each pharmacological agent. Data presented is from 6 fibres (n = 6) from 4 CB preparations (AOPCP), 6 fibres (n = 6) from 4 CB preparations (8-SPT) and 5 fibres (n = 5) from 4 CB preparations (SQ22536). Error bars indicate + S.E.M. * denotes $P < 0.05$ compared with control basal discharge frequency; paired Student's t-test

(Fig. 32.3a, b). In every fibre tested the absolute increase in hypercapnic discharge was reduced in the presence of SQ22536. Accordingly, further analysis showed that SQ22536 (200 μM) produced a 47.1 ± 9.4 % decline in CB $CO_2$ sensitivity (Fig. 32.3c). Normal hypercapnic responses

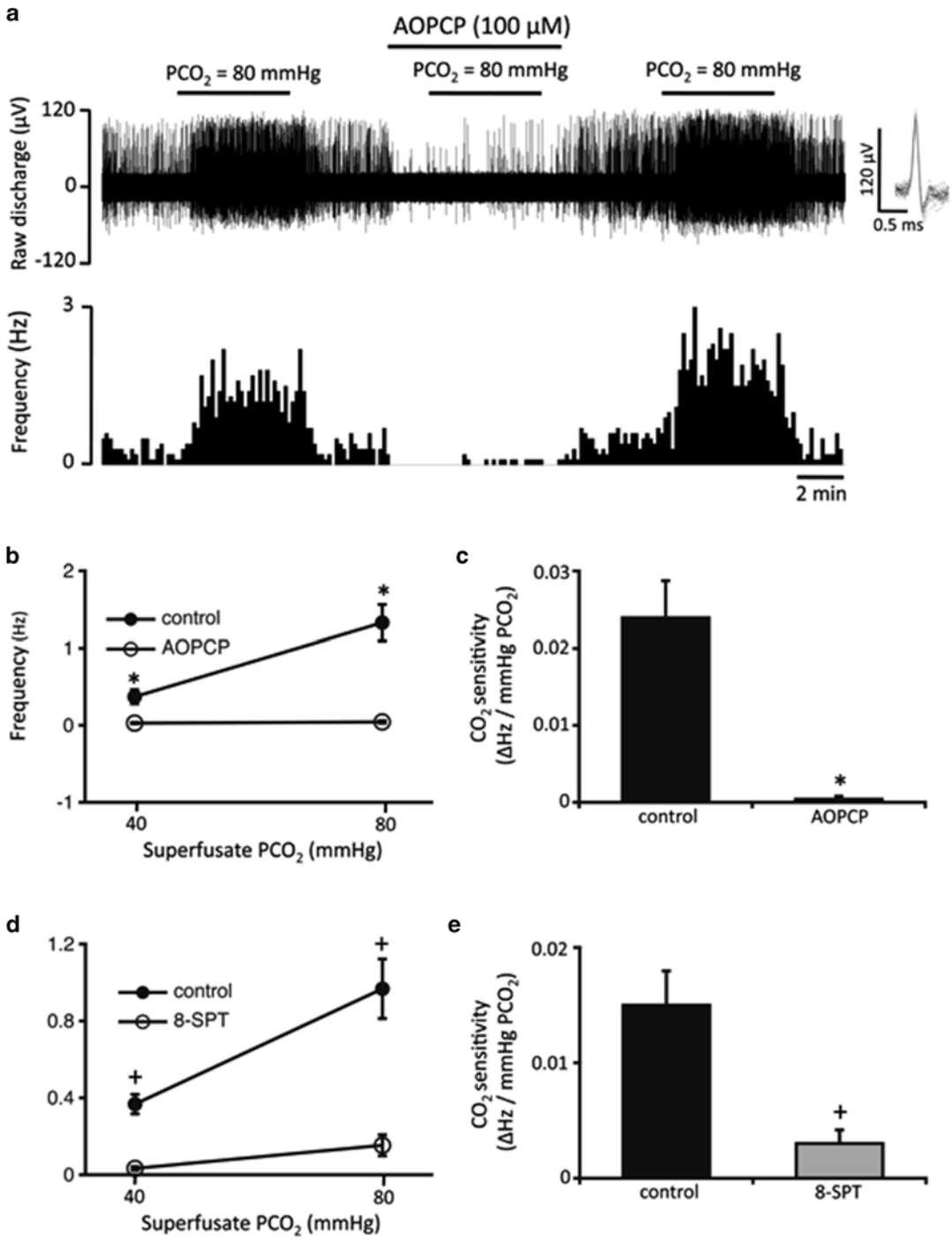


**Fig. 32.2** Carotid body (CB) responses to hypercapnia are mediated by adenosine generated from ecto-5′-nucleotidase (CD73). (**a**) An example electrophysiological recording of the CB response to 5 min of hypercapnia ($PCO_2 = 80$ mmHg) in the presence and absence of the CD73 inhibitor AOPCP. Raw discharge is shown (upper) along with frequency histograms (lower). Overdrawn action potentials are shown inset to demonstrate the single fibre discrimination used to measure frequency. The inhibitory action of AOPCP was readily reversible. (**b**) Mean discharge frequencies recorded in normocapnia ($PCO_2 = 40$ mmHg) and hypercapnia ($PCO_2 = 80$ mmHg),

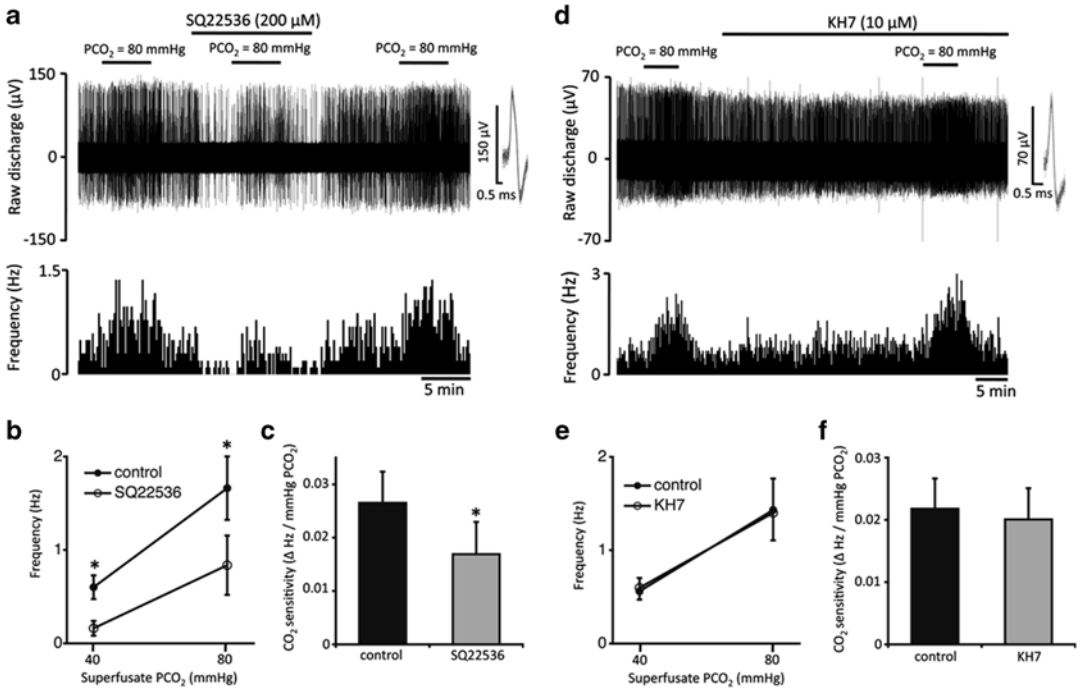


**Fig. 32.3** Rises in chemoafferent activity in hypercapnia are dependent on transmembrane (tmAC) but not soluble adenylate cyclase (sAC) activity. (**a**) Characteristic example recording of the response to hypercapnia ($PCO_2$ = 80 mmHg) in the presence and absence of the tmAC inhibitor SQ22536 (200 μM). Raw discharge is shown (*upper*) along with frequency histograms (*lower*). Overdrawn action potentials are shown inset to demonstrate the single fibre discrimination. The inhibitory impact of SQ22536 was fully reversible. (**b**) Mean single fibre discharge frequencies recorded in normocapnia ($PCO_2$ = 40 mmHg) and hypercapnia ($PCO_2$ = 80 mmHg), in control conditions and following addition of SQ22536 to the superfusate. Error bars indicate ± S.E.M. * denotes $P < 0.05$ compared with control group; one way repeated measures ANOVA with Bonferroni post hoc analysis. (**c**) Calculated mean $CO_2$ sensitivity (Δ Hz/mmHg $PCO_2$) in control conditions during SQ22536 drug application. Error bars indicate + S.E.M. * denotes $P < 0.05$ compared with control group; paired Student's t-test. For (**b**) and (**c**) the data presented is from 7 fibres (n = 7) from 4 CB preparations. (**d**) As for (**a**) but in the presence of the sAC inhibitor KH7 (10 μM). KH7 was applied for ~ 30 min to maximise delivery and uptake into the CB before exposure to hypercapnia. **(e)** Mean single fibre discharge frequencies recorded in normocapnia ($PCO_2$ = 40 mmHg) and hypercapnia ($PCO_2$ = 80 mmHg), for control and during application of KH7. Error bars indicate ± S.E.M. (**f**) Calculated $CO_2$ sensitivities (Δ Hz/mmHg $PCO_2$) for control and KH7 groups. Error bars indicate + S.E.M. For E) and F) data is from 5 fibres (n = 5) from 4 CB preparations

were readily restored following removal of the agent from the superfusate, as exemplified in Fig. 32.3a. In contrast, the soluble adenylyl cyclase (sAC) antagonist, 2-(1H-Benzo[d]imidazol-2-ylthio)-N′-(5-bromo-2-hydroxybenzylidene)propanehydrazide (KH7;

**Fig. 32.2** (continued) in control conditions and following addition of AOPCP. Error bars indicate ± S.E.M. * denotes $P < 0.05$ compared with control group; one way repeated measures ANOVA with Bonferroni post hoc analysis. (c) Calculated mean $CO_2$ sensitivity (Δ Hz/mmHg $PCO_2$) in control conditions and following AOPCP drug application. Error bars indicate + S.E.M. * denotes $P < 0.05$ compared with control group; paired Student's t-test. For B) and C) data is from 6 fibres (n = 6) from 5 CB preparations. (d) Mean discharge frequencies recorded in normocapnia and hypercapnia, in control conditions and in the presence of 8-SPT (300 μM), the non-selective adenosine receptor antagonist. Error bars indicate ± S.E.M. * denotes $P < 0.05$ compared with control group; one way repeated measures ANOVA with Bonferroni post hoc analysis. (e) Calculated mean $CO_2$ sensitivity (Δ Hz/mmHg $PCO_2$) for control and 8-SPT groups. Error bars indicate + S.E.M. * denotes $P < 0.05$ compared with control group; paired Student's t-test. For (d) and (e) data is from 7 fibres (n = 7) from 3 CB preparations

10 μM; (Nunes et al. 2013)), failed to impact on basal chemoafferent activity or the response to hypercapnia (Fig. 32.3d, e). KH7 (10 μM) did not alter CB $CO_2$ sensitivity even after prolonged incubation (Fig. 32.3d, f). These data therefore suggest that cAMP production mediates a component of the functional chemoafferent response to hypercapnia and that this is selectively dependent on tmAC rather than sAC activation.

## 32.4 Discussion

### 32.4.1 CD73, Adenosine and tmAC Signalling Mediate Basal CB Activity and the Sensitivity to Hypercapnia

The findings presented in this study indicate that extracellular adenosine formed selectively through catabolism of ATP, in the presence of ecto-5′-nucleotidase (CD73), has an important neuromodulatory role in mediating the CB sensory neuronal discharge, both under basal conditions and during stimulation by hypercapnia. In addition we show that tmAC but not sAC activity is necessary for full expression of CB hypercapnic sensitivity.

It has been previously reported that inhibition of ATP metabolism in normoxia by AOPCP decreases CB adenosine content (Conde and Monteiro 2004). Our observations suggest that this source of adenosine is functionally required in order to generate the basal chemoafferent outflow. The impact of adenosine is most likely to be conferred through modifications in cAMP, an excitatory signalling molecule in the CB (Nunes et al. 2014), given that the $A_{2A}$ and $A_{2B}$ adenosine receptor subtypes expressed in the CB (Gauda et al. 2000; Kobayashi et al. 2000; Conde et al. 2006) are coupled to tmACs (Ribeiro and Sebastiao 2010). Accordingly, in this investigation pharmacological inhibition of tmACs by SQ22536 caused a significant reduction in basal chemoafferent activity.

The basal sensory output from the CB accounts for up to 60 % of the drive to breath at rest (Blain et al. 2009) and may contribute to the resting sympathetic outflow to the vasculature (Kumar and Prabhakar 2012). Furthermore, it is the chronic rise in basal CB activity following CIH that is thought to drive the hypertension in patients with OSA (Narkiewicz et al. 1998; Peng et al. 2003). It is probable that overall chemoafferent output in normoxia is dependent on both spontaneous presynaptic (type I cell) depolarisation and neurotransmitter release, along with subsequent post-synaptic receptor activation. Chemoafferent neurones may also generate a degree of spontaneous activity. In large clusters of type I cells, spontaneous cellular depolarisation is reported to be a consequence of an attenuation of the background $K^+$ current, which is itself regulated by local 5-HT and PKC activation (Zhang and Nurse 2000; Zhang et al. 2003). The observations presented here suggest an additional signalling mechanism that is dependent on adenosine formation and tmAC mediated cAMP production.

It is becoming more apparent that the CB has a principal role in countering rises in arterial $CO_2$. As well as direct stimulation of the CB accounting for approximately 30–50 % of the reflex hypercapnic ventilatory response (Heeringa et al. 1979; Rodman et al. 2001), it has been recently shown that the CB chemoafferent outflow is necessary in establishing the $CO_2$ sensitivity of the central medullary chemoreceptors (Blain et al. 2010). Despite these important findings, the full transduction mechanisms that lead to an increase in CB discharge frequency during hypercapnia are still elusive. The results described here provide evidence that the heightened chemoafferent activity in hypercapnia is dependent on CD73 mediated catabolism of ATP to form adenosine. The principal origin of the synaptic ATP is most likely to be the type I cell given that ATP is secreted as a neurotransmitter in both normocapnic (Conde et al. 2012) and hypercapnic conditions (Zhang and Nurse 2004). Interestingly, in chemosensitive regions of the brainstem, hypercapnia-evoked ATP release occurs through the gap junctional protein, connexin26 (Cx26) (Huckstepp et al. 2010b). Direct binding of $CO_2$ prevents pore occlusion and effectively 'traps' Cx26 in an open conformation (Huckstepp et al. 2010a; Meigh et al. 2013). In the CB, recent evidence has identified a mechanism of ATP induced ATP release through pannexin channels in type II cells (Zhang et al. 2012). Whether

ATP is released from type II cells in normoxia and/or hypercapnia, thus acting as a substrate for additional adenosine formation, could be an interesting area for future investigating.

We also demonstrate that inhibitory targeting of tmACs also reduced the $CO_2$ sensitivity of the CB. This is in agreement with the idea that adenosine partially establishes the chemoafferent sensitivity of the CB to hypercapnia through tmAC dependent cAMP production. In the later instance however, a considerable proportion of the response to hypercapnia is preserved, which was in contrast to the results described using 8-SPT and AOPCP. This may have been due to incomplete run-down in tmAC function using SQ22536 or, more likely, that adenosine has additional actions that are independent of cAMP. These alternative downstream signalling pathways possibly involve activation of PKC or phospholipase C, as has been proposed for a component of the excitatory adenosine neuromodulation in the CNS (Cunha 2001).

The finding that SQ22536 but not KH7 reduces chemoafferent excitation in hypercapnia, suggests that cAMP regulation of CB $CO_2$ sensitivity is itself determined by tmAC and not sAC enzymatic activity. Although sAC is present in the CB (Nunes et al. 2009) and is directly stimulated by binding of $CO_2$ or $HCO_3^-$ (Townsend et al. 2009), it appears to have no functional contribution in moderating the chemoafferent frequency in hypercapnia. This is in accordance with our previous findings where KH7 failed to modify CB cAMP content when the organ was exposed to isohydric hypercapnia (Nunes et al. 2013). Thus we propose that rises in $CO_2$ or intracellular $HCO_3^-$ alone are insufficient to stimulate sAC enough to have functional effects on chemoafferent discharge in hypercapnia.

### 32.4.2 Conclusions

Endogenous adenosine produced from extracellular catabolism of ATP in the presence of ecto-5′-nucleotidase (CD73) is necessary for the generation of a basal chemoafferent discharge frequency. This basal discharge may be of clinical significance in a number of cardiorespiratory disorders where enhanced CB activity is associated with increased sympathetic outflow and thus with potential increase in patient morbidity and mortality. In addition this source of adenosine and tmAC generation of cAMP, acting downstream of adenosine receptors, are required for the full expression of the CB sensitivity to hypercapnia.

## References

Bianchi V, Spychala J (2003) Mammalian 5′-nucleotidases. J Biol Chem 278:46195–46198

Bin-Jaliah I, Maskell PD, Kumar P (2005) Carbon dioxide sensitivity during hypoglycaemia-induced, elevated metabolism in the anaesthetized rat. J Physiol 563:883–893

Biscoe TJ, Purves MJ, Sampson SR (1970) The frequency of nerve impulses in single carotid body chemoreceptor afferent fibres recorded in vivo with intact circulation. J Physiol 208:121–131

Black AM, McCloskey DI, Torrance RW (1971) The responses of carotid body chemoreceptors in the cat to sudden changes of hypercapnic and hypoxic stimuli. Respir Physiol 13:36–49

Blain GM, Smith CA, Henderson KS, Dempsey JA (2009) Contribution of the carotid body chemoreceptors to eupneic ventilation in the intact, unanesthetized dog. J Appl Physiol 106:1564–1573

Blain GM, Smith CA, Henderson KS, Dempsey JA (2010) Peripheral chemoreceptors determine the respiratory sensitivity of central chemoreceptors to CO(2). J Physiol 588:2455–2471

Cass CE, Young JD, Baldwin SA (1998) Recent advances in the molecular biology of nucleoside transporters of mammalian cells. Biochem Cell Biol 76:761–770

Conde SV, Monteiro EC (2004) Hypoxia induces adenosine release from the rat carotid body. J Neurochem 89:1148–1156

Conde SV, Obeso A, Vicario I, Rigual R, Rocher A, Gonzalez C (2006) Caffeine inhibition of rat carotid body chemoreceptors is mediated by A2A and A2B adenosine receptors. J Neurochem 98:616–628

Conde SV, Monteiro EC, Rigual R, Obeso A, Gonzalez C (2012) Hypoxic intensity: a determinant for the contribution of ATP and adenosine to the genesis of carotid body chemosensory activity. J Appl Physiol 112:2002–2010

Cunha RA (2001) Adenosine as a neuromodulator and as a homeostatic regulator in the nervous system: different roles, different sources and different receptors. Neurochem Int 38:107–125

Fitzgerald RS, Parks DC (1971) Effect of hypoxia on carotid chemoreceptor response to carbon dioxide in cats. Respir Physiol 12:218–229

Gauda EB, Northington FJ, Linden J, Rosin DL (2000) Differential expression of a(2a), A(1)-adenosine and D(2)-dopamine receptor genes in rat peripheral arterial chemoreceptors during postnatal development. Brain Res 872:1–10

Heeringa J, Berkenbosch A, de Goede J, Olievier CN (1979) Relative contribution of central and peripheral chemoreceptors to the ventilatory response to CO2 during hyperoxia. Respir Physiol 37:365–379

Holmes AP, Turner PJ, Carter P, Leadbeater W, Ray CJ, Hauton D, Buckler KJ, Kumar P (2014) Glycogen metabolism protects against metabolic insult to preserve carotid body function during glucose deprivation. J Physiol 592:4493–4506

Huckstepp RT, Eason R, Sachdev A, Dale N (2010a) CO2-dependent opening of connexin 26 and related beta connexins. J Physiol 588:3921–3931

Huckstepp RT, id Bihi R, Eason R, Spyer KM, Dicke N, Willecke K, Marina N, Gourine AV, Dale N (2010b) Connexin hemichannel-mediated CO2-dependent release of ATP in the medulla oblongata contributes to central respiratory chemosensitivity. J Physiol 588:3901–3920

Kobayashi S, Conforti L, Millhorn DE (2000) Gene expression and function of adenosine A(2A) receptor in the rat carotid body. Am J Physiol Lung Cell Mol Physiol 279:L273–L282

Kumar P (2009) Systemic effects resulting from carotid body stimulation-invited article. Adv Exp Med Biol 648:223–233

Kumar P, Prabhakar NR (2012) Peripheral chemoreceptors: function and plasticity of the carotid body. Compr Physiol 2:141–219

Livermore S, Nurse CA (2013) Enhanced adenosine A2b receptor signaling facilitates stimulus-induced catecholamine secretion in chronically hypoxic carotid body type I cells. Am J Physiol Cell Physiol 305:C739–C750

McQueen DS, Ribeiro JA (1986) Pharmacological characterization of the receptor involved in chemoexcitation induced by adenosine. Br J Pharmacol 88:615–620

Meigh L, Greenhalgh SA, Rodgers TL, Cann MJ, Roper DI, Dale N (2013) CO2 directly modulates connexin 26 by formation of carbamate bridges between subunits. eLife 2013;2:e01213

Narkiewicz K, van de Borne PJH, Montano N, Dyken ME, Phillips BG, Somers VK (1998) Contribution of tonic chemoreflex activation to sympathetic activity and blood pressure in patients with obstructive sleep apnea. Circulation 97:943–945

Nattie E (1999) CO2, brainstem chemoreceptors and breathing. Prog Neurobiol 59:299–331

Nunes AR, Monteiro EC, Johnson SM, Gauda EB (2009) Bicarbonate-regulated soluble adenylyl cyclase (sAC) mRNA expression and activity in peripheral chemoreceptors. Adv Exp Med Biol 648:235–241

Nunes AR, Holmes AP, Sample V, Kumar P, Cann MJ, Monteiro EC, Zhang J, Gauda EB (2013) Bicarbonate-sensitive soluble and transmembrane adenylyl cyclases in peripheral chemoreceptors. Respir Physiol Neurobiol 188:83–93

Nunes AR, Holmes AP, Conde SV, Gauda EB, Monteiro EC (2014) Revisiting cAMP signaling in the carotid body. Front Physiol 5:406

Nurse CA (2010) Neurotransmitter and neuromodulatory mechanisms at peripheral arterial chemoreceptors. Exp Physiol 95:657–667

Peng YJ, Overholt JL, Kline D, Kumar GK, Prabhakar NR (2003) Induction of sensory long-term facilitation in the carotid body by intermittent hypoxia: implications for recurrent apneas. Proc Natl Acad Sci U S A 100:10073–10078

Pepper DR, Landauer RC, Kumar P (1995) Postnatal development of CO2-O2 interaction in the rat carotid body in vitro. J Physiol 485(Pt 2):531–541

Perez-Garcia MT, Almaraz L, Gonzalez C (1990) Effects of different types of stimulation on cyclic AMP content in the rabbit carotid body: functional significance. J Neurochem 55:1287–1293

Piskuric NA, Nurse CA (2013) Expanding role of ATP as a versatile messenger at carotid and aortic body chemoreceptors. J Physiol 591:415–422

Ribeiro JA, Sebastiao AM (2010) Modulation and metamodulation of synapses by adenosine. Acta Physiol (Oxf) 199:161–169

Rocher A, Caceres AI, Almaraz L, Gonzalez C (2009) EPAC signalling pathways are involved in low PO2 chemoreception in carotid body chemoreceptor cells. J Physiol 587:4015–4027

Rodman JR, Curran AK, Henderson KS, Dempsey JA, Smith CA (2001) Carotid body denervation in dogs: eupnea and the ventilatory response to hyperoxic hypercapnia. J Appl Physiol 91:328–335

Summers BA, Overholt JL, Prabhakar NR (2002) CO(2) and pH independently modulate L-type Ca(2+) current in rabbit carotid body glomus cells. J Neurophysiol 88:604–612

Townsend PD, Holliday PM, Fenyk S, Hess KC, Gray MA, Hodgson DRW, Cann MJ (2009) Stimulation of mammalian G-protein-responsive adenylyl cyclases by carbon dioxide. J Biol Chem 284:784–791

Vidruk EH, Olson EB Jr, Ling L, Mitchell GS (2001) Responses of single-unit carotid body chemoreceptors in adult rats. J Physiol 531:165–170

Wyatt CN, Mustard KJ, Pearson SA, Dallas ML, Atkinson L, Kumar P, Peers C, Hardie DG, Evans AM (2007) AMP-activated protein kinase mediates carotid body excitation by hypoxia. J Biol Chem 282:8092–8098

Zhang M, Nurse CA (2000) Does endogenous 5-HT mediate spontaneous rhythmic activity in chemoreceptor clusters of rat carotid body? Brain Res 872:199–203

Zhang M, Nurse CA (2004) CO2/pH chemosensory signaling in co-cultures of rat carotid body receptors and petrosal neurons: role of ATP and ACh. J Neurophysiol 92:3433–3445

Zhang M, Fearon IM, Zhong H, Nurse CA (2003) Presynaptic modulation of rat arterial chemoreceptor function by 5-HT: role of K+ channel inhibition via protein kinase C. J Physiol 551:825–842

Zhang M, Piskuric NA, Vollmer C, Nurse CA (2012) P2Y2 receptor activation opens pannexin-1 channels in rat carotid body type II cells: potential role in amplifying the neurotransmitter ATP. J Physiol 590:4335–4350

# T-Type $Ca^{2+}$ Channel Regulation by CO: A Mechanism for Control of Cell Proliferation

33

Hayley Duckles, Moza M. Al-Owais, Jacobo Elies, Emily Johnson, Hannah E. Boycott, Mark L. Dallas, Karen E. Porter, John P. Boyle, Jason L. Scragg, and Chris Peers

**Abstract**

T-type $Ca^{2+}$ channels regulate proliferation in a number of tissue types, including vascular smooth muscle and various cancers. In such tissues, up-regulation of the inducible enzyme heme oxygenase-1 (HO-1) is often observed, and hypoxia is a key factor in its induction. HO-1 degrades heme to generate carbon monoxide (CO) along with $Fe^{2+}$ and biliverdin. Since CO is increasingly recognized as a regulator of ion channels (Peers et al. 2015), we have explored the possibility that it may regulate proliferation via modulation of T-type $Ca^{2+}$ channels.

Whole-cell patch-clamp recordings revealed that CO (applied as the dissolved gas or via CORM donors) inhibited all 3 isoforms of T-type $Ca^{2+}$ channels (Cav3.1-3.3) when expressed in HEK293 cells with similar $IC_{50}$ values, and induction of HO-1 expression also suppressed T-type currents (Boycott et al. 2013). CO/HO-1 induction also suppressed the elevated basal $[Ca^{2+}]_i$ in cells expressing these channels and reduced their proliferative rate to levels seen in non-transfected control cells (Duckles et al. 2015).

Proliferation of vascular smooth muscle cells (both A7r5 and human saphenous vein cells) was also suppressed either by T-type $Ca^{2+}$ channel inhibitors (mibefradil and NNC 55-0396), HO-1 induction or application

H. Duckles
Department of Cardiovascular Science, Medical School, University of Sheffield, Sheffield S10 2RX, UK

M.M. Al-Owais • J. Elies • E. Johnson • K.E. Porter J.P. Boyle • J.L. Scragg
Division of Cardiovascular and Diabetes Research, LIGHT, Faculty of Medicine and Health, University of Leeds, Leeds LS2 9JT, UK

H.E. Boycott
Life Sciences Centre, University of British Columbia, Vancouver V6T 1Z3, Canada

M.L. Dallas
School of Pharmacy, University of Reading, Reading RG6 6UB, UK

C. Peers (✉)
Leeds Institute of Cardiovascular and Metabolic Medicine, Faculty of Medicine and Health, University of Leeds, Leeds LS2 9JT, UK
e-mail: c.s.peers@leeds.ac.uk



C. Peers et al. (eds.), *Arterial Chemoreceptors in Physiology and Pathophysiology*, Advances in Experimental Medicine and Biology 860, DOI 10.1007/978-3-319-18440-1_33

of CO. Effects of these blockers and CO were non additive. Although L-type $Ca^{2+}$ channels were also sensitive to CO (Scragg et al. 2008), they did not influence proliferation. Our data suggest that HO-1 acts to control proliferation via CO modulation of T-type $Ca^{2+}$ channels.

**Keywords**
Heme oxygenase • Carbon monoxide • T-type $Ca^{2+}$ channel • Smooth muscle • Vascular disease • Proliferation

## 33.1 Introduction

Heme oxygenases (HO-1 and HO-2) are enzymes that catalyse the degradation of heme, generating biliverdin, $Fe^{2+}$ and carbon monoxide (CO). The enzymes differ in that HO-2 is widely distributed and constitutively active, whereas HO-1 (also known as heat shock protein 32) is induced by numerous forms of cellular stress, including hypoxia (Kim et al. 2006; Ryter et al. 2006). HO-1 is commonly regarded as protective through reduction of levels of heme (which is itself pro-oxidant), and formation of biliverdin which is rapidly converted to the powerful antioxidant, bilirubin.

Induction of HO-1 is associated with pathological cardiovascular conditions including myocardial infarction, hypertension, atherosclerosis and vascular injury. Although diverse, these important diseases share the common feature of increased levels of vascular smooth muscle cell (VSMC) proliferation, which can, for example in the pulmonary circulation, be promoted by hypoxia (Ryter et al. 2006; Chang et al. 2008). Evidence indicates that HO-1 has anti-proliferative effects which are likely due to its ability to generate CO (Otterbein et al. 2003; Durante et al. 2006; Durante 2003): indeed, CO inhalation reduces VSMC proliferation in intimal hyperplasia which often arises as an unwanted consequence of vessel grafting (Otterbein et al. 2003; Ramlawi et al. 2007; see also Newby and George 1996). Based in part on such findings, CO (in the form of controlled inhalation levels, or CO-releasing molecules (CORMs)), is being explored as a therapeutic approach for cardiovascular disease (Foresti et al. 2008), although it should be noted that the detailed mechanisms underlying its anti-proliferative effects remaining unknown.

Switching of VSMCs from the contractile to proliferative phenotype is a crucial step in the progression of vascular diseases, as well as in development and repair (Owens et al. 2004; Owens 1995; Wamhoff et al. 2006). Associated with this switch is a dramatic change in the expression of a restricted number of ion channels (Cidad et al. 2010), included amongst which is the T-type $Ca^{2+}$ channel (Perez-Reyes 2003). In contractile VSMCs $Ca^{2+}$ influx via L-type $Ca^{2+}$ channels is a major determinant of vascular tone, but in proliferating VSMCs L-type $Ca^{2+}$ channel expression declines substantially whilst expression of T-type $Ca^{2+}$ channels increases (Richard et al. 1992; Kuga et al. 1996). Much evidence indicates that influx of $Ca^{2+}$ via T-type $Ca^{2+}$ channels is required for proliferation and neointima formation following vascular injury (Kuga et al. 1996; Schmitt et al. 1995; Rodman et al. 2005; Lipskaia et al. 2009; Tzeng et al. 2012).

A number of research groups, including our own, have demonstrated that specific ion channels are targets of regulation by CO, and that via ion channel modulation CO exerts many of its important physiological and pathological actions (Williams et al. 2004; Jaggar et al. 2005; Telezhkin et al. 2011; Scragg et al. 2008; Dallas et al. 2012; Peers et al. 2015). In the present study, we have examined whether T-type $Ca^{2+}$ channels represent another target for modulation by CO and, if so, how this might impact on VSMC proliferation.

## 33.2 Methods

### 33.2.1 Cell Culture

Experiments were performed using HEK293 cells (Boycott et al. 2013), the aortic smooth muscle cell line A7r5 (Kimes and Brandt 1976) and human saphenous vein cells (Duckles et al. 2015). HEK293 cells were cultured in minimum essential medium containing Earle's salts and L-glutamine, and supplemented with 10 % (v/v) foetal bovine serum (FBS; Biosera, Ringmer UK), 1 % (v/v) non-essential amino acids, 1 % (v/v) antibiotic/antimycotic, and 0.1 % (v/v) gentamicin. HEK293 cells stably expressing T-type $Ca^{2+}$ channels (Cav3.1, 3.2 or 3.3; a kind gift from E. Perez-Reyes; University of Virginia, USA), were cultured in wild type (WT) HEK293 media supplemented with 1 mg/ml G-418. Cells were kept in a humidified incubator at 37 °C (95 % air: 5 % $CO_2$) and passaged weekly. A7r5 cells (from the European Collection of Cell Cultures, Porton Down UK) were grown in A7r5 complete media, consisting of DMEM containing 10 % FBS (Biosera, Ringmer UK) and 1 % glutamax (Gibco, Paisley UK). Human saphenous vein smooth muscle cells (HSVSMCs) were isolated from the saphenous vein (SV) of anonymous patients undergoing coronary artery bypass graft surgery as previously described (Duckles et al. 2015). All cells were kept in a humidified incubator at 37 °C (95 % air: 5 % $CO_2$).

### 33.2.2 Electrophysiology

$Ca^{2+}$ currents were recorded from HEK293 cells using the whole-cell configuration of the patch-clamp technique at room temperature (21–24 °C) as previously described (Boycott et al. 2013). Pipettes (4–6 MΩ) contained (in mM): CsCl (120), $MgCl_2$ (2), EGTA (10), TEA-Cl (20), HEPES (10), Na-ATP (2), pH 7.2 (adjusted with CsOH), and the perfusate was composed of (in mM): NaCl (95), CsCl (5), $MgCl_2$ (0.6), $CaCl_2$ (15), TEA-Cl (20), HEPES (5), D-glucose (10), pH 7.4 (adjusted with NaOH). Cells were voltage-clamped at −80 mV and either repeatedly depolarized to −20 mV (200 ms, 0.1 Hz) or to a series of test potentials ranging from −100 mV to +60 mV. All currents were low-pass filtered at 2 kHz and digitised at 10 kHz.

### 33.2.3 Proliferation Assay

Cells were plated in 24-well plates in complete media ($1 \times 10^4$ cells per well). HSVSMCs were allowed to adhere overnight and subjected to serum free media (SFM) for 2.5 days respectively. A7r5 and HEK293 cells were allowed to adhere for 6 h and then exposed to SFM overnight. On day 0 of the assay, SFM was removed and 1 ml of the relevant complete media added to each well, in addition to any drugs being investigated. To count cells, media was removed, cells were washed with 1 ml of Dulbecco's phosphate buffered saline (PBS) and 200 µl of 0.05 % trypsin-EDTA (Gibco, Paisley UK) was added (pre-warmed to 37 °C). Post-incubation, 800 µl of complete media was added and the cell suspension centrifuged (600 g for 6 min). Following removal of 950 µl of media, 50 µl of supernatant remained with the cell pellet, which was then re-suspended with 50 µl of 0.4 % Trypan Blue (Thermo Scientific, Rockford USA) to exclude non-viable cells. Media was retained from one well of each treatment, processed in the same manner as the cell samples, and any cells present were counted as an additional quantification of non-viable cells. Day 0 counts and media counts were performed using a hemocytometer. All other counts were performed using a TC10 Automated Cell Counter (Bio-Rad, Hemel Hempstead UK).

### 33.2.4 Western Blotting

Cells were grown to 80 % confluence in 6-well plates. Wells were replenished with 0.4 % serum-containing media plus the required drugs. Post-treatment, the cells were washed with PBS and lysed with Mammalian Protein Extraction

Reagent (M-PER™; Thermo Scientific, Rockford USA) containing Complete Mini protease inhibitors (Roche Diagnostics Ltd, Lewes UK). Protein levels were determined using a BCA protein assay kit (Thermo Scientific, Rockford USA). Next, 10–20 μg protein in 2× sample buffer (250 mM Tris/HCl, pH 6.8, 4 % (w/v) SDS, 20 % (w/v) glycerol, 1 % bromophenol blue, and 10 % β-mercaptoethanol) was loaded onto 12.5 % polyacrylamide gels and separated for ~1 h at 35 mA before being transferred onto 0.2 μm polyvinyl difluoride membranes at 30 V overnight. Membranes were blocked using 5 % (w/v) non-fat dried milk powder in Tris buffered saline (TBS)-Tween (0.05 %) for 1 h, then incubated with rabbit anti-HO-1 antibody (1:200; SC-10789; Santa Cruz, Dallas USA) for 3 h at 21–24 °C. Mouse anti-β-actin raised against the N-terminal of β-actin (1:4,000; Sigma, Gillingham UK) was used as a loading control. Membranes were then washed in TBS-Tween (0.05 %) and incubated with the corresponding peroxidase-conjugated secondary antibody (1:2,000; GE Healthcare, Amersham UK) for 1 h at 21–24 °C. Bands were detected using the enhanced chemi-luminescent method on hyperfilm. Densitometric analysis used Image J (NIH, UK).

### 33.2.5 $Ca^{2+}$ Microfluorimetry

Cells were plated on circular glass coverslips and allowed to adhere overnight. Cells were washed and incubated with 4 μM Fura 2-AM (Invitrogen, Cambridge UK) in HEPES-buffered saline (HBS) for 40 min 21–24 °C. HBS contained (in mM): NaCl (135), KCl (5), $MgSO_4$ (1.2), $CaCl_2$ (2.5), HEPES (5), glucose (10), osmolarity adjusted to 300 mOsm with sucrose, and pH adjusted to 7.4. The Fura 2-containing HBS was washed off for 15 min to allow de-esterification. Coverslip fragments were placed in a perfusion chamber on an inverted epifluorescence microscope and cells superfused via gravity at 2–3 ml/min. $[Ca^{2+}]_i$ was indicated by fluorescence emission measured at 510 nm as a result of alternating excitation at 340 nm and 380 nm using a Cairn Research ME-SE Photometry system (Cairn Research, Cambridge UK).

Statistical comparisons were made using, as appropriate, paired or unpaired student's T-tests, one way ANOVA with a multiple comparison test, or repeated measures one way ANOVA with a multiple comparison test.

## 33.3 Results

### 33.3.1 CO Inhibits T-Type $Ca^{2+}$ Channels

Whole-cell patch-clamp recordings from HEK293 cells expressing each of the major forms of T-type $Ca^{2+}$ channels (Cav3.1, 3.2 or 3.3) revealed that CO, applied as the CO donor CORM-2, inhibited all 3 isoforms (Fig. 33.1a). These effects were attributable to release of CO, since the inactive form of CORM-2 was without significant effect (not shown). Indeed, all three isoforms displayed similar sensitivity to CORM-2 ($IC_{50}$ *ca* 3 μM in each case). The time course of inhibition (Fig. 33.1b) shows that CO inhibition of currents recorded in Cav3.2-expressing HEK293 cells was irreversible. However, current amplitude recovery was observed following exposure to the reducing agent dithiothreitol (DTT; 1 mM), as exemplified in Fig. 33.1b (lower plot). The ability of DTT to reverse CO inhibition was exploited to examine whether HO-1 induction led to tonic inhibition of T-type currents: exposure of cells to hemin (iron protoporphyrin IX (200 μM)) caused a time-dependent induction of HO-1, as determined by western blot (Fig. 33.1c). Following HO-1 induction, the ability of DTT to augment currents was dramatically enhanced (Fig. 33.1c), consistent with the idea that HO-1 induction led to increased CO levels, thereby causing tonic inhibition of Cav3.2-mediated T-type currents.

### 33.3.2 CO Modulation of $[Ca^{2+}]_i$ and Proliferation in Cav3.2 Expressing Cells

To investigate the consequences of CO inhibition of T-type $Ca^{2+}$ channels on cell function, we next explored the ability of CO to regulate $[Ca^{2+}]_i$ and

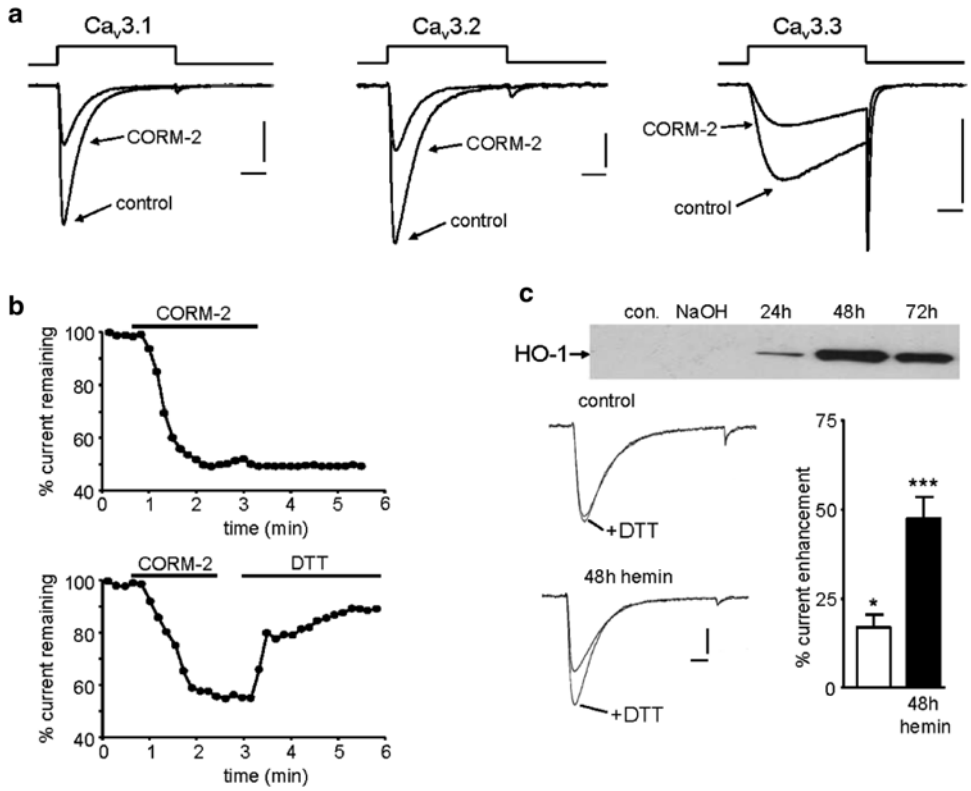


**Fig. 33.1** CO inhibits T-type channels. (**a**) currents evoked in a HEK293 cell stably expressing Cav3.1 (*left*) Cav3.2 (*middle*) or Cav3.3 (*right*) before and during exposure to CORM-2 (3 μM) as indicated. Currents were evoked by step depolarizations from −90 mV to −30 mV. Scale bars in each case: vertical, 0.5 nA, horizontal, 20 ms. (**b**) Upper; example time-series plot illustrating normalized current amplitudes evoked by step depolarizations from −90 mV to −30 mV in a Cav3.2-expressing cell. For the period indicated by the bar, CORM-2 (3 μM) was applied via the perfusate. Lower; as upper, except that, following washout of CORM-2, the cell was exposed to dithiothreitol (DTT, 1 mM) for the period indicated by the second bar. (**c**) Upper; western blot illustrating the time-dependent induction of HO-1 following exposure to hemin (200 μM). Lower, example currents showing the effects of DTT (1 mM) on untreated cells (control) or those in which HO-1 had been induced following exposure to hemin (200 μM, 48 h) . Scale bars: 0.1 nA, 10 ms. Right; plot of the mean (± s.e.m.) % enhancement of currents in control (n = 9) and hemin-treated cell caused by DTT (n = 9). Data obtained from currents evoked by step depolarizations from −90 mV to −30 mV. Statistical significance: * $P < 0.05$; *** $P < 0.001$ as compared with controls (Adapted from Boycott et al. 2013; Duckles et al. 2015 with permission)

cellular proliferation. Experiments were restricted to studying the effects of CO in Cav3.2-expressing cells. As exemplified in Fig. 33.2a, basal $[Ca^{2+}]_i$ was significantly elevated in cells expressing this channel, as compared with wild type (WT; untransfected) cells, and removal of extracellular $Ca^{2+}$ (replaced with 1 mM EGTA) caused a much greater fall of $[Ca^{2+}]_i$ as compared with WT cells, consistent with the idea that the elevated basal $[Ca^{2+}]_i$ was attributable to tonic $Ca^{2+}$ influx via T-type $Ca^{2+}$ channels. Induction of HO-1 (using cobalt protoporphyrin, CoPPIX) also reduced basal $[Ca^{2+}]_i$ (Fig. 33.2b), as did exposure to CO using the water soluble CO donor, CORM-3. This donor was without effect in WT cells (Fig. 33.2c). Proliferation was also monitored in these same cells. As shown in Fig. 33.2d, expression of Cav3.2 led to a dramatic increase in proliferation as compared with WT cells. This increase was presumably due to tonic $Ca^{2+}$ influx via Cav3.2 channels, since proliferation was reduced by the T-type $Ca^{2+}$ channel inhibitor mibefradil, and also by CORM-3. Note that (i) these agents were non-additive,

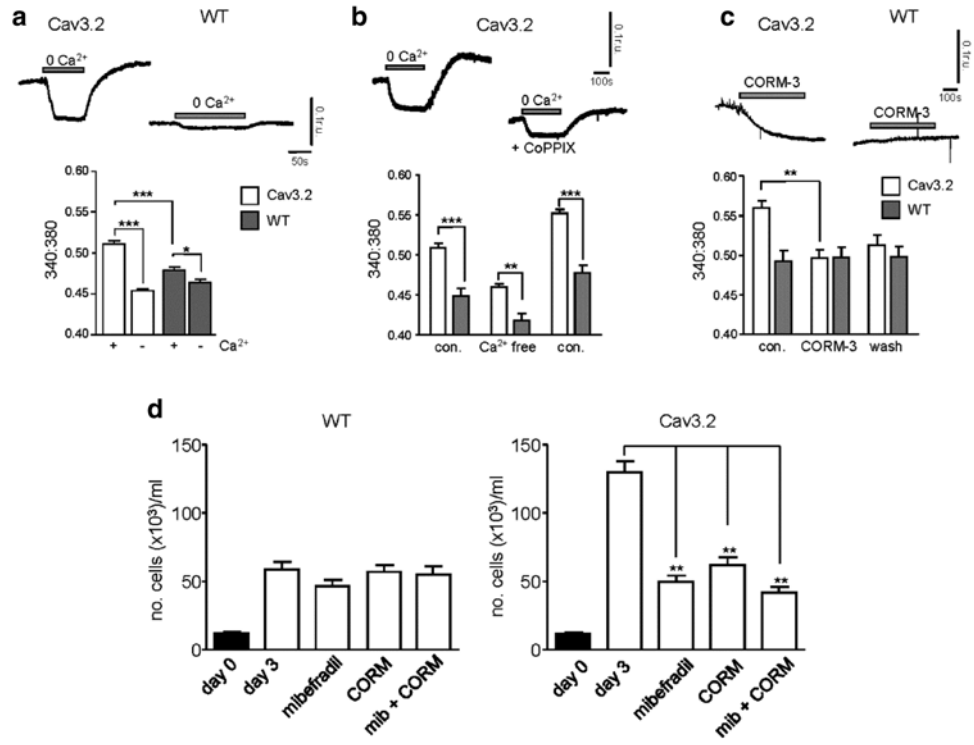


**Fig. 33.2** CO modulates $[Ca^{2+}]_i$ and proliferation in Cav3.2 expressing cells. (**a**) Upper traces show examples of basal $[Ca^{2+}]_i$ recorded in Cav3.2-expressing and WT HEK293 cells. For the periods indicated by the horizontal bars, extracellular $Ca^{2+}$ was replaced with 1 mM EGTA. Below; Bar graph illustrating the mean basal $[Ca^{2+}]_i$ levels (with s.e.m. bars) recorded in Cav3.2-expressing cells (open bars, n = 6) and WT cells (shaded bars, n = 6) in the presence and absence of extracellular $Ca^{2+}$, as indicated. (**b**) Upper traces; examples of basal $[Ca^{2+}]_i$ recorded in Cav3.2-expressing cells either with no pre-treatment, or exposed to 10 μM CoPPIX for 48 h to induce HO-1 expression (+CoPPIX). For the periods indicated by the horizontal bars, extracellular $Ca^{2+}$ was replaced with 1 mM EGTA. Below; Bar graphs illustrating the mean (± s.e.m.) basal $[Ca^{2+}]_i$ levels recorded in Cav3.2-expressing cells (n = 16) before (con.), during ($Ca^{2+}$ free) and after (con.) removal of extracellular $Ca^{2+}$. Statistical significance: ** $P < 0.01$, *** $P < 0.001$ (**c**) Upper traces show examples of basal $[Ca^{2+}]_i$ recorded in Cav3.2-expressing and WT HEK293 cells and the effects of CORM-3 (3 μM) applied for the periods indicated by the horizontal bars. Below; Bar graph illustrating the mean (± s.e.m.) basal $[Ca^{2+}]_i$ levels recorded in Cav3.2-expressing cells (open bars, n = 5) and WT cells (shaded bars, n = 6) before (con.), during (CORM-3) and after (wash) exposure to CORM-3. Statistical significance: * $P < 0.05$; ** $P < 0.01$, *** $P < 0.001$ as compared with appropriate controls. Data analysed via paired or unpaired t-test as appropriate. (**d**) Bar graphs illustrating the effects of mibefradil and CORM-3 (applied separately or together, as indicated) on proliferation measured on day 3 in WT (*left*) and Cav3.2-expressing HEK293 cells (*right*). Each bar represents mean (± s.e.m.) proliferation determined from nine repeats. Statistical significance: ** $P < 0.01$ as compared with controls. Data analysed via repeated ratio measures one way ANOVA followed by Dunnett's multiple comparison test (Taken from Duckles et al. 2015 with permission)

(ii) that either mibefradil or CORM-3 reduced proliferation rates in Cav3.2-expressing cells to levels observed in WT cells, and (iii) these agents were without effect on proliferation in WT cells, suggesting that increased proliferation was entirely attributable to T-type $Ca^{2+}$ channel activity, which in turn can be regulated by CO.

### 33.3.3 CO Modulates Proliferation in VSMCs

To examine whether CO could also modulate proliferation via modulation of native T-type $Ca^{2+}$ channels in VSMCs, we examined its effects in both A7r5 cells and HSVSMCs. As

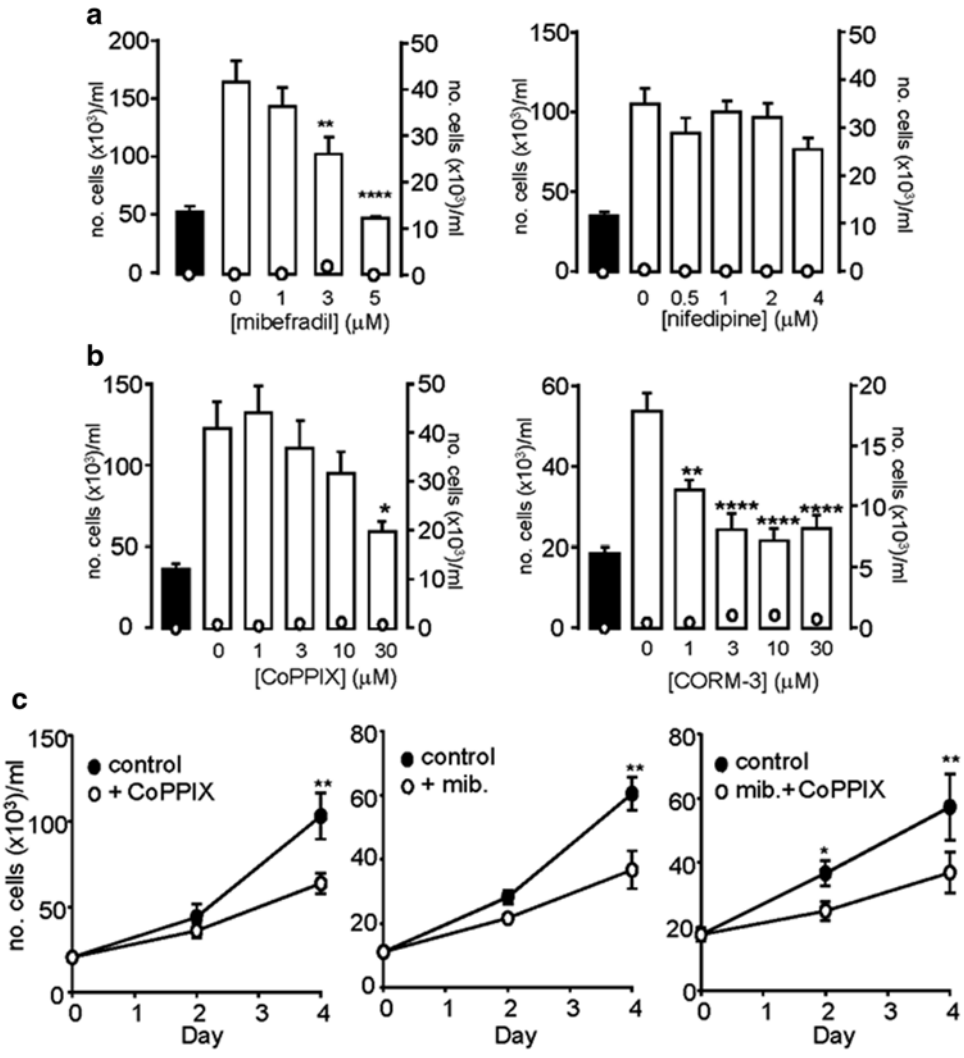


**Fig. 33.3** T-type $Ca^{2+}$ channel inhibitors suppress proliferation of A7r5 cells and HSVSMCs. (**a**) Bar graphs showing the proliferative response (mean ± s.e.m) of A7r5 cells to increasing concentrations of specified drugs. Proliferation (plotted as bar graphs, corresponding to the left-hand Y axis) was monitored on Day 0 (*solid bars*) and on Day 3 (*open bars*) in the absence or presence of mibefradil (n = 4) or nifedipine (n = 3). (**b**) as (**a**), except cells were exposed to CoPPIX to induce HO-1, or to CORM-3, as indicated. The open circles show the corresponding non-viable cell count (plotted against corresponding right-hand Y-axis). Statistical significance: * $p < 0.05$, ** $p < 0.01$, **** $p < 0.0001$ vs Day 3 Control (no drug). Data analysed via repeated ratio measures one way ANOVA followed by Dunnett's multiple comparison test. (**c**) Line graphs showing proliferation of HSVSMCs monitored over a 4-day period, in the absence of drug treatment (*solid circles*), or during HO-1 induction with 3 μM CoPPIX (open symbols, *left*), or in the presence of 3 μM mibefradil (*open circles*, *middle*), or during simultaneous application of 3 μM mibefradil and 3 μM CoPPIX (*open circles, right*). Each point represents mean ± s.e.m. (n = 5). Statistical significance: * $p < 0.05$, ** $p < 0.01$. Data analysed via repeated measures one way ANOVA followed by Sidak's multiple comparison test between control and treated groups for each timepoint (Taken from Duckles et al. 2015 with permission)

shown in Fig. 33.3a, although A7r5 cells express both L- and T-type $Ca^{2+}$ channels (Duckles et al. 2015), proliferation was only reduced by mibefradil and not nifedipine, indicating that T-type but not L-type channels regulated proliferation in these cells.

Consistent with their effects in Cav3.2-expressing HEK293 cells, HO-1 induction or CO exposure (using CORM-3) also significantly reduced proliferation (Fig. 33.3b). Similarly, in HSVSMCs both HO-1 induction and mibefradil separately reduced proliferation, and combining both maneuvers did not suppress proliferation further (Fig. 33.3c). These data are consistent with data obtained in HEK293 cells indicating that VSMC proliferation is also regulated by T-type $Ca^{2+}$ channel activity, and that CO inhibition of T-type channels could significantly suppress proliferation.

## 33.4 Discussion

The switch of VSMCs from a contractile to a proliferative phenotype is a complex process which is, in part, regulated by $Ca^{2+}$ influx (Barbado et al. 2009; Owens et al. 2004). Various routes of $Ca^{2+}$ entry into VSMCs have been proposed as important for proliferation, including TRPC channels (Kumar et al. 2006) and the STIM1/Orai pathway (Zhang et al. 2011). There is also a substantial body of evidence implicating T-type $Ca^{2+}$ channels in the process of proliferation and neointima formation following vascular injury (Kuga et al. 1996; Schmitt et al. 1995). In more recent times, Cav3.1 has been identified as the key T-type $Ca^{2+}$ channel required for VSMC proliferation (Tzeng et al. 2012). Our data in A7r5 and HSVSMCs are consistent with an important role for native T-type $Ca^{2+}$ channels in proliferation. Thus, in A7r5 cells, despite the presence of L-type $Ca^{2+}$ channels (Duckles et al. 2015), proliferation appeared selectively regulated by T-type $Ca^{2+}$ channels, and this was also the case in HSVSMCs (Fig. 33.3). The observation that proliferation was sensitive to mibefradil implies that tonic $Ca^{2+}$ influx via T-type $Ca^{2+}$ channels occurs in these cells. We present no direct evidence of this in VSMCs, but in HEK293 cells expressing Cav3.2, tonic $Ca^{2+}$ influx via these channels is indeed evident (Fig. 33.2). This presumably arises from the ability of these channels to generate a window current (Perez-Reyes 2003), which arises from a small proportion of the T-type $Ca^{2+}$ channel population being partially activated and not fully inactivated at the cell's resting membrane potential.

Our findings indicate that proliferation can be suppressed by induction of HO-1 in VSMCs, and that this occurs via formation of CO by HO-1. Thus, CO was able to mimic the suppressive effects of HO-1 induction in VSMCs (Fig. 33.3) and, in HEK293 cells expressing Cav3.2, HO-1 induction or CO reduced basal $[Ca^{2+}]_i$ and suppressed proliferation. These findings are consistent with numerous studies indicating that HO-1 induction suppresses proliferation in vascular diseases (Cao et al. 2009; Araujo et al. 2012). Furthermore, other studies implicate CO as the means by which HO-1 suppresses proliferation (Otterbein et al. 2003; Ramlawi et al. 2007). In light of the direct evidence from recombinant studies (Fig. 33.1), we propose that HO-1 regulation of VSMC proliferation is attributable to the ability of CO to inhibit T-type $Ca^{2+}$ channels. Thus, CO inhibits all three isoforms of T-type channel, and inhibition is observed when CO is applied directly, or when HO-1 is induced (Fig. 33.1). These results, coupled with the observations that CO or HO-1 induction suppresses T-type $Ca^{2+}$ channel-dependent proliferation in VSMCs (Fig. 33.3) imply that the ability of CO to inhibit T-type $Ca^{2+}$ channels is important in VSMC. This implication is further supported by the observation that the effects of HO-1 induction and mibefradil exposure on proliferation of HSVSMCs were not additive.

In summary, our data provide a novel signalling pathway to account for the anti-proliferative effects of HO-1 observed in vascular diseases. This pathway has the potential for targeting in future strategies for the treatment of vascular diseases. There are also important implications arising from our studies for other diseases including various cancers where T-type $Ca^{2+}$ channels have been shown to regulate proliferation (Panner and Wurster 2006; Heo et al. 2008).

**Acknowledgements** This work was supported by the British Heart Foundation.

## References


Araujo JA, Zhang M, Yin F (2012) Heme oxygenase-1, oxidation, inflammation, and atherosclerosis. Front Pharmacol 3:119

Barbado M, Fablet K, Ronjat M, De WM (2009) Gene regulation by voltage-dependent calcium channels. Biochim Biophys Acta 1793:1096–1104

Boycott HE, Dallas ML, Elies J, Pettinger L, Boyle JP, Scragg JL, Gamper N, Peers C (2013) Carbon monoxide inhibition of Cav3.2 T-type Ca2+ channels reveals tonic modulation by thioredoxin. FASEB J 27:3395–3407

Cao J, Inoue K, Li X, Drummond G, Abraham NG (2009) Physiological significance of heme oxygenase in hypertension. Int J Biochem Cell Biol 41:1025–1033

Chang T, Wu L, Wang R (2008) Inhibition of vascular smooth muscle cell proliferation by chronic hemin treatment. Am J Physiol Heart Circ Physiol 295:H999–H1007

Cidad P, Moreno-Dominguez A, Novensa L, Roque M, Barquin L, Heras M, Perez-Garcia MT, Lopez-Lopez JR (2010) Characterization of ion channels involved in the proliferative response of femoral artery smooth muscle cells. Arterioscler Thromb Vasc Biol 30:1203–1211

Dallas ML, Yang Z, Boyle JP, Boycott HE, Scragg JL, Milligan CJ, Elies J, Duke A, Thireau J, Reboul C, Richard S, Bernus O, Steele DS, Peers C (2012) Carbon monoxide induces cardiac arrhythmia via induction of the late Na+current. Am J Respir Crit Care Med 186:648–656

Duckles H, Boycott HE, Al-Owais MM, Elies J, Johnson E, Dallas ML, Porter KE, Giuntini F, Boyle JP, Scragg JL, Peers C (2015) Heme oxygenase-1 regulates cell proliferation via carbon monoxide-mediated inhibition of T-type $Ca^{2+}$ channels. Pflugers Arch 467:415–427. doi:10.1007/s00424-014-1503-5

Durante W (2003) Heme oxygenase-1 in growth control and its clinical application to vascular disease. J Cell Physiol 195:373–382

Durante W, Johnson FK, Johnson RA (2006) Role of carbon monoxide in cardiovascular function. J Cell Mol Med 10:672–686

Foresti R, Bani-Hani MG, Motterlini R (2008) Use of carbon monoxide as a therapeutic agent: promises and challenges. Intensive Care Med 34:649–658

Heo JH, Seo HN, Choe YJ, Kim S, Oh CR, Kim YD, Rhim H, Choo DJ, Kim J, Lee JY (2008) T-type Ca2+ channel blockers suppress the growth of human cancer cells. Bioorg Med Chem Lett 18:3899–3901

Jaggar JH, Li A, Parfenova H, Liu J, Umstot ES, Dopico AM, Leffler CW (2005) Heme is a carbon monoxide receptor for large-conductance Ca2+-activated K+ channels. Circ Res 97:805–812

Kim HP, Ryter SW, Choi AM (2006) CO as a cellular signaling molecule. Annu Rev Pharmacol Toxicol 46:411–449

Kimes BW, Brandt BL (1976) Characterization of two putative smooth muscle cell lines from rat thoracic aorta. Exp Cell Res 98:349–366

Kuga T, Kobayashi S, Hirakawa Y, Kanaide H, Takeshita A (1996) Cell cycle–dependent expression of L- and T-type Ca2+ currents in rat aortic smooth muscle cells in primary culture. Circ Res 79:14–19

Kumar B, Dreja K, Shah SS, Cheong A, Xu SZ, Sukumar P, Naylor J, Forte A, Cipollaro M, McHugh D, Kingston PA, Heagerty AM, Munsch CM, Bergdahl A, Hultgardh-Nilsson A, Gomez MF, Porter KE, Hellstrand P, Beech DJ (2006) Upregulated TRPC1 channel in vascular injury in vivo and its role in human neointimal hyperplasia. Circ Res 98:557–563

Lipskaia L, Hulot JS, Lompre AM (2009) Role of sarco/endoplasmic reticulum calcium content and calcium ATPase activity in the control of cell growth and proliferation. Pflugers Arch 457:673–685

Newby AC, George SJ (1996) Proliferation, migration, matrix turnover, and death of smooth muscle cells in native coronary and vein graft atherosclerosis. Curr Opin Cardiol 11:574–582

Otterbein LE, Zuckerbraun BS, Haga M, Liu F, Song R, Usheva A, Stachulak C, Bodyak N, Smith RN, Csizmadia E, Tyagi S, Akamatsu Y, Flavell RJ, Billiar TR, Tzeng E, Bach FH, Choi AM, Soares MP (2003) Carbon monoxide suppresses arteriosclerotic lesions associated with chronic graft rejection and with balloon injury. Nat Med 9:183–190

Owens GK (1995) Regulation of differentiation of vascular smooth muscle cells. Physiol Rev 75:487–517

Owens GK, Kumar MS, Wamhoff BR (2004) Molecular regulation of vascular smooth muscle cell differentiation in development and disease. Physiol Rev 84:767–801

Panner A, Wurster RD (2006) T-type calcium channels and tumor proliferation. Cell Calcium 40:253–259

Peers C, Boyle JP, Scragg JL, Dallas ML, Al-Owais MM, Hettiarachichi NT, Elies J, Johnson E, Gamper N, Steele DS (2015) Diverse mechanisms underlying the regulation of ion channels by carbon monoxide. Br J Pharmacol 172:1546–1556

Perez-Reyes E (2003) Molecular physiology of low-voltage-activated t-type calcium channels. Physiol Rev 83:117–161

Ramlawi B, Scott JR, Feng J, Mieno S, Raman KG, Gallo D, Csizmadia E, Yoke CB, Bach FH, Otterbein LE, Sellke FW (2007) Inhaled carbon monoxide prevents graft-induced intimal hyperplasia in swine. J Surg Res 138:121–127

Richard S, Neveu D, Carnac G, Bodin P, Travo P, Nargeot J (1992) Differential expression of voltage-gated Ca(2+)-currents in cultivated aortic myocytes. Biochim Biophys Acta 1160:95–104

Rodman DM, Reese K, Harral J, Fouty B, Wu S, West J, Hoedt-Miller M, Tada Y, Li KX, Cool C, Fagan K, Cribbs L (2005) Low-voltage-activated (T-type) calcium channels control proliferation of human pulmonary artery myocytes. Circ Res 96:864–872

Ryter SW, Alam J, Choi AM (2006) Heme oxygenase-1/carbon monoxide: from basic science to therapeutic applications. Physiol Rev 86:583–650

Schmitt R, Clozel JP, Iberg N, Buhler FR (1995) Mibefradil prevents neointima formation after vascular injury in rats. Possible role of the blockade of the T-type voltage-operated calcium channel. Arterioscler Thromb Vasc Biol 15:1161–1165

Scragg JL, Dallas ML, Wilkinson JA, Varadi G, Peers C (2008) Carbon monoxide inhibits L-type $Ca^{2+}$ channels via redox modulation of key cysteine residues by mitochondrial reactive oxygen species. J Biol Chem 283:24412–24419

Telezhkin V, Brazier SP, Mears R, Muller CT, Riccardi D, Kemp PJ (2011) Cysteine residue 911 in C-terminal tail of human BK(Ca)alpha channel subunit is crucial for its activation by carbon monoxide. Pflugers Arch 461:665–675

Tzeng BH, Chen YH, Huang CH, Lin SS, Lee KR, Chen CC (2012) The Cav3.1 T-type calcium channel is required for neointimal formation in response to vascular injury in mice. Cardiovasc Res 96:533–542

Wamhoff BR, Bowles DK, Owens GK (2006) Excitation-transcription coupling in arterial smooth muscle. Circ Res 98:868–878

Williams SE, Wootton P, Mason HS, Bould J, Iles DE, Riccardi D, Peers C, Kemp PJ (2004) Hemoxygenase-2 is an oxygen sensor for a calcium-sensitive potassium channel. Science 306:2093–2097

Zhang W, Halligan KE, Zhang X, Bisaillon JM, Gonzalez-Cobos JC, Motiani RK, Hu G, Vincent PA, Zhou J, Barroso M, Singer HA, Matrougui K, Trebak M (2011) Orai1-mediated I (CRAC) is essential for neointima formation after vascular injury. Circ Res 109:534–542

# 34 Glutamatergic Receptor Activation in the Commisural Nucleus Tractus Solitarii (cNTS) Mediates Brain Glucose Retention (BGR) Response to Anoxic Carotid Chemoreceptor (CChr) Stimulation in Rats

R. Cuéllar, S. Montero, S. Luquín, J. García-Estrada, O. Dobrovinskaya, V. Melnikov, M. Lemus, and E. Roces de Álvarez-Buylla

**Abstract**

Glutamate, released from central terminals of glossopharyngeal nerve, is a major excitatory neurotransmitter of commissural nucleus tractus solitarii (cNTS) afferent terminals, and brain derived neurotrophic factor (BDNF) has been shown to attenuate glutamatergic AMPA currents in NTS neurons. To test the hypothesis that AMPA contributes to glucose regulation *in vivo* modulating the hyperglycemic reflex with brain glucose retention (BGR), we microinjected AMPA and NBQX (AMPA antagonist) into the cNTS before carotid chemoreceptor stimulation in anesthetized normal Wistar rats, while hyperglycemic reflex an brain glucose retention (BGR) were analyzed. To investigate the underlying mechanisms, GluR2/3 receptor and c-Fos protein expressions in cNTS neurons were determined. We showed that AMPA in the cNTS before CChr stimulation inhibited BGR observed in aCSF group. In contrast, NBQX in similar conditions, did not

R. Cuéllar • O. Dobrovinskaya • M. Lemus
E.R. de Álvarez-Buylla (✉)
Centro Universitario de Investigaciones Biomédicas, Universidad de Colima, Ave. 25 de Julio 965, Col. Villas de San Sebastián, Colima, Col C.P. 28045, México
e-mail: rab@ucol.mx

S. Montero
Centro Universitario de Investigaciones Biomédicas, Universidad de Colima, Ave. 25 de Julio 965, Col. Villas de San Sebastián, Colima, Col C.P. 28045, México

Facultad de Medicina, Universidad de Colima, Colima, México

S. Luquín
Centro Universitario de Ciencias de la Salud, Universidad de Guadalajara, Guadalajara, México

J. García-Estrada
Centro Universitario de Ciencias de la Salud, Universidad de Guadalajara, Guadalajara, México

Centro de Investigaciones Biomédicas de Occidente, IMSS, Guadalajara, México

V. Melnikov
Facultad de Medicina, Universidad de Colima, Colima, México



C. Peers et al. (eds.), *Arterial Chemoreceptors in Physiology and Pathophysiology*, Advances in Experimental Medicine and Biology 860, DOI 10.1007/978-3-319-18440-1_34

modify the effects on glucose variables observed in aCSF control group. These experiments suggest that glutamatergic pathways, via AMPA receptors, in the cNTS may play a role in glucose homeostasis.

**Keywords**
AMPA • NBQX • Carotid body • Glucose homeostasis • Brain glucose retention

## 34.1 Introduction

There is strong evidence suggesting that AMPA receptors are involved in the central pathways to modulate chemoreceptor inputs, however the studies examining its role in the control of energy metabolism are scarce (Pang and Han 2012). It is known that excitatory synaptic transmission in the cardio-respiratory reflexes is mediated predominantly by the activation of AMPA receptors in the NTS to undertake a sympatho-excitation reflexes (Ozawa et al. 1998; Lin 2009). Ohtake studies (1998) suggest that AMPA ionotropic receptors are the main ventilatory response modulators. Furthermore, activation of AMPA receptor increases chemoreceptor responses evoked by stimulation in animals exposed to intermittent hypoxia (de Paula et al. 2007). In the same way, glutamate seems to be released from central terminals of glossopharyngeal afferents in the NTS [from the espinomedular junction to the caudal region of the facial motor nucleus in the rostral ventrolateral medulla (RVLM)], which plays a role in regulating sympathetic activity of baro- chemoreflex in respiratory function (Koshiya and Guyenet 1996). We addressed whether glutamate signaling, through AMPA receptors, modulates glucose homeostasis altered by anoxic stimulation of circulatorily isolated CChrs with cyanide (NaCN) (Alvarez-Buylla and Roces de Alvarez-Buylla 1994).

## 34.2 Methods

### 34.2.1 Animals and Surgical Procedures

Male Wistar rats (280–300 g) were used. All procedures were in accord to the Guide for the Care and Use of Laboratory Animals from National Institutes of Health, USA. Rats were anesthetized with a bolus injection of sodium pentobarbital (3 mg/100 g i.p.) supplemented by a continuous i.p. infusion of the same anesthetic (0.063 mg/min). Buprenorphine (0.03 mg/kg subcutaneously, Temgesic, Schering-Plough, México) 5 min before surgical procedures was used as analgesic. Body temperature was kept at 37 ± 1 °C with a heating pad. Animals were artificially ventilated, respiratory rate and tidal volume were based on pH, $pO_2$ and $pCO_2$ values in arterial blood obtained during experimental procedures, as well as 10 min before and at the end of experiment. Permanent silastic catheters filled with heparin (1,000 U/mL) were inserted into the abdominal aorta (accessed from the femoral artery) and jugular sinus (accessed from the right external jugular vein) without interrupting circulation in these vessels (Alvarez-Buylla and Alvarez-Buylla 1988). The correct placement of catheters was verified at the end of each experiment (Fig. 34.1a).

### 34.2.2 Drugs

The drugs used were: (a) sodium cyanide (NaCN); (Sigma, Mex.) at a dose of 5 μg/100 g (diluted in 100 nL of freshly prepared sterile saline-sal); (b) artificial cerebrospinal fluid (aCSF- 100 nL, containing NaCl 145 mM, KCl 2.7 mM, MgCl mM 1.0, $CaCl_2$ mM 1.2, ascorbate 2.0 mM, $NaH_2PO_4$ 2, mM, pH 7.3–7.4); (c) α-amino-3-hydroxy-5-methyl-4-isoxazolepropionate (AMPA, 2 μM/100 nL of aCSF) (Sigma, Méx.) (Müeller et al. 2005); (c) or 1,2,3,4-tetrahydro-6-nitro-2,3-dioxo-[*f*]quinoxaline-7-sulfonamide, (NBQX, 2 mM/100 nL of aCSF), (Sigma, Méx.) (Müeller et al. 2005).

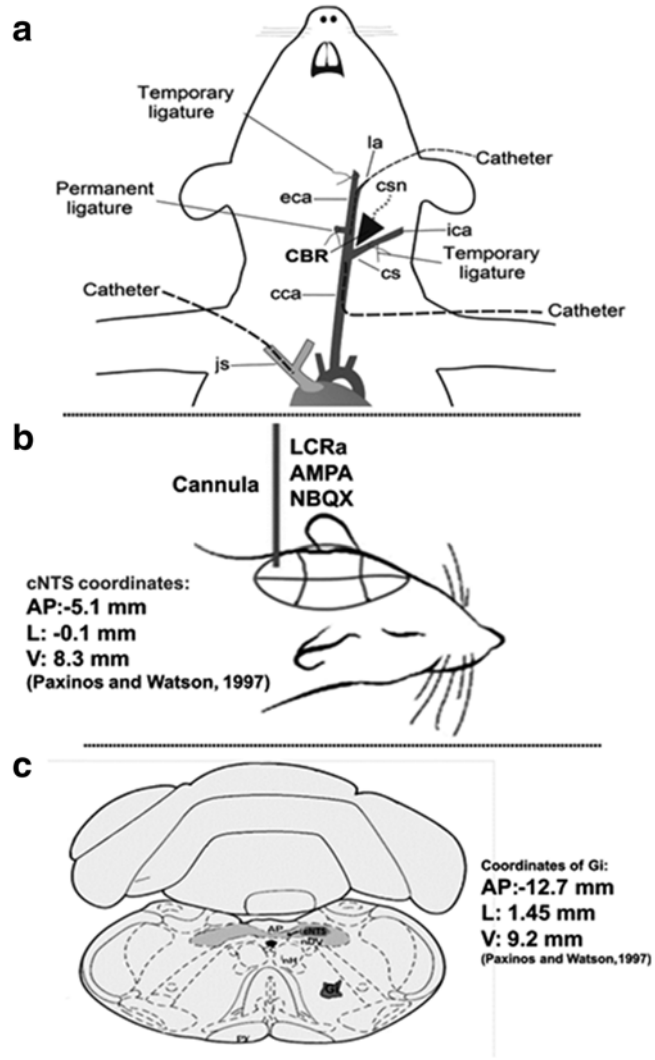


**Fig. 34.1** (**a**) Placement of catheters and ligatures to locally perfuse left carotid sinus to stimulate carotid body chemoreceptors with NaCN. *cc* common carotid artery, *CBR* carotid body receptors, *cs* circulatory isolated carotid sinus, *csn* carotid sinus nerve,*eca* external carotid artery, *ica* internal carotid artery, *js* jugular sinus, *la* lingual artery. (**b**) Placement of cannula into the cNTS. (**c**) microinjection site stained with methylene blue (cNTS) (overdraw of Paxinos and Watson 1997)

Drugs were diluted immediately before application. In sham experiments, the same volume of aCSF was injected.

### 34.2.3 CChr Stimulation

CChr stimulation was performed as previously described (Alvarez-Buylla and Alvarez-Buyllla 1988). Briefly, 5 μg/100 g NaCN in 100 μL sal./2 s was injected into the local circulation of the left carotid sinus, avoiding baroreceptor stimulation. NaCN was used as a carotid body chemoreceptor stimulator since its effects are equivalent to those observed in anoxemic anoxia (Serani et al. 1983). The left carotid sinus was temporarily isolated from the cephalic circulation, while the right carotid sinus was denervated. With this technique only the left carotid sinus is exposed to NaCN and within 10–15 s, NaCN is cleared into a washing cannula (Fig. 34.1a). Previous experiments conducted on isolated chemoreceptor fibers showed that an injection of 5 μg/100 g of NaCN into the carotid body circulation elicits electrical activity before the first signs of respiratory changes are observed. NaCN administered as described above, but after carotid nerve section did not have any effect (Alvarez-Buylla and Alvarez-Buylla 1988).

### 34.2.4 Microinjection of Drugs into the cNTS

Injections (aCSF, AMPA or NBQX) into the cNTS were done using a stereotaxic frame (Stoelting Co., Wood Dale, Il, USA) and the following coordinates from bregma: AP = −5.1 mm, L = −0.1 mm, V = 8.3 mm; incisor bar 3.3 mm above zero point (Paxinos and Watson 1997). The surface of the brain was reached with a 1/32 in. burr hole and a glass micropipette (50–60 µm external tip diameter); filled with the solution to be injected, was inserted into the left cNTS (Fig. 34.1b). The micropipette was connected to a 0.5 mL Hamilton microsyringe with polyethylene tubing (PE 20) for injections. AMPA and NBQX drugs were delivered in 100 nL of artificial cerebrospinal fluid (aCSF) during 5 s approximately. The volume of each injection was determined by measuring the movement of the fluid meniscus within the microinjector pipette. In control experiments the micropipette was directed to the gigantocellular reticular nucleus (Gi), the coordinates in this case were AP = −12.7 mm, L = 1.45 mm, V = 9.2 mm (Paxinos and Watson 1997). Once the last blood sample was drawn, the correct positioning of the micropipette tip site was corroborated by injecting 50–100 nL of methylene blue (10 %) through the same micropipette. Anesthetized rats were decapitated; the brains were removed, immediately frozen, and sectioned at 40 µm in a cryostat (CM-1800, Leica Microsystems, Nussloch, Germany). Sections were stained with cresyl violet for histological verification of the microinjection site and tissue damage (Fig. 34.1c).

### 34.2.5 Blood Sampling and Measurements

Blood samples were taken via catheters inserted into the abdominal aorta (arterial) and from the jugular sinus (venous). Blood samples were collected from each rat as follows: two basal samples at t = −10 min and t = −5 min (to obtain a basal level in t = −7.5 min). AMPA, and NBQX drugs or aCSF, as control, were injected into the NTS at t = −4 min, while CChr stimulation was done into the local circulation of the isolated carotid sinus at t = 0 min. Four experimental samples were then collected at 5, 10, 20 and 30 min. To compensate for fluid loss, rats received 0.3 mL sal. after each sample was taken (0.15 mL of arterial blood and 0.15 mL of venous blood). Blood was centrifuged and plasma was kept chilled until assayed. Plasma glucose concentration in µmol/mL was determined by the glucose-oxidase method with a glucose analyzer (Beckman Autoanalyzer, Beckman Coulter, CA USA). Brain glucose retention was determined by arterial-venous (A-V) glucose differences between abdominal aorta and jugular sinus blood in µmol/mL. Blood flow was not considered for glucose retention because it does not change significantly after CChr stimulation (Alvarez-Buylla et al. 1997). To discard any possible change in blood pressure after NaCN injection into the carotid sinus circulation, arterial blood pressure was measured in the femoral artery in two control experiments with a pressure transducer (Ohmeda Pte Ltd, Singapore), the results in these experiments did not show significant changes; Glucose, $PO_2$, $PCO_2$ and pH values were within the range of standard curves at all times.

### 34.2.6 Experimental Protocol

Animals were allowed to stabilize for 30 min after surgery, at which time they were randomized into the following groups: (a) aCSF (100 nL into the cNTS) followed by CChr, n = 8; (b) AMPA (2 µM diluted in 100 nL aCSF into de cNTS) followed by CChr stimulation, n = 9; (c) NBQX (2 mM diluted in 100 nL aCSF into the NTS) followed by CChr stimulation, n = 9 (Fig. 34.2).

### 34.2.7 Immunohistochemistry for GluR2/3 and c-Fos

In aCSF, AMPA, and NBQX groups vibratome sections were processed for immunohistochemical staining. Collected sections were

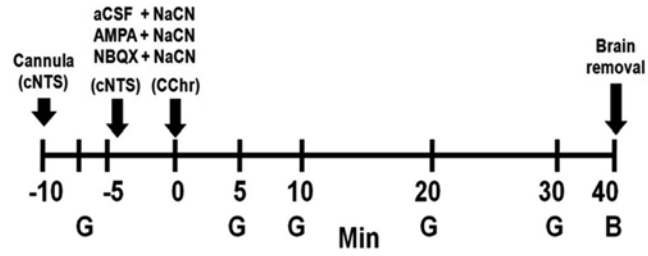


**Fig. 34.2** Time line in experimental protocol. G, glycemia

soaked in phosphate-buffered saline (PBS; pH 7.3) for 12–24 h, washed in 3 % goat serum and 0.4 % triton X (GS-T) in PBS (3 % GS-T-PBS) for 1 h, and then incubated for 16–36 h at 4 °C in rabbit anti-GluR2/3 (1:100 dilution, Chemicon, Temecula, CA) and anti-c-Fos primary antibodies (1:1,000 dilution, Santa Cruz Biotechnology, CA), diluted in 3 % GS-T-PBS. Sections rinsed extensively in 3 % GST-PBS, and incubated (in both cases) in goat anti-rabbit biotinylated IgG secondary antibody (1:250, diluted in 3 % GS-T-PBS) (Jackson Immunoresearch, Westgrove, PA) for 2 h. The tissue was placed for 1.5 h at room temperature in avidin–biotinylated- peroxidase complex (1 % GS-T-PBS, ABC Vectastin Kit) (Vector Labs., Burlingame, CA), rinsed in PBS 0.1 M without triton. The peroxidase reaction product was visualized following a 10 min incubation in a chromogen solution (3.3 diaminobencidine 0.07 % and $H_2O_2$ 0.01 %, pH 7.6) (Aldrich, St. Louis, MO) to obtain a brown color. After successive washes in PBS 0.1 M, sections were transferred to 0.05 M PBS, mounted, dehydrated, and coverslipped (Vectamount). Control sections (without the primary antibody) were processed as described. Tissue sections from each treatment group were pooled, and processed in tandem with control groups, to minimize variations in immunohistochemistry labeling. Sections were analyzed under an Axio Imager bright-field microscope equipped with a digital camera using AxioVision (version 4.8, 2009) software (Carl Zeiss, Munich, Germany). For each rat, 20 representative digital photomicrographs were taken at the same A/P coordinates using a Plan Achromat 20× objective. Positive GluR2/3 and Fos-ir cells were counted semiautomatically with a program using the Auto Measure Program Wizard (AxioVision version 4.8).

### 34.2.8 Data Analysis

Values expressed as means ± SEM. Data were analyzed using the SPSS 12.0 and ANOVA one way for multiple comparisons, and Scheffé's test to compare the data between groups. Significance was set at $p < 0.05$. Arterial glucose or BGR levels vs. their basal values (Student *t*-test), represented by an asterisk (*);plus sign (+) compares aCSF group vs. corresponding AMPA or NBQX groups. Comparison between AMPA and NBQX groups is represented by the pound sign (#). The actual basal arterial blood glucose values were 6.16 ± 0.16 µmol/mL (aCSF group), 6.0 ± 0.19 (AMPA group) and 5.88 ± 0.24 (NBQX group).

## 34.3 Results

When aCSF (100 nL) was injected into the cNTS 4 min before CChr stimulation with NaCN, an increase in arterial glucose concentration was observed at all the times studied, as previously shown (Alvarez-Buylla and Alvarez-Buylla 1988), the values rose from 6.33 ± 0.20 up to 9.88 ± 0.45 µmol/mL a t = 30 min ($p < 0.01$) (Fig. 34.3). When BGR was calculated, a prompt and significant increase was also obtained, with maximum level at t = 20 min, the values rose from 0.85 ± 0.08 µmol/mL up to 2.36 ± 0.23 µmol/mL ($p < 0.01$) (Fig. 34.4a). Rats that received an AMPA injection into the cNTS before CChr stimulation decreased their glucose levels when compared to aCSF group, with the higher decrement value at t = 5 min ($p < 0.01$), the values decreased from 6.01 ± 0.14 to 6.11 µmol/mL a t = 5 min ($p < 0.01$) (Fig. 34.4a). Similar results were observed in relation to BGR

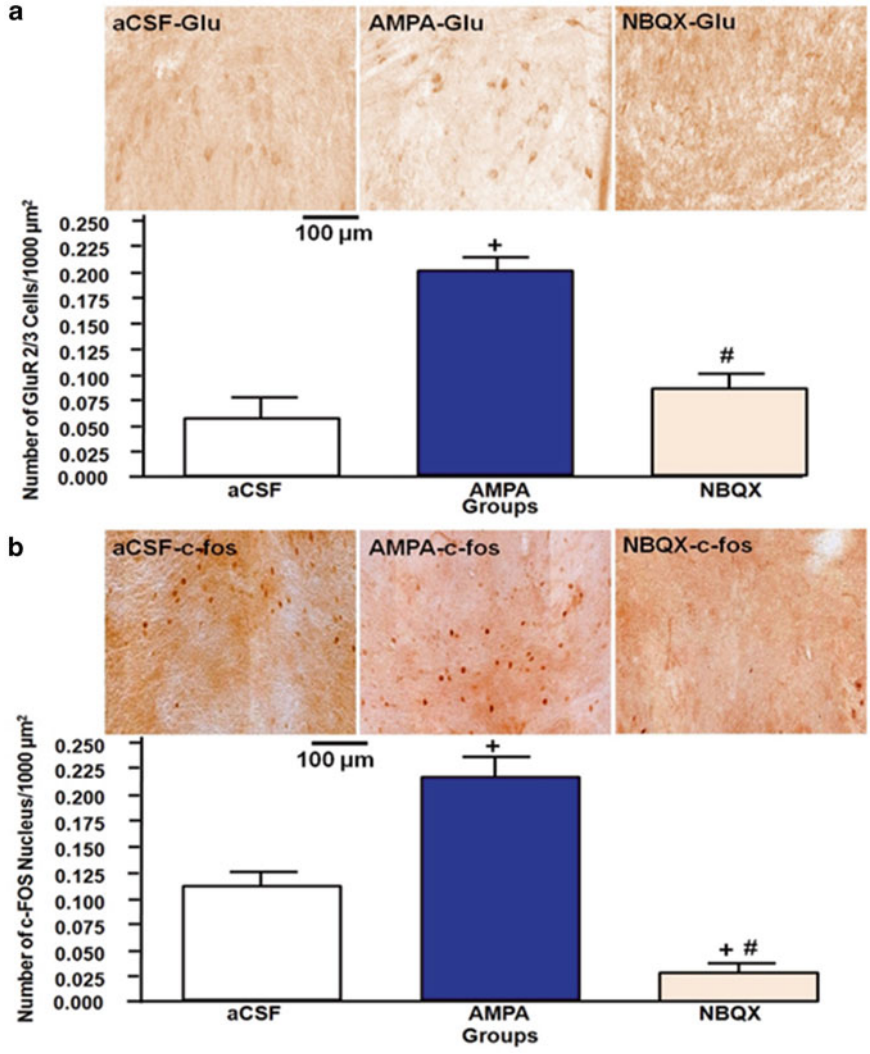


**Fig. 34.3** Effects of aCSF, AMPA or NBQX infusions into the cNTS, prior to CChr stimulation on GluR2/3 (Glu) and c-Fos expression in the cNTS (n = 8 per group). (**a**) GluR2/3-labeled cells, (**b**) number of c-Fos labeled cells in the same groups. Data are means of marked cells counted unilaterally ± S.E.M. Plus signs (+) indicate significant difference between aCSF group with their corresponding AMPA or NBQX groups. Pound sign (#) indicates significant difference between AMPA and NBQX groups

values, that decreased from 0.85 ± 0.11 down to 0.72 ± 0.14 µmol/mL a t = 5 min ($p < 0.01$) (Fig. 34.4b). By the contrary, rats injected with NBQX into cNTS 4 min before CChr stimulation, although showed a small increase at 5 and 10 min, it was not significant ($p > 0.05$, ANOVA one way), while the BGR levels decreased at 20 and 30 min (Fig. 34.4b). The comparison between AMPA and NBQX values for BGR did not yield a significant difference ($p > 0.05$, ANOVA).

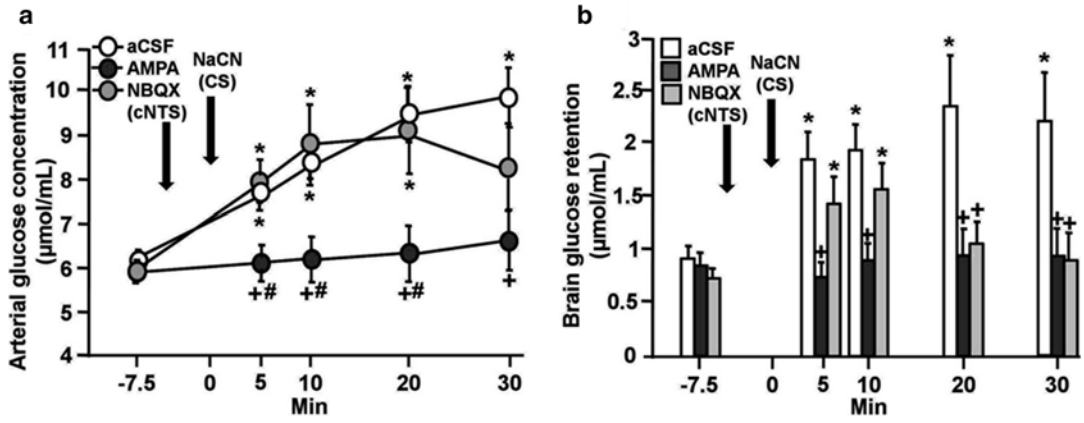


**Fig. 34.4** Effects of CChr stimulation 4 min after aCSF (n = 8), AMPA (n = 9) or NBQX (n = 8) infusions in the cNTS of anesthetized rats on: (**a**) arterial glucose concentration, and (**b**) BGR. The values are means ± S.E.M.; $*p < 0.05$ compares with its own basal (Student *t*-test); $+p < 0.05$ compares with aCSF group; $\#p < 0.5$ compares AMPA and NBQX groups (ANOVA)

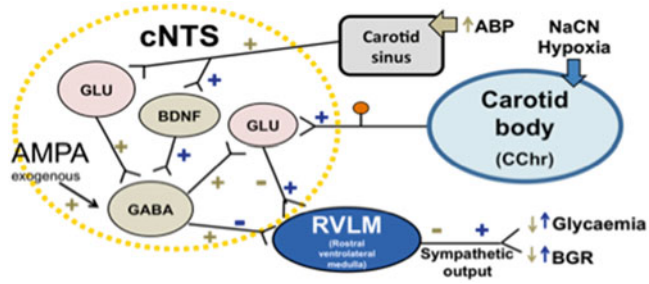


**Fig. 34.5** Proposed scheme of cNTS glutamatergic participation on hyperglycemic reflex and brain glucose retention (BGR) elicited by CChr stimulation with NaCN. +, excitation; −, inhibition; *blue* symbols, carotid chemoreceptor pathway; *gray* symbols, carotid baroreceptor pathway

## 34.4 Discussion

Arterial chemoafferent and baroreceptor neurons share a common development requirements to make their first synapses in the NTS (Brady et al. 1999; Paton et al. 2001). Recent studies in awake rats, provide evidence that the pressor response and sympathoexcitation due to the peripheral chemoreflex are mediated by ionotropic glutamate within the cNTS (Braga et al. 2007). Therefore, we hypothesized a possible involvement of ionotropic glutamate receptors in the effects presented here, after CChr stimulation and AMPA infusion into the cNTS. This study showed that AMPA in the cNTS before CChr stimulation inhibited BGR observed in aCSF group. However, an AMPA/kainate receptor blocker (NBQX) in the cNTS, preceding CChr stimulation, although did not modify the hyperglycemic reflex, significantly inhibited BGR at 20 and 30 min after CChr anoxic stimulation, as observed in aCSF group. The excitatory synaptic transmission in the cardio-respiratory reflexes is predominantly mediated by the AMPA receptors activation in the NTS to undertake a sympathoexcitation reflex (Ozawa et al. 1998; Lin 2009). Furthermore, activation of the AMPA receptor increases the chemoreceptor responses evoked by stimulation in animals exposed to intermittent hypoxia (de Paula et al. 2007), and CChr stimulation activates glutamatergic neurons in the cNTS (Takakura et al. 2006). Activation of AMPA receptors in cNTS induces GABAergic interneuron stimulation with a decrease in sympathetic output, and hyperglycemic reflex-BGR inhibition (Lemus et al. 2008). Sympathetic excitation

stimulates hepatic glycogenolysis and glucagon secretion to provide as much glucose as possible to the brain in a stressful situation (Hoffman 2007). It was previously showed that baroreceptor afferences supply glutamatergic excitatory signals to the NTS, to activate inhibitory GABAergic interneurons in the MVLC (caudal MVL) reducing the sympathetic output in response to increased arterial blood pressure in cardiovascular regulation (Clark et al. 2011). L-glutamate, also mediates the parasympathetic component of the chemoreflex (Braga and Machado 2006), and it could also explain the inhibitory effect of AMPA in the cNTS on glucose variables analyzed in these experiments. The results with NBQX infusion into cNTS indicated that another neurotransmitter might also be participating in the sympathetic component of the reflex studied (Braga and Machado 2006). Our experiments suggest that glutamatergic pathways, via AMPA receptors in the cNTS, may play a role in glucose homeostasis (Fig. 34.5).

**Acknowledgements** Supported by CONACYT 177047, and FRABA 798/12 grants.

## References

Alvarez-Buylla R, Alvarez-Buylla E (1988) Carotid sinus receptors participate in glucose homeostasis. Respir Physiol 72:347–360

Alvarez-Buylla R, Alvarez-Buylla E (1994) Changes in blood glucose concentration in the carotid body-sinus modify brain glucose retention. Brain Res 654:167–170

Alvarez-Buylla R, de Alvarez-Buylla ER, Mendoza H, Montero SA, Alvarez-Buylla A (1997) Pituitary and adrenals are required for hyperglycemic reflex initiated by stimulation of CBR with cyanide. Am J Physiol 272:R392–R399

Brady R, Katz D, Mayer C, Zaidi S (1999) BDNF is a target-derived survival factor for arterial baroreceptor and chemoafferent primary sensory neurons. J Neurosci 19:2131–2142

Braga VA, Machado BH (2006) Chemoreflex sympathoexcitation was not altered by the antagonism of glutamate receptors in the commissural nucleus tractus solitarii in the working heart-brainstem preparation of rats. Exp Physiol 91:551–559

Braga VA, Soriano RN, Braccialli AL, dePaula PM, Bonagamba LGH, Paton JF, Machado BH (2007) Involvement of L-Glutamate and ATP in the neurotransmission of the sympathoexciytatory component of the chemoreflex in the comissural nucleus tractus solitarii of awake rats and in the working heart-brainstem preparation. J Physiol 581:1129–1145

Clark CG, Hasser EM, Kunze DL, Katz DM, Kline DD (2011) Endogenous brain-derived neurotrophic factor in the nucleus tractus solitarius tonically regulates synaptic and autonomic function. J Neurosci 31:12318–12329

de Paula PM, Tolstykh G, Mifflin S (2007) Chronic intermittent hypoxia alters NMDA and AMPA-evoked currents in NTS neurons receiving carotid body chemoreceptor inputs. Am J Physiol Regul Integr Comp Physiol 292:R2259–R2265

Hoffman RP (2007) Sympathetic mechanisms of hypoglycemic counter regulation. Curr Diabetes Rev 3:185–193

Koshiya N, Guyenet PG (1996) NTS neurons with carotid chemoreceptor inputs arborize in the rostral ventrolateral medulla. Am J Physiol 270:R1273–R1278

Lemus M, Montero SA, Cadenas JL, Lara JJ, Tejeda-Chavez HR, Álvarez-Buylla R, de Álvarez-Buylla ER (2008) GabaB receptors activation in the NTS blocks the glycemic responses induced by carotid body receptor stimulation. Auton Neurosci 141:73–82

Lin L (2009) Glutamatergic neurons say NO in the nucleus tractus solitarii. J Chem Neuroanat 38:154–165

Müeller P, Foley C, Vogl H, Hay M, Hasser E (2005) Cardiovascular response to a group III mGluR agonist in NTS requires NMDA receptors. Am J Physiol Regul Integr Comp Physiol 289:R198–R208

Ohtake PJ, Torres JE, Gozal YM, Graff GR, Gozal D (1998) NMDA receptors mediate peripheral chemoreceptor afferent input in the conscious rat. J Appl Physiol 84:853–861

Ozawa S, Kamiya H, Tsuzuki K (1998) Glutamate receptors in the mammalian central nervous system. Prog Neurobiol 54:581–618

Pang ZP, Han W (2012) Regulation of synaptic functions in central nervous system by endocrine hormones and the maintenance of energy homeostasis. Biosci Rep 32:423–432

Paton JFR, Deuchars J, Li YW, Kasparov S (2001) Properties of solitary tract neurones responding to peripheral arterial chemoreceptor. Neuroscience 105:231–248

Paxinos G, Watson C (1997) The rat brain in stereotaxic coordinates. Academic, New York

Serani A, Lavados M, Zapata P (1983) Cardiovascular responses to hypoxia in the spontaneously breathing cat: reflexes originating from carotid and aortic bodies. Arch Biol Med Exp 16:29–41

Takakura AC, Moreira TS, Colombari E, West GH, Stornetta RL, Guyenet PG (2006) Peripheral chemoreceptor inputs to retrotrapezoid nucleus (RTN) CO2-sensitive neurons in rats. J Physiol 572:503–523

# Augmented 5-HT Secretion in Pulmonary Neuroepithelial Bodies from PHD1 Null Mice

35

Simon Livermore, Jie Pan, Herman Yeger, Peter Ratcliffe, Tammie Bishop, and Ernest Cutz

**Abstract**

Sustained exposure to low oxygen concentration leads to profound changes in gene expression to restore oxygen homeostasis. Hypoxia-inducible factors (HIFs) comprise a group of transcription factors which accumulate under hypoxia and contribute to the complex changes in gene expression. Under normoxic conditions HIFs are degraded by prolyl-hydroxylases (PHD), however during hypoxia this degradation is inhibited causing HIF accumulation and subsequent changes in gene expression. Pulmonary neuroepithelial bodies (NEB) are innervated serotonin (5-HT)-producing cells distributed throughout the airway epithelium. These putative $O_2$ sensors are hypothesized to contribute to the ventilatory response to hypoxia. NEB dysfunction has been implicated in several paediatric lung diseases including neuroendocrine cell hyperplasia of infancy and sudden infant death syndrome, both characterized by a marked NEB hyperplasia with unknown functional significance. We have previously reported striking NEB hyperplasia in PHD1$^{-/-}$ mice making these mice a potential model to study the role of NEBs in paediatric lung diseases. Here we report *in vitro* studies on 5-HT release from NEB using this model.

**Keywords**

Airway oxygen sensors • Hypoxia signalling • Pulmonary neuroendocrine cell hyperplasia • Paediatric lung disease

Simon Livermore and Jie Pan contributed equally with all other contributors.

S. Livermore • J. Pan • H. Yeger • E. Cutz (✉)
Division of Pathology, Department of Pediatric Laboratory Medicine, The Research Institute, The Hospital for Sick Children and Department of Laboratory Medicine and Pathobiology, University of Toronto, 555 University Avenue, M5G1X8 Toronto, ON, Canada
e-mail: ernest.cutz@sickkids.ca

P. Ratcliffe • T. Bishop
The Henry Wellcome Building for Molecular Physiology, University of Oxford, Oxford, UK



C. Peers et al. (eds.), *Arterial Chemoreceptors in Physiology and Pathophysiology*, Advances in Experimental Medicine and Biology 860, DOI 10.1007/978-3-319-18440-1_35

## 35.1 Introduction

The pulmonary neuroendocrine system consists of solitary pulmonary neuroendocrine cells (PNEC) and innervated cell clusters called neuroepithelial bodies (NEB) distributed throughout the airway epithelium of human and animal lungs. NEB density peaks in perinatal life and decreases with postnatal lung growth, suggesting a role in perinatal adaptation to air breathing (Cutz et al. 2007). These chemosensitive cells respond acutely to decreases in $pO_2$ (hypoxia) via an $O_2$-sensitive NADPH oxidase complex causing closure of $O_2$-sensitive $K^+$ channels, membrane depolarization, $Ca^{2+}$ entry, and neurosecretion of 5-HT and peptides (Fu et al. 2002). These responses are physiologically analogous to the glomus cells of the carotid body (CB), the primary arterial chemoreceptors. Glomus cells undergo $Ca^{2+}$-dependent neurosecretion of catecholamines and peptides in response to hypoxia, elevated $pCO_2$ (hypercapnia), and/or increased $[H^+]$ (acidosis). This led to a hypothesis that NEBs represent airway $O_2$-sensors during the perinatal period when CB sensors are immature, and monitor changes in airway $PO_2$ relaying this information to the CNS via vagal afferents to produce compensatory changes in the cardiorespiratory system.

In accordance with this hypothesis NEB dysfunction could lead to perinatal respiratory complications. Indeed, NEB dysfunction has been implicated in a host of paediatric respiratory diseases including neuroendocrine cell hyperplasia of infancy (NEHI) and sudden infant death syndrome (SIDS) (Cutz et al. 2007). These disorders are characterized by marked NEB hyperplasia; however the functional significance is unknown. We have previously reported that PHD1 null mice show distinct NEB hyperplasia (Pan et al. 2012). In the present study we used an *in vitro* model of NEB cells isolated from lungs of PHD1 null and control WT mice. The release of 5-HT was assessed by carbon fiber amperometry to characterize the single cell physiology and by ELISA assay. Here we show an increase in 5-HT content and enhanced 5-HT secretion in NEB cells from PHD 1 null mice when compared to WT controls. .

## 35.2 Materials and Methods

### 35.2.1 Cell Culture

Lungs were removed from wild type (WT, n = 12 litters) or prolyl-hydroxylase-1 ($PHD1^{-/-}$, n = 16 litters) knockout mice pups (P0-P5) and placed in $CO_2$-independent medium on ice. Lungs were finely minced and then placed in a salt solution containing digestive enzymes (Dispase + DNAse I + Collagenase IV). Tissue was triturated 20× and then enzymatically digested for 1 h, triturated 20× every 20 min. The digested cell suspension was centrifuged and washed with ice-cold Hanks Balanced Salt Solution 3×. Cell suspension was differentially plated and cultured on cover slips. The cultures were incubated with 5-HT precursor, L 5-hydroxytryptophan (5-HTP, 50–100 ug/ml), since earlier studies reported low endogenous levels of 5-HT in NEBs of rat and mouse lungs (Cutz et al. 1974).

### 35.2.2 5-HT Measurement

5-HT was measured using an ELISA as previously described (Pan et al. 2002) or by amperometry as previously reported (Fu et al. 2002).

### 35.2.3 Immunochemistry

NEB cells were immunostained as previously described (Cutz et al. 2004). NEBs were identified with the markers SV2 (mMab); synaptophysin (SYP) (rMab); 5-HT (goat).

## 35.3 Results

We have previously observed marked NEB hyperplasia in $PHD1^{-/-}$ compared to WT controls. In this study we tested the hypothesis that this distinct NEB morphological change affects NEB cell physiology. Thus we isolated NEBs from newborn (P1-5) $PHD1^{-/-}$ and WT control mice and cultured them on coverslips. Using immunohistochemistry we found that NEBs

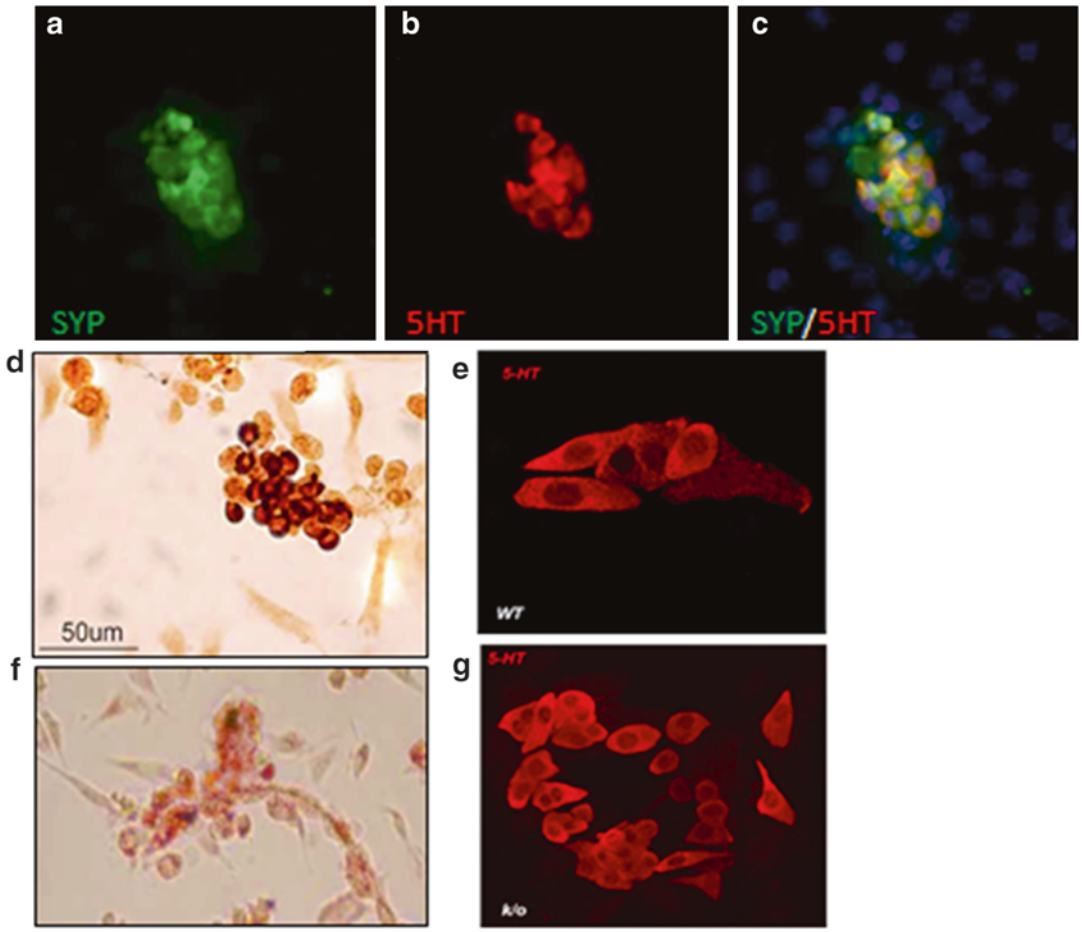


**Fig. 35.1** NEB cells in culture show classical NEB markers. *Top*, NEBs in culture are immunopositive for markers of synaptophysin (**a**) and 5-HT (**b**) and these markers are colocalized to the same cells (**c**). (**d**), NEBs in culture are also immunopositive for SV2 and live NEBs can readily be identified with neutral red staining (**f**). Comparison of 5-HT expression in NEBs isolated from wild type (**e**) and PHD1 null mice (**g**)

retain their characteristic markers under *in vitro* conditions as previously reported (Cutz et al. 2004). We observed that isolated NEBs were positive for synaptophysin (Fig. 35.1a) and 5-HT (Fig. 35.1b), both of which colocalized in the same NEB cells (Fig. 35.1c). As shown in Fig. 35.1d NEBs were also immunopositive for synaptic vesicle protein 2 (SV2) and could be readily cross-identified in culture using supravital dye, neutral red (Fig. 35.1f). NEB cells from both WT and PHD1 null mice maintained in culture for 48 h expressed strong 5-HT immunoreactivity (Fig. 35.1e, g).

Using the ELISA assay we observed increased 5-HT content in NEB cells of PHD1 null compared to WT controls under both normoxia and hypoxia conditions. As expected, exposure to hypoxia for different time periods showed increased 5-HT release at each time point, although the total amount of 5-HT was higher in NEB cells from PHD1 null mice, compared to WT controls (Fig. 35.2). As shown in Fig. 35.2, prolonged periods of hypoxia (1–12 h) augmented 5-HT release from NEBs in culture. Critically, this hypoxia-evoked secretion was augmented in NEBs from PHD1$^{-/-}$ (n = 6 cultures)

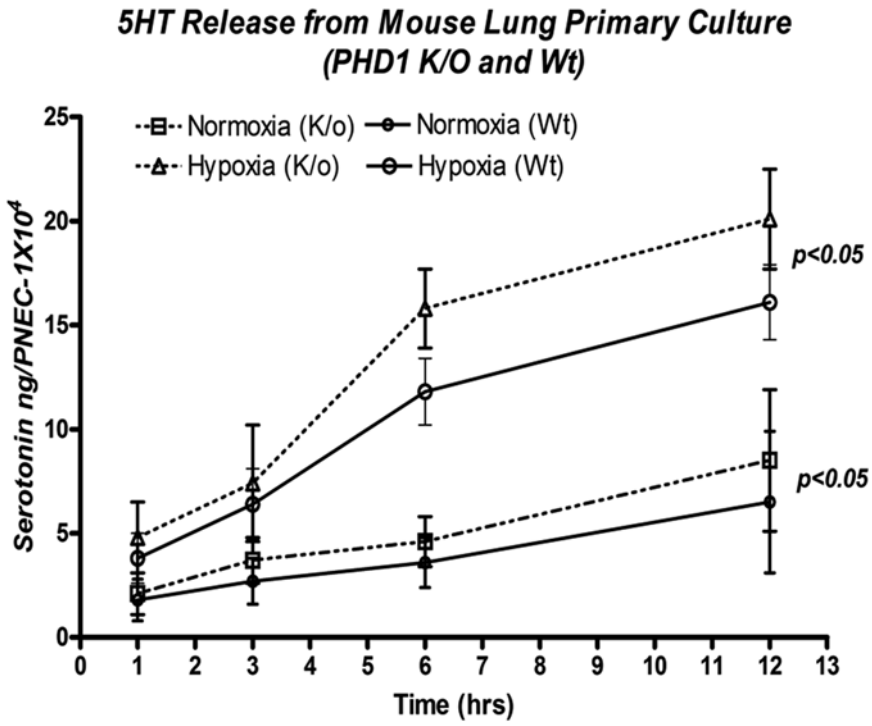


**Fig. 35.2** Time course of 5-HT secretion from NEBs isolated from PHD1$^{-/-}$ mice. As shown, in WT NEBs normoxia (*small open circles*) produces minimal 5-HT secretion over the time studied, however when exposed to hypoxia (*large open circles*) the 5-HT secretion is greatly augmented. This effect is more pronounced in NEBs from PHD1$^{-/-}$ mice where there is minimal 5-HT secretion in normoxia (*open squares*) and pronounced 5-HT secretion in hypoxia (*open triangles*)

mice vs WT (n = 4 cultures). Next, we compared 5-HT secretion from NEB cells in WT and PHD1 null mice using amperometry (n = 6 cells in each group). As shown in Fig. 35.3a, exposure of NEBs from WT mice to pO2 of 30 or 15 mmHg resulted in a burst of amperometric spikes each reflecting the oxidation of quanta of 5-HT molecules. These spikes had a greater amplitude in NEBs from PHD1 null compared to WT mice (Fig. 35.3b) indicating a greater quantal size (see scale bars). Thus, increased 5-HT synthesis and secretion seems to be a feature of NEBs from lungs of PHD1 null mice.

## 35.4 Discussion

NEB cell hyperplasia occurs in a number of paediatric respiratory diseases including SIDS and NEHI. However, until now reliable animal models to study the physiological consequences of NEB hyperplasia have been lacking. We have previously shown that NEB hyperplasia is a morphological characteristic of PHD1 null mice and in the current study we begin to characterize the physiological phenotype of PHD1 knockout in the NEB system. We demonstrate that NEBs from PHD1 null mice have increased 5-HT content under normoxic conditions. Primary lung cultures from PHD1 null mice contain well preserved NEBs expressing classical NEB markers SV2, synaptophysin, and 5-HT. Moreover, these NEBs can be readily identified with the supravital stain neutral red which makes these cultures amenable to single-cell electrophysiology.

We have previously shown that hypoxia evokes 5-HT secretion from rabbit NEBs in a lung slice preparation (Fu et al. 2002). First, we tested whether 5-HT secretion could be measured from mouse NEBs using an ELISA assay. Indeed,

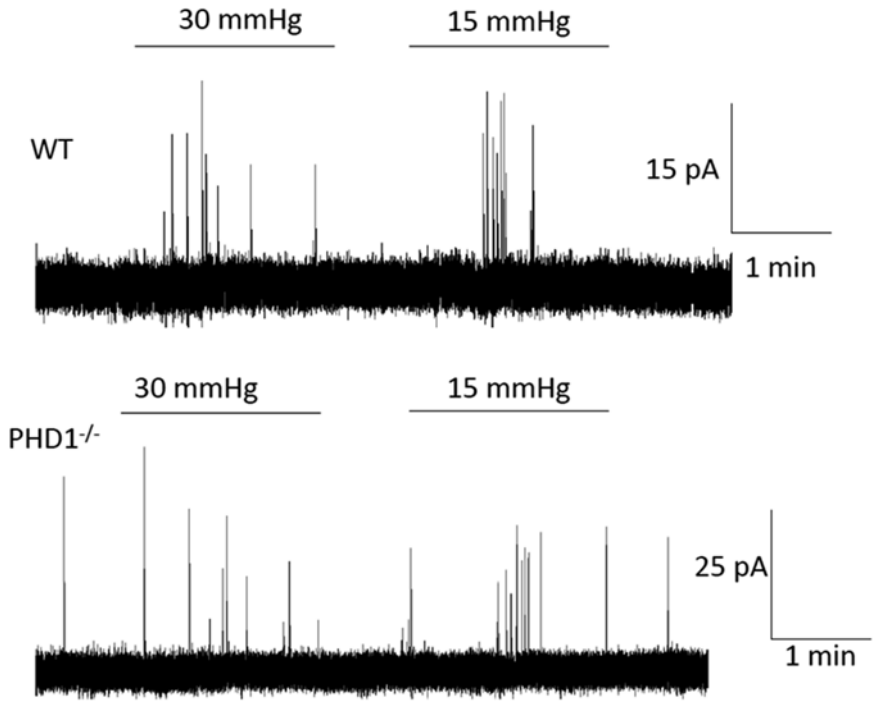


**Fig. 35.3** Comparison of 5-HT secretion from wild type NEBs (**a**) and NEBs from PHD1$^{-/-}$ mice (**b**). As shown hypoxia produces a secretory response from wild type and PHD1$^{-/-}$ NEBs; this response was greater in NEBs isolated from PHD1$^{-/-}$ mice (compare scale bars)

5-HT was released at significantly greater rate under hypoxic conditions compared to normoxic conditions from NEBs. Next, we compared 5-HT secretion in response to acute hypoxia and found 5-HT secretion was significantly greater from NEBs isolated from PHD1 null mice.

Further characterization of the physiologic responses of these animal models could provide insight into the role of NEBs in the pathobiology of paediatric respiratory diseases. For example, increased secretion of 5-HT and other mediators that may be co-released during hypoxia stimulation could be involved in a variety of activities including the modulation of the control of respiration, airway and vascular responses or inflammatory/immune processes (Cutz et al. 2007).

**Acknowledgements** Supported by grants from Canadian Institute for Health Research (MOP 15270) to EC and H.Y., and welcome trust (Programme grant #091857) to P.R. and T.B.

## References

Cutz E, Chan W, Wong V, Conen PE (1974) Endocrine cells in rat fetal lungs. Ultrastructural and histochemical study. Lab Invest 30:458–464

Cutz E, Fu XW, Yeger H (2004) Methods to study neuroepithelial bodies as airway oxygen sensors. In: Sen KS, Semenza GL (eds) Oxygen sensing, methods in enzymology, vol 381. Academic, New York, pp 26–40

Cutz E, Yeger H, Pan J (2007) Pulmonary neuroendocrine system in pediatric lung disease-recent advances. Pediatr Dev Pathol 10:419–435

Fu XW, Nurse CA, Wong V, Cutz E (2002) Hypoxia-induced secretion of serotonin from intact pulmonary neuroepithelial bodies in neonatal rabbits. J Physiol Lond 539:503–510

Pan J, Yeger H, Radcliffe P, Bishop P, Cutz E (2012) Hyperplasia of pulmonary neuroepithelial bodies in lungs of prolyl hydroxylase-1 deficient mice. Adv Exp Med Biol 758:149–155

Pan J, Bear C, Farragher S, Cutz E, Yeger H (2002) Cystic fibrosis transmembrane conductance regulator modulates neurosecretory function in pulmonary neuroendocrine cell related tumor cell line models. Am J Respir Cell Mol Biol 27:553–560

# Selective Expression of Galanin in Neuronal-Like Cells of the Human Carotid Body

36

Camillo Di Giulio, Guya Diletta Marconi, Susi Zara, Andrea Di Tano, Andrea Porzionato, Mieczyslaw Pokorski, Amelia Cataldi, and Andrea Mazzatenta

**Abstract**

The carotid body is a neural-crest-derived organ devoted to respiratory homeostasis through sensing changes in blood oxygen levels. The sensory units are the glomeruli composed of clusters of neuronal-like (type I) cells surrounded by glial-like (type II) cells. During chronic hypoxia, the carotid body shows growth, with increasing neuronal-like cell numbers. We are interested in the signals involved in the mechanisms that underlie such response, because they are not well understood and described. Considering that, in literature, galanin is involved in neurotrophic or neuroprotective role in cell proliferation and is expressed in animal carotid body, we investigated its expression in human. Here, we have shown the expression and localisation of galanin in the human carotid body.

**Keywords**

Galanin • Carotid body • Hypoxia • Oxygen sensing

C. Di Giulio • A. Di Tano • A. Mazzatenta (✉)
Department of Neurosciences, Imaging and Clinical Science, University 'G. d'Annunzio' of Chieti–Pescara, Via dei Vestini 31, 66100 Chieti, Italy
e-mail: amazzatenta@yahoo.com

G.D. Marconi • S. Zara • A. Cataldi
Department of Pharmacology, University 'G. d'Annunzio' of Chieti–Pescara, Chieti, Italy

A. Porzionato
Section of Human Anatomy, Department of Molecular Medicine, University of Padova, Via A. Gabelli 65, 35121 Padova, Italy

M. Pokorski
Laboratory of Electrophysiology, Clinical Research Center, Murayama Medical Center, 2-37-1 Gakuen, MusashiMurayama City, Tokyo 208-0011 Japan

Public Higher Medical Professional School, 68 Katowicka St., 45-060 Opole, Poland

Institute of Psychology, Opole University, Opole, Poland
e-mail: m_pokorski@hotmail.com



C. Peers et al. (eds.), *Arterial Chemoreceptors in Physiology and Pathophysiology*, Advances in Experimental Medicine and Biology 860, DOI 10.1007/978-3-319-18440-1_36

## 36.1 Introduction

The carotid body (CB) is a chemosensitive structure for acute oxygen-sensing and oxygen homeostasis that is key to life. It is a paired organ that is positioned at the bifurcation of the carotid artery, and during development it originates from the neural crest. The CB is innervated by afferent sensory nerve fibres that are connected to the glossopharyngeal nerve, which activate the brainstem respiratory centre to produce hyperventilation during hypoxaemia. The CB chemosensing core constitutes an intricate network of blood vessels that originate from a branch from the external carotid artery, and which spread into the parenchyma of the CB, where they make contact with the glomeruli. The glomeruli are the chemosensory units that are formed by a cluster of cells: the neuronal-like, or type I, cells, that are surrounded by the processes of non-excitable glial-like, sustentacular, or type II, cells. The neuronal-like cells are in tight contact with a minute branch off the capillaries, and they show some similarities to sympathetic neurons. They are electrically excitable, express oxygen-sensitive $K^+$ channels and an inward $Ca^{2+}$ current, which contributes to the membrane depolarisation that results in neurotransmitter secretion through dense-core vesicles (Lopez-Barneo et al. 2001; Peers and Buckler 1995; Weir et al. 2005).

Under chronic hypoxia, the CB can enlarge to several-fold its normal size, as also seen in patients with cardiopulmonary disease (Wang and Bisgard 2002; McGregor et al. 1984; Heath et al. 1982). This occurs through the production of new neuronal-like cells by activation of a resident population of neural-crest-derived progenitor cells. Furthermore, on returning to normoxia conditions, the original size of the CB is restored, with about half of the CB glomus cell mass replaced by these newly formed cells This thus indicates a striking regenerative power that is unusual for adult neural tissue.

These newly formed cells have the same neurochemical complex and electrophysiological properties as the mature neuronal-like cells. Consequently, the CB has been considered to be a neurogenic centre with a recognisable physiological function in adult life, because it contains such self-renewing and multipotent stem cells, which putatively represent the glial cells (Pardal et al. 2007).

In a similar chemosensory organ to the CB, the olfactory system, the generation of new olfactory neurons in adult mouse brain is driven by galanin (Cordeo-Llana et al. 2014). Furthermore, galanin has been described in the animal carotid body (Kameda 1989; Heym and Kummer 1989; Ichikawa and Helke 1993; Finley et al. 1995), and the galanin receptors GalR1 and GalR2 have been shown to be expressed in rat CB type I cells (Porzionato et al. 2010). We have therefore investigated whether galanin is expressed in the human CB.

## 36.2 Methods

Human carotid bodies (n = 12) were collected from 12-h to 72-h post-mortem, for subjects (mean age, 50 years; age range, 26.5–75.5 years) who had not shown chronic pulmonary or cardiovascular disease. The exclusion criteria were for signs at autopsy examination that the subject had undergone cardiac hypertrophy or previous myocardial infarction, and for subjects who showed any tissue degeneration or alteration detected using standard histological staining. Furthermore, the possible influence of the death-to-autopsy interval was examined statistically (for detailed method, see Porzionato et al. 2005). The study was approved by the local Ethics Committee, and was performed according to Italian laws on human autopsy tissue (Porzionato et al. 2005).

The specimens were fixed in neutral 10 % formalin, embedded in paraffin wax, sectioned (5 μm), and examined following Mallory trichrome histological staining (Bio Optica, Milan, Italy) and Azan blue staining (Bio Optica, Milan, Italy). The H-11 mouse monoclonal anti-galanin antibody (sc166431; Santa Cruz Biotechnology, CA, USA), the H1α 67 anti-hypoxia inducible factor (HIF) antibody (sc-53546; Santa Cruz Biotechnology), and developing kits (HRP Polymer/DAB Plus Chromogen, Lab Vision UltraVision LP Detection System; Thermo Scientific, CA, USA) were used for the immunohistochemistry. For light microscopy and data acquisition, a Leica DM 4000

microscope was used, which was equipped with the Leica DFC 320 digital acquisition system (Leica Cambridge Ltd., Cambridge, UK). The QWin Plus 3.5 software (Leica Cambridge Ltd.) was used to digitise the images and to compute the areas positive for the antibodies. Commercial software (i.e., SPSS, Origin) were used for the data and statistical analyses, using one-way ANOVA (α set to 0.001, unless otherwise specified).

## 36.3 Results

The anatomical organisation of the human CB was investigated using Azan blue staining (Fig. 36.1a, b). The anatomical structure highlighted in the histological staining revealed the CBs were preserved.

Mallory trichrome staining (Fig. 36.2a, b) coupled with immunostaining with an anti-HIF antibody (Fig. 36.3a, b) of the human CB sections

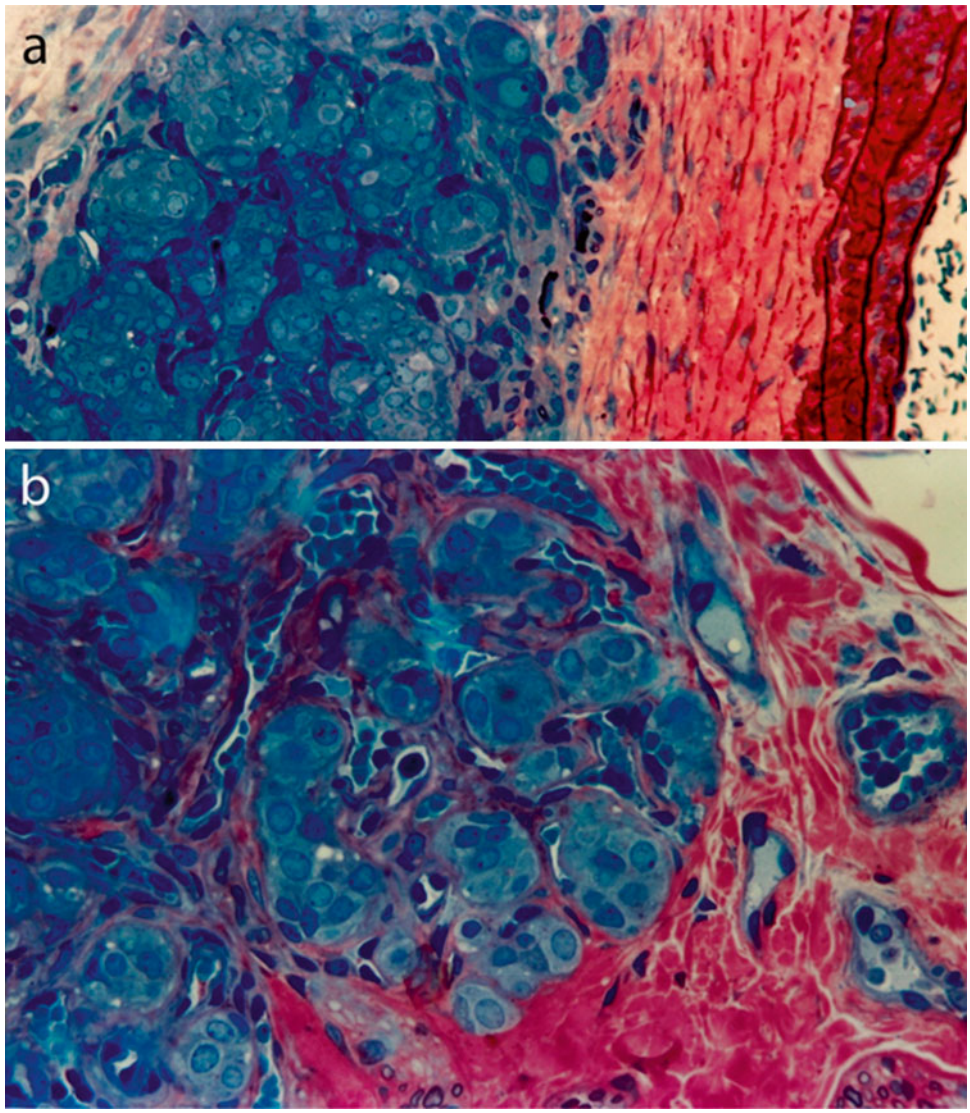


**Fig. 36.1 Representative Azan blue staining of the human carotid body (CB)** (**a**) histological sections of the human carotid bifurcation shows anatomical organization of CB, (**b**) higher magnification of the glomeruli clusters that form the functional chemosensing unit of the CB

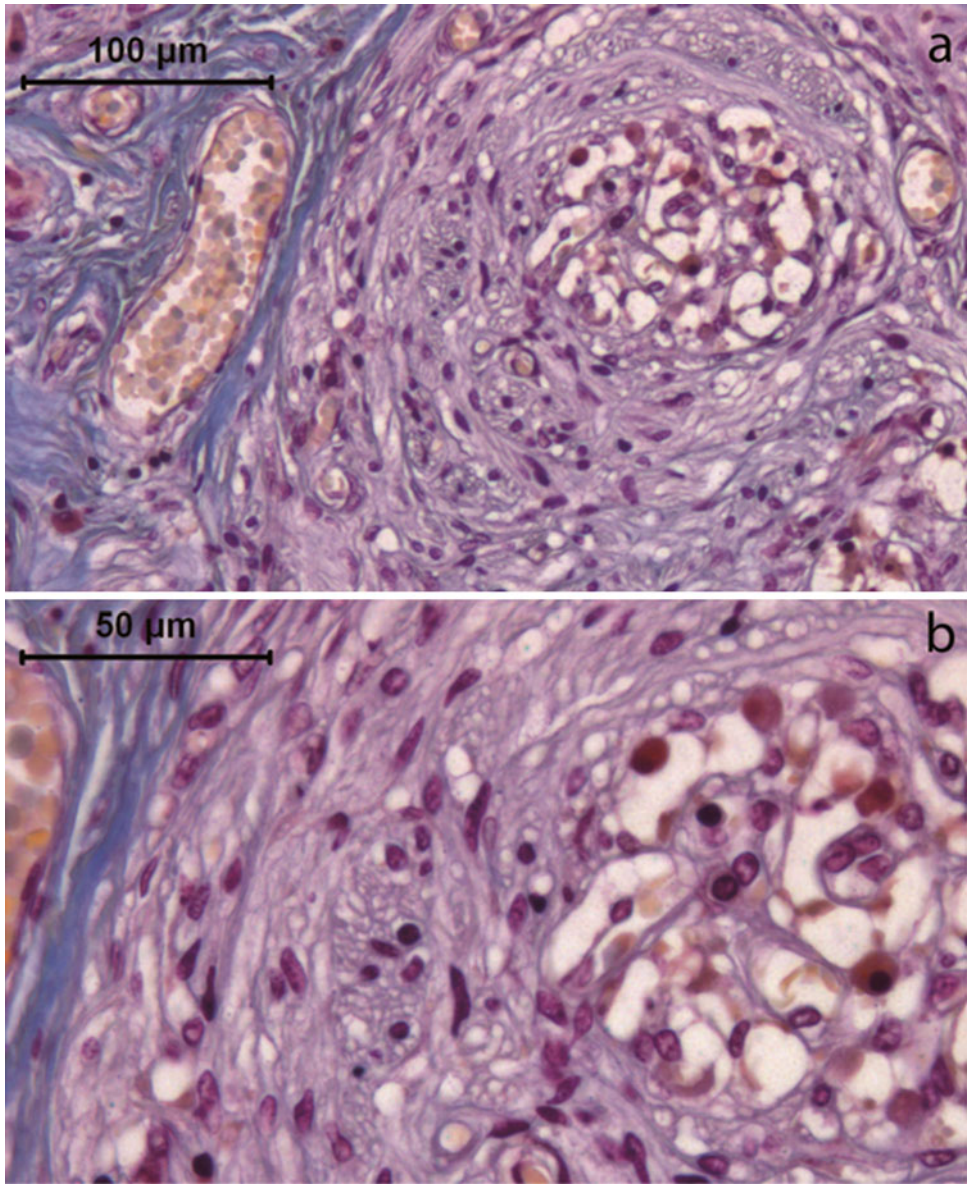


**Fig. 36.2 Mallory trichrome staining of human CB sections** (**a**) the glomerulus organisation and the blood vessel network are highlighted, (**b**) higher magnification

highlight the organisation of the glomeruli and the blood vessel network. This staining shows a detailed tissue sensorial structure of the CB. The HIF immunostaining, labels specifically the type I cells, and illustrates the functional organization of CB.

Histological sections of the human CB immunostained with an anti-galanin antibody reveal the galanin expression in type I cells, which are anatomically present in the sensorial structure of the CB (Fig. 36.4a, b).

Figure 36.5 shows high magnification of the sensorial unit of the CB highlighted using the bass-relief technique, showing the neuronal-like cells, glial cells, blood vessels and afferent sensory nerve fibres. The inset to Fig. 36.5 shows immunostaining of the neuronal-like cells.

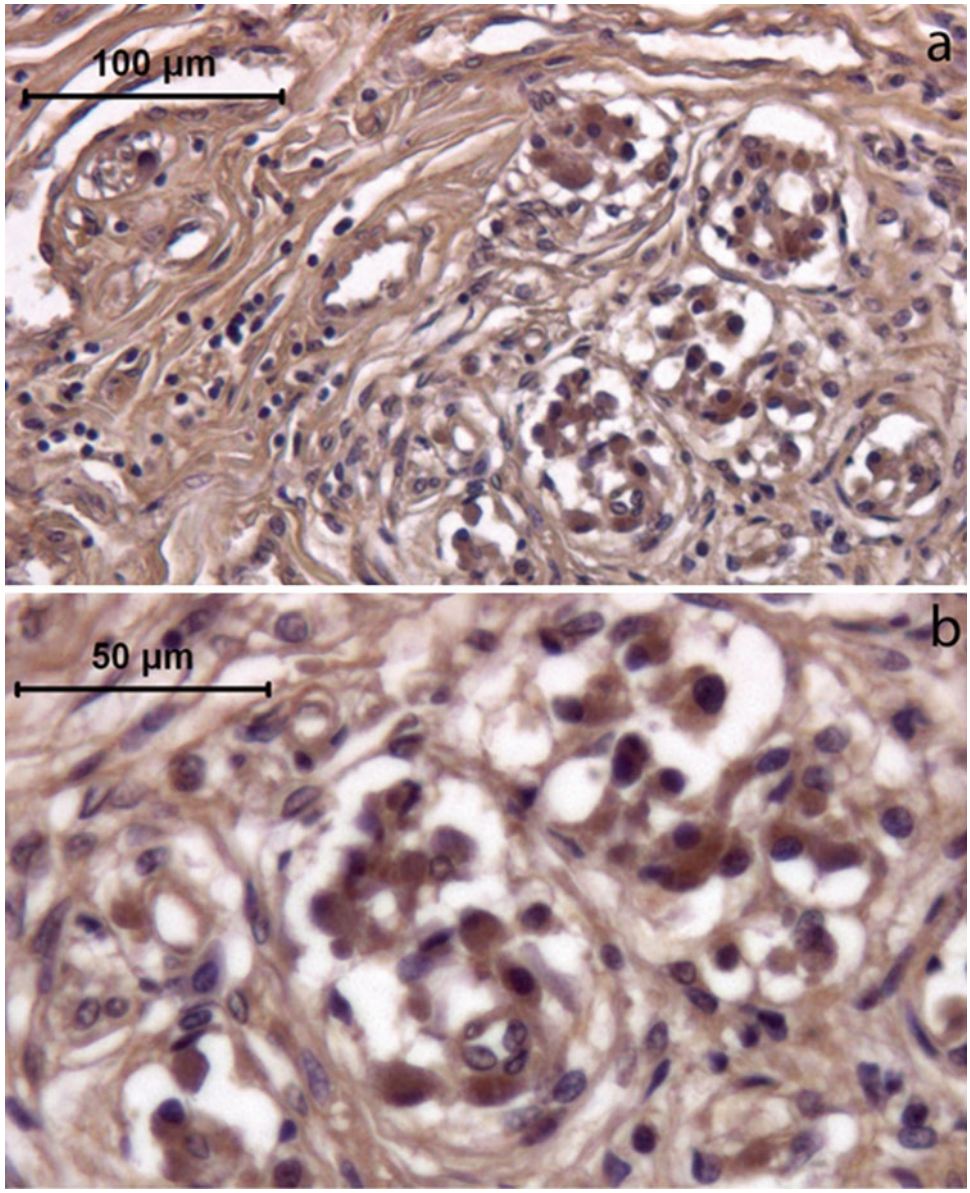


**Fig. 36.3 Immunostaining of human CB sections with an anti-HIF antibody** (**a**), HIF is selectively expressed by neuronal-like cells (**b**)

## 36.4 Discussion

We have found here the expression of the neuropeptide galanin in human CB. Galanin was first isolated from porcine intestine (Tatemoto et al. 1983) and was subsequently found in several species and tissues (Ch'ng, et al. 1985; Melander et al. 1986). Galanin expression has been shown throughout both the central and peripheral nervous systems, including the CB of rat, monkey, guinea pig and chicken (Kameda 1989; Heym and Kummer 1989; Ichikawa and Helke 1993; Finley et al. 1995).

The galanin peptide in animals consists of 29 amino acids, while it has 30 amino acids in

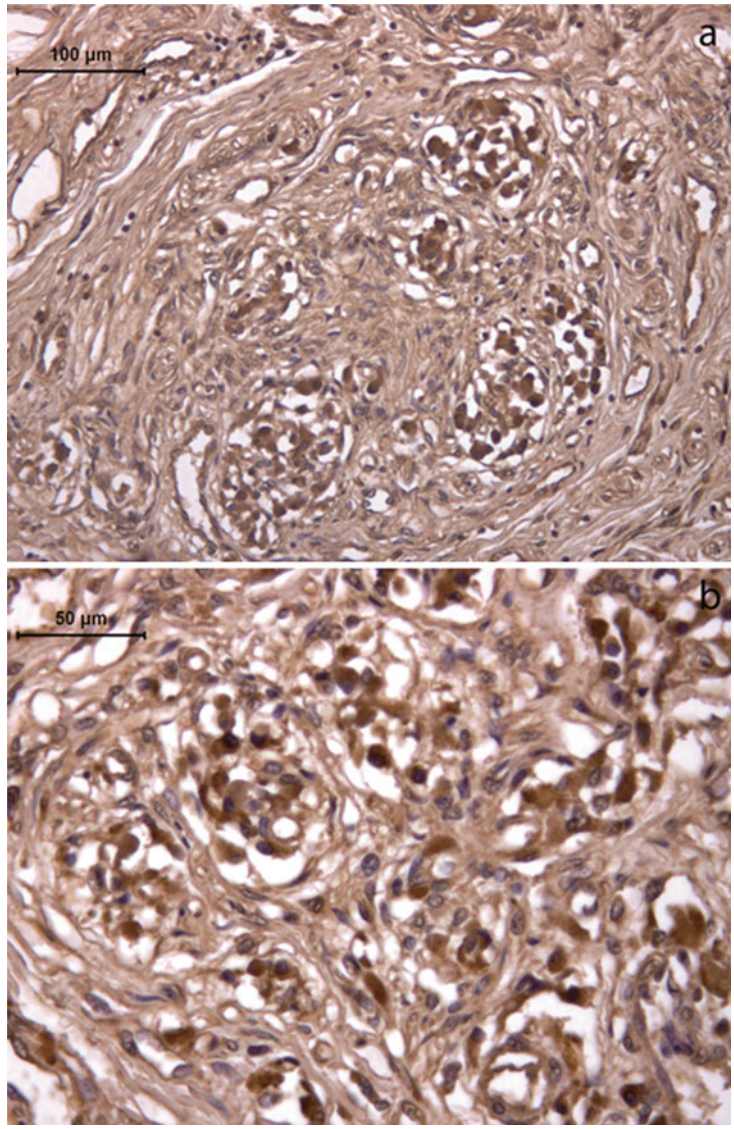


**Fig. 36.4 Immunostaining of human CB sections with an anti-galanin antibody** (**a**), higher magnification of the galanin expression (**b**)

human. Galanin is a highly inducible neuropeptide that has been conserved across species, and it has been shown to be distinctly up-regulated within the nervous system after pathological disturbance, where its N-terminal region has been shown to be crucial for its biological activity (Branchek et al. 2000). Galanin belongs to the galanin-related peptide family of neuropeptides, which is different from the other neuropeptide families (Ohtaki et al. 1999). Its biological effects are mediated through three different G-protein coupled receptors, termed GalR1, GalR2 and GalR3. Only the first two of these galanin receptors, GalR1 and GalR2, have been shown to be expressed in rat CB (Branchek et al. 2000; Florén et al. 2000; Porzionato et al. 2010).

GalR1 has been shown to be coupled to Gi/o, which acts through inhibition of adenylyl cyclase. However, GalR2 acts through another signalling pathway: via Gq/11 and the activation

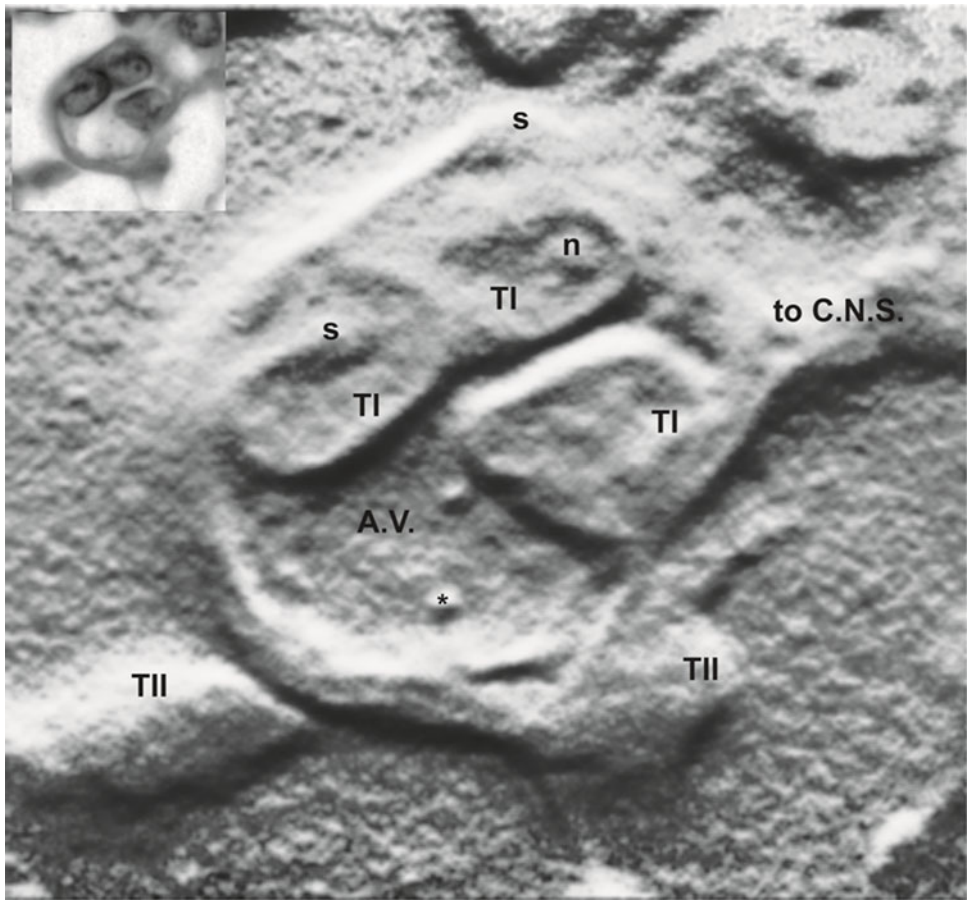


**Fig. 36.5 Bass-relief technique to highlight the sensorial unit of the CB** (**a**), which is composed of the neuronal-like cells (type I; TI), glial-like cells (type II; TII), artery vessels (*A.V.*), synapses (*s*), and afferent sensory nerve fibres (CNS). *n* nucleus, * erythrocyte. (**b**) *Inset*: Anti-galanin antibody immunostaining of a neuronal-like cell

of phospholipase C and protein kinase C (Wang et al. 1998; Wittau et al. 2000). As such, galanin can participate in the modulation of several ascending neurotransmitter systems, including cholinergic, noradrenergic, and serotonergic pathways (Tatemoto et al. 1983; Crawley et al. 2002).

Galanin acts as a neurotrophic/neuroprotective factor for several neuronal populations, and mainly for sensory neurons, and it is involved in the plasticity of the nervous system (Xu et al. 1996; Wiesenfeld et al. 1992; Hokfelt et al. 1987, 1994; Holmes et al. 2000). Moreover, in vitro galanin administration resulted in up-regulation of genes involved in the pro-survival/ pro-neuronal signalling pathways, and increased the number of neurons upon differentiation from olfactory sensory neuron progenitors (Cordeo-Llana et al. 2014).

Treatment with galanin and the specific agonist Gal2-11 in wild-type and GAL knock-out neural stem cells under differentiation conditions significantly promotes neuritogenesis, which is inhibited by the galanin antagonist M35 (Ma et al. 2008). Thus, galanin regulates differentiating neural stem cells, and in this way it can participate in the development and plasticity of the nervous system.

The CB can undergo size adaptation that leads to an increase under chronic hypoxia condition,

due to the production of new neuronal-like cells. Conversely, when returned to normoxia conditions, there is a corresponding decrease in the size of the CB, whereby the sensory cells have been renewed by the activation of a resident population of neural-crest-derived progenitors (Wang and Bisgard 2002; McGregor et al. 1984; Heath et al. 1982; Pardal et al. 2007). These adaptive phenomena have indicated the presence of self-renewing and multipotent stem cells in the CB (Pardal et al. 2007). The sustentacular cells are glial-like cells, and these express astrocyte markers and have a supportive role (Pallot 1987). When exposed to prolonged hypoxia, it has been proposed that type II cells themselves differentiate, or there is the production of stem-cell precursors of the neuronal-like cells (Pardal et al. 2007). This mechanism is crucial for the physiological role of the CB, because during adult life, this maintains a population of cells that can differentiate into neuronal-like cells.

Following the recent report that galanin is involved in neurodifferentiation of chemosensory neurons (Cordeo-Llana et al. 2014), we here investigated its potential expression in the glomeruli of the human CB, through identification of the cell type(s) that express it, and by examining the cell morphology to determine their position inside the glomeruli. There was no immunostaining for the glial like cells.

In conclusion, we have shown here the expression of galanin in human CB, with its selective expression in the neuronal-like or type I cells.

**Conflicts of Interest** The authors declare no conflicts of interest in relation to this article.

## References


Branchek TA, Smith KE, Gerald C et al (2000) Galanin receptor subtypes. Trends Pharmacol Sci 21:109–117

Ch'ng JL, Christofides ND, Anand P et al (1985) Distribution of galanin immunoreactivity in the central nervous system and the responses of galanin containing neuronal pathways to injury. Neuroscience 16:343–354

Cordeo-Llana O, Rinaldi F, Brennan PA et al (2014) Galanin promotes neuronal differentiation from neuronal progenitor cells in vitro and contributes to the generation of new olfactory neurons in the adult mouse brain. Exp Neurol 256:93–104

Crawley JN, Mufson EJ, Hohmann J et al (2002) Galanin overexpressing transgenic mice. Neuropeptides 36:145–156

Finley JC, Erickson JT, Katz DM (1995) Galanin expression in carotid body afferent neurons. Neuroscience 68:937–942

Florén A, Land T, Langel Ü (2000) Galanin receptor subtypes and ligand binding. Neuropeptides 34:331–337

Heath D, Smith P, Jago R (1982) Hyperplasia of the carotid body. J Pathol 138:115–127

Heym C, Kummer W (1989) Immunohistochemical distribution and colocalization of regulatory peptides in the carotid body. J Electron Microsc Tech 12:331–342

Hokfelt T, Wiesenfeld HZ, Villar M et al (1987) Increase of galanin-like immunoreactivity in rat dorsal root ganglion cells after peripheral axotomy. Neurosci Lett 83:217–220

Hokfelt T, Zhang X, Wiesenfeld HZ (1994) Messenger plasticity in primary sensory neurons following axotomy and its functional implications. Trends Neurosci 17:22–30

Holmes FE, Mahoney S, King VR et al (2000) Targeted disruption of the galanin gene reduces the number of sensory neurons and their regenerative capacity. Proc Natl Acad Sci U S A 97:11563–11568

Ichikawa H, Helke CJ (1993) Distribution, origin and plasticity of galanin-immunoreactivity in the rat carotid body. Neuroscience 52:757–767

Kameda Y (1989) Distribution of CGRP-, somatostatin-, galanin-, VIP- and substance P-immunoreactive nerve fibers in the chicken carotid body. Cell Tissue Res 257:623–629

Lopez-Barneo J, Pardal R, Ortega-Saenz P (2001) Cellular mechanism of oxygen sensing. Annu Rev Physiol 63:259–287

Ma J, Shan L, Yu LL et al (2008) Expression of galanin and galanin receptors in neurogenesis regions of adult mouse brain and effect of galanin on the neural stem cell differentiation. Fen Zi Xi Bao Sheng Wu Xue Bao 41(5):359–366

McGregor KH, Gil J, Lahiri S (1984) A morphometric study of the carotid body in chronically hypoxic rats. J Appl Physiol 57:1430–1438

Melander T, Hokfelt T, Rokaeus A (1986) Distribution of galanin-like immunoreactivity in the rat central nervous system. J Comp Neurol 248:475–517

Ohtaki T, Kumano S, Ishibashi Y et al (1999) Isolation and cDNA cloning of a novel galanin-like peptide (GALP) from porcine hypothalamus. J Biol Chem 274:37041–37045

Pallot DJ (1987) The mammalian carotid body. Adv Anat Embryol Cell Biol 102:1–91

Pardal R, Ortega-Saenz P, Duran R et al (2007) Glia-like stem cells sustain physiologic neurogenesis in the adult mammalian carotid body. Cell 131:364–377

Peers C, Buckler KJ (1995) Transduction of chemostimuli by the type I carotid body cell. J Membr Biol 144:1–9

Porzionato A, Macchi V, Guidolin D et al (2005) Histopathology of carotid body in heroin addiction. Possible chemosensitive impairment. Histopathology 46(3):296–306

Porzionato A, Macchi V, Barzon L et al (2010) Expression and distribution of galanin receptor subtypes in the rat carotid body. Mol Med Rep 3:37–41

Tatemoto K, Rökaeus A, Jörnvall H et al (1983) Galanin – a novel biologically active peptide from porcine intestine. FEBS Lett 164:124–128

Wang S, Hashemi T, Fried S et al (1998) Differential intracellular signalling of the GalR1 and GalR2 galanin receptor subtypes. Biochemistry 37:6711–6717

Wang ZY, Bisgard GE (2002) Chronic hypoxia-induced morphological and neurochemical changes in the carotid body. Microsc Res Tech 59:168–177

Weir EK, Lopez-Barneo J, Buckler KJ et al (2005) Acute oxygen-sensing mechanisms. N Engl J Med 353:2042–2055

Wiesenfeld HZ, Bartfai T, Hokfelt T (1992) Galanin in sensory neurons in the spinal cord. Front Neuroendocrinol 13:319–343

Wittau N, Grosse R, Kalkbrenner F et al (2000) The galanin receptor type 2 initiates multiple signalling pathways in small cell lung cancer cells by coupling to G(q), G(i) and G(12) proteins. Oncogene 19:4199–4209

Xu ZQ, Shi TJ, Hokfelt T (1996) Expression of galanin and a galanin receptor in several sensory systems and bone anlage of rat embryos. Proc Natl Acad Sci U S A 93:14901–14905

# Role of BK Channels in Murine Carotid Body Neural Responses *in vivo*

37

L.E. Pichard, C.M. Crainiceanu, P. Pashai, E.W. Kostuk, A. Fujioka, and M. Shirahata

**Abstract**

The aim of this study was to explore the role of BK channels in the hypoxic sensitivity of the *in vivo* murine carotid body (CB). Four strains of mice (DBA/2J, A/J, BKα1 knockout and BKα1 wild type – FVB background) were used. The mice were anesthetized, paralyzed and mechanically ventilated ($PaCO_2 \sim 35$ mmHg, $PO_2 > 300$ mmHg). We measured carotid sinus nerve (CSN) activity during three gas challenges ($F_IO_2$: 0.21, 0.15 and 0.10). CSN activity was analyzed with time-variant spectral analysis with frequency domain conversion (Fast Fourier Transforms). Afferent CSN activity increased with lowering $F_IO_2$ in the DBA/2J, BKKO and BKWT mice with the most robust response in 600–800 frequencies. No substantial changes were observed in the A/J mice. Although maximal neural output was similar between the BKKO and BKWT mice, the BKWT had a higher early response compared to BKKO. Thus, BK channels may play a role in the initial response of the CB to hypoxia. The contribution of BKβ subunits or the importance of frequency specific responses was unable to be determined by the current study.

**Keywords**

BK channel • Carotid sinus nerve • Chemosensitivity • Hypoxia • Mouse

## 37.1 Introduction

Several types of potassium channels in the carotid body glomus cells (GCs) have been shown to be inhibited by hypoxia. BK channels have long been recognized as modulators of hypoxic sensing cascade in the CB (Peers 1990). Evidence indicates that BK channels are critical

L.E. Pichard • C.M. Crainiceanu • P. Pashai
E.W. Kostuk • A. Fujioka • M. Shirahata (✉)
Department of Environmental Health Sciences, Johns Hopkins University, Baltimore, MD, USA
e-mail: mshiraha@jhmi.edu



C. Peers et al. (eds.), *Arterial Chemoreceptors in Physiology and Pathophysiology*, Advances in Experimental Medicine and Biology 860, DOI 10.1007/978-3-319-18440-1_37

for depolarizing GCs during hypoxia in rats (Wyatt and Peers 1995), but some species differences may be present in their role in hypoxic chemotransduction cascade (Prabhakar and Peers 2014). Species differences can be viewed as differences in genetic background. In such, we observed strain differences in BK channel expression in DBA/2J and A/J strains (Otsubo et al. 2011). In the GCs of DBA/2J, 40–50 % of the outward $K^+$ current is carried by iberiotoxin-sensitive BK channels. In the A/J mice iberiotoxin-sensitive BK current was barely recognized under our experimental conditions. The differences in BK channel expression between these strains may be reflected to the phenotypic differences in hypoxic response: DBA/2J mice are high responder and A/J mice are low responder (Tankersley et al. 1994; Rubin et al. 2003; Campen et al. 2004). To further explore the role of BK channels in the *in vivo* CB hypoxic sensitivity, we examined integrated CB function (i.e. CB afferent neural output) in four different strains of mice, the DBA/2J, A/J, BKKO and BKWT mice.

## 37.2 Methods

Mice were housed and bred in the animal facility of the Johns Hopkins Bloomberg School of Public Health (Baltimore, MD). Heterozygous BKα1 mutant mice were kindly provided by Dr. AL Meredith at University Maryland and bred in our facility. Genotype of mutant mice was determined from DNA obtained from their tails. All animal experiments were conducted in accordance with NIH guidelines and the experimental protocols were approved by the Animal Care and Use Committee of the Johns Hopkins University.

### 37.2.1 Measurements of CSN Activity in Ventilated Mice

Mice were anesthetized with urethane 1.25 g/kg (i.p.). Mice were ventilated via a tracheal tube by a modified volume-controlled Harvard animal ventilator (Model 687, Harvard Apparatus) under hyperoxia ($F_IO_2 = 1.0$) with ~3 $cmH_2O$ of positive end expiratory pressure. Respiratory rate and tidal volume were selected based on our previous experiments to maintain appropriate arterial blood gas values (see Sect. 37.2.3). The right common carotid artery was cannulated for monitoring blood pressure. The right jugular vein was cannulated for continual fluid supplementation with modified Krebs Solution (0.025 mL/g/h). Subsequently, mice were paralyzed with pancronium bromide (0.03–0.04 mg/kg, i.p.) and atropine (0.07 mg/kg, i.p.) was given to reduce tracheal secretions. The neck was incised to expose the left carotid bifurcation and the glossopharyngeal nerve. CSN was identified and the central end was sectioned. The area including the CB and CSN was filled with Krebs solution. The sectioned end was then placed into a glass suction pipette containing a silver-silver chloride electrode and Krebs solution. Additionally, a silver-silver chloride electrode was inserted into the salivary gland to serve as a biological ground. The signal was amplified (AC-Preamplifier P15, Grass Instruments Co.) and collected using digital recording software (AcqKnowledge, BioPac Systems, Inc.) together with airway pressure and arterial pressure. Baroreceptors were mechanically denervated in a manner similar to those previously described (Shirahata and Fitzgerald 1991; Van Vliet et al. 1999). Successful removal of baroreceptors was confirmed when increased blood pressure did not accompany an increase in CSN activity. Functional viability of the CB and CSN was assessed prior and at the end of the experiment by a brief exposure to 100 % inspired $N_2$ which leads to a vigorous increase in nerve activity.

### 37.2.2 Conditions of Mice

The success of the CSN recording in an *in vivo* mouse was dependent on the proper control of ventilation and fluid balance. We performed separate experiments to determine appropriate ventilatory conditions and fluid support for each strain. Strain specific respiratory rate was selected from

published data from unanesthetized mice (~145/min for DBA/2J and A/J mice, ~170/min for FVB strains) (Boudinot et al. 2002; Tankersley et al. 1994). At these respiratory rates optimal tidal volumes to maintain PaCO2 at ~35 mmHg with our ventilator were 14.9 ± 1.0, 10.7 ± 0.5, 11.7 ± 0.8 (μL/g) for DBA/2J, A/J and FVB (BKWT, BKKO) strains, respectively. Continual infusion of modified Krebs solution at a rate of 0.025 mL/g/h well maintained airway pressure and arterial pressure for 4 h.

### 37.2.3 Spectral Analysis of CSN Activity

Time-variant spectral analysis was carried out as follows. Each continuous 120 s of recording segment including 90 s of gas challenge was broken down into 2-s windows. Each 2-s window overlapped with the previous window by 50 %, which decreases the variance derived from converting finite data sets of the time domain into the frequency domain (Pesaran et al. 2002). Because the raw signal of CSN activity is non-periodic, a Hann function was applied to reduce leakage in fast Fourier transform (FFT) before transformation (Eq. 37.1).

$$w(n)=\begin{cases}\frac{1}{2}\left[1+\cos\left(\frac{2\pi n}{N}\right)\right] & n=-\frac{N}{2},\ldots,-1,0,1,\ldots,\frac{N}{2}\\ \frac{1}{2}\left[1-\cos\left(\frac{2\pi n}{N}\right)\right] & n=0,1,2,\ldots,N-1\end{cases} \tag{37.1}$$

$n$ : each individual observation within a data set of $N$ observations.

FFT transformation was performed according to the Eq. 37.2 below.

$$w(n)_{fft}=\sum_{k=0}^{N-1}w(n)\cdot e^{2\pi i\frac{kn}{N}} \tag{37.2}$$

$w(n)$: the vector containing the original time series data, $N$ : the total number of points in the vector $i=\sqrt{-1}$

Data exploration showed a significant 60 Hz noise in the raw signal. This noise was also evident in its harmonics. Thus, the raw signal was passed through a comb-pass filter set at every 60 Hz up the Nyquist frequency (2,500 Hz). Also, to further suppress any narrow band bias from this strong 60 Hz signal, we omitted frequency data contained within ±5 Hz of the 60 Hz signal and its harmonics. All frequencies below 65 Hz were also removed, because they included unwanted artifacts coming from breathing and/or heart beats (Fig. 37.1).

Subsequently, the spectrum was normalized as follows: (1) Baseline was determined as the mean spectral power during the 15-s period before the $N_2$ challenge. Baseline was subtracted from each point of spectral observation; (2) After baseline subtraction, each spectral observation was divided by the total power across all challenges in all experiments to offset the variations between the experiments; (3) Further, each spectral observation was expressed as the ratio of the maximal power during the $N_2$ response. The spectrum was broken down into 7 frequency bands for analysis. Alpha (α): 65–295 Hz, Beta (β): 305–535 Hz, Gamma (γ): 545–775 Hz, Delta (δ): 785–1,015 Hz, Epsilon (ε): 1,025–1,255, Zeta (ζ): 1,265–1,495 Hz and Eta (η): 1,505–2,500. Because the eta frequency band was wider than others, the power content of each band was normalized as follows: (the power content of each band) ÷ (the total number of frequencies in the band). ANOVA or t test was used for statistical analysis with an aid of Prizm4 software (Graphpad) and $p<0.05$ was considered significant.

## 37.3 Results

### 37.3.1 Temporal Characteristics of CSN Activity in Response to Hypoxia

In each preparation, three gas challenges ($F_IO_2=0.21$, 0.15, 0.1) were performed at a random order. DBA/2J, BKWT and BKKO mice showed a time and $F_IO_2$ dependent neural output:

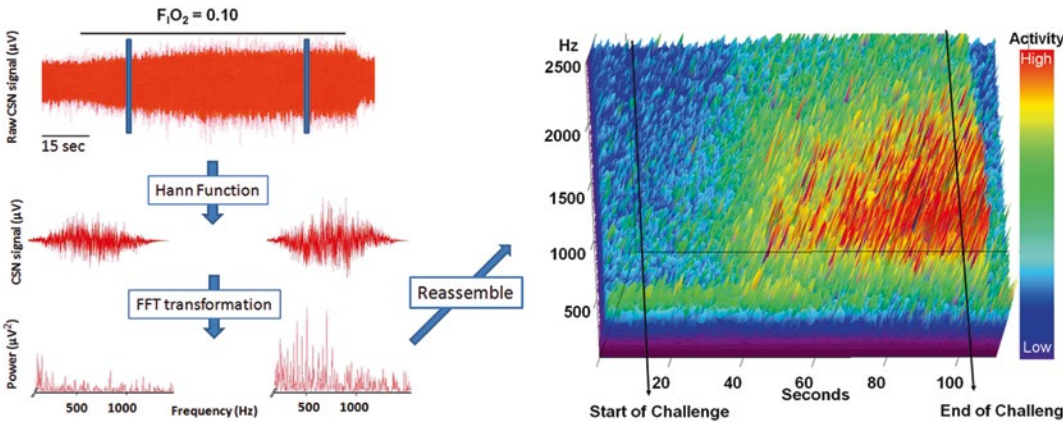


**Fig. 37.1** Time variant spectral analysis of CSN signal. Two separate 2 s-windows (*blue boxes*) were shown in the raw signal (*Top left*). Each signal was processed into frequency domain (FFT) after applying Hann function. After transformation, signals were re-assembled to mesh plot graph (*right*), which shows the temporal and spectral characteristics of CSN activity in response to a gas challenge

The lower $F_IO_2$, along with the duration of the challenge, leads to greater increases in neural output. A/J strain did not significantly respond to any of the three gas challenges, although all preparations including the A/J strain did respond to the anoxic (100 % $N_2$) challenge (data not shown). The DBA/2J mice showed a progressive and almost linear increase in neural output with each hypoxic challenge (Fig. 37.2a). BKWT mice showed faster response to all three $F_IO_2$ challenges compared to other strains (Fig. 37.2c). In the BKKO mice, hypoxic response was clearly observed, but in response to the 0.10 $F_IO_2$ challenge neural output was not sustained and a decrease was observed in the last ~30 s of the response (Fig. 37.2d).

### 37.3.2 Spectral Characteristics of CSN Activity in Response to Hypoxia

Figure 37.3 shows spectral characteristics of mean CSN activity in response to three levels of gas challenges. Robust responses were apparent in β and γ bands (305–535 Hz and 545–775 Hz, respectively) in all three responsive strains (DBA/2J, BKWT and BKKO). In all strains little response was seen in η band (1,505–2,500 Hz). The A/J strains show little response in all frequency bands.

Spectral characteristics were further examined in DBA/2J mice. An example in response to $F_IO_2$ 0.1 is shown in Table 37.1. Arterial blood samples were obtained from DBA/2J mice in separate but similar experimental settings. $PaO_2$ exponentially decreased during hypoxic ventilation. $PaO_2$ values at the baseline, 30 s after hypoxia, 60 s after hypoxia and 90 s after hypoxia were $308.8 \pm 17.3$ ($n=5$), $52.3 \pm 4.3$ ($n=10$), $48.8 \pm 3.9$ ($n=6$), $40.6 \pm 3.4$ ($n=10$), respectively. Along with the reduction of $PaO_2$, CSN activity increased over a wide frequency range. However, β (305–535 Hz) and γ (545–775 Hz) show more vigorous hypoxic responses compared to other bands at any time points examined. Maximal responses in the β and γ bands were significantly higher than other bands (ANOVA, $p<0.05$). No significant differences were observed between β and γ bands. Similar spectral characteristics were observed in other gas challenges ($F_IO_2$ 0.15 and 0.21; data not shown).

Although CSN activity increased with decreased $F_IO_2$ in DBA/2J, BKWT and BKKO

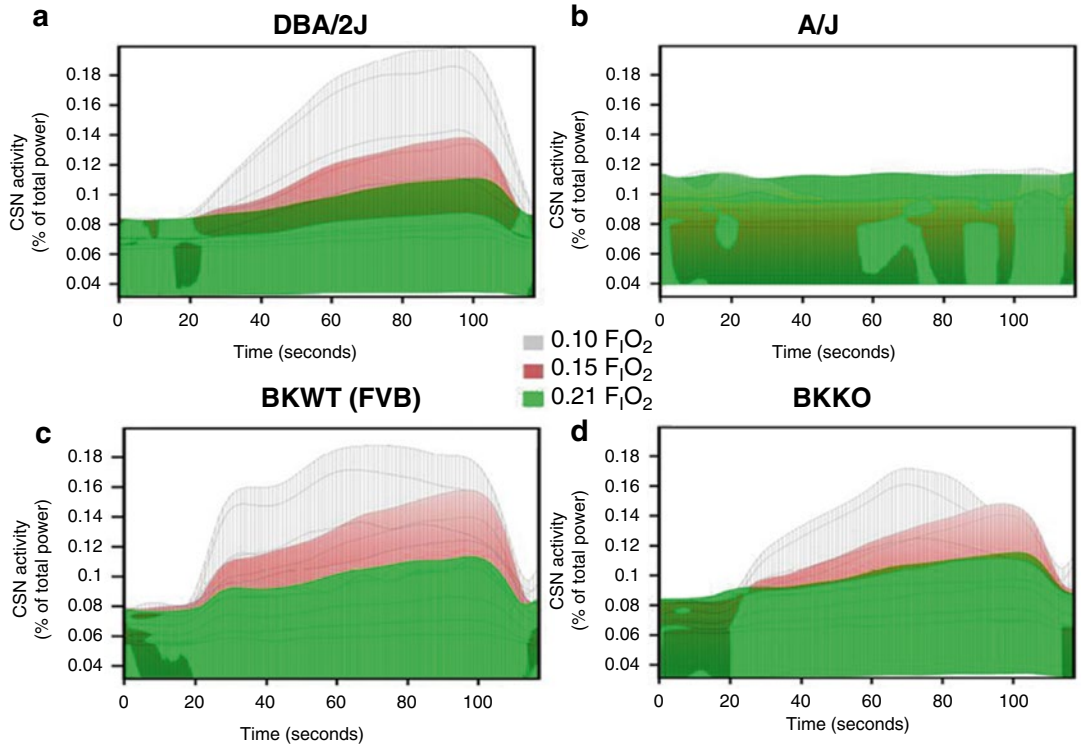


**Fig. 37.2** Strain specific temporal characteristics in response to decreased $F_IO_2$. The figure shows the mean normalized responses to the three different gas challenges. The number of experiments for DBA/2J, A/J, BKWT, and BKJO were 11, 12, 4 and 6, respectively. The responses were color-coded: $F_IO_2$ 0.21 – *green*, 0.15 – *red*, 0.1 – *grey*. To aid in comparing across challenges, we have plotted all three responses on the same panels. Gas challenges began at 15 s and ended at 105 s. The shades of colors vary because three dimensional characteristics of CSN activity, as seen in Fig. 37.1, were compressed in two dimensional forms

strains, the response speed appears different among strains (Fig. 37.2). Thus, we further explored the differences in CSN responses among the four strains using the β band. The β band is most responsive to hypoxia (Fig. 37.3, Table 37.1). As presented in Fig. 37.4, 15 s after 0.1 $F_IO_2$ exposure, CSN activity was significantly increased from the baseline in three responsive strains and it remained elevated during the hypoxic exposure (repeated ANOVA, $p<0.05$; marked as * in Fig. 37.4a). The increase at 30 s was less in BKKO mice than that of BKWT (t-test, $p<0.05$ marked as # in Fig. 37.4b). In A/J mice, the baseline CSN activity was higher than those of other strains, and no significant changes in CSN activity was seen during hypoxia.

## 37.4 Discussion

This study shows that CSN response to hypoxia is strain specific. Among the strains examined, DBA/2J and FBV mice proved to be high responders. A/J mice did not show a significant hypoxic response. These results are consistent with studies which show that the A/J strain has very attenuated cardiovascular and respiratory responses to hypoxia (Campen et al. 2004; Tankersley et al. 1994). In the study simulating sleep apnea, Rubin et al. (2003) also showed a decreased sensitivity to hypoxia in the A/J strain compared to the DBA/2J strain. The muted CB response is, at least in part, responsible for the reduced systemic response to hypoxia in A/J

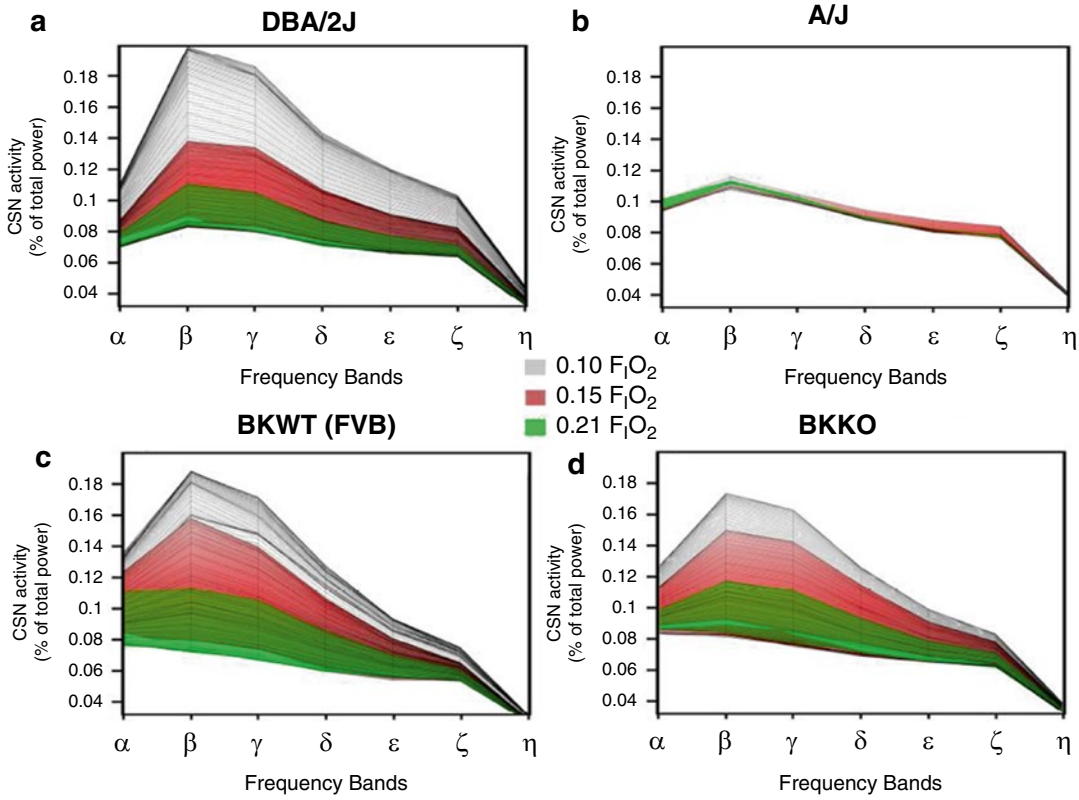


**Fig. 37.3** Strain specific spectral characteristics in response to decreased $F_IO_2$. The figure shows the mean normalized responses to the three different gas challenges. The number of experiments for DBA/2J, A/J, BKWT, and BKJO were 11, 12, 4 and 6, respectively. The responses were color-coded: $F_IO_2$ 0.21 – *green*, 0.15 – *red*, 0.1 – *grey*. Note that three dimensional characteristics of CSN activity were compressed in two dimensional forms

mice. Previously we have shown that the CB of A/J mice expresses less BK channels (Otsubo et al. 2011), suggesting that BK channels play a role in the different sensitivity to hypoxia between the DBA/2J and A/J strains. In the current study genetic elimination of BKα1 showed reduced CSN response to hypoxia at the initial phase. The data suggest that BK channels may play a role for initiating hypoxic response in the mouse CB. However, the fact that BKKO still have the hypoxic response indicates that BKα1 is not required to maintain the hypoxic neural response of the CB. The involvement of BKβ2 subunits, which was more expressed in the CB of DBA/2J mice than that of A/J mice (Balbir et al. 2007; Otsubo et al. 2011), cannot be assessed from this study.

Several types of oxygen-sensitive K channels in the CB have been identified in several species. These include BK channels (Peers 1990) and background TASK-like K channels in the rat (Williams and Buckler 2004), Kv4.1 and Kv4.3 in the rabbit (Sanchez et al. 2002), and Kv3 in the C57Bl/6J mouse (Pérez-García et al. 2004). In addition, AMP-activated protein kinase (AMPK) may link mitochondrial oxidative phosphorylation to K channel inhibition or calcium mediated signaling in the CB (Evans et al. 2005). Heme-oxygenase-2, with NADPH-cytochrome P450 reductase, functions to alter BK channel activity under different oxygen tensions (Williams et al. 2004). A component of NADPH oxidase, $p47^{phox}$, appears to be a part of chemosensory machinery (He et al. 2005). The contribution of the above

**Table 37.1** Frequency specific CSN activity in response to 10 % O2 in DBA/2J mice

| | Alpha | | Beta | | Gamma | | Delta | | Epsilon | | Zeta | | eta | |
|---|---|---|---|---|---|---|---|---|---|---|---|---|---|---|
| | Mean | SE | Mean | SE | Mean | SE | Mean | SE | Mean | SE | Mean | SE | mean | SE |
| Base | 0.0704 | 0.0026 | 0.0837 | 0.0029 | 0.0807 | 0.0027 | 0.0729 | 0.0032 | 0.0672 | 0.0034 | 0.0646 | 0.0033 | 0.0326 | 0.0017 |
| | # | | | | | | | | # | | # | | # | |
| 10% 30s | 0.0880 | 0.0037 | 0.1419 | 0.0087 | 0.1368 | 0.0044 | 0.1084 | 0.0052 | 0.0915 | 0.0050 | 0.0823 | 0.0038 | 0.0379 | 0.0018 |
| | # | | * | | * | | *,# | | *,# | | # | | # | |
| 10% 60s | 0.1069 | 0.0037 | 0.1905 | 0.0144 | 0.1798 | 0.0083 | 0.1372 | 0.0090 | 0.1133 | 0.0085 | 0.0997 | 0.0070 | 0.0435 | 0.0030 |
| | *,# | | * | | * | | *,# | | *,# | | *,# | | # | |
| 10% 90s | 0.1018 | 0.0037 | 0.1810 | 0.0157 | 0.1648 | 0.0090 | 0.1292 | 0.0089 | 0.1100 | 0.0098 | 0.0946 | 0.0083 | 0.0419 | 0.0039 |
| | *,# | | * | | * | | *,# | | *,# | | *,# | | # | |
| Post | 0.0715 | 0.0037 | 0.0922 | 0.0045 | 0.0891 | 0.0042 | 0.0746 | 0.0030 | 0.0686 | 0.0032 | 0.0655 | 0.0031 | 0.0328 | 0.0017 |
| | # | | | | | | # | | # | | # | | # | |

CSN activity was collected over 5 s at each time slot and expressed as % of total power (N = 11). For the sake of simplicity, selected statistical comparisons with ANOVA (between the base and other time points; between the beta and other frequency bands) are presented. *, significantly different from own base; # significantly different from beta band

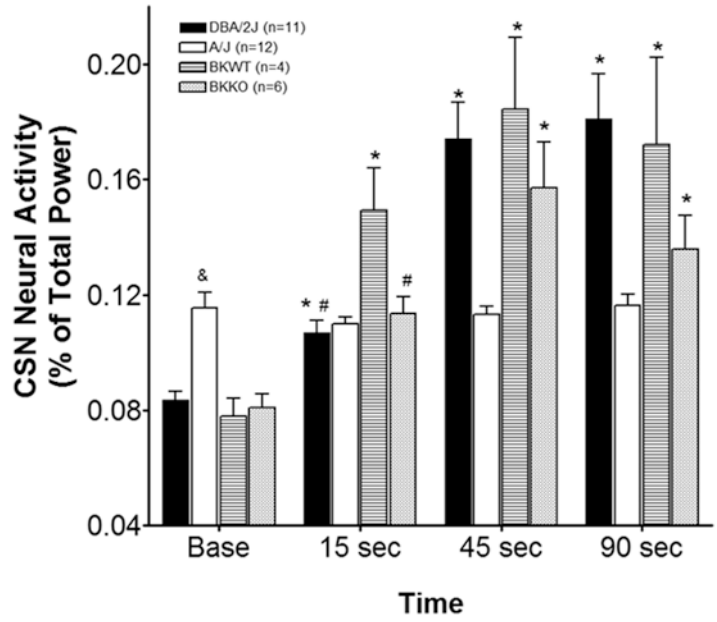


**Fig. 37.4** Summary statistics on strain-specific responses of CSN activity (beta frequency band) to 0.10 $F_IO_2$ compared to baseline. * significantly different from own baseline (one way ANOVA, repeated measures, $p<0.05$). # significantly different from BKWT at 15 s (one way ANOVA, $p<0.05$). &, significantly different from other strains at base (one way ANOVA, $p<0.05$)

mentioned components to the strain differences in the hypoxic response of the CSN activity was not examined in the current study. In our comparative gene expression study (Balbir et al. 2007), no significant transcriptional differences are seen in gene expression of these components between the A/J's CB and the DBA/2J's CB.

Traditionally, large mammals, such as cats, rabbits, dogs and goats, have been used to characterize the CB function *in vivo*. Rats and mice have been used mostly *in vitro* except for measuring the hypoxic ventilatory response. In the current study, we characterized the CB neural response to hypoxia in the *in vivo* anesthetized and ventilated mouse model. CSN response to hypoxia in *in vivo* mice resemble other large animals in the two responsive strains (DBA/2J and BKWT – i.e. FVB). In addition, spectral time-varying analysis revealed that hypoxia increased mouse CSN activity in a wide range of frequencies. However, CSN activity does not increase homogenously in different frequencies. Rather, it appears to show some synchronization towards approximately 600–800 Hz (β and γ frequency bands). A physiological importance of this synchronization is not apparent from this study. It has been shown that electrical coupling between GCs decreases during hypoxia (Eyzaguirre 2007). Eyzagurre proposed that this uncoupling enhances transmitter release from GCs. Also, electrical couplings between the GCs and the sensory nerve ending may be enhanced. The synchronization observed in this study might be downstream results from the phenomena observed in electrical coupling within the CB. In future studies, the preparation presented here can be a useful tool to understand unsolved physiological questions described above with the aid of pharmacological treatments and genetic modifications.

**Acknowledgements** This work was funded, in part, by HL081345 and F31HL096450.

## References


Balbir A, Lee H, Okumura M, Biswal S, Fitzgerald RS, Shirahata M (2007) A search for genes that may confer divergent morphology and function in the carotid body between two strains of mice. Am J Physiol Lung Cell Mol Physiol 292:L704–L715

Boudinot E, Tremblay P, Champagnat J, Foutz AS (2002) Respiratory function in mice lacking or overexpressing the prion protein. Neurosci Lett 323:89–92

Campen MJ, Tagaito Y, Li J, Balbir A, Tankersley CG, Smith P, Schwartz A, O'Donnell CP (2004) Phenotypic variation in cardiovascular responses to acute hypoxic and hypercapnic exposure in mice. Physiol Genomics 20:15–20

Evans AM, Mustard KJ, Wyatt CN, Peers C, Dipp M, Kumar P, Kinnear NP, Hardie DG (2005) Does AMP-activated protein kinase couple inhibition of mitochondrial oxidative phosphorylation by hypoxia to calcium signaling in O2-sensing cells? J Biol Chem 280:41504–41511

Eyzaguirre C (2007) Electric synapses in the carotid body-nerve complex. Respir Physiol Neurobiol 157:116–122

He L, Dinger B, Sanders K, Hoidal J, Obeso A, Stensaas L, Fidone S, Gonzalez C (2005) Effect of $p47^{phox}$ gene deletion on ROS production and oxygen sensing in mouse carotid body chemoreceptor cells. Am J Physiol 289:L916–L924

Otsubo T, Kostuk EW, Balbir A, Fujii K, Shirahata M (2011) Differential expression of large-conductance Ca-activated K channels in the carotid body between DBA/2 J and a/J strains of mice. Front Cell Neurosci 5:19

Peers C (1990) Hypoxic suppression of $K^+$ currents in type I carotid body cells: selective effect on the $Ca^{2+}$-activated $K^+$ current. Neurosci Lett 119:253–256

Pesaran B, Pezaris JS, Sahani M, Mitra PP, Anderson RA (2002) Temporal structure in neuronal activity during working memory in macaque parietal cortex. Nat Neurosci 5:805–811

Pérez-García MT, Colinas O, Miguel-Velado E, Moreno-Domínguez A, López-López JR (2004) Characterization of the Kv channels of mouse carotid body chemoreceptor cells and their role in oxygen sensing. J Physiol 557:457–471

Prabhakar NR, Peers C (2014) Gasotransmitter regulation of ion channels: a key step in O2 sensing by the carotid body. Physiology 29:49–55

Rubin AE, Polotsky VY, Balbir A, Krishnan JA, Schwartz AR, Smith PL, Fitzgerald RS, Tankersley CG, Shirahata M, O'Donnell CP (2003) Differences in sleep-induced hypoxia between A/J and DBA/2J mouse strains. Am J Respir Crit Care Med 168:1520–1527

Sanchez D, Lopez-Lopez JR, Perez-Garcia MT, Sanz-Alfayate G, Obeso A, Ganfornina MD, Gonzalez C (2002) Molecular identification of Kv subunits that contribute to the oxygen-sensitive K+ current of chemoreceptor cells of the rabbit carotid body. J Physiol 542:369–382

Shirahata M, Fitzgerald RS (1991) Dependency of hypoxic chemotransduction in cat carotid body on voltage-gated calcium channels. J Appl Physiol 71:1062–1069

Tankersley CG, Fitzgerald RS, Kleeberger SR (1994) Differential control of ventilation among inbred strains of mice. Am J Physiol 267:R1371–R1377

Van Vliet BN, Chafe LL, Montani JP (1999) Contribution of baroreceptors and chemoreceptors to ventricular hypertrophy produced by sino-aortic denervation in rats. J Physiol 516:885–895

Williams BA, Buckler KJ (2004) Biophysical properties and metabolic regulation of a TASK-like potassium channel in rat carotid body type 1 cells. Am J Physiol Lung Cell Mol Physiol 286:L221–L230

Wyatt CN, Peers C (1995) $Ca^{2+}$-activated $K^+$ channels in isolated type-I cells of the neonatal rat carotid-body. J Physiol 483:559–565

Williams SE, Wootton P, Mason HS, Bould J, Iles DE, Riccardi D, Peers C, Kemp PJ (2004) Hemoxygenase-2 is an oxygen sensor for a calcium-sensitive potassium channel. Science 306:2093–2097

# Chronic Intermittent Hypoxia Blunts the Expression of Ventilatory Long Term Facilitation in Sleeping Rats

38

Deirdre Edge and Ken D. O'Halloran

**Abstract**

We have previously reported that chronic intermittent hypoxia (CIH), a central feature of human sleep-disordered breathing, causes respiratory instability in sleeping rats (Edge D, Bradford A, O'halloran KD. Adv Exp Med Biol 758:359–363, 2012). Long term facilitation (LTF) of respiratory motor outputs following exposure to episodic, but not sustained, hypoxia has been described. We hypothesized that CIH would enhance ventilatory LTF during sleep. We examined the effects of 3 and 7 days of CIH exposure on the expression of ventilatory LTF in sleeping rats. Adult male Wistar rats were exposed to 20 cycles of normoxia and hypoxia (5 % $O_2$ at nadir; $SaO_2 \sim 80$ %) per hour, 8 h per day for 3 or 7 consecutive days (CIH, N = 7 per group). Corresponding sham groups (N = 7 per group) were subjected to alternating cycles of air under identical experimental conditions in parallel. Following gas exposures, breathing during sleep was assessed in unrestrained, unanaesthetized animals using the technique of whole-body plethysmography. Rats were exposed to room air (baseline) and then to an acute IH (AIH) protocol consisting of alternating periods of normoxia (7 min) and hypoxia ($FiO_2$ 0.1, 5 min) for 10 cycles. Breathing was monitored during the AIH exposure and for 1 h in normoxia following AIH exposure. Baseline ventilation was elevated after 3 but not 7 days of CIH exposure. The hypoxic ventilatory response was equivalent in sham and CIH animals after 3 days but ventilatory responses to repeated hypoxic challenges were significantly blunted following 7 days of CIH. Minute ventilation was significantly elevated following AIH exposure compared to baseline in sham but not in CIH exposed animals. LTF, determined as the % increase in minute ventilation from baseline following AIH exposure, was significantly blunted in CIH exposed rats. In summary, CIH leads to

D. Edge (✉) • K.D. O'Halloran
Department of Physiology, School of Medicine,
University College Cork, Cork, Ireland
e-mail: dedge@ucc.ie



C. Peers et al. (eds.), *Arterial Chemoreceptors in Physiology and Pathophysiology*,
Advances in Experimental Medicine and Biology 860, DOI 10.1007/978-3-319-18440-1_38

impaired ventilatory responsiveness to AIH. Moreover, CIH blunts ventilatory LTF. The physiological significance of ventilatory LTF is context-dependent but it is reasonable to consider that it can potentially destabilize respiratory control, in view of the potential for LTF to give rise to hypocapnia. CIH-induced blunting of LTF may represent a compensatory mechanism subserving respiratory homeostasis. Our results suggest that CIH-induced increase in apnoea index (Edge D, Bradford A, O'halloran KD. Adv Exp Med Biol 758:359–363, 2012) is not related to enhanced ventilatory LTF. We conclude that the mature adult respiratory system exhibits plasticity and metaplasticity with potential consequences for the control of respiratory homeostasis. Our results may have implications for human sleep apnoea.

**Keywords**
Long term facilitation • Chronic intermittent hypoxia • Ventilation • Obstructive sleep apnoea • Hypoxia

## 38.1 Introduction

Intermittent hypoxia (IH), the dominant feature of sleep-disordered breathing, has been shown to induce respiratory plasticity – namely long-lasting neural facilitation in the respiratory control system at multiple levels. Long-term facilitation (LTF) is characterised by a progressive increase in respiratory motor output during or following exposure to episodic, but not sustained, hypoxia (Mitchell et al. 2001; Mahamed and Mitchell 2007; Baker and Mitchell 2000). LTF has been described in multiple respiratory pathways, including carotid sinus nerve afferents (Millhorn et al. 1980; Peng et al. 2003; Iturriaga et al. 2006), phrenic (Fuller et al. 2000; Bach and Mitchell 1996), and hypoglossal motor efferents (Fuller et al. 2001a). There is growing interest in the effects of chronic intermittent hypoxia (CIH) on breathing due to its relevance to sleep-disordered breathing and other conditions characterised by intermittent hypoxia. Both ventilatory LTF as well as ventilatory adaptation to CIH have been observed in animal preparations (Cao et al. 1992; Olson et al. 2001; Turner and Mitchell 1997; McGuire et al. 2002; Reeves and Gozal 2006a, b; Skelly et al. 2012). Although animal models of IH have greatly enhanced our understanding of the mechanisms of respiratory plasticity (Baker et al. 2001; Baker and Mitchell 2000; Baker-Herman et al. 2004, 2010; Baker-Herman and Mitchell 2002, 2008; Dale-Nagle et al. 2010a, b; Fuller et al. 2000, 2001a, b, 2003, 2005; Golder et al. 2005, 2008; Hoffman et al. 2010; Hoffman and Mitchell 2011; Johnson and Mitchell 2002; Kinkead et al. 2001; Ling et al. 2001; Lovett-Barr et al. 2012; MacFarlane and Mitchell 2008; MacFarlane et al. 2008, 2009, 2011; Mahamed and Mitchell 2007, 2008a, b; McCrimmon et al. 2008; Mitchell et al. 2001; Mitchell and Johnson 2003; Vinit et al. 2009; Wilkerson et al. 2007; Wilkerson and Mitchell 2009), much of what we have learnt about IH and breathing has come from reduced preparations where animals are anaesthetized, vagotomized, and paralyzed (Mateika and Sandhu 2011) (Matiela and Sandhu 2011), making the physiological significance less clear. Recently, ventilatory LTF in sleeping rats has been demonstrated (Nakamura et al. 2010). LTF is reported to be more robust during sleep in rats, whereas LTF is most often observed in wakefulness in humans (Harris et al. 2006). LTF is most often observed in settings of manipulated and controlled $CO_2$ levels (Mateika and Narwani 2009). From these studies and the level of disparate results (Mateika and Sandhu 2011), it is somewhat difficult to ascertain how IH may affect the respiratory con-

trol system in unanaesthetized mammals, including humans under poikilocapnic conditions. The duration of the hypoxic stimulus can be a key determinant of the evoked motor response (Mitchell et al. 2001). Accordingly, we wished to test the effects of both short (3 days) and long (7 days) durations of CIH on respiratory control in sleeping rats. Specifically, we wished to determine the effects of CIH exposure on basal ventilation. We also sought to examine the effects of CIH exposure on the ventilatory response to acute intermittent hypoxia (AIH), to test the hypothesis that CIH alters the capacity for LTF expression in sleeping rats.

## 38.2 Methods

### 38.2.1 Animal Model of Chronic Intermittent Hypoxia

Adult male Wistar rats (311 ± 10 g (3 day) and 288 ± 6 g (7 day); mean ± SEM) were exposed to sham or CIH gas exposures. The gas supply to half of the environmental chambers alternated between air and nitrogen every 90s, reducing the ambient oxygen concentration to 5 % at the nadir, resulting in arterial $O_2$ saturation values of ~80 % at the nadir (CIH for either 3 or 7 days; N = 7 per group). The corresponding sham groups (N = 7 per group) were subjected to alternating cycles of normoxia under identical experimental conditions in parallel. Gas treatments were carried out for 20 cycles per hour, 8 h per day for 3 or 7 consecutive days. Rats had free access to food and water throughout the exposures. All procedures were performed under licence from the Irish Government Department of Health and Children in accordance with National and European guidelines following ethics committee approval.

### 38.2.2 Whole-Body Plethysmography

Following the chronic gas treatments, respiratory recordings were performed in unrestrained, unanaesthetized, sleeping rats using the technique of whole-body plethysmography. Rats were exposed to room air (baseline) and then to an acute IH (AIH) protocol consisting of alternating periods of normoxia (7 min) and hypoxia ($FiO_2$ 0.1, 5 min) for 10 cycles. Breathing was monitored during AIH exposure and for 1 h in normoxia following AIH exposure.

### 38.2.3 Data Analysis

#### 38.2.3.1 Normoxic and hypoxic ventilatory responses

Normoxic breathing before AIH exposure was compared between groups for each time point using Student un-paired *t* tests (baseline). During analysis of breathing during AIH exposure, the first 2 min of each normoxic and hypoxic bout were discarded to allow for circulation and mixing within the chambers of the corresponding gases. Minute ventilation ($V_E$: ml/min/100 g body weight) during 5 min of each normoxic episode, and 3 min of each hypoxic episode were averaged per bout per animal. The hypoxic ventilatory response (HVR) was also assessed during the AIH protocol. Each of the 10 hypoxic episodes was expressed as a % change from the preceding normoxic period in sham and CIH exposed rats. Values obtained were compared between sham and CIH exposed rats using Student un-paired *t* tests.

#### 38.2.3.2 Ventilation following AIH

The normoxic hour post AIH was divided into 5 min intervals and average values were obtained for each bout. Respiratory variables within the last 5 min interval of the hour post AIH period (i.e. at time 60, 1 h following the AIH protocol) were compared to the 1st normoxic bout (baseline) of AIH for sham and CIH exposed animals. Values were compared within each trial with a Student paired one-tailed *t* test, or Wilcoxin signed-rank test where appropriate, for both groups (sham and CIH) for both 3 and 7 day studies. Additionally, the last 5 min epoch of normoxic breathing during the hour post AIH was also expressed as a % of baseline values. Values were compared with a two-way ANOVA; (time × CIH) for 3 and 7 days of sham and CIH exposure with Bonferroni post-hoc tests; $p < 0.05$ was deemed significant in all cases.

## 38.3 Results

Baseline ventilation was elevated after 3 but not 7 days of CIH exposure (57 ± 4 vs. 72 ± 3 $V_E$ ml/min/100 g body weight; sham vs. 3 day CIH-exposure; Student un-paired *t* test; p = 0.0130). The hypoxic ventilatory response, expressed as a % change from the preceding normoxic episode was equivalent in sham and CIH exposed animals after 3 days (+52 ± 2 vs. +45 ± 4 %), but ventilatory responses to repeated hypoxic challenges were significantly blunted following 7 days of CIH (+63 ± 4 vs. + 50 ± 3 %, p = 0.0292, Student un-paired *t* test). Minute ventilation was significantly elevated following AIH exposure compared to baseline in sham groups (p = 0.0391, 3 day study and p = 0.0053, 7 day study; Student paired one tailed *t* test) but not in 3 or 7 day CIH exposed animals (Fig. 38.1). LTF, defined as the % increase in minute ventilation from baseline following AIH exposure, was significantly blunted in CIH exposed rats (p = 0.0238; two-way ANOVA: gas treatment, Fig. 38.2).

## 38.4 Discussion

There is growing interest in the effects of CIH on breathing due to its relevance to sleep-disordered breathing and other conditions characterised by intermittent hypoxia. Intermittent hypoxia, a key feature of sleep disordered-breathing due to recurrent apnoea, has been shown to have myriad effects on the respiratory control system – with potentially 'adaptive' and 'maladaptive' consequences for respiratory homeostasis. The main finding of this study is that enhanced normoxic breathing following AIH (i.e. LTF) was expressed in sham but not CIH exposed animals (both 3 and 7 days); indeed, contrary to expectation, CIH exposure blunted the expression of ventilatory LTF.

LTF of respiratory motor output during and following exposure to episodic (Mitchell et al. 2001), but not sustained (Baker and Mitchell 2000), hypoxia has been well described in multiple respiratory motor pathways, including phrenic (Bach and Mitchell 1996; Fuller et al. 2000), hypoglossal (Bach and Mitchell 1996), glossopharyngeal (Cao et al. 2010), and intercostal (Fregosi and Mitchell 1994) motor nerves. Sensory LTF has also been described in the carotid body chemoafferent pathway (Peng et al. 2003). In the present study, sham animals displayed a modest enhancement of breathing following AIH (LTF ~ +18 % increase in $V_E$). However in comparison, LTF was absent in CIH exposed animals. This is consistent with the notion of 'metaplasticity' (Abraham and Bear 1996), whereby pre-conditioning alters the

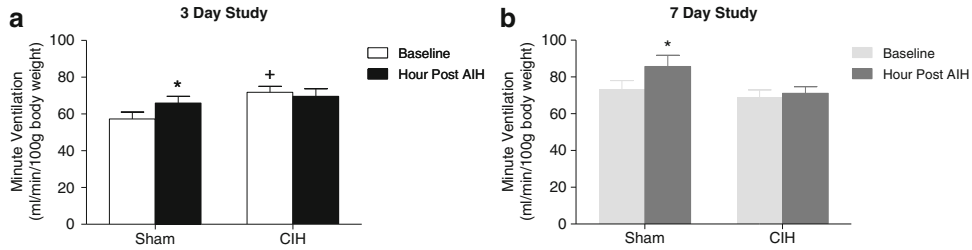


**Fig. 38.1** Values (mean ± SEM) for minute ventilation in normoxia during baseline and one hour post AIH for 3 day sham and CIH exposed rats (**a**) and 7 day sham and CIH exposed rats (**b**). * denotes significant difference from corresponding baseline; + denotes significant difference from sham baseline

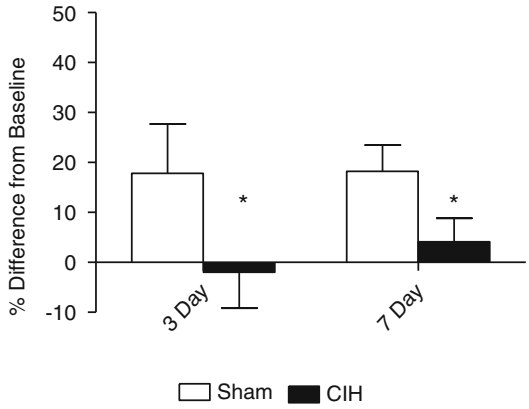


**Fig. 38.2** Values (mean ± SEM) for ventilation in normoxia one hour post AIH exposure (within the last 5 min epoch, at time 60) expressed as a % change from corresponding baseline (pre-AIH) values in 3 and 7 day sham and CIH exposed rats. *denotes significant difference from corresponding sham values; two-way analysis of variance with Bonferroni post-hoc test, $p < 0.05$

subsequent response to a 'plastic' stimulus. It has previously been reported that CIH preconditioning enhances the subsequent response to episodic hypoxia (McGuire et al. 2003). The difference observed in the effects of preconditioning with CIH between the latter study and ours most likely relates to the different stimulus paradigms employed in the two protocols. Our study utilised a CIH paradigm that more closely reflects the hypoxia-reoxygenation profile of sleep-disordered breathing. Of note, in the 3 day CIH exposed animals, normoxic ventilation (just before commencement of the AIH protocol) was significantly enhanced compared to sham controls, which may have contributed to the lack of a facilitatory effect of AIH (i.e. some form of LTF may already have been expressed). Ventilatory adaptation to CIH, however, was not evident in the 7 day CIH study (baseline ventilation was equivalent in sham and CIH exposed groups) and there was a clear blunting of the ventilatory response to hypoxia during the AIH protocol, and blunting of ventilatory LTF following AIH.

LTF has been shown to be state-dependent (Nakamura et al. 2010). A key question we wished to address was whether CIH affects ventilatory control in sleeping animals? There are disparate findings between animal and human studies on the effects of sleep state on respiratory plasticity (Mateika and Sandhu 2011). We posit that exploring ventilatory plasticity in sleep has greater relevance to sleep-disordered breathing than other experimental models, especially in light of the profound effects of sleep on the control of breathing (Douglas et al. 1982a, b, c). Our plethysmography-based study was conducted during light hours i.e. during the rats' normal sleep period. Rats were curled and asleep, albeit behaviourally-defined, throughout the study. It has been shown that in rats, unlike humans, LTF is more pronounced in sleep (Nakamura et al. 2010; Gerst et al. 2011). Here we report relatively modest effects of AIH on the expression of LTF in male Wistar rats. We did not examine the effects of AIH (or CIH) on breathing during wakefulness, therefore it is unclear the extent to which sleep state affected LTF (if at all) in our animals.

Sham rats in this study that were exposed to 10 bouts of IH displayed evidence of facilitated breathing (one hour following AIH exposure) in comparison to rats pre-treated with either 3 or 7 days of CIH. In another study, LTF of breathing during sleep was elicited in rats following an AIH protocol consisting of 5 episodes of 5 min bouts of 10.5 % $O_2$ interspersed with 5 min of normoxia (Nakamura et al. 2010). Also, in a more recent study, LTF of diaphragmatic EMG was expressed following AIH (Terada and Mitchell 2011), but this unexpectedly was not further enhanced by repeated daily exposure to IH. Similarly, in our study, CIH exposure did not enhance the expression of ventilatory LTF during sleep. In fact, contrary to expectation, LTF was blunted in CIH exposed animals suggesting habituation to IH or the emergence of a compensatory mechanism limiting the expression of LTF in response to AIH exposure.

Others have clearly demonstrated that short bouts of IH may be beneficial in treating respiratory motor impairment following spinal injury (Dale-Nagle et al. 2010b; Vinit et al. 2009). A picture is emerging that short bouts of IH can be beneficial for aspects of respiratory control (Terada and Mitchell 2011). However in cases characterised

by longer durations of IH, maladaptive phenotypes often prevail. If one considers LTF of breathing as a beneficial response, the lack of manifestation of LTF in CIH can be viewed as maladaptive. In the context of sleep-disordered breathing however, ventilatory LTF might serve to destabilize breathing and as such CIH-induced blunting of responses to AIH could be considered an adaptive or compensatory response in terms of respiratory control. Whatever the physiological significance, it is clear that the mature respiratory system exhibits hypoxic-dependent plasticity and metaplasticity, but we conclude that CIH-induced increase in apnoea index (Edge et al. 2012) is not related to enhanced ventialtory LTF.

In summary, we report that CIH alters the respiratory control system with potential consequences for respiratory homeostasis. CIH exposure blunted the response to hypoxia during AIH exposure in sleeping rats hampering the expression of AIH-induced facilitated breathing. Our findings highlight that CIH affects the neural control of breathing, with potential implications for respiratory disorders characterised by CIH such as sleep apnoea.

**Acknowledgements** Supported by the Health Research Board, Ireland (RP/2007/29).

## References

Abraham WC, Bear MF (1996) Metaplasticity: the plasticity of synaptic plasticity. Trends Neurosci 19:126–130

Bach KB, Mitchell GS (1996) Hypoxia-induced long-term facilitation of respiratory activity is serotonin dependent. Respir Physiol 104:251–260

Baker TL, Mitchell GS (2000) Episodic but not continuous hypoxia elicits long-term facilitation of phrenic motor output in rats. J Physiol 529(Pt 1):215–219

Baker TL, Fuller DD, Zabka AG, Mitchell GS (2001) Respiratory plasticity: differential actions of continuous and episodic hypoxia and hypercapnia. Respir Physiol 129:25–35

Baker-Herman TL, Mitchell GS (2002) Phrenic long-term facilitation requires spinal serotonin receptor activation and protein synthesis. J Neurosci 22:6239–6246

Baker-Herman TL, Mitchell GS (2008) Determinants of frequency long-term facilitation following acute intermittent hypoxia in vagotomized rats. Respir Physiol Neurobiol 162:8–17

Baker-Herman TL, Fuller DD, Bavis RW, Zabka AG, Golder FJ, Doperalski NJ, Johnson RA, Watters JJ, Mitchell GS (2004) BDNF is necessary and sufficient for spinal respiratory plasticity following intermittent hypoxia. Nat Neurosci 7:48–55

Baker-Herman TL, Bavis RW, Dahlberg JM, Mitchell AZ, Wilkerson JE, Golder FJ, Macfarlane PM, Watters JJ, Behan M, Mitchell GS (2010) Differential expression of respiratory long-term facilitation among inbred rat strains. Respir Physiol Neurobiol 170:260–267

Cao KY, Zwillich CW, Berthon-Jones M, Sullivan CE (1992) Increased normoxic ventilation induced by repetitive hypoxia in conscious dogs. J Appl Physiol 73:2083–2088

Cao Y, Liu C, Ling L (2010) Glossopharyngeal long-term facilitation requires serotonin 5-HT2 and NMDA receptors in rats. Respir Physiol Neurobiol 170:164–172

Dale-Nagle EA, Hoffman MS, Macfarlane PM, Mitchell GS (2010a) Multiple pathways to long-lasting phrenic motor facilitation. Adv Exp Med Biol 669:225–230

Dale-Nagle EA, Hoffman MS, Macfarlane PM, Satriotomo I, Lovett-Barr MR, Vinit S, Mitchell GS (2010b) Spinal plasticity following intermittent hypoxia: implications for spinal injury. Ann N Y Acad Sci 1198:252–259

Douglas NJ, White DP, Pickett CK, Weil JV, Zwillich CW (1982a) Respiration during sleep in normal man. Thorax 37:840–844

Douglas NJ, White DP, Weil JV, Pickett CK, Martin RJ, Hudgel DW, Zwillich CW (1982b) Hypoxic ventilatory response decreases during sleep in normal men. Am Rev Respir Dis 125:286–289

Douglas NJ, White DP, Weil JV, Pickett CK, Zwillich CW (1982c) Hypercapnic ventilatory response in sleeping adults. Am Rev Respir Dis 126:758–762

Edge D, Bradford A, O'Halloran KD (2012) Chronic intermittent hypoxia increases apnoea index in sleeping rats. Adv Exp Med Biol 758:359–363

Fregosi RF, Mitchell GS (1994) Long-term facilitation of inspiratory intercostal nerve activity following carotid sinus nerve stimulation in cats. J Physiol 477(Pt 3):469–479

Fuller DD, Bach KB, Baker TL, Kinkead R, Mitchell GS (2000) Long term facilitation of phrenic motor output. Respir Physiol 121:135–146

Fuller DD, Baker TL, Behan M, Mitchell GS (2001a) Expression of hypoglossal long-term facilitation differs between substrains of Sprague-Dawley rat. Physiol Genomics 4:175–181

Fuller DD, Zabka AG, Baker TL, Mitchell GS (2001b) Phrenic long-term facilitation requires 5-HT receptor activation during but not following episodic hypoxia. J Appl Physiol 90:2001–2006; Discussion 2000

Fuller DD, Johnson SM, Olson EB Jr, Mitchell GS (2003) Synaptic pathways to phrenic motoneurons are enhanced by chronic intermittent hypoxia after cervical spinal cord injury. J Neurosci 23:2993–3000

Fuller DD, Baker-Herman TL, Golder FJ, Doperalski NJ, Watters JJ, Mitchell GS (2005) Cervical spinal cord

injury upregulates ventral spinal 5-HT2A receptors. J Neurotrauma 22:203–213
Gerst DG 3rd, Yokhana SS, Carney LM, Lee DS, Badr MS, Qureshi T, Anthouard MN, Mateika JH (2011) The hypoxic ventilatory response and ventilatory long-term facilitation are altered by time of day and repeated daily exposure to intermittent hypoxia. J Appl Physiol 110:15–28
Golder FJ, Zabka AG, Bavis RW, Baker-Herman T, Fuller DD, Mitchell GS (2005) Differences in time-dependent hypoxic phrenic responses among inbred rat strains. J Appl Physiol 98:838–844
Golder FJ, Ranganathan L, Satriotomo I, Hoffman M, Lovett-Barr MR, Watters JJ, Baker-Herman TL, Mitchell GS (2008) Spinal adenosine A2a receptor activation elicits long-lasting phrenic motor facilitation. J Neurosci 28:2033–2042
Harris DP, Balasubramaniam A, Badr MS, Mateika JH (2006) Long-term facilitation of ventilation and genioglossus muscle activity is evident in the presence of elevated levels of carbon dioxide in awake humans. Am J Physiol Regul Integr Comp Physiol 291:R1111–R1119
Hoffman MS, Mitchell GS (2011) Spinal 5-HT7 receptor activation induces long-lasting phrenic motor facilitation. J Physiol 589:1397–1407
Hoffman MS, Golder FJ, Mahamed S, Mitchell GS (2010) Spinal adenosine A2(A) receptor inhibition enhances phrenic long term facilitation following acute intermittent hypoxia. J Physiol 588:255–266
Iturriaga R, Rey S, Alcayaga J, Del Rio R (2006) Chronic intermittent hypoxia enhances carotid body chemosensory responses to acute hypoxia. Adv Exp Med Biol 580:227–232; Discussion 351–9
Johnson SM, Mitchell GS (2002) Activity-dependent plasticity in descending synaptic inputs to respiratory spinal motoneurons. Respir Physiol Neurobiol 131:79–90
Kinkead R, Bach KB, Johnson SM, Hodgeman BA, Mitchell GS (2001) Plasticity in respiratory motor control: intermittent hypoxia and hypercapnia activate opposing serotonergic and noradrenergic modulatory systems. Comp Biochem Physiol A Mol Integr Physiol 130:207–218
Ling L, Fuller DD, Bach KB, Kinkead R, Olson EB Jr, Mitchell GS (2001) Chronic intermittent hypoxia elicits serotonin-dependent plasticity in the central neural control of breathing. J Neurosci 21:5381–5388
Lovett-Barr MR, Satriotomo I, Muir GD, Wilkerson JE, Hoffman MS, Vinit S, Mitchell GS (2012) Repetitive intermittent hypoxia induces respiratory and somatic motor recovery after chronic cervical spinal injury. J Neurosci 32:3591–3600
Macfarlane PM, Mitchell GS (2008) Respiratory long-term facilitation following intermittent hypoxia requires reactive oxygen species formation. Neuroscience 152:189–197
Macfarlane PM, Wilkerson JE, Lovett-Barr MR, Mitchell GS (2008) Reactive oxygen species and respiratory plasticity following intermittent hypoxia. Respir Physiol Neurobiol 164:263–271
Macfarlane PM, Satriotomo I, Windelborn JA, Mitchell GS (2009) NADPH oxidase activity is necessary for acute intermittent hypoxia-induced phrenic long-term facilitation. J Physiol 587:1931–1942
Macfarlane PM, Vinit S, Mitchell GS (2011) Serotonin 2A and 2B receptor-induced phrenic motor facilitation: differential requirement for spinal NADPH oxidase activity. Neuroscience 178:45–55
Mahamed S, Mitchell GS (2007) Is there a link between intermittent hypoxia-induced respiratory plasticity and obstructive sleep apnoea? Exp Physiol 92:27–37
Mahamed S, Mitchell GS (2008a) Respiratory long-term facilitation: too much or too little of a good thing? Adv Exp Med Biol 605:224–227
Mahamed S, Mitchell GS (2008b) Simulated apnoeas induce serotonin-dependent respiratory long-term facilitation in rats. J Physiol 586:2171–2181
Mateika JH, Narwani G (2009) Intermittent hypoxia and respiratory plasticity in humans and other animals: does exposure to intermittent hypoxia promote or mitigate sleep apnoea? Exp Physiol 94:279–296
Mateika JH, Sandhu KS (2011) Experimental protocols and preparations to study respiratory long term facilitation. Respir Physiol Neurobiol 176:1–11
Mccrimmon DR, Mitchell GS, Alheid GF (2008) Overview: the neurochemistry of respiratory control. Respir Physiol Neurobiol 164:1–2
Mcguire M, Zhang Y, White DP, Ling L (2002) Effect of hypoxic episode number and severity on ventilatory long-term facilitation in awake rats. J Appl Physiol 93:2155–2161
Mcguire M, Zhang Y, White DP, Ling L (2003) Chronic intermittent hypoxia enhances ventilatory long-term facilitation in awake rats. J Appl Physiol 95:1499–1508
Millhorn DE, Eldridge FL, Waldrop TG (1980) Prolonged stimulation of respiration by a new central neural mechanism. Respir Physiol 41:87–103
Mitchell GS, Johnson SM (2003) Neuroplasticity in respiratory motor control. J Appl Physiol 94:358–374
Mitchell GS, Baker TL, Nanda SA, Fuller DD, Zabka AG, Hodgeman BA, Bavis RW, Mack KJ, Olson EB Jr (2001) Invited review: intermittent hypoxia and respiratory plasticity. J Appl Physiol 90:2466–2475
Nakamura A, Olson EB Jr, Terada J, Wenninger JM, Bisgard GE, Mitchell GS (2010) Sleep state dependence of ventilatory long-term facilitation following acute intermittent hypoxia in Lewis rats. J Appl Physiol 109:323–331
Olson EB Jr, Bohne CJ, Dwinell MR, Podolsky A, Vidruk EH, Fuller DD, Powell FL, Mitchel GS (2001) Ventilatory long-term facilitation in unanesthetized rats. J Appl Physiol 91:709–716
Peng YJ, Overholt JL, Kline D, Kumar GK, Prabhakar NR (2003) Induction of sensory long-term facilitation in the carotid body by intermittent hypoxia: implications for recurrent apneas. Proc Natl Acad Sci U S A 100:10073–10078

Reeves SR, Gozal D (2006a) Changes in ventilatory adaptations associated with long-term intermittent hypoxia across the Age spectrum in the rat. Respir Physiol Neurobiol 150:135–143

Reeves SR, Gozal D (2006b) Respiratory and metabolic responses to early postnatal chronic intermittent hypoxia and sustained hypoxia in the developing rat. Pediatr Res 60:680–686

Skelly JR, Edge D, Shortt CM, Jones JF, Bradford A, O'halloran KD (2012) Tempol ameliorates pharyngeal dilator muscle dysfunction in a rodent model of chronic intermittent hypoxia. Am J Respir Cell Mol Biol 46:139–148

Terada J, Mitchell GS (2011) Diaphragm long-term facilitation following acute intermittent hypoxia during wakefulness and sleep. J Appl Physiol 110:1299–1310

Turner DL, Mitchell GS (1997) Long-term facilitation of ventilation following repeated hypoxic episodes in awake goats. J Physiol 499(Pt 2):543–550

Vinit S, Lovett-Barr MR, Mitchell GS (2009) Intermittent hypoxia induces functional recovery following cervical spinal injury. Respir Physiol Neurobiol 169:210–217

Wilkerson JE, Mitchell GS (2009) Daily intermittent hypoxia augments spinal BDNF levels, ERK phosphorylation and respiratory long-term facilitation. Exp Neurol 217:116–123

Wilkerson JE, Macfarlane PM, Hoffman MS, Mitchell GS (2007) Respiratory plasticity following intermittent hypoxia: roles of protein phosphatases and reactive oxygen species. Biochem Soc Trans 35:1269–1272

# Heme Oxygenase-1 Influences Apoptosis via CO-mediated Inhibition of $K^+$ Channels

39

Moza M. Al-Owais, Mark L. Dallas, John P. Boyle, Jason L. Scragg, and Chris Peers

**Abstract**

Hypoxic/ischemic episodes can trigger oxidative stress-mediated loss of central neurons via apoptosis, and low $pO_2$ is also a feature of the tumor microenvironment, where cancer cells are particularly resistant to apoptosis. In the CNS, ischemic insult increases expression of the CO-generating enzyme heme oxygenase-1 (HO-1), which is commonly constitutively active in cancer cells. It has been proposed that apoptosis can be regulated by the trafficking and activity of $K^+$ channels, particularly Kv2.1. We have explored the idea that HO-1 may influence apoptosis via regulation of Kv2.1. Overexpression of Kv2.1 in HEK293 cells increased their vulnerability to oxidant-induced apoptosis. CO (applied as the donor CORM-2) protected cells against apoptosis and inhibited Kv2.1 channels. Similarly in hippocampal neurones, CO selectively inhibited Kv2.1 and protected neurones against oxidant-induced apoptosis. In medulloblastoma sections we identified constitutive expression of HO-1 and Kv2.1, and in the medulloblastoma-derived cell line DAOY, hypoxic HO-1 induction or exposure to CO protected cells against apoptosis, and also selectively inhibited Kv2.1 channels expressed in these cells. These studies are consistent with a central role for Kv2.1 in apoptosis in both central neurones and cancer cells. They also suggest that HO-1 expression can strongly influence apoptosis via CO-mediated regulation of Kv2.1 activity.

**Keywords**

Heme oxygenase • Carbon monoxide • Kv2.1 $K^+$ channel • Neurone • Medulloblastoma • Apoptosis

M.M. Al-Owais • J.P. Boyle • J.L. Scragg
C. Peers (✉)
Leeds Institute of Cardiovascular and Metabolic Medicine, Faculty of Medicine and Health, University of Leeds, Leeds LS2 9JT, UK
e-mail: c.s.peers@leeds.ac.uk

M.L. Dallas
School of Pharmacy, University of Reading, Reading RG6 6UB, UK



C. Peers et al. (eds.), *Arterial Chemoreceptors in Physiology and Pathophysiology*, Advances in Experimental Medicine and Biology 860, DOI 10.1007/978-3-319-18440-1_39

## 39.1 Introduction

Central neuronal death arising from conditions such as stroke, cerebral ischemia, neurodegenerative diseases or aging (Droge and Schipper 2007; Reynolds et al. 2007; Niizuma et al. 2009; Robertson et al. 2009) commonly involves apoptosis (Hou and MacManus 2002; Okouchi et al. 2007). Also associated with many of these conditions is the increased expression of heme oxygenase-1 (HO-1) in both central neurones and astrocytes (Pappolla et al. 1998; Dennery 2000; Schipper et al. 2009).

Like the constitutively expressed HO-2, HO-1 degrades heme, liberating biliverdin, ferrous iron ($Fe^{2+}$) and carbon monoxide (CO). This reaction breaks down the pro-oxidant heme and generates the antioxidant bilirubin (produced from biliverdin via bilirubin reductase). Furthermore, CO is now widely recognized as an additional important signalling molecule, interacting with various intracellular signalling pathways (Wu and Wang 2005; Kim et al. 2006). Heme oxygenases protect the brain against acute glutamate excitotoxicity (Ahmad et al. 2006) and in various *in vitro* and *in vivo* models of stroke (Ferris et al. 1999). Whilst it is not yet established how such protection arises, it is noteworthy that CO inhalation is neuroprotective against experimental stroke (Zeynalov and Dore 2009), and that astrocyte-derived CO protects neighbouring neurones from hypoxic/ischemic-induced apoptosis (Imuta et al. 2007).

Intracellular $K^+$ regulates caspase activation, mitochondrial membrane potential and volume and cell volume (Yu et al. 1997; 2001), and its loss from the cytosol can initiate the apoptotic cascade including cell shrinkage, mitochondrial cytochrome c release and caspase activation (Hughes Jr. et al. 1997; Bortner and Cidlowski 2002; Yu 2003; Yu et al. 1997), the latter via relieving inhibition of key components of the apoptotic cascade, including pro-caspase 3 (Yu 2003; Yu et al. 2001; Prevarskaya et al. 2010). In addition, $K^+$ channels are fundamental to the regulation of membrane potential, their activity also regulates $Ca^{2+}$ influx and excessive intracellular $Ca^{2+}$ levels can also trigger apoptosis (Prevarskaya et al. 2010). $K^+$ loss occurs via $K^+$ channels, and $K^+$ channel inhibitors can protect against apoptosis triggered by many insults, including oxidative stress (Pal et al. 2006). In neurones, the voltage-gated channel Kv2.1 has been proposed to play a prominent in this regard: cortical neurones experimentally lacking functional Kv2.1 channels are protected against apoptosis, and expression of Kv2.1 in CHO cells increases their vulnerability to apoptosis, via a process involving a rapid increase in the surface expression of Kv2.1 channels (Pal et al. 2006).

In contrast to non-cancerous tissues, HO-1 is constitutively active in many cancers (Jozkowicz et al. 2007) and tumor growth often requires HO-1 (Fang et al. 2004; Jozkowicz et al. 2007). Down-regulation of HO-1 inhibits tumor growth and increases sensitivity to radiotherapy and chemotherapy (Kinobe et al. 2008). Whilst there is undoubtedly a role for biliverdin in this regard, increasing attention has been given to CO as a signalling molecule in cancer progression since it can strongly influence proliferation and apoptosis (Wu and Wang 2005; Kim et al. 2006). However, the mechanisms underlying the role of CO in these processes remain to be determined. In the present study, we have explored the possibility that CO can provide protection for central neurones in the face of oxidative stress by inhibiting Kv2.1, and have also investigated whether such a mechanistic pathway exists in tumor cells, focusing on the central nervous system medulloblastoma tumor commonly occurring in young patients. Such tumors have produced the experimentally amenable DAOY cell line (Taillandier et al. 2011).

## 39.2 Methods

### 39.2.1 Cell Culture

Wild type (WT) and Kv2.1 (rat; *KCNB1*)-transfected HEK293 cells were maintained at 37 °C (5 % $CO_2$) in Dulbecco's Modified Eagle's Medium (DMEM) containing 2 mM glutamine,

10 % fetal bovine serum, 1 % Glutamax and 1 % penicillin/streptomycin. Cells were plated either onto coverslips for electrophysiology or polylysine-coated 96 well plates for MTT and caspase activity assays, as required. Primary cultures of hippocampal neurones were prepared from hippocampi of 6–8 day old Wistar rats by mechanical and enzymatic dissociation as described previously (Dallas et al. 2011). Cells were maintained in a humidified incubator at 37 °C, 95 % air: 5 % $CO_2$ for 14 days, replacing medium every 5–7 days. All experiments were performed with cells cultured for between 5 and 14 days. The DAOY human medulloblastoma cell line was maintained in DMEM supplemented with 10 % (v/v) fetal calf serum, 1 % penicillin-streptomycin and 1 mM glutamine. Cells were cultured at 37 °C in a humidified atmosphere containing 95 % air and 5 % $CO_2$, and passaged when 80–90 % confluent.

### 39.2.2 Cell Death Assays

Cells grown in 96-well plates were exposed to varying concentrations of the oxidant dithiodipyridine (DTDP) or diamide for 10 min (37 °C, 95 % air: 5 % $CO_2$), after which the media was replaced with 110 µl medium containing 5 mg/ml thiazolyl blue tetrazolium bromide (MTT) with or without additional drugs and left for 3 h in culture at 37 °C. After this incubation period 111 µl of acidic isopropanol solution was added to each well to dissolve the formazan crystals. The plate was then scanned using a spectrophotometer (570 nm). Statistical significance was determined using one way ANOVA with Bonferroni multiple comparison test. Caspase 3/7 activity was measured using the fluorimetric Apo-ONE homogeneous caspase 3/7 assay kit (Promega UK), according to manufacturer's instructions.

### 39.2.3 Electrophysiology

Coverslip fragments with attached cells were transferred to a perfused (3–5 ml/min) recording chamber mounted on the stage of a Nikon T1-SM inverted microscope (Nikon, Tokyo, Japan). $K^+$ currents were monitored by whole-cell voltage-clamp recordings, using pipette and perfusate solutions as previously described (Dallas et al. 2011; Al-Owais et al. 2012). Patch pipette resistance was 4–6 MΩ and series resistance was compensated (60–80 %) after breaking into the whole-cell configuration. Signals were sampled at 10 kHz and low-pass filtered at 2 kHz. Voltage-clamp and analysis protocols were performed using an Axopatch 200A amplifier/Digidata 1200 interface controlled by Clampex 9.0 software (Molecular Devices, Foster City, CA, USA). Offline analysis was performed using Clampfit 9.0 (Molecular Devices). In some studies, an anti-Kv2.1 antibody was added to the pipette solution (0.5 µg/ml; Neuromab, Davis, CA, USA).

### 39.2.4 Western Blotting

Protein concentrations in cleared cell lysates (200 µl) were determined using a BCA assay kit according to manufacturers' instructions (Pierce, IL). Four volumes of cell lysate sample were added to one volume of 5× sample buffer (60 mM Tris-Cl pH 6.8, 2 % SDS, 10 % glycerol, 5 % 2-mercaptoethanol, 0.01 % bromophenol blue). Samples (20–30 µg protein) were loaded on to polyacrylamide-SDS gels (0.75-mm thick, 7 % for high MW proteins or 12.5 % for mid-range MW proteins) and separated at 200 V (45 min) before being transferred on to PVDF membranes (30 V, overnight). Membranes were blocked with 5 % non-fat milk protein in TBS-Tween (TBST, 0.05 %) for 1 h and immunostained with anti-HO-1 antibodies (1:500 dilution, Santa Cruz Biotechnology, UK) in 1 % non-fat milk protein in TBST (3 h at 21–24 °C). Membranes were then washed (6×5 min in TBST) and incubated (1 h) with secondary antibody conjugated to horseradish peroxidase (1:2,000 dilution; Amersham Pharmacia Biotech UK). Finally, membranes were again washed in TBST and bands visualized using the enhanced chemiluminescence (ECL) detection system and hyperfilm

ECL (GE Healthcare, UK). Band intensities were measured using Scion Image analysis software.

Data are presented as mean ± s.e.m.. Statistical comparisons were made using paired Student's *t*-tests or one-way ANOVA with Bonferroni's multiple-comparison test, as appropriate, with $P < 0.05$ taken as statistically significant in each case (Graphpad Prism).

## 39.3 Results

Over-expression of Kv2.1 in HEK293 cells increased their vulnerability to oxidant (DTDP)-induced cell death, as determined by MTT assays (Fig. 39.1a). Interestingly, this increased sensitivity was at least partially reversed in the presence of the CO donor molecule, CORM-2 (100 μM;

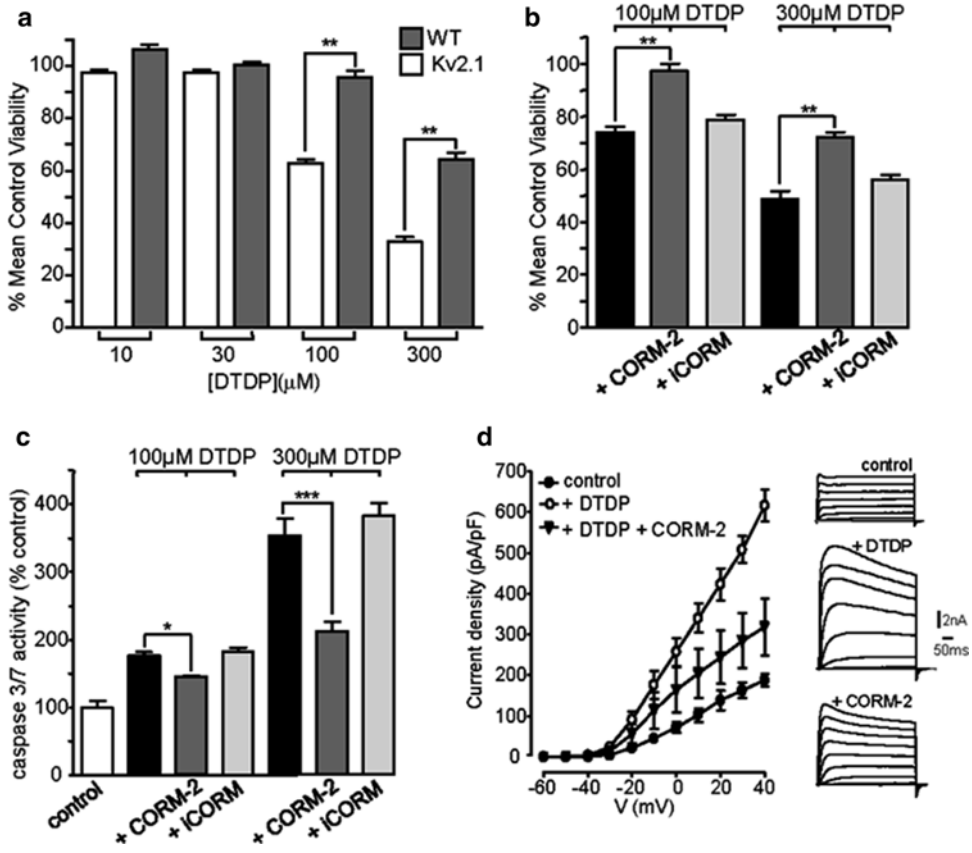


**Fig. 39.1** CO suppresses the Kv2.1-dependent susceptibility to oxidant-induced apoptosis (**a**) Cell viability assays (MTT assays), illustrating the concentration-dependent effects of the oxidant DTDP on viability determined in wild-type (WT) and Kv2.1-expressing HEK293 cells. (**b**) Viability of Kv2.1-expressing HEK293 cells following exposure to DTDP in the absence and presence of 100 μM CORM-2 or iCORM, as indicated. (**c**) Caspase 3/7 assay from Kv2.1-expressing HEK293 cells. Cells were exposed to DTDP in the absence and presence of 100 μM CORM-2 or iCORM, as indicated. (**d**) *Left*: mean ± s.e.m. current density *vs.* voltage relationships determined in control cells ($n = 14$), following exposure to DTDP in the absence and presence of 30 μM CORM-2 or iCORM, as indicated (both $n = 6$). *Right*: example families of currents evoked by step depolarizations (−100 to +40 mV) applied to representative HEK293 cells stably expressing Kv2.1. Scale bars apply to all traces. $^{*}P < 0.05$, $^{**}P < 0.01$, $^{***}P < 0.001$; 1-way ANOVA with Bonferroni multiple-comparison test

Fig. 39.1b), and this action of CORM-2 is likely to occur via CO release since the inactive form of the donor (iCORM; 100 μM) was without effect. That DTDP-induced cell death occurred at least in part via apoptosis is strongly suggested by the fact that it led to caspase 3/7 activation, which was, again, suppressed by CO, applied as CORM-2 (Fig. 39.1c). Whole-cell patch-clamp recordings from Kv2.1-expressing HEK293 cells revealed that DTDP induced a dramatic 3-fold increase in current density, consistent with the previously reported increased surge in $K^+$ channel insertion into the plasma membrane, and this was markedly suppressed by CORM-2 (Fig. 39.1d).

These results obtained in HEK293 cells were largely recapitulated in cultured hippocampal neurones. Thus, whole-cell $K^+$ currents in these cells were significantly attenuated in the presence of CORM-2 (Fig. 39.2a). However, since hippocampal neurones express a variety of

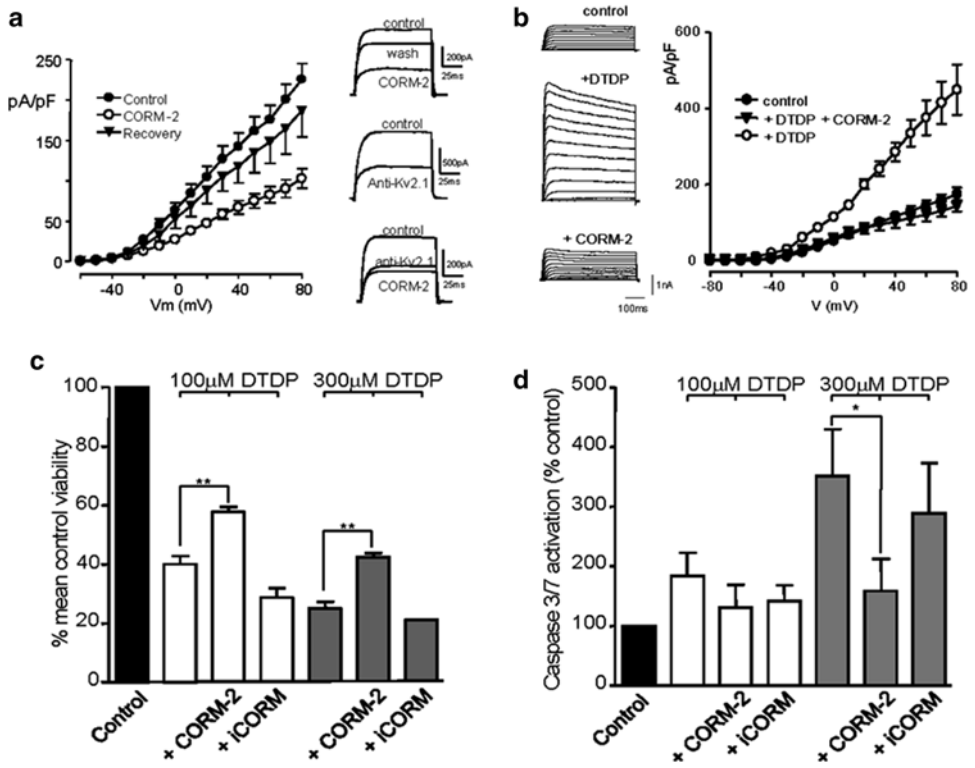


**Fig. 39.2** CO inhibits native Kv2.1 and oxidant-induced $K^+$ current surge in hippocampal neurones. (**a**) *Left*: mean ± s.e.m. ($n = 8$ cells) current density *vs.* voltage relationships obtained from hippocampal neurones, indicating the reversible inhibitory effects of CORM-2. *Right*: top traces; example currents before (control), during (CORM-2) and after exposure (wash) to 30 μM CORM-2. *Middle* traces exemplify the effects of 10-min intracellular dialysis with an anti-Kv2.1 antibody (0.5 μg/ml). *Bottom* traces show the modest effects of CORM-2 (30 μM) following 10 min dialysis with anti-Kv2.1 antibody. Currents were obtained by step depolarizations from −70 to +50 mV. (**b**) *Left*: example families of currents evoked by step depolarizations (−100 to +80 mV) applied to example hippocampal neurones. Currents were recorded in a control cell (top traces), a cell exposed to 25 μM DTDP or DTDP in the presence of 30 μM CORM-2 (*bottom* traces). Scale bars apply to all traces. *Right*: mean ± s.e.m. current density *vs.* voltage relationships determined in control cells, following exposure to DTDP and following exposure to DTDP in the presence of 30 μM CORM-2 ($n = 8$ in each case). (**c**) Normalized viability measurements made from primary hippocampal neurone preparations. Cells were exposed to DTDP in the absence of additional drugs, or in the presence of 100 μM CORM-2 or iCORM. (**d**) Caspase 3/7 activity assay in which cells were exposed to DTDP in the absence of additional drugs, but in the presence of 100 μM CORM-2 or iCORM, as indicated. *Bars* represent mean ± s.e.m. viability determined from three experiments, each repeated in triplicate. $^*P < 0.05$, $^{**}P < 0.01$; 1-way ANOVA with Bonferroni multiple-comparison test

voltage-gated $K^+$ channel types, we aimed to determine whether CO was selective in its ability to inhibit Kv2.1. To do this, we dialyzed cells with an anti-Kv2.1 antibody, which caused partial block of whole-cell $K^+$ currents due to inhibition of the Kv2.1 component. In the presence of this antibody, CORM-2 inhibited only a small fraction of the residual current, suggesting it was largely selective for Kv2.1 despite the presence of multiple $K^+$ channel types (Fig. 39.2a). More strikingly, CO (applied as CORM-2) fully reversed the oxidant-(DTDP)-induced increase of $K^+$ current amplitudes in hippocampal neurones (Fig. 39.2b). The consequences of these effects for cell viability was similar to that seen in HEK293 cells over-expressing Kv2.1; thus, loss of cell viability in hippocampal cultures was partially reversed by CORM-2 (but not iCORM; Fig. 39.2c), as was the activation of caspase 3/7 (Fig. 39.2d).

We next sought for evidence for a functional role of the CO/Kv2.1 pathway. Our previous study was the first to identify constitutive HO-1 expression and Kv2.1 expression in the medulloblastoma-derived DAOY cell line (Al-Owais et al. 2012). As shown in Fig. 39.3a, following heme-mediated HO-1 induction, DAOY cells genetically engineered to repress HO-1 expression in a doxycycline-inducible manner (+Dox; through increased HO-1 targeting shRNA production) exhibited decreased resistance to oxidant-(diamide)-induced loss of viability when compared with control (−Dox) cells. Furthermore, this protective effect of HO-1 induction was mimicked by application of the CO-donor CORM-2, but not iCORM (Fig. 39.3b). CORM-2 also inhibited whole-cell $K^+$ currents in DAOY cells (Fig. 39.3c), and reversed the oxidant-induced increase in $K^+$ current amplitudes (Fig. 39.3d) – thus, all the effects observed in HEK293 cells expressing Kv2.1, and in hippocampal neurones expressing native Kv2.1, were found in the medulloblastoma cell line DAOY.

## 39.4 Discussion

Although a number of different $K^+$ channel types have been proposed as having important roles in apoptosis (Prevarskaya et al. 2010; Lehen'kyi et al. 2011), the voltage-gated, delayed rectifier $K^+$ channel Kv2.1 has received much attention for its role in neuronal apoptosis. Pro-apoptotic agents trigger $K^+$ loss from neurones by causing a rapid increase in their surface expression via a mechanism involving p38 MAP kinase phosphorylation of Ser-800 in the intracellular C-terminal of the channel protein and additional phosphorylation of an N-terminal tyrosine (Y124) regulated via Src kinase. The process appears driven by oxidant-induced mobilization of intracellular $Zn^{2+}$ (McCord and Aizenman 2013). The present study suggests that this pathway can be counteracted by HO-1 derived CO, which acts to inhibit Kv2.1 via a mechanism which remains to be fully elucidated, but is clearly potent, especially as observed in native hippocampal neurones (see Fig. 39.2b). This provides a novel mechanism which is likely to contribute to the known protective central effects of CO administration in experimental ischemia (Zeynalov and Dore 2009).

Importantly, we have also demonstrated that the Kv2.1/CO protective pathway against oxidant-induced apoptosis is also active in the medulloblastoma cell line DAOY (Fig. 39.3). These findings present a possible mechanistic explanation as to why HO-1 (constitutively active in many tumor types) may provide tonic protection against apoptosis. Exactly why HO-1 is constitutively expressed in cancer cells is not known, although it is noteworthy that the tumor microenvironment is hypoxic (Harris 2002), and hypoxia can drive HO-1 expression (Was et al. 2010). Interestingly, in this and previous studies detailed above, the role of Kv2.1 in apoptosis assumes that this channel (or a significant fraction of the channel popultaiton) must be active

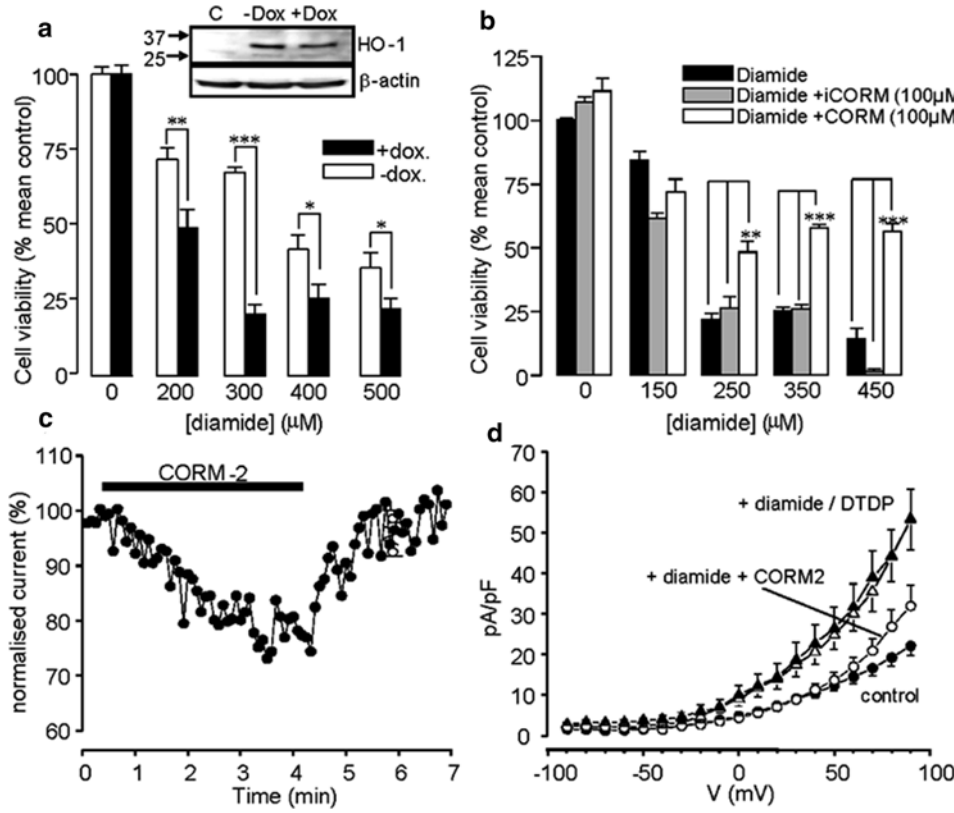


**Fig. 39.3** CO is anti-apoptotic via $K^+$ channel inhibition in DAOY medulloblastoma cells. (**a**) Mean effect on viability of diamide in DAOY cells stably expressing doxycycline-inducible HO-1 targeting shRNA. Cells were pre-exposed to hemin (200 μM, 48 h) with (+Dox) or without (−Dox) doxycycline (Dox; 2 μg/ml), as indicated. The inset shows a Western blot of HO-1 levels in control (C) cells and in cells pre-exposed to hemin (200 μM, 48 h) with or without Dox (2 μg/ml). (**b**) Mean effect on viability of DAOY cells treated with diamide with and without the subsequent incubation of CORM-2 (100 μM, 3 h) or iCORM (100 μM, 3 h). Each experiment in (**a**) and (**b**) was repeated three times in triplicate (*, $P<0.05$; **, $P<0.01$, ***, $P<0.001$; two-way ANOVA with Bonferroni multiple-comparison test). (**c**) Example time-course of the reversible inhibitory effect of CORM-2. Currents were evoked by successive step-depolarizations from −80 to +50 mV and CORM-2 (30 μM) was applied as indicated by the bar. (**d**). (D) mean (± s.e.m.) current density versus voltage relationships determined in control cells (*solid circles*, n = 10), following exposure to diamide or DTDP (*open circles* and *solid triangles*, respectively; n = 10 for each) and following exposure to diamide in the presence of CORM-2 (30 μM, *open circles*, n = 8), as indicated

not only in neurones, but also in DAOY cells, as well as in HEK293 cells when it is over-expressed (Dallas et al. 2011). This remains to be demonstrated clearly in each case.

These findings also point to a possible mechanism by which HO-1 expressing cancers might be treated, since pharmacological inhibition of HO-1 might be expected to increase vulnerability of cancer cells to apoptosis, or chemotherapeutic agents. However, caution should be taken over such an approach since CO also inhibits T-type $Ca^{2+}$ channels (Boycott et al. 2013) which can stimulate proliferation of cancers cells (Panner and Wurster 2006), and so their disinhibition by suppression of HO-1 could potentially promote cancer growth. Investigation of the overall effects of HO-1 suppression in specific cancer types would have to thoroughly investigated before such approaches to treatment can be considered.

**Acknowledgements** This work was supported by the Yorkshire Cancer Research and The Wellcome Trust.

## References


Ahmad AS, Zhuang H, Dore S (2006) Heme oxygenase-1 protects brain from acute excitotoxicity. Neuroscience 141:1703–1708

Al-Owais MM, Scragg JL, Dallas ML, Boycott HE, Warburton P, Chakrabarty A, Boyle JP, Peers C (2012) Carbon monoxide mediates the anti-apoptotic effects of heme oxygenase-1 in medulloblastoma DAOY cells via K+ channel inhibition. J Biol Chem 287:24754–24764

Bortner CD, Cidlowski JA (2002) Cellular mechanisms for the repression of apoptosis. Annu Rev Pharmacol Toxicol 42:259–281

Boycott HE, Dallas ML, Elies J, Pettinger L, Boyle JP, Scragg JL, Gamper N, Peers C (2013) Carbon monoxide inhibition of Cav3.2 T-type Ca2+ channels reveals tonic modulation by thioredoxin. FASEB J 27:3395–3407

Dallas ML, Boyle JP, Milligan CJ, Sayer R, Kerrigan TL, McKinstry C, Lu P, Mankouri J, Harris M, Scragg JL, Pearson HA, Peers C (2011) Carbon monoxide protects against oxidant-induced apoptosis via inhibition of Kv2.1. FASEB J 25:1519–1530

Dennery PA (2000) Regulation and role of heme oxygenase in oxidative injury. Curr Top Cell Regul 36:181–199

Droge W, Schipper HM (2007) Oxidative stress and aberrant signaling in aging and cognitive decline. Aging Cell 6:361–370

Fang J, Akaike T, Maeda H (2004) Antiapoptotic role of heme oxygenase (HO) and the potential of HO as a target in anticancer treatment. Apoptosis 9:27–35

Ferris CD, Jaffrey SR, Sawa A, Takahashi M, Brady SD, Barrow RK, Tysoe SA, Wolosker H, Baranano DE, Dore S, Poss KD, Snyder SH (1999) Haem oxygenase-1 prevents cell death by regulating cellular iron. Nat Cell Biol 1:152–157

Harris AL (2002) Hypoxia–a key regulatory factor in tumour growth. Nat Rev Cancer 2:38–47

Hou ST, MacManus JP (2002) Molecular mechanisms of cerebral ischemia-induced neuronal death. Int Rev Cytol 221:93–148

Hughes FM Jr, Bortner CD, Purdy GD, Cidlowski JA (1997) Intracellular K+ suppresses the activation of apoptosis in lymphocytes. J Biol Chem 272:30567–30576

Imuta N, Hori O, Kitao Y, Tabata Y, Yoshimoto T, Matsuyama T, Ogawa S (2007) Hypoxia-mediated induction of heme oxygenase type I and carbon monoxide release from astrocytes protects nearby cerebral neurons from hypoxia-mediated apoptosis. Antioxid Redox Signal 9:543–552

Jozkowicz A, Was H, Dulak J (2007) Heme oxygenase-1 in tumors: is it a false friend? Antioxid Redox Signal 9:2099–2117

Kim HP, Ryter SW, Choi AM (2006) CO as a cellular signaling molecule. Annu Rev Pharmacol Toxicol 46:411–449

Kinobe RT, Dercho RA, Nakatsu K (2008) Inhibitors of the heme oxygenase – carbon monoxide system: on the doorstep of the clinic? Can J Physiol Pharmacol 86:577–599

Lehen'kyi V, Shapovalov G, Skryma R, Prevarskaya N (2011) Ion channels in control of cancer and cell apoptosis. Am J Physiol Cell Physiol 301:1281–1289

McCord MC, Aizenman E (2013) Convergent Ca2+ and Zn2+ signaling regulates apoptotic Kv2.1 K+ currents. Proc Natl Acad Sci U S A 110:13988–13993

Niizuma K, Endo H, Chan PH (2009) Oxidative stress and mitochondrial dysfunction as determinants of ischemic neuronal death and survival. J Neurochem 109(Suppl 1):133–138

Okouchi M, Ekshyyan O, Maracine M, Aw TY (2007) Neuronal apoptosis in neurodegeneration. Antioxid Redox Signal 9:1059–1096

Pal SK, Takimoto K, Aizenman E, Levitan ES (2006) Apoptotic surface delivery of K+ channels. Cell Death Differ 13:661–667

Panner A, Wurster RD (2006) T-type calcium channels and tumor proliferation. Cell Calcium 40:253–259

Pappolla MA, Chyan YJ, Omar RA, Hsiao K, Perry G, Smith MA, Bozner P (1998) Evidence of oxidative stress and in vivo neurotoxicity of beta-amyloid in a transgenic mouse model of Alzheimer's disease: a chronic oxidative paradigm for testing antioxidant therapies in vivo. Am J Pathol 152:871–877

Prevarskaya N, Skryma R, Shuba Y (2010) Ion channels and the hallmarks of cancer. Trends Mol Med 16:107–121

Reynolds A, Laurie C, Mosley RL, Gendelman HE (2007) Oxidative stress and the pathogenesis of neurodegenerative disorders. Int Rev Neurobiol 82:297–325

Robertson CL, Scafidi S, McKenna MC, Fiskum G (2009) Mitochondrial mechanisms of cell death and neuroprotection in pediatric ischemic and traumatic brain injury. Exp Neurol 218:371–380

Schipper HM, Song W, Zukor H, Hascalovici JR, Zeligman D (2009) Heme oxygenase-1 and neurodegeneration: expanding frontiers of engagement. J Neurochem 110:469–485

Taillandier L, Blonski M, Carrie C, Bernier V, Bonnetain F, Bourdeaut F, Thomas IC, Chastagner P, Dhermain F, Doz F, Frappaz D, Grill J, Guillevin R, Idbaih A, Jouvet A, Kerr C, Donadey FL, Padovani L, Pallud J, Sunyach MP (2011) [Medulloblastomas: review]. Rev Neurol (Paris) 167:431–448

Was H, Dulak J, Jozkowicz A (2010) Heme oxygenase-1 in tumor biology and therapy. Curr Drug Targets 11:1551–1570

Wu L, Wang R (2005) Carbon monoxide: endogenous production, physiological functions, and pharmacological applications. Pharmacol Rev 57:585–630

Yu SP (2003) Regulation and critical role of potassium homeostasis in apoptosis. Prog Neurobiol 70:363–386

Yu SP, Yeh CH, Sensi SL, Gwag BJ, Canzoniero LM, Farhangrazi ZS, Ying HS, Tian M, Dugan LL, Choi DW (1997) Mediation of neuronal apoptosis by enhancement of outward potassium current. Science 278:114–117

Yu SP, Canzoniero LM, Choi DW (2001) Ion homeostasis and apoptosis. Curr Opin Cell Biol 13:405–411

Zeynalov E, Dore S (2009) Low doses of carbon monoxide protect against experimental focal brain ischemia. Neurotox Res 15:133–137

# Inhibition of T-type $Ca^{2+}$ Channels by Hydrogen Sulfide

40

Jacobo Elies, Jason L. Scragg, Mark L. Dallas, Dongyang Huang, Sha Huang, John P. Boyle, Nikita Gamper, and Chris Peers

**Abstract**

T-type $Ca^{2+}$ channels are a distinct family of low voltage-activated $Ca^{2+}$ channels which serve many roles in different tissues. Several studies have implicated them, for example, in the adaptive responses to chronic hypoxia in the cardiovascular and endocrine systems. Hydrogen sulfide ($H_2S$) was more recently discovered as an important signalling molecule involved in many functions, including $O_2$ sensing. Since ion channels are emerging as an important family of target proteins for modulation by $H_2S$, and both T-type $Ca^{2+}$ channels and $H_2S$ are involved in cellular responses to hypoxia, we have investigated whether recombinant and native T-type $Ca^{2+}$ channels are a target for modulation by $H_2S$. Using patch-clamp electrophysiology, we demonstrate that the $H_2S$ donor, NaHS, selectively inhibits Cav3.2 T-type $Ca^{2+}$ channels heterologously expressed in HEK293 cells, whilst Cav3.1 and Cav3.3 channels were unaffected. Sensitivity of Cav3.2 channels to $H_2S$ required the presence of the redox-sensitive extracellular residue H191, which is also required for tonic binding of $Zn^{2+}$ to this channel. Chelation of $Zn^{2+}$ using TPEN prevented channel inhibition by $H_2S$. $H_2S$ also selectively inhibited native T-type channels (primarily Cav3.2) in sensory dorsal root ganglion neurons. Our data demonstrate a novel target for $H_2S$ regulation, the T-type $Ca^{2+}$ channel Cav3.2. Results have important implications for the proposed pro-nociceptive effects of this gasotransmitter. Implications for the control of cellular responses to hypoxia await further study.

J. Elies • J.L. Scragg • J.P. Boyle • C. Peers (✉)
Leeds Institute of Cardiovascular and Metabolic Medicine, Faculty of Medicine and Health, University of Leeds, Leeds LS2 9JT, UK
e-mail: c.s.peers@leeds.ac.uk

M.L. Dallas
School of Pharmacy, University of Reading, Reading RG6 6UB, UK

D. Huang • S. Huang
Department of Pharmacology, Hebei Medical University, Shijiazhuang, China

N. Gamper
School of Biomedical Sciences, Faculty of Biological Sciences, University of Leeds, Leeds, UK



C. Peers et al. (eds.), *Arterial Chemoreceptors in Physiology and Pathophysiology*, Advances in Experimental Medicine and Biology 860, DOI 10.1007/978-3-319-18440-1_40

**Keywords**
Hydrogen sulfide • T-type $Ca^{2+}$ channel • HEK293 cells • Sensory neuron • Zinc • Patch clamp

## 40.1 Introduction

$H_2S$ is a "gasotransmitter", with biological importance and influence becoming comparable to that of carbon monoxide and nitric oxide in both the brain and periphery (Szabo 2007; Li et al. 2011; Wang 2012; Paul and Snyder 2012). $H_2S$ is generated primarily from cysteine by cystathionine γ lyase (CSE) and cystathionine β synthetase (CBS), the former most important in peripheral tissues whilst the latter predominates in the central nervous system (CNS). 3-mercaptopyruvate sulfurtransferase (3MST) along with cysteine aminotransferase also generate $H_2S$ in the brain and vasculature (Shibuya et al. 2009a, b).

$H_2S$ acts as an anti-inflammatory and anti-apoptotic agent within the CNS (Gong et al. 2011), enhancing cognitive function and protecting neurons against oxidative stress (Kimura et al. 2012; Kimura and Kimura 2004). It was suggested that in the peripheral nervous system, $H_2S$ is involved in pain sensation, exerting hyperalgesic properties (Takahashi et al. 2010; Maeda et al. 2009; Kawabata et al. 2007). $H_2S$ is also an important regulatory factor in the cardiovascular system, influencing cardiac pre- and post-conditioning (Calvert et al. 2009; Predmore and Lefer 2011). Furthermore it is also generated in vascular smooth muscle cells (VSMCs) and causes vasodilation through activation of smooth muscle $K_{ATP}$ channels (Zhao et al. 2001; Yang et al. 2008). $H_2S$ is also an important factor in oxygen sensing: in the carotid body, levels of $H_2S$ generated by CSE expressed in type I cells increase in hypoxia (Makarenko et al. 2012; Peng et al. 2010). Interestingly, $H_2S$ donors stimulate carotid body sensory activity in a manner at least superficially reminiscent of hypoxia (Li et al. 2010; Peng et al. 2010). Most importantly, carotid body responses to hypoxia were dramatically reduced in both CSE knockout mice and in rats treated with pharmacological inhibitors of $H_2S$ generating enzymes (Peng et al. 2010).

T-type $Ca^{2+}$ channels are a family of voltage-gated $Ca^{2+}$ channels; encoded by three genes (*CACNA1G, CACNA1H* and *CACNA1I*) they give rise to voltage-sensing, pore-forming Cav3.1, Cav3.2 and Cav3.3 subunits, respectively. These channels are widely and differentially expressed, serving a variety of functions. This arises in part because they can contribute to tonic $Ca^{2+}$ influx (Perez-Reyes 2003), thereby controlling proliferation of smooth muscle (Kuga et al. 1996; Rodman et al. 2005) and cancer (Santoni et al. 2012) cells. In the nervous system, T-type $Ca^{2+}$ channels control neuronal burst firing and hence excitability (Talley et al. 1999), which is crucial to, for example, nociception (Jevtovic-Todorovic and Todorovic 2006; Todorovic and Jevtovic-Todorovic 2011). Interestingly, $H_2S$ is reported to exert hyperalgesic effects (Kawabata et al. 2007), the latter supposedly via sensory neuronal T-type $Ca^{2+}$ channel augmentation (Takahashi et al. 2010). T-type $Ca^{2+}$ channels are also associated with cellular responses to hypoxia. For example, they strongly influence hypoxia-evoked catecholamine release from immature adrenal chromaffin cells (Levitsky and Lopez-Barneo 2009), and their expression is augmented during development of hypoxic pulmonary hypertension (Wan et al. 2013; Chevalier et al. 2014).

Given the common areas of physiological importance of both T-type $Ca^{2+}$ channels and those emerging for $H_2S$, coupled with the increasing awareness that ion channels are a major target for modulation by $H_2S$ (Peers et al. 2012), we have investigated the possibility that $H_2S$ may exert at least some of its actions via regulation of these channels.

## 40.2 Methods

### 40.2.1 Cell Culture

HEK293 cells stably transfected to express T-type $Ca^{2+}$ channels (rat Cav3.1 and Cav3.3, human Cav3.2; kind gifts from Dr E. Perez-Reyes, University of Virginia) were cultured as previously described (Fearon et al. 2000; Boycott et al. 2013) in minimum essential growth medium (MEM) with Earle's salts and L-glutamine supplemented with 9 % (v/v) fetal bovine serum (FBS; Biosera, Ringmer, East Sussex, UK), 1 mg/ml geneticin G-418 sulphate, 1 % (v/v) non-essential amino acids, 50 µg/ml gentamicin, 100 units/ml penicillin G, 100 µg/ml streptomycin and 0.25 µg/ml amphotericin in a humidified atmosphere of air/$CO_2$ (19:1) at 37 °C. Cells were passaged when 80–90 % confluent. We also generated stable cell lines expressing the Cav3.2 mutant H191Q and the Cav3.1 mutant Q172H, exactly as previously reported (Boycott et al. 2013): these cells were maintained under antibiotic (G-418, 1 mg/ml) selection throughout the cloning process. G-418 concentration was then reduced to 400 µg/ml in all subsequent passages once stable clones had been positively identified.

Dorsal root ganglion (DRG) neurons were cultured as described previously (Kirton et al. 2013) from ganglia of adult (150–200 g) Wistar rats (killed by isoflurane overdose). Ganglia were incubated (ca. 20 min) in Hank's balanced salt solution (HBSS) containing collagenase (1 mg/ml, Sigma) and dispase (10 mg/ml, Invitrogen) at 37 °C. Ganglia were gently triturated 10–20 times using a 1 ml Gilson pipette, and the resulting cells were washed twice in 10 ml cold, fresh growth media (DMEM with GlutaMAX I (Invitrogen)), supplemented with 10% fetal calf serum, penicillin (50 U/ml) and streptomycin (50 µg/ml) and collected by centrifugation (800 g for 5 min at 4 °C). No nerve growth factor was added. The cell pellet was then resuspended in pre-warmed growth media and plated onto glass coverslips coated with poly-D-lysine and laminin. Neurons were cultured for 2–5 days in a humidified incubator (37 °C, 5 % $CO_2$).

### 40.2.2 Electrophysiology

Conventional whole-cell patch-clamp recordings were used to record $Ca^{2+}$ currents from HEK293 cells expressing Cav3.1, Cav3.2 or Cav3.3 and DRG neurons. For HEK293 cells, an Axopatch 200 A amplifier was employed (Molecular Devices, Sunnyvale, CA, USA), and data were acquired via a Digidata 1200 interface controlled by Clampex 9.0 software. Offline analysis was performed using Clampfit 9.0 (Molecular Devices). Cells were either repeatedly step depolarized to −20 mV from −80 mV for 200–400 ms (0.2 kHz), or a series of 100 ms depolarizing steps from −100 to +50 mV in 10 mV increments were applied. Signals were low-pass filtered at 2 kHz and sampled at 10 kHz.

Glass coverslips with attached cells were placed at the bottom of a small recording chamber (0.5 ml) on the stage of an inverted microscope and constantly perfused by gravity. The standard perfusate (pH 7.4, 22 ± 1 °C) was composed of (in mM): (95) NaCl, (5) CsCl, (0.6) $MgCl_2$, (15) $CaCl_2$, (20) TEA-Cl, (5) HEPES, and (10) glucose (pH 7.4 adjusted with NaOH). Patch pipettes were made from borosilicate glass and had resistances ranging from 3 to 6 MΩ when filled with the internal solution, containing (in mM): (120) CsCl, (2) $MgCl_2$, (10) HEPES, (10) EGTA, (20) TEA-Cl, (2) Na-ATP, and (2) Mg-ATP (pH 7.2 adjusted with CsOH).

For DRG neurons, currents were evoked by 75 ms square voltage pulses to −40 mV (0.1 Hz) from a holding potential of −90 mV, or to 0 mV to evoke high-voltage activated $Ca^{2+}$ currents. They were amplified using an Axopatch 700B patch clamp amplifier (Axon Instruments, USA), recorded using pClamp 10.4 software (Axon Instruments, USA) and sampled at a frequency of 4 kHz. The extracellular solution contained (in mM): (150) TEA-Cl, (2) $CaCl_2$, (10) HEPES, (10) glucose (pH 7.4 with CsOH). Intracellular solution contained (in mM): (135) CsCl, (3) $MgCl_2$, (10) EGTA, (10) HEPES, (3) Mg-ATP, (0.6) GTP (pH 7.4 with CsOH). Pipettes with resistance of 2–4 MΩ were used.

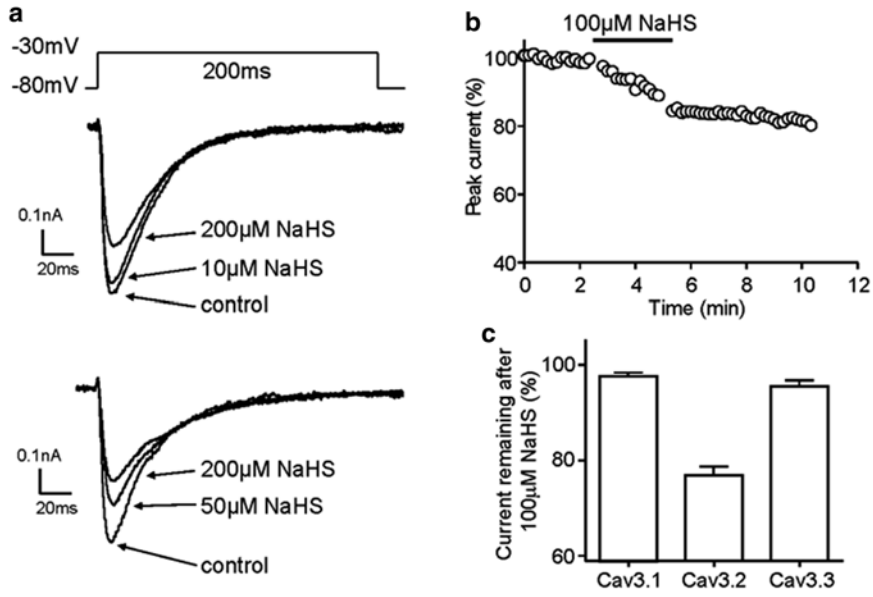


**Fig. 40.1** $H_2S$ inhibits Cav3.2 T-type $Ca^{2+}$ currents. (**a**) Currents recorded from two example HK293 cells expressing Cav3.2 T-type $Ca^{2+}$ channels. Currents were evoked by successive step depolarizations as indicated before and during application of the $H_2S$ donor NaHS at the concentrations indicated. (**b**) Time-series plot illustrating normalized current amplitudes evoked by step depolarizations from −80 mV to −30 mV in a Cav3.2-expressing cell. For the period indicated by the bar, NaHS was applied via the perfusate. (**c**) Bar graph showing mean (±s.e.m.; n > 5 in each case) % current remaining following exposure to NaHS (100 μM) as determined in cells expressing the three major isoforms of T-type $Ca^{2+}$ channel, as indicated

In all experiments, cells were exposed to $H_2S$ by dissolving NaHS directly into the perfusate. These solutions generated offset potentials, and so a 3 % agar-salt (1M KCl) bridge was employed.

## 40.3 Results

Whole-cell patch-clamp recordings from HEK293 cells expressing Cav3.2 channels revealed expected transient inward currents characteristic of this class of voltage-gated $Ca^{2+}$ channel (Fig. 40.1a), as we and others have previously shown (Perez-Reyes 2003; Fearon et al. 2000; Boycott et al. 2013). As the example traces demonstrate, currents were inhibited in a concentration-dependent manner by the $H_2S$ donor, NaHS, which was tested over the concentration range 1 μM–1 mM. An example time series indicates the rate of current inhibition, and shows that the effects of NaHS were largely irreversible (Fig. 40.1b). At a concentration of 100 μM, inhibition of Cav3.2 was near maximal. However, currents recorded from cells expressing either Cav3.1 or Cav3.3 channels were unaffected by this concentration of NaHS, suggesting that $H_2S$ specifically modulated Cav3.2 channels (Fig. 40.1c).

Cav3.2 is distinguished from other T-type $Ca^{2+}$ channels by its enhanced sensitivity to redox modulators (Todorovic et al. 2001; Nelson et al. 2005) which act at least in part via modulation of a region of the extracellular S3/S4 linker of domain I (Fig. 41.2a, inset) containing a histidine residue (H191): substitution of this residue with glutamine (H191Q) abolishes increased redox sensitivity in Cav3.2 (Nelson et al. 2007a, b). We examined the sensitivity to NaHS of Cav3.2 (H191Q) and found that 100 μM NaHS was unable to inhibit this mutant (exemplified in Fig. 40.2a). Since this residue has been implicated in tonic, inhibitory binding of $Zn^{2+}$ (Nelson

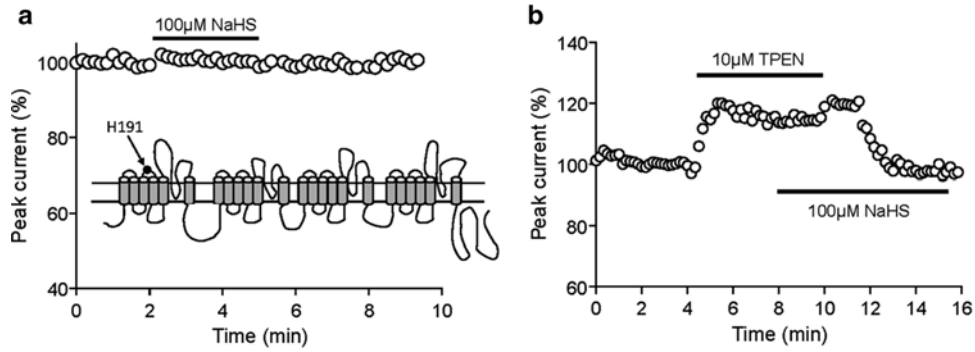


**Fig. 40.2** Involvement of H191 in the sensitivity of Cav3.2 T-type $Ca^{2+}$ currents to $H_2S$. (**a**) Time-series plot illustrating normalized current amplitudes evoked by step depolarizations from −80 mV to −30 mV in a H191Q mutant Cav3.2-expressing HEK293 cell. For the period indicated by the bar, NaHS was applied via the perfusate. Inset; cartoon of the T-type $Ca^{2+}$ channel, showing the location of the H191 residue. (**b**) Time-series plot illustrating normalized current amplitudes evoked by step depolarizations from −80 mV to −30 mV in a Cav3.2-expressing HEK293 cell. For the periods indicated by the bars, TPEN and NaHS were applied via the perfusate. Note the lack of effect of NaHS in the continued presence of TPEN

et al. 2007b), and $H_2S$ has previously been proposed to chelate $Zn^{2+}$ (Matsunami et al. 2011), we examined whether $Zn^{2+}$ chelation might alter responses of Cav3.2 to $H_2S$ (note; chelation is of contaminant $Zn^{2+}$ as none was added to the solutions. The concentration of this contaminant $Zn^{2+}$ is unknown). As exemplified in Fig. 40.2b, the $Zn^{2+}$ chelator TPEN (N,N,N′,N′-tetra-2-picolylethylenediamine; 10 μM) augmented currents generated in Cav3.2 expressing cells and, in its continued presence, $H_2S$ was without further effect. Only upon removal of TPEN was the ability of $H_2S$ to inhibit currents restored. These results are consistent with a role for $Zn^{2+}$ in channel inhibition by $H_2S$ but argue against $H_2S$ acting as a $Zn^{2+}$ chelator.

To investigate regulation of native T-type $Ca^{2+}$ channels by $H_2S$, we employed sensory neurons isolated from DRGs, since the dominant channel isoform in this tissue is Cav3.2 (Nelson et al. 2006). Small depolarizing steps applied to these cells evoked largely transient inward currents which were sensitive to inhibition by the T-type $Ca^{2+}$ channel inhibitor mibefradil (3 μM), as illustrated in Fig. 40.3a.

These currents were also partially inhibited by $H_2S$; 100 μM NaHS inhibited native T-type current in DRGs by 18.6 ± 0.7% (e.g. Fig. 40.3a, representative of 5 recordings). By contrast, larger step depolarizations evoked currents arising from high voltage activated (HVA) currents, due to activation of N-, P/Q- and L-type $Ca^{2+}$ channels (Rola et al. 2003). These currents were unaffected by NaHS (Fig. 40.3b). Thus, $H_2S$ inhibits native T-type $Ca^{2+}$ channels in DRG neurons, and appears to discriminate between these and HVA currents.

## 40.4 Discussion

The present study identifies Cav3.2 as a novel target for modulation by $H_2S$. This gasotransmitter is emerging as an important regulator of diverse ion channels, including cardiac L-type $Ca^{2+}$ channels, ATP-sensitive $K^+$ channels and high conductance $Ca^{2+}$ sensitive $K^+$ (BK) channels (Peers et al. 2012), and its ability to modulate Cav3.2 suggests the possibility that this gasotransmitter may exert physiological effects via this channel. $H_2S$ clearly discriminates between voltage-gated $Ca^{2+}$ channels, being selective in its ability to modulate Cav3.2 but not Cav3.1 or Cav3.3 (Fig. 40.1). Furthermore, it was without effect on HVA currents in sensory neurons (Fig. 40.3). Discrimination between subtypes of T-type $Ca^{2+}$ channels appears to centre on the extracellular H191 residue which is responsible for the striking

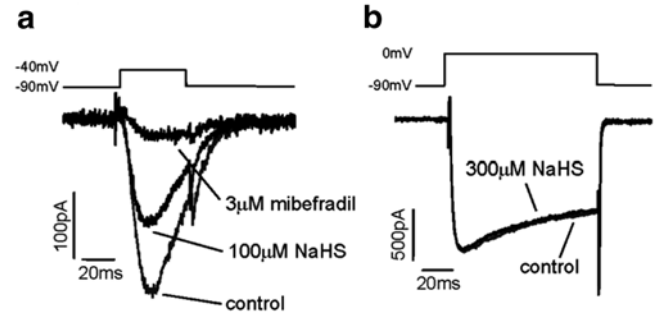


**Fig. 40.3** $H_2S$ inhibits native T-type $Ca^{2+}$ currents in DRG neurons. (**a**) Currents recorded from an example DRG neuron in response to a small test depolarization (to −40 mV) before and during application of NaHS (100 μM), as indicated. (**b**) Similar to (**a**) but a larger depolarization (to 0 mV) is used instead. Currents were evoked by successive step depolarizations before and during application of the $H_2S$ donor NaHS at the concentrations indicated, and also following bath application of mibefradil (in **a**)

sensitivity of this channel to redox modulators (Todorovic et al. 2001; Nelson et al. 2005). Thus, the mutant H191Q was insensitive to $H_2S$ (Fig. 40.2). Chelation of $Zn^{2+}$ with TPEN augmented current amplitudes in Cav3.2-expressing cells, as previously described (Nelson et al. 2007b) and in the presence of TPEN, $H_2S$ was without effect (Fig. 40.2). This finding suggests that $Zn^{2+}$ binding via H191 is involved in the ability of $H_2S$ to inhibit Cav3.2, but is not consistent with the suggestion that $H_2S$ acts to modulate this channel via $Zn^{2+}$ chelation (Matsunami et al. 2011), since this would lead to current augmentation, not inhibition, by $H_2S$. The mechanism by which $H_2S$ inhibits Cav3.2 remains to be fully determined.

Previous studies have suggested that $H_2S$ augments rather than inhibits T-type $Ca^{2+}$ channel activity, at least when applied at high (mM) concentrations, and that such an effect may account for the hyperalgesic effects of $H_2S$ (Maeda et al. 2009; Takahashi et al. 2010). These suggestions conflict with the present study which demonstrates Cav3.2 inhibition at lower concentrations, and remain to be reconciled. Exactly what levels of $H_2S$ can be achieved within cellular compartments via the activity of endogenous enzymes remains to be determined accurately, since measurement of $H_2S$ is not trivial (Papapetropoulos et al. 2015) but circulating levels in humans are believed to be in the submicromolar range (Peter et al. 2013), suggesting that experimental application of $H_2S$ may commonly be excessive. However, our findings suggest that at the lower concentrations studied thus far, $H_2S$ exerts inhibitory effects on Cav3.2. The physiological consequences of such an action in sensory neurons or elsewhere remain to be fully examined.

**Acknowledgements** This work was supported by The British Heart Foundation.

## References

Boycott HE, Dallas ML, Elies J, Pettinger L, Boyle JP, Scragg JL, Gamper N, Peers C (2013) Carbon monoxide inhibition of Cav3.2 T-type Ca2+ channels reveals tonic modulation by thioredoxin. FASEB J 27:3395–3407

Calvert JW, Jha S, Gundewar S, Elrod JW, Ramachandran A, Pattillo CB, Kevil CG, Lefer DJ (2009) Hydrogen sulfide mediates cardioprotection through Nrf2 signaling. Circ Res 105:365–374

Chevalier M, Gilbert G, Roux E, Lory P, Marthan R, Savineau JP, Quignard JF (2014) T-type calcium channels are involved in hypoxic pulmonary hypertension. Cardiovasc Res 103:597–606

Fearon IM, Randall AD, Perez-Reyes E, Peers C (2000) Modulation of recombinant T-type Ca2+ channels by hypoxia and glutathione. Pflugers Arch 441:181–188

Gong QH, Shi XR, Hong ZY, Pan LL, Liu XH, Zhu YZ (2011) A new hope for neurodegeneration: possible role of hydrogen sulfide. J Alzheimers Dis 24(Suppl 2):173–182

Jevtovic-Todorovic V, Todorovic SM (2006) The role of peripheral T-type calcium channels in pain transmission. Cell Calcium 40:197–203

Kawabata A, Ishiki T, Nagasawa K, Yoshida S, Maeda Y, Takahashi T, Sekiguchi F, Wada T, Ichida S, Nishikawa H (2007) Hydrogen sulfide as a novel nociceptive messenger. Pain 132:74–81

Kimura Y, Kimura H (2004) Hydrogen sulfide protects neurons from oxidative stress. FASEB J 18:1165–1167

Kimura H, Shibuya N, Kimura Y (2012) Hydrogen sulfide is a signaling molecule and a cytoprotectant. Antioxid Redox Signal 17:45–57

Kirton HM, Pettinger L, Gamper N (2013) Transient overexpression of genes in neurons using nucleofection. Methods Mol Biol 998:55–64

Kuga T, Kobayashi S, Hirakawa Y, Kanaide H, Takeshita A (1996) Cell cycle–dependent expression of L- and T-type Ca2+ currents in rat aortic smooth muscle cells in primary culture. Circ Res 79:14–19

Levitsky KL, Lopez-Barneo J (2009) Developmental change of T-type Ca2+ channel expression and its role in rat chromaffin cell responsiveness to acute hypoxia. J Physiol 587:1917–1929

Li Q, Sun B, Wang X, Jin Z, Zhou Y, Dong L, Jiang LH, Rong W (2010) A crucial role for hydrogen sulfide in oxygen sensing via modulating large conductance calcium-activated potassium channels. Antioxid Redox Signal 12:1179–1189

Li L, Rose P, Moore PK (2011) Hydrogen sulfide and cell signaling. Annu Rev Pharmacol Toxicol 51:169–187

Maeda Y, Aoki Y, Sekiguchi F, Matsunami M, Takahashi T, Nishikawa H, Kawabata A (2009) Hyperalgesia induced by spinal and peripheral hydrogen sulfide: evidence for involvement of Cav3.2 T-type calcium channels. Pain 142:127–132

Makarenko VV, Nanduri J, Raghuraman G, Fox AP, Gadalla MM, Kumar GK, Snyder SH, Prabhakar NR (2012) Endogenous H2S is required for hypoxic sensing by carotid body glomus cells. Am J Physiol Cell Physiol 303:C916–C923

Matsunami M, Kirishi S, Okui T, Kawabata A (2011) Chelating luminal zinc mimics hydrogen sulfide-evoked colonic pain in mice: possible involvement of T-type calcium channels. Neuroscience 181:257–264

Nelson MT, Joksovic PM, Perez-Reyes E, Todorovic SM (2005) The endogenous redox agent L-cysteine induces T-type Ca2+ channel-dependent sensitization of a novel subpopulation of rat peripheral nociceptors. J Neurosci 25:8766–8775

Nelson MT, Todorovic SM, Perez-Reyes E (2006) The role of T-type calcium channels in epilepsy and pain. Curr Pharm Des 12:2189–2197

Nelson MT, Joksovic PM, Su P, Kang HW, Van DA, Baumgart JP, David LS, Snutch TP, Barrett PQ, Lee JH, Zorumski CF, Perez-Reyes E, Todorovic SM (2007a) Molecular mechanisms of subtype-specific inhibition of neuronal T-type calcium channels by ascorbate. J Neurosci 27:12577–12583

Nelson MT, Woo J, Kang HW, Vitko I, Barrett PQ, Perez-Reyes E, Lee JH, Shin HS, Todorovic SM (2007b) Reducing agents sensitize C-type nociceptors by relieving high-affinity zinc inhibition of T-type calcium channels. J Neurosci 27:8250–8260

Papapetropoulos A, Whiteman M, Giuseppe C (2015) Pharmacological tools for hydrogen sulfide research: a brief, introductory guide for beginners. Br J Pharmacol 172(6):1633–1637

Paul BD, Snyder SH (2012) H(2)S signalling through protein sulfhydration and beyond. Nat Rev Mol Cell Biol 13:499–507

Peers C, Bauer CC, Boyle JP, Scragg JL, Dallas ML (2012) Modulation of ion channels by hydrogen sulfide. Antioxid Redox Signal 17:95–105

Peng YJ, Nanduri J, Raghuraman G, Souvannakitti D, Gadalla MM, Kumar GK, Snyder SH, Prabhakar NR (2010) H(2)S mediates O(2) sensing in the carotid body. Proc Natl Acad Sci U S A 107:10719–10724

Perez-Reyes E (2003) Molecular physiology of low-voltage-activated t-type calcium channels. Physiol Rev 83:117–161

Peter EA, Shen X, Shah SH, Pardue S, Glawe JD, Zhang WW, Reddy P, Akkus NI, Varma J, Kevil CG (2013) Plasma free H2S levels are elevated in patients with cardiovascular disease. J Am Heart Assoc 2:e000387

Predmore BL, Lefer DJ (2011) Hydrogen sulfide-mediated myocardial pre- and post-conditioning. Expert Rev Clin Pharmacol 4:83–96

Rodman DM, Reese K, Harral J, Fouty B, Wu S, West J, Hoedt-Miller M, Tada Y, Li KX, Cool C, Fagan K, Cribbs L (2005) Low-voltage-activated (T-type) calcium channels control proliferation of human pulmonary artery myocytes. Circ Res 96:864–872

Rola R, Szulczyk PJ, Witkowski G (2003) Voltage-dependent Ca2+ currents in rat cardiac dorsal root ganglion neurons. Brain Res 961:171–178

Santoni G, Santoni M, Nabissi M (2012) Functional role of T-type calcium channels in tumour growth and progression: prospective in cancer therapy. Br J Pharmacol 166:1244–1246

Shibuya N, Mikami Y, Kimura Y, Nagahara N, Kimura H (2009a) Vascular endothelium expresses 3-mercaptopyruvate sulfurtransferase and produces hydrogen sulfide. J Biochem 146:623–626

Shibuya N, Tanaka M, Yoshida M, Ogasawara Y, Togawa T, Ishii K, Kimura H (2009b) 3-Mercaptopyruvate sulfurtransferase produces hydrogen sulfide and bound sulfane sulfur in the brain. Antioxid Redox Signal 11:703–714

Szabo C (2007) Hydrogen sulphide and its therapeutic potential. Nat Rev Drug Discov 6:917–935

Takahashi T, Aoki Y, Okubo K, Maeda Y, Sekiguchi F, Mitani K, Nishikawa H, Kawabata A (2010) Upregulation of Ca(v)3.2 T-type calcium channels targeted by endogenous hydrogen sulfide contributes to maintenance of neuropathic pain. Pain 150:183–191

Talley EM, Cribbs LL, Lee JH, Daud A, Perez-Reyes E, Bayliss DA (1999) Differential distribution of three members of a gene family encoding low voltage-activated (T-type) calcium channels. J Neurosci 19:1895–1911

Todorovic SM, Jevtovic-Todorovic V (2011) T-type voltage-gated calcium channels as targets for the development of novel pain therapies. Br J Pharmacol 163:484–495

Todorovic SM, Jevtovic-Todorovic V, Meyenburg A, Mennerick S, Perez-Reyes E, Romano C, Olney JW, Zorumski CF (2001) Redox modulation of T-type calcium channels in rat peripheral nociceptors. Neuron 31:75–85

Wan J, Yamamura A, Zimnicka AM, Voiriot G, Smith KA, Tang H, Ayon RJ, Choudhury MS, Ko EA, Wang J, Wang C, Makino A, Yuan JX (2013) Chronic hypoxia selectively enhances L- and T-type voltage-dependent Ca2+ channel activity in pulmonary artery by upregulating Cav1.2 and Cav3.2. Am J Physiol Lung Cell Mol Physiol 305:L154–L164

Wang R (2012) Physiological implications of hydrogen sulfide: a whiff exploration that blossomed. Physiol Rev 92:791–896

Yang G, Wu L, Jiang B, Yang W, Qi J, Cao K, Meng Q, Mustafa AK, Mu W, Zhang S, Snyder SH, Wang R (2008) H2S as a physiologic vasorelaxant: hypertension in mice with deletion of cystathionine gamma-lyase. Science 322:587–590

Zhao W, Zhang J, Lu Y, Wang R (2001) The vasorelaxant effect of H(2)S as a novel endogenous gaseous K(ATP) channel opener. EMBO J 20:6008–6016

# 41

# GAL-021 and GAL-160 are Efficacious in Rat Models of Obstructive and Central Sleep Apnea and Inhibit $BK_{Ca}$ in Isolated Rat Carotid Body Glomus Cells

Mark L. Dallas, Chris Peers, Francis J. Golder, Santhosh Baby, Ryan Gruber, and D. Euan MacIntyre

**Abstract**

GAL-021 and GAL-160 are alkylamino triazine analogues, which stimulate ventilation in rodents, non-human primates and (for GAL-021) in humans. To probe the site and mechanism of action of GAL-021 and GAL-160 we utilized spirometry in urethane anesthetized rats subjected to acute bilateral carotid sinus nerve transection (CSNTX) or sham surgery. In addition, using patch clamp electrophysiology we evaluated ionic currents in carotid body glomus cells isolated from neonatal rats. Acute CSNTX markedly attenuated and in some instances abolished the ventilatory stimulant effects of GAL-021 and GAL-160 (0.3 mg/kg IV), suggesting the carotid body is a/the major locus of action. Electrophysiology studies, in isolated Type I cells, established that GAL-021 (30 μM) and GAL-160 (30 μM) inhibited the $BK_{Ca}$ current without affecting the delayed rectifier $K^+$, leak $K^+$ or inward $Ca^{2+}$ currents. At a higher concentration of GAL-160 (100 μM), inhibition of the delayed rectifier $K^+$ current and leak $K^+$ current were observed. These data are consistent with the concept that GAL-021 and GAL-160 influence breathing control by acting as peripheral chemoreceptor modulators predominantly by inhibiting $BK_{Ca}$ mediated currents in glomus cells of the carotid body.

M.L. Dallas
School of Pharmacy, University of Reading, Reading RG6 6UB, UK

C. Peers
Leeds Institute of Cardiovascular and Metabolic Medicine, Faculty of Medicine and Health, University of Leeds, Leeds LS2 9JT, UK

F.J. Golder • S. Baby • R. Gruber
D.E. MacIntyre (✉)
Galleon Pharmaceuticals Inc., Horsham, PA 19044, USA
e-mail: emacintyre@galleonpharma.com



C. Peers et al. (eds.), *Arterial Chemoreceptors in Physiology and Pathophysiology*, Advances in Experimental Medicine and Biology 860, DOI 10.1007/978-3-319-18440-1_41

**Keywords**
GAL-021 • GAL-160 • $BK_{Ca}$ channel • Carotid body • Carotid sinus nerve • Peripheral chemoreceptor modulators

## 41.1 Introduction

Predicated on the concept that agents which modulate the drive to breathe represent a rational approach towards the development of therapeutics for breathing control disorders such as drug-induced respiratory depression and sleep apnea, a phenotypic screening approach was used to identify ventilatory stimulant compounds. Starting from precedented agents, such as doxapram and almitrine, that are effective ventilatory stimulants in humans (Golder et al. 2013), a diversity of molecular scaffolds were designed, constructed, evaluated and further optimized to incorporate drug-like properties relating to potency, efficacy, specificity and tolerability. These efforts culminated in the identification of 2 development candidate compounds, the alkylamino triazine derivatives GAL-021 and GAL-160.

Upon intravenous administration by bolus or infusion to rats (Baby et al. 2012a) or cynomolgus monkeys (Golder et al. 2012) GAL-021 elicits dose-dependent increases in minute ventilation and shows robust, dose-dependent, reversal of opioid (morphine/fentanyl/alfentanil), benzodiazepine (midazolam), and anaesthetic (isoflurane/propofol)-induced respiratory depression (Baby et al. 2012a; Golder et al. 2013). GAL-021 recently has been shown to stimulate ventilation and to reverse opioid-induced respiratory depression in human volunteers (McLeod et al. 2014; Roozekrans et al. 2014). Unlike opioid receptor antagonists, GAL-021 does not reverse or compromise opioid analgesia in rats or humans (Baby et al. 2012a; Roozekrans et al. 2014). GAL-160 displays a similar profile of activity to GAL-021 with respect to spirometry and opioid-induced respiratory depression in rodents, but has higher oral bioavailability in preclinical species. In rodent models of central and obstructive sleep apnea, both GAL-021 and GAL-160 demonstrate beneficial effects on apnea frequency and duration, and reduce the desaturation sequelae without compromising sleep architecture (Gruber et al. 2013; Hewitt et al. 2014).

We have shown previously that GAL-021-induced ventilatory stimulation in rats is associated with increased carotid sinus nerve and phrenic motoneuron activity (Baby et al. 2012b), suggesting that these alkylamino triazine derivatives may act, at least in part, at the carotid body to promote afferent signaling to the brainstem respiratory centers and resultant efferent signaling to the upper airways and diaphragm, consistent with increased respiratory drive. Key to this signaling cascade are the complement of hypoxic sensing ion channels expressed in the carotid body. The molecular identity of the carotid body $K^+$ channel(s) which is/are inhibited by hypoxia remains a matter of debate. Controversies and interpretation conflicts arise *inter alia* because of species and age differences in the isolated type I cells evaluated, type of preparation used for investigation (e.g. single cell vs cluster), and configuration used for single channel recording (Buckler and Honore 2004; Peers et al. 2010; Kim 2013). In the rat carotid body much evidence points to the presence and functional importance of $BK_{Ca}$ and TASK channels in chemotransduction (Buckler 2007; Peers et al. 2010; Kim et al. 2012). There are few reports relating to human carotid body chemotransduction, although a recent report documents that the human carotid body transcriptome contains $BK_{Ca}$ and TASK-1 channels (Mkrtchian et al. 2012). To probe further the site and mechanism of action of GAL-021 and GAL-160, we compared the evoked ventilatory stimulation in rats subjected to acute bilateral carotid sinus nerve transection or sham surgery. In addition we evaluated the effects of GAL-021 and GAL-160 on $K^+$ and $Ca^{2+}$ currents using whole cell patch clamp electrophysiology in isolated rat carotid body type I glomus cells.

## 41.2 Methods

### 41.2.1 Spirometry Studies

Male adult Sprague Dawley rats were used for these studies. Animals were initially anesthetized with 2 % isoflurane. The femoral artery and vein were cannulated to permit monitoring blood pressure and drug administration. The cervical trachea was cannulated and connected to a pneumotachometer (MLT1L, AD Instruments, CO) to measure respiratory flow. The respiratory flow waveform was used to measure respiratory rate (RR) from cycle period, and integrated to calculate tidal volume ($V_T$). Minute volume ($\dot{V}_E$) was calculated as the product of RR and $V_T$. After these procedures, isoflurane was discontinued and replaced by urethane anesthesia (1.8 g/kg IV). Stable baseline values of cardiorespiratory parameters and arterial blood gases were confirmed before commencing the experimental protocol. Minute ventilation was measured before and after vehicle (saline), GAL-021 (0.3 mg/kg IV) and GAL-160 (0.3 mg/kg IV) injection. GAL-021 and GAL-160 were administered by slow IV bolus to separate groups of animals. Next, the carotid sinus nerves were transected bilaterally at the point where they branch off from the glossopharyngeal nerve and the protocol repeated. Sham-operated animals were included as controls. The ventilatory response to hypoxia ($FiO_2 = 0.10$, 3 min duration) was used to confirm functional denervation of the carotid bodies.

### 41.2.2 Glomus (Type I) Cell Isolation

To obtain carotid body glomus cells, neonatal rats (10–14 days) were killed and carotid bodies rapidly removed and placed in ice cold, phosphate buffered saline without $Ca^{2+}$ or $Mg^{2+}$ (Invitrogen). These were then enzymatically dissociated and cultured as described previously (Peers 1990; Wyatt and Peers 1993).

### 41.2.3 Electrophysiology

Fragments of coverslip with attached cells were transferred to a continuously perfused (3–5 ml/min) recording chamber mounted on the stage of an Olympus CK40 inverted microscope. All experiments were carried out at room temperature (22 ± 1 °C). Whole cell patch clamp recordings were then obtained from type I cells in voltage clamp mode. Patch pipettes had resistances of 4–6 MΩ. Series resistance was monitored after breaking into the whole cell configuration throughout the duration of experiments. If a significant increase occurred (>20 %), the experiment was terminated. Signals were acquired using a Axopatch 200B (Axon Instruments, Inc., Foster City, CA) controlled by Clampex 9.0 software via a Digidata 1322A interface (Axon Instruments, Inc., Foster City, CA). Data were filtered at 1 kHz and digitized at 5 kHz.

#### 41.2.3.1 $K^+$ Currents

To determine the effects of the test compounds on the $K^+$ currents we employed several protocols and solutions. For all experiments unless stated the standard perfusate (pH 7.4) was composed of (in mM): NaCl (135); KCl (5); $MgCl_2$ (1.2); Hepes (5); $CaCl_2$ (2.5); D-glucose (10). The intracellular solution (pH 7.2) consisted of in (mM): KCl (117); NaCl (10); EGTA (11); $MgCl_2$ (2); $CaCl_2$ (1); HEPES (11); NaATP (2). All cells were voltage clamped at −70 mV and $K^+$ currents were evoked with a series of depolarising steps from −80 mV to +60 mV (100 ms, 10 mV increments). In order to examine the effects on the $BK_{Ca}$ current, a ramp protocol −100 mV to +60 mV (1 s) was also employed, followed by a 250 ms step depolarisation to +60 mV. In addition a similar perfusate with the exception of 6 mM $MgCl_2$ and 0.1 mM $CaCl_2$ was used to inhibit the $BK_{Ca}$ component of the whole cell $K^+$ current, as described previously (Peers 1990; Peers and Green 1991). To investigate the 'leak' $K^+$ current, a ramp protocol (−100 mV to +40mV) was employed as described previously (Wyatt et al. 2007). 10 mM $BaCl_2$ was used to block of the leak $K^+$ current component.

#### 41.2.3.2 $Ca^{2+}$ Currents

For $Ca^{2+}$ channel experiments the standard perfusate (pH 7.4) was composed of (in mM): NaCl (110); CsCl (5); $MgCl_2$ (0.6); Hepes (5); $BaCl_2$ (10); D-glucose (10); TEA (20 mM). The intracellular solution (pH 7.2) consisted of in (mM): CsCl (130); NaCl (10); EGTA (11); $MgCl_2$ (2); $CaCl_2$ (0.1); HEPES (10); MgATP (2). To determine the effects of the test compounds on the $Ca^{2+}$ currents cells were clamped at −80 mV and $Ca^{2+}$ currents evoked with a series of depolarising steps from −80 mV to +40 mV.

#### 41.2.3.3 Chemicals

All chemicals were from Sigma-Aldrich (Poole, UK) unless stated otherwise. All test compounds were provided by Galleon Pharmaceuticals and made up as stock solutions on the day of the experiment and diluted (DMSO) to the stated concentration in the perfusate.

#### 41.2.3.4 Data Analysis

Offline analysis was carried out using the data analysis package Clampfit 9 (Axon Instruments) and data are expressed as mean ± SEM. *P* values are from 2-tailed Student's *t*-test, where $P<0.05$ was considered significant.

## 41.3 Results

### 41.3.1 Role of the Carotid Body/Carotid Sinus Nerve in the Ventilatory Stimulant Effects of GAL-021 and GAL-160

In rats subjected to sham surgery ventilatory stimulation was evident following hypoxia ($FiO_2=0.1$, 3 min duration), and following administration of GAL-021 (0.3 mg/kg IV) or GAL-160 (0.3 mg/kg IV). When compared to responses evoked in the sham surgery animals, the ventilatory stimulant effects of hypoxia and of GAL-021 and GAL-160 were markedly inhibited (GAL-021) or virtually abolished (GAL-160, hypoxia) in rats subjected to acute carotid sinus nerve transection (Fig. 41.1).

Abrogation of the $\dot{V}_E$ increase elicited by hypoxia is confirmation that the acute carotid sinus nerve transection procedure was successful. Thus, attenuation of responses evoked by GAL-021 and GAL-160 in carotid sinus nerve transected animals suggests that afferent signaling from the carotid body to the brainstem is prerequisite for a major component of the ventilatory stimulation elicited by these agents.

### 41.3.2 GAL-021 and GAL-160 Inhibit $K^+$ Currents in Glomus Cells

Whole cell $K^+$ currents were recorded from glomus cells before and during exposure to GAL-021 (30 μM) and GAL-160 (30 μM). As shown in Fig. 41.2 GAL-021 (30 μM) and GAL-160 (30 μM) significantly inhibited outward $K^+$ currents in glomus cells. GAL-021 caused a 62.3 ± 8.8 % inhibition at +60 mV ($n=8$, $P<0.001$ compared to vehicle control), in a similar fashion GAL-160 elicited 58.6 ± 11.3 % inhibition at +60 mV ($n=12$, $P<0.005$ compared to vehicle control). Under standard recording conditions, these $K^+$ currents are composed of $BK_{Ca}$ channels and a delayed rectifier component, and the magnitude of the $BK_{Ca}$ component is determined, at least in part, by influx of $Ca^{2+}$ via voltage gated $Ca^{2+}$ channels (Peers 1990).

### 41.3.3 GAL-021 and GAL-160 Inhibit $BK_{Ca}$ Currents in Glomus Cells

To evaluate potential effects of GAL-021 and GAL-160 on the delayed rectifier component independent of the $BK_{Ca}$ component, studies were conducted in a high $Mg^{2+}$/low $Ca^{2+}$ milieu to inactivate $BK_{Ca}$. As shown in Fig. 41.3, during $BK_{Ca}$ inhibition, GAL-021 (30 μM) and GAL-160 (30 μM) do not significantly impair outward $K^+$ current, suggesting that at these concentrations their major effects are on $BK_{Ca}$. When tested

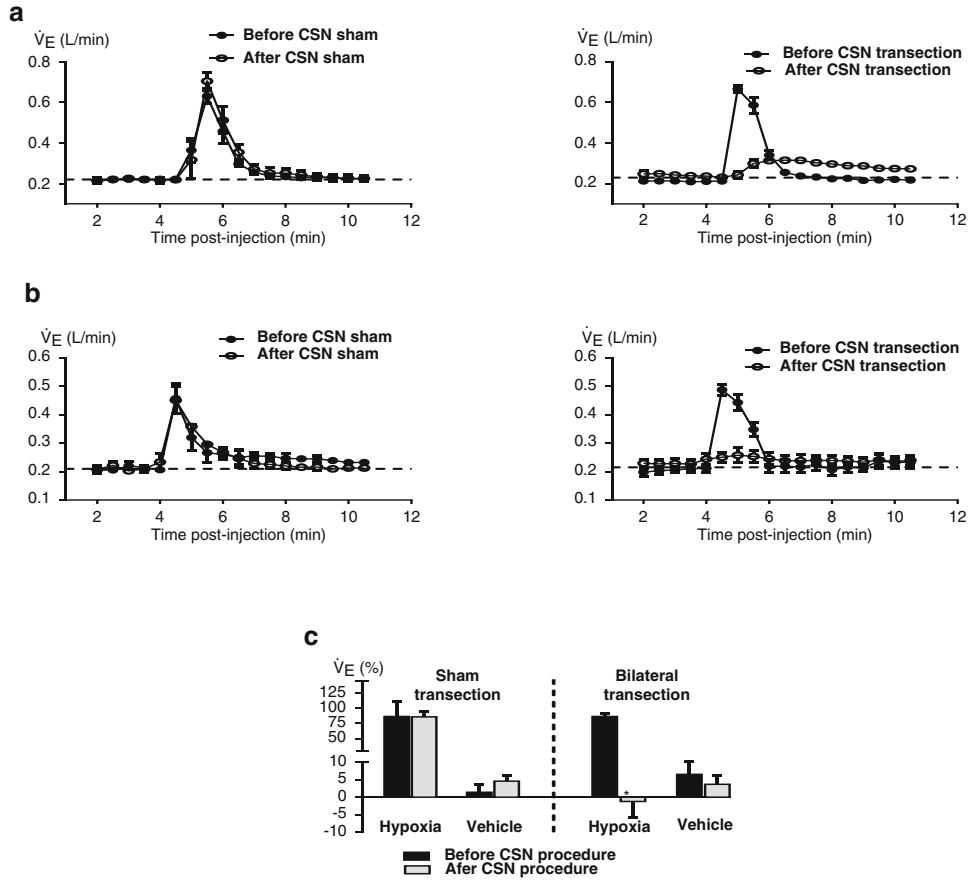


**Fig. 41.1 The effects of GAL-021, GAL-160, vehicle (saline) and hypoxia on minute ventilation in anesthetized rats before and after sham transection or bilateral transection of the carotid sinus nerve (CSN).** The ventilatory stimulant effects of GAL-021 (0.3 mg/kg IV) (**a**), GAL-160 (0.3 mg/kg IV) (**b**) and Hypoxia ($FiO_2$=0.10, 3 min duration) (**c**) were markedly reduced after denervation of the carotid bodies. * significantly different to the intact state

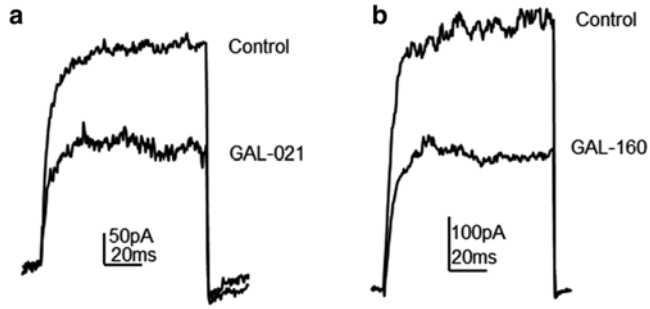


**Fig. 41.2 GAL-021 and GAL-160 inhibit whole cell $K^+$ currents in glomus cells.** (**a**) Example whole-cell $K^+$ currents evoked by a step depolarization (−80 mV to +60 mV, 100 ms) before (control) and during exposure to 30 μM GAL-021. (**b**) Example whole-cell $K^+$ currents evoked by a step depolarization (−80 mV to +60 mV, 100 ms) before (control) and during exposure to 30 μM GAL-160

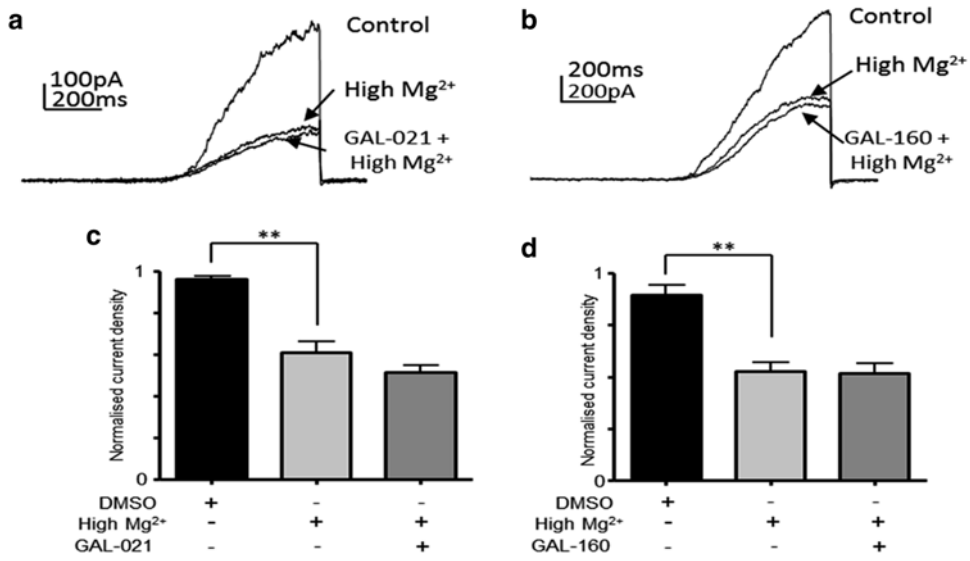


**Fig. 41.3 GAL-021 and GAL-160 inhibit $BK_{Ca}$ currents in glomus cells.** (**a**) Example traces showing ramp depolarizations (−100 mV to +60 mV, 1 s) in control, in the presence of high $Mg^{2+}$/low $Ca^{2+}$ solution (High $Mg^{2+}$) and in presence of GAL-021 and (**b**) another example utilizing GAL-160. In both examples cells were exposed initially to the high $Mg^{2+}$/low $Ca^{2+}$ solution, and then GAL-021 and GAL-160 in the continued presence of the high $Mg^{2+}$/low $Ca^{2+}$ solution. (**c**, **d**) Bar graph showing mean normalized current densities (determined at +60 mV from 4 to 6 cells in each case) and the relative effects of DMSO, high $Mg^{2+}$/low $Ca^{2+}$ solution alone, and GAL-021 and GAL-160 in the presence of high $Mg^{2+}$/low $Ca^{2+}$ solution as indicated. ** indicates $P<0.01$

at a higher concentration, modest inhibition of outward $K^+$ current by GAL-160 (100 μM) was evident (data not shown).

### 41.3.4 GAL-021 and GAL-160 Do Not Inhibit $Ca^{2+}$ Currents in Type I Cells

As, under the recording conditions utilized, $BK_{Ca}$ activity is dependent upon $Ca^{2+}$ influx (Peers 1990), it remained possible that inhibition of $BK_{Ca}$ by GAL-021 and GAL-160 could arise secondarily to effects on $Ca^{2+}$ influx. When effects on whole-cell $Ca^{2+}$ currents were measured in type I cells, neither GAL-021 (30 μM) nor GAL-160 (30 μM) altered $Ca^{2+}$ current. GAL-021 led to −5.6±4.8 % change from control (n=3, $P>0.01$, at 0 mV). GAL-160 led to a −3.9±6.1 % change from control (n=5, $P>0.01$, at 0 mV) (Fig. 41.4).

### 41.3.5 GAL-021 and GAL-160 Do Not Inhibit Leak $K^+$ Currents in Glomus Cells

Leak $K^+$ currents, carried by TASK-channels are implicated in carotid body activation by physiological stimuli, such as hypoxia (Buckler and Turner 2013; Kim et al. 2012), as well as by doxapram (Cotten et al. 2006). Moreover, small molecule TASK inhibitors are ventilatory stimulant in rats (Cotten 2013). Accordingly, we evaluated the effects of GAL-021 and GAL-160 on the $Ba^{2+}$ sensitive leak $K^+$ current in glomus cells. In comparison to vehicle (DMSO) treatment, neither GAL-021 (30 μM) nor GAL-160 (30 μM) exerted significant effects on the $Ba^{2+}$ sensitive leak $K^+$ current. In the presence of GAL-160 (100 μM), this current was significantly reduced (Fig. 41.5).

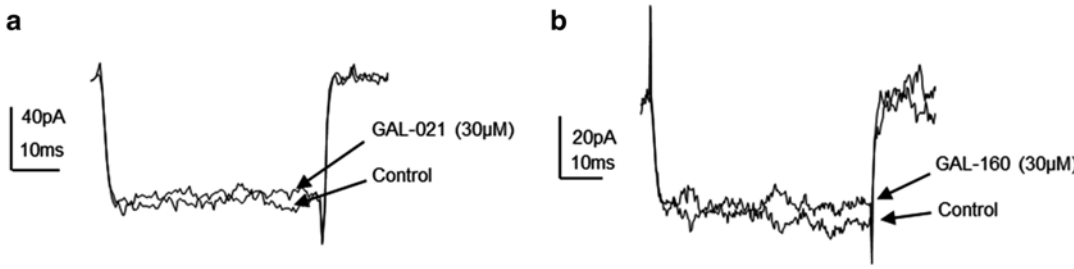


**Fig. 41.4 GAL-021 and GAL-160 do not alter $Ca^{2+}$ currents in type I cells.** (**a**, **b**) Example $Ca^{2+}$ currents recorded before and during exposure to GAL-021 (30 μM) and GAL-160 (30 μM)

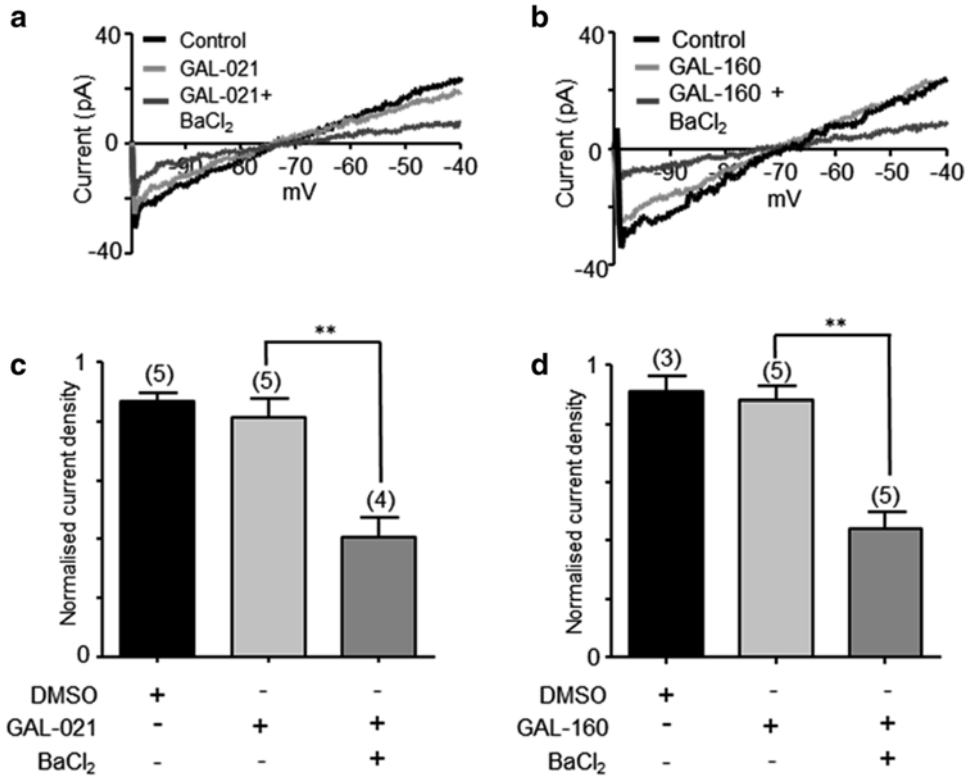


**Fig. 41.5 GAL-021 and GAL-160 do not inhibit leak $K^+$ currents in glomus cells.** (**a**, **b**) Example leak currents evoked by ramp depolarizations around the resting membrane potential (−100 mV to +40 mV) under control conditions, in the presence of (**a**) GAL-021 (30 μM) and (**b**) GAL-160 (30 μM) and in the subsequent presence of $BaCl_2$ (10 mM). (**c**) Bar graph showing mean normalized current densities and the relative effects of vehicle (DMSO), GAL-021 (30 μM) and $BaCl_2$ (10 mM) in the presence of GAL-021 (30 μM). (**d**) Bar graph showing mean normalized current densities and the relative effects of vehicle (DMSO), GAL-160 (30 μM) and $BaCl_2$ (10 mM) in the presence of GAL-160 (30 μM). Numbers of cells recorded are indicated above each bar. ** indicates $P<0.01$

## 41.4 Discussion

Marked attenuation (as with GAL-021) or abolition (as with GAL-160) of the ventilatory stimulant effects of these alkylamino triazine analogues following acute bilateral carotid sinus nerve transection in rats, allied to increases in carotid sinus nerve activity during GAL-021 administration in rats (Baby et al. 2012b) indicate that the carotid body is a/the major peripheral site of action of these agents.

Although the molecular mechanisms underlying carotid body activation are not fully understood, they are generally accepted to converge on exocytotic release of neurotransmitters (e.g. acetylcholine, dopamine, ATP, neuropeptides) some of which activate the carotid sinus nerve (Nurse 2010). Exocytosis is triggered by an elevation in the intracellular free $Ca^{2+}$ concentration. This derives predominantly via influx of extracellular $Ca^{2+}$ though L-type $Ca^{2+}$ channels, which are activated by membrane depolarization. Such depolarization is believed to arise from inhibition of certain $K^+$ channels, the expression of which varies across species (Weir et al. 2005; Peers et al. 2010). There is consensus that $BK_{Ca}$ and TASK/leak channels are expressed in rodent and human carotid bodies, although these have only been characterized electrophysiologically in glomus cells of rodents (Buckler 2007; Peers et al. 2010; Turner and Buckler 2013).

GAL-021 and GAL-160 exerted inhibitory effects on ionic currents in rat carotid body glomus cells. At 30 μM both compounds inhibited $BK_{Ca}$ currents without affecting the delayed rectifier $K^+$ current or leak $K^+$ current. At higher concentrations GAL-160 (100 μM) showed some inhibition of the delayed rectifier $K^+$ current and the leak $K^+$ current. GAL-021 and GAL-160 had no effect on the inward $Ca^{2+}$ current. Hence, the effects of both compounds on $BK_{Ca}$ cannot be secondary to an inhibition of $Ca^{2+}$ influx. Thus, these data suggest that GAL-021 and GAL-160 influence breathing control in rats by acting as peripheral chemoreceptor modulators predominantly by inhibiting $BK_{Ca}$ channels in glomus cells of the carotid body. In this regard, GAL-021 and GAL-160 share some similarity with almitrine and doxapram. Almitrine inhibits rat glomus cell $BK_{Ca}$ currents ($IC_{50} \sim 200$nM) without altering voltage dependent $K^+$, $Na^+$, or $Ca^{2+}$ currents (Peers and O'Donnell 1990; Lopez-Lopez et al. 1998). To our knowledge, the effects of almitrine on leak $K^+$ currents or TASK channels have not been tested. $BK_{Ca}$ current in rat glomus cells is also inhibited by doxapram ($IC_{50} \sim 5$ μM) (Peers 1991), which also inhibits current through cloned rat TASK channels expressed in oocytes with $IC_{50} \sim 400$nM for TASK-1 and $IC_{50} \sim 47$ μM for TASK-3 (Cotten et al. 2006).

One area of controversy regarding glomus cell $BK_{Ca}$ involvement in chemotransduction elicited by hypoxia relates to uncertainty as to whether the $BK_{Ca}$ channel contributes to glomus cell resting membrane potential under physiological conditions and whether channels are open and operative, and hence subject to modulation/inhibition, at the negative resting membrane potentials (Buckler 2007; Peers and Wyatt 2007). One might question whether this concern also applies to carotid body activation and afferent nerve signaling elicited by exogenous small molecule $BK_{Ca}$ inhibitors. Recently, there has been described a family of leucine-rich repeat containing proteins that act as auxiliary or accessory subunits, termed γ subunits, of the $BK_{Ca}$ channel. These γ subunits regulate the gating properties of $BK_{Ca}$ channels leading to channel opening even at negative resting membrane potential and, depending upon the subunit expressed, confer tissue or cell specificity in channel modulation (Yan and Aldrich 2012). Moreover, γ subunits reportedly also impact the pharmacology of channel opening, but whether they modify channel inhibition remains to be determined. The presence of γ subunits or their profile of expression in carotid body glomus cells remains to be determined. This adds an additional layer of complexity to our quest towards understanding the pharmacology and biophysics of $BK_{Ca}$ channel modulation which are already known to be influenced by the subunit composition of the channel, by splice variants in the α subunit, by the nature of the β auxiliary subunit, where β1–β4 subunits are

expressed in a tissue-specific manner, and by the basal phosphorylation status (Widmer et al. 2003; Ross et al. 2011; Hoshi et al. 2013).

In aggregate, the data suggest that $BK_{Ca}$ inhibition is a major component of the mechanism of action of GAL-021 and GAL-160, but do not preclude that additional mechanism(s) may also be operative. Whether GAL-160 affects other processes (e.g. mitochondrial bioenergetics, AMPK activation) implicated in chemoreception (Ross et al. 2011; Buckler and Turner 2013) remains to be determined. In addition, whether these actions of GAL-021 and GAL-160 on carotid body $BK_{Ca}$ channels underlie all of their effects on indices of breathing control will require more detailed correlative pharmacokinetic-pharmacodynamic studies in which biological effects at free drug concentrations in the relevant biological compartment are related to concentrations which affect electrophysiological parameters in the putatively relevant native ion channels.

**Acknowledgements** This work was supported by Galleon Pharmaceuticals, Inc.

## References

Baby SM, Gruber RB, Puskovic V, Peng S, Dax SL, Golder FJ, MacIntyre DE, Mannion JC (2012a) GAL-021, a novel respiratory stimulant, attenuates opioid-induced respiratory depression without compromising analgesia. FASEB J 26:704–728

Baby SM, Golder FJ, Peng S, Dax SL, MacIntyre DE, Mannion JC (2012b) GAL-021-induced respiratory stimulation is associated with increases in carotid sinus nerve and phrenic motoneuron activity in rats. FASEB J 26:704–729

Buckler KJ (2007) TASK like potassium channels and oxygen sensing in the carotid body. Respir Physiol Neurobiol 157:55–64

Buckler K, Honore E (2004) Molecular strategies for studying oxygen-sensitive $K^+$ channels. Methods Enzymol 381:233–257

Buckler KJ, Turner PJ (2013) Oxygen sensitivity of mitochondrial function in rat arterial chemoreceptor cells. J Physiol 591:3549–3563

Cotten JF (2013) TASK-1 (KCNK3) and TASK-3 (KCNK9) tandem pore potassium channel antagonists stimulate breathing in isoflurane anesthetized rats. Anesth Analg 116:1–16

Cotten JF, Keshavaprasad B, Laster MJ, Eger EI, Yost CS (2006) The ventilatory stimulant doxapram inhibits TASK tandem pore (K2P) potassium channel function but does not affect minimum alveolar anesthetic concentration. Anesth Analg 102:779–785

Golder FJ, Wardle RL, Van Scott MR, Hoskins PA, Dax SL, Peng S, MacIntyre DE, Mannion JC (2012) GAL-021 acts as a novel respiratory stimulant in non-human primates. FASEB J 26:704–727

Golder FJ, Hewitt MW, McLeod JF (2013) Respiratory stimulant drugs in the post- operative setting. Respir Physiol Neurobiol 189:395–402

Gruber RB, Golder FJ, MacIntyre DE (2013) GAL-021 stabilizes breathing and decreases the frequency of central apneas in morphine tolerant rats. Am J Respir Crit Care Med 187:A5681

Hewitt MM, Baby S, Golder FKJ, Mardirosian S, Peng S, MacIntyre DE (2014) GAL-160, a novel orally bioavailable modulator of breathing control, decreases the severity of obstructive apneas in rats. Sleep 37:A1 – 0004

Hoshi T, Pantazis A, Olcese R (2013) Transduction of voltage and Ca2+ signals by Slo1 BK channels. Physiology 28:172–189

Kim D (2013) $K^+$ channels in $O_2$ sensing and postnatal development of carotid body glomus cell response to hypoxia. Respir Physiol Neurobiol 185:44–56

Kim D, Cavanaugh EJ, Kim I, Carroll JL (2012) Heteromeric TASK-1/TASK-3 is the major oxygen sensitive background $K^+$ channel in rat carotid body glomus cells. J Physiol 587:2963–2975

Lopez-Lopez JR, Perez-Garcia MT, Canet E, Gonzalez C (1998) Effects of almitrine bismesylate on the ionic currents of chemoreceptor cells from the carotid body. Mol Pharmacol 53:330–339

McLeod JF, Leempoels JM, Peng SX, Dax SL, Myers LJ, Golder FJ (2014) GAL-021, a new intravenous BKCa -channel blocker is well tolerated and stimulates ventilation in health volunteers. Br J Anesth 113:875–883

Mkrtchian S, Kahlin J, Ebberyd A, Gonzalez C, Sanchez D, Balbir A, Kostuk EW, Shirahata M, Fagerlund MJ, Eriksson LI (2012) The human carotid body transcriptome with focus on oxygen sensing and inflammation - a comparative analysis. J Physiol 59:3807–3819

Nurse C (2010) Neurotransmitter and neuromodulatory mechanisms at peripheral arterial chemoreceptors. Exp Physiol 95:657–667

Peers C (1990) Hypoxic suppression of $K^+$ currents in type-I carotid body cells – selective effect on the $Ca^{2+}$ -activated $K^+$ current. Neurosci Lett 119:253–256

Peers C (1991) Effects of doxapram on ionic currents recorded in isolated type I cells of the neonatal rat carotid body. Brain Res 568:116–122

Peers C, Green FK (1991) Inhibition of Ca(2+)-activated K+ currents by intracellular acidosis in isolated type I cells of the neonatal rat carotid body. J Physiol 437:589–602

Peers C, O'Donnell J (1990) Potassium currents recorded in type I carotid body cells from the neonatal rat and their modulation by chemoexcitatory agents. Brain Res 522:259–266

Peers C, Wyatt CN (2007) The role of maxiK channels in carotid body chemotransduction. Respir Physiol Neurobiol 157:75–82

Peers C, Wyatt CN, Evans AM (2010) Mechanisms for acute oxygen sensing in the carotid body. Respir Physiol Neurobiol 174:2920–2928

Roozekrans M, van der Schrier R, Okkerse P, Hay J, McLeod JF, Dahan A (2014) Two studies on reversal of opioid-induced respiratory depression by BK-channel blocker GAL021 in human volunteers. Anesthesiology 121:459–468

Ross FA, Rafferty JN, Dallas ML, Ogunbayo O, Ikematsu N, McClafferty H, Tian L, Widmer H, Rowe ICM, Wyatt CN, Shipston MJ, Peers C, Hardie DG, Evans AM (2011) Selective expression in carotid body type I cells of a single splice variant of the large conductance calcium- and voltage-activated potassium channel confers regulation by AMP-activated protein kinase. J Biol Chem 286:11929–11936

Turner PJ, Buckler KJ (2013) Oxygen and mitochondrial inhibitors modulate both monomeric and heteromeric TASK-1 and TASK-3 channels in mouse carotid body type-1 cells. J Physiol 591:5977–5998

Weir EK, Lopez-barneo BKJ, Archer SL (2005) Acute oxygen-sensing mechanisms. N Engl J Med 353:2042–2055

Widmer HA, Rowe ICM, Shipston MJ (2003) Conditional protein phosphorylation regulates BK channel activity in rat cerebellar Purkinje neurons. J Physiol 552:379–391

Wyatt CN, Peers C (1993) Nicotinic acetylcholine-receptors in isolated type-I cells of the neonatal rat carotid-body. Neuroscience 5:275–281

Wyatt CN, Mustard KJ, Pearson SA, Dallas ML, Atkinson L, Kumar P, Peers C, Hardie DG, Evans AM (2007) AMP-activated protein kinase mediates carotid body excitation by hypoxia. J Biol Chem 282:8092–8098

Yan J, Aldrich RW (2012) BK potassium channel modulation by leucine-rich repeat-containing proteins. Proc Natl Acad Sci U S A 109:7917–7922

# The Human Carotid Body Gene Expression and Function in Signaling of Hypoxia and Inflammation

42

Jessica Kåhlin, Souren Mkrtchian, Anette Ebberyd, Lars I Eriksson, and Malin Jonsson Fagerlund

**Abstract**

Although animal carotid body oxygen sensing and signaling has been extensively investigated, the human carotid body remains essentially uncharacterized. Therefore, we aimed to study the human carotid body in terms of morphology, global and specific expression of sensing and signaling genes as well as inflammatory genes. The human carotid body response to brief or prolonged hypoxia was studied in carotid body slices from adult surgical patients and ACh, ATP and cytokine release was analyzed. We demonstrate that the human carotid body expresses key oxygen sensing and signaling genes in similarity with animal carotid bodies with a few diverging data. The human carotid body moreover shows enrichment of genes in the inflammatory response and releases pro and anti-inflammatory cytokines in response to prolonged hypoxia. In response to acute hypoxia the human carotid body releases ACh and ATP and we thus translate previous findings in animal models to human tissue. We conclude that by releasing pro- and anti-inflammatory cytokines during hypoxia the human carotid body displays a structural and functional capacity to participate in sensing and mediating systemic inflammation.

**Keywords**

Carotid body • Hypoxia • Neurotransmitter • ACh • ATP • Inflammation • Cytokine • Human • Gene expression

Lars I Eriksson and Malin Jonsson Fagerlund contributed equally.

J. Kåhlin (✉) • S. Mkrtchian • A. Ebberyd
L.I. Eriksson • M.J. Fagerlund
Department of Anesthesiology, Surgical Services and Intensive Care Medicine, Department of Physiology and Pharmacology, Section for Anesthesiology and Intensive Care Medicine, Karolinska University Hospital and Karolinska Institutet, Nanna Svartz Väg 2, 171 77 Stockholm, Sweden
e-mail: jessica.kahlin@karolinska.se

## 42.1 Introduction

As a master in global sensing of hypoxemia, the carotid body molecular structure and function has over the years been a primary focus for an array of advanced cellular and whole animal



C. Peers et al. (eds.), *Arterial Chemoreceptors in Physiology and Pathophysiology*,
Advances in Experimental Medicine and Biology 860, DOI 10.1007/978-3-319-18440-1_42

investigations. Despite considerable efforts, the prime *oxygen sensor* is still under debate and several theories prevail such as a membrane-bound, mitochondrial or metabolic origin (Kumar and Prabhakar 2012). On the other hand, there is more of consensus on the steps of the *oxygen signaling* cascade, involving down-stream sensing hypoxia-induced depolarization of the carotid body type 1 cell followed by $Ca^{2+}$-influx and subsequent release of multiple excitatory and inhibitory neurotransmitters, ultimately leading to increased sinus nerve discharge and neuronal signalling to the brain. In this context, acetylcholine (ACh) and ATP are generally accepted as primary CB excitatory neurotransmitters in most animals, although there are indications of specific species differences regarding their exact role in the carotid body signaling pathway, (Nurse 2005; Shirahata et al. 2007). Lately, there is a growing body of evidence pointing towards the carotid body as peripheral sensor of inflammation. In rodents, it is shown that cytokines and endotoxin administered intraperitoneally induce an increased expression of cytokines and cytokine receptors in the carotid body (Fernandez et al. 2011; Zhang et al. 2007). Furthermore, chronic hypoxia induces inflammatory changes in the carotid body with increased mRNA expression of pro-inflammatory cytokines and their corresponding receptors (Lam et al. 2008).

In contrast to the major advances in the field of carotid body function in animal models (also in relation to evolving cardiorespiratory disease) the *human* carotid body remains largely unexplored. With its vital and intricate location in the bifurcation of the carotid artery, the human carotid body has previously been mainly investigated in post mortem-tissue, revealing detection of dispersed receptors and proteins. In a recent publication, it was demonstrated that human carotid body tissue exposed to hypoxia releases neurotransmitters dependent on $Ca^{2+}$ influx in type 1 cells but the identity of such neurotransmitters is unknown (Ortega-Saenz et al. 2013).

In a series of three consecutive studies we have characterized human carotid body oxygen sensing and signaling molecules and function by investigating freshly harvested human carotid bodies from surgical patients targeting morphology and global as well as specific expression of human genes in oxygen sensing and signaling and release of specific neurotransmitters in response to hypoxia. We further examined the human carotid body in relation to inflammation by comparing the human carotid body inflammatory transcriptome to that of other species and by analyzing cytokine release in response to extended hypoxia.

## 42.2 Methods

### 42.2.1 Patients

After institutional human ethical committee approval at the Karolinska Institutet, we identified a group of patients for this project where denervation of the carotid body by the surgery was a prerequisite for removal of the carotid body. All patients included in the studies were scheduled for a modified radical neck dissection due to head and neck malignancies where the surgical procedure with a removal of all lymph nodes and muscle, nerve, gland and vascular tissue within several of the regions of the neck leaves the carotid body with no remaining innervation.

We included thirteen male and one female patient 36–80 years of age with a body mass index of $26 \pm 6$, with no severe cardio-pulmonary disease (New York Heart Association >3) or neurological disorder, not exposed to radiation therapy and with no tumor involvement of the carotid body. After written consent, the carotid body was removed unilaterally during sevoflurane and opioid-based general anesthesia at normoxia and normocarbia as provided by mechanical ventilation during the whole surgical procedure (Fagerlund et al. 2010; Kahlin et al. 2014; Mkrtchian et al. 2012).

### 42.2.2 Descriptive Analysis

Immediately after surgical removal the carotid body was placed in pre-oxygenated Krebs Ringer

Solution (KRS) and further analyses were ensued within 15 min of removal.

Fixated and frozen carotid body tissue was sectioned and stained with Hematoxylin-Eosin to evaluate morphology and immunohistochemistry (IHC) with appropriate antibodies was used to demonstrate protein expression in the human carotid body, as described previously (Fagerlund et al. 2010). Snap-frozen carotid body tissue was studied with microarray and PCR to evaluate global and specific gene expression (Mkrtchian et al. 2012). With computational models the human carotid body transcriptome was compared to carotid body transcriptomes from two mouse strains (Balbir et al. 2007; Ganfornina et al. 2005) and to transcriptomes of functionally related tissues in order to define the global human carotid body transcriptome and to demonstrate enrichment of specific gene groups (Mkrtchian et al. 2012).

### 42.2.3 Functional Analysis

Fresh carotid body tissue incubated in pre-oxygenated KRS after extraction was exposed to either brief (5-min) or prolonged (60-min) hypoxia to detect subsequent release of ACh and ATP as measured with high performance liquid chromatography (HPLC) and inflammatory signalling molecules using a Luminometric assay, respectively and as described earlier (Kahlin et al. 2014).

## 42.3 Results

### 42.3.1 The Human Carotid Body Transcriptome

We found that the human carotid body expresses approximately 13,500 genes, which is comparable to the number of genes expressed in most human tissues, but larger in comparison to earlier findings in the mouse carotid body transcriptome showing around 10,000 genes (Balbir et al. 2007; Ganfornina et al. 2005). This is indicative of a proposed higher complexity in the human carotid body.

In comparison with human adrenal gland and brain, the carotid body overexpresses genes in inflammation and angiogenesis and in single comparison to adrenal gland the human carotid body shows a distinct neurological profile with up-regulation of genes in neurological processes. The differential expression of selected genes in comparison with the two mouse carotid body transcriptomes revealed a similar expression pattern albeit with a few specific discrepancies (Fagerlund et al. 2010; Mkrtchian et al. 2012).

### 42.3.2 Human Carotid Body Oxygen Sensing and Signaling

Microarray and PCR analysis revealed specific human carotid body mRNA expression of genes proposed to be involved oxygen sensing (Table 42.1). In oxygen sensing the human carotid body expresses key oxygen sensing $K^+$ channels and genes involved of the standard theories on the oxygen sensing mechanism (Table 42.1). The specific expression is in line with corresponding data on animal carotid body chemosensory genes with divergence for TASK-1 and the $H_2S$-synthesizing enzyme cystathionine γ-lyase (CSE), being expressed in the human carotid body but not when comparing one or both mouse strain.

Using PCR we discovered that the human carotid body exclusively expresses the more hypoxia sensitive ZERO isoform of the $O_2$-sensitive $K^+$ channel Maxi-K, whereas rat carotid bodies express both Maxi-K isoforms (Ross et al. 2011).

In the oxygen signaling pathway, $GABA_A$, nicotinic ACh and purine receptors and receptor subunits were demonstrated as well as the dopamine $D_2$ receptor (Table 42.1).

When testing carotid body *functionality* in our ex vivo model of brief acute hypoxia, we demonstrate an approximately three-fold instantaneously increased release of the neurotransmitters ACh and ATP from human carotid body slices. The levels of ACh and ATP returned to baseline

**Table 42.1** A schematic presentation of our findings in the human carotid body where p is present, a absent and u uncertain due to conflicting results from multiple probe sets and unfilled not studied or not applicable

| Functional group | Gene | | mRNA | | Protein | Hypoxia induced release |
|---|---|---|---|---|---|---|
| | | | Microarray | PCR | IHC | HPLC, ATP-assay, multiplex |
| Oxygen sensing | AMPK | | p | p | | |
| | HO-2 | | p | p | p | |
| | NOX-2 | | p | p | | |
| | NOX-4 | | p | | | |
| | SOD-2 | | p | | | |
| | CAT | | p | | | |
| | CSE | | p | p | | |
| | CBS | | u | p | | |
| | HIF-1α | | p | | p | |
| | HIF-2α | | p | | p | |
| | NOS-1 | | u | | | |
| | NOS-2 | | a | | | |
| | NOS-3 | | a | | | |
| K+−channels | TASK-1 | | p | p | p | |
| | BK (Maxi-K) | | p | p | p | |
| | Kv 1.5 | | p | | | |
| | Kv 2.1 | | p | | | |
| Oxygen signaling | ACh | | | | | ↑ |
| | ATP | | | | | ↑ |
| | nAChR | α3 | p | p | p | |
| | | α7 | a | p | p | |
| | | β2 | a | p | p | |
| | GABAA | α2 | p | p | p | |
| | | β3 | p | p | p | |
| | | γ2 | a | a | p | |
| | GABAB1 | | p | | | |
| | A2A | | p | p | p | |
| | P2X2 | | a | p | p | |
| | D2 | | p | p | p | |
| Inflammatory response | Mediators | IL-1α | a | | | |
| | | IL-1β | p | | | ↑ |
| | | IL-4 | a | | | ↑ |
| | | IL-6 | p | | | ↑ |
| | | IL-8 | p | | | ↑ |
| | | IL-10 | a | | | ↑ |
| | | HMGB1 | p | | | |
| | | NFkB | p | | | |
| | Receptors | IL-1R1 | p | | p | |
| | | IL-6R | p | | p | |
| | | IL-10RA | p | | p | |
| | | TLR1 | p | | | |
| | | TLR4 | p | | a | |
| | | TNF-R1A | p | | | |
| | | TNF-R1B | p | | | |
| | | TGFB-R1 | p | | a | |

The abbreviations are explained in the corresponding publication (Fagerlund et al. 2010; Kahlin et al. 2014; Mkrtchian et al. 2012)

following 15 min of re-oxygenation (Kahlin et al. 2014).

### 42.3.3 Human Carotid Body Inflammation Sensing and Signaling

In comparison with functionally related tissues the human carotid body overexpressed genes in the inflammatory response and we could demonstrate specific gene and protein expression of inflammatory signaling molecules and corresponding receptors (see Table 42.1).

The release of a multitude of cytokines was monitored from human carotid body slices exposed to prolonged hypoxia for 1 h. Release of the cytokines IL-1β, IL-4, IL-6, IL-8 and IL-10 was induced by prolonged hypoxia (Kahlin et al. 2014).

## 42.4 Discussion

In a series of studies on the human carotid body the global human carotid body transcriptome was characterized and specific oxygen sensing and signaling as well as inflammatory response gene expression was uncovered. Besides comparative analysis of human and rodent morphology and gene expression, we also demonstrate that the human carotid body releases classical neurotransmitters such as ACh and ATP as well as key inflammatory signalling molecules in response to more prolonged hypoxia.

Oxygen sensing and signaling is preserved and refined during evolution from dispersed sensors in fish to primary chemosensors along the major arteries in higher species (Milsom and Burleson 2007). Through multiple water and land-living species, sensing of acute hypoxia serves to rapidly reverse an adverse chemostimuli by eliciting purposeful hyperventilation and appropriate cardiovascular responses to regain adequate oxygenation.

The mechanism of oxygen sensing remains an enigma although a number of plausible different molecular oxygen sensors have been suggested by animal experiments. Gene expression of the components of the dominating oxygen sensing theories emerging from animal studies is now also demonstrated in the human carotid body. Apart from a limited number of detected differences, for example $K^+$ channel splicing and identity of the $H_2S$-synthesizing enzyme, the expression patterns of oxygen sensing genes in rodent and human carotid body were comparable, suggesting an oxygen sensing mechanism that can be translated between species. The oxygen signaling cascade in the human carotid body includes ACh and ATP release. In line with the demonstrated presence of nicotinergic, purinergic, GABA-ergic and dopaminergic receptors in the human carotid body it is likely that a combination of excitatory and inhibitory neurotransmitters exert effects on their corresponding receptors in a direct, autocrine and/or paracrine manner. This would result in the balanced "push-pull" mechanism in carotid body activity proposed in animals (Prabhakar 2006). Considering the extensive similarities in human and animal carotid body molecular structure and function it seems reasonable to extrapolate animal data to humans given the restriction in available fresh carotid body tissue. This deficit is related to the small size and complex location of the organ and the conjunction with sparse type 1 cell cluster distribution and low RNA-yield in the human carotid body calls for a complementary animal model.

There is a growing body of evidence for a role of the carotid body in immune-to-brain signaling. The carotid body is located strategically to sense and transfer information on inflammatory molecules to the central nervous system with cardiorespiratory responses as a consequence. Systemic endotoxin induces tachypnea, tachycardia and hypotension in cats while these physiological responses was attenuated after neurotomy of the carotid sinus nerve (Fernandez et al. 2008). This finding underscores the potential relay function of the carotid body between the peripheral immune system and the brain. This connection may be important in early stages of inflammation by inducing appropriate cardiorespiratory responses, supported by findings in rodents

where rats following carotid sinus denervation exhibit a shorter survival time in endotoxin-induced sepsis (Tang et al. 1998).

Our findings of release of the pro- and anti-inflammatory cytokines IL-1β, IL-4, IL-6, IL-8 and IL-10 from the human carotid body upon extended hypoxia most importantly suggest a paracrine rather than endocrine function. Combined with the demonstration of corresponding receptors and over-expression of genes in the inflammatory response and expression of several early and late inflammatory mediators (Kahlin et al. 2014; Mkrtchian et al. 2012), we believe that fundamental prerequisites for an immune-to-brain signalling link are established in the human carotid body.

In addition, carotid body inflammation may also have a role in the progression of pathology in obstructive sleep apnea (OSA) (Fung 2014). In OSA, repetitive upper airway obstruction causing chronic intermittent hypoxia induces up-regulation of cytokine gene expression, corresponding cytokine receptors and an imbalance in the levels of hypoxia inducible factor subunits, resulting in augmentation of carotid body chemoreceptor output (Prabhakar and Semenza 2012). OSA is furthermore an independent risk factor for systemic hypertension (Diogo and Monteiro 2014) and an intact carotid body chemoreceptor response is a prerequisite for the development of hypertension in animal models of chronic intermittent hypoxia (Diogo and Monteiro 2014; Fletcher et al. 1992). Altogether, there is a need for further studies in both animals and humans to further elucidate the role of the carotid body in the pathogenesis of OSA in order to predict complications such as hypertension, and to find targets for future pharmacological and non-pharmacological treatment of OSA.

In conclusion, we have described human carotid body morphology, gene expression and hypoxia induced neurotransmitter and cytokine release. We found many similarities in the expression of key genes in oxygen and inflammation sensing and signaling. Finally, the human carotid body contains the essential components and functions to be a sensor and mediator of systemic inflammation.

## References


Balbir A, Lee H, Okumura M, Biswal S, Fitzgerald RS, Shirahata M (2007) A search for genes that may confer divergent morphology and function in the carotid body between two strains of mice. Am J Physiol Lung Cell Mol Physiol 292(3):L704–L715

Diogo LN, Monteiro EC (2014) The efficacy of antihypertensive drugs in chronic intermittent hypoxia conditions. Front Physiol 5:361. doi:10.3389/fphys.2014.00361

Fagerlund MJ, Kahlin J, Ebberyd A, Schulte G, Mkrtchian S, Eriksson LI (2010) The human carotid body: expression of oxygen sensing and signaling genes of relevance for anesthesia. Anesthesiology 113(6):1270–1279

Fernandez R, Gonzalez S, Rey S et al (2008) Lipopolysaccharide-induced carotid body inflammation in cats: functional manifestations, histopathology and involvement of tumour necrosis factor-alpha. Exp Physiol 93(7):892–907. doi:10.1113/expphysiol.2008.041152

Fernandez R, Nardocci G, Simon F et al (2011) Lipopolysaccharide signaling in the carotid chemoreceptor pathway of rats with sepsis syndrome. Respir Physiol Neurobiol 175(3):336–348. doi:10.1016/j.resp.2010.12.014

Fletcher EC, Lesske J, Behm R, Miller CC 3rd, Stauss H, Unger T (1992) Carotid chemoreceptors, systemic blood pressure, and chronic episodic hypoxia mimicking sleep apnea. J Appl Physiol (Bethesda, Md : 1985) 72(5):1978–1984

Fung ML (2014) Pathogenic roles of the carotid body inflammation in sleep apnea. Mediators Inflamm 2014:354279. doi:10.1155/2014/354279

Ganfornina MD, Perez-Garcia MT, Gutierrez G et al (2005) Comparative gene expression profile of mouse carotid body and adrenal medulla under physiological hypoxia. J Physiol 566(Pt 2):491–503

Kahlin J, Mkrtchian S, Ebberyd A et al (2014) The human carotid body releases acetylcholine, ATP and cytokines during hypoxia. Exp Physiol 99(8):1089–1098. doi:10.1113/expphysiol.2014.078873

Kumar P, Prabhakar NR (2012) Peripheral chemoreceptors: function and plasticity of the carotid body. Compr Physiol 2(1):141–219. doi:10.1002/cphy.c100069

Lam SY, Tipoe GL, Liong EC, Fung ML (2008) Chronic hypoxia upregulates the expression and function of proinflammatory cytokines in the rat carotid body. Histochem Cell Biol 130(3):549–559. doi:10.1007/s00418-008-0437-4

Milsom WK, Burleson ML (2007) Peripheral arterial chemoreceptors and the evolution of the carotid body. Respir Physiol Neurobiol 157(1):4–11. doi:10.1016/j.resp.2007.02.007

Mkrtchian S, Kahlin J, Ebberyd A et al (2012) The human carotid body transcriptome with focus on oxygen sensing and inflammation–a comparative analysis. J

Physiol 590(Pt 16):3807–3819. doi:10.1113/jphysiol.2012.231084

Nurse CA (2005) Neurotransmission and neuromodulation in the chemosensory carotid body. Auton Neurosci 120(1–2):1–9

Ortega-Saenz P, Pardal R, Levitsky K et al (2013) Cellular properties and chemosensory responses of the human carotidbody.JPhysiol.doi:10.1113/jphysiol.2013.263657

Prabhakar NR (2006) O2 sensing at the mammalian carotid body: why multiple O2 sensors and multiple transmitters? Exp Physiol 91(1):17–23

Prabhakar NR, Semenza GL (2012) Adaptive and maladaptive cardiorespiratory responses to continuous and intermittent hypoxia mediated by hypoxia-inducible factors 1 and 2. Physiol Rev 92(3):967–1003. doi:10.1152/physrev.00030.2011

Ross FA, Rafferty JN, Dallas ML et al (2011) Selective expression in carotid body type I cells of a single splice variant of the large conductance calcium- and voltage-activated potassium channel confers regulation by AMP-activated protein kinase. J Biol Chem 286(14):11929–11936. doi:10.1074/jbc.M110.189779

Shirahata M, Balbir A, Otsubo T, Fitzgerald RS (2007) Role of acetylcholine in neurotransmission of the carotid body. Respir Physiol Neurobiol 157(1):93–105

Tang GJ, Kou YR, Lin YS (1998) Peripheral neural modulation of endotoxin-induced hyperventilation. Crit Care Med 26(9):1558–1563

Zhang XJ, Wang X, Xiong LZ, Fan J, Duan XL, Wang BR (2007) Up-regulation of IL-1 receptor type I and tyrosine hydroxylase in the rat carotid body following intraperitoneal injection of IL-1beta. Histochem Cell Biol 128(6):533–540. doi:10.1007/s00418-007-0346-y

# The Carotid Body Does Not Mediate the Acute Ventilatory Effects of Leptin

43

E. Olea, M.J. Ribeiro, T. Gallego-Martin, S. Yubero, R. Rigual, J.F. Masa, A. Obeso, S.V. Conde, and C . Gonzalez

**Abstract**

Leptin is a hormone produced mostly in adipose tissue and playing a key role in the control of feeding and energy expenditure aiming to maintain a balance between food intake and metabolic activity. In recent years, it has been described that leptin might also contributes to control ventilation as the administration of the hormone reverses the hypoxia and hypercapnia commonly encountered in ob/ob mice which show absence of the functional hormone. In addition, it has been shown that the carotid body (CB) of the rat expresses leptin as well as the functional leptin-B receptor. Therefore, the possibility exists that the ventilatory effects of leptin are mediated by the CB chemoreceptors. In the experiments described below we confirm the stimulatory effect of leptin on ventilation, finding additionally that the CB does not mediate the instant to instant control of ventilation.

**Keywords**

Leptin • Carotid body • Ventilation • Catecholamine hypoxia

## 43.1 Introduction

Leptin is a hormone expressed in adipose tissue and secreted in direct proportion to adipose tissue mass (Cao 2014). Leptin function is to adjust food intake to energy expenditure. Circulating

E. Olea (✉) • T. Gallego-Martin • S. Yubero
R. Rigual • A. Obeso • C. Gonzalez
Department of Biochemistry, Molecular Biology and Physiology, Medicine School, University of Valladolid and IBGM/CSIC, Valladolid, Spain

CIBERES. Instituto de Salud Carlos III, Madrid, Spain
e-mail: olea@ibgm.uva.es

M.J. Ribeiro • S.V. Conde
Chronic Diseases Research Center (CEDOC), Nova Medical School Faculdade Ciências Médicas, University of Nova Lisboa, Lisbon, Portugal

J.F. Masa
CIBERES. Instituto de Salud Carlos III, Madrid, Spain

Pulmonary Division, Hospital San Pedro de Alcántara, Cáceres, Spain


C. Peers et al. (eds.), *Arterial Chemoreceptors in Physiology and Pathophysiology*, Advances in Experimental Medicine and Biology 860, DOI 10.1007/978-3-319-18440-1_43

leptin traverses blood brain barrier and reaches all peripheral tissues. Acting centrally, leptin tends to decrease food intake activating hypothalamic satiety centers, and acting peripherally facilitates nutrients oxidation. Centrally, leptin also activates the sympathetic system (acting at the nucleus arcuatus and at the nucleus tractus solitarius (NTS; Mark 2013), and this activation also contributes to augment the oxidative metabolism in peripheral tissues (Aguer and Harper 2012) as well as to augment blood pressure and to create a certain status of insulin resistance. Also, recent research has been published concerning the role of leptin in the respiratory system, with leptin's involvement in the most common disorders of the respiratory system including obstructive sleep apnoea-hypopnoea syndrome (OSAHS), asthma, chronic obstructive pulmonary disease (COPD) and lung cancer (Malli et al. 2010).

The CB are small arterial chemoreceptor organs which sense blood $O_2$ and $CO_2$/pH levels and are formed by clusters of cells surrounded by a dense net of capillaries that facilitates the presentation of the blood-borne stimuli to chemoreceptor cells. Chemoreceptor cells are synaptically connected with the sensory nerve endings of the carotid sinus nerve (CSN), whose central projections terminate in the brainstem, in the nucleus of solitary tract (Katz et al. 1997; Gonzalez et al. 1994), and activate adaptive responses in the respiratory and cardiovascular systems, involving also the participation of endocrine and sympathetic nervous systems (Kumar 2009). Models of CB functioning consider that chemoreceptor express $O_2$-sensor(s) which are coupled to certain $K^+$ channels in such a manner that a decrease in $PO_2$ leads to inhibition of $K^+$ channels, cell depolarization, activation of voltage dependent $Ca^{2+}$ channels, and augmentation of the release of neurotransmitters. These drive the chemoreceptor cell-nerve ending synapses to an increase in the action potential frequency in the CSN (see González et al. 1992, 2009; Peers 1997; Kemp 2005). The end result being that in hypoxia (or in hypercapnia/acidosis) the initiation of cardio respiratory reflexes, most significantly hyperventilation, aimed to normalize arterial blood gases.

Recently, two different laboratories have demonstrated the presence of leptin and leptin receptors ObRb in the CB chemoreceptor cells (Porzionato et al. 2011; Messenger and Ciriello 2013; Messenger et al. 2013). This fact, combined with the observation that increased circulating leptin levels induce the expression of phosphorylated signal transducer and activator of transcription 3 (pSTAT3) and the immediate early gene Fra-1 within these chemoreceptor cells (Messenger et al. 2012) suggest that leptin may play an important role in modulating CB function, and thereby ventilation. Along these lines, it has been observed administration of leptin have increases ventilation (Inyushkin et al. 2009; O'Donnell et al. 1999; Chang et al. 2013). In this context, the aim of our study has been to investigate the contribution of the CB to the ventilatory responses elicited by leptin. To achieve this aim, we have combined *in vivo* and *in vitro* experiments to explore effects of leptin on ventilation and direct effects of leptin in the CB chemoreceptor cells.

## 43.2 Methods

### 43.2.1 Animals and Anesthesia

Experiments were performed in adult Wistar rats 12 weeks of age following the European Community Council directive of 24 of November 1986 (86/609/EEC) for the Care and Use of Laboratory Animals. Rats were housed four per cage, with free access to food and water and maintained in the vivarium of the University of Valladolid and at the vivarium of NOVA Medical School under controlled conditions of temperature and humidity and a stationary light–dark cycle.

### 43.2.2 Intravenous Administration of Leptin in Anaesthetised Animals

Animals were anaesthetized with sodium pentobarbital (60 mg/kg, i.p.) dissolved in physiological saline. Anaesthetized rats were given

intravenous boluses of leptin at doses of (300, 600 and 900 ng/Kg) spaced 15 min from each other.

We recorded respiratory frequency (bpm) and tidal volume (TV, ml/kg) and basal minute ventilation (ml/kg/min) was calculated. The stimulation of the CB was achieved by 5 and 15 s of carotid bilateral occlusion applied immediately prior to each leptin injection and 15 min after the last. The 5 s occlusion would represent an almost pure hypoxic stimulus while the 15 s occlusion would be more an ischemic stimulus combining hypoxia, hypercapnia and acidosis in the CB and likely some central effects (Monteiro et al. 2011). We performed a bilateral carotid occlusion during 5 and 15 s prior to leptin infusions. Once recovered basal respiratory patterns a blood sample was taken to measure blood glucose and leptin levels; leptin was assayed by an ELISA provided by Cusabio Biotech; bioNova Cientifica, Madrid, Spain, following the instructions of the supplier**.** Blood pressure and heart rate was continuously monitored all along the experiments.

### 43.2.3 $^{3}$H-Catecholamine ($^{3}$H-CA) Release Experiments Using Freshly Isolated Intact CBs

General procedures used to label chemoreceptor cells $^{3}$H-catecholamine ($^{3}$H-CA) (CA) deposits and later to study their release have been described in previous publications (Vicario et al. 2000; Gonzalez-Martín et al. 2011). And analytical methods have been described in detail in Conde et al. (2006). The experiments included pairs of control *vs.* experimental CBs. Solutions were pre-equilibrated at 37 °C with a water vapour-saturated gas mixture (21 % $O_2$, normoxia, or 7 % $O_2$, hypoxic stimulation, 5 % $CO_2$, balanced $N_2$) and all along the experiments the vials atmospheres were gassed with the same gas mixture. Hypoxic and depolarizing stimuli consisted of 10 min incubations, with low $PO_2$-equilibrated (7 % $O_2$; $PO_2 \approx 46$ mmHg) and high $K^+$-containing solutions (35 mM; equiosmolar $Na^+$ was removed). Control organs were stimulated with the hypoxic and high external potassium stimulus and experimental CBs were similarly stimulated but the solutions contained 40 ng of leptin from 20 min before hypoxic stimulation and leptin was kept until the end of the experiments. Data were presented as means ± SEM of release evoked (% content). Statistical significance of differences was assessed using a two-tailed t-test for unpaired data.

## 43.3 Results

### 43.3.1 Effects of Leptin in Ventilation

Figure 43.1a depicts typical recordings of respiratory rate and TV in basal conditions and in response to ischemic hypoxia, induced by occlusions of common carotid artery (CCO) lasting 5 and 15 s in a control rat. Recordings were made before any leptin injection and 15 min after leptin bolus injection (300 ng/Kg). Control MV amounting to 365.2 ± 26.67 mL/min/kg was dose-dependently increased by leptin (Fig. 43.1b). Leptin increased in about the same percentage breathing frequency and TV. Figure 43.1c shows the increase in MV produced by bilateral carotid artery occlusions during 5 and 15 s. Note that the 5 s occlusion augmented MV by approximately by around 50 % and again leptin, injected 15 min in advance, further increased ventilation in a dose-related manner reaching 25–30 % with the highest dose employed. Fifteen seconds occlusion augmented MV by over 150 % and again leptin augmented the occlusion effect.

### 43.3.2 Plasma Leptin and Glucose Levels

Figure 43.2a depicts the levels of leptin found in blood during our experimental protocol. As it can be seen, the basal leptin levels were 11.3 ± 2.0 ng/ml (n = 6), being these levels surprisingly higher than the levels reported by other laboratories (2.2 ng/ml, Zeng et al. 1997; ca. 2 ng/ml, Simler et al. 2007; 0.78 ng/ml, Chaiban et al. 2008; ca. 4 ng/ml, Messenger et al. 2012). In additional studies from our laboratory and using ELISA kits of the same suppliers we have obtained the basal

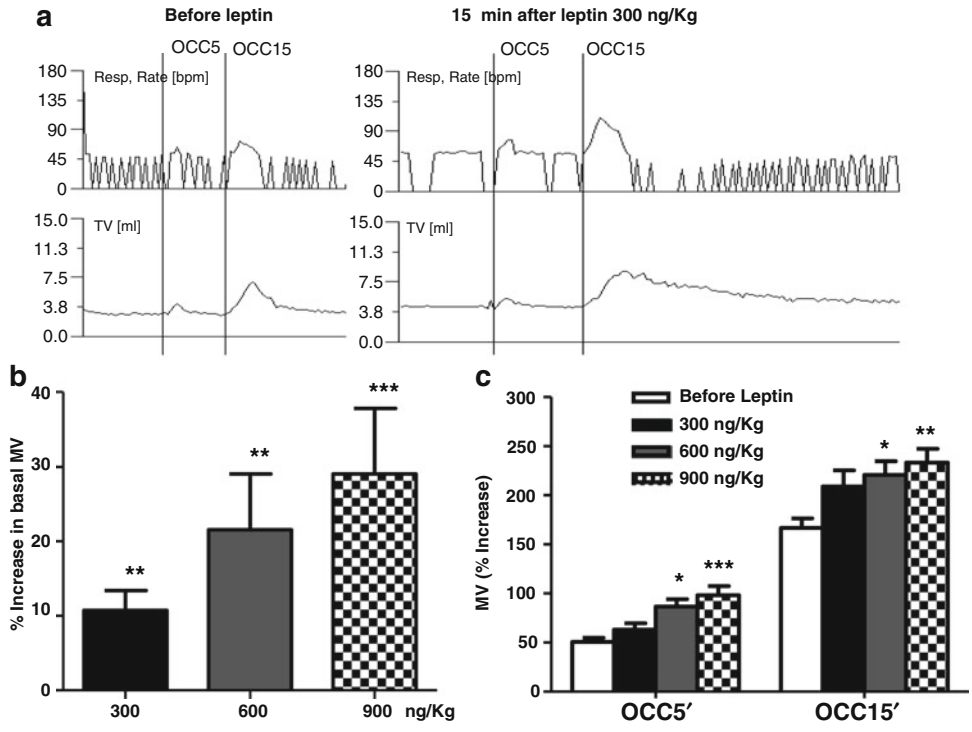


**Fig. 43.1** (**a**) Typical recordings of respiratory rate (Resp. Rate) (bpm) and tidal volume (TV; mL), in basal conditions and in response to ischemic hypoxia, induced by occlusions of common carotid arteries (*CCO*) in a control rat. Recording was made before and after leptin infusion. (**b**) Percent increase in basal (normoxic) ventilation after leptin infusion in awake control rat. (**c**) MV (% increase) resulting from both common carotid arteries occlusion (*CCO*) in basal conditions and after leptin infusions. Data are means ± SEM of eight individual values (*p < 0.05, ** p < 0.01, ***p < 0.001)

levels of leptin found have been 8.9 ± 0.5 ng/ml (Olea et al. 2014) being these values statistically identical to the values found in the present study.

Also, herein we found that with increasing doses of leptin there was a trend for the hormone levels to increase, although only with the highest dose of leptin infused the levels reached a statistical significance (16.8 ± 2.8 ng/ml; n = 6; p = 0.05). None of the doses of leptin tested in the present study altered glycaemia (Fig. 43.2b).

### 43.3.3 Leptin Does Not Activate Basal Nor Hypoxic and High $K^+$ Induced Release of $^3H$ Catecholamine in CBs

Figure 43.3a, b show the general protocol and mean time course of $^3H$-CA release experiments in four control and in four experimental CBs incubated with leptin (40 ng/ml) as marked by dashed bars. No apparent differences were observed in the time course of $^3HCA$ release in control vs. experimental organs, being the transition of the release from the leptin-free to leptin-containing media identical to control CBs. Similarly, the hypoxia and high $K^+$ induced release showed no apparent differences in the time course or in the magnitude of the evoked responses (Fig. 43.3b).

## 43.4 Discussion

Herein we have found that leptin increased spontaneous and ischemic hypoxia-induced ventilation in a dose-dependent manner although without affecting basal or stimuli-evoked catecholamines release from the CB. Leptin is a pleiotropic hormone whose actions extend from

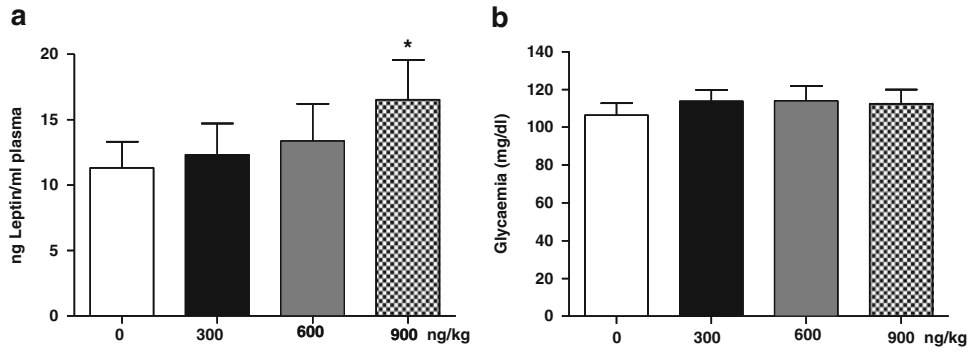


**Fig. 43.2** Plasma leptin levels (**a**) and glycaemia (**b**) in basal conditions and after leptin infusions. Means ± SEM of six individual values (*p = 0.05)

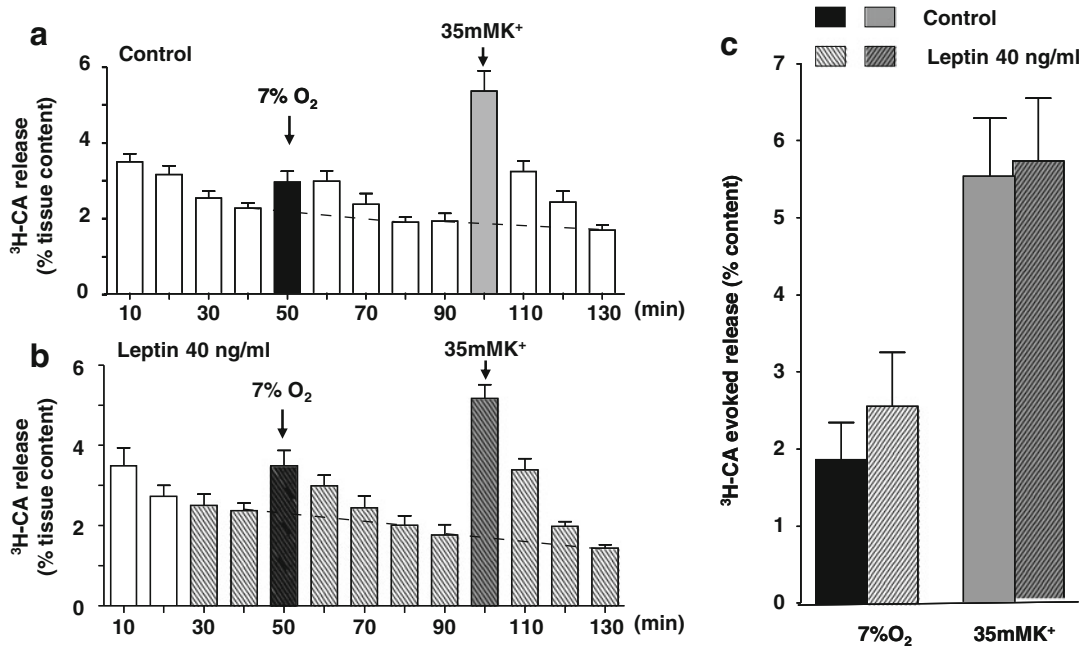


**Fig. 43.3** (**a**) and (**b**) show the time course of the release of $^{3}$H-catecolamines by the CB of control rats in control incubating solution (**a**) and in solution containing leptin (40 ng/ml; **b**). (**c**) shows the evoked release of $^{3}$H-catecolamines induced by hypoxia and high external K+

immune system homeostasis to reproduction and angiogenesis, but in the past years, a growing number of studies have examined the potential role of leptin in the respiratory system (Malli et al. 2010). These studies further suggest a significant impact of leptin on specific respiratory diseases, indicating that the pathophysiological significance of leptin regarding respiratory function in humans remains to be clarified.

Early on, obesity and leptin lack in *ob/ob* mice was related to hypoventilation encountered in obese humans, with its maximal expression in the obesity hypoventilation syndrome (Pickwick syndrome) defined by the combination of obesity, night hypoxia and permanent hypercapnia (Bickelmann et al. 1956; see Olson and Zwillich 2005).

Laboratory studies of O'Donnell and colleagues in animal models have provided evidence

indicating that systemic administration of leptin to leptin deficient Ob/Ob mice increased breathing frequency, tidal volume and minute ventilation, also leading to a significant decrease in the pre-treatment elevated arterial $P_aCO_2$ when compared to wild-type mice (O'Donnell et al. 1999). Also, quite recently it has been shown that systemic intravenous administration of leptin in rats also augments ventilation in a $CO_2$-independent manner (Chang et al. 2013).

These results along with the fact that has been demonstrated the presence of leptin and leptin receptors ObRb in the CB chemoreceptor cells (Porzionato et al. 2011; Messenger and Ciriello 2012; Messenger et al. 2013) suggested that leptin might control ventilation via the CB.

In this work, we have found that administration of leptin in anaesthetised animals augmented basal VE and potentiated the ischemic hypoxia-induced VE in a dose-dependent manner, with a latency of several min (6–8 min) and a long lasting effect (≥15 min). We should mention that the dose of leptin administered to our animals is low as evidenced by the slight modifications of basal leptin levels. In this regard we should clarify that the experiments were designed based on the lower basal leptin levels reported in the literature (Zeng et al. 1997; Simler et al. 2007; Chaiban et al. 2008; Messenger et al. 2012) and the thorough study on whole body leptin kinetics and renal metabolism in vivo by Zeng et al. (1997).

These findings indicate that leptin does indeed augment the ventilatory responses elicited by hypoxia as well as basal ventilation. To explore direct effects of leptin in the CB, we studied in vitro the time course of the release of $^3$H-CA using intact CBs, and we observed that leptin at concentrations ×4 basal endogenous levels does not affect the release of $^3$H-CA either in basal conditions or during hypoxic or high external $K^+$. Owing that the release of CA is very reliable index of chemoreceptor cell activation (González et al. 1992) data would indicate that leptin must exert its ventilatory effects acting centrally, probably at the nucleus of the tractus solitarious where the sensory nerve of the CB projects and where Ciriello and Moreau (2013) have demonstrated the existence a set of neurons that expressing leptin receptors receive inputs from CB chemoreceptors. It is worth noting, that these neurons expressing leptin receptors project to the vasopressor sites of the rostroventrolateral medulla, and thereby contribute with the hypothalamic nuclei with neurons (arcuate, ventromedial, paraventricular and dorsomedial nuclei) to control sympathetic activity (particularly renal sympathetic activity; Ciriello and Moreau 2012), heart rate and blood pressure (Harlan and Rahmouni 2013). Thus, the NTS provides a direct link between CB chemoreceptor activity and sympathetic activation.

In this line, Inyushkin et al. (2009) showed that leptin microinjections into the NTS in the brain of rats is associated with increased pulmonary ventilation and respiratory volume and enhanced bioelectrical activity of the inspiratory muscles suggesting that leptin may be implicated in ventilatory control through direct effects on respiratory control centres.

In conclusion, our data indicate that leptin augments basal and hypoxic-ischemic ventilation in a dose manner acting centrally, presumably at the NTS. Leptin does not appear to participate in the minute to minute chemoreception process in the CB, but owed the expression of the hormone and its receptors in chemoreceptor cells, it surely participates in long term regulation of CB function, probably contributing to the sensitization of this chemoreceptor know to occur in chronic hypoxia.

**Acknowledgements** Supported by grants BFU2012-37459 and CIBER CB06/06/0050 to CG (Spain) and EXPL/NEU-SCC/2183/ 2013 to SVC from Portugal. Many thanks to Ana Gordillo for her technical support.

## References

Aguer C, Harper ME (2012) Skeletal muscle mitochondrial energetics in obesity and type 2 diabetes mellitus: endocrine aspects. Best Pract Res Clin Endocrinol Metab 26:805–819

Bickelmann AG, Burwell CS, Robin ED, Whaley RD (1956) Extreme obesity associated with alveolar hypoventilation; a Pickwickian syndrome. Am J Med 21:811–818

Cao H (2014) Adipocytokines in obesity and metabolic disease. J Endocrinol 220:T47–T59

Chaiban JT, Bitar FF, Azar ST (2008) Effect of chronic hypoxia on leptin, insulin, adiponectin, and ghrelin. Metabolism 57:1019–1022

Chang Z, Ballou E, Jiao W, McKenna KE, Morrison SF, McCrimmon DR (2013) Systemic leptin produces a long-lasting increase in respiratory motor output in rats. Front Physiol 4:16

Ciriello J, Moreau JM (2012) Leptin signaling in the nucleus of the solitary tract alters the cardiovascular responses to activation of the chemoreceptor reflex. Am J Physiol Regul Integr Comp Physiol 303:R727–R736

Ciriello J, Moreau JM (2013) Systemic administration of leptin potentiates the response of neurons in the nucleus of the solitary tract to chemoreceptor activation in the rat. Neuroscience 229:88–99

Conde SV, Obeso A, Rigual R, Monteiro EC, Gonzalez C (2006) Function of the rat carotid body chemoreceptors in ageing. J Neurochem 99:711–723

González C, Almaraz L, Obeso A, Rigual R (1992) Oxygen and acid chemoreception in the carotid body chemoreceptors. Trends Neurosci 15:146–153

Gonzalez C, Almaraz L, Obeso A, Rigual R (1994) Carotid body chemoreceptors: from natural stimuli to sensory discharges. Physiol Rev 74:829–898

Gonzalez C, Vaquero LM, López-López JR, Pérez-García MT (2009) Oxygen-sensitive potassium channels in chemoreceptor cell physiology: making a virtue of necessity. Ann N Y Acad Sci 1177:82–88

Gonzalez-Martín MC, Vega-Agapito MV, Conde SV, Castañeda J, Bustamante R, Olea E, Perez-Vizcaino F, Gonzalez C, Obeso A (2011) Carotid body function and ventilatory responses in intermittent hypoxia. Evidence for anomalous brainstem integration of arterial chemoreceptor input. J Cell Physiol 226:1961–1969

Harlan SM, Rahmouni K (2013) Neuroanatomical determinants of the sympathetic nerve responses evoked by leptin. Clin Auton Res 23:1–7

Inyushkin AN, Inyushkina EM, Merkulova NA (2009) Respiratory responses to microinjections of leptin into the solitary tract nucleus. Neurosci Behav Physiol 39:231–240

Katz M, Finley J, Erickson J, Brosenitsch T (1997) Organization and development of chemoafferent input to the brainstem. In: Gonzalez C (ed) Carotid body chemoreceptors. Springer, NY, pp 159–170

Kemp PJ (2005) Hemeoxygenase-2 as an $O_2$ sensor in $K^+$ channel-dependent chemotransduction. Biochem Biophys Res Commun 338:648–652

Kumar P (2009) Systemic effects resulting from carotid body stimulation-invited article. Adv Exp Med Biol 648:223–233

Malli F, Papaioannou AI, Gourgoulianis KI, Daniil Z (2010) The role of leptin in the respiratory system: an overview. Respir Res 11:152

Mark AL (2013) Selective leptin resistance revisited. Am J Physiol Regul Integr Comp Physiol 305:R566–R581

Messenger SA, Ciriello J (2012) Effects of intermittent hypoxia on leptin signalling in the carotid body. Neuroscience 232:216–225

Messenger SA, Ciriello J (2013) Effects of intermittent hypoxia on leptin signalling in the carotid body. Neuroscience 232:216–225

Messenger SA, Moreau JM, Ciriello J (2012) Intermittent hypoxia and systemic leptin administration induces pSTAT3 and Fos/Fra-1 in the carotid body. Brain Res 1446:56–70

Messenger SA, Moreau JM, Ciriello J (2013) Effect of chronic intermittent hypoxia on leptin and leptin receptor protein expression in the carotid body. Brain Res 1513:51–60

Monteiro TC, Batuca JR, Obeso A, González C, Monteiro EC (2011) Carotid body function in aged rats: responses to hypoxia, ischemia, dopamine, and adenosine. Age (Dordr) 33:337–350

O'Donnell CP, Schaub CD, Haines AS, Berkowitz DE, Tankersley CG, Schwartz AR, Smith PL (1999) Leptin prevents respiratory depression in obesity. Am J Respir Crit Care Med 159:1477–1484

Olea E, Agapito MT, Gallego-Martin T, Rocher A, Gomez-Niño A, Obeso A, Gonzalez C, Yubero S (2014) Intermittent hypoxia and diet-induced obesity: effects on oxidative status, sympathetic tone, plasma glucose and insulin levels, and arterial pressure. J Appl Physiol (1985) 117:706–719

Olson AL, Zwillich C (2005) The obesity hypoventilation syndrome. Am J Med 118:948–956

Peers C (1997) Oxygen-sensitive ion channels. Trends Pharmacol Sci 18:405–408

Porzionato A, Rucinski M, Macchi V, Stecco C, Castagliuolo I, Malendowicz LK, De Caro R (2011) Expression of leptin and leptin receptor isoforms in the rat and human carotid body. Brain Res 1385:56–67

Simler N, Malgoyre A, Koulmann N, Alonso A, Peinnequin A, Bigard AX (2007) Hypoxic stimulus alters hypothalamic AMP-activated protein kinase phosphorylation concomitant to hypophagia. J Appl Physiol (1985) 102:2135–2141

Vicario I, Rigual R, Obeso A, Gonzalez C (2000) Characterization of the synthesis and release of catecholamine in the rat carotid body in vitro. Am J Physiol Cell Physiol 278:C490–C499

Zeng J, Patterson BW, Klein S, Martin DR, Dagogo-Jack S, Kohrt WM, Miller SB, Landt M (1997) Whole body leptin kinetics and renal metabolism in vivo. Am J Physiol 273:E1102–E1106

# Concluding Remarks

ISAC XIX
The Pearls and Perils of the Carotid Body

It is a pleasure and privilege for me to write the concluding remarks for the XIX ISAC (June 29-July 3, 2014) meeting hosted by Professor Chris Peers at the University of Leeds, Leeds, UK with co-host Professor Prem Kumar, University of Birmingham, Birmingham UK. Again it was a reunion of friends and colleagues across the world sharing new ideas, discoveries and new interpretations of old findings related to how the carotid body contributes to health and disease. The meeting was smaller than past ISAC conferences with 45 participants, but remained rich in information, comfortable in setting, and fun for all who attended. The conference included 6 1-h plenary lectures, 33 oral communications and 19 posters. Below, I summarize the key findings and take away message from each of the presentations and posters, but encourage you to read the full manuscripts included in this book. Professor Chris Peers, president of ISAC XIX, was not able to physically attend but his presence was palpable throughout the conference as many communicated with him daily; *the wonderfulness of technology*. His students along with the conference organizers ensured that things ran smoothly, and Professor Prem Kumar effortless took the helm sailing us through a great week culminating in a Gala Dinner and celebration at the Royal Armories. A special thanks goes out to Sue Tattersall and her staff who were always there to help the delegates arrange housing, transportation, finding lost luggage and reprinting lost badges and making sure no one was left behind in York or downtown Leeds.

Leeds is a city with much history and can have a reputation for its overcast skies and misty rainy. However, although many of the delegates were welcomed by a misty rain on Sunday, the weather cleared with gorgeous, sunny days for the remainder of the conference. The conference was kicked off by Professor Michael Spyer who took us on short scientific journey with his introductory plenary lecture "Chemoreceptors past, present and future". He reminded us of the combined contributions of Corneille Heymans and Fernando de Castro who characterized the part of the respiratory reflex that was mediated by the carotid body. Corneille Heymans, physiologist, won the Nobel Prize in Physiology or Medicine in 1938 for his discovery that oxygen concentration and blood pressure were sensed peripherally with information transmitted to the brain. But it was Fernando de Castro, the histologist, who carefully identified the histology of the aortic-carotid region which led to the clear distinction of baroreceptors in the carotid sinus, and peripheral chemoreceptors in the carotid body. Similarly Professor Spyer reviewed the series of experiments performed in adult cats by Professors Mitchell, Schlafke and Loeschcke in the 1960s that identified the three distinctive regions central chemoreceptors located on the ventrolateral surface of the medulla that are responsive to $PCO_2/[H^+]$, and which, when stimulated, increased ventilation. Professor Spyer and colleagues have focused their work on characterizing the key role of



C. Peers et al. (eds.), *Arterial Chemoreceptors in Physiology and Pathophysiology*,
Advances in Experimental Medicine and Biology 860, DOI 10.1007/978-3-319-18440-1

purinergic systems in mediating chemotransmission in peripheral and central chemoreceptors. Conducting experiments using genetically altered mice, they identified a key role for the P2X2/3 receptors in mediating hypoxic chemoreception in the carotid body. Additional experiments in adult rats, showed that adenosine triphosphate (ATP) is also involved in central chemosensory transduction mediated by P2 receptors. Neurons in the chemosensitive regions in the medulla are encapsulated by a network of astroglia. Building on this observation, Professor Spyer et al. in series of elegant experiments showed that these astrocytes were highly chemosensitive and released ATP. Optogenetic stimulation of brainstem astrocytes leads to depolarization of chemosensitive neurons and an increase in ventilation. Lastly, Professor Spyer finished his presentation showing that cardiac protection from preconditioning is mediated by reflex pathway involving vagal pre-ganglionic neurons. These findings are driving future therapies. Current clinical trials using vagal nerve stimulation in patients with chronic heart failure show that this intervention improves left ventricular function. By the way, regular yoga practice also increases parasympathetic tone. Professor Spyer's talk was followed by the welcoming reception in Charles Morris Hall, Storm Jameson Court.

**Monday**: the first day of the conference, and Professor Prem Kumar chaired the first session which was kicked off by an eloquent overview of the Epigenetic Regulation of Hypoxic Sensing by Professor Nanduri Prabhakar. Professor Prabhakar reviewed his earlier discoveries that neonatal animals that are exposed to chronic intermittent hypoxia (IH) from 0 to 10 days of postnatal age have enhanced hypoxic sensitivity of the carotid sinus nerve, hypertension and elevated plasma catecholamine levels. These adverse effects are sustained in to adulthood, are mediated by oxidant stress, and are blocked by pretreatment with antioxidants. Recent experiments led by Jayasri Nanduri show that IH during the neonatal period leads to long lasting transcriptional dysregulation of genes that encode for pro and antioxidant enzymes. In the carotid body of adult animals who had been exposed to IH, enzymes that methylate DNA (DNM) specifically DNMT1, DNM3b were upregulated, and the promoter region of a potent antioxidant, superoxide dismutase 2 (SOD) 2 was hypermethylated associated with lower blood levels of SOD2. Anticancer drugs such as decitabine prevents DNA hypermethylation which reduced the oxidative burden, inhibited hypoxic hypersensitivity and hypertension in neonatal animals who were exposed to IH. These findings led to an interesting discussion among the ISAC members as to whether such a treatment could be given to human infants specifically premature infants who have chronic intermittent hypoxia. DNA methylation is a key regulator of gene expression during normal development of many organs and system thus alternative pharmacological agents such as antioxidants for the treatment of adverse effect of IH and/or preventing the consequences of IH in premature infants may be a safer alternative in this population.

Professor Prabhakar's presentation was followed by several short presentations. The first explored the biological significance of hydrogen sulfide ($H_2S$) in the carotid body chemoreception presented by Teresa Gallego-Martin a trainee from the laboratories of Professor Constancio Gonzalez and Ana Obeso. Teresa presented experimental evidence that added to the controversy concerning the source of $H_2S$ production in the carotid body and whether $H_2S$ is involved in oxygen sensing. Cystathionine β-synthase (CBS) and cystathionine γ-lyase (CSE) are the two major enzymes that catalyze the production of $H_2S$. Taking a pharmacological approach and using surrorgate markers of activation: catecholamine release [$^3$H-CA] and increase in intracellular i[$Ca^{2+}$], Teresa showed that exogenous exposure of carotid bodies from adult Wister rats to NaHS (sulfide donor) *in vitro* augmented 3H-CA release and increased i[$Ca^{2+}$]. These responses where inhibited by hydroxocolbalamine (OHCb), a scavenger of nitric oxide (NO) and aminooxyacetic acid (AOAA) a CBS blocker, but not by blockade of CSE. While the authors did not explore the pathway by which $H_2S$ is involved in oxygen sensing, their data suggest that CBS participates in the generation of $H_2S$,

and $H_2S$ participates in signaling within the carotid body. The poster presentation by J. Elies (working with Professor Peers) showed that $H_2S$ inhibits Cav3.2, T-type $Ca^{2+}$ channels in three different cell lines and the dorsal root ganglia primarily by increasing the affinity of the channel for $Zn^{2+}$. Voltage gated T-type $Ca^{2+}$ channels are expressed in many tissues during early embryonic development but are undetectable in adults. These channels appear to be important in remodeling tissues during hypoxia. P. González-Rodríguez presented experiments in neonatal rats showing that hypoxic exposure (in vivo and in vitro) specifically induced the expression T-type $Ca^{2+}$ involving the HIF-RhoA/ROCK signaling cascade in right ventricular myocytes. The RhoA/Rock pathway is primarily involved in cellular proliferation, actin organization and is key pathway in important in tissue remodeling. This pathway also induces constriction of pulmonary artery smooth muscle cells perhaps also contributing hypoxic induced pulmonary hypertension. How this signaling pathway (HIF-RhoA/ROCK → modulation of expression of T-type $Ca^{2+}$ channels) may be involved in remodeling of the carotid body during chronic hypoxia is unknown. T-type $Ca^{2+}$ channel mRNAs are expressed in the rat carotid body. Cellular proliferation does not go unchecked and within the hypoxic microenvironment hemooxygenase-1 activity and carbon monoxide (CO) levels increase. We learned from the poster presentation by H. Duckles, also working with Professor Peers, that yes, hypoxic exposure upregulates T-type $Ca^{2+}$ channels and this is linked to cellular proliferation of smooth muscle cells (SMCs), but the *production of CO* in the microenvironment inhibits T-type $Ca^{2+}$ channels that controls proliferation of SMCs.

The following short oral communication by J.G Jurcsisn was presented by Professor Chris Wyatt reminds us of an important lesson: when the signal is beautiful and too good to be true, it most likely isn't true. To determine the role of AMP-activated protein kinase (AMPK) in cell signaling using $Ca^{2+}$ imaging, they performed a nice series of control experiments showing that STO609 an inhibitor of calmodulin-dependent protein kinase β (CAMKKβ) interacts with calcium dyes generating autofluorescence with Fluro-2 and quenching fluorescence when used with Rhod 1. However, in experiments using whole-cell configuration perforated patch, STO609 inhibited outward macroscopic currents, a response that was inhibited by a selective $BK_{Ca}$ channel blocker. This result was not predicted and they interpret these finding as an off target effect of STO609 on the channel itself and may not be acting specifically on CAMKKβ activity. Session one was concluded with a presentation by Professor Andrea Porzionato showing reconstructions of the carotid body using computer modeling techniques. Modeling tissue dynamics they can determine the volume of the different cell types within the carotid body. Specifically he and colleagues created a 2 step mathematical model that simulates the hypothetical sequence of cellular events that would occur in the carotid body during chronic hypoxia. The first step models macroscopic features of the carotid body focusing on changes in cell populations, rate of expansion and differentiation. The next step uses a "cell-centered" modeling strategy to further describe the alterations in the cytoskeleton, cell proliferation, differential and apoptosis. The model accurately predicted the cellular and structural changes that occur in the rat carotid body after 16 days of hypoxia. These data demonstrate how modeling can be used to predict how the carotid body may change during health and disease across the life span. Modeling in other systems can be a powerful approach in predicting cellular and tissues changes and can be an effective high throughput system to test potential therapies that target the carotid body directly or indirectly.

The second session of the first day, chaired by Professor Rodrigo Iturriaga, included presentations by Professors Colin Nurse and Chris Wyatt, Jessica Kåhlin and two student presentations by E. Metzen and Richard L. Pye. Professor Nurse explained how the type I, II cells and nerve fibers cross communicate in the carotid body via purinergic signaling pathways; ATP and adenosine have paracrine and autocrine effects. Using the experimental method that he developed, co-culture of clusters of type I and II cells with

petrosal ganglion neurons, he and colleagues were able to show that chemoexcitation of type I cells release ATP that activates $P2X_{2/3}$ receptors on carotid sinus nerve terminals and P2Y2 receptors on type II cells. Moreover, reciprocal crosstalk occurs between type I and type II cells such that activation of type I cells can elicit different response in type II cells. Excitatory adenosine A2a receptors are expressed on both carotid sinus nerve fibers and type I cells allowing for parallel activation of this excitatory pathway together with activation of P2X and Y receptors forming a tripartite network. Additional data on the topic of adenosine signaling in the carotid body from Professor Prem Kumar's laboratory was presented in a poster (Andrew Holmes first author). They show that extracellular generation of ATP, by the enzyme CD73, is important in modulating basal and hypercapnic induced chemoafferent discharge.

The next oral presentation by Professor Wyatt, was on the topic of how the carotid body contributes to opiate induced ventilatory depression. He showed, for the first time, that isolated rat type I cells are immunopositive for mu and kappa-opioid receptors, and that these receptors signal via guanine inhibitory nucleotide-binding proteins (Gi), inhibiting $K^+$-induced depolarization of type 1 cells. While we are familiar with the work of McDonald and Ribeiro that showed exogenous opiates depressed and naloxone increased single fiber activity of carotid sinus nerve in adult cats, direct actions of opiates on type 1 cells had not been previously described. Next, E. Metzen from the University of Duisburg-Essen in Germany present her work using fluorescence resonance energy transfer (FRET), showed that in response to hypoxia, in approximately 50 % of the animals, ROS levels increased and in the remaining 50 % ROS levels decreased. This heterogeneity was attributed to the differences in the animal's diet. This is an intriguing finding that may account for discrepancy in the literature about how ROS contributes to hypoxic chemotransduction in the carotid body. Measuring cell membrane potential in response to hypoxia, she also showed that NADPH-oxidase played a key in oxygen signaling in the carotid body.

Richard Pye, a Ph.D. student working with Professor Wyatt, presented recent work exploring the cellular mechanisms of leptin signaling in isolated type I cells from rats. While acute exposure to leptin depolarizes isolated type 1 cells and inhibits $BK_{ca}$ channels, leptin did not alter the cellular responses to hypoxic or acidic depolarization. Hypoxia also depolarizes type 1 cells and inhibits $BK_{ca}$ channels. Professor Shirahata (Luis Pichard, first author) determined whether the functional differences in carotid body hypoxic sensitivity in two strains of mice: DBA/2 J (who have a high level hypoxic chemosensitivity) and A/J mice (who have excessively low level of hypoxic chemosensitivity) might be related to differences in the sensitivity of the BK channels. Hypoxic induced afferent activity from the carotid body, was lowest in the A/J mice, pharmacological inhibition of BK channels in the DBA/2 J mice increased neural activity while agonist or antagonist to the BK channel had no effect on neural output from A/J mice. Comparisons were also made in knockout mice for the BK channel gene, and wild type mice. Neural response to hypoxia was delayed in the BKKO when compared to DBA/2 J and wild type mice but maximum response was similar between the three groups. The structure, catecholaminergic content and function of the carotid body is maldeveloped in A/J mice; these additional data suggest that BK channels may be affected as well.

The new respiratory stimulant, GAL-021 which is being marketed to reduce opioid-induced respiratory depression, also appears to affect $BK_{ca}$ channel activity. Professor Peers in collaboration with Galleon Pharmaceuticals, Inc in their poster (M. Dallas first author), that at low doses GAL-021 inhibits BKCa channels and at higher doses inhibits the delayed rectifier $K^+$ and leak $K^+$ currents at higher doses in type 1 cells and that carotid sinus nerve denervation essentially abolished the respiratory stimulant effects of the drug in rats.

The morning session was concluded with a presentation by Dr. Jessica Kåhlin who presented results from experiments that she recently completed for her Ph.D. thesis. She characterized the

transcriptome profile for cytokines and cytokine receptors in the carotid bodies removed from five adult humans who were undergoing unilateral neck dissection for head and neck cancer. These patients were nonsmokers and without known cardiorespiratory morbidities. Transcripts for the toll-like receptors 1 and 4, interleukin (IL) receptors 1 and 6, tumor necrosis factor (TNF) receptor, nuclear factor kappa B (NF-κB) and high mobility group protein β-1 (HMGB-1) were found but transcripts for TNFα and IL-10 were not This work was well received by the ISAC members because the study was performed in human tissue. For her work and the clear delivery of the communication, Jessica was selected along with 2 other students to receive the Fernando de Castro, Heymans and Neil award for ISAC XIX. Professor Camillo Di Giulio and collaborators presented a poster showing that the neuropeptide, galanin is expressed in the human carotid body. Galanin, co-exist with catecholamines in neurons in the central nervous system and it inhibits the release of dopamine from hypothalamic neurons. Thus, these investigators hypothesize that galanin could mediate catecholamine transmission in the carotid body inhibiting dopamine release. It would be important to know if receptors for galanin are expressed in the human carotid body. Knockout mice for each of the 3 galanin receptors exist as do selective antagonists.

Professor Keith Buckler was the afternoon plenary speaker who started the session walking us through the "metabolic hypothesis" for oxygen sensing in type 1 cells. This hypothesis states that oxygen sensing is linked to oxidative phosphorylation, placing the oxygen sensor in the mitochondria. While the metabolic hypothesis of oxygen sensing was originally proposed in 1972, experiments to date had not demonstrated that the mitochondrial membrane potential was depolarized at oxygen levels that stimulated an increase in ventilation. To place the experiments in context, all cells have the capacity to "sense" changes in oxygen tension in order to switch from aerobic to anaerobic metabolism to conserve energy optimizing the chance for cell survival during oxygen deprivation. An essential role for the carotid body is to increase ventilation in response to hypoxia in order to provide sufficient oxygen to tissues and cells to allow for aerobic metabolism, the most energy producing pathway. Thus, it is reasonable to hypothesize that the mitochondria in type 1 cells would be the starting point for sensing changes in oxygen tension at the level that may become detrimental to the organism. However, it is essential that the mitochondria in type 1 cells be able to initiate a cascade of events that will depolarize the type 1 cell at higher levels of hypoxia that normally depolarize mitochondria membrane potential. When oxygen is available, fats and carbohydrates are broken down in the cytoplasm and electrons are stored by NADH. In the presence of oxygen, NADH is oxidized by the electron transport chain in the mitochondria where *oxygen* at complex IV (cytochrome oxidase c) is the terminal electron acceptor. NADH is fluorescent when excited by ultraviolet light. Exploiting the autofluorescence of NADH and using rhodamine 123 to assess mitochondrial membrane depolarization, Professor Buckler and colleagues performing a series of well-designed integrated experiments show data supporting the metabolic hypothesis of oxygen sensing that appears to be unique to the type 1 cells. In response to moderate hypoxia, the mitochondrial membrane in type 1 cells are depolarized (electron transport chain is inhibited) and this is primarily because cytochrome oxidase activity was inhibited during hypoxia. This process occurs at oxygen levels that inhibit K+ channel and increase i[$Ca^{2+}$]. He concludes that type-1 cell mitochondria have extraordinary oxygen sensitivity commensurate with a role in oxygen sensing.

Professor Buckler's talk was followed by several short communications related to the oxygen sensing in the pulmonary artery smooth muscle cells and pulmonary neuroepithelial bodies (NEBs). Professor Aaronson presented the communication by J. Preto-Loret and colleagues revisiting whether $H_2S$ mediates hypoxic pulmonary vasoconstriction (HPV) in intrapulmonary arteries. Using small vessel myography and pharmacological approach, they show that supraphysiological doses of exogenous cysteine

enhanced HPV response. However, by blocking synthesis of $H_2S$ in the presence of physiological concentrations of cysteine, cysteine and glutamate, he concluded that endogenously produced $H_2S$ does *not* induce or mediate HPV. Professor Mark Evans uses pulmonary artery smooth muscle cells as the model system to determine how oxygen is sensed in specialized cells. Using recombinant molecular techniques in stably transfected HEK 293 cells, Professor Evans presented experiments characterizing how AMP-activated protein kinase (AMPK) interacts with oxygen sensing channels and shows that AMPK phosphorylates the oxygen sensing component of the hypoxia-sensitive channels such a $BK_{Ca}$ and others. He also presented exciting and novel preliminary experiments in transgenic mice using echocardiogram to assess pulmonary hypertension.

The last talks of the day focused on molecular mechanisms of sensing in neuroepithelial bodies (NEBs) in the lung. Professor Dirk Andriaensen in collaboration with R. Lembrechts and colleagues, presented data showing that NEBs express calcium sensing receptors (CaSR) which allow the NEBs to sense calcium levels in the microenvironment, depolarizing and raising $[Ca^{2+}]i$ levels. Lastly, Simon Liverman (Ph.D student) who is co-mentored by Colin Nurse and Ernest Cutz, characterized the stimulus response of the NEBs to hypoxia and acidic hypercapnia in lung slices from neonatal hamsters. He found that exposure to hypoxia and acidic hypercapnia increased $[Ca^{2+}]i$ levels in and serotonin release from NEB via activation of L-type $Ca^{2+}$ channels. Additional data from the laboratory of Professor Cutz was presented in the poster session (S. Livermore first author) examining the structure and function of NEBs in PHD-1 knock out (KO) mice. These mice have accumulation of constitutively expressed hypoxic-inducible-factor (HIF). They report that NEBs in PHD-1 KO mice are hyperplastic, are positive for HIF immunoreactivity, and have increased hypoxic-induced 5-HT secretion.

We concluded the first day of the conference with a wonderful walk through sunny downtown Leeds to enjoy a pie and pint (s) at Whitelocks Pub, Leed's oldest Public House built in 1715. Whitelocks Pub feels very Victorian with its long marble topped bar, cast-iron tables and red leather seats. Many of us would agree with English Poet Betjeman who described Whitelock as "the heart of Leeds." At Whitelocks we all enjoyed the fruits of Leeds: great food and spirits in the Turk's Head Yard "aka" beer garden. The buzz was infectious as ISAC members with family and friends continued conversations about the science while others shared personal stories of how women balance science and discovery with raising children. The key ingredients to making it work was (1) having understanding spouses/partners who pick up and carry on, and (2) mentors who encourage, support and sponsor their success.

**Tuesday**: I chaired Session 4 of the scientific program. Professor Robert Fitzgerald, the invited plenary speaker presented a comprehensive review of his work in cats investigating contribution of aortic and carotid body chemoreceptors on blood flow to the adrenals, eyes, spleen, pancreas, diaphragm, heart, and brain during systemic hypoxia. I highlight some of his findings. During systemic hypoxia, blood flow significantly increased in most of the organs examined, while blood flow to the pancreas and spleen significantly decreased. Careful dissection of the contribution of the carotid and aortic bodies in concert or separately to changes in blood flow differed between organs. For example: (1) aortic or carotid bodies did not significantly influence blood flow to the heart during hypoxia, (2) carotid bodies but not aortic bodies contributed significantly to the vasodilatory effect during hypoxia in the adrenal glands, (3) carotid and aortic bodies acting together attenuated blood flow to the stomach during systemic hypoxia, and lastly, input from the carotid and aortic bodies substantially contributes to increase in vascular resistance in the spleen during hypoxia. These observations coupled with the fact that the peripheral chemoreceptors are strategically placed to be first responders to adverse physiological events, emphasize the importance of peripheral chemoreceptor input in regulating blood flow to most organs during illness or

conditions that lead to hypoxia. The role of "first responders" by peripheral chemoreceptors begs the question as to what would be the unintended consequences of therapeutic carotid nerve resection in humans.

The remaining short communications in session 4 focused on the contribution of progesterone in newborn and adult female mice presented by Professors Aida Bairam and Vincent Joseph, respectively. We learned that progesterone signals through both nuclear and membrane bound receptors and both signaling pathways contribute to control of breathing at baseline and response to natural stimuli. Professor Bairam, using knockout mice for the nuclear progesterone receptor (nPR) showed the importance of this hormone in regulating breathing during early development. While baseline apnea frequency was similar between wild type and knockout mice, the hypoxic ventilatory response (HVR) in both female and male knockout mice was attenuated in animals tested at postnatal day 10. However, on postnatal 1 and 4, the contribution of nPR to HVR was influenced by gender. Professor Joseph described the contribution of the membrane progesterone receptor β (mPR-β) to breathing stability during sleep and on HVR in adult *female* mice. siRNA techniques were used to reduce the expression of mPR-β in the brain. Treated animals had a higher frequency of apnea, and marked reduction in HVR and ventilatory responses to hypoxic-hypercapnia. Two additional studies were presented in the poster session by these investigators. S. Laouafa investigated the contribution of the nPR to breathing stability during sleep and hypercapnic ventilatory responses of adult male mice, and F. Marcouiller reported their findings in adult female mice. Using wild type and nPRKO mice they show that nPR stabilized breathing during non-REM sleep, reduced post sigh apneas, and enhanced the hypercapnic ventilation in both male and female mice. These basic studies contribute to our understanding of possible mechanisms underlying the epidemiological association between the increase frequency of sleep apnea in postmenopausal women. These studies also highlight the importance of exploring gender specific effects on physiological outcomes. Remoco Berendesen working with Professor Teppema presented data in their poster disputing conclusions from previous studies suggesting that another hormone, erythropoietin, increased acute HVR in women and not men. Results from their placebo-controlled, double-blind cross over study using clinical relevant doses of EPO (50 I.U/kg) in seven male (23 ± 3 years) and seven female (22 ± 2 years) subjects failed to show any effect of EPO on differences in HVR or hypoxic pulmonary vascular responses in either sex.

My presentation completed the morning session. I shared findings from our work demonstrating the effect of inflammation during early postnatal development on the structure and function of the carotid body in newborn rats. Our studies were designed to better understand the association between preterm birth, inflammation and unstable breathing that persist beyond the immediate inflammatory episode. Exposure to lipopolysaccharide (LPS) at postnatal day 2 in newborn rats was associated with disrupted histology of the carotid body, attenuated hypoxic chemosensitivity of the carotid sinus nerve (in vitro) at and higher hypoxic threshold to increase ventilation at postnatal day 9–10, 7 days after exposure to LPS exposure.

Professor Colin Nurse chaired the next session (5). The next series of communications explored the role of the carotid body in glucose homeostasis. Maria Riberio a Ph.D student working with Professor Silvia Conde, presented her work determining whether Kv1.3 channels may play a role in insulin signaling in the carotid body similar to its role in the central nervous system. Using a comprehensive series of techniques ranging from whole cell patch voltage clamping to immunohistochemistry in slices of the carotid body and acutely dissociated type 1 cells, Ms. Riberio showed that Kv1.3 channels are expressed in type 1 cells and are involved in insulin induced depolarization of type 1 cells. This work was also recognized by the award of the Fernando de Castro, Heymans and Neil award. Maria's presentation was followed by the communication by Professor Mieczyslaw

Pokorski who presented a collaborative project with Italian colleagues: Professor Camillo Di Giulio at the University of Chieti-Pescara and Professor Mazzatenta at the University of Teramo. They describe changes in structure and function of the carotid body in a rat (Wister) model of diabetes. Diabetic rats had attenuated HVR and hypoxic sensitivity. The carotid body was remodeled similarly to what is observed in chronic hypoxia with clear evidence of neovascularization, increase in connective tissue volume and degenerative changes in glomus cells. It would be interesting to know the molecular/cellular mechanisms mediating these ultrastructural changes in the carotid body and whether the changes in the carotid body are primarily responsible for the altered HVR.

The corollary to hyperglycemia is hypoglycemia. Professor Prem Kumar presented the work performed by his former graduate student Andrew Holmes. Exploring the effects of hypoglycemia on carotid body function, they found that during hypoglycemia the carotid body metabolizes glycogen which preserves chemoafferent activity. Glycogen granules and immunoreacitivty for glycolytic enzymes were found in the carotid body, and blocking these enzymes lead to earlier failure of carotid sinus nerve activity during glucose deprivation. Additional data from Professor Kumar's laboratory on this topic was presented in the poster session (Emma L. Thompson first author). They showed that hyperventilation associated with hypoglycemia is mediated by adrenaline being released from the adrenal glands that then binds to β-adrenergic receptors in the carotid body increasing in $pCO_2$ sensitivity. What about preservation of brain glucose levels during anoxia, and the neurotransmitters systems involved brain glucose retention during anoxia? Professor Sergio Montero (R. Cuéllar first author) presenting in the poster session, showed that AMPA receptors in the commissural nucleus of the nTS (location of chemoreceptor input) are the key glutamatergic receptors that are involved in brain glucose retention during anoxic stimulation of the carotid body. Ok, the carotid body is important in glucose homeostasis; that's good, maybe?

The last oral communication of session 5 suggested that the carotid body does not always behave well, and thus its removal may be a viable, reasonable therapeutic approach for some human disorders. Professor Silvia Conde and colleagues had recently published the observation that carotid sinus nerve sectioning (CSN) restores insulin sensitivity in a pre-diabetic animal model. Joana Sacramento, a student in the laboratory sought to determine the mechanism underlying the restoration of insulin sensitivity after CSN. Insulin stimulates glucose reuptake by inducing translocation of the glucose transporter, GLUT4, to the plasma membrane and AKT, once activated, leads to inactivation of glycogen synthase which catalyzes the final step in glycogen synthesis. Thus, AKT allows for more glucose to be stored as glycogen. In diabetes GLUT 4 (Glut4), and phosphorylated Akt are reduced skeletal muscle and adipose tissue. Joana reported that these levels are restored after CSN denervation in their rat model of diabetes. J.P. Iturri (poster presentation) working with Professors Joseph and Bairam also investigated the role of AKT and ERK 1 and 2 signaling pathways in hypoxic chemosensitivity in the carotid body. Using AKT and ERK1 and 2 inhibitors, they show that carotid sinus nerve activity at baseline and in response to hypoxia was partially inhibited by AKT and blunted when ERK1/2 was blocked. At the start of the morning, we heard from Professor Fitzgerald that carotid and aortic bodies regulate blood flow to key organs during hypoxia and we finished the morning learning that the (1) carotid body is a glycolytic organ, (2) the ultrastructure of carotid body is completely disrupted in animal models of diabetes, (3) carotid body contributes to the development of insulin resistance and that its removal will restore this important function. So is the carotid body beneficial in acute stress, but in chronic stress is it detrimental and worsens disease? This question will be revisited several more times before the end of the conference.

Session 6, chaired by Professor Nanduri Prabhakar, was started by Professor José López-Barneo who presented a collective series of eloquent experiments detailing the molecular and cellular mechanisms of carotid body responsive-

ness to acute and chronic hypoxia. The carotid body in response to chronic hypoxia undergoes significant morphological changes associated with acclimatization, such as neovascularization and proliferation of type 1 cells. Professor López-Barneo reminded us that the type II cells in the carotid body are neural crest derived multipotent stems cells and are key players in the remodeling of the carotid body during chronic hypoxia. However, experiments show that these neural stem cells when grown alone on neurospheres are not directly affected by hypoxia. Experiments in his laboratory have focused on characterizing the microenvironment to identify niche factors that are involved in inducing differentiation of progenitor cells (type II). Using state-of-the art molecular and cellular techniques, they show that type I and progenitor cells within the carotid body signaling through the endothelin pathways interact and interaction via this pathway is required for cellular differentiation of progenitors into mature type 1 cells during hypoxia. Specifically, in response to chronic hypoxia, type 1 cells release endothelin-1 which binds to endothelin B receptors on undifferentiated cells and proliferating carotid body progenitors, which induces proliferative and antiapoptotic genes via the MAP kinase signaling pathway.

Professor López-Barneo's presentation was followed by four short communications. Professor Shirahata revised the question of the role of the carotid body in metabolism. She and colleagues explored whether the carotid body is in fact a metabolic sensor responding to and regulating blood glucose levels. In experiments using young mice (<14 postnatal days), she demonstrated the association between reduced HVR and plasma glucose levels. To better determine the specific carotid body responses to glucose, leptin and insulin, additional experiments were performed in superfused carotid body preparations from adult mice. In agreement with other reports in adult rats, in this preparation, the carotid sinus nerve responses were not altered by different concentrations of glucose. It was not affected by insulin at baseline or in response to hypoxia. Leptin did not change basal activity but did augment responses during hypoxia, which was partially mediated by transient receptor potential (TRP) channels.

Professor Shirahata's talk was followed by a short communication by Professor Richard Wilson, who is also interested in TRP channels and the development of sensory long-term facilitation (sLTF) of the carotid sinus nerve. Using an ex vivo perfused carotid body preparation, he reported that TRP channels, specifically the heat sensitive, TRPV1 channels partially and purinergic receptors substantially contribute to the development sLTF. sLTF was induced by repetitive short exposures to hypoxic-hypercapnia. sLTF contributes to the development of hypertension and is the link between sleep apnea and cardiovascular morbidity. Two commonly used antihypertensive agents, losartan and ketanserin, blockers of the angiotensin type II, and serotonin 5-$HT_{2A}$ receptor, respectively, block sLTF. The renin-angiotensin system, specifically angiotensin II receptors are upregulated in the adult rat carotid body after 7 days of intermittent hypoxia; an effect that is blocked by pretreatment with losartan. It is not known if losartan or ketanserin can be used as adjunct therapy to CPAP in patients with sleep apnea to decrease the risk of developing hypertension. In addition to inducing sLTF, chronic intermittent hypoxia (CIH) can also affect ventilatory responses, specifically by inducing LTF of respiratory motor outputs. D. Edge working with Professor O'Halloran showed in the poster session that ventilatory LTF was observed after 3 days of CIH but blunted after 7 days of exposure in Wister rats.

We had learned from several members of the ISAC society that intermittent and chronic hypoxia induces an inflammatory response within the carotid body. Professor José R. Fernandez and colleagues have studied the role of the carotid body in modulating systemic inflammatory responses. He shared their newest observations that in response to LPS-induced inflammation, chemo/baro-denervated adult rats have worse hypocalcaemia, greater elevation of biomarkers for acute kidney and cardiac injury, and die sooner than animals with intact chemo and baroreceptors. Session 6 concluded with, Tara Janes, who working with her thesis advisor

Professor Naweed Syed at the University of Clagary, characterized how the central and peripheral nervous system shapes hypoxic-driven behavior in *Lymnaea stegnalis,* pond snails. During moderate to severe hypoxia, snails increase breathing frequency and breath duration. This response is mediated by multiple peripheral $O_2$-chemoceptors that have a different threshold for activations. These chemoreceptors provide excitatory input into the respiratory central pattern generator. She showed that in the reduced preparation without peripheral input, hypoxia reduces the burst time of CPG in the snail.

**Wednesday**: In keeping with tradition, on the 3rd day of the conference, the ISAC members left their pens, pencils and notepads in their rooms and enjoyed a day of adventure and informal conversations and friendly exchanges as they traveled to York, UK a short 34 km from Leeds. Leaving the bus, we soon parceled ourselves into small parties of two or more and toured York. York is a beautiful, historical city that is surrounded by a wall where the Ouse and Foss rivers join in North Yorkshire, England. It has rich history, founded by the Romans in 71 AD, and today has unitary authority. Because of its strategic location and being a hub for railway networks, it became a prosperous trading center and thrived. It has many historical sites and at any one of them one could spend several days. York was once the home of over 45 medieval parish churches of which 12 are still places of worship. The York Minster, the largest Gothic cathedral in Northern Europe, where the Archbishop of York resides is a very popular tourist attraction with a remarkable history behind each breathtaking view which include towers and bells and shrines and 128 stained glassed windows that was constructed over 200 years. Professor Emilia Monteiro and I climbed the 275 steps, 230 feet to the top of the medieval central tower, an exhilarating experience that satisfied my exercise requirement for the week. Certainly worth the climb because at the top there is a breathtaking panoramic view of the picturesque city centre with hidden alleyways and surrounding beautiful countryside. I climbed it in tennis shoes; Professor Monteiro climbed it in high heels. The elegance and grace of European women, how do they do it?! In the city center, there is an intricate network of shops and confectionaries that satisfied the shoppers in the group. The day culminated in a lovely cocktail hour and dinner at the National Railway Museum.

For those who didn't get lost in a public house on the trip back to Leeds, we returned rested for the last day of scientific exchange with colleagues and friends. Professor Buckler, chaired the 7th session of the conference and Professor Harold Schultz started the morning to share with the ISAC members his comprehensive physiological studies characterizing the contribution of the carotid body to heart failure. As he began his presentation, we all waited with bated breath to see if the time fairy had visited him during the night and left him with an accurate sense of time; she had. To briefly summarize, using a rabbit model of congestive heart failure, Professor Schultz and his colleagues showed how persistence of elevated carotid body sensitivity in congestive heart failure sustains oscillatory breathing, which exacerbates tonic and chemoreflex-evoked augmented sympathetic nerve activity thereby worsening congestive heart failure and contributing to renal insufficiency. Carotid body denervation in rabbits with congestive heart failure, reduced breathing instability, reduced sympathetic tone and improved survival. The altered physiology that they describe in their model is quite representative of the humans with Cheyne-Stokes respiration and heart failure. We circle back again to the question as to whether the carotid body should stay or go. Pharmacological interventions have promise; drugs that improve endothelial function such as statins, exercise and caloric restriction all decrease carotid body sensitization.

Professor Schultz's presentation was followed by three short communications by Professors Shirahata, Ganesh Kumar and student presenter, M. C. Fernández-Agüera. Professor Shirahata presented her preliminary findings linking short term fasting in neonatal mice to long term breathing instability. Newborn animals were fasted for

3–12 h between P6 and P14. In fact, the younger the animal and the longer the fast, the more apnea and breathing instability was observed immediate and 24 h post fasting. Fasting-induced breathing instability was also associated with reduced carotid sinus nerve hypoxic sensitivity and increase in epigenetic changes. Methylation of leptin and the suppressor of cytokine signal gene was increased, a finding specific to DNA from the carotid body. Maternal hypoglycemia during pregnancy is associated with decrease fetal breathing movements, and hypoglycemia is a well-known cause of apnea in newborn infants, particularly premature infants. Apropos to Professor Shirahata's findings, it is now known that infants who are born small for gestational age, suggesting a decrease in nutrition and/or oxygen supply in utero, have greater frequency of apnea and periodic breathing postnatally.

The next presentation was by Carmen Fernández-Agüera, a student working with Professor López-Barneo. She explored how von Hippel-Lindau (Vhl) gene influences sympatho-adrenal chemoreceptor function and tolerance to hypoxia. VHL protein degrades hypoxia inducible factor (HIF1-α) a major transcription factor for a multiple hypoxic inducible genes including tyrosine hydroxylase. Genetically engineered mice, with conditional targeted deletion of Vhl gene in catecholaminergic cells throughout the body, have both atrophic carotid bodies and adrenal medulla and reduction in plasma catecholamine levels. The knockout mice, when exposed to chronic hypoxia, develop cardiomegaly, polycythemia, splenomegaly and die after 11 days of hypoxic exposure. Cells in the neurospheres generated from the carotid body from these animals showed elevated nestin-positive cells along with autophagy of TH-positive glomus cells. For this work and excellent presentation, Carmen was selected also to receive the Fernando de Castro, Heymans and Neil award. Professor Ganesh Kumar concluded Session 7 describing how elevated neural activity from the carotid body during CIH contributes to the physiological consequences of CIH: elevated sympathetic drive and systemic hypertension. Adult rats with carotid sinus nerve or sympathetic nerve denervation did not develop hypertension and elevated sympathetic activity in response to CIH when compared to sham controls.

Professor Ganesh Kumar chaired the 8th session of the meeting. A student presenter, Lucillia Diogo working with Professor Emilia Monteiro, led the session presenting results from a large prospective cohort study in adult humans (n = 250) with obstructive sleep apnea and hypertension. She showed that many anti-hypertensive treatment regimens are used to treat hypertension in this patient population, but none of these regimes were effective either before or after the patient had adapted to continuous partial airway pressure (CPAP) for the treatment of sleep apnea. Similarly, in a parallel animal experiment, carvedilol, a nonselective beta-blocker with intrinsic anti-α1 adrenergic and antioxidant properties could not reverse the CIH induced hypertension in adult animals. We had heard from Professor Ganesh Kumar that CIH-induced hypertension can be prevented with prior denervation of the carotid body, and from Professor Wilson that blockade of renin-angiotensin system can prevent the sensory long term facilitation which is believed to be key development of systemic hypertension. The communication by Ms. Diogo suggested that after hypertension is developed in humans, therapeutic interventions that decrease activity from the carotid body do not appear to reverse hypertension needing therapy.

In this session, Professor Bairam expanded on the topic of the role of progesterone and respiratory control and presented data showing that chronic caffeine administration in newborn rat pups inhibits the respiratory stimulatory effect of progesterone. Elena Olea, working with Professor Constancio Gonzalez explored the specific role of the carotid body in leptin induced ventilatory response. Her data showed that leptin given chronically or acutely in intact animals augments basal and ischemic hypoxic-induced ventilation in Wister rats. However, *in vitro*, leptin exposure applied to the carotid body did not modify any parameter of hypoxic- or high $K^+$-induced activation. These data suggest that to them that leptin may augment hypoxic ventilation via central

mechanisms. Professor Kim closed the morning session describing results of her experiments using a detailed pharmacological approach to determine the role TRP channels in hypoxic-signaling in glomus cells. Her data suggest that (transient receptor potential channel) TRP channels may provide an alternative pathway for calcium influx in glomus cells during depolarization in response to hypoxia.

Thursday afternoon was the last session (9) of the meeting. Professor Silvia Conde, chaired the session and it started with a plenary talk by Professor Julian Paton, who presented data on humans who have had unilateral carotid body removal for the treatment of intractable hypertension. Studies supporting this approach are the observations that chemoreflex-evoked sympathetic activity responses are enhanced in humans and animal models of systemic hypertension. Professor Paton and colleagues performed a key experiment showing that denervation of the carotid body (CBD) in the spontaneously hypertensive rat (SHR) prior to the development of hypertensive t 4 weeks of age delays the development of hypertension and reduces the magnitude of hypertension when it does develop. Moreover, when performed in adult SHR rats with established hypertension, CBD significantly decreased systolic blood pressure and vasomotor tone. Professor Paton presented their experience with patients who had therapeutic removal of the carotid body for the treatment of severe congestive heart failure. This treatment was associated with improved cardiovascular function. In the poster session, additional data from his laboratory presented by Wioletta Pijacka further characterized the cardiovascular and respiratory responses to hypoxia in SHR after bilateral carotid body ablation. In response to hypoxia, heart rate increased while respiratory rate did not change but carotid body ablation did not affect the cardiorespiratory response during exercise. During exercise blood pressure, heart rate and respiratory rate increased in sham and animals with carotid body ablation.

Professor Paton's presentation followed short communication by Professor Man Lung Fung. In response to CIH in adult Sprague-Dawley rats, the renin-angiotensin system was upregulated and associated with lower levels of nitric oxide (NO) in the carotid body. Since NO is a vasodilator, lower levels were not able to counterbalance the vasoconstriction from elevation of angiotensin and endothelin in the carotid body. Duchenne Muscular dystrophy (DMD) causes progressive muscle weakness that also affects the diaphragm contributing to hypoventilation. The mdx mouse has muscle weakness and reduced diaphragmatic function and is animal model for human DMD. Professor O'Halloran and colleagues presented data showing that in comparison to control animals, mdx animals have hypoventilation at baseline; but, mdx mice have a greater increase in the ventilatory response to hypoxia and similar response to hypercapnia. Whether hypersensitivity of the carotid body is contributing to this selective HVR is being explored. Professor Prem Kumar and his colleagues raised the question, "is there an obligatory role for carotid bodies in the effects of CIH." For many of us who had been listening intently throughout the conference would have answered this question with an unequivocal, yes; however, many of the paradigms of hypoxic exposure were designed to mimic severe OSA. Professor Kumar and his colleagues, Drs Andy Coney and Clare Ray used low frequency of cycles of CIH 6 cycles/h vs 30 cycles/h in adult Wister rats. This paradigm of CIH significantly increase systemic blood pressure, heart rate and cardiac mass; however, the ventilatory response to graded hypoxia in animals exposed to CIH, when tested under anesthesia, did not differ from control animals. Professor Iturriaga completed the last session of the conference, again confirming that carotid bodies are crucial to the development and maintenance of systemic hypertension. He showed that cryoablation of the carotid bodies decreased blood pressure in animals who had developed CIH-induced systemic hypertension after 2 weeks. Similarly, ebselen, an ONOO- scavenger was also able to reduce blood pressure in this model.

As with tradition, the conference ends with a GALA celebration with ISAC members dressed in their finest. The conference did culminate in a wonderful GALA event at the Royal Armories

but because of unexpected road closures to accommodate the Tour de France Grand Depart Presentation in Leeds, many of the ISAC delegates were prevented from returning to their rooms and donning their finest but arrived nevertheless at the Royal Armories in the best of spirits. Professor Prem Kumar, the master of ceremonies, was in full brigade with humor and wit that kept many of us laughing into the night. The De Castro awards were formally presented to three student awardees Maria Joao Ribeiro, communication: Kv1.3 channels mediates insulin action in the rat carotid body; supervisor Silvia Conde. Carmen Fernández-Agüera; Ablation of the von Hippel-Lindau gene impairs sympathoadrenal chemoreceptor function and tolerance to hypoxia; supervisor José López-Barneo; and Jessica Kåhlin, M.D, communication: The human carotid body with a focus on oxygen sensing and inflammation thesis advisor: MJ Fagerlund

For me, ISAC XIX, conference in Leeds will be remembered as a smaller gathering of nuclear group of basic biologist, physiologist, and physicians who with tenacity and perseverance, collaborations and friendships over decades have contributed to understanding the pearls and perils of the carotid body. The science has seamlessly moved from the bench to bedside and back to the bench on multiple occasions. This conference moved the bedside from the medical units to the operating room. While we are still searching for the holy grail the "oxygen-sensor" we continue to put the tiny pieces of a big puzzle together, we moved to a different place of significance of the carotid body in its contribution to disease, specifically diabetes, heart failure and persistent intractable hypertension in the presence of continued intermittent hypoxemia. While it is uncertain as to the contribution of the carotid body to initial onset of these diseases, it appears to be clear, that it takes full charge of the progression of the disease once given control. But, didn't we hear that the carotid body is a first line of defense to multiple forms of stress? It is beneficial in regulating blood flow to critical organs during hypoxia; it is key in hypoxic arousal in adults and infants, and it helps and modulates the systemic sepsis responses, all of which are lifesaving. On the other hand, the carotid body is also vulnerable to the very conditions that it protects the organism against, hypoxemia. Specifically chronic intermittent hypoxemia induces metaplasticity in the carotid body and higher structures leading to persistent sympathetic activation. To come to the realization that removal of these small nuggets of tissue could reverse severe heart failure, diabetes, and hypertensive is sad but true. I have always adored the carotid body. It is a beautiful organ: small, glistening, with intricate weaving of nerve fibers, blood vessels, slender cells, and oval cells, all touching, communicating and transmitting signals that regulate essentially every organ in the body. There must be a sweet spot; arresting the process of maladaptation of the carotid body to chronic stress such that carotid body can retain its life saving properties and not develop life taking properties. I don't think this will come from a pill in a box, but it might come from good diet and exercise early to prevent the development of obesity, diabetes hypertension and obstructive sleep apnea in some individuals. I look forward to continuing the conversation at ISAC XX, and invite you to join us and bring your family, friends and scientific colleagues to Baltimore, Maryland, USA 2017.

With respect to all the brilliant scientists who have contributed and continue to contribute and to the students who will contribute to our understanding of the contribution of the carotid body to health and disease.

Estelle B. Gauda, M.D.
Professor of Pediatrics
President, ISAC 2014–2017.

# Index





C. Peers et al. (eds.), *Arterial Chemoreceptors in Physiology and Pathophysiology*,
Advances in Experimental Medicine and Biology 860, DOI 10.1007/978-3-319-18440-1